Republic of Turkey
Ministry of Public Works and Settlement

General Directorate of Disaster Affairs

Seismic Microzonation for Municipalities

Pilot Studies: Adapazarı, Gölcük, İhsaniye and Değirmendere

January 2004

Prepared by:

DRM
world institute for
disaster risk management

With financial support from:

DEZA DIREKTION FÜR ENTWICKLUNG UND ZUSAMMENARBEIT
DDC DIRECTION DU DÉVELOPPEMENT ET DE LA COOPÉRATION
DSC DIREZIONE DELLO SVILUPPO E DELLA COOPERAZIONE
SDC SWISS AGENCY FOR DEVELOPMENT AND COOPERATION
COSUDE AGENCIA SUIZA PARA EL DESARROLLO Y LA COOPERACIÓN

Seismic Microzonation for Municipalities

This documentation is the result of a collaborative effort, led by the World Institute for Disaster Risk Management, Inc. (DRM) and the General Directorate of Disaster Affairs (GDDA), Ministry of Public Works and Settlement, Republic of Turkey, and financed by the Swiss Agency for Development and Cooperation (SDC) of the Federal Department of Foreign Affairs.

The following institutions and individuals contributed to this effort:

General Directorate of Disaster Affairs, Ministry of Public Works and Settlement (GDDA); Bogazici University, Kandilli Observatory and Earthquake Research Institute (BU-KOERI), Istanbul; Middle East Technical University (METU), Ankara; Sakarya University (SAU), Adapazari; Swiss Federal Institute of Technology Zurich - Institute for Geotechnical Engineering (ETHZ-IGT); Swiss Federal Institute of Technology Zurich - Institute of Geophysics (ETHZ-IG); Swiss Federal Institute of Technology Lausanne - Institut de Structures (EPFL-IS); Swiss Federal Institute for Snow and Avalanche Research (SLF), Davos; Studer Engineering, Zurich; Virginia Institute of Technology and State University (VT), College of Architecture and Urban Studies; University of Pennsylvania (UP), Wharton School – Risk Management and Decision Processes Center.

H. Akman (BU-KOERI), Walter J. Ammann (SLF), Atilla Ansal (BU-KOERI), Sami Arsoy (SAU), Marc Badoux (EPFL-IS), Sadık Bakır (METU), Murat Balamir (METU), Pierre-Yves Bard (University of Grenoble), Jonathan Bray (University of California, Berkeley), Juliane Buchheister (ETHZ-IGT), K. Önder Çetin (METU), Andreas Christen (ETHZ-IG), Barbara Dätwyler (SDC), A. Demir (GDDA), S. Demir (GDDA), Ekrem Demirbas (formerly GDDA, currently General Directorate of Technical Research and Application), M. Demircioğlu (BU-KOERI), M. E. Durgun (GDDA), Muzaffer Elmas (SAU), Mustafa Erdik (BU-KOERI), Ayfer Erken (Istanbul Technical University, ITU), Donat Fäh (ETHZ-IG), Yasin Fahjan (BUKOERI), Liam Finn (Kagawa University), Domenico Giardini (ETHZ-IG), Oktay Gökçe (GDDA), Christian Greifenhagen (EPFL-IS), A. Güldemir (GDDA), Ümit Gülerce (ITU), Polat Gülkan (METU), Jürg Hammer (DRM), Walter Hofmann (Brandenberger & Ruosch), İ. Kayakıran (GDDA), Rusen Keles (Ankara University), S. Kök (GDDA), M. Dinçer Köksal (DRM), Oliver Korup (SLF), Frederick Krimgold (DRM, VT), Howard Kunreuther (UP), Aslı Kurtuluş (ITU), Jan Laue (ETHZIGT), Pierino Lestuzzi (EPFL-IS), George G. Mader (Spangle Associates), Alberto Marcellini (CNR-IDPA, Milan), Roberto Meli (National University of Mexico), E. Nebioğlu (GDDA), Heinrich Neukomm (Board of the Swiss Federal Institutes of Technology), Akin Önalp (SAU), K. Özener (GDDA), Rocco Panduri (Studer Engineering), Karin Şeşetyan (BU-KOERI), Bilge Siyahi (BU-KOERI), Sarah Springman (ETHZ-IGT), Franz Stössel (SDC), Jost Studer (Studer Engineering), Mustafa Taymaz (GDDA), M. K. Tüfekçi (GDDA), Natasha Udu-gama (DRM), Robert Whitman (MIT, Massachusetts Institute of Technology), S. Yağcı (GDDA), A. Yakut (METU), Susumu Yasuda (Tokyo Denki University), U. Yazgan (METU), T. Yılmaz (METU).

The principal authors of "Pilot Studies: Adapazari, Gölcük, İhsaniye and Değirmendere" are: Coordinators: Atilla Ansal and Sarah Springman; Earthquake Hazard: Mustafa Erdik and Domenico Giardini; Microtremor Measurements: Donat Fäh; Geological and Geotechnical Tasks: Akin Önalp, Sarah Springman, Jan Laue, K. Önder Çetin, and Bilge Siyahi; Structural Damage Assessment: Polat Gülkan, Muzaffer Elmas and Pierino Lestuzzi; Data Processing and GIS plotting: Mustafa Taymaz, Ekrem Demirbaş, M. Dinçer Köksal, and Oktay Gökçe.

Citation: World Institute for Disaster Risk Management, Inc., 2004: Seismic Microzonation for Municipalities. Pilot Studies: Adapazari, Gölcük, İhsaniye and Değirmendere.

www.DRMonline.net

January 2004

Foreword

The Kocaeli Earthquake of August 17, 1999 revealed the devastating consequences that earthquakes can have for society and economy. In the aftermath of this earthquake, the General Directorate of Disaster Affairs started initiatives with the objective to mitigate the earthquake risk in Turkey.

The General Directorate of Disaster Affairs (GDDA), Ministry of Public Works and Settlement, undertook an endeavor entitled "Microzonation for Earthquake Risk Mitigation" (MERM).

The World Institute for Disaster Risk Management, Inc. (DRM) executed the project with financial support from the Swiss Agency for Development and Cooperation (SDC), of the Federal Department of Foreign Affairs, Switzerland.

Project design commenced in September 1999. The project was executed between March 2002 and February 2004.

This endeavor resulted in the following project documentation, under the generic title of "Seismic Microzonation for Municipalities": (1) Executive Summary; (2) The Seismic Microzonation Manual; and, (3) Reference information, consisting of pilot studies, a state-of-the-art report, and supporting documentation for sustainable implementation.

DRM executed the MERM Project with Turkish and international participation:

Bogazici University, Kandilli Observatory and Earthquake Research Institute (BU-KOERI), Istanbul; Middle East Technical University (METU), Ankara; Sakarya University (SAU), Adapazari; Swiss Federal Institute of Technology Zurich - Institute for Geotechnical Engineering (ETHZ-IGT); Swiss Federal Institute of Technology Zurich - Institute of Geophysics (ETHZ-IG); Swiss Federal Institute of Technology Lausanne -Institut de Structures (EPFL-IS); Swiss Federal Institute for Snow and Avalanche Research (SLF), Davos; Studer Engineering, Zurich; Virginia Institute of Technology and State University (VT), College of Architecture and Urban Studies; University of Pennsylvania (UP), Wharton School - Risk Management and Decision Processes Center.

The present document is entitled "Pilot Studies: Adapazari, Gölcük, İhsaniye and Değirmendere." It is part of the reference information and shows the application of the guidelines in the manual. The microzonation studies were conducted in two pilot areas: (1) Adapazari, (2) Gölcük, İhsaniye and Değirmedere. The activities can be described in different phases: acquisition and analysis of the geological and geotechnical data, determination of the earthquake hazard, microtremor measurements, evaluation of the liquefaction susceptibility and landslide hazard, mapping and final data evaluation. The damage encountered during the 1999 earthquakes is evaluated for comparison with the seismic microzonation..

Acknowledgements

A project of such dimensions, involving local and governmental authorities as well as several university institutions of worldwide reputation, and consisting of intensely interconnected tasks, can only be accomplished with the volition of all involved parties. Special thanks must be given to:

- The General Directorate of Disaster Affairs (GDDA), General Director Dr. Mustafa Taymaz, former Deputy General Director Ekrem Demirbas, Oktay Gökçe and the staff of GDDA for their cooperation in the development and implementation of the project.
- The Swiss Agency for Development and Cooperation (SDC) of the Federal Department of Foreign Affairs for funding the project, and for valuable contributions towards the improvement of project sustainability and implementation, in particular by Ms. Barbara Dätwyler and Dr. Franz Stössel.
- The Governors of the provinces of Kocaeli and Sakarya, as well as the authorities of the municipalities involved in the pilot studies, for their assistance given to the project team.
- The President of Sakarya University, Prof. Mehmet Durman, for helping the project in all stages with great effort.
- The members of the Technical Advisory Board for their comments on the manual, making it possible to achieve an international standard that includes state-of-the-art methodologies based on latest research results.
- All members of the project team for the constancy shown in the preparation of the assigned tasks.

TABLE OF CONTENTS

TABLE OF FIGURES

TABLE OF TABLES

1. INTRODUCTION

Atilla Ansal, Department of Earthquake Engineering, Kandilli Observatory and Earthquake Research Institute, Boğaziçi University

1.1. SCOPE

The microzonation studies were conducted in two pilot areas (1) Adapazarı, (2) Gölcük, İhsaniye and Değirmedere for the purpose of testing and demonstrating the applicability of the proposed microzonation procedure recommended in the Microzonation Manual. It was decided jointly on July 30, 2001 in a meeting held with General Directorate of Disaster Affairs (GDDA) to select two areas (Adapazarı and Gölcük-İhsaniye-Değirmedere) for the pilot studies. The location and general geology of the pilot areas are shown in Figure 1.1.

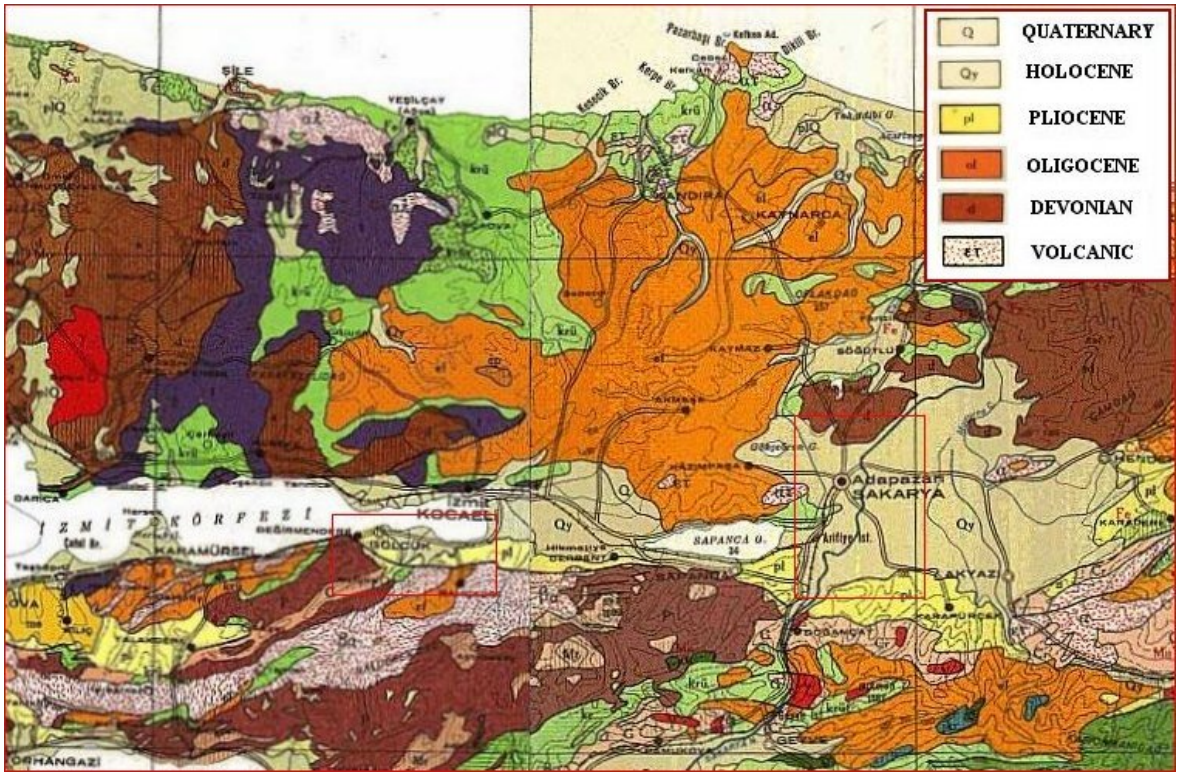

Figure 1.1. Location of the pilot areas over the Geology Map of the region

The microzonation studies in the pilot areas were carried out by the participation of researchers from Boğaziçi, Middle East Technical, and Sakarya Universities and Directorate of Disaster Affairs from Turkey, Institute of Geophysics and Institute of Geotechnical Engineering of the Swiss Federal Institute of Technology in Zurich, Structural Engineering Institute of the Swiss Federal Institute of Technology in Lausanne, Studer Engineering from Switzerland, and World Institute of Disaster Risk Management.

The procedure adopted was based on the consensus reached among the researchers involved in the study during the Concept (Ansal et al., 2002a) and Synthesis (Ansal et al., 2003) meetings held at Kandilli Observatory and Earthquake Research Institute of Boğaziçi University, in Istanbul during 13-14 June 2002 and 25-26 January 2003.

The final revisions on the Research Task Group Report (Part 2C - Case Studies dated May 7, 2003) were implemented after the Technical Advisory Board Meeting held in Zurich, Switzerland during June 2 and 3, 2003 in accordance with the Report of Technical Advisory Board (TAB, 2003). These revisions were mainly related to the definition of the

zoning parameters with respect to ground shaking and with the method applied for determining the liquefaction susceptibility. The methodologies followed are explained in detail in Chapter 11.

The related activities concerning the microzonation studies were carried out in seven partly simultaneous and partly consecutive phases. The first phase involved the compilation of the available geological and geotechnical data that was previously obtained for different purposes. A major portion of the available data was supplied by Prof. Önalp of Sakarya University. Limited numbers of additional subsurface explorations were also carried out under the supervision of Prof. Önalp to supplement the available data. The second group of data was supplied by Mr. Demirbaş of General Directorate of Disaster Affairs. These data were forwarded to Institute of Geotechnical Engineering of the Swiss Federal Institute of Technology in Zurich for analysis and evaluation. At the same time, all the available geotechnical data was converted to GIS format at the General Directorate of Disaster Affairs (GDDA) under the supervision of Dr. Köksal of DRM and Mr.Gökçe of GDDA.

The second phase of the study was the evaluation of the earthquake hazard for the microzonation study. In this phase, as previously decided, both pilot areas were divided into approximately 500 x 500 m grids to evaluate earthquake hazard parameters for each grid. The determination of the regional hazard for the pilot areas was one of the important contributions of this study to the state-of-the-practice of microzonation in Turkey. Since the region has experienced a very severe earthquake in the near past, basically two types of assessment were carried out, as explained in detail in Chapter 3 of this report. The first assessment was the estimation of the hazard parameters with respect to the Poisson model for a probability of exceedance of 10% in 50 years. The second assessment was the estimation of the hazard parameters with respect to time dependent probability by a renewal model taking into account the recent earthquakes of 1999. Since the major purpose for the microzonation study is for land use and city planning it was decided to determine the required earthquake hazard parameters based on the Poisson model for a return period of 100 years that corresponds approximately to 40% probability of exceedance in 50 years. This third assessment methodology is adopted as the method to be used for the estimation of the regional hazard parameters for the microzonation studies carried in the pilot areas.

The third phase of the study involved microtremor measurements in the pilot areas and interpretation of the results obtained, as explained in detail in Chapter 4 of this report.

The fourth phase of the study was the evaluation and analysis of the available geotechnical data to determine the necessary parameters for conducting the microzonation with respect to different parameters. Representative soil profiles and site conditions for each grid were determined, as explained in detail in Chapter 5. Site response analysis were conducted for each grid point using the simulated earthquake time histories obtained based on the seismic hazard study, as explained in detail in Chapter 6. However, even though it is recommended to use at least 6 simulated time histories for each grid point in the Microzonation Manual (Part 2B) only one simulated earthquake time history was used in site response analysis due to the time limitations.

The fifth phase involved the evaluation of the liquefaction susceptibility and landslide hazard based on the results obtained in the fourth phase of the study. The procedures adopted and the results obtained are explained in Chapter 7 and Chapter 8, respectively.

The sixth phase was the mapping of the results for the pilot areas taking into consideration the results obtained in the previous phases. A GIS mapping procedure was adopted to evaluate the variation of the calculated parameters in both pilot areas as summarized in Chapter 10.

The last phase involved the final evaluation of all the findings obtained from the studies conducted for specifying the microzonation with respect to site amplification, liquefaction susceptibility and landslide hazard as summarized, in the last chapter (Chapter 11) of this report.

Even though it may be considered not within the scope of a standard microzonation study, since two major earthquakes had taken place in the region, an attempt is also made, as summarized in Chapter 9, to evaluate and assess the damage encountered during these earthquakes for the purpose of comparison with respect to the microzonation that was obtained. The damage data was obtained from different studies conducted in the region after the 1999 earthquakes.

The work done in the different phases are explained in the following chapters of this report. The details concerning the microtremor study and the GIS based program developed for landslide hazard as well as the results obtained from site characterization, site response analysis, and microtremor measurements are given in the Appendix. In addition NEHRP summary pages and a study conducted by P.Lestuzzi on vulnerability of the structures are also given in Appendix.

1.2. BACKGROUND

Seismic microzonation requires multi-disciplinary contributions as well as comprehensive understanding of the effects of earthquake generated ground motions on man-made structures. It can be considered as the process for estimating the response of soil layers under earthquake excitations and thus the variation of earthquake ground motion characteristics on the ground surface. The key issue affecting the applicability and thus feasibility of any microzonation study is the suitability and reliability of the parameters selected for zonation.

The main reason behind a microzonation study is to use the obtained variation of the selected parameters for land use and city planning. Therefore it is crucial that the selected microzonation parameters should be meaningful for city planners as well as for public officials and should not lead to controversial arguments among the property owners and city administrators.

The purpose of seismic microzonation is to minimize the damage to the man-made environment. Thus, selection of the zonation parameters should be in accordance with this objective. Different zones could be delineated with respect to selected parameters to provide city planners with some guidelines for specifying population and building density, and, more specifically, building characteristics. All of these analyses have to be considered within a probabilistic framework in order to account for all possibilities that may arise due different earthquake source mechanisms attached with relevant exceedance probabilities (risk) levels that are suitable for the purpose.

Seismic microzonation can be considered as being composed of three main phases. In the first phase, the earthquake source characteristic for the study area needs to be determined more accurately in a probabilistic manner to satisfy the requirements of the civil engineering and urban planning. The second phase is the investigation of the geological and geotechnical site conditions taking into consideration all the relevant factors

(i.e. topographical and basin effects, variations in the soil stratifications, soil nonlinearity, etc.). This information is an essential ingredient for the assessment of site dependent seismic hazard studies. The third phase is the analysis and interpretation of the accumulated data in the first two phases to establish suitable and applicable microzonation parameters that could be utilized for urban planning and thus for earthquake risk mitigation.

The national seismic zoning maps are mostly at small scales such as 1:1,000,000 or less and are mostly based on seismic source zones defined at similar scales. However, seismic microzonation for a town requires 1:5,000 or even 1:1,000 scale studies and needs to be based on seismic hazard studies at similar scales. There appears to be a significant gap between the two zonation approaches in Turkey. The earthquake code utilizes national seismic macrozonation maps in specifying the minimum design requirements. Even though the purpose of earthquake codes are to deliver more site specific related estimation of the induced earthquake forces in accordance with the selected exceedance probability for the structural design, there are incompatibilities regarding the differences among the map scales adopted for estimating the earthquake hazard and the site characterization. Thus one purpose of the seismic microzonation could be to supply input for the structural design by replacing national macrozonation maps. However, the applicability of this approach is questioned by engineers and scientists as well as by public officials in charge of design and construction control, because the reliability and uniformity of these microzonation studies can not be assured. While the country wide macrozonation maps are produced by national experts and go through a careful review process, the same approach can not be followed for the large number of seismic microzonation studies. One possible solution for this scale incompatibility is to increase the scales of seismic zonation maps steadily with the accumulation of geological and seismological data as implemented by USGS in USA (Frankel et al., 2000; Leyendecker et al., 2000).

The general trend in conventional microzonation studies was to simplify the applied methodology by adopting the macrozonation seismic hazard maps as the primary source to estimate the earthquake hazard. In addition, due to the lack of sufficient geological and geotechnical data, a second simplification is to define the site conditions with respect to local geological units. It is important, as pointed out by Wills & Silva (1998) and Willis et al., (2000), to base this classification on accumulated data concerning the characteristics of each geologic unit. However, when conducting a seismic microzonation study at a scale of 1:5000, it is also essential to appreciate the possible variations in each geologic unit. The deviations from the mean values obtained for each geologic unit can exceed the permissible limits to justify its use for assessing the effects of local soil conditions. Wills & Silva (1998) suggested and utilized the average shear wave velocity in the upper 30 m as one parameter to characterize the geologic units while also admitting the importance of other factors such as impedance contrast, 3-dimensional basin and topographical effects, and source effects such as rupture directivity on ground motion characteristics. In the compiled database, they have encountered significant variations in the equivalent shear wave velocities especially in the case of alluvium deposits. These variations were deduced to be mainly due to the age and grain size characteristics, which are not always indicated in the geologic maps. Wills & Silva (1998) suggested using shear wave velocity for classifying site conditions rather than geological units, even though the determination of shear wave velocities requires extensive field investigations.

Even though these two simplifications may appear logical to many engineers and scientists, they are the main source of incorrectness in any microzonation study conducted at a scale of 1:5,000 and thus reduce the reliability and applicability of microzonation.

The increase in the accumulated instrumental and experimental data, as well as the advances in site evaluation and response analyses (Hartzell et al, 1997a), has led to extensive modifications of the microzonation methodology especially during the last decade. It was shown over and over again in the literature (Gazetas et al., 1990; Faccioli, 1991; Ansal et al., 1993; Bard, 1994; Chavez-Garcia et al., 1996; Chin-Hsiung et al., 1998; Gueguen et al., 1998; Kawase, 1998; Athanasopoulus et al., 1999; Hartzell et al., 2001) based on the encountered earthquake damage and strong ground motion records that there are numerous source and site factors (i.e. near field effects, directivity, duration, focusing, topographical and basin effects, soil nonlinearity, etc.) that are neglected in most conventional microzonation studies. However, these are the important parameters in assessing ground motion characteristics. Thus the main deficiency of any conventional microzonation study lies in its simplistic approach.

The response of man-made structures during earthquakes are not only related to structural features but also are controlled by two main factors: earthquake ground motion and local site conditions. Any seismic microzonation study neglecting the probable earthquake ground motion characteristics would be incomplete. In addition, the observed data and accumulated information in recent earthquakes and improved analysis methods available at the present have shown that zonation studies based only on geological formations would lead to limited assessment of the earthquake source and local site effects, thus would not yield accurate and comprehensive information that may be needed for city and urban planning.

One possible reason for this weakness and multiplicity in the seismic microzonation studies is the necessity for interdisciplinary interpretation of the obtained results. However, in most cases, seismic zonation studies, whether they are at macro or micro scale are generally conducted by earth scientists. Unlike seismic macrozonation, seismic microzonation requires an essential input from civil engineering, especially in the field of geotechnical engineering.

The results obtained from microzonation studies need to be treated as time dependent parameters and they have to be updated at regular intervals. And as more data becomes available, the reliability of the microzonation maps and their impact in city and land use planning will increase.

Geological formations, local site classification, equivalent shear wave velocity, peak ground acceleration, spectral amplification and their variation are some of the parameters studied during a seismic microzonation. A consistent approach has to be implemented to assess each parameter with respect to all other parameters. The objective of seismic zonation is to establish a seismic hazard map at a scale of 1:5000 taking into account earthquake source and local site conditions. Thus estimation of the earthquake induced forces and their variation in the investigated area must be the main target in seismic microzonation (Hartzell et al., 1997b). Even though seismic microzonation contains important information for city and urban planning, considering different structures with different functions, site specific studies need to be performed at each site to evaluate the effects of local soil conditions.

The geological and geotechnical site characterization requires detailed studies based on in-situ and laboratory tests, in order to have an accurate database to estimate site response characteristics (Abeki et al., 1995). The reliability of the result of the seismic microzonation study depends directly on how well the site characterization studies were conducted.

The simplest approach is to adopt the seismic macrozonation maps that delineate different seismic regions neglecting all the geological and geotechnical parameters. In this case, the whole city or the whole region would be in the same zone and thus land use and city planning would be identical for all regions and could even be considered as independent of seismic factors. In this case, the earthquake risk mitigation issue is reduced to designing and construction of more earthquake resistant structures in accordance with earthquake codes. The improvements in earthquake risk mitigation can be achieved with the advances in the earthquake codes and with the enhancement in the effectiveness of the design and construction control. However, all the available instrumental and damage data indicates that the earthquake ground motion characteristics could be very variable (Field & Hough, 1997), and in some cases could be stronger than those specified in the existing earthquake codes.

Even though the earthquake ground motion characteristics may be higher than those specified in the earthquake codes, this approach can still be considered as one possible alternative for new construction. However, in most of the highly seismic regions the existing cities have a long history with a large building stock that would not fit into this category. Thus in assessing the vulnerability of these buildings, it appears essential to have a more accurate estimate of the earthquake ground motion characteristics that may take place in the future. Therefore, it is necessary to conduct a comprehensive seismic microzonation for such cities and regions. Considering the legal and financial issues of rehabilitation, the accuracy and the reliability of the microzonation is a crucial parameter. Therefore, it appears necessary to improve the seismic microzonation methodologies to achieve improvements in earthquake risk mitigation policies. This would increase the cost of the seismic microzonation study and may seem to reduce the feasibility of adopting such a methodology. But any improvement in the accuracy and reliability of seismic microzonation would directly affect the rehabilitation costs. The savings that may be accumulated through a more comprehensive microzonation study could justify the increase in the cost of the microzonation study.

The seismic microzonation could be defined as the zonation with respect to ground motion characteristics taking into account source and site conditions (AFPS, 1995; ISSMGE/TC4, 1999). Therefore the major purpose is to estimate the variation of the earthquake ground motion characteristics (Marcellini et al., 1995; Lachet et al., 1996; Fäh et al., 1997; Lungu et al., 2000). But this purpose does not include the estimation of the structural damage distribution. The structural damage during an earthquake may be modelled as a complex function of three interacting factors; source, site and structural characteristics. Since microzonation only involves the first two factors, it may not be possible to model or estimate the structural damage distribution in any region during any earthquake.

1.3. PILOT STUDY AREAS

Since no detailed geological investigations were carried out within the scope of the DRM project an attempt is made here to review some of the observations in the literature by various researchers.

According to Rathje et al. (2000) "*The Adapazarı basin is a former Plio-Pleistocene lake. The lake sediments are overlain by Pleistocene and early Holocene alluvium transported from the mountains north and south of the basin. This older alluvium is overlain in some areas by recent (mid-to late Holocene) alluvium deposited by the Sakarya River and its tributaries. The City Adapazarı lies essentially on the active flood plains of the Sakarya River, and the river has deposited the soft near-surface sediments underlying*

the majority of the city. Additionally, ground water is very shallow in Adapazarı (i.e. less than 2 to 3 meters) due to the proximity of the city to the Sakarya River."

According to Bray et al., (2000) "*The city of Adapazarı is located over Holocene alluvial sediments created by the Sakarya River, which originally flowed westward through Lake Sapanca into the Sea of Marmara but now flows northward through the Adapazarı basin to the Black Sea. As evidence of the active fluvial processes in the Adapazarı basin, a masonry bridge built in a.d.559 on the old alignment of the Sakarya River is now 4 km west of the current river (Ambraseys and Zatopek, 1969). Due to active sedimentation and fluvial action, the subsurface conditions at Adapazarı are such that large variations of soil type and state are to be expected in both the vertical and horizontal directions. The soils reported in typical boring logs include fine sands, silty sands, silty clays, and gravels. The ground water varies seasonably but it is typical at a depth of 1 to 2 meters. As stated previously ……., the surface geology of Adapazarı consists generally of young alluvium but transition into Upper Cretaceous flysch in hills at the southwest part of the city. The Cretaceous bedrock consists primarily of marls, conglomerates, and limestone*."

One of the important studies conducted involved gravity survey in Adapazarı to estimate the bedrock topography by Komazawa et al., (2002). According to the authors "*Adapazarı is located in a basin of about 25 x 40 km^2. The alluvial plain is very flat. The downtown of Adapazarı is on the northeastern foot of hills. The hills form a row which looks like a peninsula extending eastward into the basin. Sakarya River runs from south to north in the basin, and enters into Black Sea. The main North Anatolia fault of E–W strike forms the southern boundary, and the Duzce fault of NE–SW strike, the southeastern boundary. There are steep mountain ranges of about 1000 m high on the south of the faults. The era of the basement rocks is different between the northern and southern parts: Devonian and Silurian in the northern part and Cretaceous in the southern part. Various rocks such as metamorphic, intrusive and volcanic rocks are observed along the faults. Volcanic ash–soil of Eocene covers these basement rocks. During the 1999 earthquake, surface ruptures with displacement up to 5 m appeared along the North Anatolia fault suggesting at least two narrow depressions of bedrock in the basin. Moreover, it is very noticeable that, dense distribution of linear contours extends in nearly E–W direction along about 40°48´N. The rate of change in gravity is comparable to those along the North Anatolia faults.*"

The topography of the region was given by Komazawa et al., (2002) as shown in Figure 1.2. The bedrock topography determined by Komazawa et al., (2002) is used to understand the situation below the Adapazarı pilot area as shown in Figure 1.3.

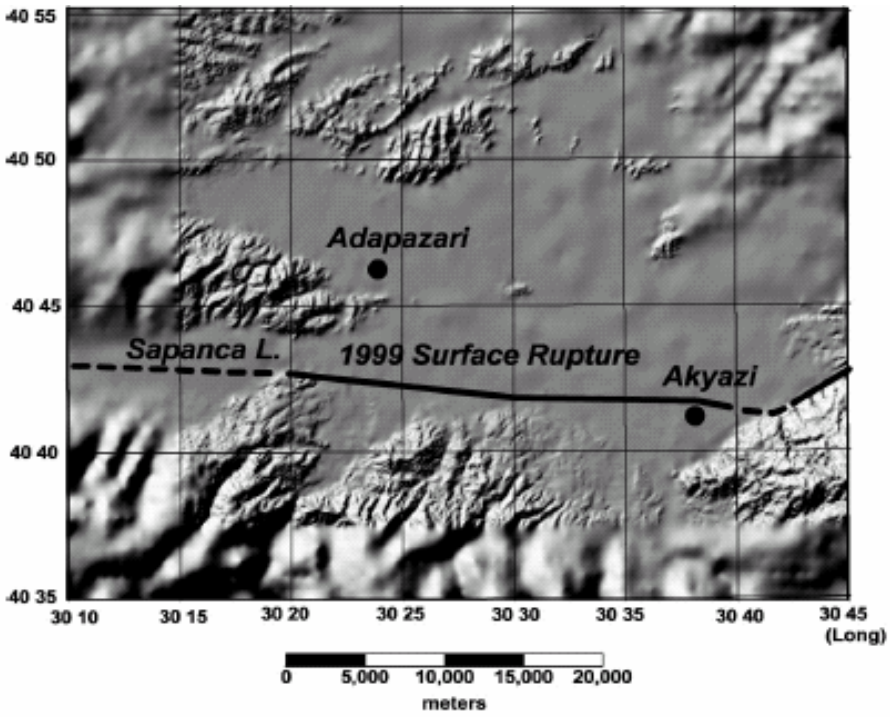

Figure 1.2. Topography around Adapazarı drawn using GTOPO30 and available local maps. Adapazarı is located on the foot of peninsula-like hills (After Komazawa et al., 2002)

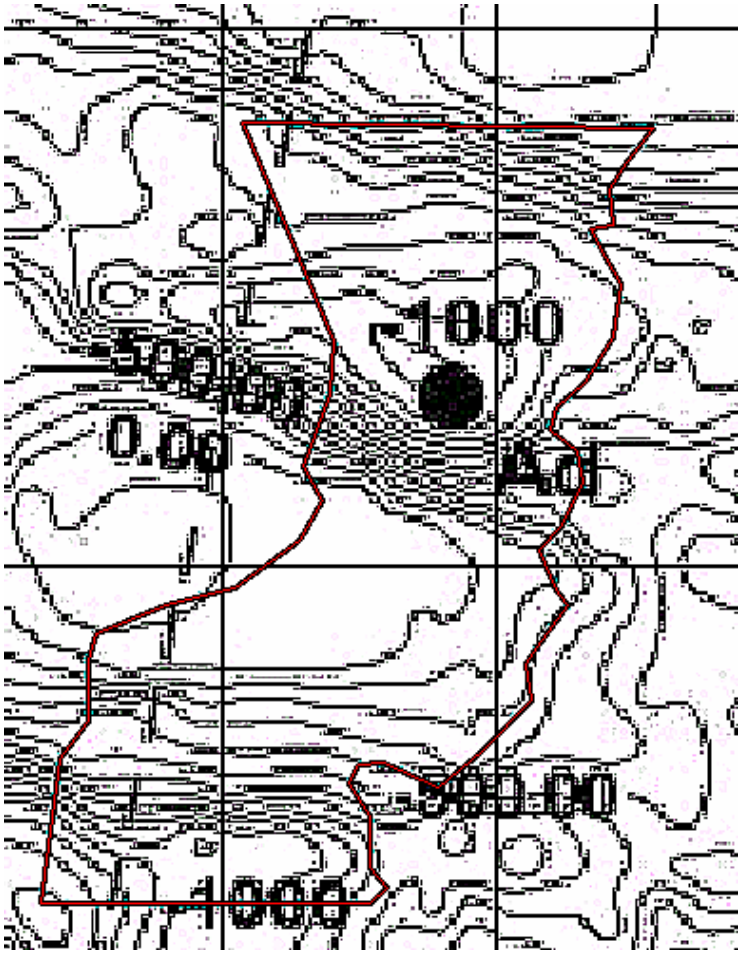

Figure 1.3. The variation of basin depth in Adapazarı based on the findings of Komazawa et al. (2002)

2. THE GEOLOGY AND GEOTECHNICAL CHARACTERISTICS OF THE PILOT AREAS

Akın Önalp, Professor of Geotechnical Engineering, Istanbul Kültür University

2.1. INTRODUCTION

The main purpose of this Project had been designated as preparing a manual for microzonation studies to be used by the municipalities within the earthquake hazard zones of Turkey. There was no hesitation among the parties concerned at the inception as to which pilot areas to choose, because the region to the east of Marmara Sea offered all possible variations of geology and earthquake conditions for an instructive study such as this Project. The locations were therefore selected to be Adapazarı, İhsaniye, Gölcük, and Değirmendere which had all suffered heavily during the 1999 earthquake and yet possess different geological and geotechnical characteristics owing to their position to the south and the north of the North Anatolian Fault (NAF) as shown in Figure 2.1.

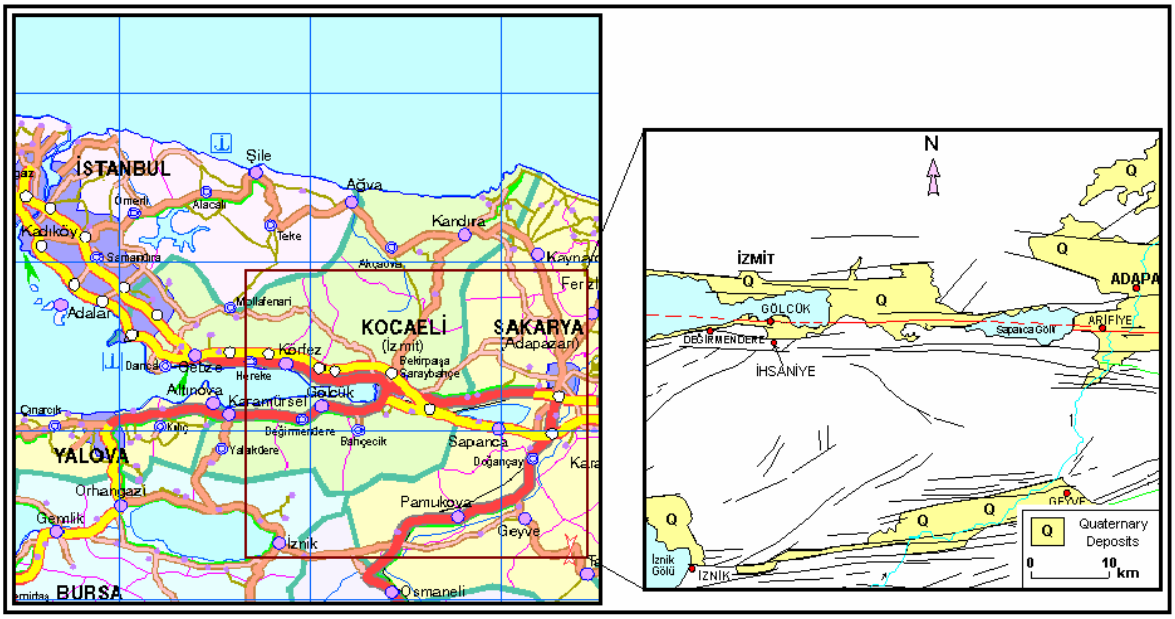

Figure 2.1. Location and general geology of the pilot areas

2.2. ADAPAZARI AREA

2.2.1 Geology

The geological studies done in the past have determined that the oldest unit in the region is the Sultaniye metamorphites dating back to Permian-Triassic. This unit consists of volcano-sedimentary and volcano-clastic rocks metamorphosed to schists, quartzites, marble and phyllites. This unit can be observed to the south of the town of Sapanca by the lake.

Akçay metamorphites of the Cretaceous outcrop to the south and southeast of Sapanca.

The Akveren formation of Upper Cretaceous and Lower Eocene, consisting of marl, clayey limestone, mudstone, siltstone, claystone and recifal limestone can be seen on the hills to the west of Adapazarı.

Miocene and Pliocene is represented by the Örencik formation comprising loosely cemented conglomerate, limestone and mudstones.

The Quaternary is the dominant formation in and around Adapazarı which is represented by Holocene and recent sediments, with thicknesses up to several hundred meters.

One widespread speculation is that the Black Sea was formerly connected to the Marmara through the "Strait of Adapazarı-Izmit" when the current Bosporus had not been incised, thus the extreme depth of the basin. It is nevertheless difficult to explain how the basin was filled with sediments up to 1000 m within a short geological time period of seven to ten thousand years.

The groundwater table (GWT) in the region is believed to be closely related to the rivers surrounding the city, thus indicating seasonal fluctuations up to a meter. The average GWT depth in the city is around – 2 m at the present time and construction of the sewage and water supply lines appears to have caused a general drop of about 0.5 m since the earthquake, probably due to the extensive permeable backfill used. The claims that GWT rose markedly shortly before the earthquake are unfounded.

The North Anatolian Fault (NAF) is the dominant geomorphological feature in the area. The NAF runs in an east-west fashion and is known to become active at intervals of approximately a decade. This transform fault generates earthquakes of magnitude 7.2 or higher resulting in widespread damage in Arifiye and Adapazarı city.

2.2.2 Soils of Adapazarı

Among the sites chosen, Adapazarı-Arifiye area is the most perplexing and peculiar from the point of view of ground conditions. This city, with a history going back over 1000 years, is located in the vicinity of the River Sakarya. Its name translates as "island market", indicating a long past of annual flooding and river meandering, which frequently necessitated the use of boats to reach the central market here. Flooding by the river Sakarya was last recorded on the Adapazarı plain in 1963, after which dams constructed upstream have checked the excessive flows of the past. The other stream, Çark, currently flows along the west side of the city, draining the nearby Lake Sapanca northwards. No record of flooding caused by this stream is available, but evidence exists to suggest that it has periodically altered course towards the city centre, leaving behind marshes. The altitudes on the axis from Arifiye to the Northern limits of the city of Adapazarı vary between 28 and 32 meters and the area of study can, for most practical purposes, be assumed to be a flat site. The hills to the west of Adapazarı rise up to 250 m.

The upper cretaceous flysch bedrock makes a notch shaped valley along a North-South axis under the city centre which has been filled with fluvial and lacustrine sediments for the past 7000 years. The current depth of the basin is estimated to be over 1000 m with the result that earthquakes that hit at intervals of a decade have had devastating effects, possibly due to ground amplification effects. The sediments are soft and loose with the ground water table rising to the surface in spring months in many locations. Carbon dating on fragments of a reed found at a depth of 7.5 m revealed that it could not be older than 700 years. This corresponds to an excessive rate of sedimentation in the Holocene. Overwhelmingly green and occasionally brown non-plastic silts are liquefiable and are found in the top 10 m. The color indicates the genetic property, which are metamorphic rocks along the Geyve Valley through which River Sakarya flows. The brown clays are found below 6 m and are deposits in shallow lakes. Grey clays of high plasticity are sediments likely to be deposits of temporary swamps of the past. A majority of soils in

Arifiye appear to be predominantly clays of high plasticity and organic content, suggesting the presence of large marshes in the past.

A total of about 600 high quality boreholes and soundings have been implemented since the 1999 earthquake by Sakarya University. Most of the boreholes were 15m deep with several selected spots reaching 30 m. Additionally, a pilot borehole of 200 m was drilled in the middle of the city. The information collected from the work during the past three years indicates that the soil conditions in the city can be summarized as follows.

- The soil layering is exceptional: The velocity and the duration of flooding formed layers as thin as a few centimeters and the thickness of most layers rarely exceed a few meters.
- The top 5 m is dominated by silts and their age is between 100 and 1000 years.
- Clays and sands appear as bands, high plasticity clays being sedimented in former marshes or possibly shallow lakes, and the sands and silty sands along former and buried streams.
- Gravel is rarely encountered, and its presence is a clear indication of the former beds of Sakarya and Çark streams.

A total of 3850 samples mostly from the top 15 m depth were classified according to the Turkish Standard TS1500/2000 and 1210 were found to be silts and 1659 clays. All the data available points out to the fact that Adapazarı-Arifiye region is a fine soil zone.

The NAF is approximately 3 km from Arifiye village and 8 km from the centre of Adapazarı. Proximity to the fault, however, appeared not to be proportional to building damage.

2.3. IZMIT AREA

Izmit area has a unique geological past. The Sea of Marmara has inundated the region during the Triassic and receded in the upper Triassic only to return by the Upper Cretaceous. This marine character of the deposits has persisted until the late Cretaceous. The continental shelves to the North and South of Marmara Sea define a geological and geomorphologic lineation. This linearity is probably a continental meeting region, which joins the abyssal plane that forms the base of the sea and the Palaeozoic island arc of Kocaeli peninsula. This connection has subsequently yielded to form the North Anatolian Fault (NAF). The stratigraphy of the region to the North and the South of the NAF is shown in Figure 2.2.

2.3.1 Gölcük and İhsaniye

The town of Gölcük and the village of İhsaniye are located on the Armutlu Peninsula which has two basic tectono-stratigraphic units brought together during the Mesozoic. These are the Pamukova and İznik metamorphites. These units are covered by an Upper Cretaceous limestone later overlain by the Bakacak Formation comprising sandstone-siltstone and gravelstone. All these units are covered by land and coastal sediments represented by claystone-sandstone-and limestones of the Kılınç Formation aged Miocene.

The Pliocene (Cenozoic) Aslanbey Formation that is found discordantly over the Kılınç Formation is formed by lightly cemented claystone-sandstone-siltstone and gravelstone. Its thickness has been estimated to be in excess of 700 m.

North flank			NAF	**South flank**	
Age	Formation	Properties	Age	Formation	Properties
Quaternary	Alluvium	Gravel, Sand, Silt, Clay	Quaternary	Alluvium	Gravel, Sand, Silt, Clay
Pliocene	Örencik Fm.	Gravelstone, Sandstone, Mudstone, Claystone	Pliocene	Arslanbey Fm.	Conglomerate, Sandstone, Mudstone, Marl
Upper Miocene Bottom Pliocene	Meşetepe Fm.	Gravelstone, Sandstone, Claystone, Coal	Eocene	Sarısu Fm.	Agglomerate, Tuff, Andezite, Basalt
Lower-Middle Eocene	Çaycuma Fm.	Sandstone, Mudstone, Marl, Limestone	Paleocene	İncebel Flysch	Sandstone, Mudstone, Marl, Conglomerate
Paleocene Lower Eocene	Atbaşı Fm.	Marl, Shale, Sandstone	Upper Cretaceous	Bakacak Fm.	Olistostromal rocks, Flysch
Upper Cretaceous Paloecene	Akveren Fm.	Fragmented limestone, Clayey limestone, Marl	Permo-Triassic	Pamukova Metamorphic Group	Amphibolite, Metagranite, Shale
Upper Cretaceous	Teksen Fm.	Conglomerate, Sandstone with carbonate levels	Upper Triassic and earlier	İznik Metamorphic Group	Shale, Marble, Meta fragments
Lower Triassic	Erikli Fm.	Siltstone, Shale, Sandstone			
Permo-Triassic	Çakraz Fm.	Conglomerate, Sandstone, Mudstone			
Upper Ordovician Lower Silurian	Gözdağ Fm.	Sandstone, Shale, Limestone			
Lower-Middle Ordovician	Aydos Fm.	Quartz, Quartzarenite, Quartz conglomerate			
Lower Ordovician	Kurtköy Fm.	Conglomerate,Arkose Mudstone			

Figure 2.2. Stratigraphic Column from the Region Studied

2.3.2 Gölcük

The area studied in Gölcük is about 600 ha and can be typified by two main geological units: The Aslanbey formation representing the Pliocene is observed to the north of the main highway roughly bisecting the town, rising from about 10 to 350 m; and the Quaternary sediments over the Pliocene mainly on the north side of the highway extending into the sea.

The Aslanbey formation is known to contain sandstone-siltstone-claystone, and rarely gravelstone, and can be described as a soft rock although its appearance is of soil rather than a rock. It is nevertheless considered a reliable stratum for foundations,

especially when it is found in the form of sandy-gravely clay. This formation is not permeable and groundwater is not always present, especially on the slopes south of the town.

The quaternary sediments have been supplied by the Selimiye (Kazıklıdere) creek, now reaching the sea on the eastern limit of Gölcük and contain sand-silt and clay. Boreholes on the flat northern part of Gölcük supplied samples which contained organic marine sediments occasionally include shells. The depth of groundwater was measured to be between 2 to 6 m. The thickness of the sediments changes from 15 m along the shore to 1 m in vicinity of the highway. The thickness of the alluvium increases to 50 m towards the east near Kavaklı.

The most important ground feature in and around Gölcük is the presence of the active faults one of which traverses the town along the north coast and another along Atatürk Street within the town centre. They have caused widespread damage during the 1999 earthquake. Notably in the military zone where the Turkish Navy was based, evidence of liquefaction is rare and confined to the narrow band along the coast line.

2.3.3 İhsaniye

The municipality of İhsaniye is the next centre of settlement to the east of Gölcük. The village is about two kms inland from the main highway and is characterized by the presence of two streams of Selimiye (Kazıklı) and Asar (Hisar).

The area of study of about 490 ha contains the geological units Iznik metamorphites (Triassic-Lower Cretaceous), Limestone members of the Bakacak formation aged Upper Cretaceous-Mesozoic, Pliocene-Cenozoic aged Aslanbey Formation and the Quaternary alluvium.

The Iznik metamorphites represented by meta-sandstones, meta-siltstones, chert, radiolarite and shales cover a limited area and their thickness has been estimated to be more than 1000 m.

Bakacak Formation consisting mainly of limestones is frequently encountered in the southern limits of the study area. Weathered sections have clayey limestones with a cover of residual soil. The thickness of this formation is around 100 m.

The Aslanbey formation covers significant areas. It consists of loose and lightly cemented sandstones-siltstones-claystones and gravelstones (conglomerates). It often behaves as soil due to past extensive weathering and degradation. Its thickness is in the order of 100 m.

The older geological units of the study area have degraded; they have been eroded and transported by the two streams forming the east and the western limits of the municipality. The alluvium may contain two different compositions, one with boulders and the other with not such coarse material.

Another special feature of Ihsaniye is the presence of deposits of talus, that cover parts of Bakacak and Aslanbey formations and contains the gravels of these rocks (D_{max} up to 200 mm), being lightly cemented by carbonates and clay. Their recorded thickness reaches 10 m.

The Kavaklı fault which is 8 kms from Gölcük is the main structural defect in İhsaniye and has caused significant damage in 1999.

2.3.4 Değirmendere

It is known that the oldest units of the Izmit Bay region are the Yedigoller formation consisting of metasandstones, shales, meta volcanites and metagranotoids of the Paleozoic. These rocks are encountered in the mountains to the south and the southwest of Değimendere. This is overlain by the Pontian aged weakly cemented gravel-sand-claystone-conglomerate series (Örencik Fm.) and the younger deposits including talus and scree.

Limited parts of the town are located on the Paleozoic Yedigöller formation. Pontian aged reddish or yellowish brown land sediments cover the central and the eastern part of the town. Current steep slopes and the Pliocene cover are located over the Pontian aged conglomerates.

Holocene coastal and fluvial sediments cover wide areas on the North part of Değirmendere. The contact between the alluvium and the Pontian is exhibited by the presence of a terrace along the present coast, possibly parallel to the former shoreline, a clear evidence of a tectonic subsidence. Such terraces are commonplace along the coast of Marmara and their presence is an indication of past of earthquake activity. A large alluvial fan has been formed in the Holocene when sea level was much lower and the Değirmendere stream was able to break through the Upper Pleistocene terrace, providing ample sediments to the shore and the sea.

Taluvium is another deposit particular to Değirmendere which was formed along the toe zones of the Paleozoic metamorphite slopes.

The 1999 earthquake has caused several calamities including heavy damage by tsunami-like waves and subsidence of a substantial portion of the shoreline. This subsidence has been attributed to the throw of the fault and submarine slope failure as well as lateral spreading.

The typical geotechnical profile of Değirmendere can be summarized as scree at the toe of the slopes, alluvium of the Quaternary and lightly cemented terrigenous (land) sediments deposited on Paleozoic metamorphics. Ground failure therefore has mainly been observed to be to be limited to the coastal strip. The near surface groundwater table has accordingly also been restricted to the flat areas near the sea.

3. ASSESSMENT OF THE SEISMIC HAZARDS IN ADAPAZARI, GÖLCÜK, DEĞİRMENDERE AND İHSANİYE PROVINCES IN NORTHWESTERN TURKEY

M. Erdik, K. Şeşetyan, M. Demircioğlu, B. Siyahi and H. Akman, Department of Earthquake Engineering, Kandilli Observatory and Earthquake Research Institute, Boğaziçi University

3.1. INTRODUCTION

This report presents the essential ingredients of the assessment of the seismic hazard for Adapazarı, Gölcük, Değirmendere and İhsaniye regions conducted in connection with the Earthquake Hazard Task of DRM-MERM Project (Figure 3.1). The study involves a probabilistic estimate of the expected ground motions at the sited locations for the next 50 years. The methodology used in this study is similar to the one used by the U. S. Geological Survey to develop the current seismic hazard maps for the United States. The program utilized in the assessment of the seismic hazard is also the code developed by A. Frankel and used by USGS (Frankel et al., 1996). Necessary tools and examples for the construction of the response spectra and for the simulation of the spectrum compatible design basis ground motion are also presented.

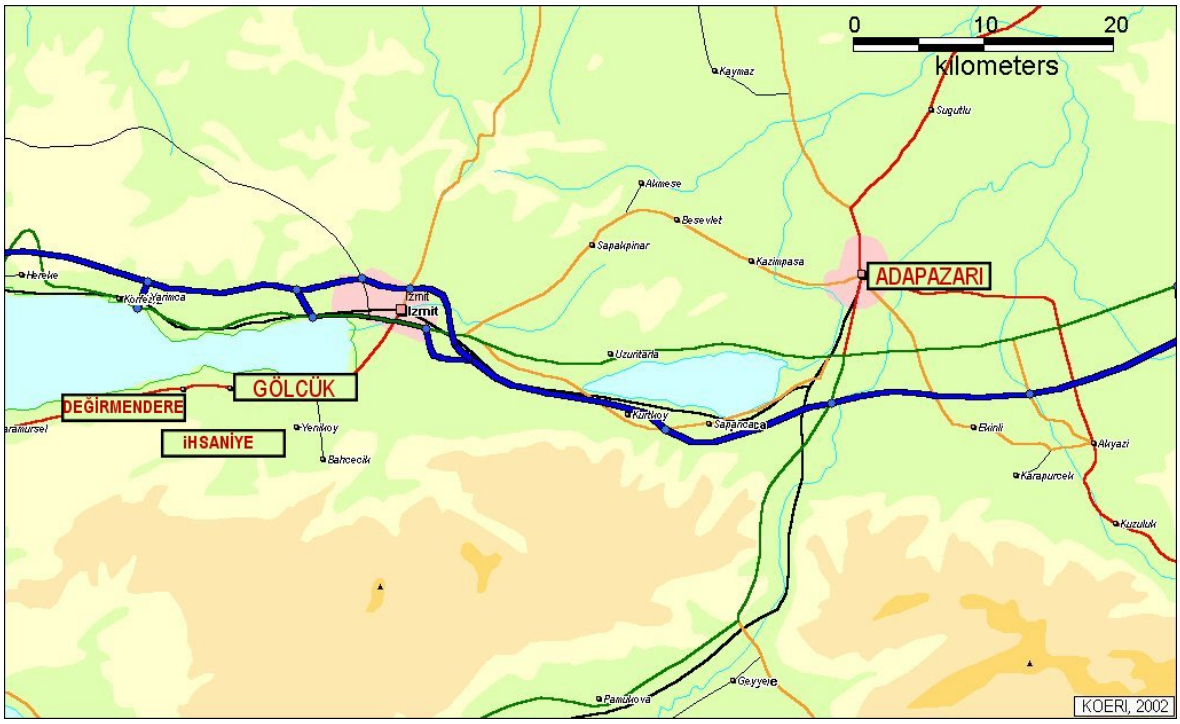

Figure 3.1. Location map of the study regions.

3.2. TECTONICS

The fault segmentation model used in this study is based on a compilation of data from various studies (Barka and Kadinsky-Cade, 1988; Şaroğlu et al., 1992; Akyüz et al., 2000; LePichon et al., 2001; Yaltırak, 2002). Various fault models developed in the mentioned studies are given in Figure 3.2 through Figure 3.6. The fault segmentation model developed for this study is presented in Figure 3.7.

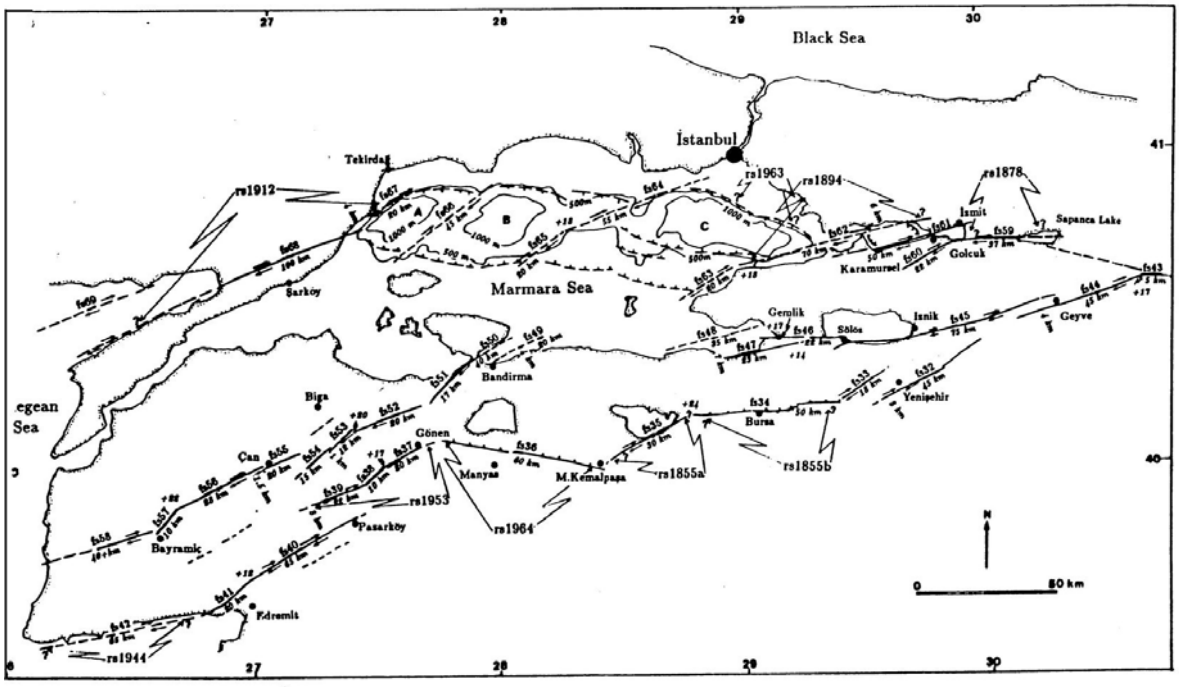

Figure 3.2. Active fault segments in the western section of the North Anatolian Fault Zone, in the Marmara Sea region (Barka and Kadinsky-Cade, 1988)

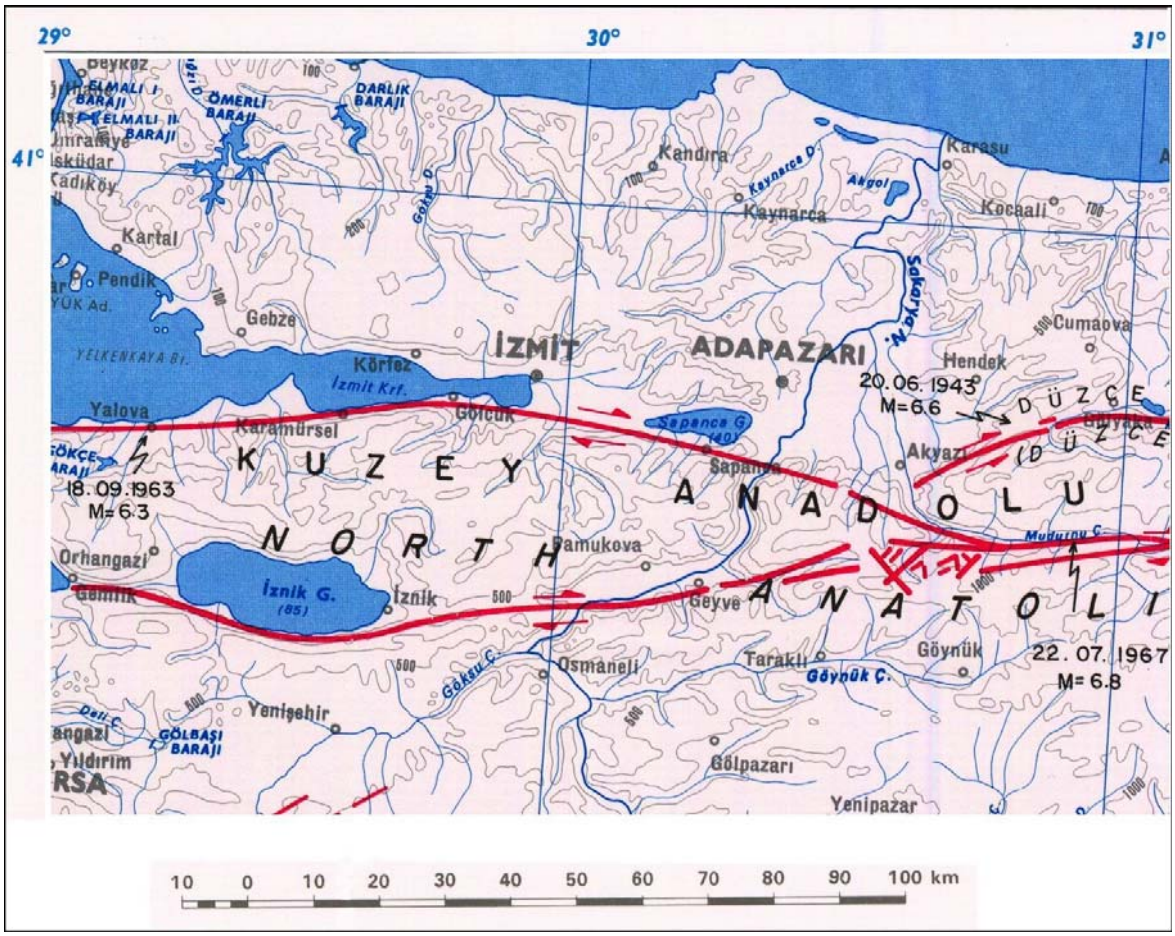

Figure 3.3. Active fault map of the region (Şaroğlu et al., 1992)

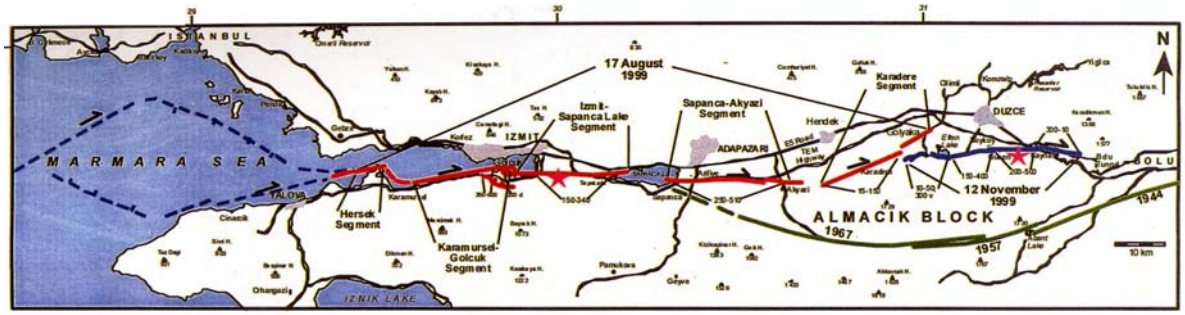

Figure 3.4. Active faults of eastern Marmara region during the last century (Akyüz et al., 2000)

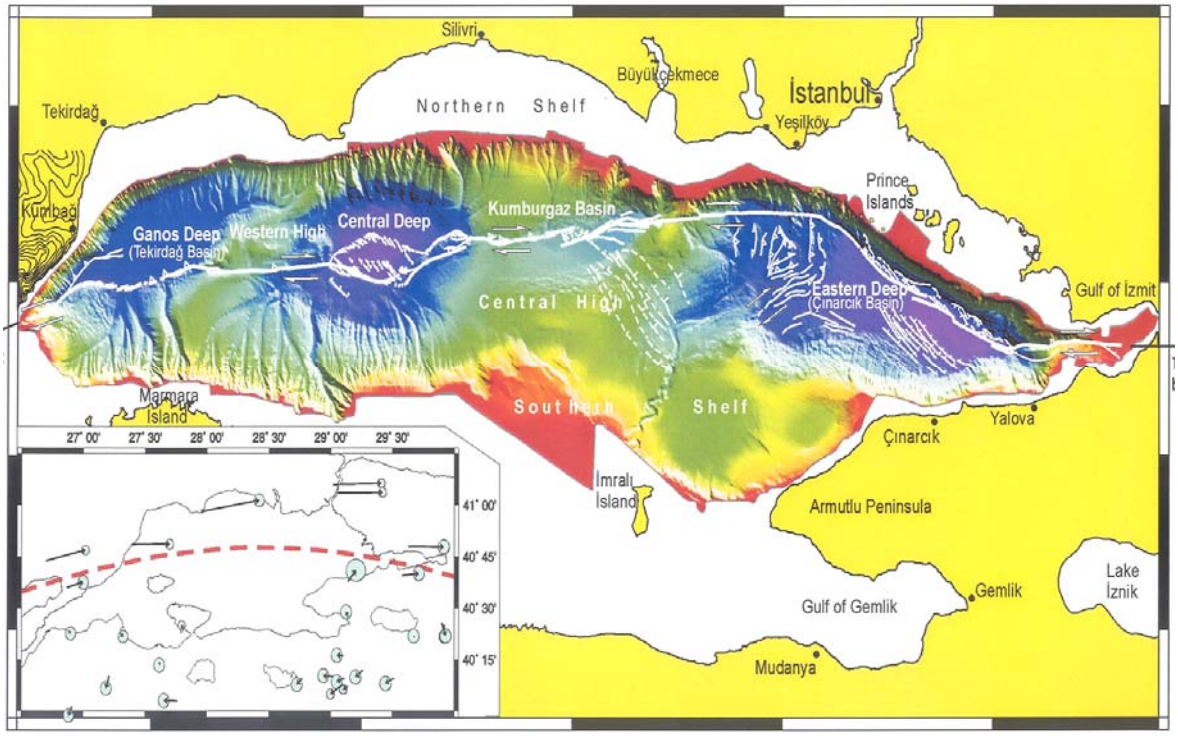

Figure 3.5 The recent high-resolution bathymetric map obtained from the survey of the Ifremer RV Le Suroit vessel that indicates a single, thorough going strike-slip fault system (LePichon et al., 2001).

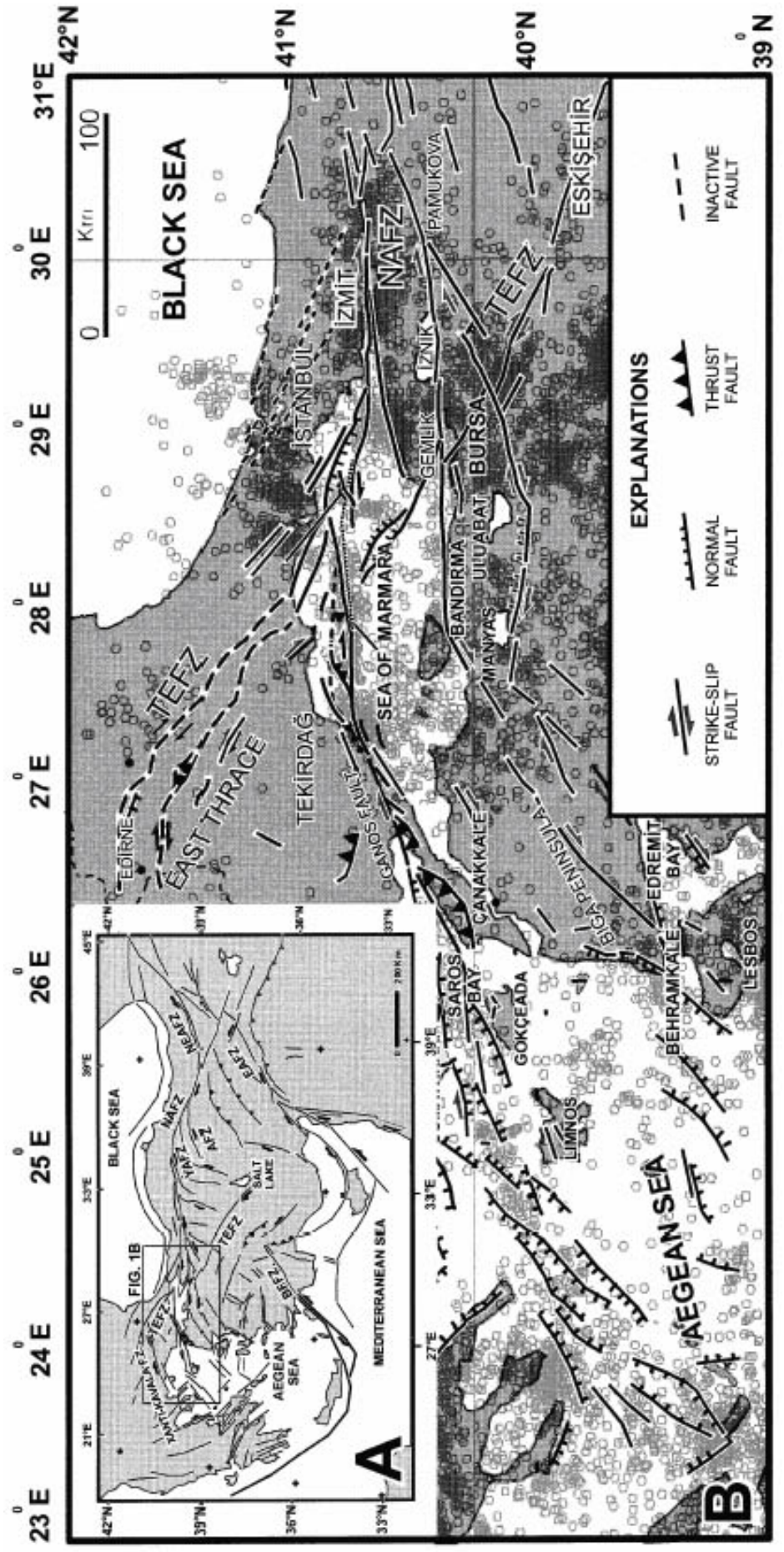

Figure 3.6. (A) Simplified tectonic map of eastern Mediterranean region, (B) Seismotectonic map of the Marmara Sea Region (Yaltırak, 2002)

Figure 3.7 Fault segmentation model developed for this study.

3.3. SEISMICITY

The historic and instrumental seismicity of the Marmara region has been thoroughly investigated in the report named "Earthquake Risk Assessment in Istanbul Metropolitan Area" prepared by the Earthquake Eng. Dept. of B.U. KOERI (Erdik et al., 2002). The historical seismicity and the seismicity of the 20th century in the Marmara region are illustrated in Figure 3.8 and Figure 3.9 respectively.

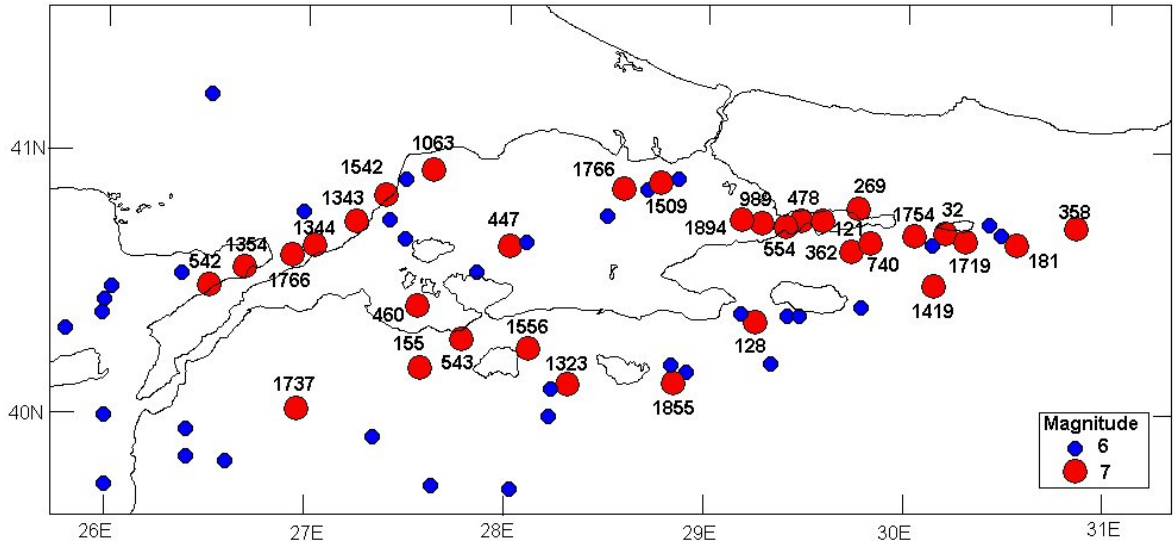

Figure 3.8. Historical Earthquakes in the Marmara Sea region
(from Ambraseys & Finkel, 1991)

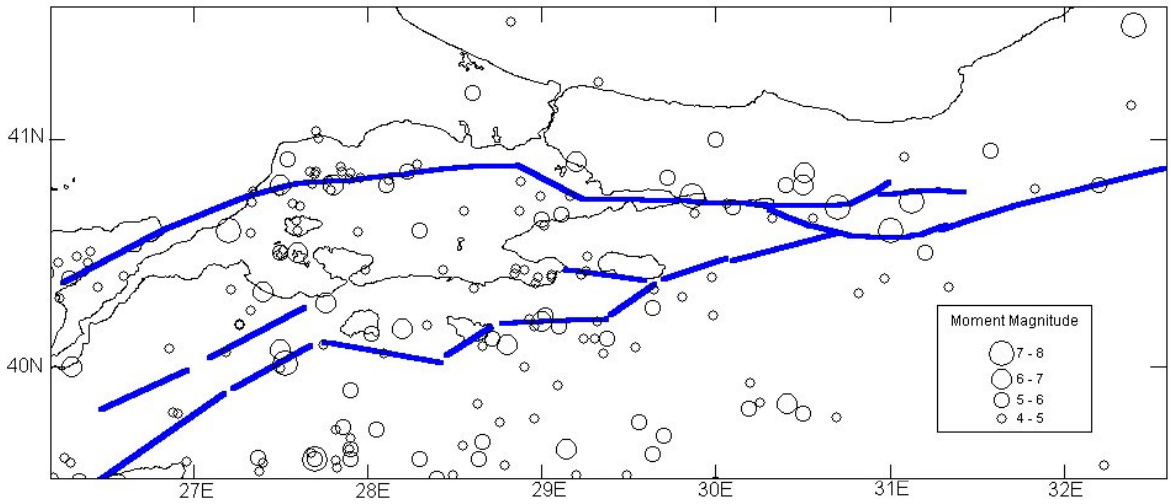

Figure 3.9. Seismicity of the last century

The association of earthquakes between 1500-present with the segmentation proposed for the Northern Portion of the North Anatolian Fault in the Marmara Region is given in Table 3.1. The historical events, characteristic earthquakes, recurrence intervals and annual probabilities associated with each segment of the model are given in Table 3.2.

Table 3.1. Association of earthquakes between 1500-present with the segmentation proposed for the Northern Portion of the North Anatolian Fault in the Marmara Region.

Earthquake	Fault Segment
10.9.1509 (Ms= 7.2)	7, 8
10.5.1556 (Ms=7.2)	9
25.5.1719 (Ms=7.4)	2, 3, 4, 5
2.9.1754 (Ms=6.8)	6
22.5.1766 (Ms=7.1)	7, 8
5.8.1766 (Ms=7.4)	11
10.7.1894 (Ms=7.3)	3, 4, 5
9.8.1912 (Ms= 7.3)	11
17.8.1999 (Ms=7.8)	1, 2, 3, 4

Table 3.2. Characteristic and renewal model parameters associated with the segments.

						Time dependent		Characteristic
Segment	Last Characteristic Earthquake	COV	Mean Recurrence Time	Maximum Magnitude	Time since Last Eq	50 year prob.	Annual Rate	Annual Rate
1	1999	0.5	140	7.2	3	0.0344	0.0007	0.0071
2	1999	0.5	140	7.2	3	0.0344	0.0007	0.0071
3	1999	0.5	140	7.2	3	0.0344	0.0007	0.0071
4	1999	0.5	140	7.2	3	0.0344	0.0007	0.0071
5	1894	0.5	175	7.2	108	0.3734	0.0093	0.0057
6	1754	0.5	210	7.2	248	0.4095	0.0105	0.0048
7	1766	0.5	250	7.2	236	0.3374	0.0082	0.0040
8	1766	0.5	250	7.2	236	0.3374	0.0082	0.0040
9	1556	0.5	200	7.2	446	0.5212	0.0147	0.0050
10		0.5	200	7.2	1000	0.3340	0.0081	0.0050
11	1912	0.5	150	7.5	90	0.4206	0.0109	0.0067
12	1967	0.5	250	7.2	35	0.0203	0.0004	0.0040
13		0.5	600	7.2	1000	0.1771	0.0039	0.0017
14		0.5	600	7.2	1000	0.1771	0.0039	0.0017
15		0.5	1000	7.2	1000	0.0974	0.0020	0.0010
16	1855	0.5	1000	7.2	147	0.0006	0.0000	0.0010
17	1855	0.5	1000	7.2	147	0.0006	0.0000	0.0010
19	1944	0.5	250	7.5	58	0.0597	0.0012	0.0040
21	1999	0.5	250	7.2	3	0.0012	0.0000	0.0040
22	1957	0.5	250	7.2	45	0.0347	0.0007	0.0040
25		0.5	1000	7.2	1000	0.0974	0.0020	0.0010

3.4. METHODOLOGY

The earthquake hazards in the region are assumed to be the result of the following contributions, computed in following two steps:

a. Ground motions that would occur as the result from the earthquakes in the magnitude range from 5.0 to 6.9.
b. Ground motions that would result from larger magnitude events in the magnitude range 7.0 and higher.

Part (a) is termed as “background activity”, i.e. the activity not associated with the main tectonic entities. In the computation of part (a), an earthquake catalogue of magnitude 5.0 and higher events are used. These events are not assigned to specific faults (the resolution of the neo-tectonic studies that we have compiled from literature does not allow such an association), but they are assigned to cells of a grid (of size 0.005° x 0.005°), in other words each cell of the grid is assumed to be a potential source for moderately sized events. It is also assumed that a Gutenberg-Richter type recurrence relationship governs the earthquake recurrence in the background.

To compute the seismic activity in each cell first an overall “b” value is calculated for the entire region. Although the maximum likelihood method (Weichert, 1980) yielded a “b” value of 0.8 for the Marmara region, mainly to account for the deficiently reported earthquakes at lower magnitudes, a “b” value of 1.0 is preferred for the analysis. Following

that, the "a" value in each source cell is obtained using the earthquake catalogue considered to be complete since 1900 and 1940 for magnitudes greater than 5.5 and 5.0 respectively. As such, the background activity is assumed to be Poissonian. The girded rates are spatially smoothed with a two-dimensional Gaussian filter with a decay distance of 50 km. This approach is in conformity with what is currently been done by USGS for the assessment of earthquake hazard in California.

Part (b) is related with the seismic energy release along well-defined faults. For this part, a fault segmentation model is developed and it is assumed that energy along these faults is released by characteristic events characterized by magnitude and recurrence time. Two models have been used to determine the seismic activity along these linear source zones: these are a Poisson model using a characteristic earthquake recurrence relationship and a time dependent (renewal) model. The Poisson and the renewal models differ in that in the Poisson model the probability of occurrence of the characteristic event does not change in time, whereas in the renewal model it increases as a function of the time elapsed since the last characteristic event.

The characteristic earthquake recurrence rates are determined by assigning characteristic magnitude and recurrence intervals to each fault segment in the region. The model assumes that seismic energy along the segments ate released by characteristic earthquakes. In this study, the Young and Coppersmith (1985) model is used to determine the magnitude distribution. In this model, the fault generates moderate magnitude earthquake as well as characteristic earthquakes. Figure 3.10 represents the magnitude density function of this model.

Figure 3.11 compares the recurrence relationships that would result from the assumption of "Truncated Exponential (i.e. Gutenberg-Richter) Model" and the "Characteristic Model" based on the Young and Coppersmith (1985) study.

The historical seismicity, the tectonic models and the known slip rates along the faults constitute the main data used in the assignment. The annual rates are then calculated as:

$$R = 1 / \text{mean recurrence interval} \tag{3.1}$$

The model is Poissonian since the calculated annual probability of occurrence (R) does not change with time.

For the renewal model, the conditional probability for each fault segment is calculated from the mean recurrence interval of the characteristic earthquake determined as explained previously, the elapsed time since the last major earthquake and the exposure period (taken as 50 years). The probabilities are said to be conditional since they change as a function of the time elapsed since the last earthquake. A lognormal distribution with a covariance of 0.5 is assumed to represent the earthquake probability density distribution. The 50 year conditional probabilities thus calculated are converted to effective Poissonian annual probabilities (P_{cond}) such that (WGCEP, 1995):

$$R_{eff} = -\ln(1 - P_{cond}) / T \tag{3.2}$$

The sensitivity of the conditional probabilities to various covariance values for the renewal as well as for the Poisson models for exposure periods of 50 and 5 years is given in Figure 3.12. It can be observed from Figure 3.12 that the probability remains constant for the Poisson model and that as the covariance becomes larger, the conditional probability approaches the Poisson probability.

The total hazard in the region is calculated as the summation of hazards computed in steps (a) and (b).

The ground motion parameters used in the quantification of the earthquake hazard for this study are the peak ground acceleration (PGA) and the spectral accelerations (SA) for natural periods of 0.2 and 1.0 seconds. The ground motions are determined for soft rock (NEHRP B/C boundary) conditions. Boore et al. (1997), Campbell (1997) and Sadigh et al. (1997) have proposed the attenuation relationships used in the assessment of PGA, whereas those of Boore et al. (1997) and Sadigh et al. (1997) have been used for SA. Although the initial choice of these attenuation relationships follow that of USGS studies for California, nevertheless, these Western US–based attenuation relationships have been found to provide good correlation with the attenuation characteristics of ground motion in the Northwestern Anatolia Region (Özbey, 2001; Erdik et al., 2002).

3.5. RESULTS

The results of the North-west of Turkey region for 10% probability of exceedance in 50 years for PGA are illustrated in order to give an idea in Figure 3.13.

The results obtained for 10% probability of exceedance in 50 years for PGA and SA at 0.2 sec and 1.0 sec. natural periods at NEHRP B/C boundary site class for the Poissonian and renewal models are presented in Figure 3.14 through Figure 3.19 and Figure 3.20 through Figure 3.25 for (A) Adapazarı and (B) Gölcük, Değirmendere and İhsaniye regions respectively. For display purposes, the hazard maps are overlain with the grids to be used in the quantification (lumping) of the microzonation information in this study, supplied and used by the other teams.

After the last meeting, the result acquired for 40% probability of exceedance in 50 years (about 100 return period) for PGA and SA at 0.2 sec. and 1.0 sec natural periods at NEHRP B/C boundary site class for the Poissonian model and are presented in Figure 3.26 through Figure 3.28 for (A) Adapazarı and in Figure 3.29 through Figure 3.31 for (B) Gölcük, Değirmendere and İhsaniye regions.

3.6. DISCUSSION

We would like to put some emphasis on the following points about the hazard assessment results:

Hazard in the region has been assessed for “b” values of both 0.8 (obtained as the result of the maximum likelihood method) and 1.0 (adopted to account for the deficiency in small magnitude events) but the results did not show much difference, since the hazard in the region is essentially controlled by the faults.

Various statistical models have been proposed for the computation of the probability density function, such as Gaussian, log-normal, Weibull, Gamma and Brownian. Among those, the log-normal distribution is the most commonly used in the engineering practice. The Brownian Passage Time (BPT) model is a more recently proposed model and is also assumed to adequately represent the earthquake distribution. The probability density functions of the two models are similar, but the conditional probabilities begin to diverge around the mean recurrence time. However, the BPT distribution yields higher conditional probabilities for large elapsed times since the last earthquake. We have investigated the sensitivity of the annual rates to the model chosen, and to the aperiodicity (alpha, BPT model) and to the coefficient of variation (COV, Lognormal model). The annual rates are highly sensitive to the alpha/COV values, larger values yielding smaller annual rates. The

BPT and Lognormal distributions give considerable differences only for large elapsed times since the last characteristic event. A small COV (i.e. 0.3 or less) indicates that the characteristic earthquakes are highly periodic. As the COV grows larger (i.e. 0.7 or higher) the conditional probabilities approach those of the Poisson probabilities. As such, we have to decide on the appropriate choice of alpha/COV values. Following the California practice, we have used a value of 0.5.

We have experimented with cascade models. It is well known that, even though segments can be mapped separately at the surface, they could combine and be a single structure at depth, or a rupture on one segment could trigger ruptures on others in a cascade model. So two scenarios are envisioned: (1) faults rupture independently, producing characteristic-size earthquakes (the model incorporated in the report reviewed), or (2) fault segments rupture together as a cascade, producing earthquakes of M>7. The Cascade assumption increases the Maximum Magnitude but reduces the rate of occurrence of the more moderate events. Previous rupturing cycles around the Marmara Sea indicate that, on average, one out of three ruptures were multiple segments. The probabilistic results based on cascade models provided about the same earthquake hazard levels obtained from non-cascading models.

Although the comparison between Poissonian and renewal models shows large hazard differences, it does not indicate that the seismic potential in the region (say Adapazarı) is depleted or exhausted. The current "Earthquake Hazard Zoning Map" of Turkey provides an effective PGA of 0.4 g for Adapazarı, which compares favourably with the results obtained from the renewal model.

Finally we would like to note that the methodology adopted causes the concentration of the hazard at some segment junction points such as the junction region of segments S3, S2 and S12 in Figure 3.14 through Figure 3.16. If segment S12 was removed from the model, this "mapping" would disappear.

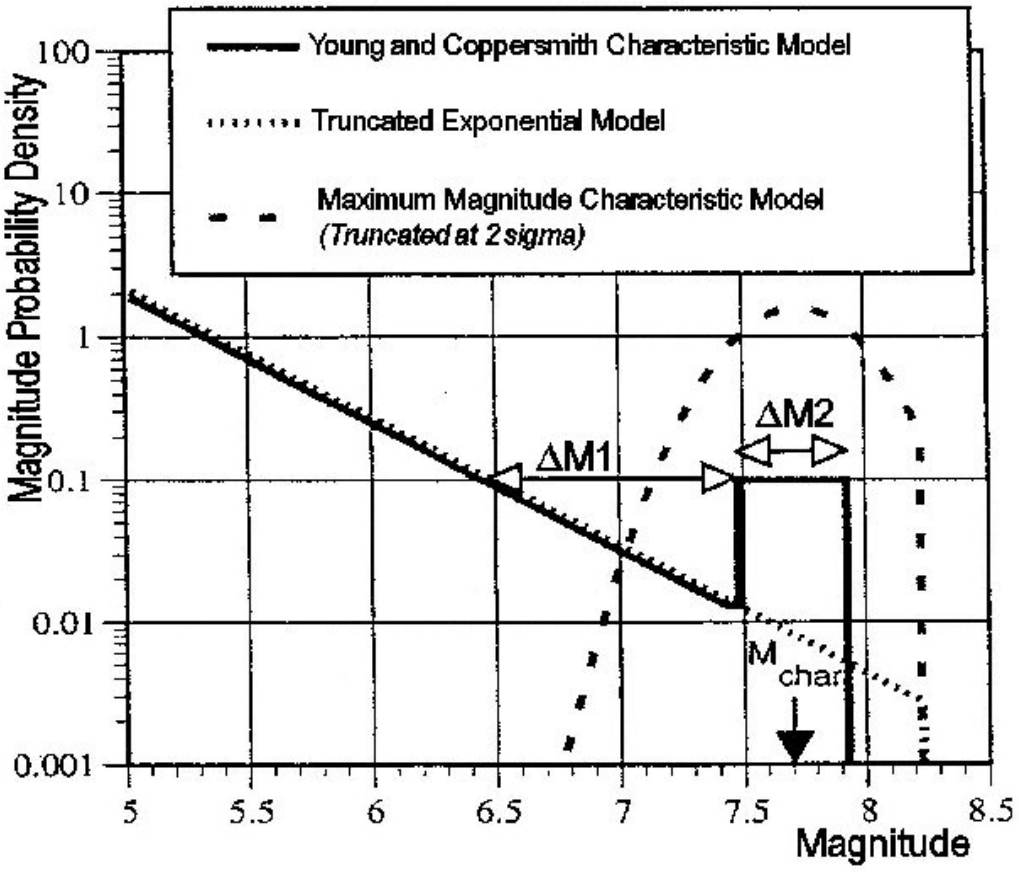

Figure 3.10. The definition of the magnitude probability density for characteristic earthquake model

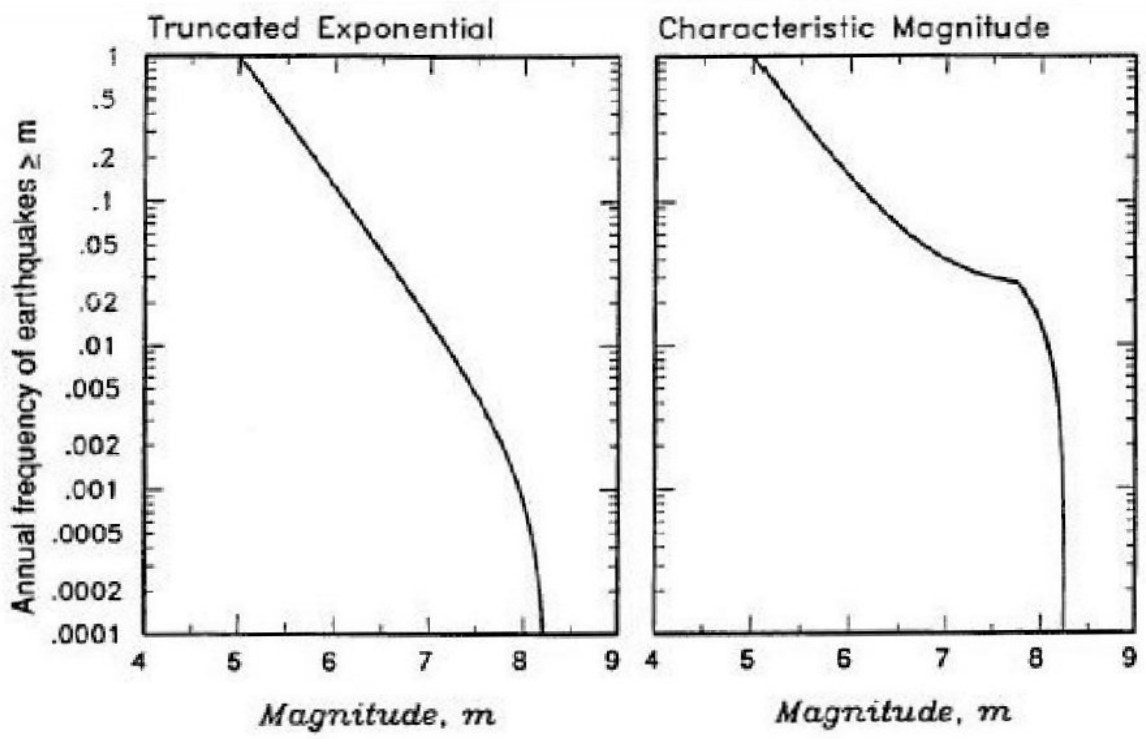

Figure 3.11. An illustrative comparison of recurrence relationships

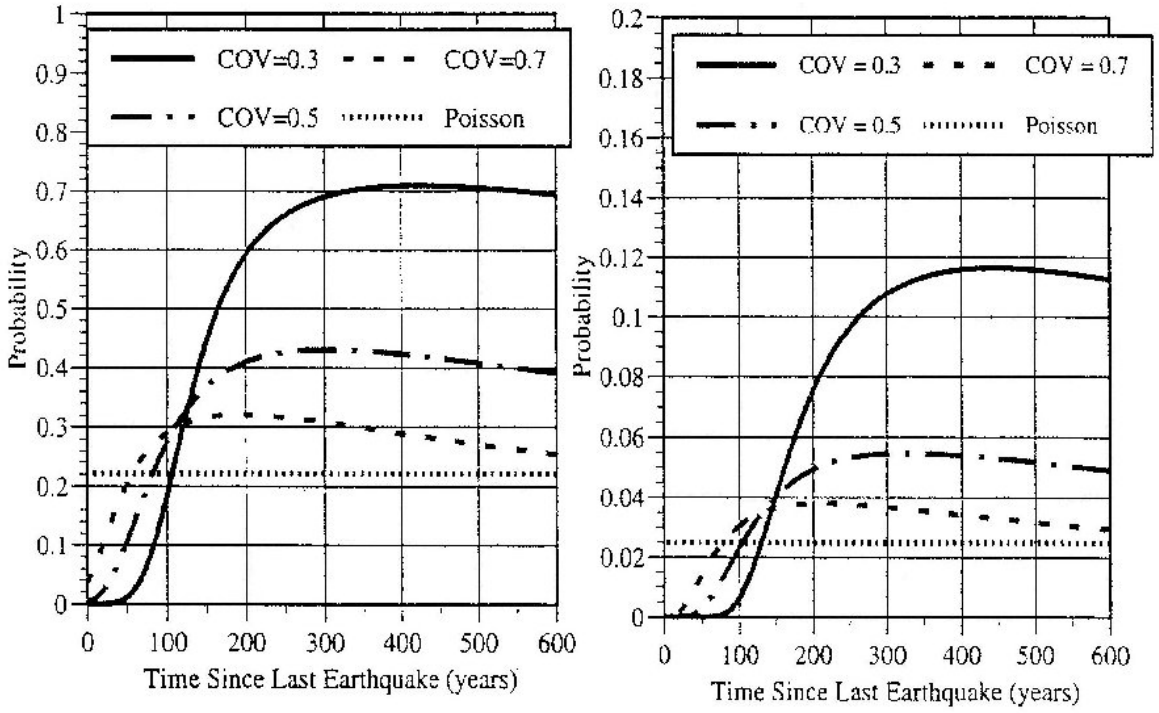

Figure 3.12. Sensitivity of the time dependent probabilities for a renewal model with 50 and 5 year exposure periods (After Abrahamson, 2000)

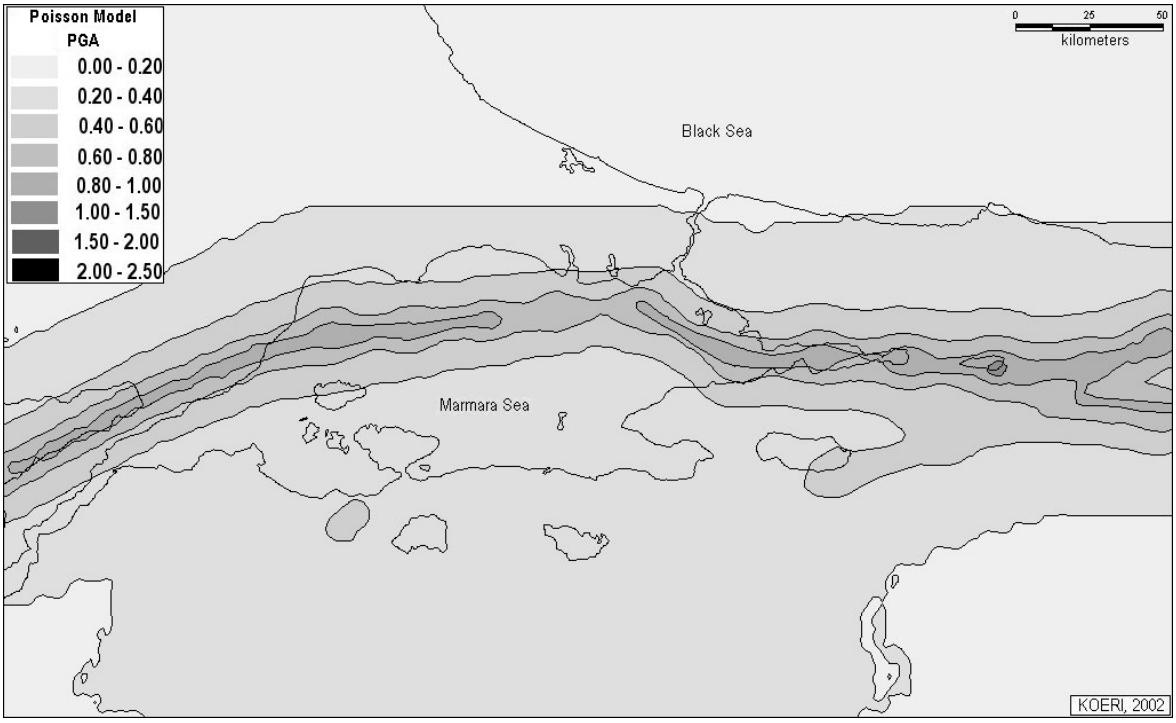

Figure 3.13. PGA contour map at NEHRP B/C boundary site class for 10% probability of exceedance in 50 years (Poissonian model)

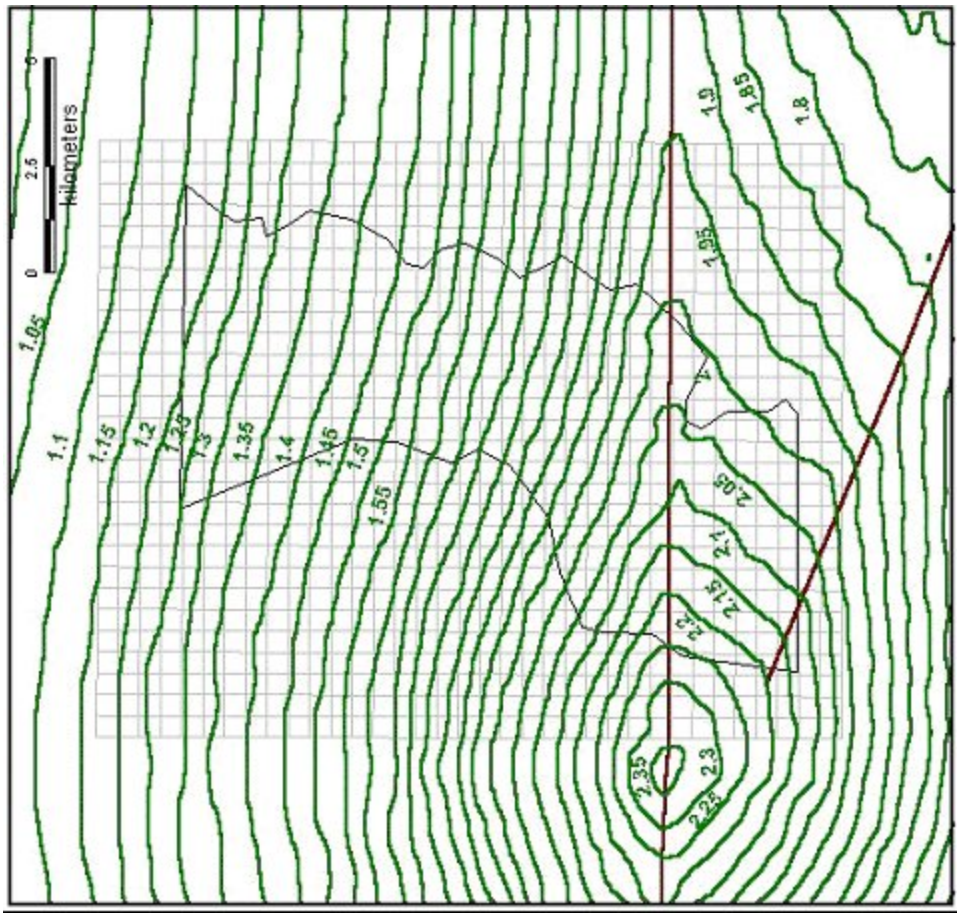

Figure 3.15. SA (T=0.2sec) contour map at NEHRP B/C boundary site class for 10% probability of exceedance in 50 years for Adapazarı region (Poissonian model)

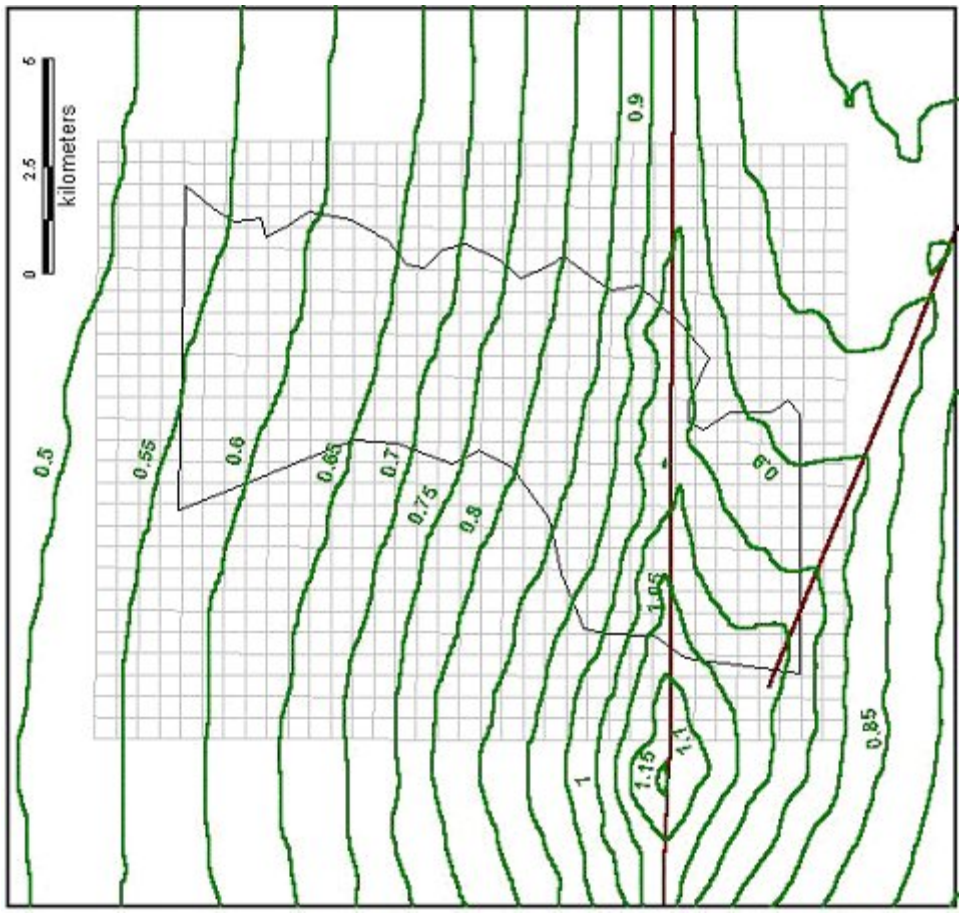

Figure 3.14. PGA contour map at NEHRP B/C boundary site class for 10% probability of exceedance in 50 years for Adapazarı region (Poissonian model)

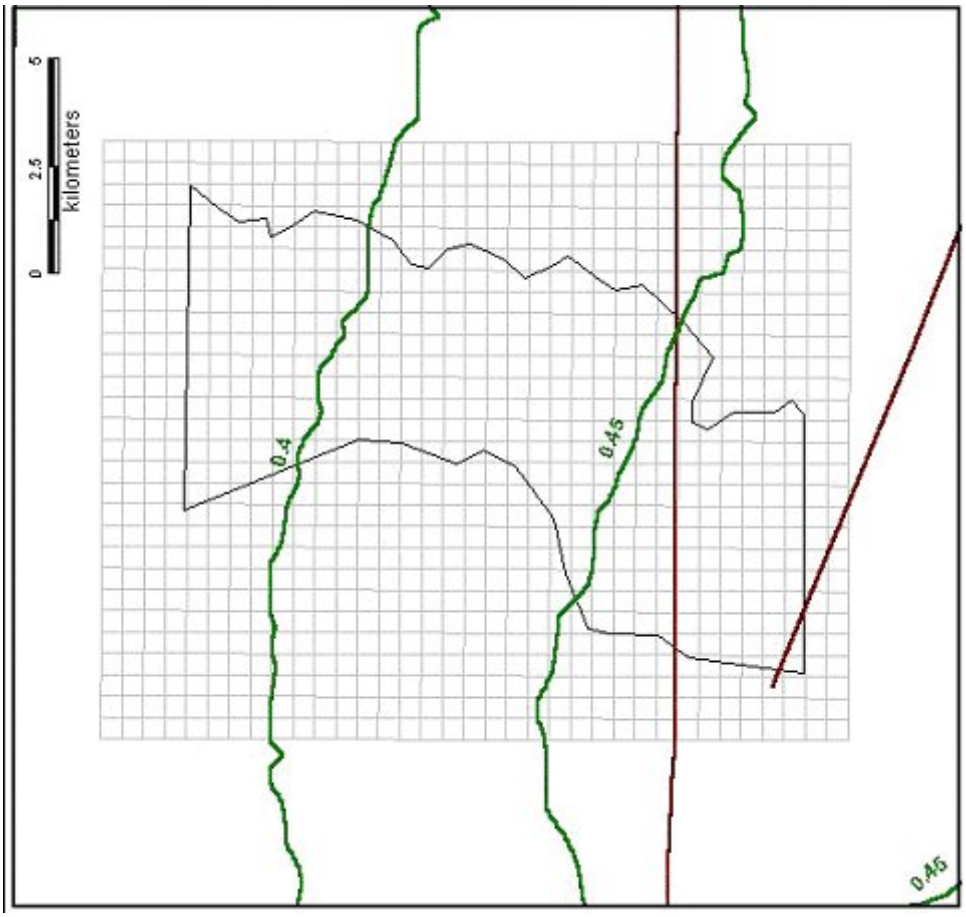

Figure 3.17. PGA contour map at NEHRP B/C boundary site class for 10% probability of exceedance in 50 years for Adapazarı region (Renewal model)

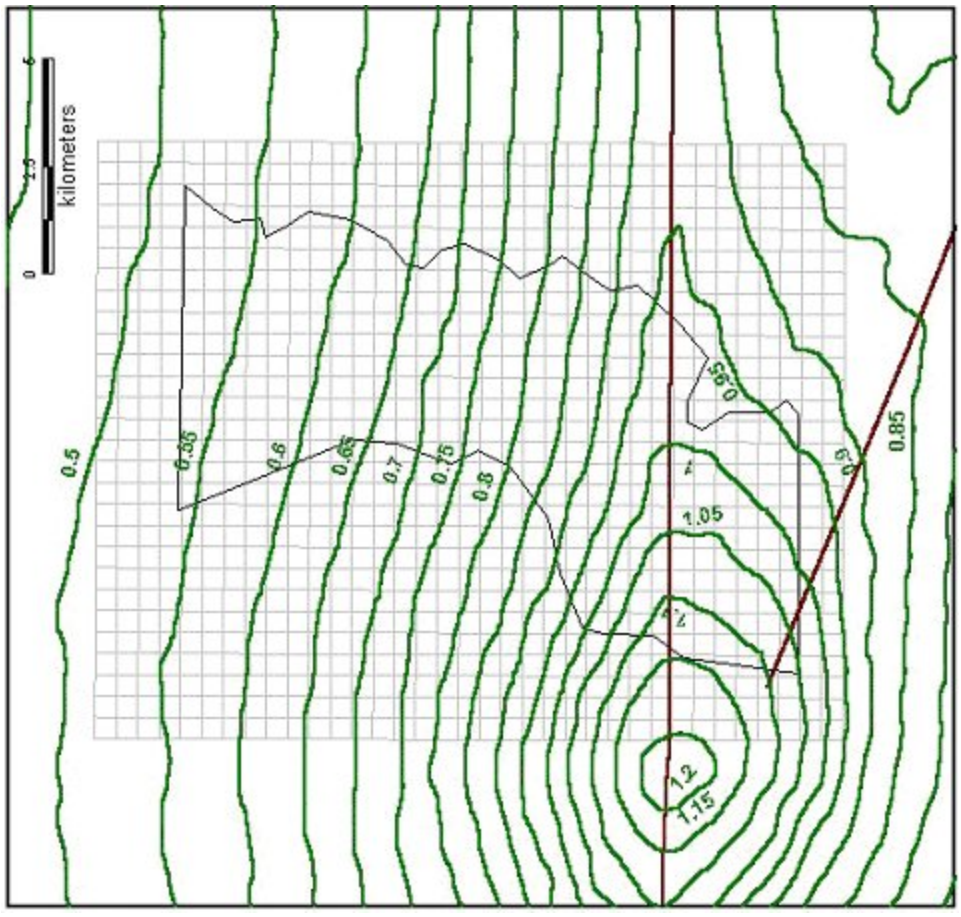

Figure 3.16. SA (T=1.0sec) contour map at NEHRP B/C boundary site class for 10% probability of exceedance in 50 years for Adapazarı region (Poissonian model)

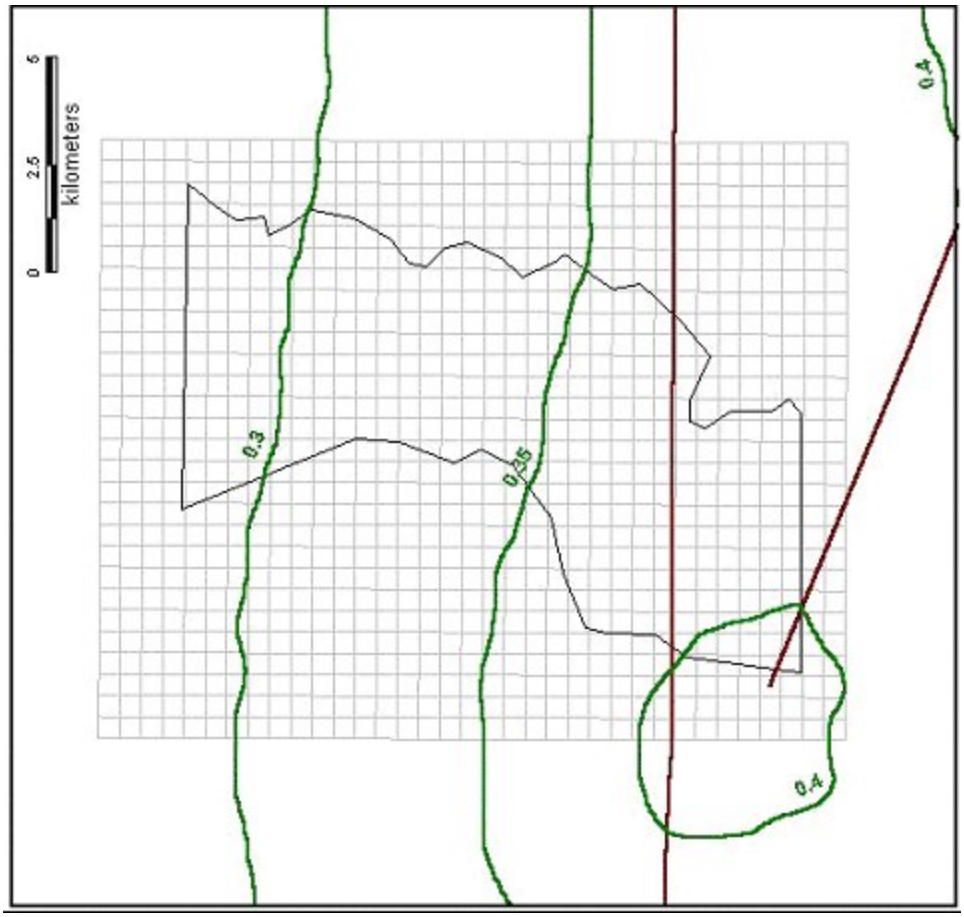

Figure 3.19. SA (T=1.0sec) contour map at NEHRP B/C boundary site class for 10% probability of exceedance in 50 years for Adapazarı region (Renewal model

Figure 3.18. SA (T=0.2sec) contour map at NEHRP B/C boundary site class for 10% probability of exceedance in 50 years for Adapazarı region (Renewal model)

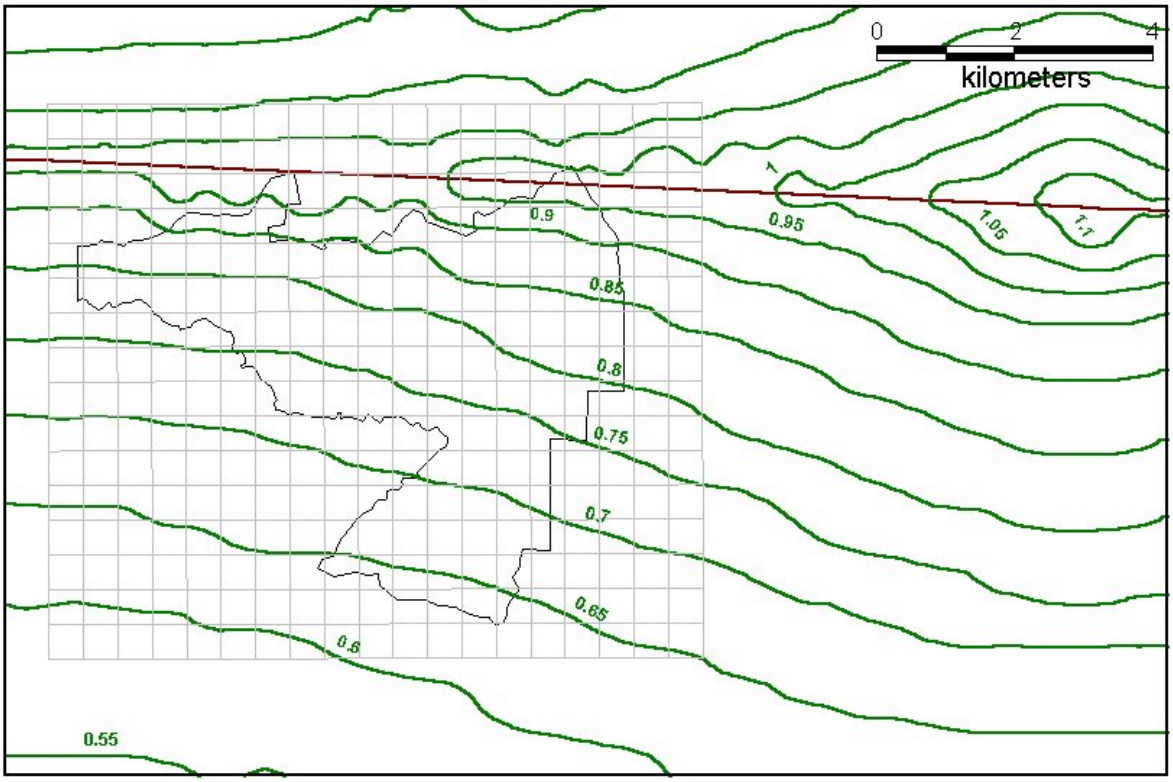

Figure 3.20. PGA contour map at NEHRP B/C boundary site class for 10% probability of exceedance in 50 years for Gölcük region (Poissonian model)

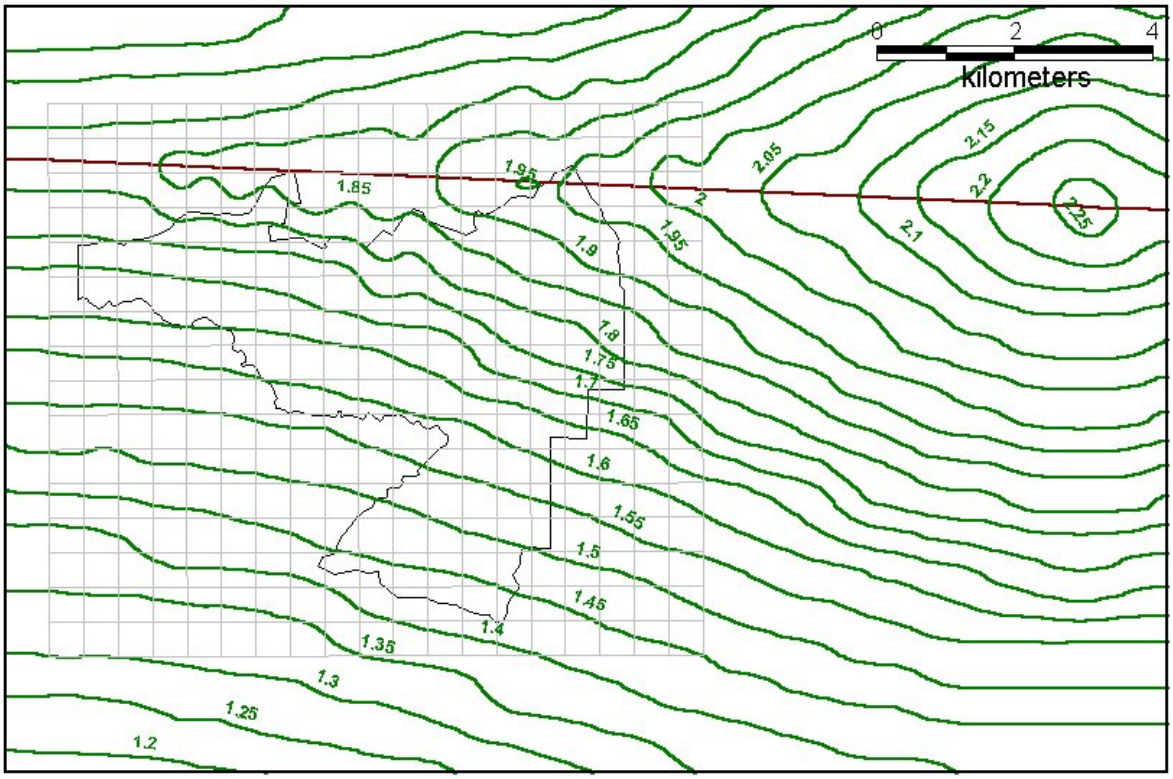

Figure 3.21. SA (T=0.2sec) contour map at NEHRP B/C boundary site class for 10% probability of exceedance in 50 years for Gölcük region (Poissonian model)

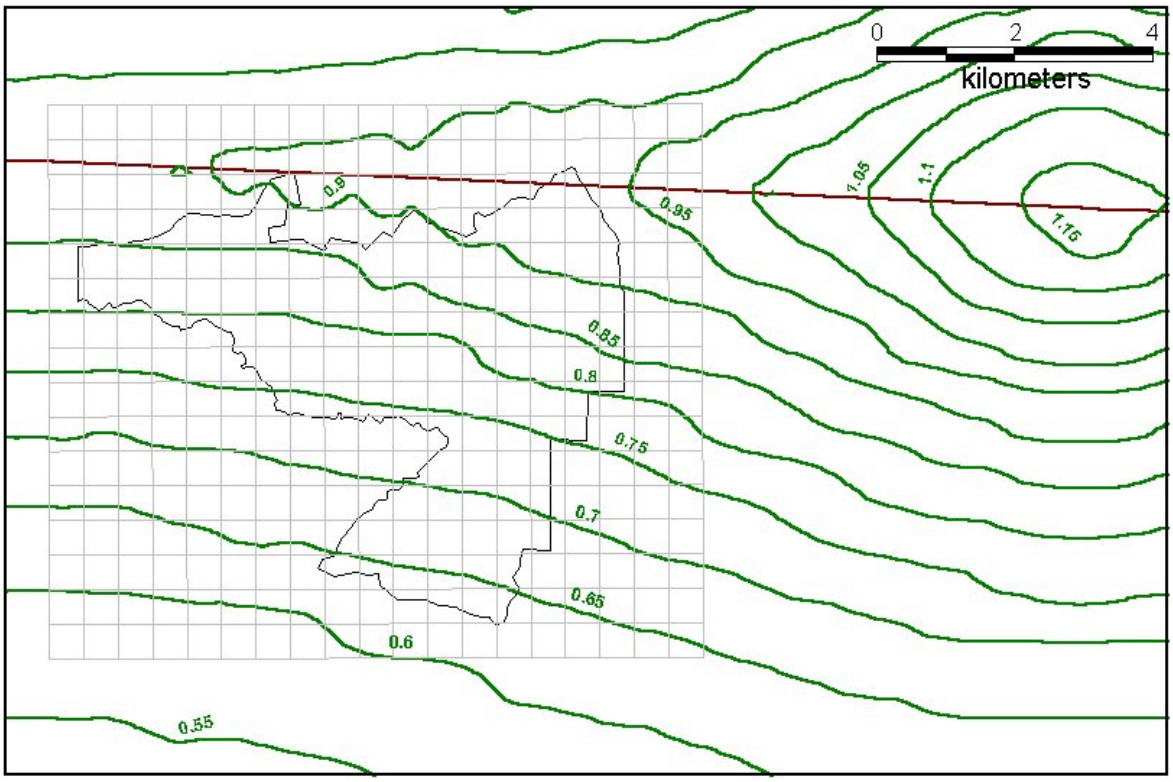

Figure 3.22. SA (T=1.0sec) contour map at NEHRP B/C boundary site class for 10% probability of exceedance in 50 years for Gölcük region (Poissonian model)

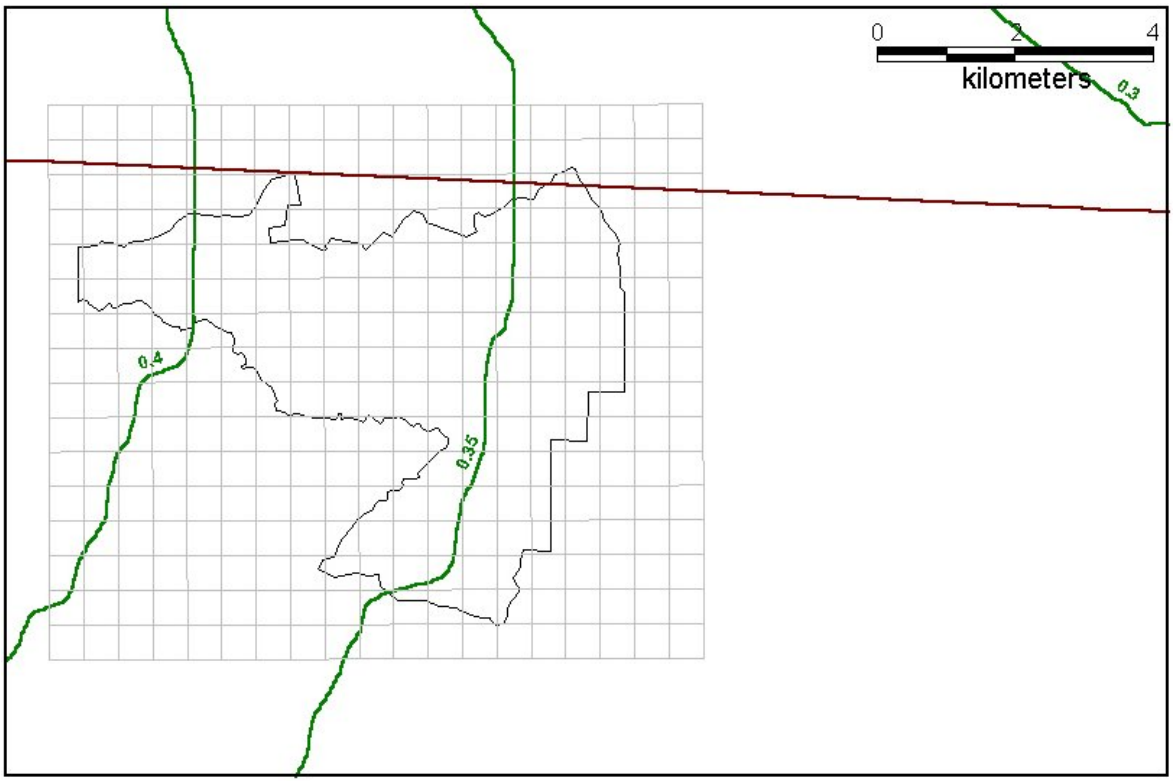

Figure 3.23. PGA contour map at NEHRP B/C boundary site class for 10% probability of exceedance in 50 years for Gölcük region (Renewal model)

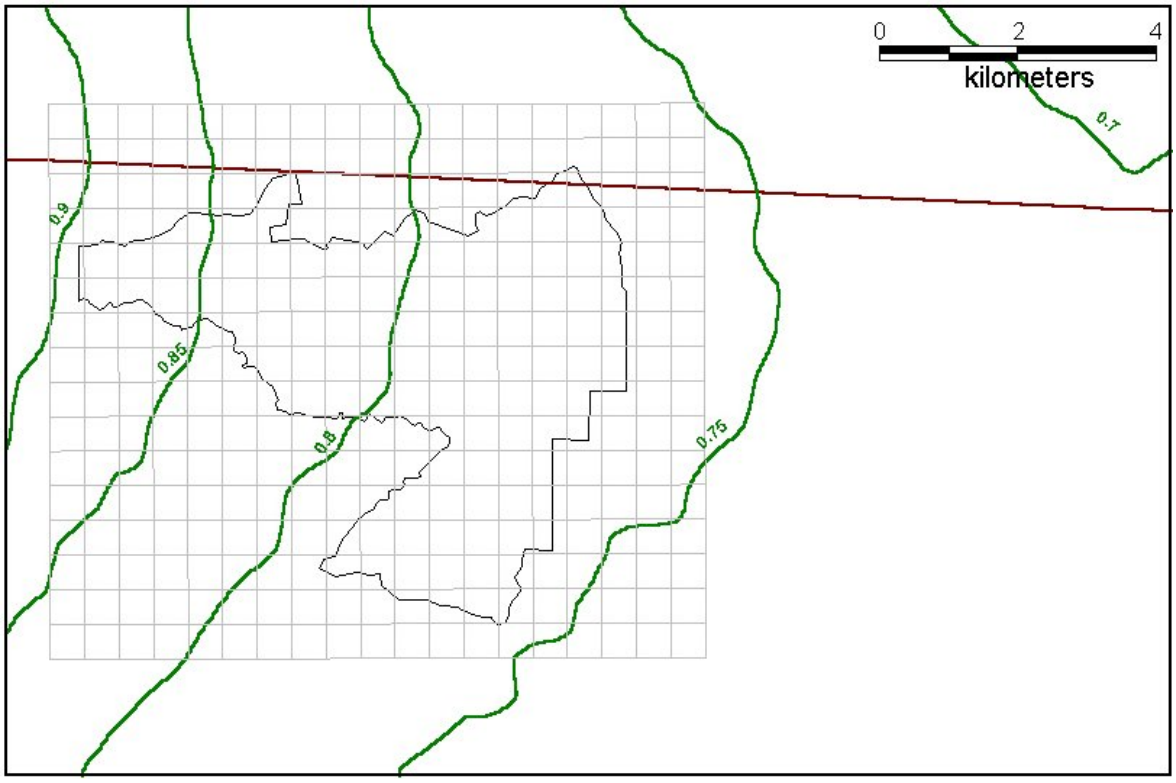

Figure 3.24. SA (T=0.2sec) contour map at NEHRP B/C boundary site class for 10% probability of exceedance in 50 years for Gölcük region (Renewal model)

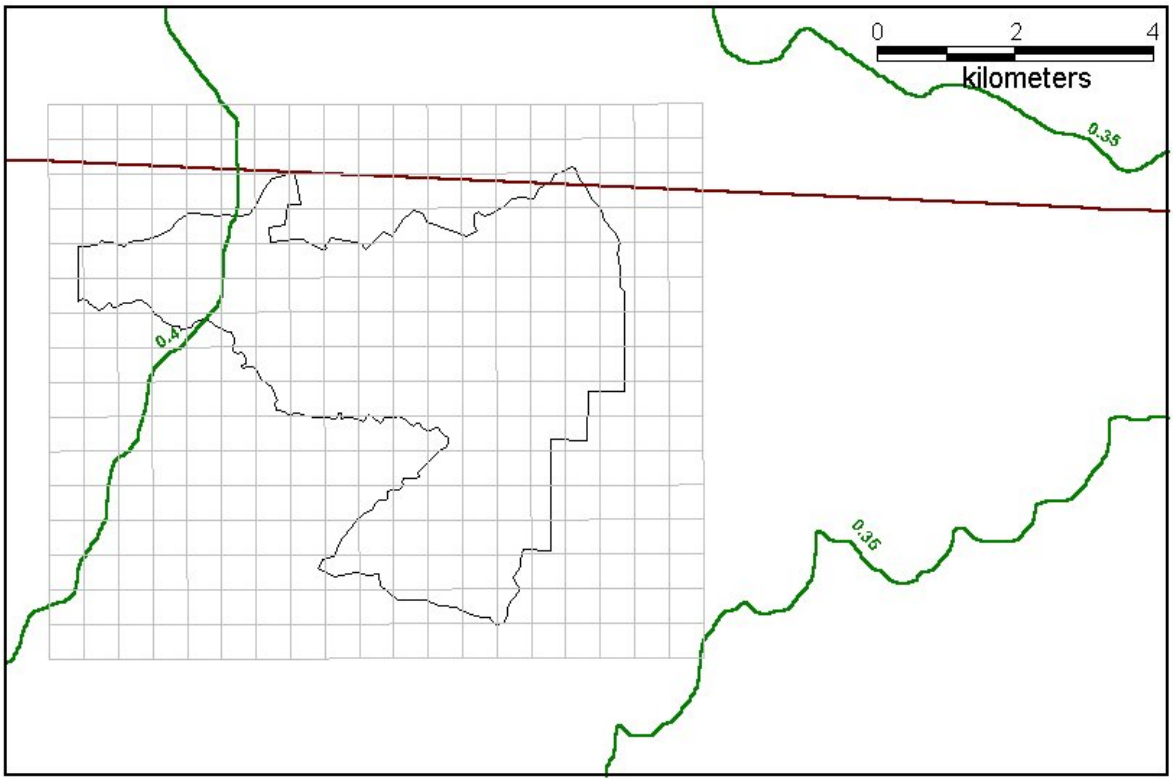

Figure 3.25. SA (T=1.0sec) contour map at NEHRP B/C boundary site class for 10% probability of exceedance in 50 years for Gölcük region (Renewal model)

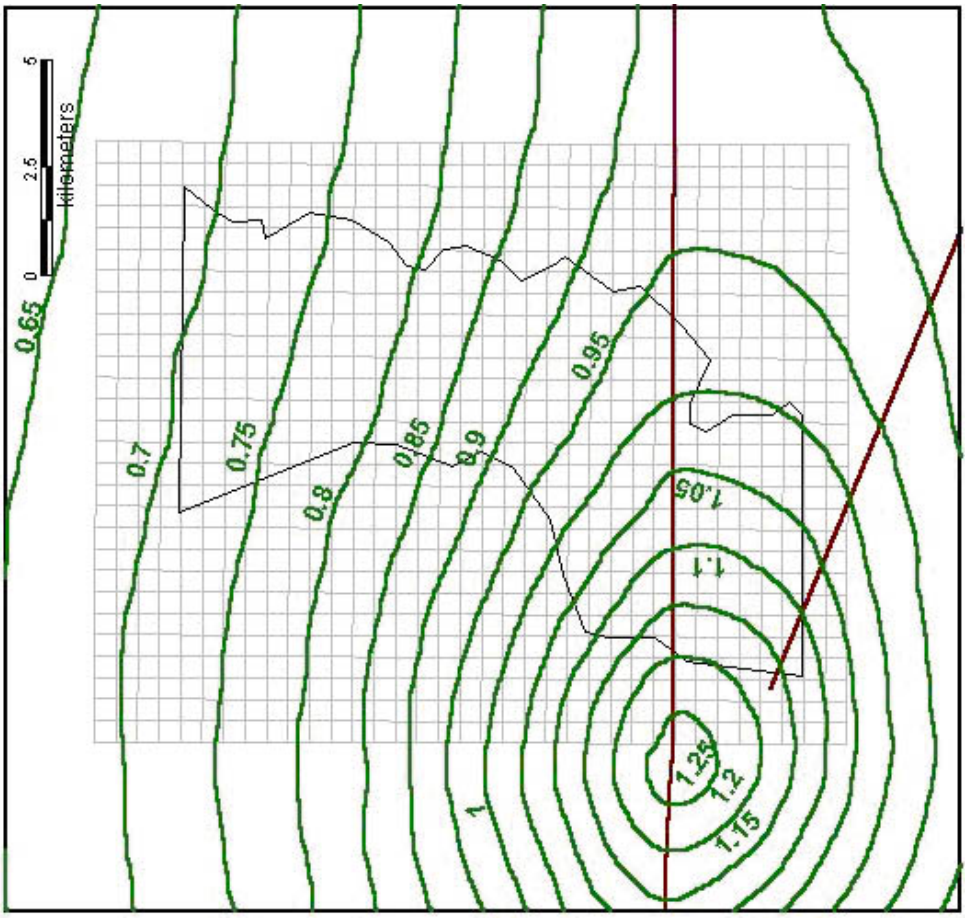

Figure 3.27. SA (T=0.2 sec) contour map at NEHRP B/C boundary site class for 40% probability of exceedance in 50 years for Adapazarı region (Poissonian model)

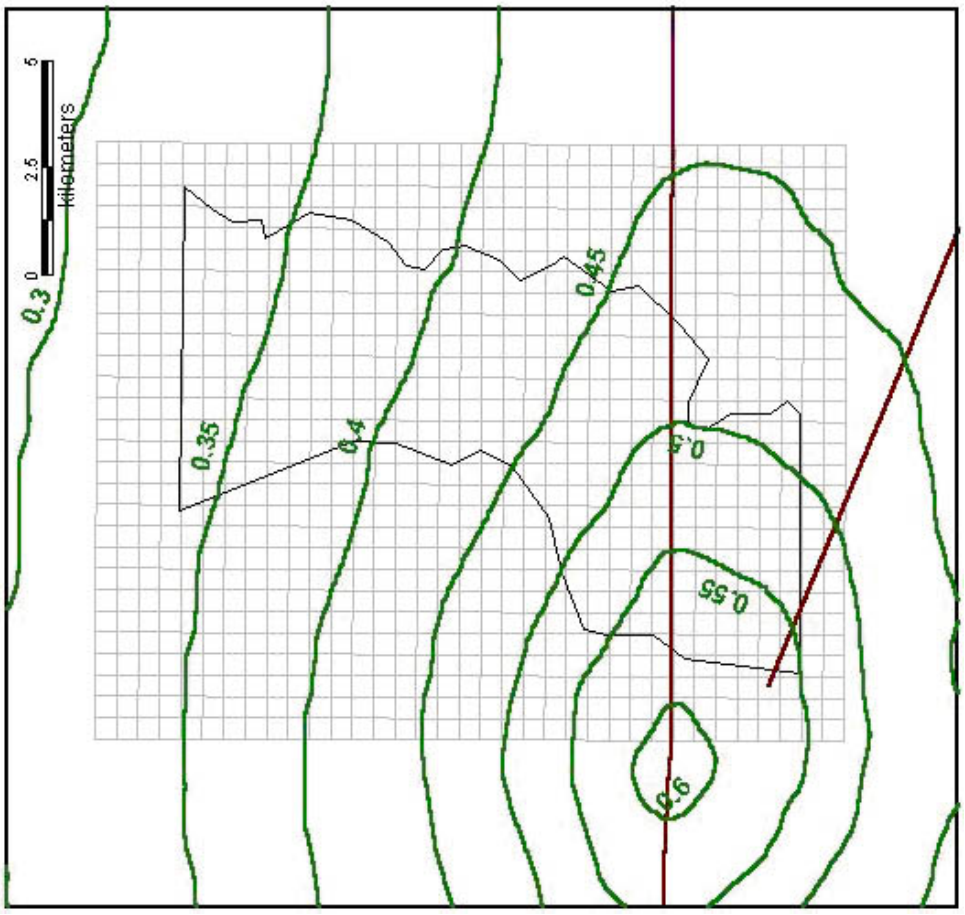

Figure 3.26. PGA contour map at NEHRP B/C boundary site class for 40% probability of exceedance in 50 years for Adapazarı region (Poissonian model)

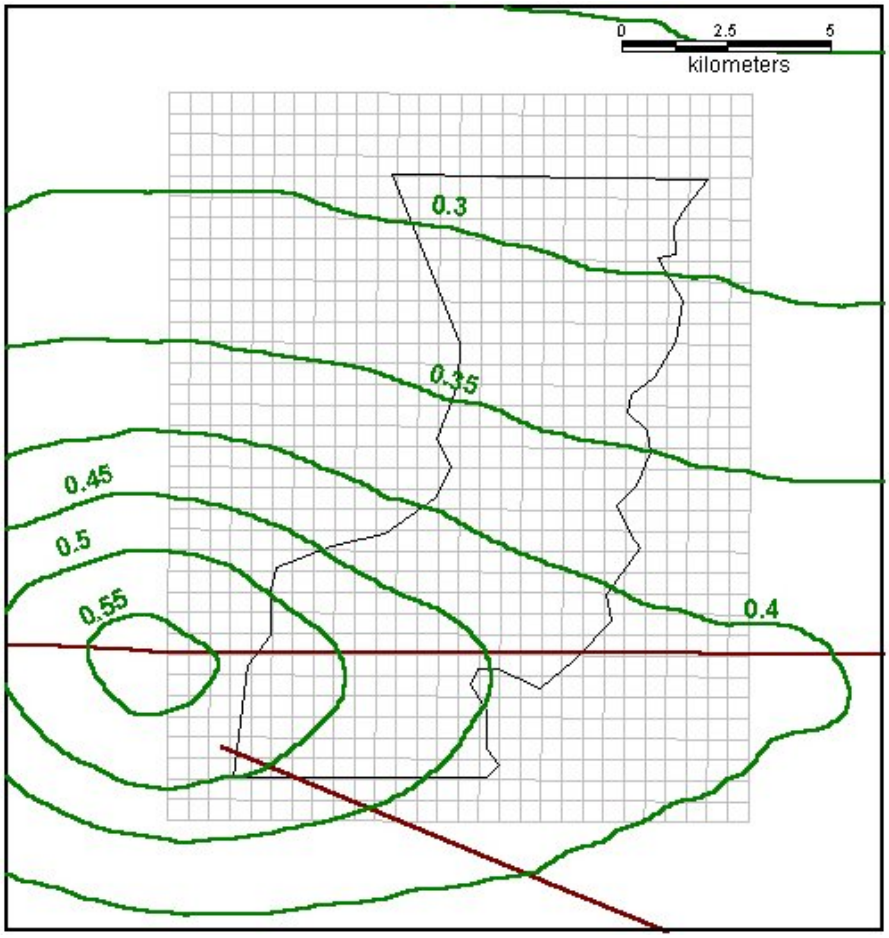

Figure 3.28. SA (T=1.0 sec) contour map at NEHRP B/C boundary site class for 40% probability of exceedance in 50 years for Adapazarı region (Poissonian model).

Figure 3.29. PGA contour map at NEHRP B/C boundary site class for 40% probability of exceedance in 50 years for Gölcük region (Poissonian model)

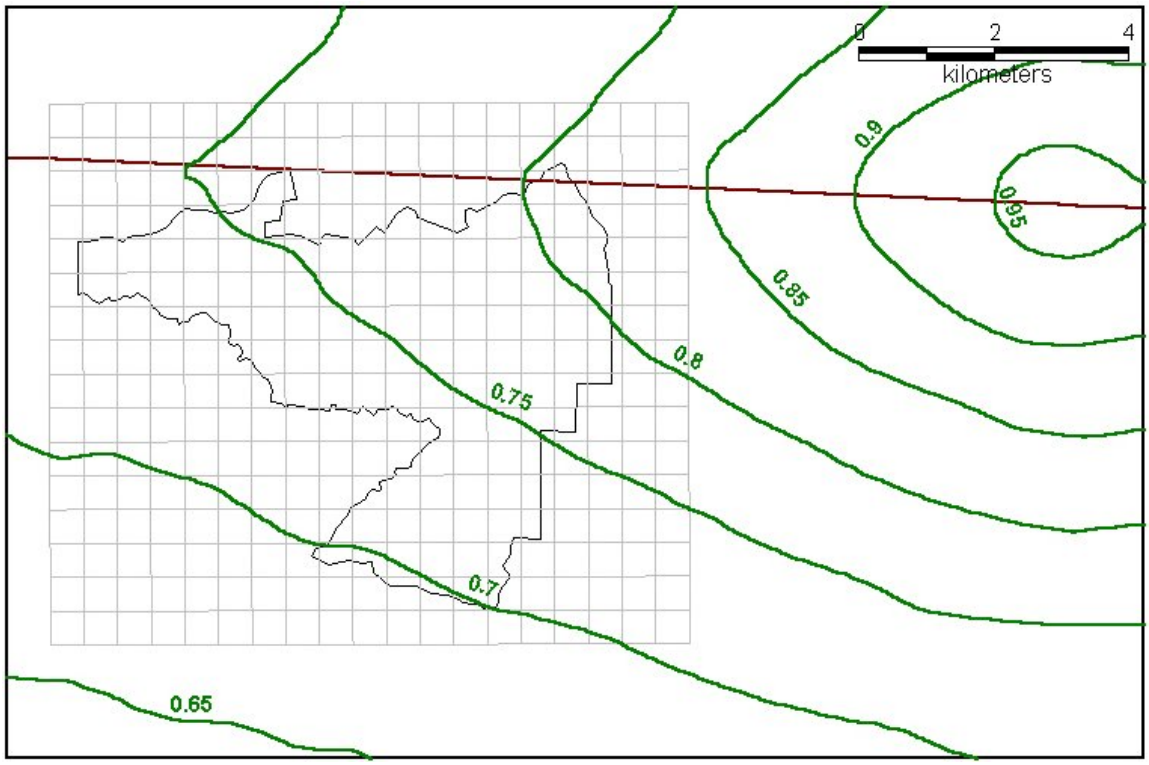

Figure 3.30. SA (T=0.2 sec) contour map at NEHRP B/C boundary site class for 40% probability of exceedance in 50 years for Gölcük region (Poissonian model).

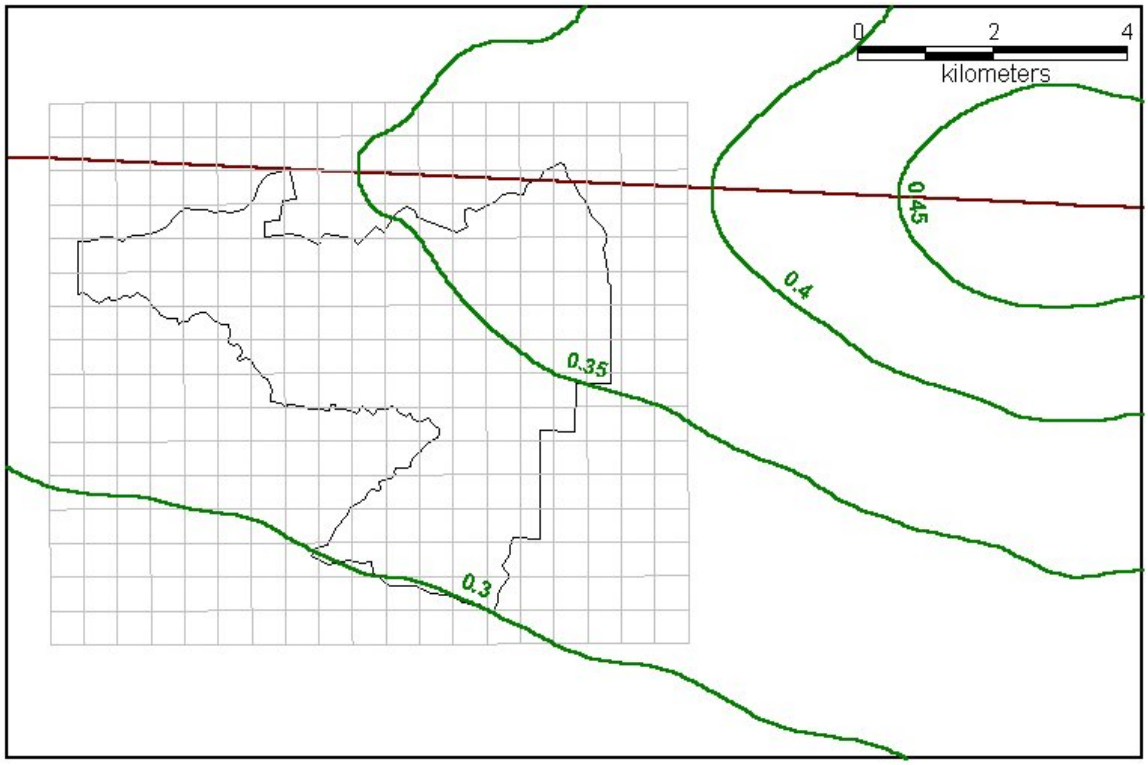

Figure 3.31. SA (T=0.1 sec) contour map at NEHRP B/C boundary site class for 40% probability of exceedance in 50 years for Gölcük region (Poissonian model).

3.7. RESPONSE SPECTRA

The shape of the response spectrum (5% damped) will be taken equal to the so-called "Uniform Hazard Response Spectrum" provided in NEHRP (1997) Provisions. This spectrum is determined on the basis of the site-specific short-period (Sms) and medium-period (Sm1) spectral accelerations as illustrated in Figure 3.32.

$$Sms = Fa \cdot Ss \quad (3.3)$$

$$Sm1 = Fv \cdot S1 \quad (3.4)$$

S_s and S_1 are represented by the SA calculated, respectively, at T=0.2 s and T=1.0 s periods for NEHRP Site Class B/C Boundary and plotted in Figures 3.15, 3.16, 3.18, 3.19, 3.27, 3.28 for Adapazarı region and in Figures 3.21, 3.22, 3.24, 3.25, 3.30, 3.31 for Gölcük region. Fa and Fv are respectively the Short and Medium Period Amplification Factors, originally defined in NEHRP (1997). For the ground motion defined at NEHRP Site Class B/C Boundary, Fa = Fv =1.

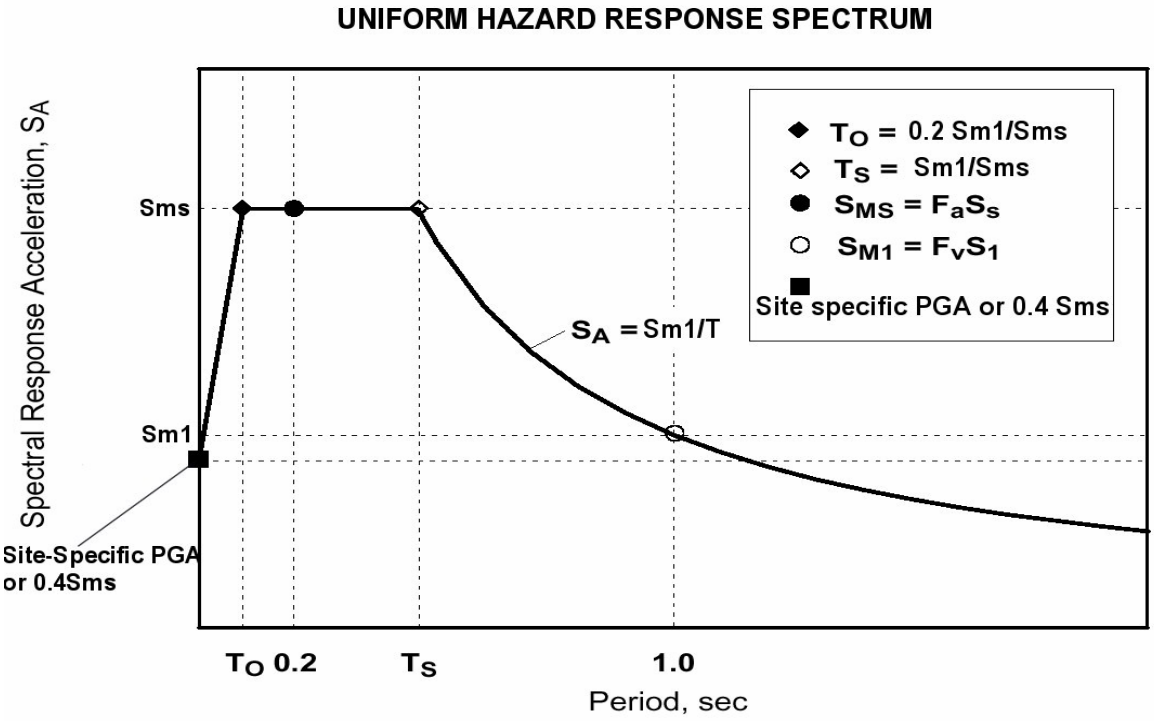

Figure 3.32. NEHRP (1997) Uniform Hazard Response Spectrum

3.8. SPECTRUM COMPATIBLE DESIGN BASIS GROUND MOTION

For simulation of time domain ground motion compatible with the response spectra presented, the procedure developed by Deodatis (1996) and coded by Papageorgiou et. al. (2000) will be utilized. The target acceleration spectra compatible time history is a ground motion simulation program generating a synthetic time history of ground acceleration. The time domain simulations are non-stationary with random phase.

Please note that this may not be the perfect methodology since the spectrum on which the simulation is based may not correlate with a physically realizable earthquake and we are fully aware of the issues associated with such an approach. However, other more rigorous approaches (e.g. deterministic simulation of ground motion after de-

aggregation of the probabilistic hazard) are suited more to site-specific studies and are not compatible with the scope and the depth of this investigation.

As an example simulation was done for the centroid of the cell R16 in Adapazarı study area. As a result of the simulation, the acceleration time history, velocity and displacement motions, which depend on acceleration time history, were obtained using the spectral acceleration values at t=0.2 sec and t=1 sec belonging to cell R16. Based on these two parameters, horizontal and vertical components of the simulated time history were obtained as presented in Figure 3.33 and Figure 3.34.

The spectral acceleration values at t=0.2 sec and t=1.0 sec, obtained from the hazard study for 40% probability of exceedance in 50 years, were assigned to the microzonation study cells as Sms and Sm1 respectively and input files for every cell in Adapazarı and Gölcük regions were prepared (Annex 2C.1).

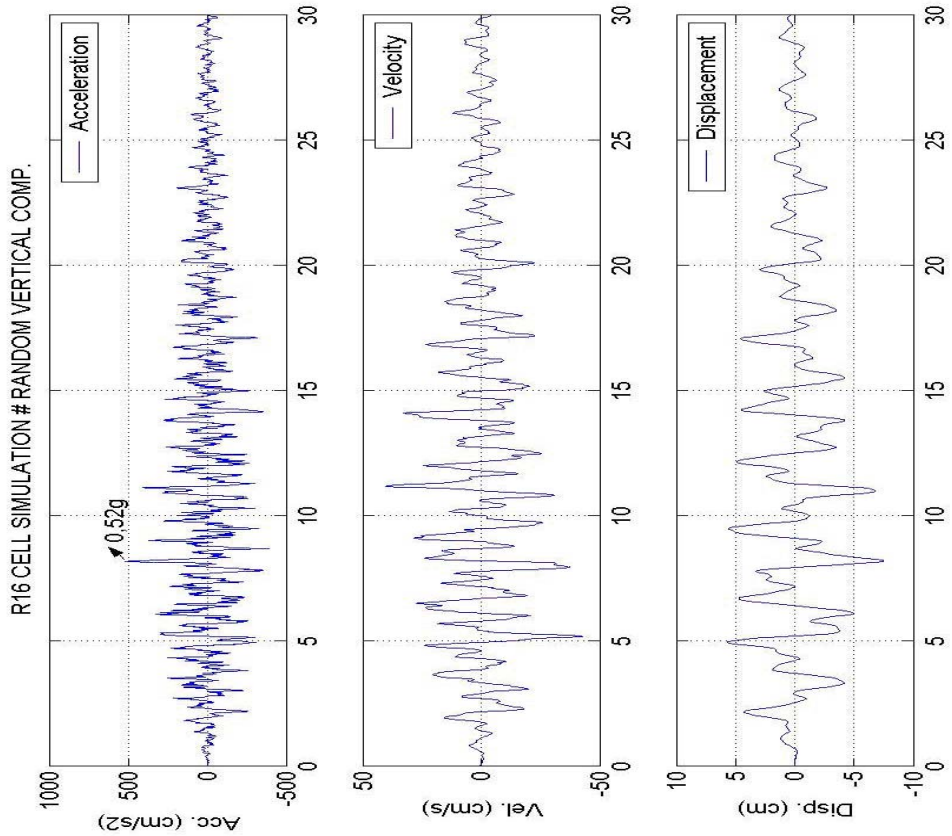

Figure 3.34. Response Spectrum Compatible Vertical Ground Motion at Cell R16 (Free-field outcrop of NEHRP B/C Boundary)

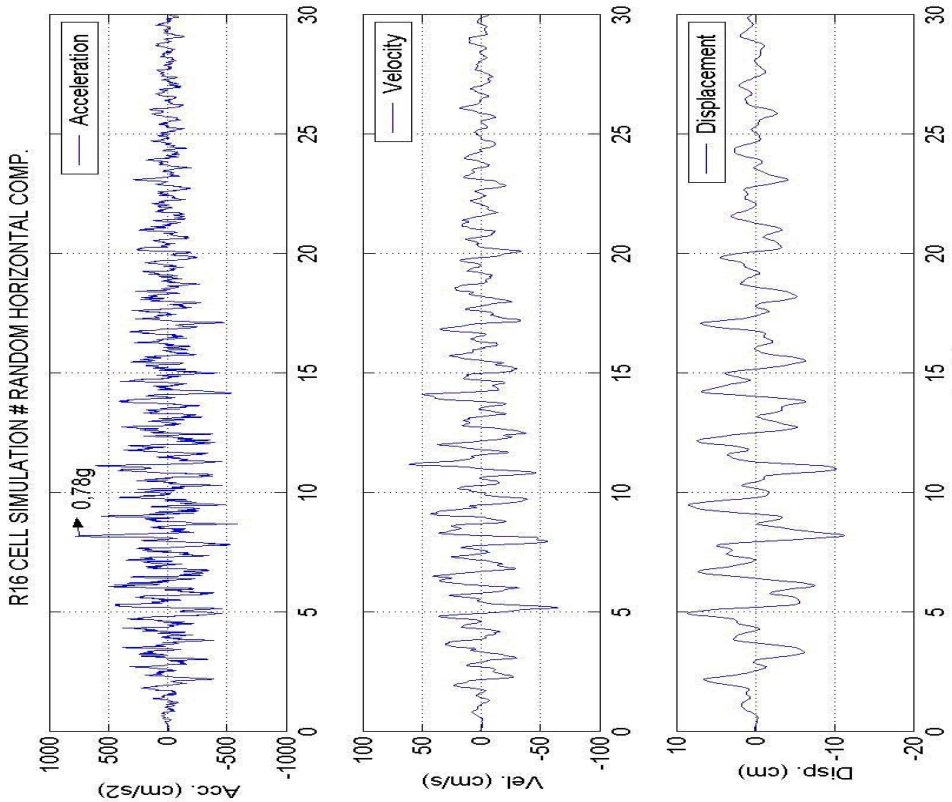

Figure 3.33. Response Spectrum Compatible Random Horizontal Ground Motion at Cell R16 (Free-field outcrop of NEHRP B/C Boundary)

4. SINGLE-STATION AMBIENT VIBRATION MEASUREMENTS AND INTERPRETATION FOR THE CITIES OF ADAPAZARI AND GÖLCÜK, TURKEY

D. Fäh and A. Christen (Swiss Seismological Service, ETH Zürich, Switzerland) with the cooperation of Ü. Gülerce (Istanbul Technical University, Turkey) and C. Greifenhagen (ETH Lausanne, Switzerland).

4.1. SUMMARY

Single station ambient vibration measurements have been performed in the two cities Adapazarı and Gölcük in Turkey. These cities suffered heavy damage during the 1999 Kocaeli earthquake. The work presented here is a contribution to the DRM-MERM Project. The main goals of our work are to determine the fundamental frequencies of resonance of the soils within the studied areas, to provide a preliminary interpretation of the subsurface structure and its variation, and to propose a zonation based on the shape of the observed ambient vibration H/V spectral ratios. Published S-wave velocity profiles have been used to compute synthetic H/V spectral ratios, which are then compared to the observation.

4.2. INTRODUCTION

The investigation of the local ground condition is an important part of any site-specific hazard assessment. One of the key parameters is the S-wave velocity structure of the unconsolidated sediments and the S-wave contrast between bedrock and sediments. These parameters together with the geometry of the bedrock-sediment interface mainly control the amplification of seismic waves during earthquakes. By knowing the structure, a prediction of amplification effects can be performed with numerical simulation techniques.

The S-wave velocity structure can be obtained through active in-situ measurements such as S-wave seismics, surface-wave measurements with single stations or arrays, and down-hole and cross-hole techniques. Passive methods based on ambient vibrations or microtremors are of special interest. These methods can be applied in urban areas where in general it is not possible to carry out active measurements due to the lack of space for the experimental setup or restrictions on using explosion sources. Array methods were established by Horike (1985) after the pioneering work done by Aki (1957). These methods make use of the dispersive character of surface waves, and allow determining shear-wave velocity profiles from the inversions of dispersion curves. The waves involved in the microtremors are surface waves as well as body waves of P and S-type, and observed wave fields are composed of several different modes that are in general not separated in time. This unknown composition of the wavefield is a major problem in microtremor methods. Array measurements of ambient vibrations have been performed in the target areas by Kudo et al. (2002) and Yamanaka et al. (2001). Their results will be evaluated within our study, and are used for the interpretation of the subsurface structure and its variation.

The fundamental frequency of resonance f_0 is a quantity that can be derived from the S-wave velocity structure of the site. Amplification of waves as a function of frequency is therefore directly related to f_0. The fundamental frequency can be obtained from a single-station ambient vibration measurement using the H/V method proposed by Nakamura (1989). This method has proven to be the most convenient technique to estimate the fundamental frequency of soft deposits (Lachez and Bard, 1994; Lermo and Chavez-Garcia, 1994) and is applied in this study using an algorithm described in Fäh et al. (2001). If borehole data can be used for calibration, the procedure has the potential to allow estimates

of shear-wave velocity of the unconsolidated sediments. In one-dimensional structures, average H/V spectral ratios can be assumed to measure the ellipticity of the fundamental mode Rayleigh wave. The ellipticity at each frequency is defined as the ratio between the horizontal and vertical displacement eigenfunctions in the P-SV case, at the free surface. Hence the shape of H/V ratios can be used to estimate the shear-wave velocity profile. Yamanaka et al. (1994) and Satoh et al. (2001) applied this idea for deep sedimentary basins, Fäh et al. (2001) and Yamanaka et al. (2001) for shallow sites. Such methods have not been applied in this study, due to the lack of borehole information.

H/V spectral ratios can be considered as the fingerprint of the local structure. By comparing measurements within an area, similar H/V curves are observed on similar local structures. Such comparison therefore allows for a zonation. Each site within one zone is expected to show similar amplification effects during earthquakes. This idea will be applied for the two cities in order to propose a zonation based on the shape of the observed ambient vibration H/V spectral ratios.

4.3. FIELD CAMPAIGN AND INSTRUMENTATION

In August 2002 an ambient-vibration measurement campaign was carried out in the area of Adapazarı and Gölcük. The campaign was prepared in Zurich and included a training course for the use of the instruments and analysis software. One of the major difficulties for the planning of the campaign was the lack of geographical maps. This problem could be only partly resolved during the field campaign.

The ambient-vibration measurements were performed with Mars88 recorders and Lennartz 5sec sensors. A standard set-up of the recorders has been used the details of which is given in Appendix 1.1. Three sets of instruments were provided by the Swiss Seismological Service. The equipment was shipped by DEZA. The DRM-MERM project management provided field assistance, and organized accommodation and transportation during the campaign.

During the 20 days of the campaign, 211 measurements were performed inside the Adapazarı area and 31 in Gölcük. Three independent teams performed the measurements. The meaning of the point names is described in Appendix 1.2. An overview of the measuring sites is given in Figures 4.1 and 4.2. During the campaign, the recorded signals were analyzed in order to check their quality. The decision was made for the next day's measurements based on the latest set of results.

The entire dataset has been analyzed at the Swiss Seismological Service in order to perform a quality control, and to provide a homogeneous dataset and interpretation. Possible flawed parts of the recording and signals caused by near-sensor sources were removed. The dataset is available on CD-ROM; the content of the CD-ROM is described in Appendix 1.4. The data are provided in SAF format. The format is described in Appendix 1.3. The H/V method is shortly described in the following chapter.

4.4. COMPUTATION OF H/V RATIOS

Two methods are applied to compute average H/V ratios. The combination of both then allows for a future inversion of the H/V ratio for the S-wave velocity structure of the site, in case borehole information or seismic measurements may become available.

In the classical polarization analysis in the frequency domain, the polarization is defined as the ratio between the Fourier spectra of the horizontal components and the spectrum of the vertical component. In this study the H/V polarization at a site is computed

as the average from many windows of noise data, each with fixed length. For each window the Fourier spectra are computed and no smoothing is applied to the spectra. The ratio is formed and the polarizations are averaged over all windows using log10 of the single H/V ratios. Finally the average spectral ratio is slightly smoothed. The result for the classical H/V ratio is always shown in blue in the figures.

The SH part of the wavefield contributes to the horizontal component of motion in the measurements. The SH-wave contribution cannot be determined from a single station measurement, because source locations and mechanisms of ambient vibrations are in general unknown. This requires some assumptions concerning the spectral content of SH-waves. A reasonable assumption is that the transverse part of the wave field has a similar spectrum and energy content to the radial part (Fäh et al., 2001). This results in a reduction factor of the square root of 2 for the H/V ratio when considering only P-SV waves. The classical H/V curves in this study are all corrected with this factor.

The second method for H/V ratios tries to reduce the SH-wave influence by identifying P-SV-wavelets from the signal and taking the spectral ratio only from these wavelets. This is done by means of a frequency-time analysis (FTAN) of each of the three components of the ambient vibrations (Fäh et al., 2001). In a frequency-time representation of the vertical signal, the most energetic sections are identified in time for each frequency. We assume that this maximum is related to a single P-SV wavelet.

Because the horizontal component of the wavelet may be phase shifted with respect to the vertical component, it is selected from a time window centered at the arrival time of the maximum energy on the vertical component and with a width of one wave period. The horizontal component is selected as the maximum of the quadratic mean of the spectral values from both components and the H/V ratio is formed for the wavelet with this value. The polarization spectra with this technique are computed for different windows of the noise data and averaged without any smoothing.

In the figures, the result with this FTAN based method is always shown in a green color. The similarity in shape and amplitude of the two H/V curves supports the assumptions made for the SH-wave content for the classical method. We provide an interpretation only for frequencies above 0.2 Hz, because this frequency is the eigenfrequency of the sensor.

The software that has been used to compute H/V spectral ratios (Matlab Routine Analyse13SAF.m) and to visualize the results (Matlab Routine Bild1DRMA.m) are provided on the CD-ROM. The amplitudes of the H/V spectral ratios are always given at log10 scale.

Adapazarı

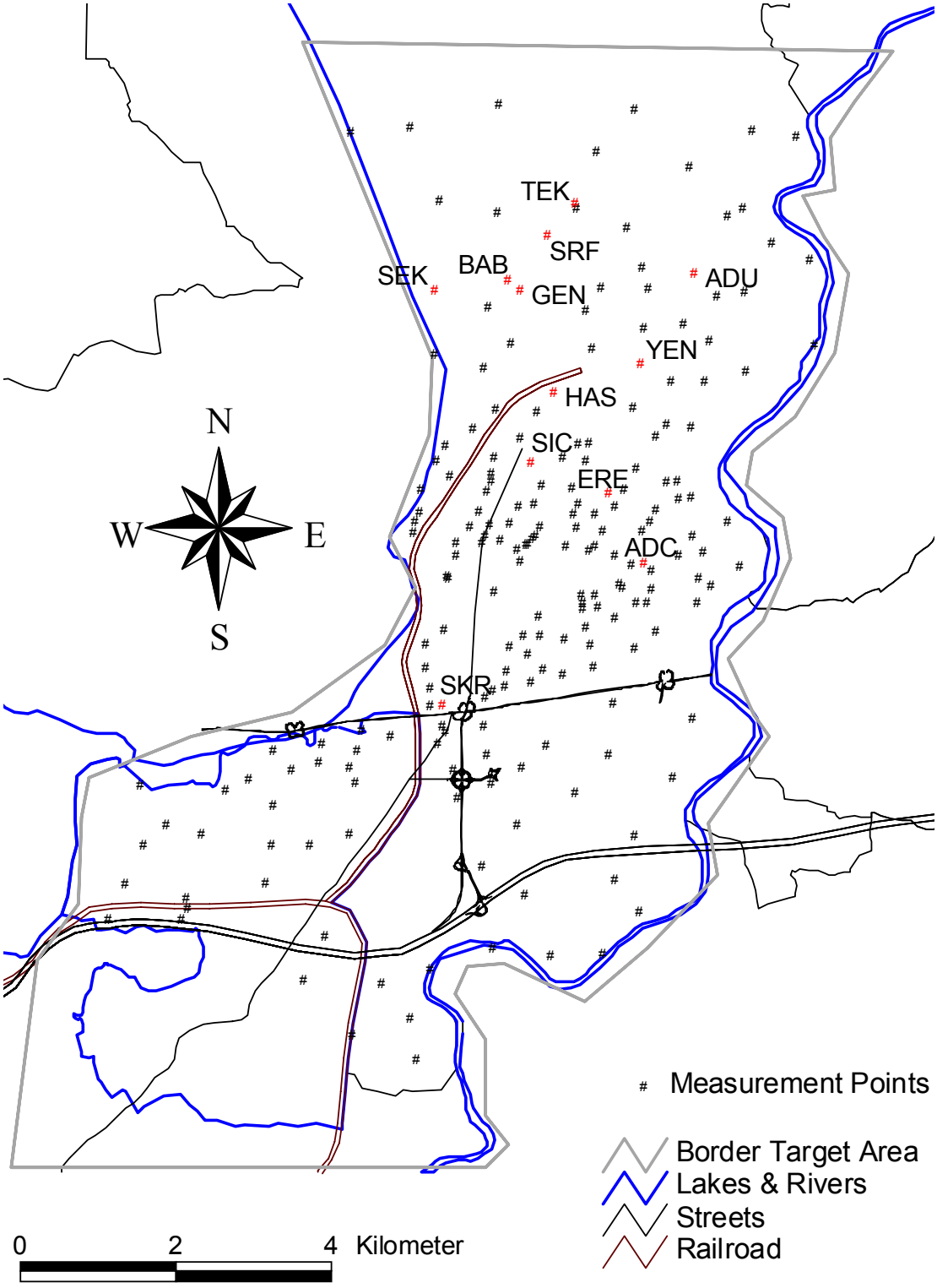

Figure 4.1. Microtremor measurements in Adapazarı; S-wave velocity profiles are available from ambient-vibration array measurements at sites ADU and ADC (Kudo et al., 2002) and YEN, SRF, TEK, ERE, SIC (Yamanaka et al., 2001). BAB, HAS, GEN, SEK and SKR are the strong-motion recording sites.

Gölcük

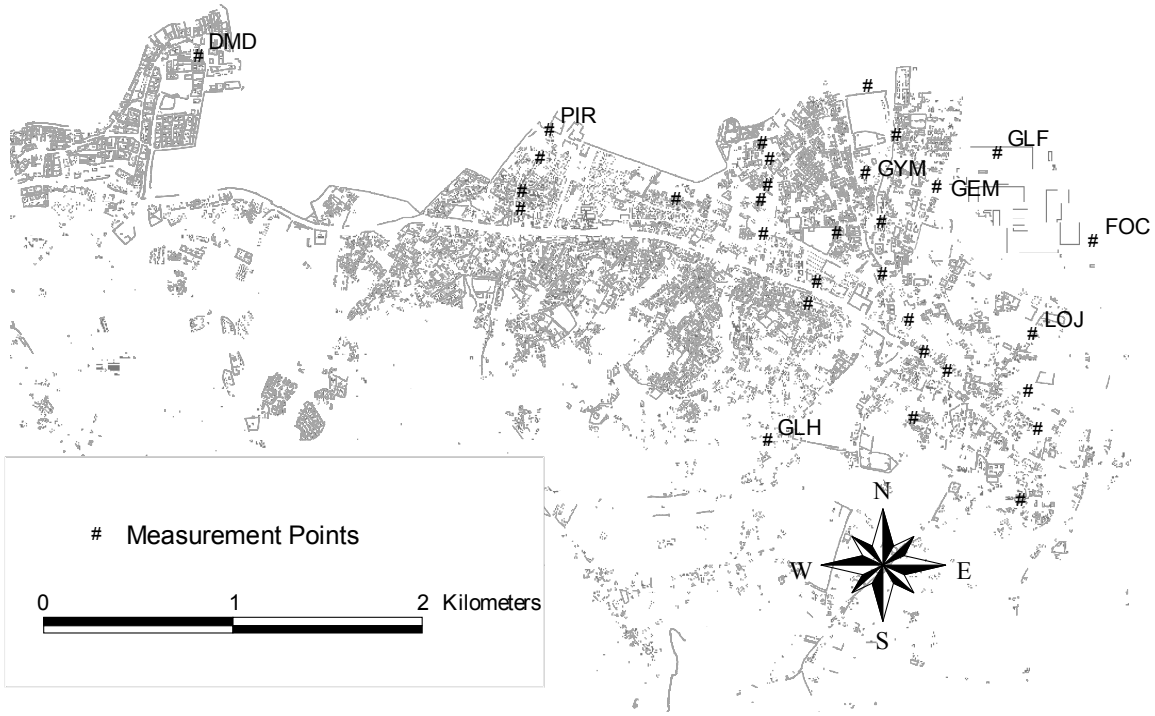

Figure 4.2. Microtremor measurements in Gölcük; S-wave velocity profiles are available from ambient-vibration array measurements at sites GLF and GLH (Kudo et al., 2002). DMD, FOC, LOJ, GYM, GEM and PIR are the strong-motion recording sites.

4.5. RESULTS FOR THE AREA OF ADAPAZARI

All ambient vibration records have been analyzed and the fundamental frequency of resonance has been determined for all sites (Figure 4.3). In general, a careful geological investigation of the site is a prerequisite to ensure that the investigated peak in the H/V ratio is related to the fundamental mode Rayleigh wave, and therefore to the fundamental frequency of resonance. In structures with two, or maybe three strong impedance contrasts, we can expect to obtain several peaks related to the fundamental and higher modes Rayleigh waves.

The two-layer case can be observed for the northern part in the Adapazarı area. For this area, array measurements provide S-wave velocity profiles down to bedrock. As we will show later on, numerical simulation of H/V spectral ratios with such profiles show good agreement with measured H/V curves. In the southern part of the Adapazarı area, we have no information about the thickness and layering of the soft sediments. The interpretation given for this area is therefore not unique.

The area of Adapazarı can be divided into several zones with similar shape of the H/V spectral ratios. The zones are shown in Figure 4.3 and examples of H/V spectral ratios for each zone are given in Figure 4.4 to Figure 4.8. The amplitudes are given at log10 scale. The following zones can be distinguished:

A. The fundamental frequency of resonance is between 0.22 and 0.50 Hz, with a second peak at around 0.7-0.8 Hz. For this area, S-wave velocity profiles are available from ambient-vibration array measurements (Kudo et al., 2002; Yamanaka

et al., 2001), and the velocity profiles will be discussed further on. The H/V spectral ratio shown in Figure 4.4 is a typical example of a structure with two layers. The surface sediments are composed of clays and silts, inter-bedded with gravel layers. The thickness of this layer is between 20 and 80 m. The large amplitude of the second peak (0.7-0.8 Hz) is due to the large S-wave velocity contrast between the surface sediments and the deep sediments. The deep sediments have a maximum thickness of about 300 to 400 m.

B. The observed H/V spectral ratios are characterized by one peak at the fundamental frequency of resonance. An example of a measured H/V spectral ratio is given in Figure 4.5. This type of spectrum is observed at the borders of the sedimentary basins. The frequency of the peak is varying from 0.7 Hz to values above 10 Hz, depending of the thickness of the soft sediments. Close to the foot of the hills, the fundamental frequency is high and it is decreasing towards the sedimentary basins. This spatial variation of the structure might be responsible for the excitation of local surface waves during earthquakes. Due to the smooth variation of the fundamental frequency of resonance, we can approximate the structure by a model composed of one-layer of soft sediments over bedrock. An inversion applied to the observed H/V ratios could define the gradient in S-wave velocity of this layer. A prerequisite would be borehole information down to the bedrock layer. The transition between zone B and A is very abrupt, which indicates that the deep sedimentary layer appears at this transition with a rapid increase of the thickness of the deep sediments.

C. Hill area, no clear peak is visible in the H/V spectral ratios. An example of a measured H/V spectral ratio is given in Figure 4.6. This zone can be considered as bedrock. Between the different small hills, small deposits of soft sediments can be identified, with observed fundamental frequency of resonance above 3 Hz. The density of measurements is not sufficient to resolve these small areas.

D. At all stations in this zone, the H/V spectral ratios show a clear peak around 0.4 to 0.5 Hz. An example of a measured H/V spectral ratio is given in Figure 4.7. For some stations an additional peak is seen below 0.2 Hz. For the deep sediments in this zone no geophysical information is available to us, and two possible basin models can be proposed: a deep and a shallow basin with fundamental frequency of resonance below 0.2 Hz or in the 0.4-0.5 Hz range respectively. The deep-basin model would require an interpretation of the observed H/V ratios at low frequencies with a two-dimensional structural model in order to explain the frequency distribution (Steimen et al., 2003). Due to the very clear peak in the H/V ratio, the shallow-basin model is favored. The large amplitudes of the H/V spectral ratio at the fundamental frequency around 0.4 Hz indicate a strong velocity contrast between sediments and bedrock. This can be explained by the presence of a thick layer of lake sediments with very low S-wave velocities. The small variation of the fundamental frequencies indicates a homogeneous layering of the soil deposit, with a maximum thickness of about 150-200 m.

E. The H/V spectral ratios measured in this zone show a double peak with one peak at 0.5 Hz and the other at around 1Hz. These two frequencies correspond to the ones of the neighboring sites to the west in zone D (0.5 Hz) and to the east in zone B (1 Hz). We might expect in zone E a change of the structure, and it may be possible that the layer of very soft lake sediments appear. An interpretation of the H/V spectral ratios with one-dimensional structural models is considered to be not valid anymore.

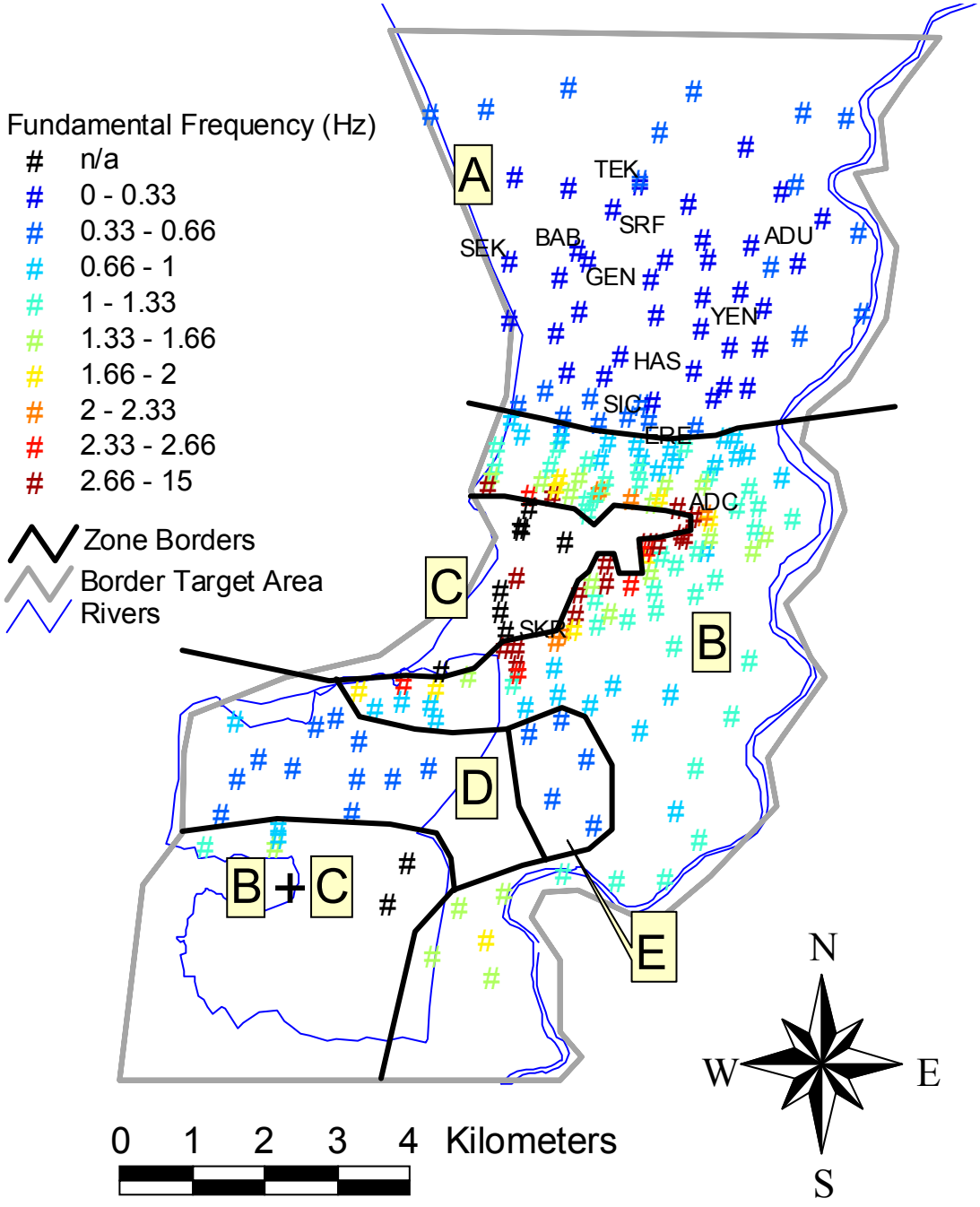

Figure 4.3. Measured fundamental frequencies of resonance in the Adapazarı area (Values in Hz); The zones with similar H/V spectral ratios are given with an index from A to E.

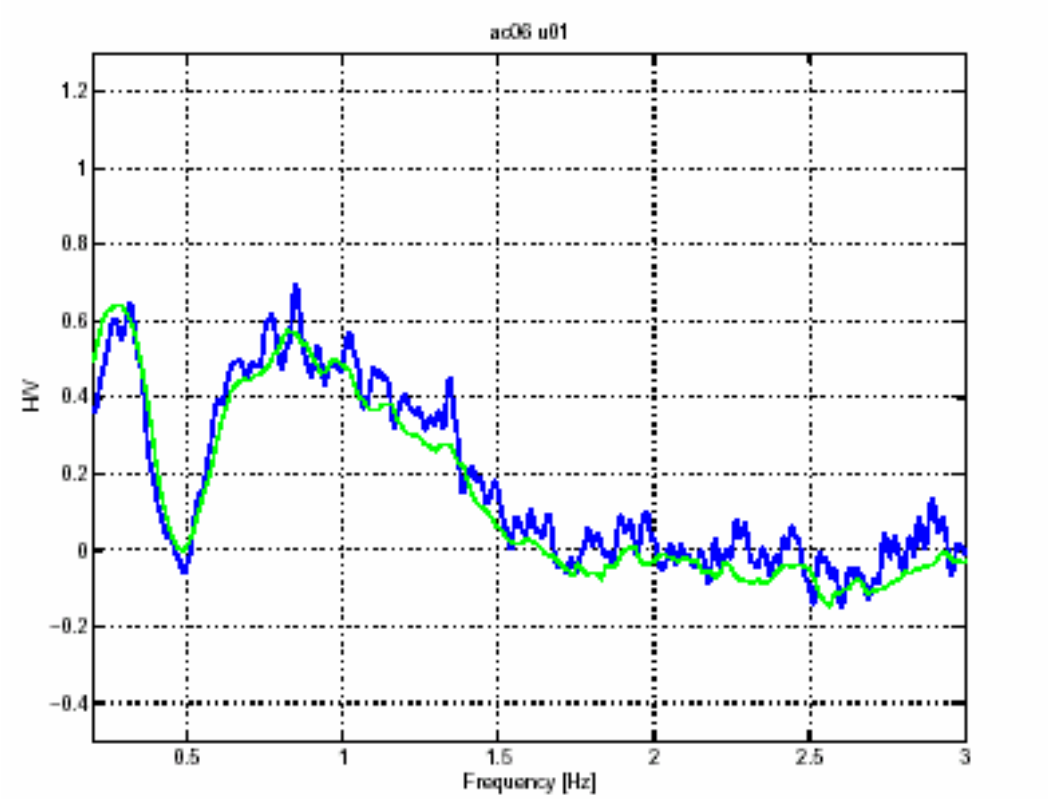

Figure 4.4. Example of an H/V spectral ratio observed in zone A. (Site: ac06_u01)

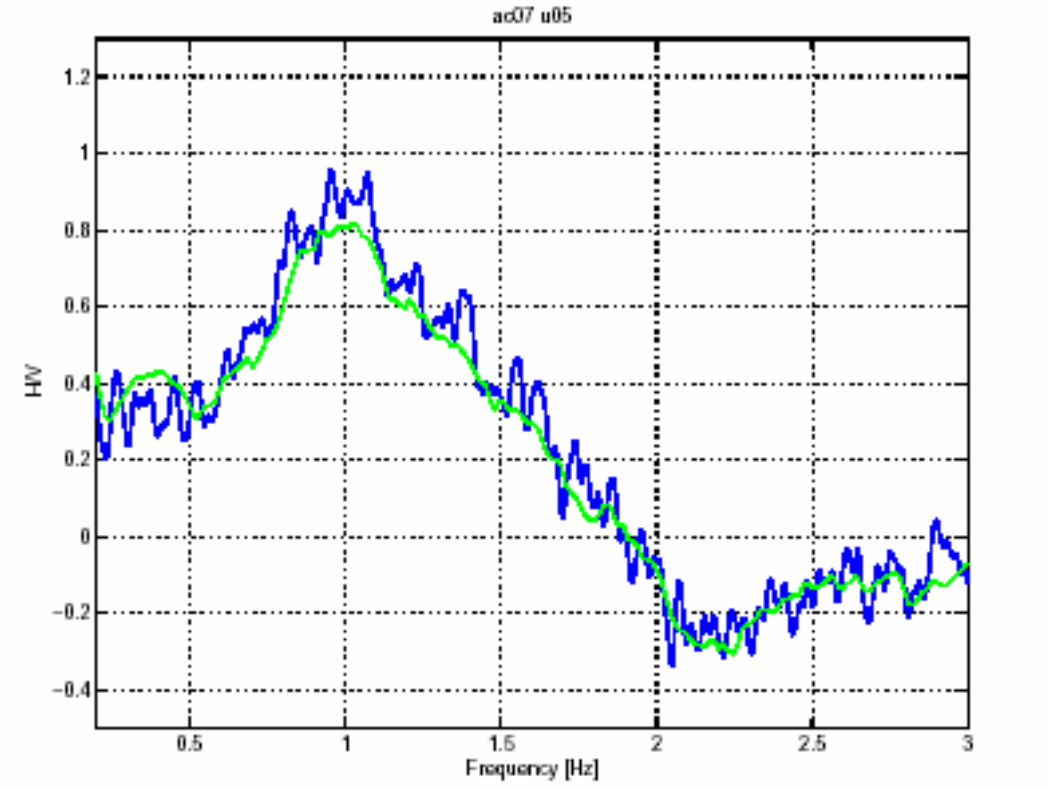

Figure 4.5. Example of an H/V spectral ratio observed in zone B. (Site: ac07_u05)

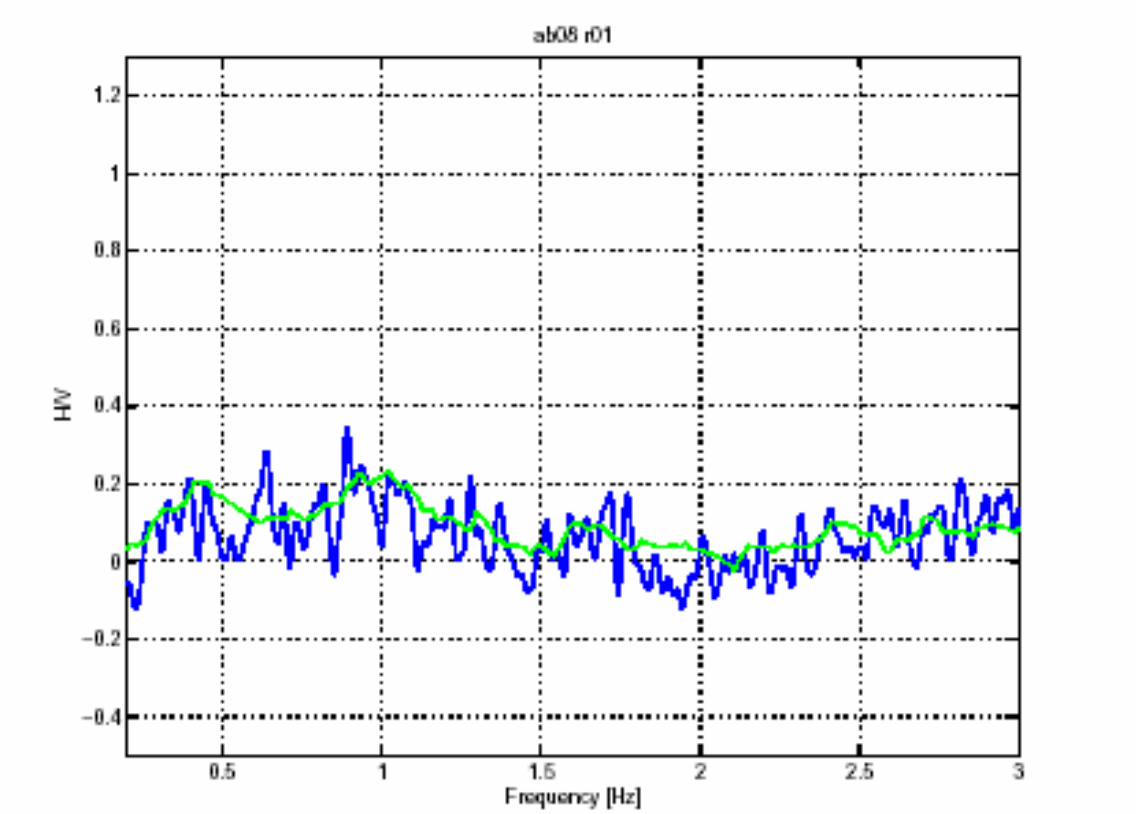

Figure 4.6. Example of an H/V spectral ratio observed in zone C. (Site: ab08_r01)

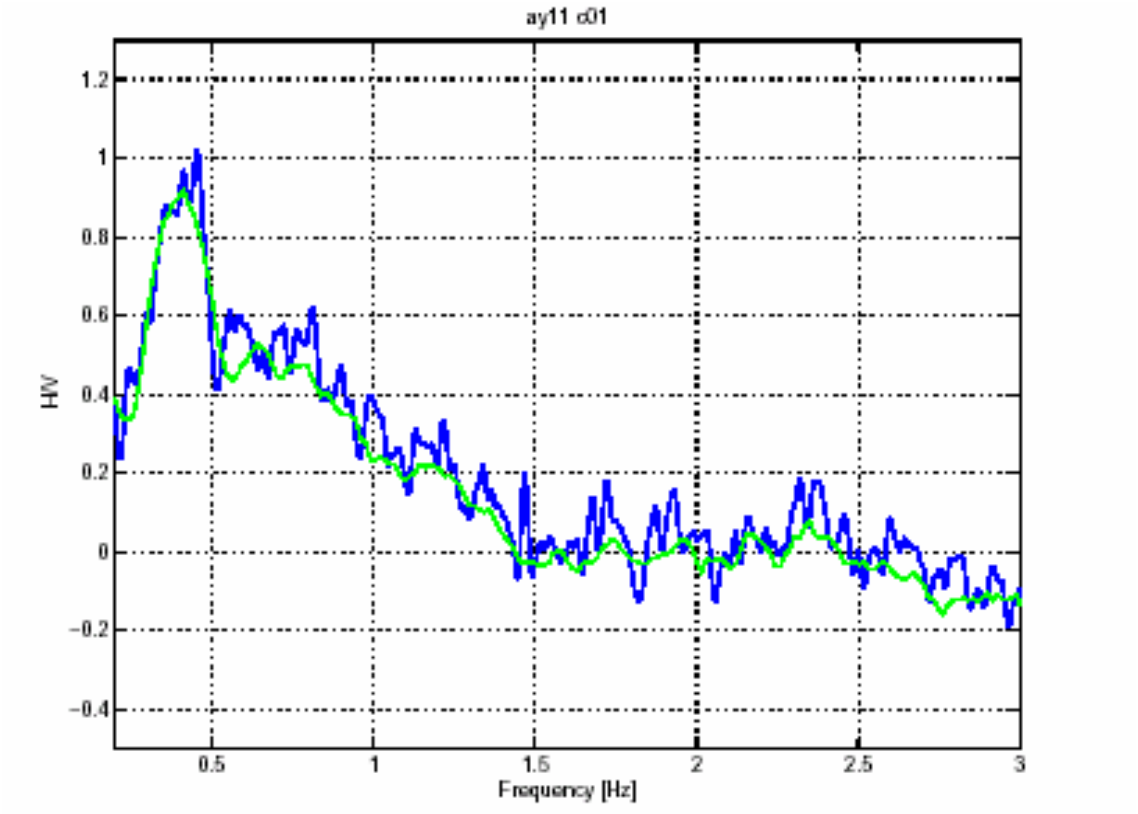

Figure 4.7. Example of an H/V spectral ratio observed in zone D. (Site: ay11_c01)

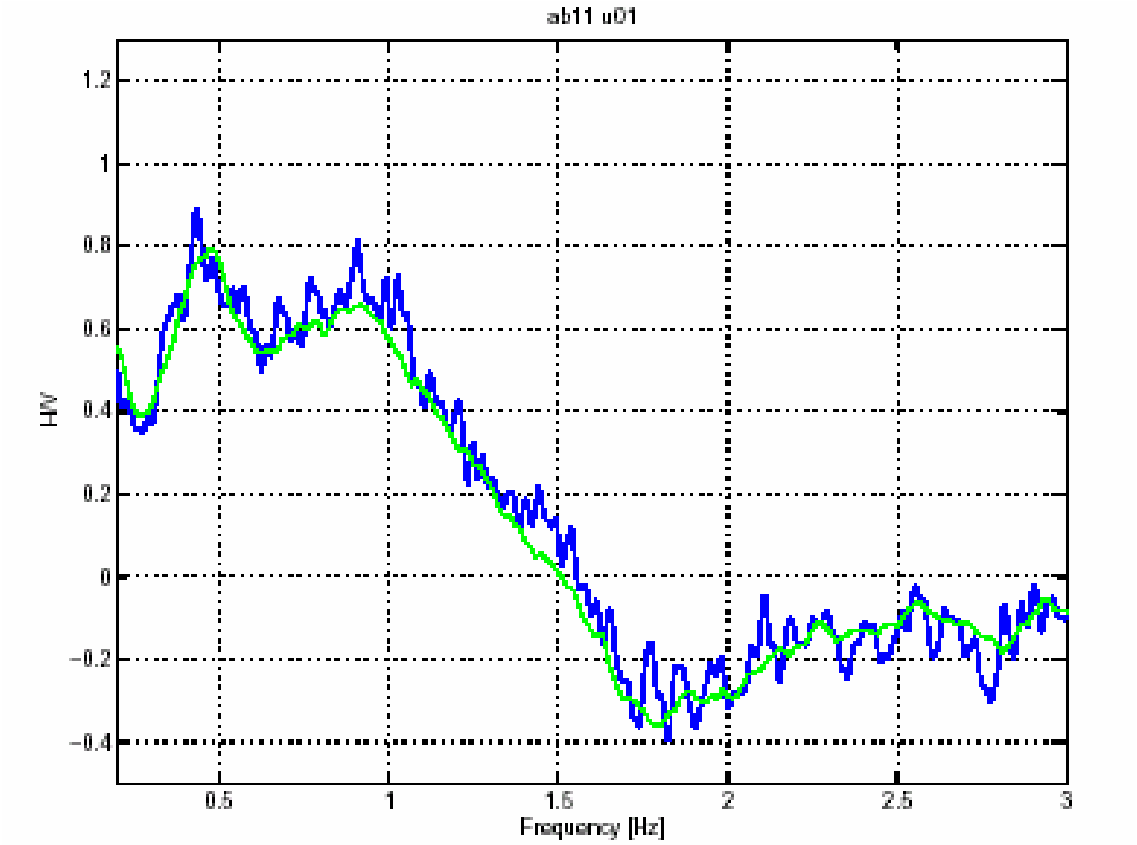

Figure 4.8. Example of an H/V spectral ratio observed in zone E. (Site: ab11_u01)

The f_0 values at each site are finally interpolated linearly and slightly smoothed, resulting in a fundamental frequency map shown in Figure 4.9. The fundamental frequency follows the main geologic features and allows a qualitative description of expected amplification of waves as a function of frequency. At frequencies much below f_0 there is no amplification of waves when compared to the hill zone. In our case of a strong impedance contrast between bedrock and sediment, amplification around f_0 can be very strong. The amplification at frequencies above f_0 depends on the layering of the soils and the incident wave field.

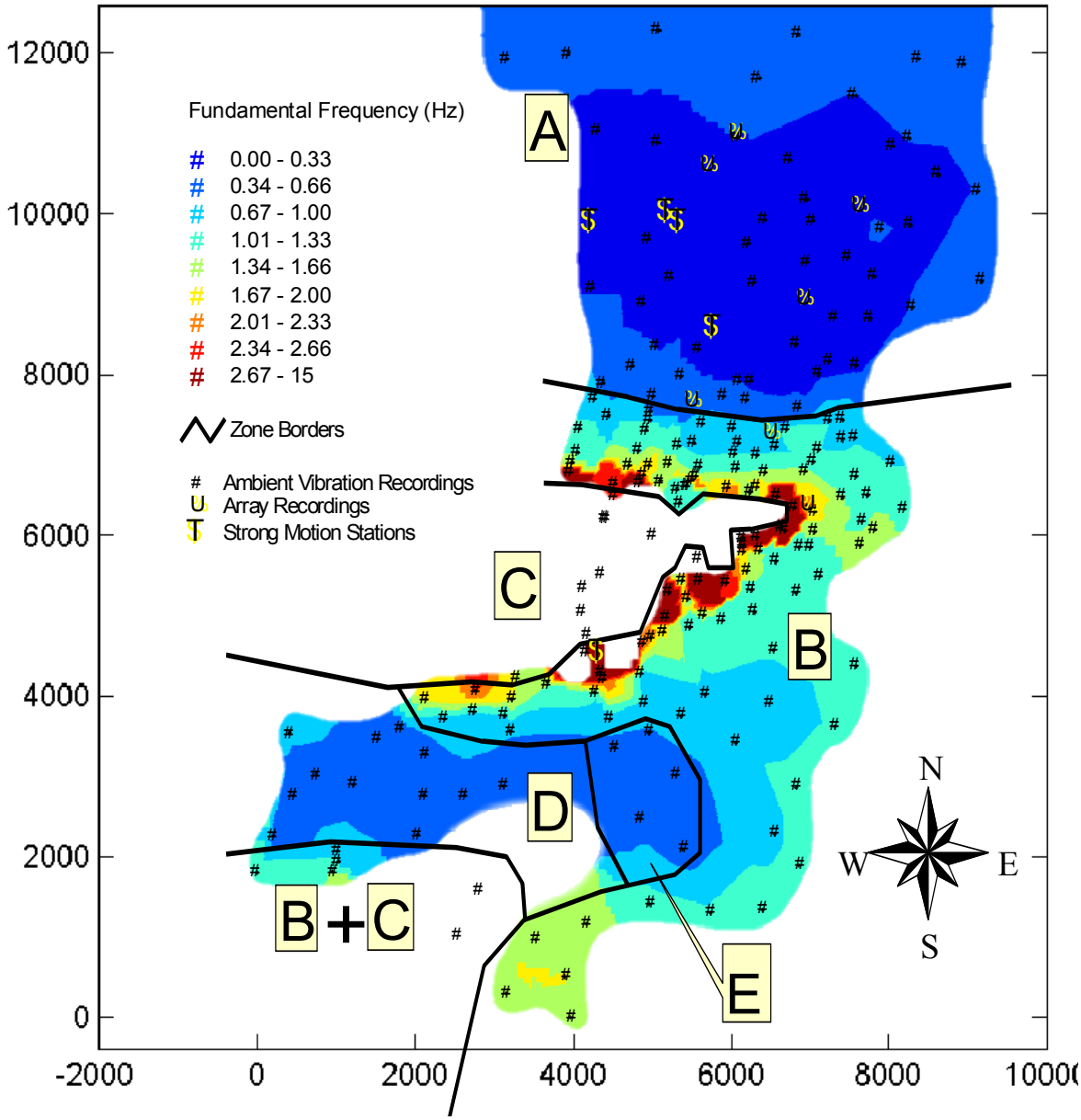

Figure 4.9. Map of fundamental frequencies in Adapazarı. Sites at which array measurements have been performed are given as yellow squares, sites of the strong motion aftershock recordings are given as yellow triangles.

The amplitude of the H/V spectral ratio at the fundamental frequency f_0 is an indicator for the S-wave velocity contrast between bedrock and sediments, and therefore provides some information on the severity of the resonance effects. The higher the amplitudes the larger is the velocity contrast. The amplitude values of the H/V ratios at each site are interpolated linearly and slightly smoothed, resulting in a map shown in Figure 4.10 at a log10 scale. The amplitude depends on the source-depth distribution and source-distance distribution. Amplitudes of the H/V ratio therefore provide only a qualitative indicator of the possible resonance effects. The largest amplitudes are observed in the zone D, where the layer of very soft sediments causes the large amplitudes of the H/V spectral ratios. The other areas with high amplitude are located in zone B, close to the transition between bedrock and sediments.

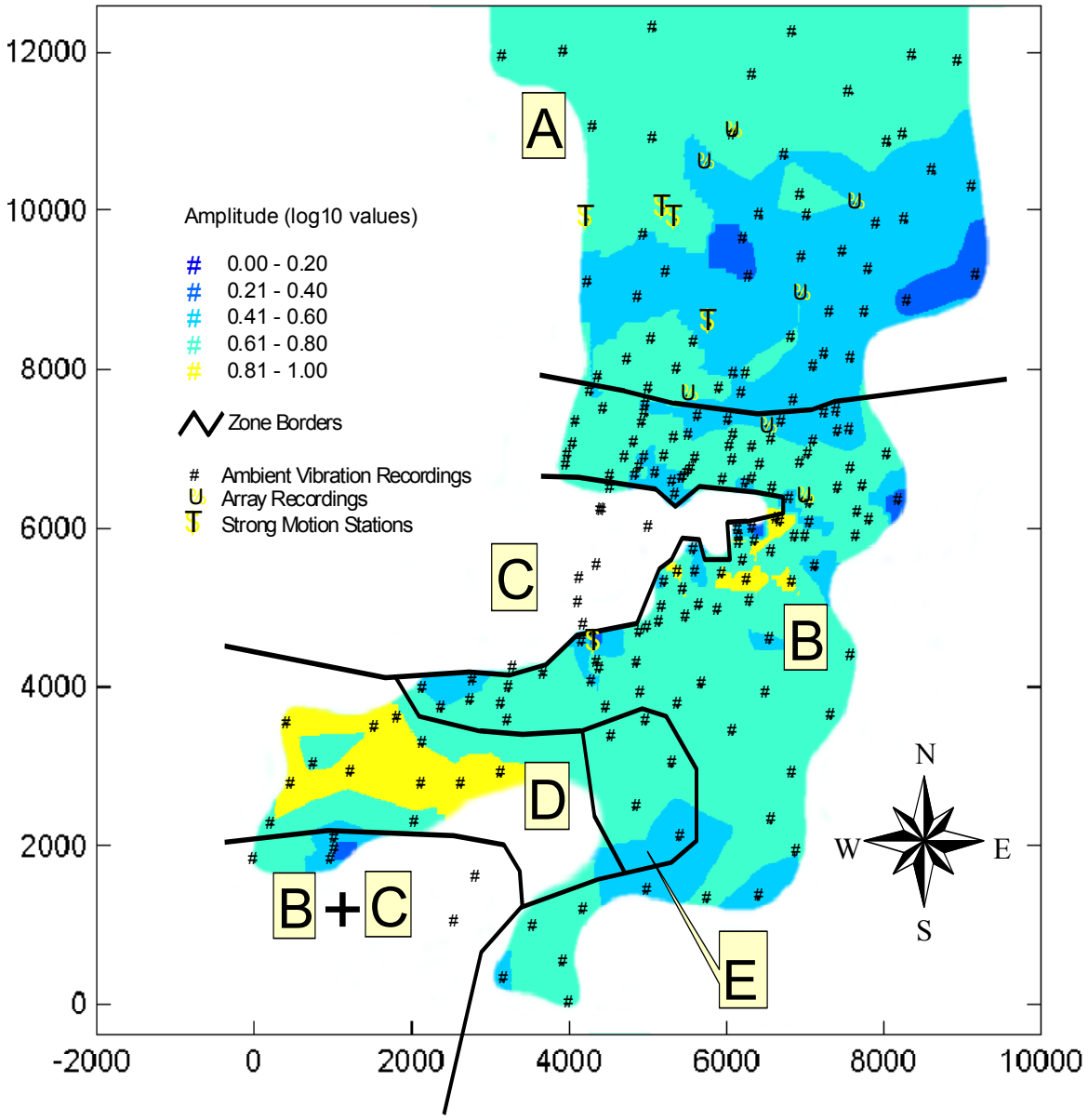

Figure 4.10. Map of the amplitude of the H/V spectral ratio at the fundamental frequency in Adapazarı

The amplitude of the second peak of the H/V spectral ratio provides some information about the velocity contrast between the surface sediments and the deep sediments (in the two-layer over bedrock case). The larger the amplitude of the ratio, the higher is the velocity contrast. An example is the H/V ratio shown in Figure 4.4 with the second peak at 0.7-0.8 Hz. In zone A, we have evidence for this two-layer structure from the array measurements performed by Kudo et al. (2002) and Yamanaka et al. (2001). This interpretation of the second peak is only allowed as long as the f_0 of the surface low-velocity layer is considerably larger than the fundamental frequency of the entire soil column.

4.5.1 Comparison between synthetic H/V spectral ratios and observations

S-wave velocity profiles are available from ambient-vibration array measurements at sites ADU and ADC (Kudo et al., 2002) and YEN, SRF, TEK, ERE, SIC (Yamanaka et al.,

2001). The models proposed by Kudo are given in Table 4.1. The sites of the arrays could not be exactly reconstructed, and the location error of the site is within a radius of about 50 m. Yamanaka does not provide station coordinates and velocity profiles in tabular form. Our modeling results for these sites are therefore only indicative, and are not shown here.

We have used the proposed structural models in Table 4.1 to compute synthetic H/V spectral ratios, and to compare them to the observed ratios at the sites. The modeling of synthetic H/V ratios requires some assumptions to be made about the distribution of the source positions, and we try to keep the assumptions as general as possible by superposing a multitude of sources over a wide distance range.

Table 4.1. S-wave velocity profiles proposed by Kudo et al. (2002) for two sites in Adapazarı

ADC		ADU	
Vs (m/sec)	Thickness (m)	Vs (m/sec)	Thickness (m)
243	38	166	44
441	97	331	88
728	242	500	281
1500	70	878	63
2000	halfspace	1050	100
		1500	halfspace

The numerical technique used is the mode summation method (Panza, 1985; Panza and Suhadolc, 1987) for the P-SV part of the wavefield. The method allows the investigation of signals from well-defined sources and source-receiver distances. For a given structure the P-SV modes are first calculated. From the defined source the energy content of each mode in the Fourier domain is computed, and then summed to derive the actual wavefield. In order to generate synthetic ambient vibration wave fields, multiple sources are considered. Randomly distributed sources are assumed over a certain distance range [x, x+250m] and depth range [0m, 250m]. Twenty distance ranges are treated, namely [250m, 500m], [500m, 750m], ..., [5000m, 5250m] with 100 different random source mechanisms for each range. Finally the average H/V ratio is computed directly in the frequency domain from the 20 times 100 H/V ratios of the single runs with different sources.

The synthetic average H/V spectral ratio for the site ADU is shown in Figure 4.11 as thick black line. The H/V ratio is similar to the observations given in blue and green color. The ellipticity of the fundamental mode Rayleigh wave is shown in red and the first higher mode in magenta. In the modeling, the average H/V ratios are determined by the fundamental mode ellipticity in the frequency band 0.22-0.5 Hz This has been generally observed for structural models with a large velocity contrast between bedrock and sediments for frequencies between the fundamental frequency of resonance f_0 of the unconsolidated sediments and the first minimum of the average H/V ratio (Fäh et al., 2001). The shape of H/V ratios in this frequency band depends mostly on the layering of the sediments. The peak of the first higher mode at about 0.6 Hz seems to be present in the observed H/V ratio. The difference in the high frequency range is most probably due to the limited number of layers in the structure used for the modeling and the complexity of the real ambient vibration wavefield.

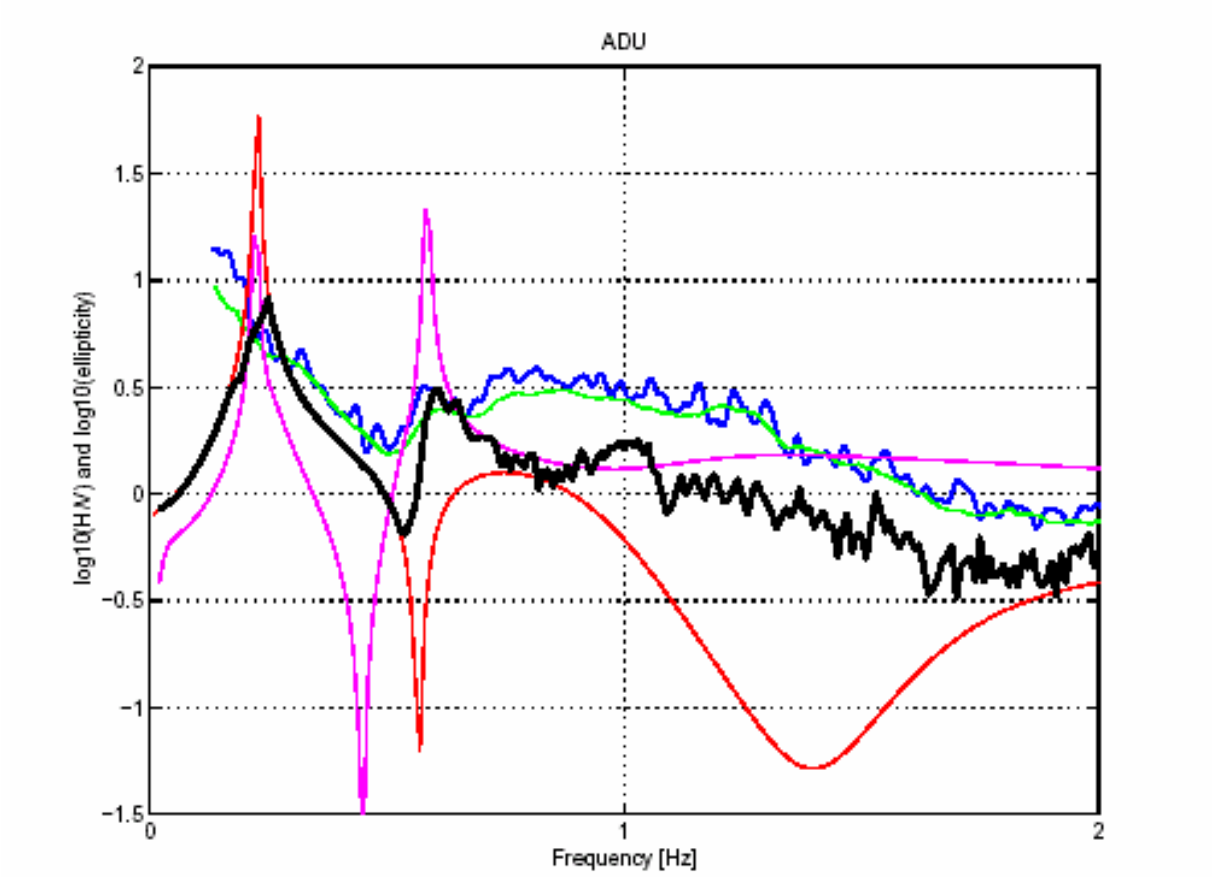

Figure 4.11. Comparison between H/V ratios of observed noise at observation site ADU (blue line: classical method; green line: FTAN based) and synthetic H/V spectral ratios (Black curve). The ellipticity of the fundamental-mode Rayleigh wave (red curve) and the first higher mode (magenta curve) are given. The H/V spectral ratios are given at log10 values.

In Kudo et al. (2002), site ADC is classified as a structure with deep sediments. This cannot be confirmed by the measured H/V ratio (Figure 4.12). The fundamental frequency of resonance is around 2.0-2.3 Hz, which is not consistent with the structure ADC given in Table 4.1. Referring to Kudo et al. (2002), site ADC is located in the heavily damaged area of Adapazarı, and a fundamental frequency of about 2 Hz would give a good reason for this damage.

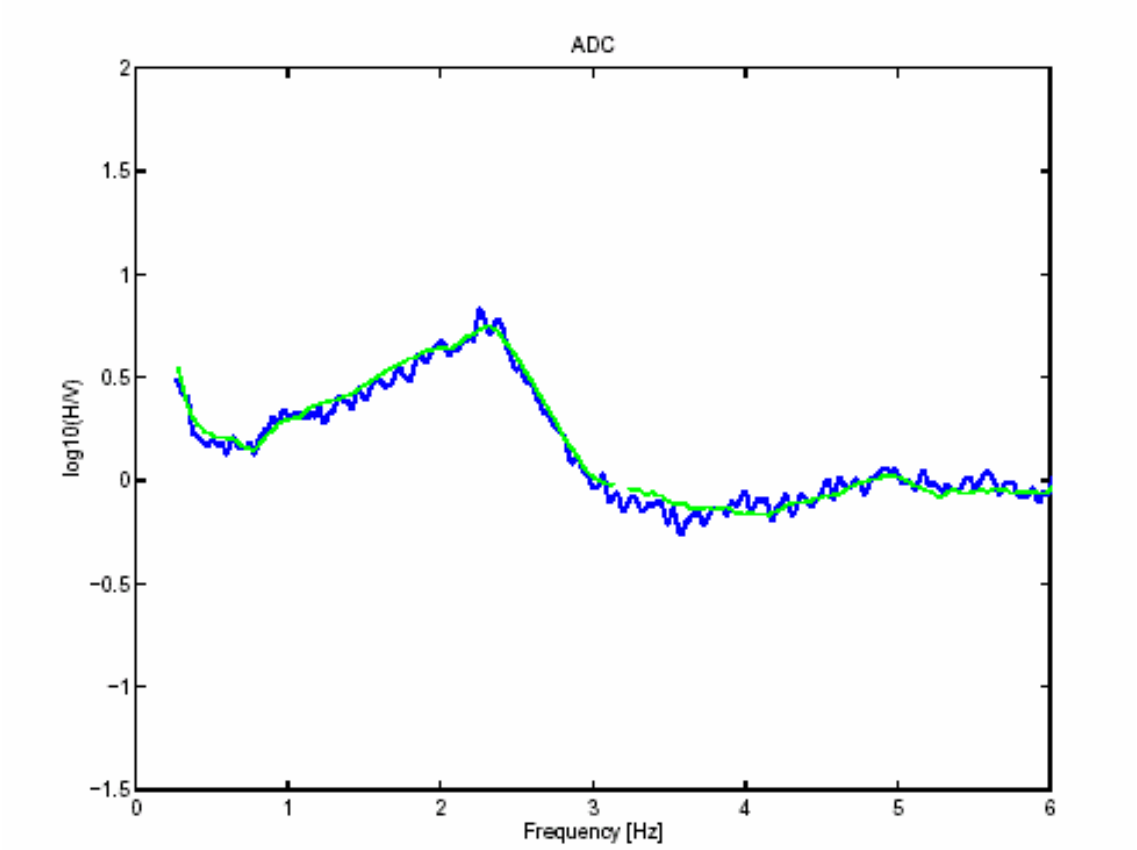

Figure 4.12. H/V ratios observed at site ADC (blue line: classical method; green line: FTAN based).

For the sites described in Yamanaka et al. (2002) the total thickness of the soft sediments is overestimated leading to a lower fundamental frequency of resonance than measured in Adapazarı. This is due to the fact that only the phase velocity curve of the fundamental mode Rayleigh wave, measured on vertical component recordings, are used to invert for the S-wave velocity profile. This curve is not sufficient to resolve the thickness of the soft sediments. A combined inversion using the phase velocity curves, and the fundamental frequency or ellipticity would resolve this problem. The comparison between the velocity profiles at sites ERE and SIC (Fig. 5 in Yamanaka et al. (2002)) confirms the very rapid increase in the thickness of the soft sediments between zone B and A.

4.5.2 Comparison between H/V spectral ratios from strong motion recordings and ambient vibrations

Acceleration and velocity time histories recorded in Adapazarı and Gölcük area after the main shock were collected and organized in the DRM-MERM project by the Kandilli Observatory and Earthquake Research Institute in Istanbul. The dataset includes motions recorded at 19 stations: 13 in Adapazarı and 6 in Gölcük. All of these stations were temporary stations (except station SKR), which were installed after the Kocaeli Earthquake, and currently uninstalled. Stations were operated by the Earthquake Engineering Department of Bogazici University, Kandilli Observatory and Earthquake Research Institute (KOERI), by the Istanbul Technical University (ITU), by Earthquake Research Department of General Directorate of Disaster Affairs (ERD), by Geological Hazards Team, United States Geological Survey, Golden, Colorado, by Earthquake Hazards Team, United States Geological Survey, Menlo Park, California.

From this dataset, recordings have been selected with a certain level of peak ground motion. The selected recordings have been used to compute average H/V spectral ratios. The entire waveforms (P waves, S waves and coda) were used. Only one example is given here for the recording site HAS in Adapazarı. Four events with peak ground accelerations greater than 50 mg were selected for the analysis. Figure 4.13 provides the comparison between H/V ratios from ambient vibrations and H/V ratios from the earthquake data. In the frequency band between f_0 and 1.2 Hz, there is good correspondence between the H/V curves. The variability in the curves obtained from the strong motion recordings is higher due to the limited number of records. Above 1.2 Hz the H/V curves differ considerably, which is due to difference in the composition of the wavefields.

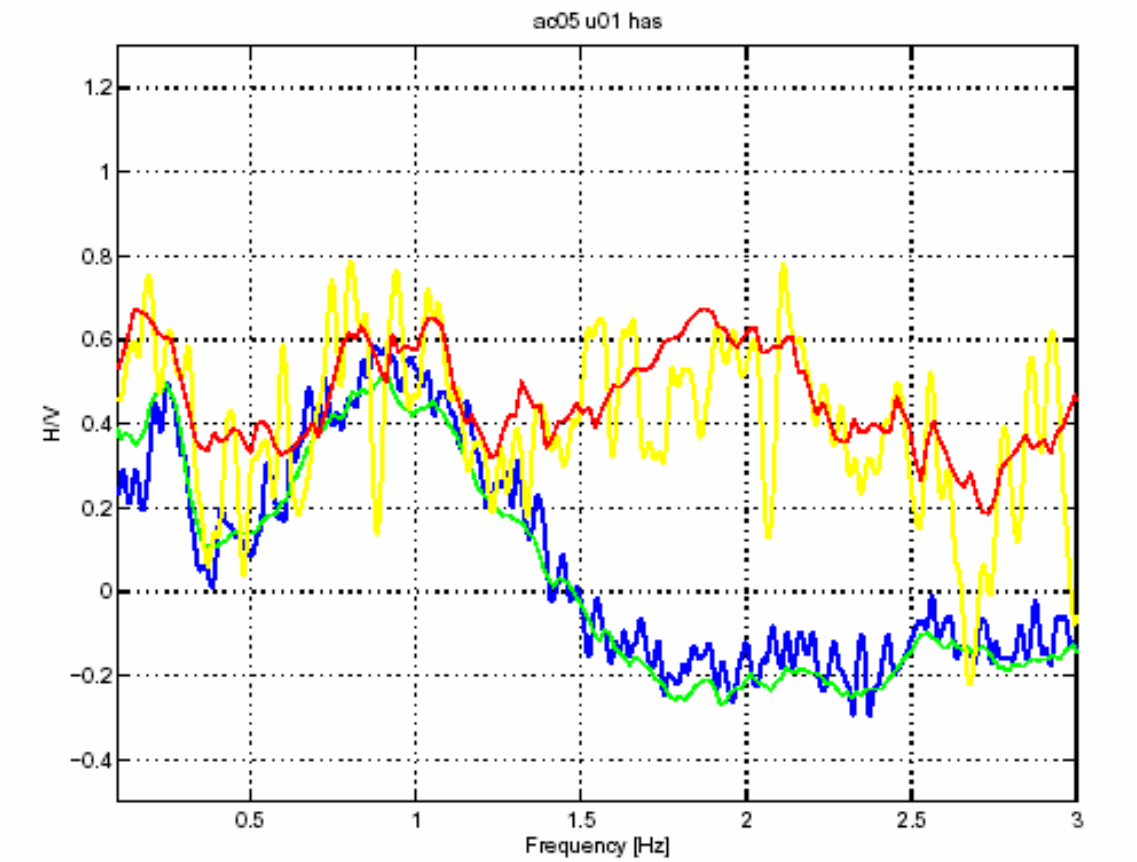

Figure 4.13. Comparison between H/V ratios from ambient vibrations site HAS (blue line: classical method; green line: FTAN based) and H/V ratios from strong motion recordings (yellow line: classical method, red line: FTAN based) provided by KOERI.

4.6. RESULTS FOR THE AREA OF GÖLCÜK

All ambient vibration records have been analyzed and the fundamental frequency of resonance has been determined for all sites (Figure 4.14).

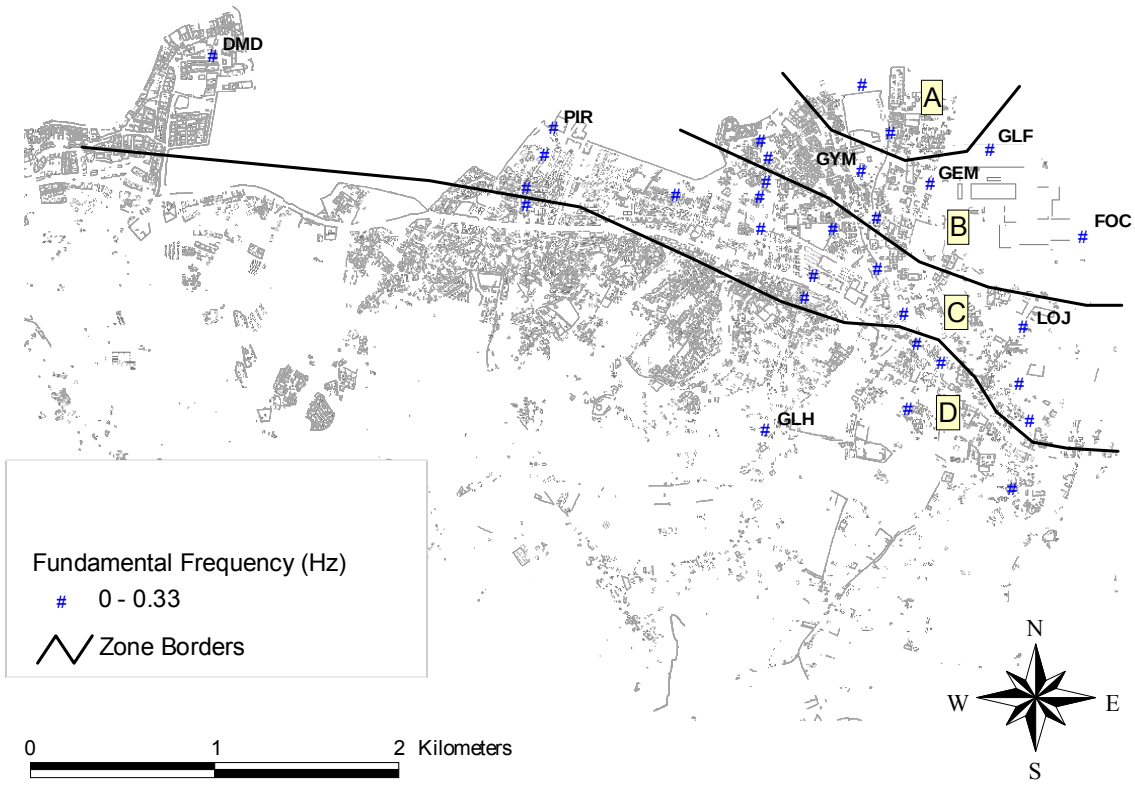

Figure 4.14. Measured fundamental frequencies of resonance in the Gölcük area (Values in Hz)

The measured fundamental frequencies of resonance are rather constant (0.2-0.3 Hz) for the sites within the area composed of unconsolidated sediments. Different zones can be distinguished. Examples of H/V spectral ratios for the different zones are shown in Figure 4.15 to Figure 4.18. The amplitudes are given at log10 scale. The change from one zone to the next is very smooth, especially between zones C and D. The borders between the zones are only rough indications.

A. This area shows a particular signal, due to the fact that this area was settled and flooded during the Kocaeli earthquake, and refilled later on. One can see a peak at 0.35 Hz, quickly followed by a second peak at around 0.7 Hz (Figure 4.15). The large amplitude of the second peak is due to the low S-wave velocity of the refill material. The fundamental frequency of resonance is expected around 0.2 Hz.

B. The measurements in this area show the fundamental frequency at 0.25 Hz, and a second, wide peak with the maximum in at frequencies around 0.7 (in the north-east) and 1.2 Hz (in the south-west) (Figure 4.16). The large amplitude of this second peak indicates a surface layer of soft sediments with low S-wave velocity. This is confirmed by the array measurements at site GLF (see below).

C. The fundamental frequency is around 0.25 Hz (Figure 4.17). The second peak becomes very wide and flat when compared to zone B, with the maximum around 1.5 Hz and a second minimum at about 3.5 Hz. In this zone, the surface layer with soft sediments is disappearing.

D. The fundamental frequency is around 0.25 to 0.3 Hz (Figure 4.18). There is no second peak visible, due to the absence of the soft surface layer. This is confirmed by the array measurements at station GLH (see below).

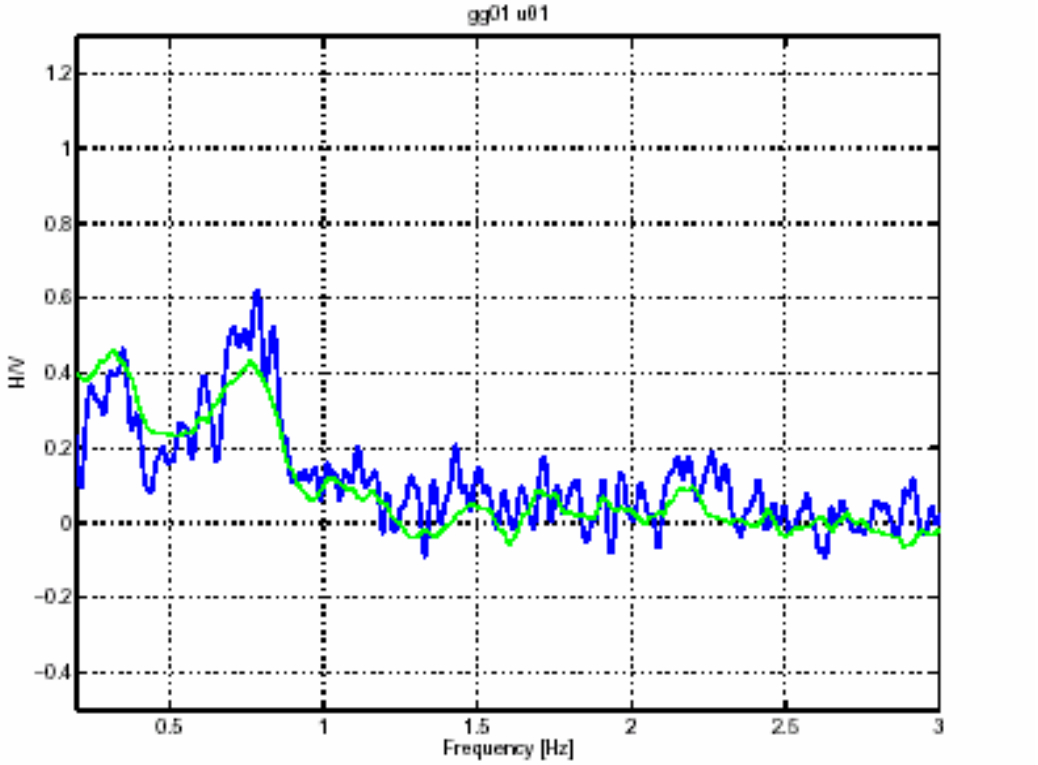

Figure 4.15. Example of an H/V spectral ratio observed in zone A (Site: gg01_u01)

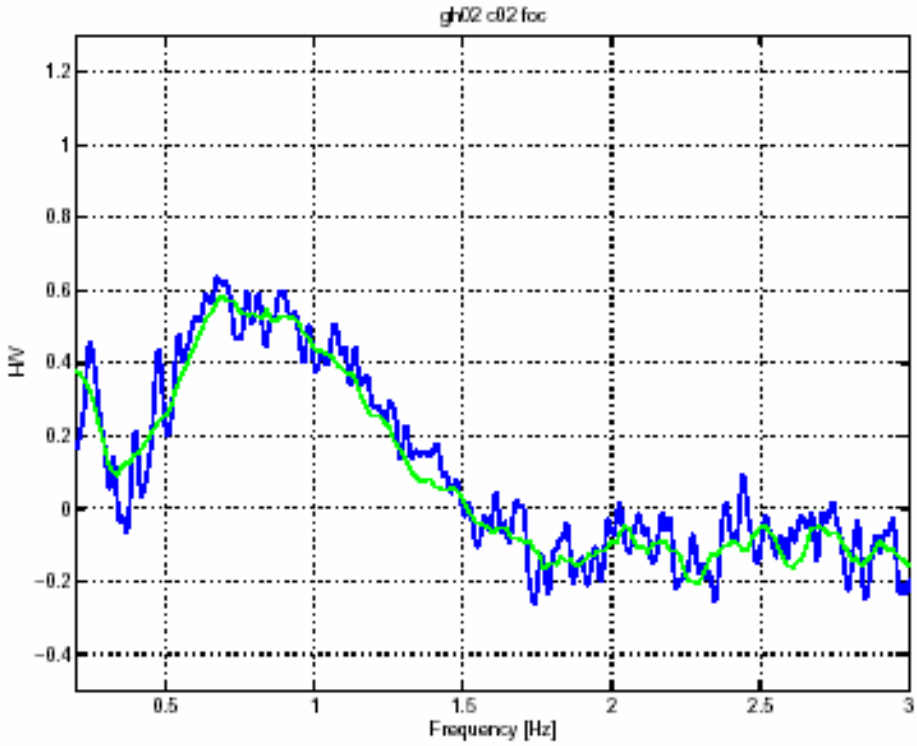

Figure 4.16. Example of an H/V spectral ratio observed in zone B (Site: gh02_c02_foc)

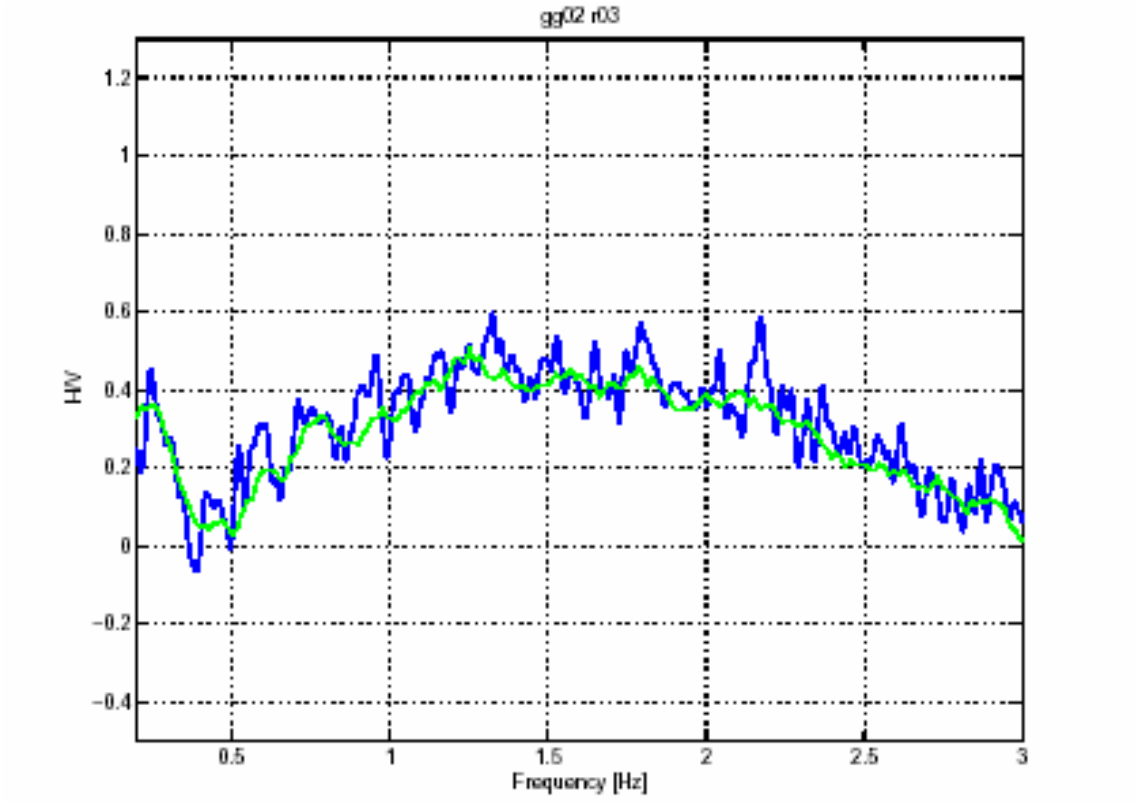

Figure 4.17. Example of an H/V spectral ratio observed in zone C (Site: gg02_r03)

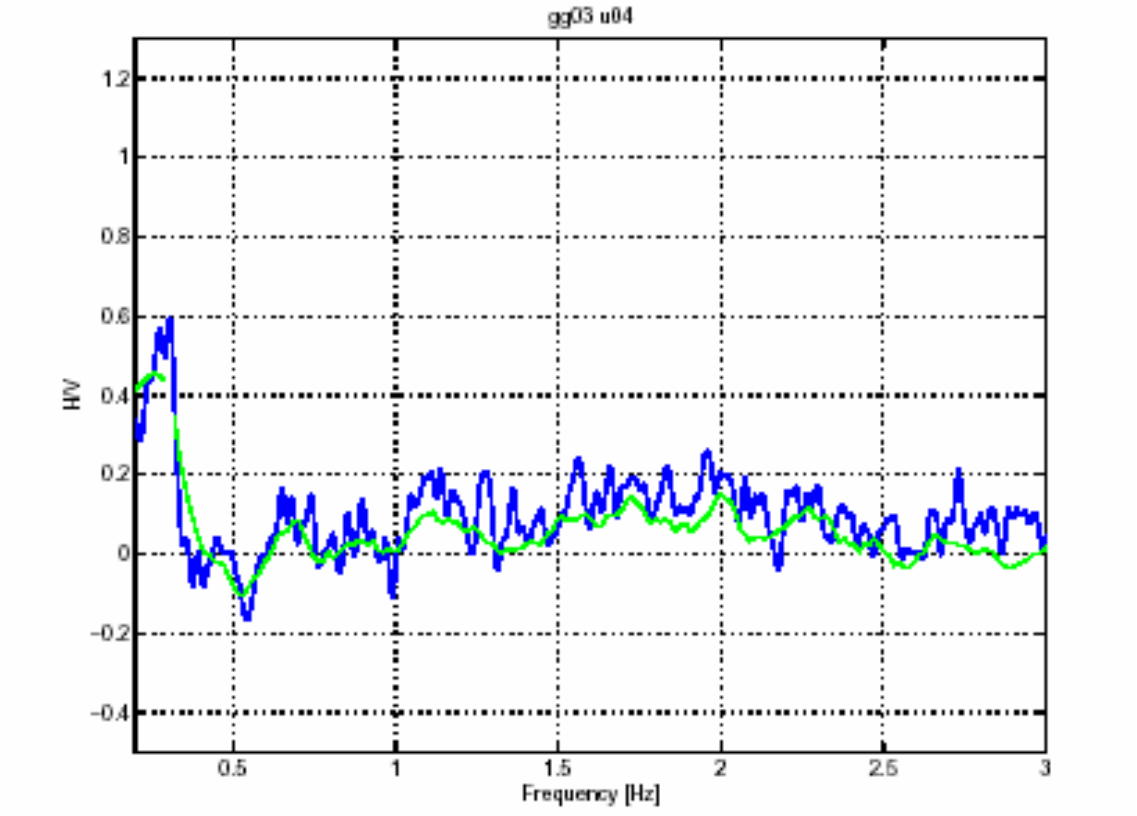

Figure 4.18. Example of an H/V spectral ratio observed in zone D (Site: gg03_u04)

The decay of the second peak in the H/V spectral ratio shown in Figure 4.16 to Figure 4.18 is an expression of the disappearing of the surface layer with very low S-wave velocity. This is the reason why we cannot draw sharp boundaries between the different zones.

The f_0 values at each site are finally interpolated linearly and slightly smoothed, resulting in a fundamental frequency map shown in Figure 4.19, which once again shows the constant values of the fundamental frequency of resonance.

The amplitude of the H/V spectral ratio at the fundamental frequency f_0 is shown in Figure 4.20. The amplitudes do not show the large differences like in the Adapazarı area. The largest amplitudes are observed in the zone A and D. One reason for the lower amplitudes in zone B and C could be that the fundamental mode Rayleigh wave is not the dominant mode in the ambient vibration wavefield (see below).

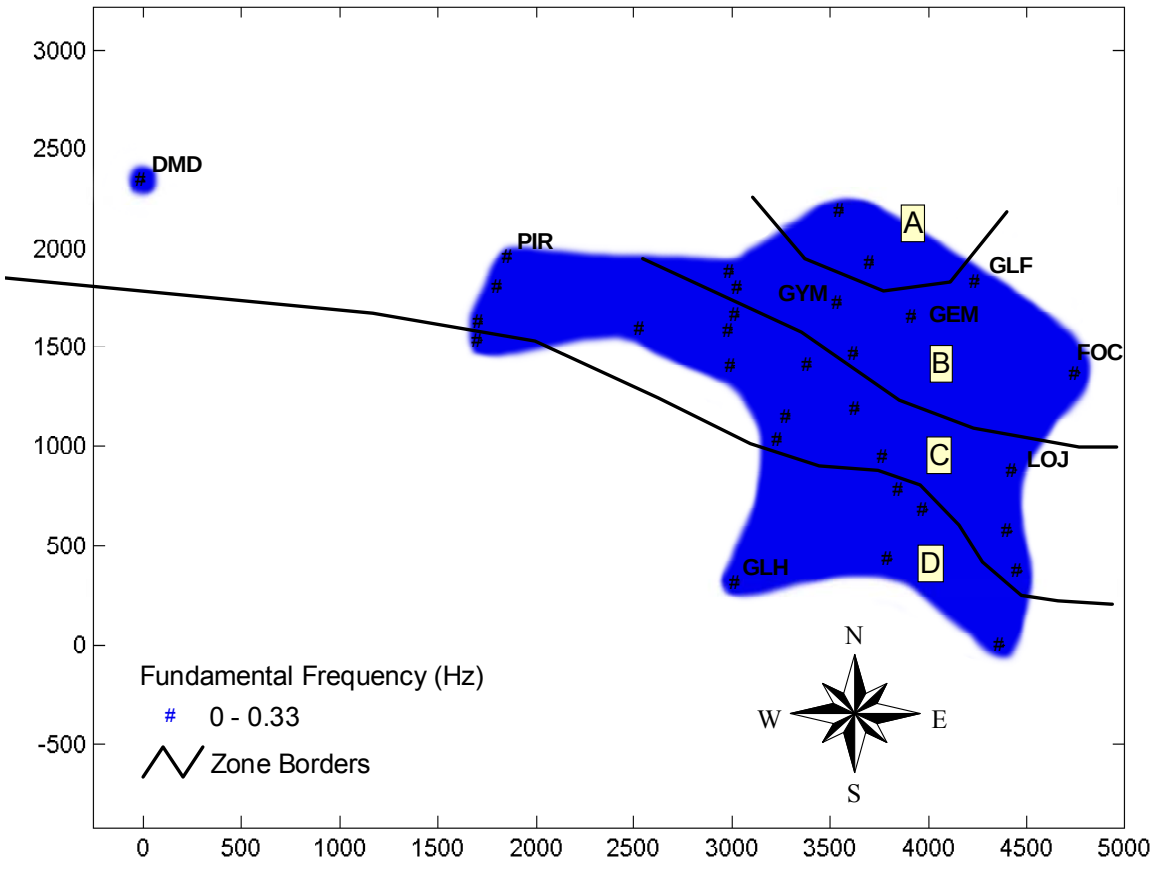

Figure 4.19. Map of fundamental frequencies in Gölcük.

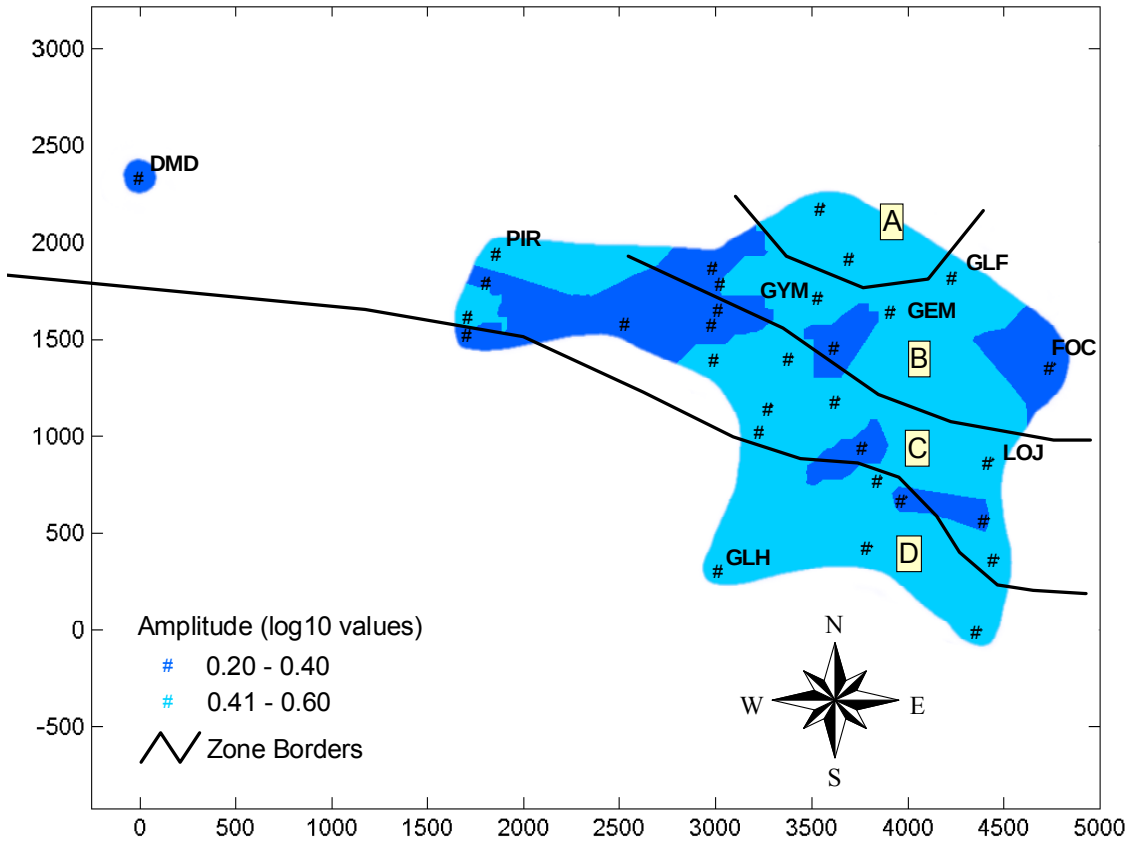

Figure 4.20. Map of the amplitude of the H/V spectral ratio at the fundamental frequency in Adapazarı.

4.6.1 Comparison between synthetic H/V spectral ratios and observations

S-wave velocity profiles are available from ambient-vibration array measurements at sites GLF and GLH (Kudo et al., 2002). The models proposed by Kudo are given in Table 4.2. Site GLF is located in zone B where we observe a surface layer of soft sediments. Site GLH is characterized by the absence of this layer. The sites of the arrays could not be exactly reconstructed, and the location error of the site is within a radius of about 50 m. We have used the proposed structural models in Table 4.2 to compute synthetic H/V spectral ratios, and to compare them to the observed ratios at the sites. The modeling is described in Section 4.5.1.

Table 4.2. S-wave velocity profiles proposed by Kudo et al. (2002) for two sites in Gölcük.

GLF		GLH	
Vs (m/sec)	Thickness (m)	Vs (m/sec)	Thickness (m)
150	14	303	22
259	70	455	60
531	270	594	295
950	300	950	halfspace
1120	halfspace		

The synthetic average H/V spectral ratio for the site GLF is shown in Figure 4.21 as thick black line, and for site GLH in Figure 4.22. The fundamental frequency is f_0 of synthetic H/V spectral ratios are in agreement with the observations given in blue and green color. The ellipticity of the fundamental mode Rayleigh wave is shown in red and

the first higher mode in magenta. For both sites the general shape of the observed H/V ratios can be explained by the numerical modeling.

From the observed H/V curves, we may expect that not only the fundamental mode Rayleigh wave is excited around the fundamental frequency of resonance, but also the first higher mode. For site GLF (Figure 4.21) the first higher mode seems to be dominant around f_0. For this frequency band, the modeling does not explain the observations due to the selection of only near-surface sources that excite the ambient vibrations. This selection will excite mostly the fundamental mode Rayleigh waves and not the higher modes.

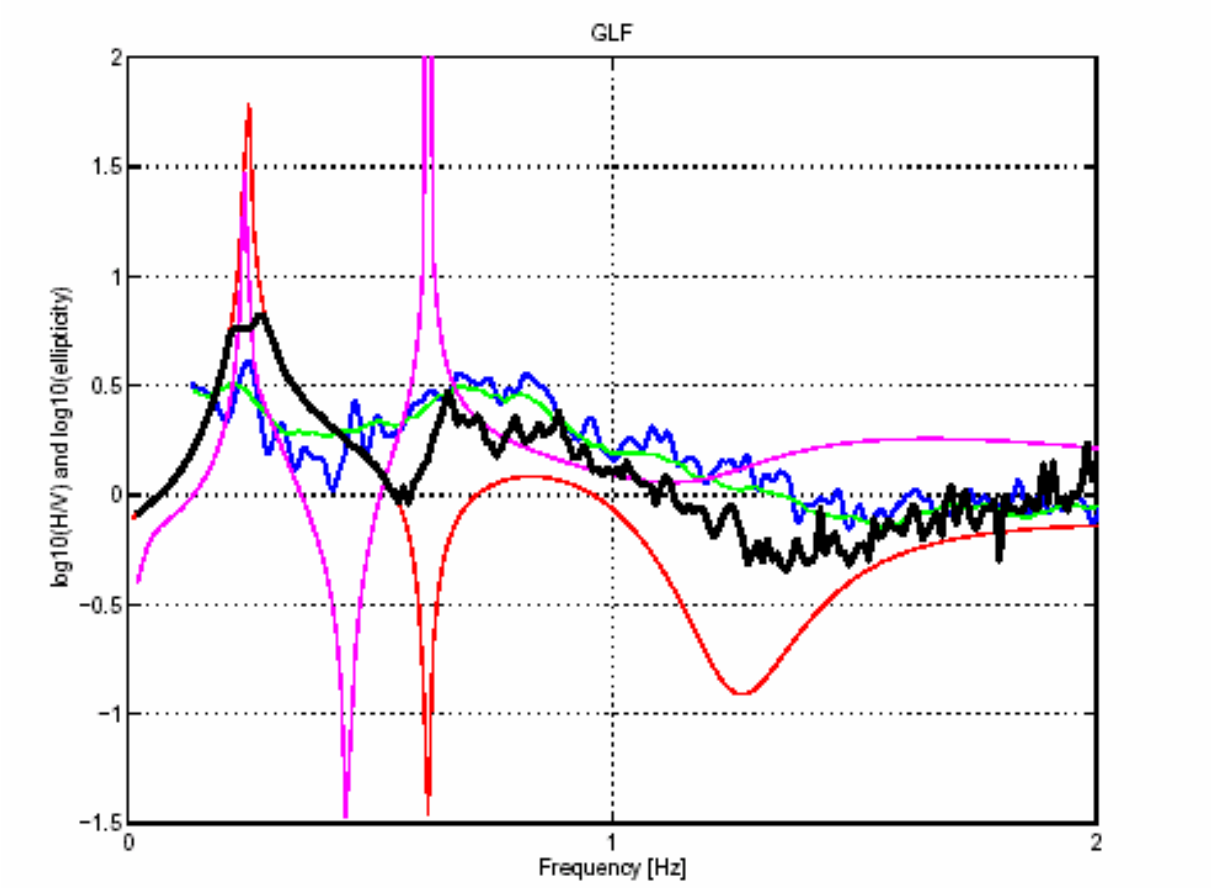

Figure 4.21. Comparison between H/V ratios of observed noise at observation site GLF (blue line: classical method; green line: FTAN based) and synthetic H/V spectral ratios (Black curve). The ellipticity of the fundamental-mode Rayleigh wave (red curve) and the first higher mode (magenta curve) are given.

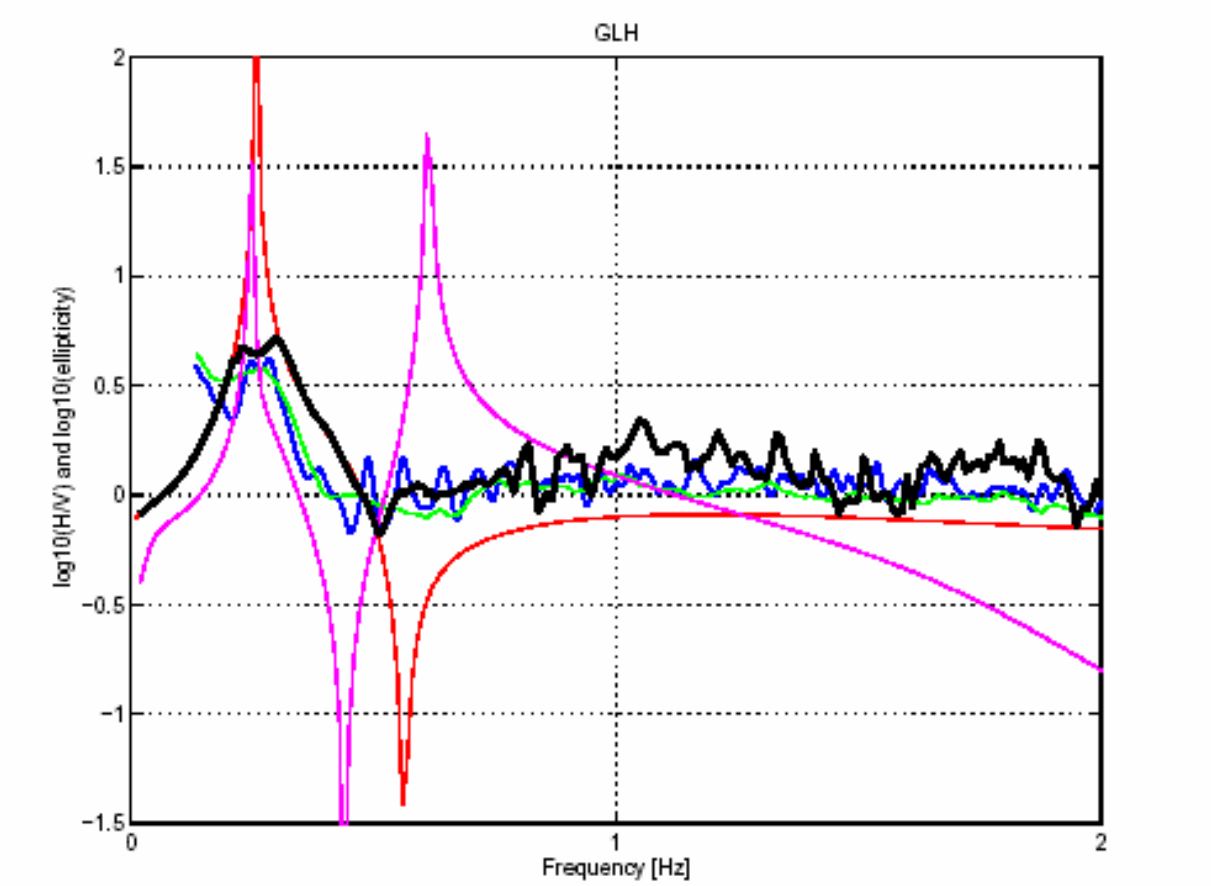

Figure 4.22. Comparison between H/V ratios of observed noise at observation site GLH (blue line: classical method; green line: FTAN based) and synthetic H/V spectral ratios (Black curve). The ellipticity of the fundamental-mode Rayleigh wave (red curve) and the first higher mode (magenta curve) are given.

4.6.2 Comparison between H/V spectral ratios from strong motion recordings and ambient vibrations

Only one example is given here for the recording site FOC in Gölcük (Figure 4.23). The comparison between H/V ratios obtained from ambient vibrations and strong motion recordings show some agreement below 0.8 Hz. The variability in the curves obtained from the strong motion recordings is very high due to the limited number of records. Above 0.8 Hz, the H/V curves differ considerably, which is due to difference in the composition of the wavefields.

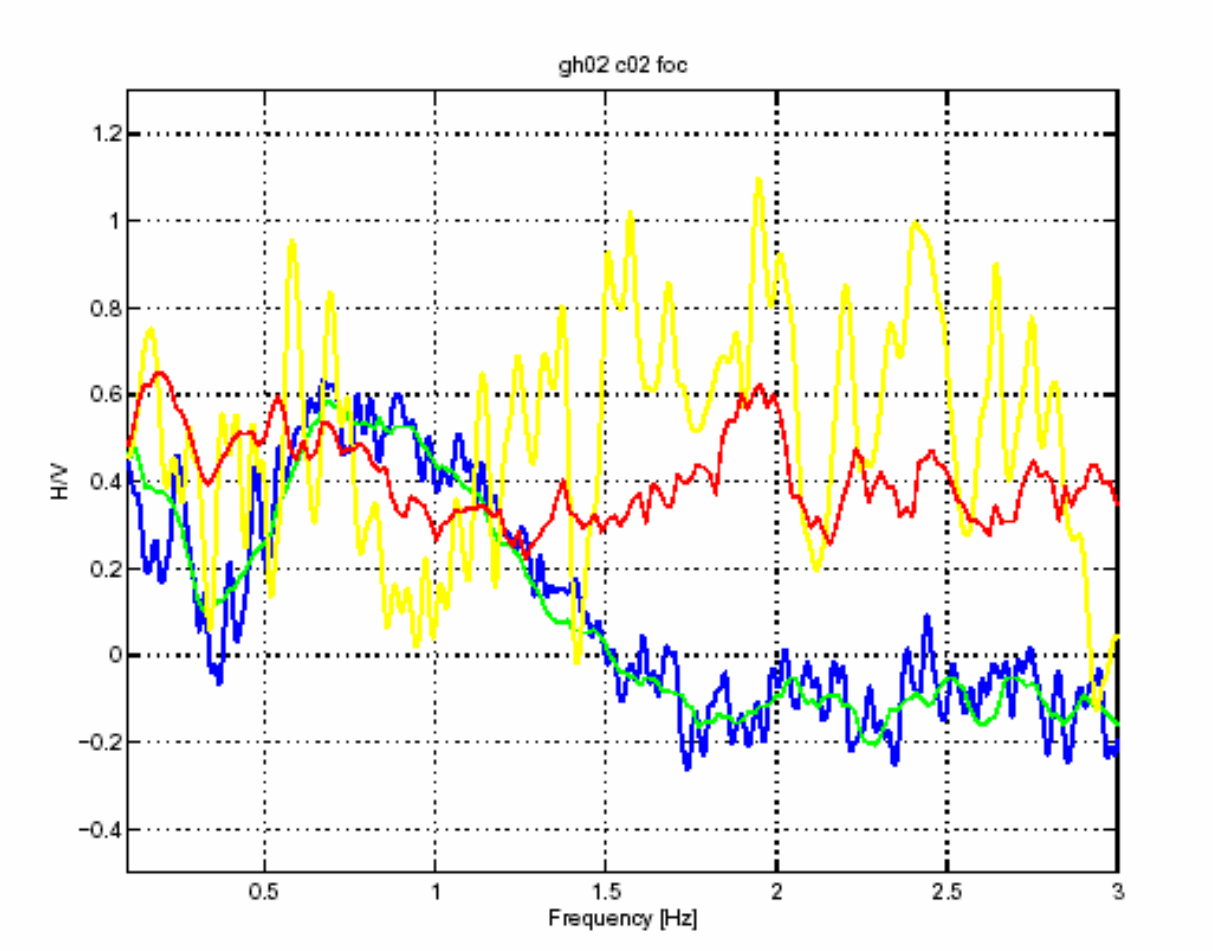

Figure 4.23. Comparison between H/V ratios from ambient vibrations at observation site FOC (blue line: classical method; green line: FTAN based) and H/V ratios from strong motion data (yellow line: classical method, red line: FTAN based) provided by USGS. From the strong motion data six events with peak ground acceleration larger than 15mg were selected for the analysis.

5. GEOTECHNICAL SITE CHARACTERIZATION

Jan Laue, Juliane Buchheister, Sarah M. Springman, Institute of Geotechnical Engineering (IGT) of the Swiss Federal Institute of Technology (ETH)

5.1. INTRODUCTION

The Institute of Geotechnical Engineering (IGT) of the Swiss Federal Institute of Technology (ETH) has been taking part in the Research Task Group. It has conducted the tasks "establishing the local soil conditions" together with "site classification" and "site response analyses". The tasks have been conducted for the pilot study areas in Adapazarı and Gölcük. The following section deals first with the determination of the local soil condition. The following part covers the task site classification.

5.2. LOCAL SOIL CONDITIONS

5.2.1 General Remarks

The aim of the task "Local Site Conditions" is to define hypothetical boreholes, which can be assumed to be located at the centre of the grids. A hypothetical borehole should be an idealized borehole, which will be the most representative for the soil conditions in the specific area of interest. In an ideal project, new site investigations might be conducted, almost in the centre of each of the grids. In the case of the two pilot areas for this microzonation study, it was not possible to carry out many additional boreholes in areas where there were few or even no information given. The reasons will not be discussed here. The location of the project areas can be seen in other parts of the Report on Pilot studies (e.g. Erdik, 2002).

5.2.2 Available Data

For the identification of the local soil conditions, an approach was chosen by taking available existing data into account. Data were available from different sources for the two project areas, with varying degree of information on the site investigations being conducted, reliability and quality of the derived data. This initial situation will be most likely to be the state for every area with existing infrastructure and buildings. Thus this information should be dealt with great care and a plausibility check of the available data is essential prior to carrying out the microzonation procedure. Direct use of this kind of data from such a variety of different sources might lead to an unrealistic scenario, and might not be comparable or even withstand a subsequent confirmation of this approach in terms of the hypothetical boreholes. Nonetheless data from different sources should be taken into account if the quality appears to be acceptable so that it is possible to benefit from an independent view of the soil conditions in overall terms and the reliability of a single site investigation in particular.

Several resources of site investigations were available. Additionally, some site investigations, mainly conducted after the earthquake of 1999, are reported in the literature or are published (e.g. Ansal et al. ed. 2001) or are available on the Internet (e.g. PEER, Figure 5.1). The use of these data in terms of a definition of the representative boreholes, however promising, has not been possible because significant necessary information such as exact coordinates of the location of the site investigations, topographical conditions, depth of groundwater table, information about the site investigation techniques, etc. has not been available. These data have already been interpreted, and only the essence of the results of the original soundings is given in the publications. Thus, they can be used for

comparison and for checking plausibility only but they cannot be used as basic data for the microzonation study.

Mainly two sources of data have been used for the pilot study. The first, and in our view, the most reliable source were data sheets of existing and new boreholes based on drilling work, SPT and CPT data, and some additional laboratory tests summarized by Prof. A. Önalp from Sakarya University. The second source was the GDDA datafiles, which were transformed into a database at the DRM local office by Dr. Köksal. The second source included some of the data available from the first source, but also soundings, which have been used as a base for other publications, and of other origins. The reliability, the density and the quality of the information were, compared with the first source, somewhat variable. Thus the overall quality of this database was difficult to judge and sometimes it would have been easier to conduct new soundings.

The available data from Sakarya University included data sheets of each location (Figure 5.2) giving summarized information of the site investigation conducted including the results of laboratory investigation for some areas. Additionally, the borehole log from the site was available (Figure 5.3), and for some locations, CPT or CPTU data was also included (Figure 5.6).

In total there were 120 sets of data for Adapazarı and 97 sets for Gölcük, which were available from Sakarya University. Additionally 22 (Adapazarı) and 6 (Gölcük) CPT loggings were available, but without further drilling information. Not all of these data sets cover a single 500m * 500m grid point. In some cases, there is more than one borehole available for each grid. Other grids of the original pilot study area were not covered.

306 data sets were available in the database of GDDA in total for Adapazarı, while 66 turned out to be similar sets of boreholes, which already have been received by Sakarya University but with reduced information. 260 sets were included (70 have are reduced versions of the data already been received by Sakarya University) for the Gölcük area. The variation of the information was crucial. For some of the boreholes, a similar amount of data to that given by Sakarya University was available. For other locations, only limited and very simplified information is given. As it is difficult to show the content of the database in this report, Figure 5.2 gives a summary of the data that is included, although originally created by (http://peer.berkeley.edu/turkey/Adapazarı). A simplification of the original site investigation data has already been made before the data was included in the GDDA datafiles. Figure 5.5 shows information in the form it has been stored in the GDDA database.

Initially, 3 different coordinate systems had been used, which complicated any comparisons between the various sets of data. After transferring all coordinates to UTM coordinates, all available boreholes have been plotted for the two areas of the pilot study (Figure 5.6 and 5.7).

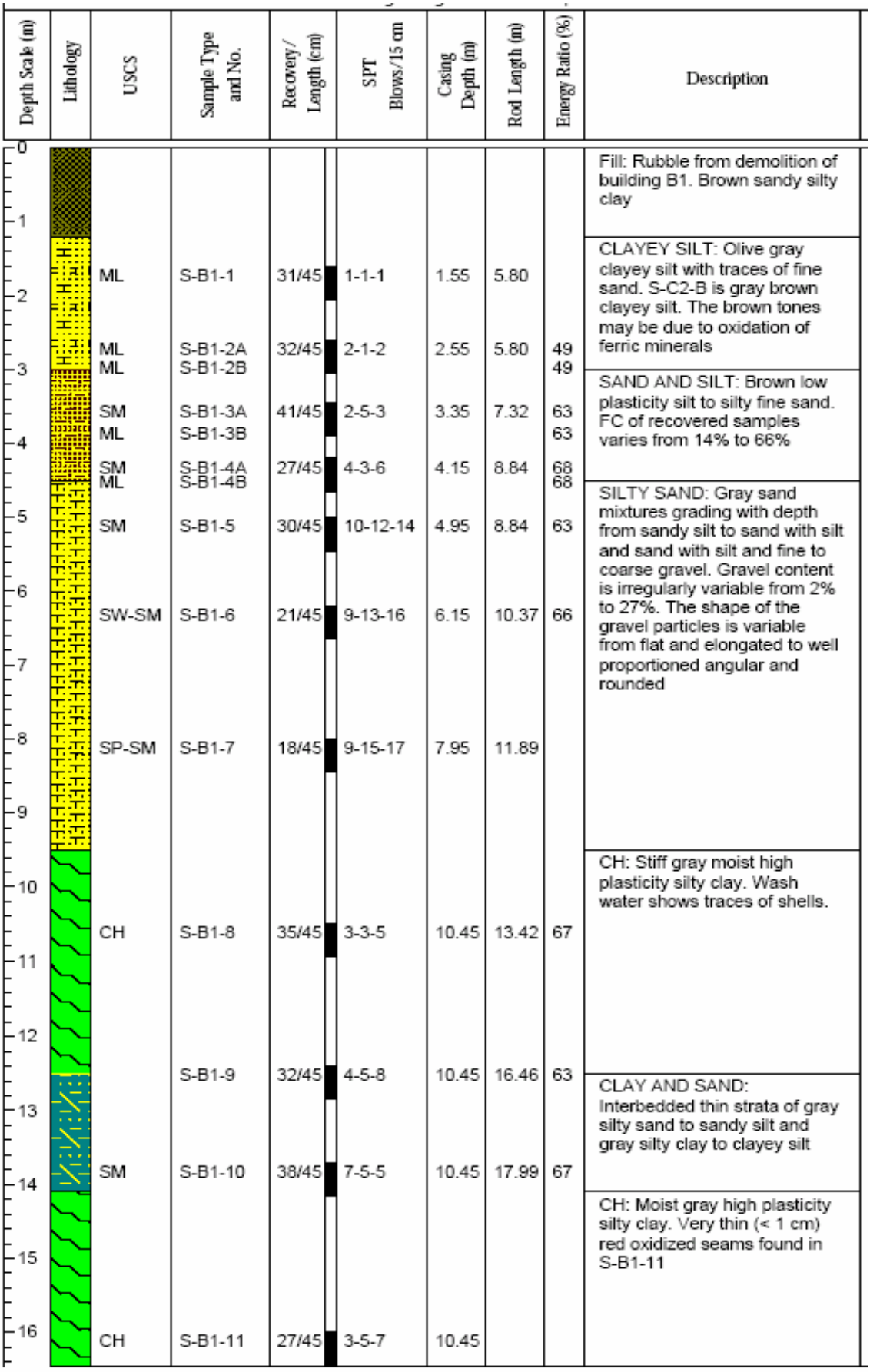

Depth Scale (m)	USCS	Sample Type and No.	Recovery / Length (cm)	SPT Blows/15 cm	Casing Depth (m)	Rod Length (m)	Energy Ratio (%)	Description
0–1								Fill: Rubble from demolition of building B1. Brown sandy silty clay
1–2	ML	S-B1-1	31/45	1-1-1	1.55	5.80		CLAYEY SILT: Olive gray clayey silt with traces of fine sand. S-C2-B is gray brown clayey silt. The brown tones may be due to oxidation of ferric minerals
2–3	ML	S-B1-2A	32/45	2-1-2	2.55	5.80	49	
	ML	S-B1-2B					49	
3–4	SM	S-B1-3A	41/45	2-5-3	3.35	7.32	63	SAND AND SILT: Brown low plasticity silt to silty fine sand. FC of recovered samples varies from 14% to 66%
	ML	S-B1-3B					63	
4–5	SM	S-B1-4A	27/45	4-3-6	4.15	8.84	68	
	ML	S-B1-4B					68	
5–6	SM	S-B1-5	30/45	10-12-14	4.95	8.84	63	SILTY SAND: Gray sand mixtures grading with depth from sandy silt to sand with silt and sand with silt and fine to coarse gravel. Gravel content is irregularly variable from 2% to 27%. The shape of the gravel particles is variable from flat and elongated to well proportioned angular and rounded
6–7	SW-SM	S-B1-6	21/45	9-13-16	6.15	10.37	66	
7–8								
8–9	SP-SM	S-B1-7	18/45	9-15-17	7.95	11.89		
9–10								
10–11	CH	S-B1-8	35/45	3-3-5	10.45	13.42	67	CH: Stiff gray moist high plasticity silty clay. Wash water shows traces of shells.
11–12								
12–13		S-B1-9	32/45	4-5-8	10.45	16.46	63	CLAY AND SAND: Interbedded thin strata of gray silty sand to sandy silt and gray silty clay to clayey silt
13–14	SM	S-B1-10	38/45	7-5-5	10.45	17.99	67	
14–15								CH: Moist gray high plasticity silty clay. Very thin (< 1 cm) red oxidized seams found in S-B1-11
15–16								
16	CH	S-B1-11	27/45	3-5-7	10.45			

Figure 5.1. Summary of a single borehole (http://peer.berkeley.edu/turkey/adapazarı); this borehole has not been used in the further work. Therefore the location is not given.

DRM-World Institute for Disaster Risk Management
206 North Washington Street
Suite 400
Alexandria, VA 22314
USA www.DRMonline.net

PROJECT: MICROZONATION FOR EARTHQUAKE RISK MITIGATION

BORING DATA SHEET **NO** :	City	District	Pafta/Ada/Parsel	Boring No.
105	ADAPAZARI	OZANLAR	118/775/10	SOZ363

				SPT	CPT				SCPTU (m/s)		Seismic Profile(m/s)		natural		atterberg limits (%)			sieve analysis						
depth (m)	description of soil	soil classification	Sample type	N/30 cm	point resistance (MPa)	friction ratio	pore pressure (MPa)	Soil type behaviour index I_c	(V_s)shear wave velocity	(V_p)P wave velocity	(V_s)shear wave velocity	(V_p)P wave velocity	water content (%)	unit weight (t/m^3)	liquid limit w_L	Plastic limit w_P	plasticity index Ip	gravel (%)	sand (%)	fines content (%)	0.002-0.076mm (%)	<0.002mm (%)	D_{50} mm	C_u
0.00					0	2.381	0.001																	
0.50					0.726	4.85	0.026																	
1.00					0.98	1.484	0.028																	
1.50	Low Plasticity Silt	ML	SPT	6	0.544	4.233	0.035						37		32	25	7			85				
2.00					0.526	4.755	0.033																	
2.50					0.798	1.079	0.027																	
3.00	Low Plasticity Clay	CL	SPT	6	0.472	2.248	0.02		112				32		35	23	12			59				
3.50					0.29	6.374	0.014																	
4.00	Low Plasticity Silt	ML	UD		2.558	3.324	0.041		154				33		32	NP	NP			68			0.015	
4.50	Low Plasticity Clay	CL	SPT	11	1.034	2.616	0.188						41		47	24	23			90				
5.00					0.708	2.754	-0.023		127															
5.50					1.161	2.427	-0.009																	
6.00				25	0.544	4.558	0.007		86															
6.50					2.104	1.784	0.027																	
7.00																								
7.50	Low Plasticity Clay	CL	SPT	21									31		35	22	13			79				
8.00																								
8.50																								
9.00				59																				
9.50																								
10.00																								
10.50	Well Graded Sand-Silty Sand	SW-SM	SPT	54									18		NP	NP	NP			7			0.6	
11.00																								
11.50																								
12.00	Uniform Sand	SP	SPT	55									18		NP	NP	NP			4			0.68	
12.50																								
13.00																								
13.50	Intermediate Plasticity Clay	CI	SPT	33									30		40	24	16			94				
14.00																								
14.50																								
15.00				35																				
15.50																								

Figure 5.2. Data Sheet for the grid Q10 in Adapazarı

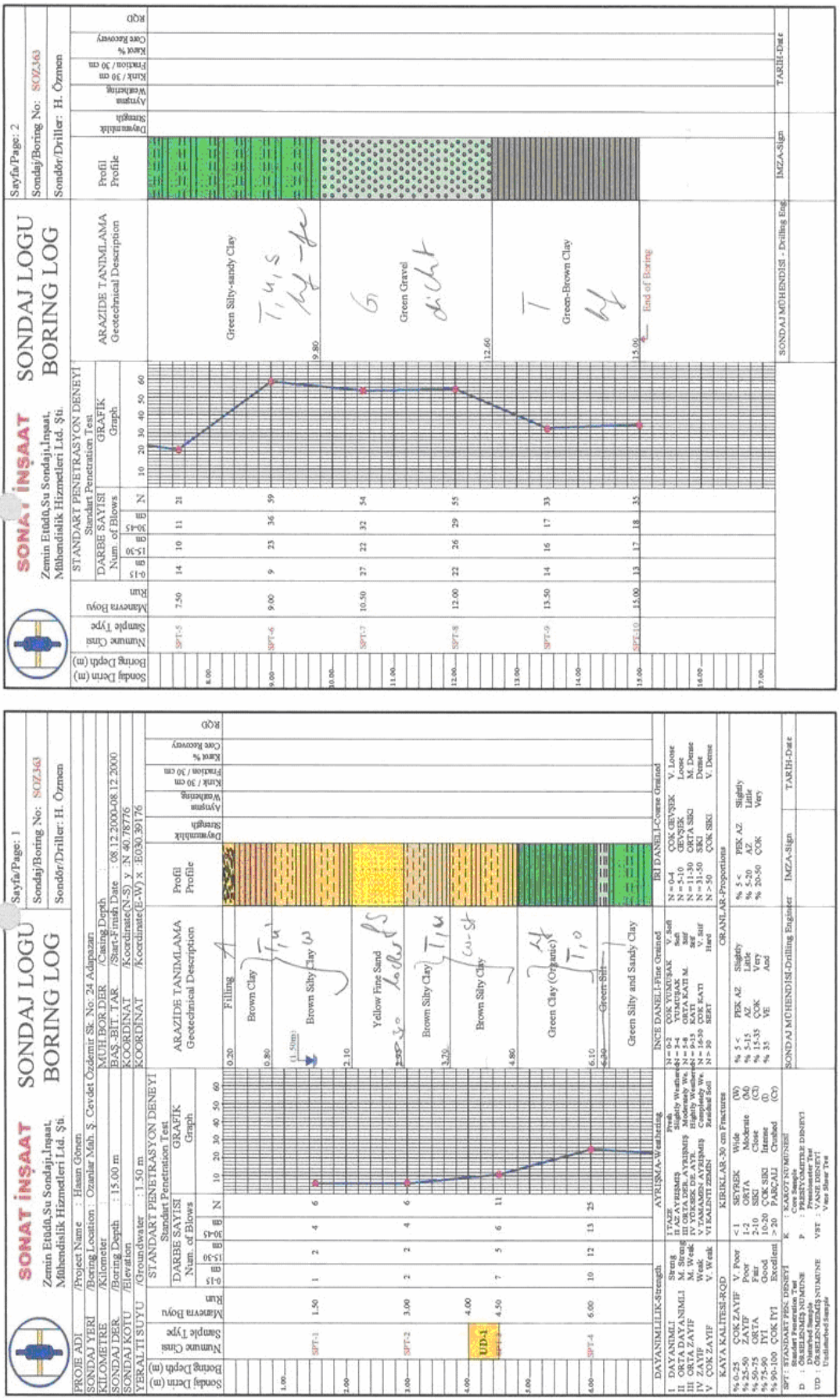

Figure 5.3. Borehole log for the grid Q10 in Adapazarı

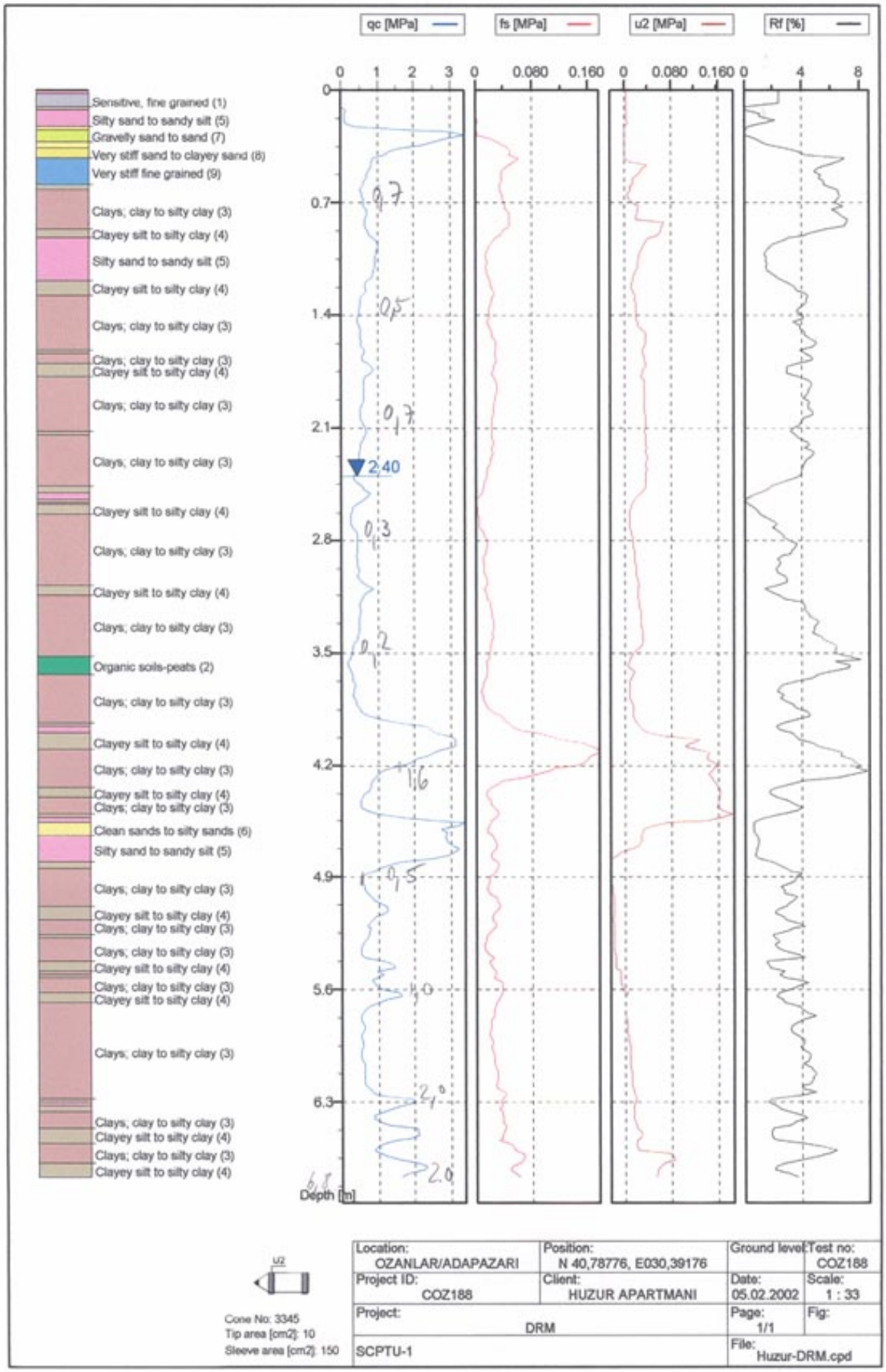

Figure 5.4. CPTU data for grid Q10 Adapazarı

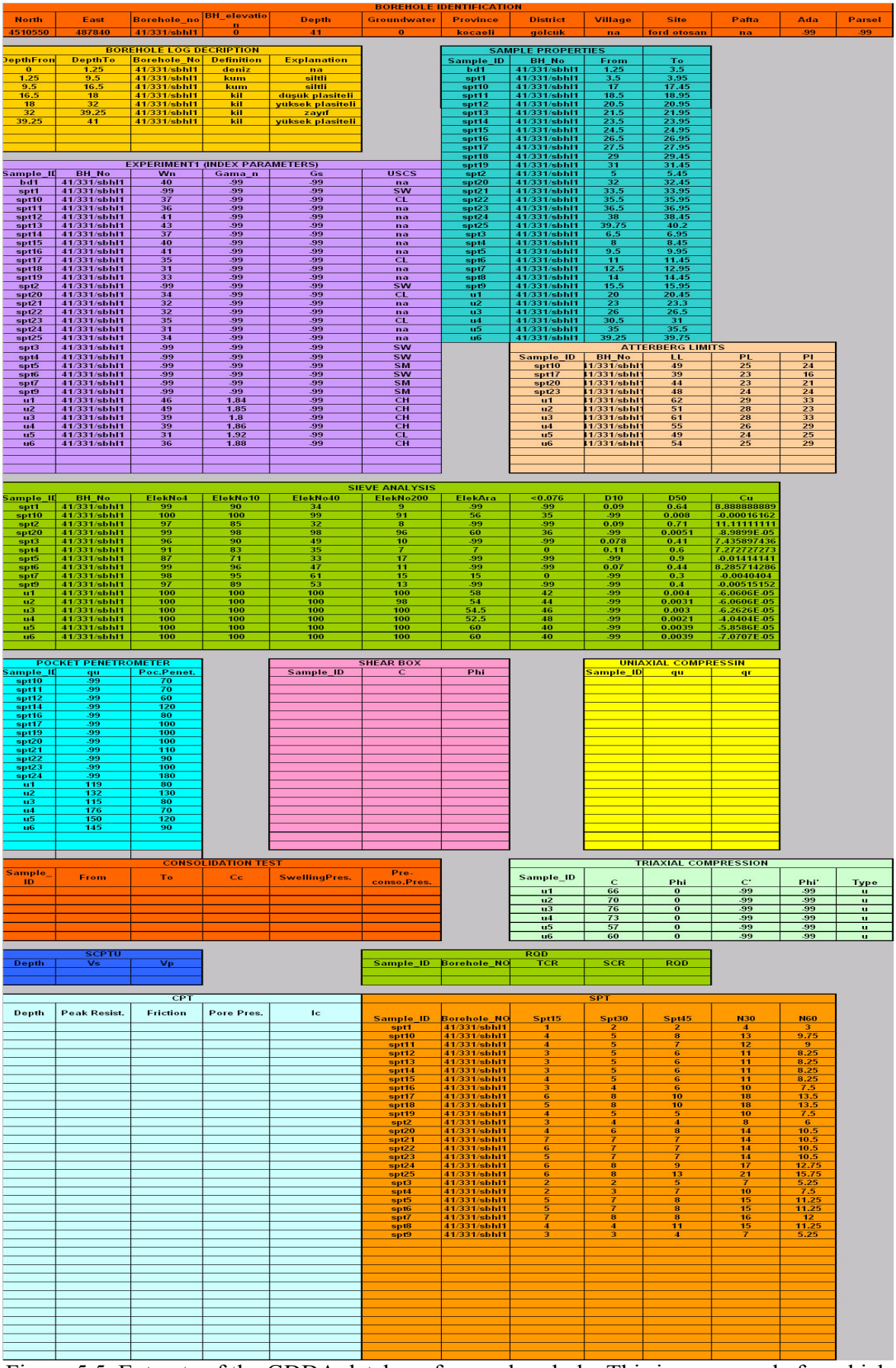

BOREHOLE IDENTIFICATION

North	East	Borehole_no	BH_elevation	Depth	Groundwater	Province	District	Village	Site	Pafta	Ada	Parsel
4510550	487840	41/331/sbh1	0	41	0	kocaeli	gölcuk	na	ford otosan	na	99	99

BOREHOLE LOG DECRIPTION

DepthFron	DepthTo	Borehole_No	Definition	Explanation
0	1.25	41/331/sbh1	deniz	na
1.25	9.5	41/331/sbh1	kum	silttli
9.5	16.5	41/331/sbh1	kum	silttli
16.5	18	41/331/sbh1	kil	düşük plasiteli
18	32	41/331/sbh1	kil	yüksek plasiteli
32	39.25	41/331/sbh1	kil	zayıf
39.25	41	41/331/sbh1	kil	yüksek plasiteli

SAMPLE PROPERTIES

Sample_ID	BH_No	From	To
bd1	41/331/sbh1	1.25	3.5
spt1	41/331/sbh1	3.5	3.95
spt10	41/331/sbh1	17	17.45
spt11	41/331/sbh1	18.5	18.95
spt12	41/331/sbh1	20.5	20.95
spt13	41/331/sbh1	21.5	21.95
spt14	41/331/sbh1	23.5	23.95
spt15	41/331/sbh1	24.5	24.95
spt16	41/331/sbh1	26.5	26.95
spt17	41/331/sbh1	27.5	27.95
spt18	41/331/sbh1	29	29.45
spt19	41/331/sbh1	31	31.45
spt2	41/331/sbh1	5	5.45
spt20	41/331/sbh1	32	32.45
spt21	41/331/sbh1	33.5	33.95
spt22	41/331/sbh1	35.5	35.95
spt23	41/331/sbh1	36.5	36.95
spt24	41/331/sbh1	38	38.45
spt25	41/331/sbh1	39.75	40.2
spt3	41/331/sbh1	6.5	6.95
spt4	41/331/sbh1	8	8.45
spt5	41/331/sbh1	9.5	9.95
spt6	41/331/sbh1	11	11.45
spt7	41/331/sbh1	12.5	12.95
spt8	41/331/sbh1	14	14.45
spt9	41/331/sbh1	15.5	15.95
u1	41/331/sbh1	20	20.45
u2	41/331/sbh1	23	23.3
u3	41/331/sbh1	26	26.5
u4	41/331/sbh1	30.5	31
u5	41/331/sbh1	35	35.5
u6	41/331/sbh1	39.25	39.75

EXPERIMENT1 (INDEX PARAMETERS)

Sample_ID	BH_No	Wn	Gama_n	Gs	USCS
bd1	41/331/sbh1	40	-99	-99	na
spt1	41/331/sbh1	-99	-99	-99	SW
spt10	41/331/sbh1	37	-99	-99	CL
spt11	41/331/sbh1	36	-99	-99	na
spt12	41/331/sbh1	41	-99	-99	na
spt13	41/331/sbh1	43	-99	-99	na
spt14	41/331/sbh1	37	-99	-99	na
spt15	41/331/sbh1	40	-99	-99	na
spt16	41/331/sbh1	41	-99	-99	na
spt17	41/331/sbh1	35	-99	-99	CL
spt18	41/331/sbh1	31	-99	-99	na
spt19	41/331/sbh1	33	-99	-99	na
spt2	41/331/sbh1	-99	-99	-99	SW
spt20	41/331/sbh1	34	-99	-99	CL
spt21	41/331/sbh1	32	-99	-99	na
spt22	41/331/sbh1	32	-99	-99	na
spt23	41/331/sbh1	35	-99	-99	CL
spt24	41/331/sbh1	31	-99	-99	na
spt25	41/331/sbh1	34	-99	-99	na
spt3	41/331/sbh1	-99	-99	-99	SW
spt4	41/331/sbh1	-99	-99	-99	SW
spt5	41/331/sbh1	-99	-99	-99	SM
spt6	41/331/sbh1	-99	-99	-99	SW
spt7	41/331/sbh1	-99	-99	-99	SM
spt9	41/331/sbh1	-99	-99	-99	SM
u1	41/331/sbh1	46	1.84	-99	CH
u2	41/331/sbh1	49	1.85	-99	CH
u3	41/331/sbh1	39	1.8	-99	CH
u4	41/331/sbh1	39	1.86	-99	CH
u5	41/331/sbh1	31	1.92	-99	CL
u6	41/331/sbh1	36	1.88	-99	CH

ATTERBERG LIMITS

Sample_ID	BH_No	LL	PL	PI
spt10	41/331/sbh1	49	25	24
spt17	41/331/sbh1	39	23	16
spt20	41/331/sbh1	44	23	21
spt23	41/331/sbh1	48	24	24
u1	41/331/sbh1	62	29	33
u2	41/331/sbh1	51	28	23
u3	41/331/sbh1	61	28	33
u4	41/331/sbh1	55	26	29
u5	41/331/sbh1	49	24	25
u6	41/331/sbh1	54	25	29

SIEVE ANALYSIS

Sample_ID	BH_No	ElekNo4	ElekNo10	ElekNo40	ElekNo200	ElekAra	<0.076	D10	D50	Cu
spt1	41/331/sbh1	99	90	34	9	-99	-99	0.09	0.64	8.888888889
spt10	41/331/sbh1	100	100	99	91	56	35	-99	0.008	-0.000161616
spt2	41/331/sbh1	97	85	32	8	-99	-99	0.09	0.71	11.11111111
spt20	41/331/sbh1	99	98	98	96	60	36	-99	0.0051	-8.9899E-05
spt3	41/331/sbh1	96	90	49	10	-99	-99	0.078	0.41	7.435897436
spt4	41/331/sbh1	91	83	35	7	7	0	0.11	0.6	7.272727273
spt5	41/331/sbh1	87	71	33	17	-99	-99	-99	0.9	0.01414141
spt6	41/331/sbh1	99	96	47	11	-99	-99	0.07	0.44	8.285714286
spt7	41/331/sbh1	98	95	61	15	15	0	-99	0.3	-0.0040404
spt9	41/331/sbh1	97	89	53	13	-99	-99	-99	0.4	-0.00515152
u1	41/331/sbh1	100	100	100	100	58	42	-99	0.004	-6.0606E-05
u2	41/331/sbh1	100	100	100	98	54	44	-99	0.0031	-6.0606E-05
u3	41/331/sbh1	100	100	100	100	54.5	46	-99	0.003	-6.2626E-05
u4	41/331/sbh1	100	100	100	100	52.5	48	-99	0.0021	-4.0404E-05
u5	41/331/sbh1	100	100	100	100	60	40	-99	0.0039	-5.8586E-05
u6	41/331/sbh1	100	100	100	100	60	40	-99	0.0039	-7.0707E-05

POCKET PENETROMETER

Sample_ID	qu	Poc.Penet.
spt10	-99	70
spt11	-99	70
spt12	-99	60
spt14	-99	120
spt16	-99	80
spt17	-99	100
spt19	-99	100
spt20	-99	100
spt21	-99	110
spt22	-99	90
spt23	-99	100
spt24	-99	180
u1	119	80
u2	132	130
u3	115	80
u4	176	70
u5	150	120
u6	145	90

SHEAR BOX

Sample_ID	C	Phi

UNIAXIAL COMPRESSIN

Sample_ID	qu	qr

CONSOLIDATION TEST

Sample_ID	From	To	Cc	SwellingPres.	Pre-conso.Pres.

TRIAXIAL COMPRESSION

Sample_ID	C	Phi	C'	Phi'	Type
u1	66	0	-99	-99	u
u2	70	0	-99	-99	u
u3	76	0	-99	-99	u
u4	73	0	-99	-99	u
u5	57	0	-99	-99	u
u6	60	0	-99	-99	u

SCPTU

Depth	Vs	Vp

RQD

Sample_ID	Borehole_NO	TCR	SCR	RQD

CPT

Depth	Peak Resist.	Friction	Pore Pres.	Ic

SPT

Sample_ID	Borehole_NO	Spt15	Spt30	Spt45	N30	N60
spt1	41/331/sbh1	1	2	2	4	3
spt10	41/331/sbh1	4	5	8	13	9.75
spt11	41/331/sbh1	4	5	7	12	9
spt12	41/331/sbh1	3	5	6	11	8.25
spt13	41/331/sbh1	3	5	6	11	8.25
spt14	41/331/sbh1	3	5	6	11	8.25
spt15	41/331/sbh1	4	5	6	11	8.25
spt16	41/331/sbh1	3	4	6	10	7.5
spt17	41/331/sbh1	6	8	10	18	13.5
spt18	41/331/sbh1	5	8	10	18	13.5
spt19	41/331/sbh1	4	5	5	10	7.5
spt2	41/331/sbh1	3	4	4	8	6
spt20	41/331/sbh1	4	6	8	14	10.5
spt21	41/331/sbh1	7	7	7	14	10.5
spt22	41/331/sbh1	6	7	7	14	10.5
spt23	41/331/sbh1	5	7	7	14	10.5
spt24	41/331/sbh1	6	8	9	17	12.75
spt25	41/331/sbh1	6	8	13	21	15.75
spt3	41/331/sbh1	2	2	5	7	5.25
spt4	41/331/sbh1	2	3	7	10	7.5
spt5	41/331/sbh1	5	7	8	15	11.25
spt6	41/331/sbh1	5	7	8	15	11.25
spt7	41/331/sbh1	7	8	8	16	12
spt8	41/331/sbh1	4	4	11	15	11.25
spt9	41/331/sbh1	3	3	4	7	5.25

Figure 5.5. Extracts of the GDDA database for one borehole. This is an example for which more information was available

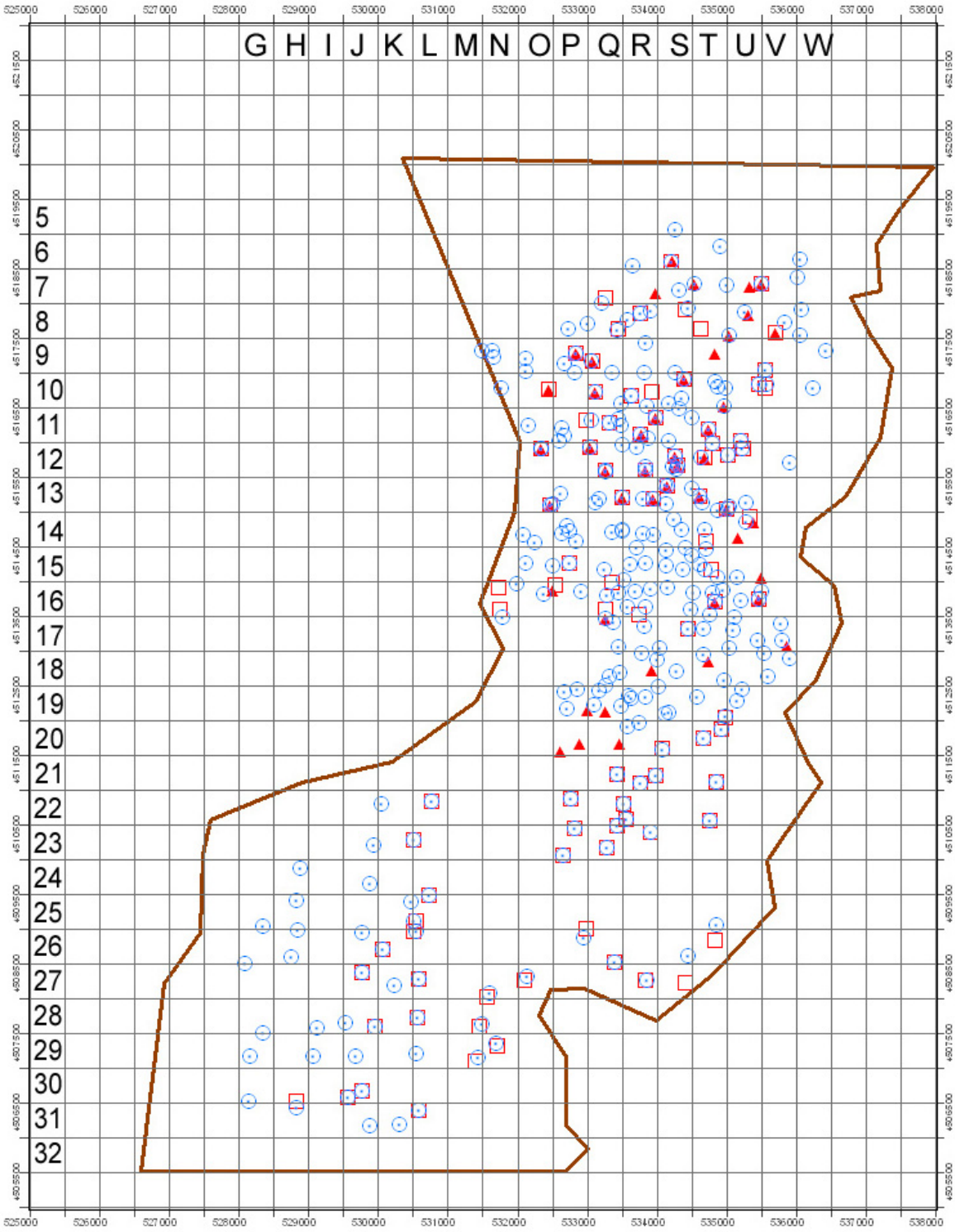

Figure 5.6. Locations of all available boreholes for Adapazarı; Blue points (circles with dots) are data locations from the GDDA database. Red points are all other data from Sakarya University (triangles are CPT data and squares are borehole data).

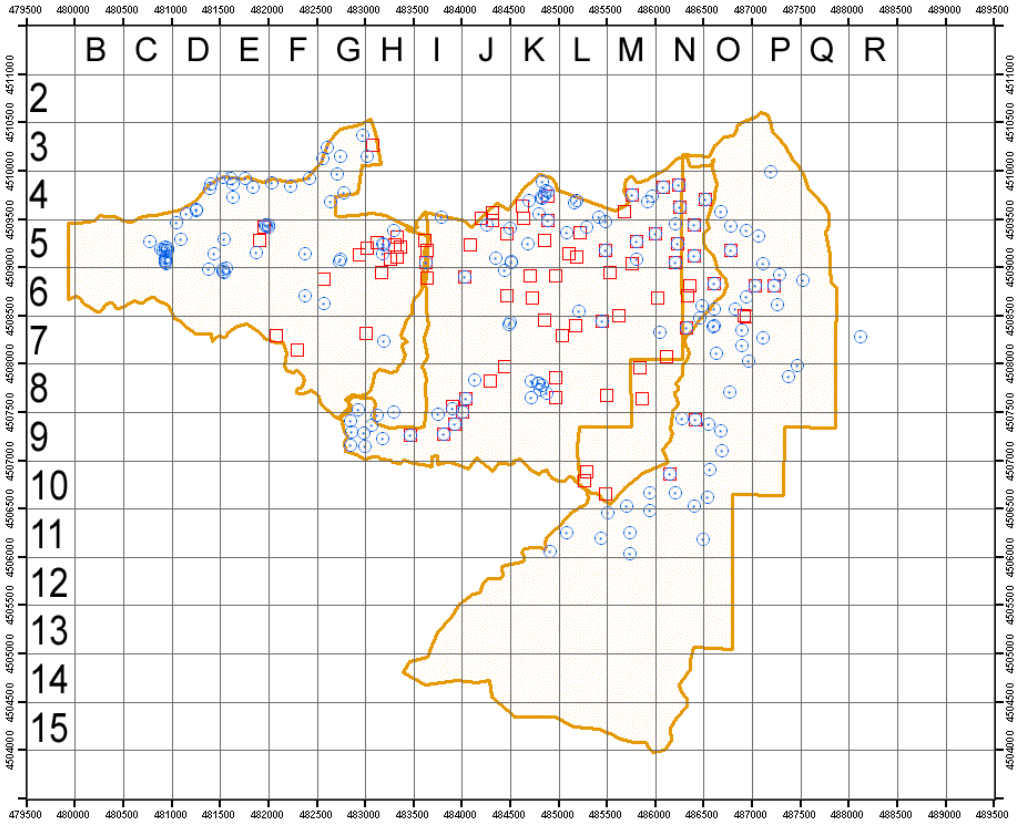

Figure 5.7. Locations of all available boreholes for Gölcük; Blue points (circles with dots) indicate location of sounding from the GDDA data base. Red points show locations of the data received from Sakarya University (squares are borehole data).

5.2.3 Data consistency and choice of representative boreholes

All of the available data about the borehole information available for each location has been checked first for consistency. Secondly data from each grid has been compared. Thirdly, a representative borehole has been chosen.

The following bullet points will give an overview of the problems faced with this procedure:

- Case of "double data". Difficulties occur when a data sheet and original data was available from one borehole, simplifications have already been made and assumption included, which cannot be followed by a third party. Therefore data from this borehole was usually classified as doubtful and a remark has been made in case it has been included for further use.
- Unique numbering system. No unique numbering e.g. Adapazarı Grid Q10, borehole SOZ363 = 54_sau_soz363 in the GDDA database and CPT COZ188 all have the same coordinates, which has not been documented in the available database from the beginning.
- Contradictory information. On some data sheets, a soil was identified as solid (meaning very stiff or hard) but the Atterberg limit test showed a liquid limit that was less than the natural water content. This would indicate that the consistency would be

liquid (e.g. Adapazarı Grid R12). Usually the interpreted consistency of the SPT values was trusted more than a single test result.

- Soil description. The soil description in the borehole logs varies according to the borehole company. For some data sets, borehole data are simplified to one single layer without any other components e.g. Adapazarı Grid K23: "hard clay". There were additional contradictions with the results of laboratory tests if they were available (Results of tests giving soil mechanical parameter are rare. Sieve analysis results (or at least amount of fines) were more often available for proof checking).
- Often, especially in Adapazarı, the available information showed no predominant component of soil type. These were then identified as a mixture of two soil types e.g. Adapazarı Grid P9: "silt – clay".
- Difference in details. Borehole information can consist of very thin layers e.g. Adapazarı Grid V19 (layers every 20 cm, 14 layers for 15 m). Sometimes the borehole information has already been summarized to give the main predominant layers e.g. Adapazarı Grid R23 (3 layers for 15 m).
- Nomenclature. There was no consistent description of soils and soil classes according to the e.g. ASCE classification. In some cases, assumptions were necessary for a unified description. Some information on classification has been only available in Turkish. These have been translated as far as possible. Some definition for soil descriptions were still not consistent, so the following interpretation was assumed:

  little = slightly

  block = cobbles
- In some cases the description of the consistency is missing. The description of the density of coarse soils is usually missing too. As an example Adapazarı Grid U20: "little brown silty CLAY, light brown clayey GRAVEL". Usually a correlation with the SPT values was made for interpretation of this borehole information.
- Comparability of soundings and borehole log description. SPT values – firmness/ strength of soil as well as consistency were often not consistent. Thus the following SPT N 30 interpretation was assumed for further use:

  Fine grained soils

  Interpretation of SPT N30 values

  N 30 values - interpretation

0-2	very soft
2-8	soft
8-15	stiff
15-30	semi-solid
>30	semi-solid to solid

  Coarse-grained soils

Density – SPT N30 value diagrams have been adopted according to the German industry standard DIN 4094. An example is given in Figure 5.8 (http://www.grundbau.tu-berlin.de/download/skripte/gb1/kap02.pdf).

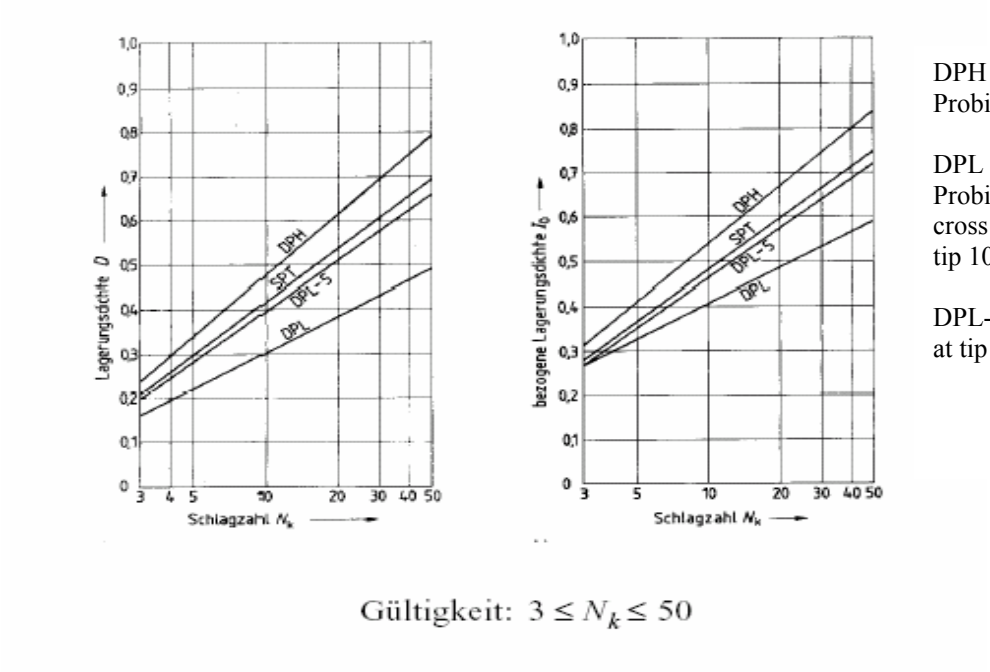

DPH (Dynamic Probing Heavy)

DPL (Dynamic Probing Light)- cross section at the tip 10 cm^2

DPL-S cross section at tip 5 cm^2

Figure 5.8: Relationship between number of blows from different energy rated penetration tests (while the curve of DPH, DPL and DPL-S are of no account for the current scenario) and density (left) or relative density (right) for narrowly graded sands (DIN 4094). The curve SPT has been used for this study. Note that the chart is only valid for N_k between 3 and 50.

The following decisions have been made in terms of the definition of the representative boreholes:

- The data from borehole logs have been preferred before those available from the data sheet.
- Summarized versions of the borehole log were preferred.
- Unique soil description was preferred e.g. “silty clay” instead of “silt-clay”
- Locations where only CPT data were available were rarely used (only at locations where other information of the soil strata was available).
- Little gravelly sandy clay was usually interpreted as little gravelly and sandy clay and not as little gravelly and little sandy clay e.g. Gölcük Grid I6.

In addition to the influencing factors mentioned above for choice and establishment of the representative boreholes, the topographical conditions (elevation) as well as information on the groundwater situation was needed. For most of the boreholes in Adapazarı, and for some of the boreholes in the Gölcük area, the elevation of the site of the soil investigation was not given. It had to be derived by a more complicated and time-consuming approach using rarely available topographical maps. Information on the groundwater situation was only available for approximately half of the data locations. In addition, seasonal changes could not be taken into account as in most cases (at least for the GDDA database), no time and date of the site investigation was given. The groundwater maps given by the GDDA data base are not included here, since they were submitted late and were only available towards the end of the project, and are also misleading as all

available information on the groundwater condition was included independent of the time of the derivation, and are only given in layers of 2.5m thickness.

Taking into account the challenges mentioned above, representative boreholes have been chosen for each grid close to the available existing data. Layer simplification and choice of the representative borehole has been carried out based on engineering judgment. It should not be forgotten that these representative boreholes have been chosen for the microzonation study and not for any other purpose (e.g. replacing site investigation for new buildings).

It has been decided to transmit all representative data in graphical format, which can be transferred into the database. The graphical format allows an easy overview of the data to be used in the next steps of the microzonation project. In addition, a graphical sheet forces further users to be confronted with comments on reliability and the details of the background of data. Also, further users of the hypothetical boreholes are directed to the original borehole numbers and the respective database (GDDA data starts usually with a two digit number, data from Sakarya with a three letter code).

Figure 5.9 shows the representative borehole for the grid Q10, of which the different data sets were already given in the earlier figures. Figure 5.10 – 5.13 show different situations for grid locations in Gölcük.

The soil notation as well as description of the consistency or the density is given in German due to limitations of the program. A translation of all German terms used into English is available at the bottom of each data sheet. A further text block indicates necessary information, which is crucial to be included for each borehole. This information includes the grid number, location of the original borehole chosen to be the representative one, the complete range of boreholes and their distribution within specific grid, and information on the groundwater level. When necessary, comments on reliability of this information are added. The last block indicates the plausibility of the data. It is marked red if there are restrictions in plausibility as well as if there is only one borehole in a grid, which could not be cross – checked with other data.

Figure 5.10 and 5.11 show an example where good correlation could be found among the existing boreholes. Figure 5.12 and 5.13 shows the opposite. Here, three different boreholes could be established within one grid. A river valley could be identified crossing the grid. The slopes on both sides show different topsoil layers. In such cases, the representative borehole has been chosen by means of topographic maps as well as the distribution of soils in the neighboring grids. The main influence is the majority of area represented by the chosen hole in the grid. More than half of the grid is located on the eastern slope for J6 in Gölcük (shown in the Figures 5.12 and 5.13),. The other possibilities are indicated in the text marked in red together with the chosen representative borehole.

Using existing data offers a good opportunity to start a microzonation project without spending too much money on additional data derivation. Nevertheless, this has to be done with great care and knowledge of the local soil conditions. Thus some of the decisions taken by IGT for the two project areas, in terms of the choice of the hypothetical boreholes and their interpretation, might be questionable for local geotechnical engineers, but will be exact enough to fit the purpose of the microzonation study for the project areas and to give examples for future users.

Institut für Geotechnik	Projekt:	DRM
ETH Hönggerberg	Gebiet:	Adapazari area - city
CH-8093 Zürich	Koordinaten:	532108 / 4517006
SCHWEIZ	Maßstab:	1: 100

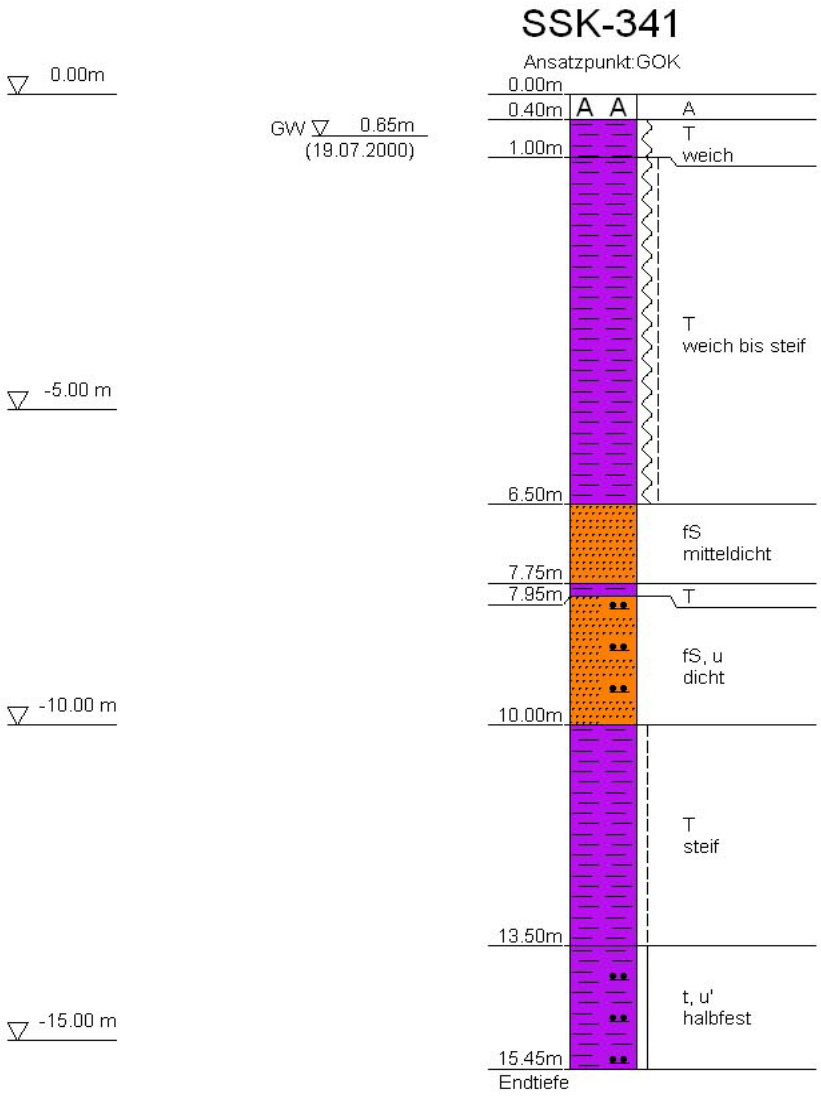

Grid:	O 10
Coordinates:	x=532.000-532.499, y=4.517.000-4.517.499
Borehole points (BH):	SSK-341 (=54_sau_ssk341), 54_230_sk30
Elevation of BHs:	n.a.
comments to the BHs:	
Groundwater:	ca. 0.6 - 0.7 m below surface
Data plausibility:	characteristic boring log: up to a depth of 15.5 m clay underneath a thin layer of fill, including a ca. 3 - 4 m thick sand layer in between.

Layers:	Mu=Top soil, A=Fill, U=Silt, S=Sand, G=Gravel, X=Cobbles
Density:	locker=loose, mitteldicht=medium dense, dicht=dense, sehr dicht=very dense or hard
Consistency:	breiig=viscous,weich=soft, steif=stiff,halbfest=semi-solid or very stiff, fest=solid or very hard

Figure 5.9. Representative borehole for grid Q10 Adapazarı

Grid:	P 4
Coordinates:	x=487.000-487.500, y=4.509.500-4.510.000
Region:	relatively even land
Elevation:	ca. 0 - 8 m
Borehole points (BH):	41/331/bhy01, 41/331/bhy02, 41/331/bhy03, 41/331/bhy04, 41/331/bhy05, 41/331/bh3, 41/331/bh4, 41/331/bh7, 41/331/bh8, 41/331/bh8a, 41/331/bha1, 41/331/bha2, 41/331/bha3, 41/331/sk8, 41/331/sk10, 41/331/sk11, 41/331/sk12, 41/331/sk13, 41/331/sk14, 41/331/sk15, 41/331/sk16, 41/331/sk17, 41/331/sk18, 41/331/sk20, 41/331/sk21, 41/331/sk23,
Region of BHs:	BHs are well distributed in the grid
Elevation of BHs:	0.7 - 7.5 m (above sea level)
Groundwater:	0 - 1.5 m below surface, sometimes ca. 11 m below surface mainly in the west - northwest of the grid (mainly in a sand layer underneath a clay layer)
Data plausibility:	characteristic boring log: interbedded strata of clay and sand, part of sand ca. 60-70% and part of clay ca. 30-40%, thin silt layers in between do appear rarely, silt layers in the interbedded strata show in the south east corner of the grid (e.g. 41/331/bh3, 41/331/bh4, 41/331/sk8)

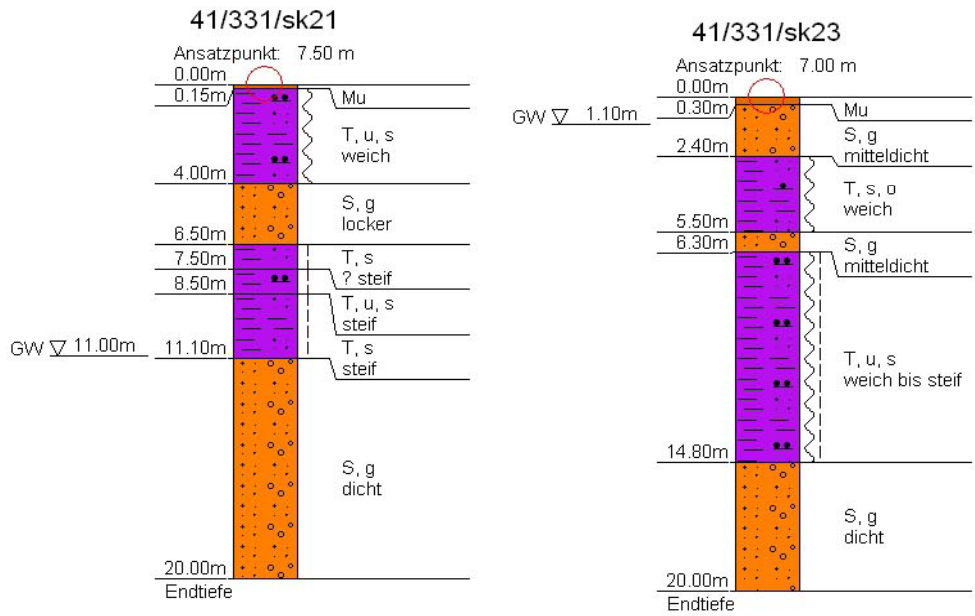

Institut für Geotechnik	Auftraggeber : DRM	Massstab : 1:250/1:5000	Plan-Nr.:
ETH-Hönggerberg	Project : Gölcük area	Datum : 12.11.2002	Grid P4
CH-8093 Zürich	Ihsaniye	Layers: A=Fill, U=Silt, S=Sand, G=Gravel, X=Cobbles	
SCHWEIZ			
Consistency: breiig=viscous, weich=soft, steif=stiff, halbfest=semi-solid or very stiff, fest=solid or very hard			
Density: locker=loose, mitteldicht=medium dense, dicht=dense, sehr dicht=very dense or hard			DC

Figure 5.10. Two different available boreholes for grid P4 Gölcük

Institute for Geotechnical Engineering	Project : MERM DRM
Swiss Federal Institute of Technology Zurich	Area : Gölcük
ETH Hönggerberg	Coordinates : 487090 / 4509930
CH-8093 Zurich SWITZERLAND	Scale : 1: 100

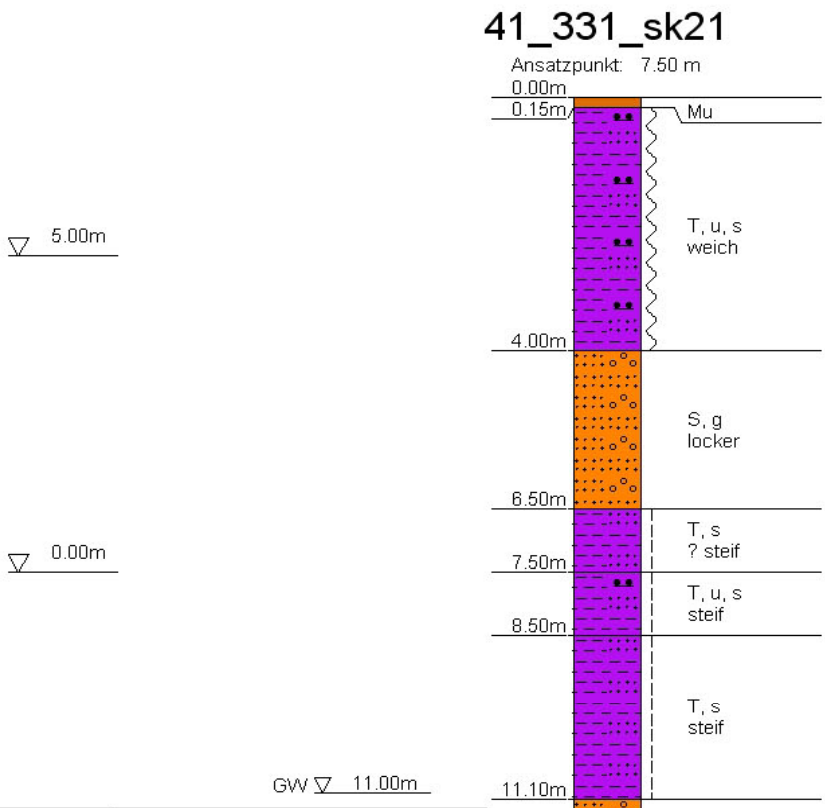

Grid:	P 4
Coordinates:	x=487.000-487.499, y=4.509.500-4.509.999
Region:	relatively even land
Elevation:	ca. 0 - 8 m
Borehole points (BH):	41_331_bhy01, 41_331_bhy02, 41_331_bhy03, 41_331_bhy04, 41_331_bhy05, 41_331_bh3, 41_331_bh4, 41_331_bh7, 41_331_bh8, 41_331_bh8a, 41_331_bha1, 41_331_bha2, 41_331_bha3, 41_331_sk8, 41_331_sk10, 41_331_sk11, 41_331_sk12, 41_331_sk13, 41_331_sk14, 41_331_sk15, 41_331_sk16, 41_331_sk17, 41_331_sk18, 41_331_sk20, 41_331_sk21, 41_331_sk23,
Region of BHs:	BHs are very well distributed in the grid
Elevation of BHs:	0.7 - 7.5 m (above sea level)
Groundwater:	0 - 1.5 m below surface, sometimes ca. 11 m below surface mainly in the west - northwest of the grid (mainly in a sand layer underneath a clay layer)
Data plausibility:	characteristic boring log: interbedded strata of clay and sand, part of sand ca. 60-70% and part of clay ca. 30-40%, thin silt layers in between do appear rarely, silt layers in the interbedded strata show in the south east corner of the grid (e.g. 41_331_bh3, 41_331_bh4, 41_331_sk8)

Layers : **Mu = Top Soil, A = Fill, T = Clay, U = Silt, S = Sand, G = Gravel, X = Cobbles**
Density : **locker = loose, mitteldicht = medium dense, dicht = dense, sehr dicht = very dense**
Consistency : **breiig = viscous, weich = soft, steif = stiff, halbfest = semi-solid, fest = solid**

Figure 5.11. Representative borehole selected for grid P4 Gölcük

Grid:	J 6
Coordinates:	x=484.000-484.500, y=4.508.500-4.509.000
Region:	land, very hilly
Elevation:	ca. 38 -103 m, to the middle and south of the grid is the highest elevation
Borehole points (BH):	AS-19, Sk-21, 41/329/sk19
Region of BHs:	BHs to the left and to the right of the hightest point close to the border of the grid
Elevation of BHs:	38.5 - 56.0 m (above sea level)
Groundwater:	2.5 m below surface (only measured in Sk-21)
Data plausibility:	characteristic boring log: to the east side of the grid (Sk-21) a 16 m clay layer is above a dense gravel layer, to the west side of the grid (AS-10) silt layers a predominant and to the north west (41/329/sk19) a 11m thick layer of gravel and sand covers a hard clay layer.

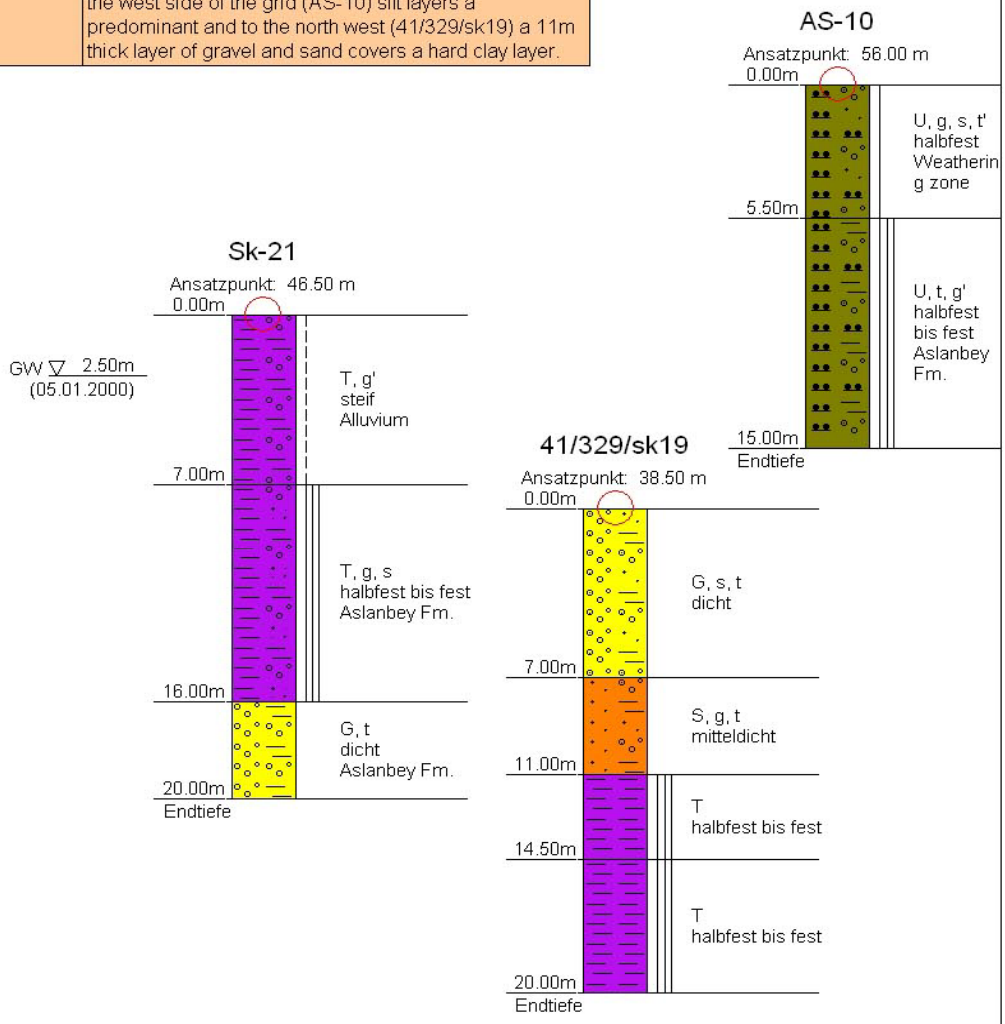

Institut für Geotechnik ETH-Hönggerberg CH-8093 Zürich SCHWEIZ	Auftraggeber : DRM	Massstab : 1:250/1:7500	Plan-Nr.:
	Project : Gölcük area	Datum : 09.11.2002	Grid J6
	Gölcük	Layers: A=Fill, U=Silt, S=Sand, G=Gravel, X=Cobbles	
Consistency: breiig=viscous, weich=soft, steif=stiff, halbfest=semi-solid or very stiff, fest=solid or very hard			
Density: locker=loose, mitteldicht=medium dense, dicht=dense, sehr dicht=very dense or hard			DC

Figure 5.12. Three different boreholes for grid J6 in Gölcük

Institute for Geotechnical Engineering	Project : MERM DRM
Swiss Federal Institute of Technology Zurich	Area : Gölcük
ETH Hönggerberg	Coordinates : 484463 / 4508705
CH-8093 Zurich SWITZERLAND	Scale : 1: 100

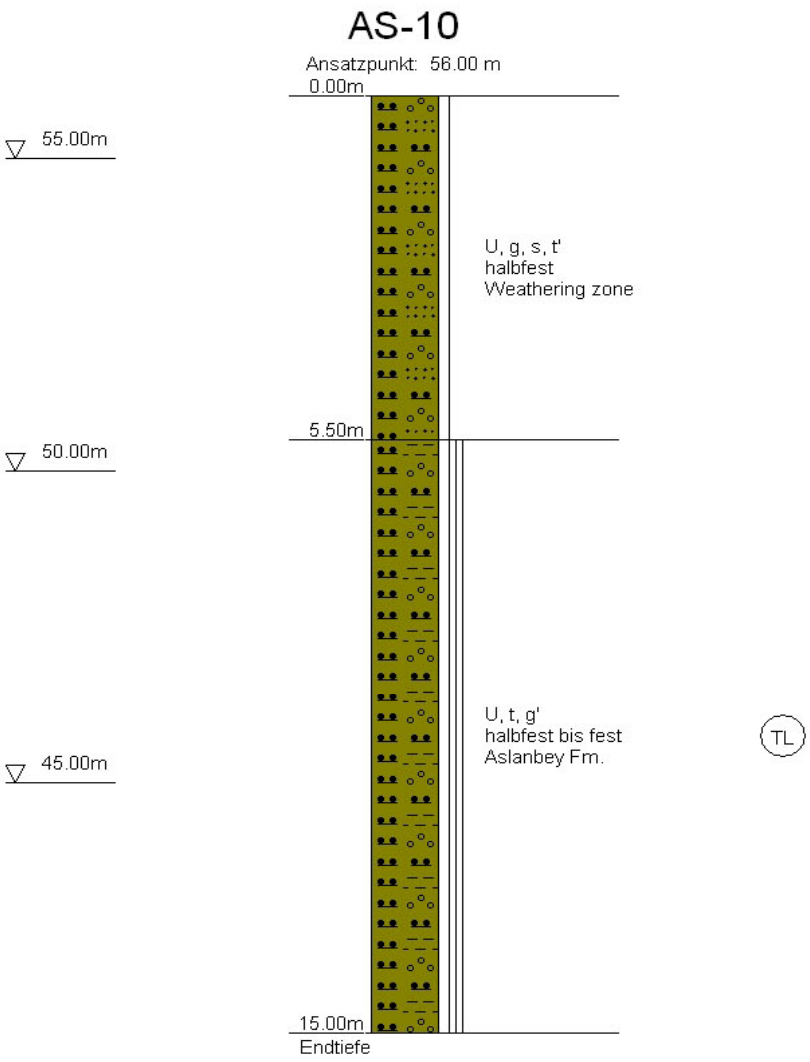

Grid:	J 6
Coordinates:	x=484.000-484.499, y=4.508.500-4.508.999
Region:	land, very hilly
Elevation:	ca. 38 -103 m, to the middle and south of the grid is the highest elevation
Borehole points (BH):	AS-19, Sk-21, 41_329_sk19
Region of BHs:	BHs to the left and to the right of the hightest point close to the border of the grid
Elevation of BHs:	38.5 - 56.0 m (above sea level)
Groundwater:	2.5 m below surface (only measured in Sk-21)
Data plausibility:	characteristic boring log: to the east side of the grid (Sk-21) a 16 m clay layer is above a dense gravel layer, to the west side of the grid (AS-10) silt layers a predominant and to the north west (41_329_sk19) a 11m thick layer of gravel and sand covers a hard clay layer.

Layers	: Mu = Top Soil, A = Fill, T = Clay, U = Silt, S = Sand, G = Gravel, X = Cobbles
Density	: locker = loose, mitteldicht = medium dense, dicht = dense, sehr dicht = very dense
Consistency	: breiig = viscous, weich = soft, steif = stiff, halbfest = semi-solid, fest = solid

Figure 5.13. Representative borehole selected for grid J6 in Gölcük

5.2.4 Interpolation of non-filled grids and hypothetical boreholes

Based on the available data, additional hypothetical boreholes were identified or interpolated as basis for the other tasks. Interpolation of data to fill empty grid points has been carried out very carefully and was omitted for doubtful cases as well as for cases where extrapolation of borehole data would have been needed. For Adapazarı, the grids G28, H28, H29, H30, I25, I26, I27; I28, I31, I32, J26, K24, K25, K26, K30, K31, L25, L31, M28, N29, O27, P21, P25, P27, Q21, R8, R27, S10, S22, S23, T10, U10, U19, V8 and V12 where interpolated. The interpolated areas for Gölcük are shown in 5.14. In addition to the restricted area, of which no data was available, two grids are shown (Grid G7 and M9) where interpolation has not been carried out due to topographical reasons as well as contradictory data from the neighboring grids. The selected representative boreholes, which will be used as hypothetical data for local soil conditions as well as the detailed input data can be found in the Appendix 2.2.

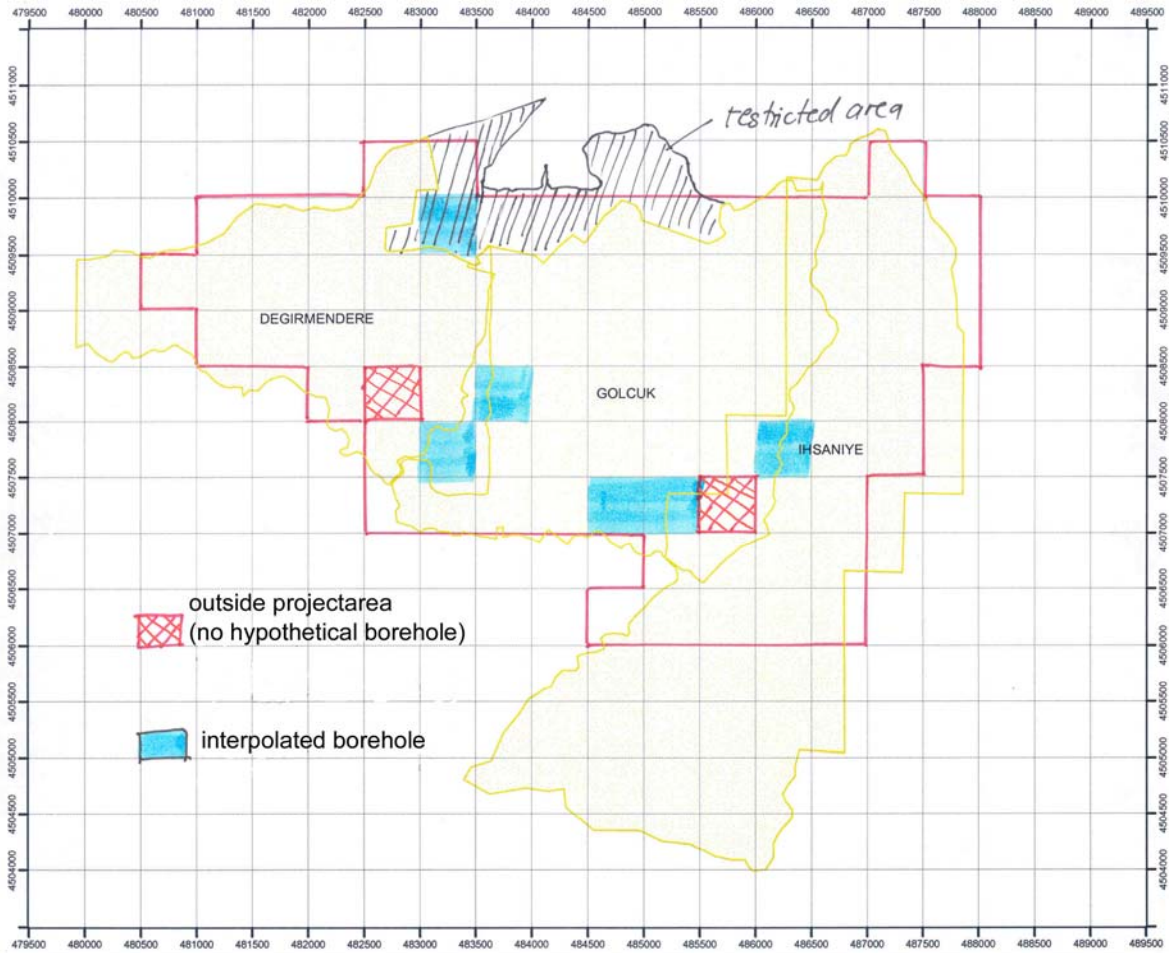

Figure 5.14. Area of interpolated boreholes shown in blue in Gölcük. Note that the crossed areas show areas with no data extrapolation.

5.3. SITE CLASSIFICATION

The task site classification is based on the use of the Turkish Code and the NEHRP approach. The boundary information needed for both procedures are the local soil conditions and, in particular the distribution of shear wave velocities in the topmost 30

meters. To conduct this part in a structured manner, firstly the shear wave distribution in the upper layers has been established. The details of how the site classification was carried out will be introduced in the following sections, if they are not already described in more detail in part D of the manual (Ansal 2003). All results of shear wave velocity distributions as well as the classification, can be found in the Appendix 2.2.

5.3.1 Distribution of shear wave velocity for the topmost 30 meters

Several procedures can be used to establish the shear wave velocity (Vs) distribution with depth. Aside from measurements in the borehole, which were only available very rarely, several empirical correlations between SPT and CPT data and shear wave velocity can be used. Different approaches are given in Chapter D of the Manual of the MERM project, and the different methods have been studied in comparison. This comparison included mainly correlation with CPT results, measured data from Bakır (2002), linear extrapolation of known data, and SPT correlations. As a result, the correlation of the shear wave velocity with the SPT values seemed to offer the best fit and it has been decided to choose one of these methods. The results of this comparison are not shown and nor are they discussed here in detail due to space restrictions. Figure 5.15 gives an example of the differences in the resulting velocities. The Iyisan method (Iyisan 1996) was used for the pilot study. This relationship is valid for all soil types to estimate shear wave velocity from SPT tests:

$$V_s = 51.5\, N^{0.516} \qquad (5.1.)$$

The following procedure was established for the estimation of a shear wave velocity profile for the hypothetical boreholes.

If an SPT profile is available for the hypothetical borehole, then the procedure is as follows:

1. Check if there are borehole measurements for shear wave velocity (Seismic Profile or SCPTU) available

   <u>for Adapazarı:</u>

   If yes, these test results were used. Usually, the test results were available only for the upper layers so that the deeper layers had to be correlated with the SPT values (see 2.). It has to be noted, that the measured shear wave velocities are smaller than the shear wave velocities determined from the Iyisan method.

   <u>for Gölcük:</u>

   There are no measured shear wave velocities available for the Gölcük area.

2. Check if an SPT profile is available for the whole depth of the borehole.

   The SPT profile has been transferred via the Iyisan method to a shear wave velocity profile. As further procedure requires constant shear wave velocity for layer of predefined thickness, a medium value has been chosen for each layer. Idealizations and assumption have to be made for certain situations.

   2.1. If the SPT profile is not available for the last layer, it was linearly extrapolated for this last layer up to a depth of 30 meters below surface. In most cases, this extrapolation was constant for fine-grained soils. A slightly increasing shear wave velocity distribution was chosen for coarse-grained material. The soil type of the unknown layer was adopted from the last known layer of the borehole profile.

2.2. If the SPT profile is not available for the top layer (i.e. fill or topsoil layer), an assumption of the shear wave velocity of 100 m/s was made.

2.3. If no SPT results were available only in one intermediate layer, a correlation with the existing measurement data seemed appropriate (comp. 3).

Some additional remarks on the available data from the different data sources are given here:

- The SPT value R was found to be an N_{70} value rather than an N_{30} value. This was concluded from the graphical presentation of the SPT values from the data sheets of the borehole company in data sheets from Sakarya University.
- SPT values were extrapolated for 30 cm penetration depth when 50 hits or more were obtained for less than 30 cm penetration. The maximum extrapolated SPT value of $N_{30} = 157$ was equal to a shear wave velocity of 700 m/s and this was determined for each case.
- If the SPT value presented in the GDDA database equals 198 it means that no SPT tests were carried out. The value is just a big number since one is needed for the database.

3. No SPT profile exists for the upper 30 m:

<u>for Adapazarı:</u>

If there are no SPT test results available, which is always the case for interpolated boreholes, a correlation between the soil type and the existing v_s measurements with depth was used. This correlation works well for the soil types clay, silt and sand. No measurements have been available for gravel so that an assumption has to be made.

<u>for Gölcük:</u>

Shear wave velocities were interpolated between neighboring boreholes if these had been interpolated. No interpolation has been incorporated for the groundwater table.

4. SPT profile exists up to the surface of bedrock in the upper 30 m

The shear wave distribution has to be determined for the topmost 30 meters or up to bedrock or competent layer. The value of the shear wave velocity for the competent layer was chosen to be v_s = 700 m/s. Therefore shear wave velocities were interpolated to define the depth of the competent layer. This layer is then shown as weathered bedrock = Gravel-Cobbles.

The shear wave velocity reached a value of 700 m/s in the upper 30 m through the linear interpolation process only in few of the boreholes (e.g. Adapazarı Grid G 28, Q18).

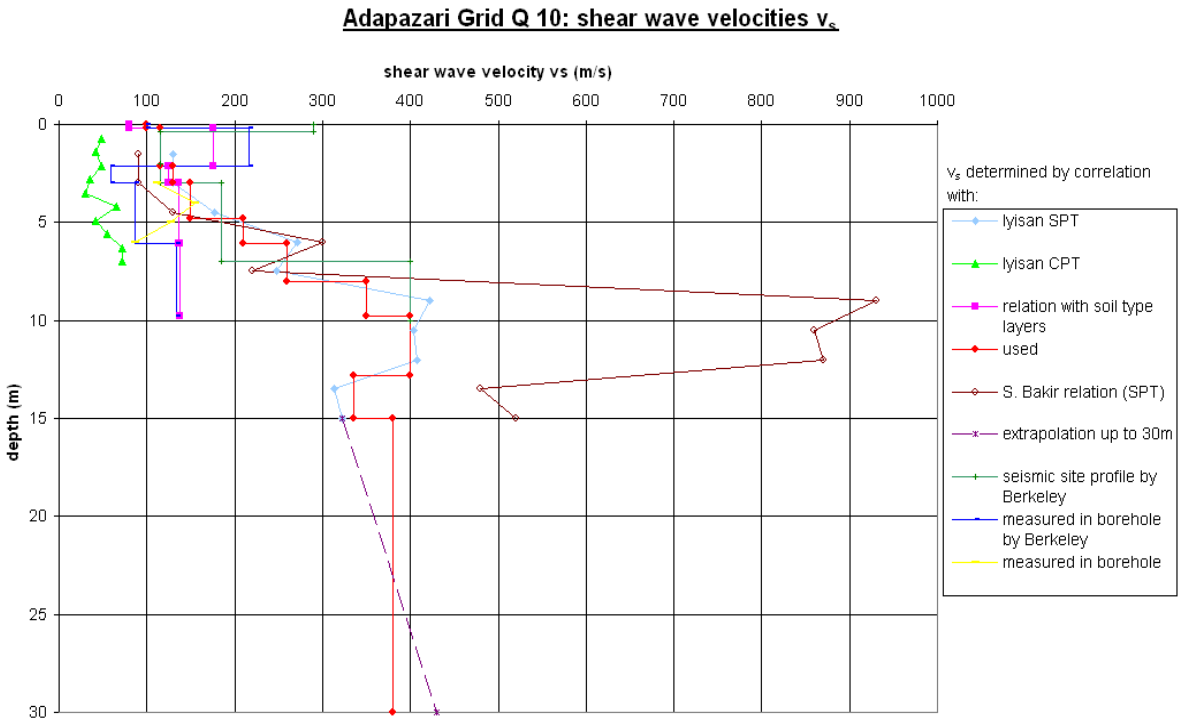

Figure 5.15. Comparison of different methods adopted to derive the shear wave velocity for the grid Q10 in Adapazarı

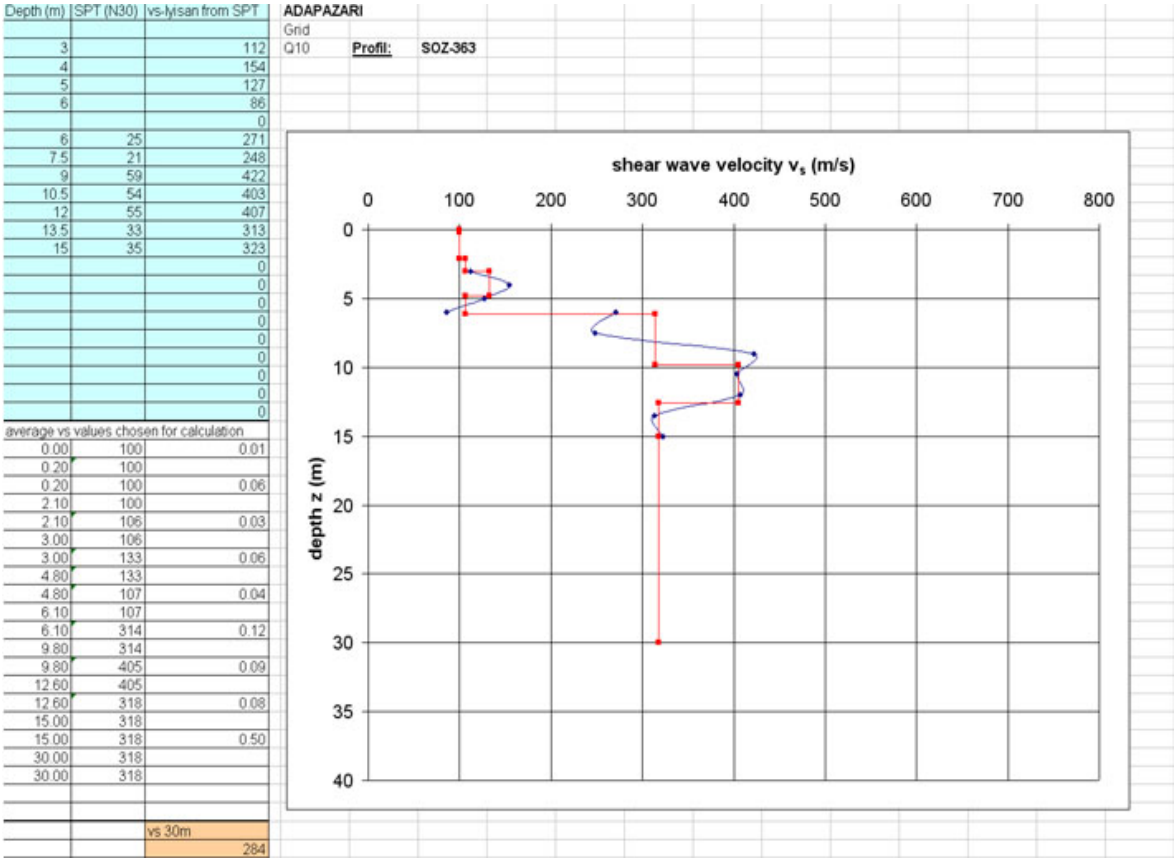

Figure 5.16. Derived and idealized shear wave distribution for grid Q10. The derivation procedure can be seen in a table format on the left of the figure. All shear wave velocity determination are summarized in single Excel sheets and can be found in the Appendix 2.2

5.4. PROCEDURE FOR THE CLASSIFICATION OF HYPOTHETICAL BOREHOLES ACCORDING TO THE TURKISH CODE

Site classification according to the Turkish Code is given in detail in the state of the art report (Ansal 2003) as well as being fully documented in the code. A two-step procedure for site classification is established. Figure 5.17 shows the table summarizing the classification. A description of their use can be found in the Turkish Code.

The Turkish Code subdivides the classification in two areas. Initially the soil group A-D has to be determined so that a local site class can be derived. It is clear from Table 12.1 (Figure 5.17) that there are 4 different possibilities for identifying the soil group, which are all equivalent. In terms of comparability of the results of the classification, it has to be decided before the beginning of the classification to follow a certain sequence of decisions. For the pilot study here, it has been decided to focus on SPT – values first and use the shear wave velocities only if there are no SPT values available. The second classification of the Turkish Code "site class" (Table 12.2 in Figure 5.17) correlates the soil group with the expansion of the different layers in the topmost 30 meters.

Some examples will be given under the following bullet points, which might be of use for further applications. In terms of practical use, the check for the soil group should be made from the bottom (& most critical) soil class D to the top A (& least critical). Some special rules for describing the "site class" have to be applied also, which were given here when necessary for the pilot areas.

- Grid N11 from Gölcük is one of the examples where shear wave velocity has been used for site classification.
- There are values given in the tables, which allow the classification in two different groups. This is the case if N30 =16 for silt and clay, N30 =30 for sand and gravel, V_s = 300 m/s for silt and clay, V_s = 400 m/s for sand and gravel (e.g. Gölcük grids O10 or Q6).
- Silt is treated as silty clay.
- In the case of more than one SPT N30 value for one layer, the lowest value is taken to classify the soil group of this layer (on the safe side). e.g. Gölcük Grid E6, M7.
- Fill and top soil cannot be chosen as a classifying layer, even if they would fulfill the requirements. e.g. Gölcük Grid L10.
- The layer that should be the most critical for the classification is usually a soft silt/clay or loose sand/gravel.
- It might be that more than one single layer will be characterized together as a classifying layer. e.g. Gölcük Grid K4.
- Topmost Layer Thickness h1 is the thickness of the "classifying layer" in the first 30 m below surface. In case the classifying type of material (e.g. clay) appears twice, both layers do count for the thickness h1.
- A range of Local Site Classes e.g. from Z1-Z2 is given if the thickness of the "classifying layer" is not clearly defined through the borehole profile. No precise decision has been made.
- A range of Local Site Classes is given if there is already a range specified for the Soil Group (e.g. Gölcük Grid O10). Again, no precise classification has been made.

- In some cases, the last layer of the hypothetical borehole is chosen as the "classifying layer", so the thickness of the layer is not known and therefore the range indicates this (e.g. Gölcük Grid C5).
- If the "classifying" type of material is found at the top, somewhere in the middle of the borehole profile and in the last layer as well, all layers sum up to the full height of the classifying layer (e.g. Gölcük Grid G9).
- If more than one layer is characterized as the classifying layer, a range in the local site class is given (e.g. Gölcük Grid K4).
- Soil Group A is always classified as Local Site Class Z1 since no term for the topmost layer thickness (h1) is given for this soil group.
- As to the definition of the topmost layer thickness, for this study, the soil group C can never be classified as the local site class Z4 due to the fact that the topmost layer thickness h1 has to be greater than 50 m (h1 > 50 m), whereas the depth of the representative boreholes was always less than 30 meters.

TABLE 12.1 - SOIL GROUPS

Soil Group	*Description of Soil Group*	*Stand. Penetr.* (N/30)	*Relative Density* (%)	*Unconf. Compres. Strength* (kPa)	*Shear Wave Velocity* (m/s)
(A)	**1.** Massive volcanic rocks, unweathered sound metamorphic rocks, stiff cemented sedimentary rocks	—	—	> 1000	> 1000
	2. Very dense sand, gravel...	> 50	85–100	—	> 700
	3. Hard clay, silty lay……..	> 32	—	> 400	> 700
(B)	**1.** Soft volcanic rocks such as tuff and agglomerate, weathered cemented sedimentary rocks with planes of discontinuity……	—	—	500–1000	700–1000
	2. Dense sand, gravel.....	30–50	65–85	—	400–700
	3. Very stiff clay, silty clay..	16–32	—	200–400	300–700
(C)	**1.** Highly weathered soft metamorphic rocks and cemented sedimentary rocks with planes of discontinuity	—	—	< 500	400–700
	2. Medium dense sand and gravel.....……	10–30	35–65	—	200–400
	3. Stiff clay, silty clay.....	8–16	—	100–200	200–300
(D)	**1.** Soft, deep alluvial layers with high water table.....…….	—	—	—	< 200
	2. Loose sand.....…...	< 10	< 35	—	< 200
	3. Soft clay, silty clay.....…...	< 8	—	< 100	< 200

TABLE 12.2 - LOCAL SITE CLASSES

Local Site Class	*Soil Group according to Table 12.1 and Topmost Layer Thickness* (h_1)
Z1	Group **(A)** soils Group **(B)** soils with $h_1 \leq 15$ m
Z2	Group **(B)** soils with $h_1 > 15$ m Group **(C)** soils with $h_1 \leq 15$ m
Z3	Group **(C)** soils with $15 \text{ m} < h_1 \leq 50$ m Group **(D)** soils with $h_1 \leq 10$ m
Z4	Group **(C)** soils with $h_1 > 50$ m Group **(D)** soils with $h_1 > 10$ m

Figure 5.17. Table for Site classification from Turkish Code (Ministry of public Health, 1997)

The Figures 5.18 and 5.19 show the results of the classification according to the Turkish Code. Note that a plot of the local soil groups might be reasonable but it will be misleading as the determination of the local soil group is just an interim step of the classification procedure.

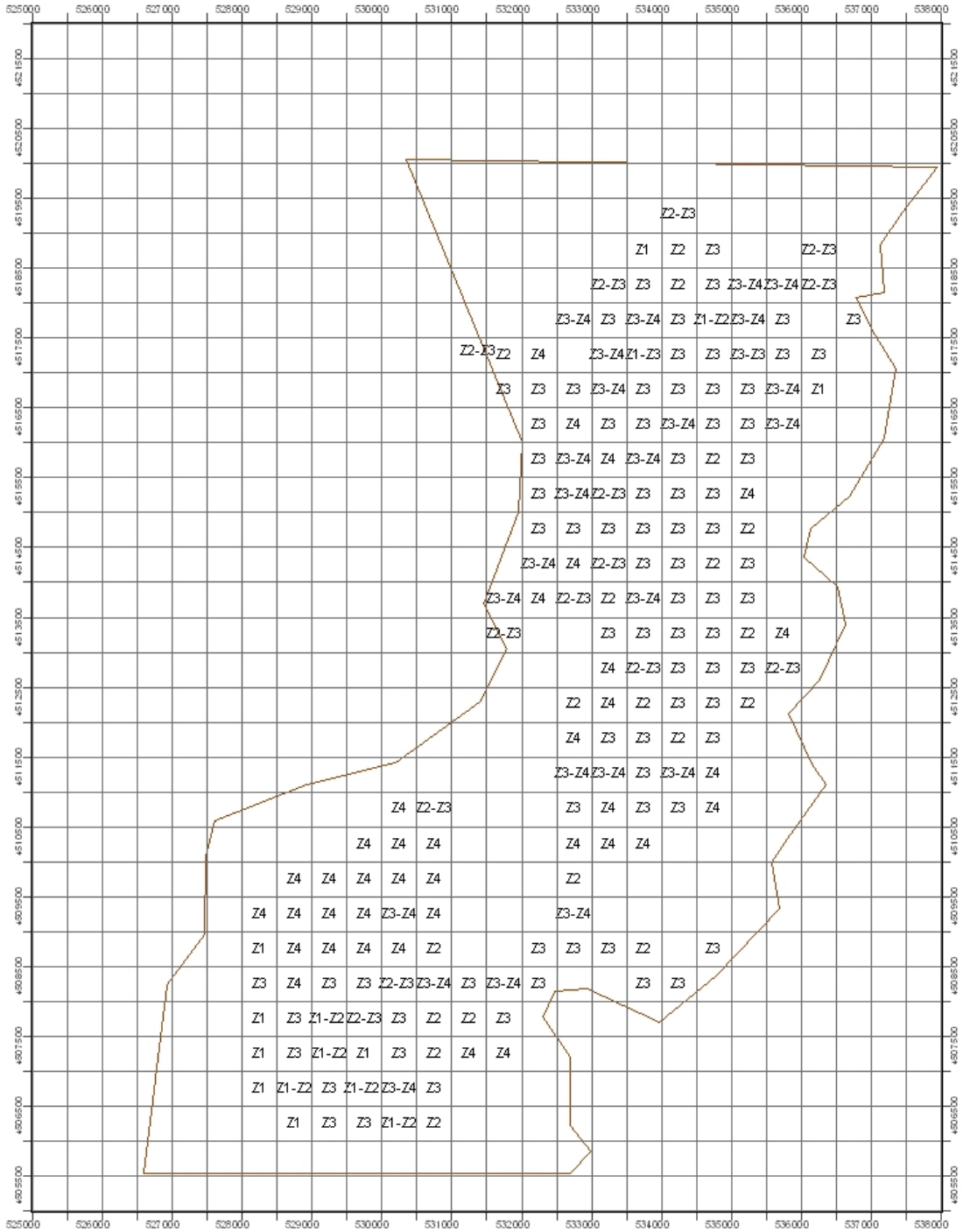

Figure 5.18. Local Site Classes for Adapazarı

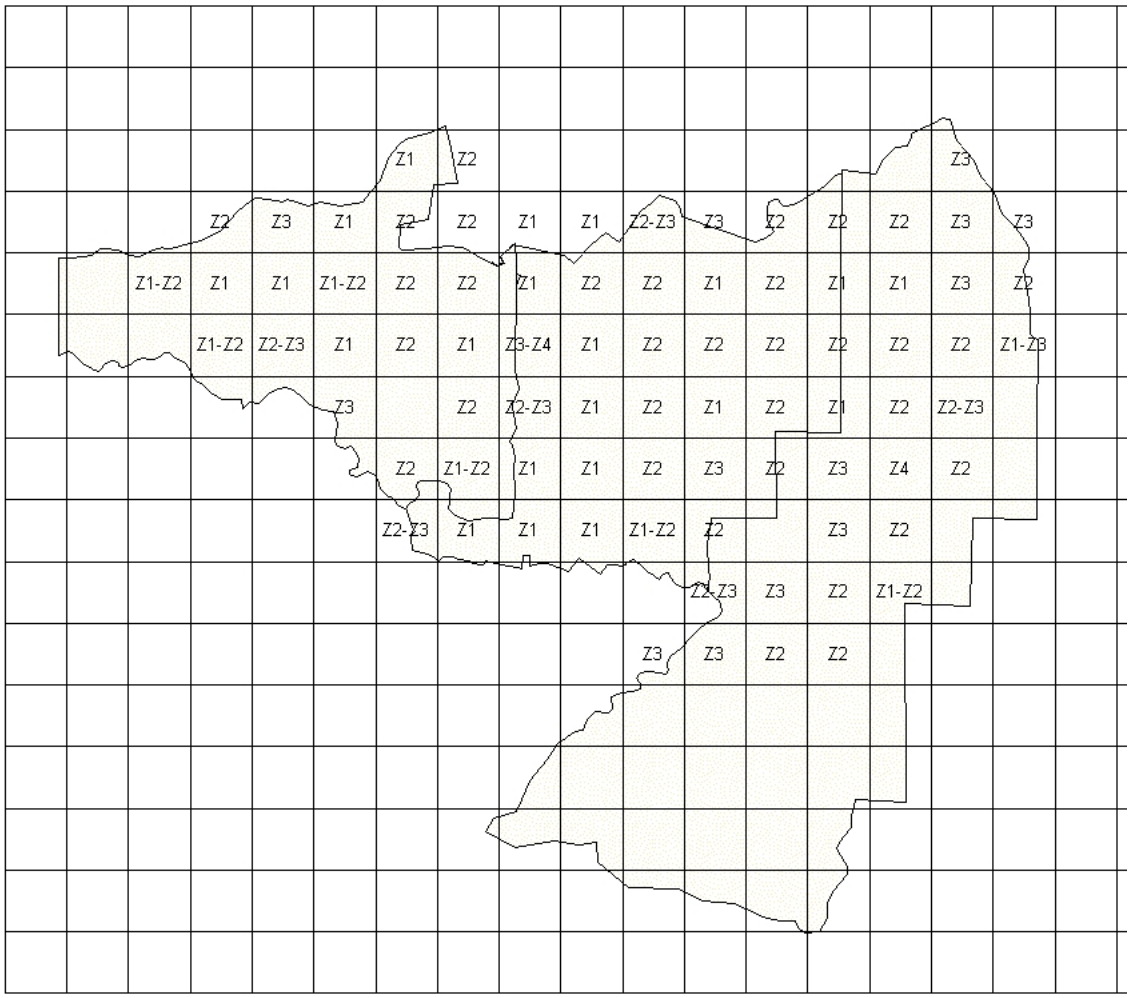

Figure 5.19 Local Site Class for Gölcük

5.5. PROCEDURE FOR THE CLASSIFICATION OF HYPOTHETICAL BOREHOLES ACCORDING TO THE NEHRP APPROACH (BSSC 2001)

The relevant four pages of the NEHRP approach are given in the Appendix 2.1, so that the procedure can be followed. It is based on a stepwise approach. Firstly it has to be decided if there is any danger of liquefaction. If so, a grid would be classified as Site Class F. This has not been done here. If any such decision is taken in the liquefaction chapter, the map will be updated accordingly.

A classification into Site Class A and B could not be done for the pilot studies as it has been decided in the project to identify the shear wave velocity for the competent bed rock with V_s = 700 m/s. The average shear wave velocity for Site Class A and B has to rise significantly over 760 m/s to represent hard rock and rock respectively according to NEHRP.

The classification between Site Classes C-E is given in the Figure 5.20. Three possibilities are given for this classification in terms of, $\overline{Vs}$, $\overline{N}$ or $\overline{N}_{ch}$, $\overline{s_u}$. The definition for the values can be found in the NEHRP approach. The method proposed by NEHRP, which is based directly on the results of the SPT soundings for the top 30 m has not been chosen since measurements were not available for the whole depth and the existing measurements were already included in the available values of the shear wave velocities,

which are based on the Iyisan relationship. The s_u method was not taken into account because the necessary values are mostly not available.

TABLE 4.1.2.2 Site Classification

Site Class	$\bar{v}_s$	N or N_{ch}	$\bar{s}_u$
E	< 600 fps (< 180 m/s)	< 15	< 1,000 psf (< 50 kPa)
D	600 to 1,200 fps (180 to 360 m/s)	15 to 50	1,000 to 2,000 psf (50 to 100 kPa)
C	> 1,200 to 2,500 fps (360 to 760 m/s)	> 50	> 2,000 (> 100 kPa)

NOTE: If the $\bar{s}_u$ method is used and the $\bar{N}_{ch}$ and $\bar{s}_u$ criteria differ, select the category with the softer soils (e.g., use *Site Class* E instead of D).

Figure 5.20. Classification of Site classes C-E following the NEHRP approach (BSSC, 2001)

The basis for the classification for the pilot areas is therefore based on an average shear wave velocity for the first 30-meters of the soil strata. This weighted average of the shear wave velocity $\overline{Vs}$ for the top 30m is derived using the following formula (formula 4.1.2.3-1 of BSSC 2001):

$$\overline{Vs} = \frac{\sum_{i=1}^{n} d_i}{\sum_{i=1}^{n} \frac{d_i}{v_{si}}} \tag{5.2}$$

v_{si} is the shear wave velocity (m/s) of each layer of defined thickness

d_i is the thickness of any layer between 0 m and 30 m.

As mentioned before only a classification for the site classes C, D and E is presented here. The sequence is given in the following two steps.

1. Check if there is a soft soil layer of more than 3 m thickness present in one of the borehole profiles. If yes, check if it is a soft clay layer and if additional information is available about the plasticity index PI, water contents w and undrained shear strength s_u. If PI > 20, w > 40% and s_u < 25 kPa classify as site class E. If no, continue with the categorization from point 2 below. Soft soil layers thinner than 3 m, that might add up in the hypothetical borehole to a layer thickness greater than 3 m, are taken into account as well.
    - In most cases the undrained shear strength is not known for the pilot areas. In many grids, two controversial experimental results of the considered clay layer may be found, one that satisfy the above mentioned criteria and one that may not do so, are available (e.g. Adapazarı Grid S18).
    - To indicate that a soft clay layer thicker than 3 m is present in the hypothetical borehole (even though the limiting criteria concerning PI, w and s_u (as mentioned in the previous paragraph) are not completely fulfilled),

a minus is added "– E" to the site class. This is based on the weighted average shear wave velocity.

2. Derivation of the average shear wave velocity (see above) and determination of the site class.

The results of the classification are given in the Figures 5.21 and 5.22.

A table of the classification is included in the Appendix 2.2. For Gölcük, soft layers appear seldom, with the exception of the grids I6, N8 (silt), N9 (silt), P3, P4, P5 (silt), P6 (silt) and Q4, in total these include 8 out of 82 grids. Some of the grids mentioned above have a soft layer thicker than 3 m, some of them have a lower PI and w than necessary for the classification of site class E, and some of them show no additional information for PI and w. Therefore none of these grids were classified as site class E, due to the presence of a soft clay layer.

In the Adapazarı area soft layers (clay and silt) appear in the grids G26, H25, H26, H27, I25, I26, I27, I28 (silt), J24, J25, J26 (silt), J28 (silt), K23, K24, K25, K26, K27 (silt), L24, L25, L26, N8, N11, O10, O11, O13, O14, O15, O17 (silt), O27 (silt), O28 (silt), P9 (silt-clay), P10, P11 (silt-clay), P12, P16, P22, Q9, Q10, Q11, Q12 (soft silt and clay layers alternating), Q13, Q15, Q18 (silt), R8, R9, R11, R12, R13, R14, R16, R17, S7, S9, S10, S11, S12 (silt-clay and silt), S13, S14, S15 (silt), S16 (silt-clay), S17 (silt-clay), S18, S19, S20, T8, T10 (silt), T11 (silt), T12, T13 (silt), T14, T15 (clay and silt), T16, T17, T18, T19, T20, T21, U8, U10 (silt), U11 (silt), U12 (clay and silt), U13, U14, U16, U17, U18, V9, V10, V11, V12 (clay and silt), V18 (clay and clay-silt), W9. Thus almost half of the grids have a soft layer of a varying thickness.

The north of Adapazarı shows a varying distribution in terms of a classification towards site classes, although potential for liquefaction (class F) has not been adjusted here. The southern areas show a more significant area denoted as class E, which lie south of a hill site and another, which is classified as class C and is next to the lake. The classification for Gölcük is less variable showing class C in most cases for Degirmendere and Gölcuk, whereas class D more prominent for Ihsaniye.

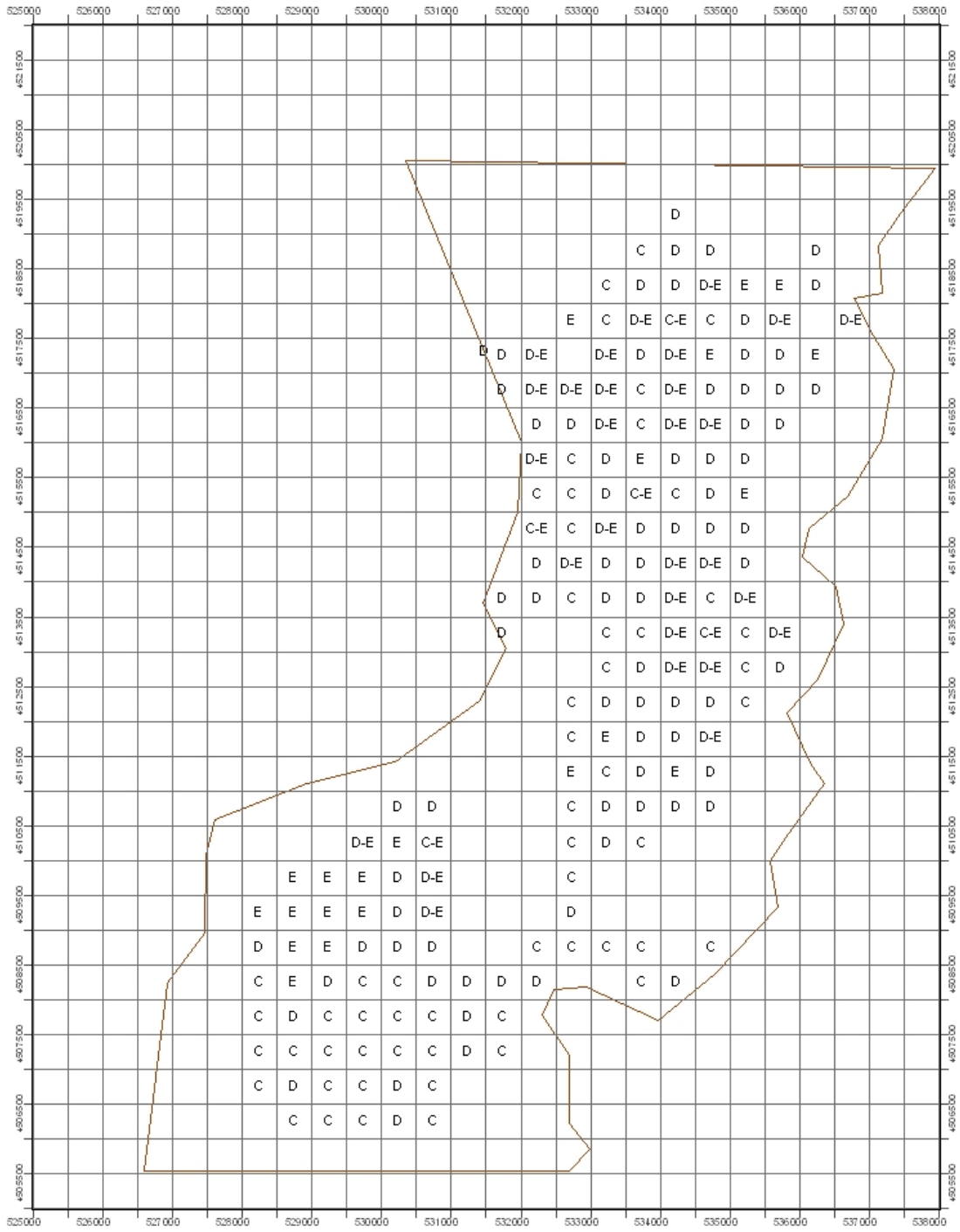

Figure 5.21. Classification according to NEHRP for Adapazarı. Note that a classification of potentially liquefiable zones (class F) has not been done at this stage as a cause of the internal task distribution of this project.

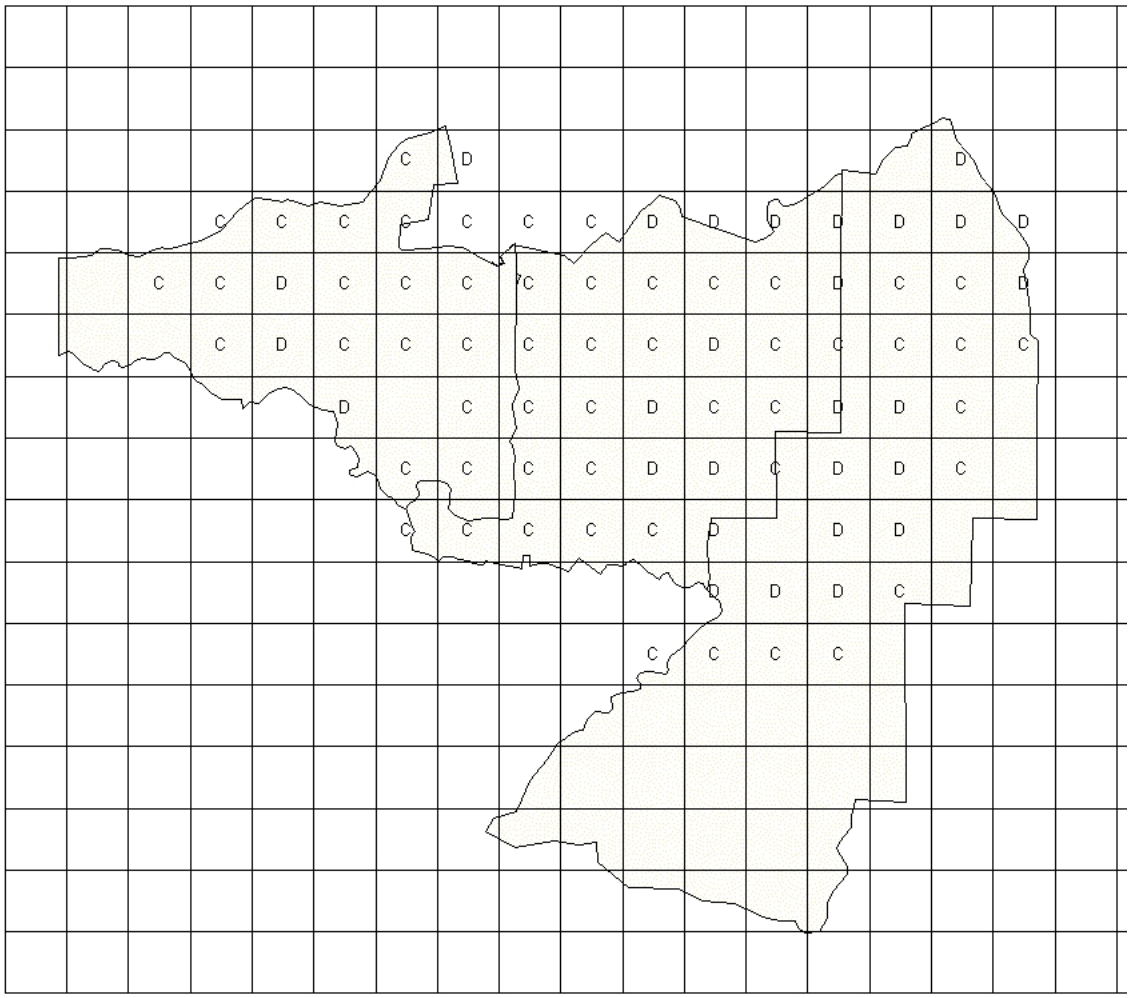

Figure 5.22. Classification according to NEHRP for Gölcük. Note that a classification of potentially liquefiable zones (class F) has not been done at this stage as a cause of the internal task distribution of this project.

6. SITE RESPONSE ANALYSES

Jan Laue, Juliane Buchheister, Sarah M. Springman, Institute for Geotechnical Engineering (IGT) of the Swiss Federal Institute of Technology (ETH), Zurich

The site response analysis determines the main frequencies and amplification that the surface of the ground will experience. There are several ways of achieving this, including simple empirical methods using analogies given in Codes. A more sophisticated method has been chosen for this project, based on a one dimensional analysis, in which an earthquake is introduced to the base rock or a competent layer from where the waves are permitted to travel vertically up through the soil column. This and other similar methods are described in the manual and the state of the art report. The procedure of input and output will be described here in Excel sheets based on the program SHAKE (Schnabel et al. 1972, Idriss & Sun, 1991) to make the analysis easier for inexperienced users (based on version SHAKE91) and will be more suitable, as the newer versions of SHAKE (1999) require a license fee to be paid, which might not be affordable (or necessary) for further use.

Some assumptions have to be made for the analysis. During the work on the pilot area, it has been decided to introduce the earthquake to the top most layers at the height of the competent layer. As described in the chapter on Soil Conditions, only a few of the grids show a competent layer in the topmost 30 meters. Thus, data from the literature had to be taken into account to derive the soil strata up to the competent layer. It was only necessary to represent the soil profile between 30 m and the competent layer with the selected shear wave velocity distribution. Thus the first paragraph will deal with the determination of the shear wave velocities between a depth of 30 m below the surface and the competent layer. The next section summarises the other input parameters required while the last section gives the results.

6.1. SHEAR WAVE VELOCITY BETWEEN 30 M AND THE TOP OF THE BEDROCK

When no site-specific soundings are available to identify the competent layers, geophysical methods have to be used. Results of array measurements conducted and described by Kudo et al. (2002) were used here. Kudo (comp. Ansal et al. 2003) describes average shear wave velocities over larger areas of soil up to bedrock. Two stations reported for both of the pilot areas are in the area of interest. In Gölcük, the stations GLF and GLH are the stations located in the pilot area, where the stations are ADC and ADU in Adapazarı. The shear wave velocity is given in an average manner for these stations. As the depth at which a value of v_s= 700 m/s has been reached is essential a linear increase of v_s was assumed in order to derive the depth of the competent layer, so that the shear wave velocity profile with depth could be linearly interpolated between two layers to reach the competent layer. The depths of the surface of the bedrock layer for the 4 relevant stations are given below:

ADU: 281 m

ADC: 126 m

GLH: 171 m

GLF: 193 m

The allocation of the two stations to each grid in the pilot areas has been done based on the results of the microtremor measurements, which are described in the research task group report (Fäh et al. 2003).

The zones determined where relatively constant fundamental frequencies may be found, could be correlated with one of the stations previously described by Kudo et al (2002), so that each grid could be related to one of the stations. Thus a shear wave velocity profile could be established up to the competent layer.

The following figures show the allocation of grid points to the respective stations of the array measurements with respect to the areas defined by Fäh et al. (2003). The Figures 6.1 and 6.2 show the allocation of the different grids to the station given by Kudo.

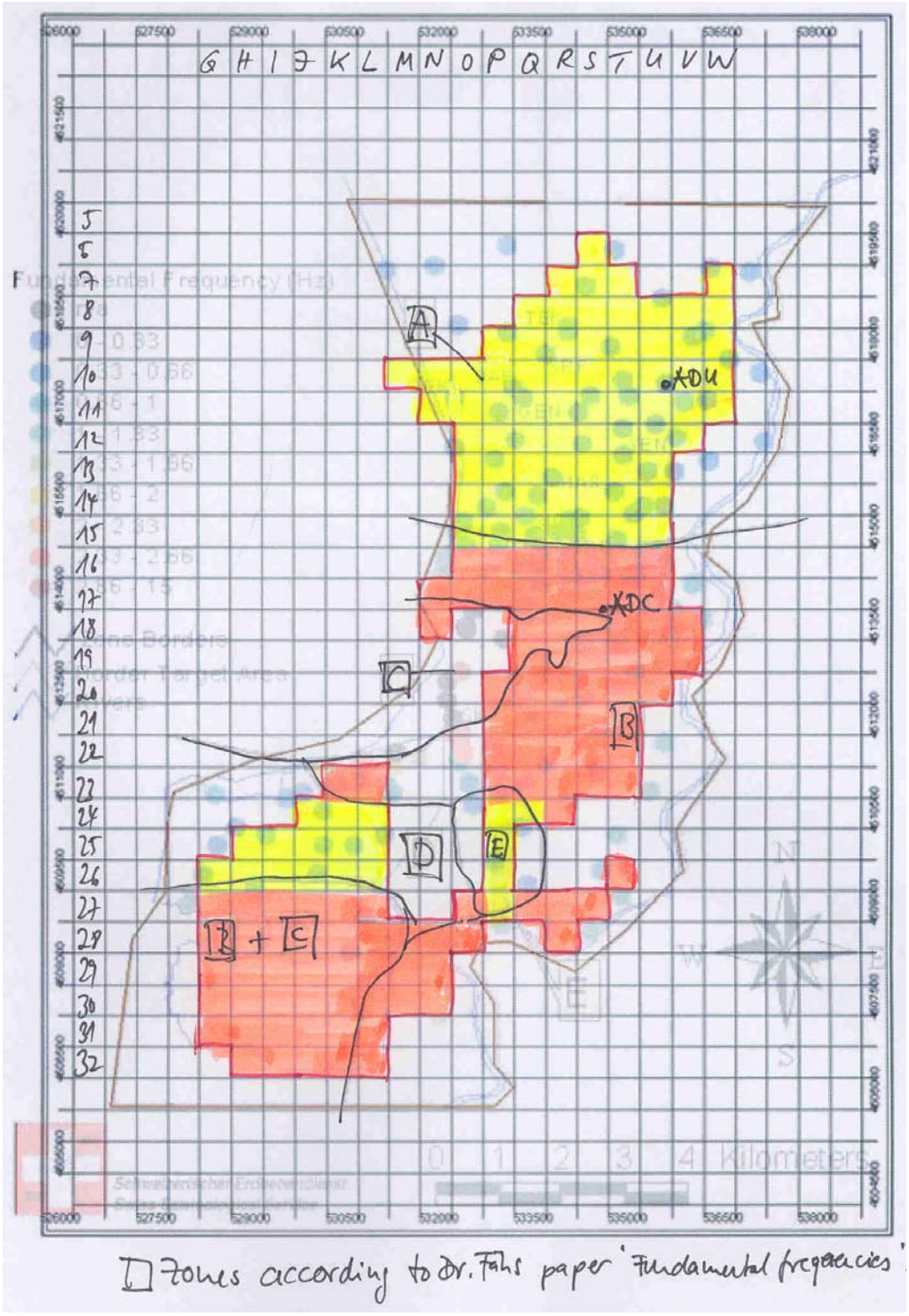

Figure 6.1. Allocation of the Kudo stations ADU and ADC to the grids in the pilot area of Adapazarı (Laue et al. 2003).

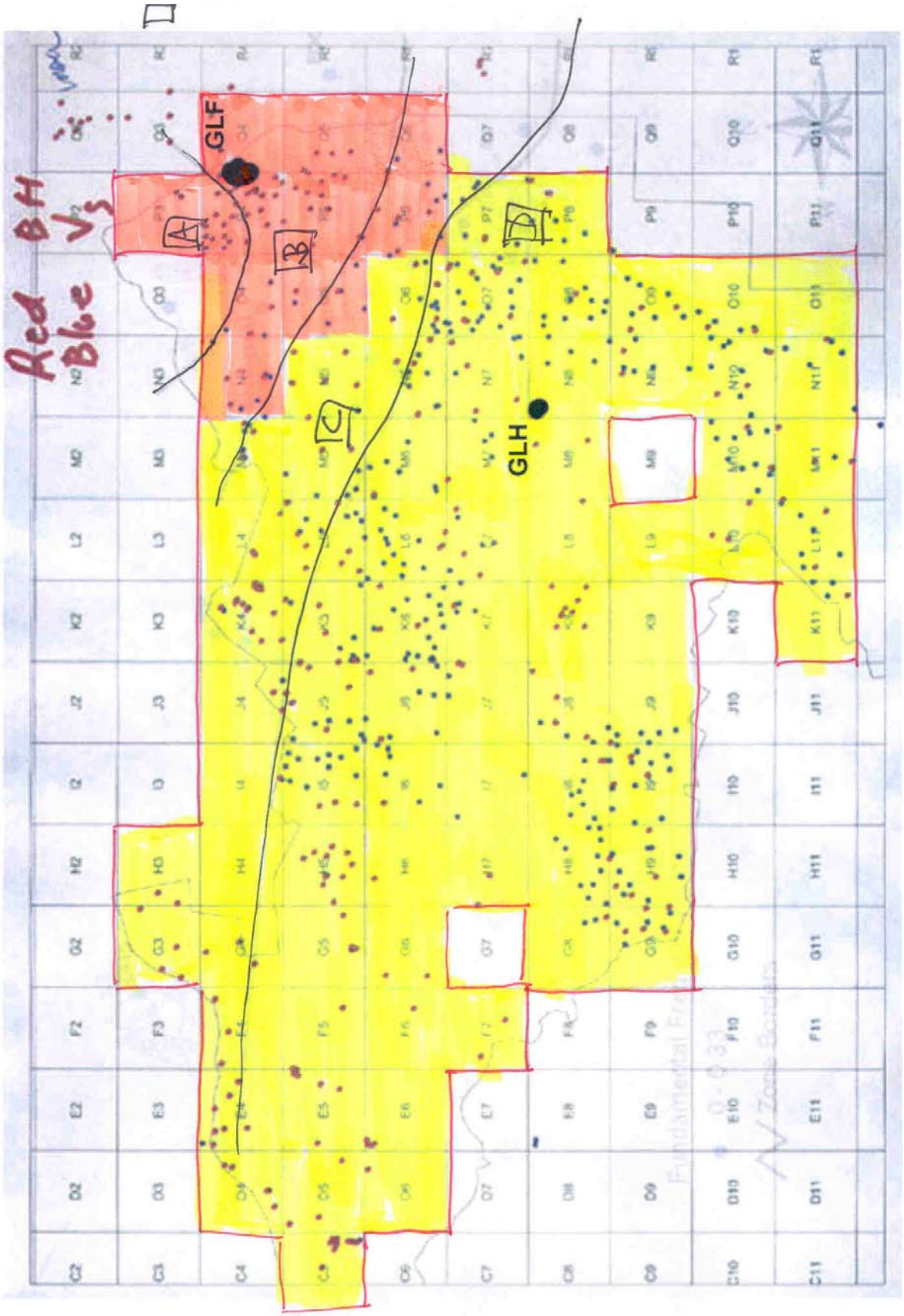

Figure 6.2. Allocation of the Kudo stations GLF and GLH to the grids in the pilot area of Gölcük (Laue et al., 2003).

6.2. INPUT REQUIREMENTS

6.2.1 Earthquake input file

The earthquake data has been introduced as an outcrop motion. Earthquake data has been received from another task group and reference should be made to the respective chapter (Erdik et al. 2003). A single earthquake for each grid was used for the analysis conducted here. Usually, several different earthquake files should be studied and an average result should be established. The earthquake has been introduced into the calculation in the time domain.

6.2.2 Soil profile

The hypothetical borehole was introduced for each grid as the soil profile, including the extension up to competent layer. In case of mixed layers (e.g. sand and silt S+U), the softer layer has been chosen as the representative one.

The following boreholes in Adapazarı had these mixed layers (S=sand, T=clay, U=silt)

Grid number	Layer	Material parameter
G26	S+U	U
G31	U+S	U
H32	S+U	S
P9	T+U	T
P11	T+U	T
Q11	T+U	T
Q16	T+U	T
R11	T+S	T
	S+T	S
	U+T	U
S6	T+S	T
S16	T+U	T
S17	T+U	T
S19	T+U	T
T7	T+U	T
U9	U+S	U
U16	T+U	T
V18	T+U	T

6.2.3 Material parameters

The shear wave velocity distribution has to be included for each of the materials. In addition, the strain dependency of the material properties has to be allocated to each soil. A brief mention is included in the text, while the respective figures and details can be found in the Annex. The names are given herein (according to the notation given in the SHAKE program series) and their allocation. Several material types have been defined for the Excel sheet calculations.

Mat 1 Top soil: Chosen strain dependent approach: G: Vucetic & Dobry with PI=0% D: Vucetic & Dobry with PI=0%	Mat 2 Fill: Chosen strain dependent approach: G: Seed & Idriss average D: Seed & Idriss average
Mat 3 Silt: Chosen strain dependent approach: G: Vucetic & Dobry mit PI=15% D: Vucetic & Dobry mit PI=15%	Mat 4 Clay: Chosen strain dependent approach: G: Vucetic & Dobry mit PI=30% D: Vucetic & Dobry mit PI=30%
Mat 5 Sand: Chosen strain dependent approach: G: Seed & Idriss average D: Seed & Idriss average	Mat 6 Gravel: Chosen strain dependent approach: G: Seed & Idriss average D: Seed & Idriss average
Mat 7 Kudo unknown material layer: Chosen strain dependent approach: G: Seed & Idriss average D: Seed & Idriss average	Mat 8 Bedrock: Chosen strain dependent approach: G: Rock Idriss D: Rock Idriss

6.2.4 Total unit weight

A total unit weight has to be introduced in the calculation. Due to the lack of availability of representative data, the unit weight had to be estimated. Please note that the density given is the saturated bulk density

Mat 1 Top soil:	18 kN/m^3
Mat 2 Fill:	19 kN/m^3
Mat 3: Clay	20 kN/m^3
Mat 4: Silt	20 kN/m^3
Mat 5: Sand	21 kN/m^3
Mat 6: Gravel	22 kN/m^3
Mat 7: unknown Kudo	21 kN/m^3
Mat 8: Bedrock	26 kN/m^3

6.2.5 Groundwater level

The groundwater level has to be introduced in the calculations. Again assumptions have to be made according to the different data available.

For both of the Adapazarı and Gölcük areas, data based on the GDDA database and given to public on a map (Köksal, 2003) have been used, even if no differentiation between the date of the derivation has been made. The following tables give the input data for the grids. For Adapazarı, only grids are mentioned where the groundwater table does not lie in the topmost 2.5 meters. The groundwater level is given for all grids for the Gölcük area.

Adapazarı:

Grid number	Groundwater level range (m)	Grid number	Groundwater level range (m)
G26	2.5 – 5	G27	7.5 – 10
G28	12.5 – 15	G29	n.a.
G30	n.a.	G31	n.a.
H25	2.5 – 5	H26	2.5 – 5
H27	7.5 – 10	H28	10 – 12.5
H29	n.a.	H30	n.a.
H31	n.a.	H32	n.a.
I27	5 – 7.5	I28	7.5 – 10
I29	10 – 12.5	I30	n.a.
I31	12.5 – 15	I32	12.5 – 15
J28	5 – 7.5	J29	7.5 – 10
J30	7.5 – 10	J31	10 – 12.5
J32	10 – 12.5	K28	2.5 – 5
K29	2.5 – 5	K30	5 – 7.5
K31	5 – 7.5	K32	5 – 7.5
L28	2.5 – 5	L29	2.5 – 5
L30	2.5 – 5	L31	2.5 – 5
L32	2.5 – 5	M29	2.5 – 5
M30	2.5 – 5	N18	5 – 7.5
N30	2.5 – 5	O20	7.5 - 10
O21	7.5 – 10	O22	7.5 – 10
O23	2.-5 - 5	P13	2.5 – 5
P14	2.5 – 5	P20	7.5 – 10
P21	7.5 – 10	P22	2.5 – 5
P23	2.5 – 5	Q13	2.5 – 5
Q14	2.5 – 5	Q17	7.5 – 10
Q18	10 – 12.5	Q19	7.5 – 10
Q20	2.5 – 5	Q21	2.5 – 5
R16	7.5 – 10	R17	12.5 – 15
R18	n.a.	R19	5 – 7.5
S16	10 – 12.5	S17	n.a.
S18	n.a.	S19	12.5 – 15
S20	2.5 – 5	S21	2.5 – 5
T15	2.5 – 5	T16	n.a.
T17	n.a.	T18	n.a.
T19	12.5 – 15	T20	5 – 7.5
T21	5 – 7.5	T22	2.5 – 5
U15	2.5 – 5	U16	7.5 – 10
U17	n.a.	U18	12.5 – 15
U19	10 – 12.5	U20	5 – 7.5
V18	5 – 7.5	V19	5 – 7.5

Gölcük:

Grid number	Groundwater level range (m)	Grid number	Groundwater level range (m)
D4	0 - 2.5	E4	0 - 2.5
F4	10 - 12.5	G3	5 - 7.5
G4	10 – 12.5	G8	7.5 – 10
G9	5 – 7.5	H3	10 – 12.5
H7	10 – 12.5	H8	7.5 – 10
H9	5 – 7.5	I5	12.5 - 15
I7	12.5 - 15	J4	12.5 - 15
K4	2.5 – 5	K5	7.5 – 10
K11	5 – 7.5	L4	0 – 2.5
L5	7.5 – 10	L10	5 – 7.5
L11	5 – 7.5	M4	2.5 – 5
M5	5 – 7.5	M6	10 – 12.5
M8	10 – 12.5	M10	2.5 – 5
M11	2.5 – 5	N4	2.5 – 5
N5	5 – 7.5	N6	5 – 7.5
N7	5 – 7.5	N8	7.5 - 10
N9	2.5 – 5	N10	5 – 7.5
N11	5 – 7.5	O4	2.5 – 5
O5	2.5 – 5	O6	2.5 – 5
O7	5 – 7.5	O8	5 – 7.5
O9	2.5 – 5	O10	2.5 – 5
P3	0 – 2.5	P4	0 – 2.5
P5	0 – 2.5	P6	2.5 – 5
P7	5 – 7.5	P8	5 – 7.5
Q4	0 – 2.5	Q5	0 – 2.5
Q6	2.5 – 5		

6.3. RESULTS OF THE SITE RESPONSE ANALYSIS

The following Figures 6.3 and 6.4 show the distribution of Peak horizontal Ground Acceleration (PGA) for both areas of the pilot studies. This map is given here to illustrate that all results used later on for microzonation purposes are based on numbers. The values for each grid show the result for 1 special scenario and have no physical meaning for any other use than building one of the basis for microzonation. The interpreted maps will be included in Chapter 11 of this report. All calculations are available in an electronic version and are added to the Annex. They are summarized in additional tables, which are also included in printed version of the Appendix 2.3.

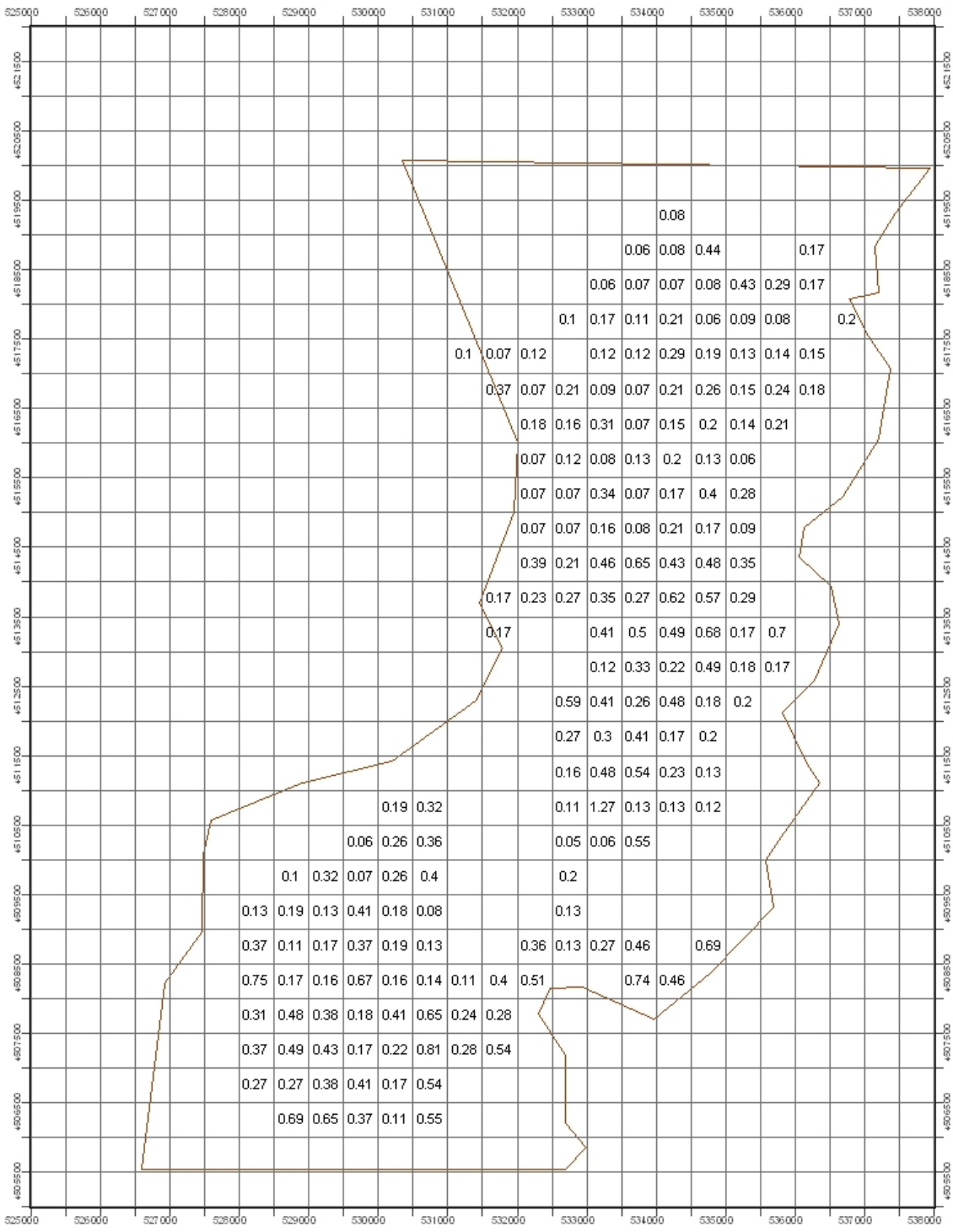

Figure 6.3. Peak horizontal Ground Acceleration shown as multiples of g (m/s^2) for Adapazarı

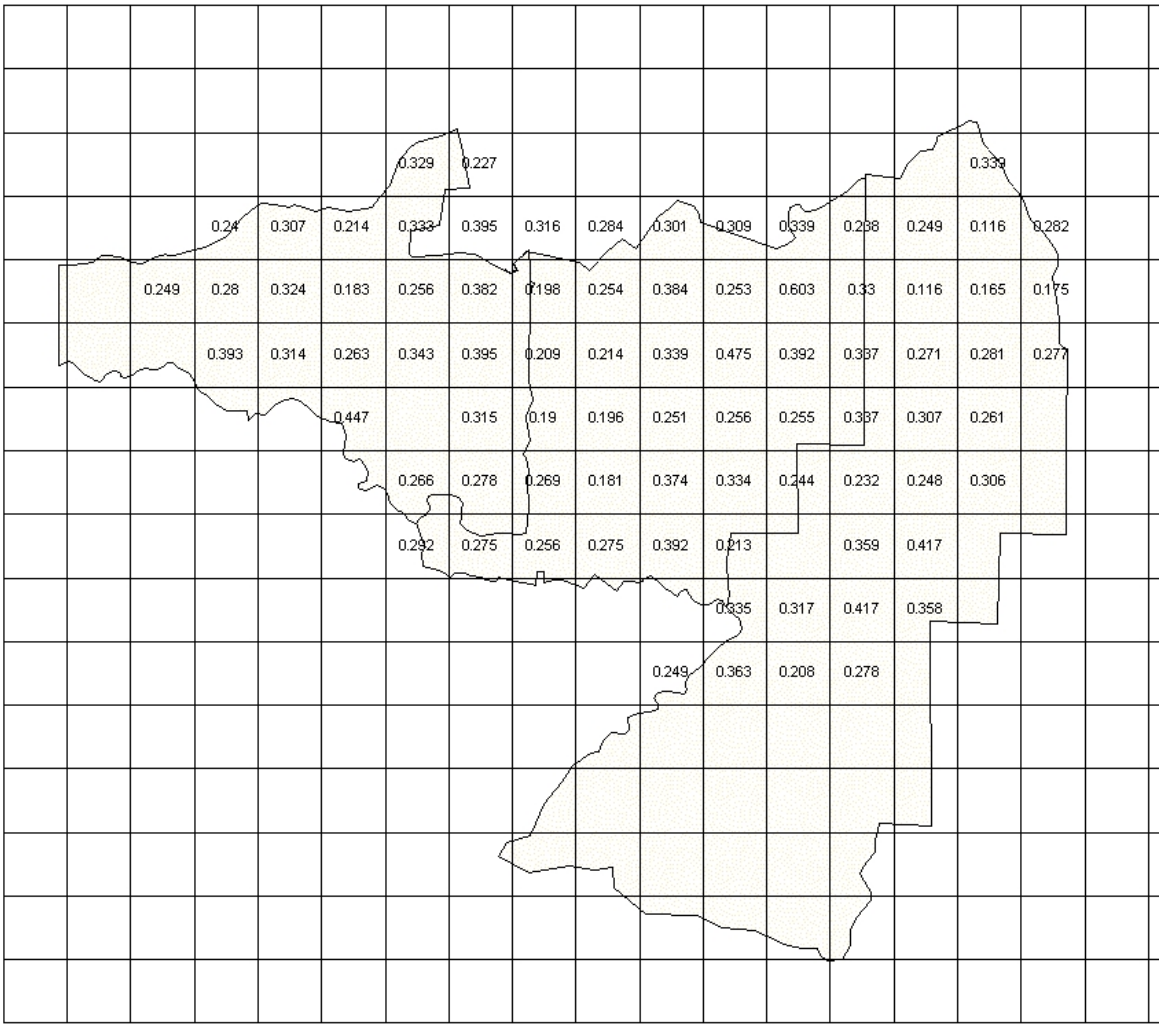

Figure 6.4. Peak horizontal Ground Accelerations shown as multiples of g (m/s^2) for Gölcük.

In addition to the Peak Ground Accelerations, the summary tables in the Appendix 2.3 indicate the spectral acceleration and the predominant period resulting from the calculation for the specific input earthquake. Also added into the table are the amplitude of shear strain and the respective depth. The results are not given here, as they are part of chapter 11. The necessity of including the maximum amplitude of shear strain and the related depth will also be discussed in chapter 11.

7. SEISMIC SOIL LIQUEFACTION ASSESSMENT METHODOLOGIES

K. Önder Çetin, Middle East Technical University, Civil Engineering Department, Ankara

7.1. INTRODUCTION

Soil liquefaction is a major cause of damage during earthquakes. "Modern" engineering treatment of liquefaction-related issues evolved initially in the wake of the two devastating earthquakes of 1964, the 1964 Niigata and 1964 Great Alaska Earthquakes, in which seismically-induced liquefaction produced spectacular and devastating effects.

Over the nearly four decades that have followed, significant progress has occurred. Initially, this progress was largely confined to improved ability to assess the likelihood of initiation (or "triggering") of liquefaction in clean, sandy soils. As the years passed, and earthquakes continued to provide lessons and data, researchers and practitioners became increasingly aware of the additional potential problems associated with both silty and gravely soils and the issues of post-liquefaction strength and stress-deformation behavior also began to attract increased attention.

Today, the area of "soil liquefaction engineering" is emerging as a semi-mature field of practice in its own right. This area now involves a number of discernable sub-issues or sub-topics, as illustrated schematically in Figure 7.1, showing that the first step in most engineering treatments of soil liquefaction continues to be (1) assessment of "liquefaction potential", or the risk of "triggering" (initiation) of liquefaction. There have been major advances here in recent years, and some of these will be discussed.

Once it is determined that occurrence of liquefaction is a potentially serious risk/hazard, the consequences of the potential liquefaction will be assessed. This, now, increasingly involves (2) assessment of available post-liquefaction strength and resulting post-liquefaction overall stability (of a site, and/or of a structure or other built facility, etc.). There has been considerable progress over the past fifteen years in evaluation of post-liquefaction strengths. If post-liquefaction stability is found wanting, then deformation/displacement potential is large, and engineered remediation is typically warranted.

If post-liquefaction overall stability is not unacceptable, then attention is next directed towards (3) assessment of anticipated deformations and displacements. This is a very "soft" area of practice, and much remains to be done here with regard to development and calibration/verification of engineering tools and methods. Similarly, relatively little is known regarding (4) the effects of liquefaction-induced deformations and displacements on the performance of structures and other engineered facilities, and criteria for "acceptable" performance are not well established.

Finally, in cases in which the engineer(s) conclude that satisfactory performance cannot be counted on, (5) engineered mitigation of liquefaction risk is generally warranted. This, too, is a rapidly evolving area, and one rife with potential controversy. Ongoing evolution of new methods for mitigation of liquefaction hazard provides an ever increasing suite of engineering options, but the efficacy and reliability of some of these remain contentious and accurate and reliable engineering analysis of the improved performance provided by many of these mitigation techniques continues to be difficult.

It is not possible, within the confines of this report, to address fully all of these issues (a textbook would be required). Instead, methodologies regarding liquefaction triggering

assessment will be highlighted, and GIS-based applications of these liquefaction triggering methodologies will be demonstrated for the cities of Sakarya and Gölcük after August 17, 1999 Kocaeli Earthquake with $M_w = 7.4$.

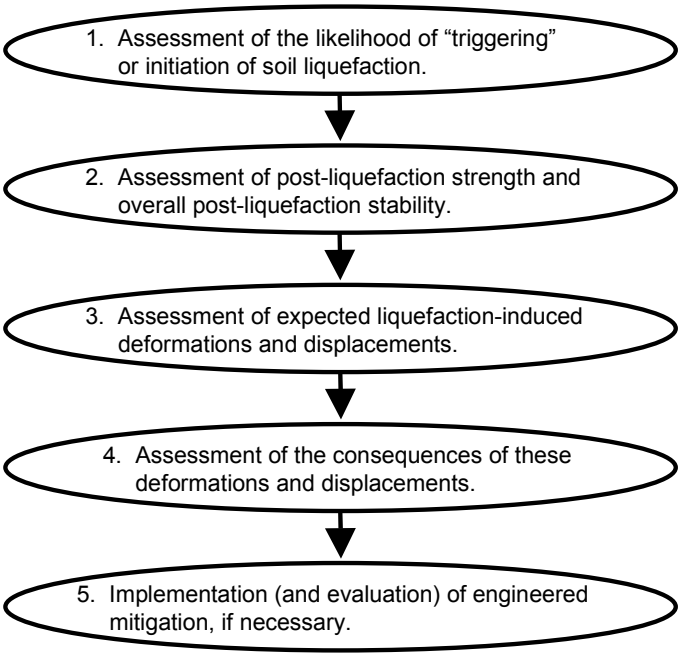

Figure 7.1. Key Elements of Soil Liquefaction

7.2. ASSESSMENT OF LIQUEFACTION POTENTIAL

7.2.1 Liquefiable Soils

The first step in engineering assessment of the potential for "triggering" or initiation of soil liquefaction is the determination of whether or not soils of "potentially liquefiable nature" are present at a site. This, in turn, raises the important question regarding which types of soils are potentially vulnerable to soil liquefaction.

It has long been recognized that relatively "clean" sandy soils, with few fines, are potentially vulnerable to seismically-induced liquefaction. There has, however, been significant controversy and confusion regarding the liquefaction potential of silty soils (and silty/clayey soils), and also of coarser gravely soils and rock fills.

Coarser, gravely soils are the easier of the two to discuss, so we will begin there. The cyclic behavior of coarse gravely soils differs little from that of "sandy" soils, as Nature has little or no respect for the arbitrary criteria established by the standard #4 sieve. Coarse, gravely soils are potentially vulnerable to cyclic pore pressure generation and liquefaction. There are now a number of well-documented field cases of liquefaction of coarse gravely soils (e.g., Evans, 1987; Harder, 1988; Hynes, 1988; Andrus, 1994). These soils do, however, often differ in behavior from their finer, sandy brethren in two ways: (1) they can be much more pervious, and so can often rapidly dissipate cyclically generated pore pressures, and (2) due to the mass of their larger particles, the coarse gravely soils are seldom deposited gently and so do not often occur in the very loose states more often encountered with finer sandy soils. Sandy soils can be very loose to very dense, while the very loose state is uncommon in gravely deposits and coarser soils.

The apparent drainage advantages of coarse, gravely soils can be defeated if their drainage potential is circumvented by either; (1) their being surrounded and encapsulated by finer, less pervious materials, (2) if drainage is internally impeded by the presence of finer soils in the void spaces between the coarser particles (it should be noted that the D_{10} particle size, not the mean or D_{50} size, most closely correlates with the permeability of a broadly graded soil mix), or (3) if the layer or stratum of coarse soil is of large dimension, so that the distance over which drainage must occur (rapidly) during an earthquake is large. In these cases, the coarse soils should be considered to be of potentially liquefiable type, and should be evaluated accordingly.

Questions regarding the potential liquefiability of finer, "cohesive" soils (especially "silts") are increasingly common at meetings and professional short courses and seminars. Over the past five years, a group of approximately two dozen leading experts has been attempting to achieve consensus regarding a number of issues involved in the assessment of liquefaction potential. This group, referred to hereafter as the NCEER Working Group, have published many of their consensus findings (or at least near-consensus findings) in the NSF-sponsored workshop summary paper (NCEER, 1997), and additional views are coming in a second paper scheduled for publication this year in the ASCE Journal of Geotechnical and Geoenvironmental Engineering (Youd et al., 2001). The NCEER Working Group addressed this issue, and it was agreed that there was a need to reexamine the "Modified Chinese Criteria" (Finn et al., 1994) for defining the types of fine "cohesive" soils potentially vulnerable to liquefaction, but no improved consensus position could be reached, and more study was warranted.

Some of the confusion here is related to the definition of liquefaction. In this paper, the term "liquefaction" will refer to significant loss of strength and stiffness due to cyclic pore pressure generation, in contrast to "sensitivity" or loss of strength due to monotonic shearing and/or remolding. By making these distinctions, we are able to separately discuss "classical" cyclically-induced liquefaction and the closely-related (but different) phenomenon of strain-softening or sensitivity.

Figure 7.2 illustrates the "Modified Chinese Criteria" for defining potentially liquefiable soils. According to these criteria, soils are considered to be of potentially liquefiable type and character if: (1) there are less than 15% "clay" fines (based on the Chinese definition of "clay" sizes as less than 0.005 mm), (2) there is a Liquid Limit of LL $\leq$ 35%, and (3) there is a current in situ water content greater than or equal to 90% of the Liquid Limit.

Andrews and Martin (2000) have re-evaluated the liquefaction field case histories from the database of Seed et al. (1984, 1985), and have transposed the "Modified Chinese Criteria" to standard conventions (with clay sizes defined as those less than about 0.002 mm). Their findings are largely summarized in Figure 7.3. Andrews and Martin recommend that soils with less than about 10% clay fines (< 0.002 mm) and a Liquid Limit (LL) in the minus #40 sieve fraction of less than 32% be considered potentially liquefiable, that soils with more than about 10% clay fines and LL $\geq$ 32% are unlikely to be susceptible to classic cyclically-induced liquefaction, and that soils intermediate between these criteria should be sampled and tested to assess whether or not they are potentially liquefiable.

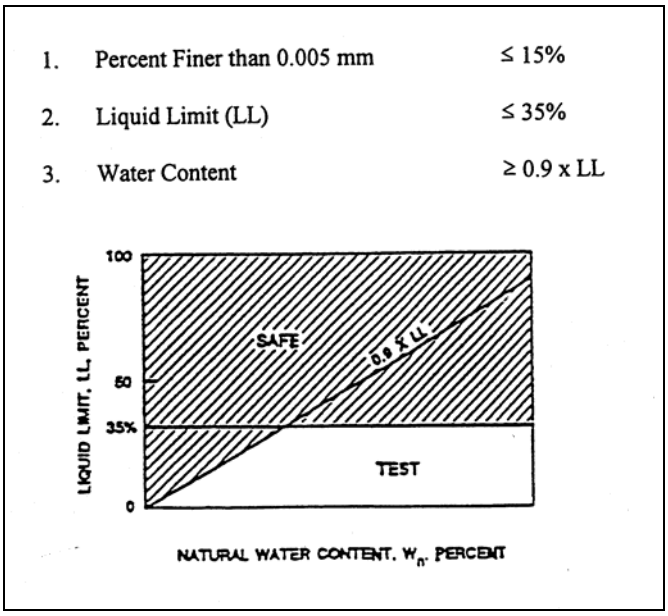

Figure 7.2. Modified Chinese Criteria (after Finn et al., 1994)

	Liquid Limit[1] < 32%	Liquid Limit ≥ 32%
Clay Content[2] < 10%	Susceptible	Further Studies Required *(Considering plastic non-clay sized grains – such as Mica)*
Clay Content[2] ≥ 10%	Further Studies Required *(Considering non-plastic clay sized grains – such as mine and quarry tailings)*	Not Susceptible

Notes:
1. Liquid limit determined by Casagrande-type percussion apparatus.
2. Clay defined as grains finer than 0.002 mm.

Figure 7.3. Liquefaction Susceptibility of Silty and Clayey Sands (after Andrews and Martin, 2000)

This is a step forward, as it somewhat simplifies the previous "Modified Chinese" criteria, and transposes it into terms more familiar to Turkish practitioners. We note, however, that there is a common lapse in engineering practice inasmuch as engineers often tend to become distracted by the presence of potentially liquefiable soils, and then often neglect cohesive soils (clays and plastic silts) that are highly "sensitive" and vulnerable to

major loss of strength if sheared or remolded. These types of "sensitive" soils often co-exist with potentially liquefiable soils, and can be similarly dangerous in their own right.

Both experimental research and review of liquefaction field case histories show that for soils with sufficient "fines" (particles finer than 0.074 mm, or passing a #200 sieve) to separate the coarser (larger than 0.074 mm) particles, the characteristics of the fines control the potential for cyclically-induced liquefaction. This separation of the coarser particles typically occurs as the fines content exceeds about 12% to 30%, with the precise fines content required being dependent principally on the overall soil gradation and the character of the fines. Well-graded soils have lesser void ratios than uniformly-graded or gap-graded soils, and so require lesser fines contents to separate the coarser particles. Similarly, clay fines carry higher void ratios than silty particles and so are more rapidly effective at over-filling the void space available between the coarser (larger than 0.074 mm) particles.

In soils wherein the fines content is sufficient as to separate the coarser particles and control behavior, cyclically-induced soil liquefaction appears to occur primarily in soils where these fines are either non-plastic or are low plasticity silts and/or silty clays (PI $\leq$ 10 to 12%). In fact, low plasticity or non-plastic silts and silty sands can be among the most dangerous of liquefiable soils, as they not only can cyclically liquefy; they also "hold their water" well and dissipate excess pore pressures slowly due to their low permeability.

Soils with more than about 15% fines and with fines of "moderate" plasticity (8% $\leq$ PI $\leq$ 15%) fall into an uncertain range. These types of soils are usually amenable to reasonably "undisturbed" (e.g.: thin-walled, or better) sampling, however, and so can be tested in the laboratory. It should be remembered to check for "sensitivity" of these cohesive soils as well as for potential cyclic liquefiability.

The criteria of this section do not fully cover all types of liquefiable soils. As an example, well-studied clayey sand (SC) at a site in the south-eastern U.S. has been clearly shown to be potentially susceptible to cyclic liquefaction, despite a clay content on the order of 15 %, and a Plasticity Index of up to 30% (Riemer et al., 1993). This is a highly unusual material, however, as it is ancient sand that has weathered in place, with the clay largely coating the individual weathered grains, and the overall soil state is unusually "loose". Exceptions must be anticipated, and judgment will continue to be necessary in evaluating whether or not specific soils are potentially liquefiable.

Two additional conditions necessary for potential liquefiability are: (1) saturation (or at least near-saturation), and (2) "rapid" (largely "undrained") loading. It should be remembered that phearatic conditions are variable both with seasonal fluctuations and irrigation, and that the rapid cyclic loading induced by seismic excitation represents an ideal loading type.

7.3. ASSESSMENT OF TRIGGERING POTENTIAL

Quantitative assessment of the likelihood of "triggering" or initiation of liquefaction is the necessary first step for most projects involving potential seismically-induced liquefaction. There are two general types of approaches available for this: (1) use of laboratory testing of "undisturbed" samples, and (2) use of empirical relationships based on correlation of observed field behavior with various in-situ "index" tests.

The use of laboratory testing is complicated by difficulties associated with sample disturbance during both sampling and reconsolidation. It is also difficult and expensive to perform high-quality cyclic simple shear testing, and cyclic triaxial testing poorly represents the loading conditions of principal interest for most seismic problems. Both sets

of problems can be ameliorated, to some extent, by use of appropriate "frozen" sampling techniques, and subsequent testing in a high quality cyclic simple shear or torsional shear apparatus. The difficulty and cost of these delicate techniques, however, places their use beyond the budget and scope of most engineering studies.

Accordingly, the use of in-situ "index" testing is the dominant approach in common engineering practice. As summarized in the recent state-of-the-art paper (Youd et al., 1997, 2001), four in-situ test methods have now reached a level of sufficient maturity as to represent viable tools for this purpose, and these are (1) the Standard Penetration Test (SPT), (2) the cone penetration test (CPT), (3) measurement of in-situ shear wave velocity (V_s), and (4) the Becker penetration test (BPT). The oldest and still the most widely used of these is the SPT, and this will be the focus of the next section of this report.

7.3.1 Existing SPT-Based Correlations

The use of SPT as a tool for evaluation of liquefaction potential first began to evolve in the wake of a pair of devastating earthquakes that occurred in 1964; the 1964 Great Alaskan Earthquake (M = 8+) and the 1964 Niigata Earthquake (M ≈ 7.5), both of which produced significant liquefaction-related damage (e.g.: Kishida, 1966; Koizumi, 1966; Ohsaki, 1966; Seed and Idriss, 1971). Numerous additional researchers have made subsequent progress, and these types of SPT-based methods continue to evolve today.

As discussed by the NCEER Working Group (NCEER, 1997; Youd et al., 2001), one of the most widely accepted and used SPT-based correlations are the "deterministic" relationship proposed by Seed, et al. (1984, 1985). This relationship, with minor modification at low CSR (as recommended by the NCEER Working Group; NCEER, 1997). This familiar relationship is based on comparison between SPT N-values, corrected for both effective overburden stress and energy, equipment and procedural factors affecting SPT testing (to $N_{1,60}$-values) vs. intensity of cyclic loading, expressed as magnitude-weighted equivalent uniform cyclic stress ratio (CSR_{eq}). The relationship between corrected $N_{1,60}$-values and the intensity of cyclic loading required to trigger liquefaction is also a function of fines content in this relationship, as shown in Figure 7.4.

Although widely used in practice, this relationship is dated, and does not make use of an increasing body of field case history data from seismic events that have occurred since 1984. It is particularly lacking in data from cases wherein peak ground shaking levels were high (CSR > 0.25), an increasingly common design range in regions of high seismicity. This correlation also has no formal probabilistic basis, and so provides no insight regarding either uncertainty or probability of liquefaction.

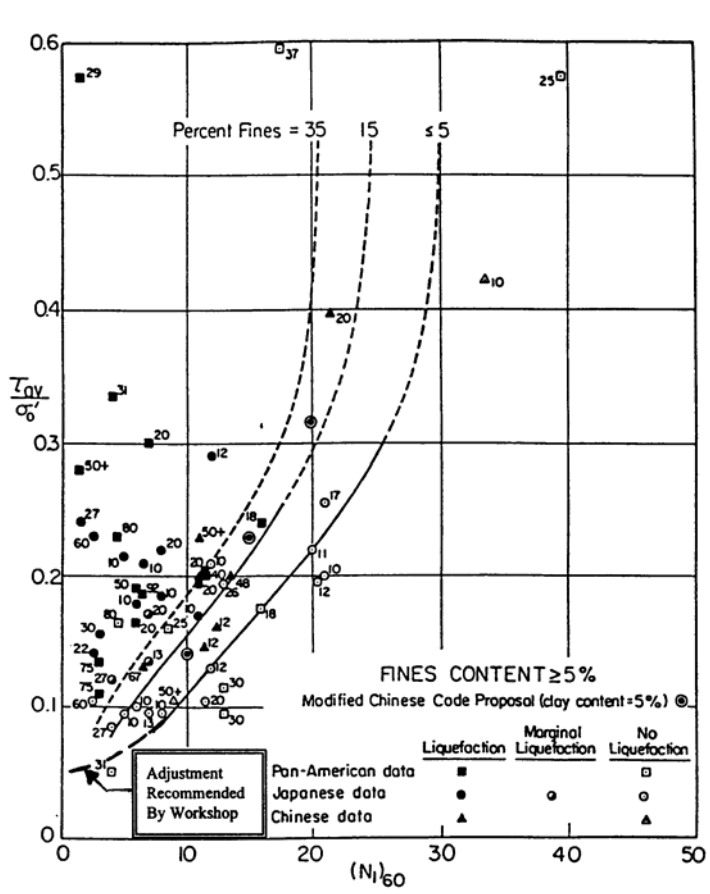

Figure 7.4 Correlation Between Equivalent Uniform Cyclic Stress Ratio and SPT $N_{1,60}$-Value for Events of Magnitude, $M_W \approx 7.5$ for Varying Fines Contents, with Adjustments at Low Cyclic Stress Ratio as Recommended by NCEER Working Group (Modified from Seed, et al., 1986)

Efforts at development of similar, but formally probabilistically-based, correlations have been published by a number of researchers, including Liao et al. (1988), Liao and Lum (1998), and more recently Youd and Noble (1997), and Toprak et al. (1999).

The probabilistic relationship proposed by Liao et al. employs a larger number of case history data points than were used by Seed et al. (1984), but this larger number of data points is the result of less severe screening of points for data quality, and so includes some low quality data. This relationship was developed using the maximum likelihood estimation method for probabilistic regression (binary regression of logistic models). The way the likelihood function was formulated did not permit separate treatment of aleatory and epistemic sources of uncertainty, and so overstates the overall variance or uncertainty of the proposed correlation. This can lead to large levels of over-conservatism at low levels of probability of liquefaction. An additional shortcoming was that Liao et al. sought, but failed to find, a significant impact of fines content on the regressed relationship between SPT penetration resistance and liquefaction resistance, and so developed reliable curves only for sandy soils with less than 12% fines.

The relationship proposed by Youd and Noble employs a number of field case history data points from earthquakes which have occurred since the earlier relationships were developed, and excludes the most questionable of the data used by Liao et al. The basic methodology employed, maximum likelihood estimation, is the same, however, and

as a result this correlation continues to overstate the overall uncertainty. The effects of fines content were judgmentally prescribed, a priori, in these relationships, and so were not developed as part of the regression. This correlation is applicable to soils of variable fines contents, and so can be employed for both sandy and silty soils, however, uncertainty (or variance) is high.

The relationship proposed by Toprak et al. also employs an enlarged and updated field case history database, and deletes the most questionable of the data used by Liao et al. As with the studies of Youd et al., the basic regression tool was binary regression, and the resulting overall uncertainty is again very large. Similarly, fines corrections and magnitude correlated duration weighting factors were prescribed a priori, rather than regressed from the field case history data, further decreasing model "fit" (and increasing variance and uncertainty).

Overall, these four prior relationships presented above are all excellent efforts, and are among the best of their types. It is proposed that more can now be achieved, however, using more powerful and flexible probabilistic tools, and taking fullest possible advantage of the currently available field case histories and current knowledge affecting the processing and interpretation of these.

7.3.2 Proposed SPT-Based Correlation

This section presents proposed correlations for assessment of the likelihood of initiation (or "triggering") of soil liquefaction (Cetin, et al., 2000; Seed et al., 2001). These new correlations eliminate several sources of bias intrinsic to previous, similar correlations, and provide greatly reduced overall uncertainty and variance. Indeed, the uncertainty is now sufficiently reduced that the principal uncertainty now resides where it belongs; in the engineer's ability to assess suitable CSR and representative $N_{1,60}$ values for design cases.

Key elements in the development of this new correlation were: (1) accumulation of a significantly expanded database of field performance case histories, (2) use of improved knowledge and understanding of factors affecting interpretation of SPT data, (3) incorporation of improved understanding of factors affecting site-specific ground motions (including directivity effects, site-specific response, etc.), (4) use of improved methods for assessment of in-situ cyclic shear stress ratio (CSR), (5) screening of field data case histories on a quality/uncertainty basis, and (6) use of higher-order probabilistic tools (Bayesian Updating). These Bayesian methods (a) allowed for simultaneous use of more descriptive variables than most prior studies, and (b) allowed for appropriate treatment of various contributing sources of aleatory and epistemic uncertainty. The resulting relationships not only provide greatly reduced uncertainty, they also help to resolve a number of corollary issues that have long been difficult and controversial, including: (1) magnitude-correlated duration weighting factors, (2) adjustments for fines content, and (3) corrections for effective overburden stress.

As a starting point, all of the field case histories employed in the correlations were obtained and studied. Additional cases were also obtained, including several proprietary data sets. Eventually, approximately 450 liquefaction (and "non-liquefaction") field case histories were evaluated in detail. A formal rating system was established for rating these case histories on the basis of data quality and uncertainty, and standards were established for inclusion of field cases in the final data set used to establish the new correlations. In the end, 201 of the field case histories were judged to meet these new and higher standards, and were employed in the final development of the proposed new correlations.

A significant improvement over previous efforts was the improved evaluation of peak horizontal ground acceleration at each earthquake field case history site. Specific details are provided by Cetin et al. (2000). Significant improvements here were principally due to improved understanding and treatment of issues such as (a) directivity effects, (b) effects of site conditions on response, (c) improved attenuation relationships, and (d) availability of strong motion records from recent (and well-instrumented) major earthquakes. In these studies, peak horizontal ground acceleration (a_{max}) was taken as the geometric mean of two recorded orthogonal horizontal components. Whenever possible, attenuation relationships were calibrated on an earthquake-specific basis, based on local strong ground motion records, significantly reducing uncertainties. For all cases wherein sufficiently detailed data and suitable nearby recorded ground motions were available, site-specific site response analyses were performed. In all cases, both local site effects and rupture-mechanism-dependent potential directivity effects were also considered.

A second major improvement was better estimation of in-situ CSR within the critical stratum for each of the field case histories. All of the previous studies described so far used the "simplified" method of Seed and Idriss (1971) to estimate CSR at depth (within the critical soil stratum) as

$$CSR_{peak} = \left(\frac{a_{\max}}{g}\right) \cdot \left(\frac{\sigma_v}{\sigma'_v}\right) \cdot (r_d) \tag{7.1}$$

where

a_{max} = the peak horizontal ground surface acceleration,
g = the acceleration due to gravity,
σ_v = total vertical stress,
σ'_v = effective vertical stress, and
r_d = the nonlinear shear mass participation factor.

Recognition that r_d is nonlinearly dependent upon a suite of factors led to studies by Cetin and Seed (2001a) to develop improved correlations for estimation of r_d. The results of 2,153 seismic site response analyses performed to assess the variation of r_d over ranges of (1) site conditions, and (2) ground motion excitation characteristics. It was observed that the earlier r_d proposal of Seed and Idriss (1971) understates the variance, and provides biased (generally high) estimates of r_d at depths of between 3 to 15 m. Unfortunately, it is in this depth range that the critical soil strata for most of the important liquefaction (and non-liquefaction) earthquake field case histories occur. This, in turn, creates some degree of corresponding bias in relationships developed on this basis.

Cetin and Seed (2001b) propose a new, empirical basis for estimation of r_d as a function of; (1) depth, (2) earthquake magnitude, (3) intensity of shaking, and (4) site stiffness (as expressed in Equation 7.2).

d < 65 ft:

$$r_d(d, M_w, a_{max}, V^*_{s,40'}) = \frac{\left[1 + \frac{-23.013 - 2.949 \cdot a_{max} + 0.999 \cdot M_w + 0.016 \cdot V^*_{s,40'}}{16.258 + 0.201 \cdot e^{0.104 \cdot (-d + 0.0785 \cdot V^*_{s,40'} + 24.888)}}\right]}{\left[1 + \frac{-23.013 - 2.949 \cdot a_{max} + 0.999 \cdot M_w + 0.016 \cdot V^*_{s,40'}}{16.258 + 0.201 \cdot e^{0.104 \cdot (0.0785 \cdot V^*_{s,40'} + 24.888)}}\right]} \pm \sigma_{\varepsilon r_d} \quad (7.2a)$$

d ≥ 65 ft:

$$r_d(d, M_w, a_{max}, V^*_{s,40'}) = \frac{\left[1 + \frac{-23.013 - 2.949 \cdot a_{max} + 0.999 \cdot M_w + 0.016 \cdot V^*_{s,40'}}{16.258 + 0.201 \cdot e^{0.104 \cdot (-65 + 0.0785 \cdot V^*_{s,40'} + 24.888)}}\right]}{\left[1 + \frac{-23.013 - 2.949 \cdot a_{max} + 0.999 \cdot M_w + 0.016 \cdot V^*_{s,40'}}{16.258 + 0.201 \cdot e^{0.104 \cdot (0.0785 \cdot V^*_{s,40'} + 24.888)}}\right]} - 0.0014 \cdot (d - 65) \pm \sigma_{\varepsilon r_d} \quad (7.2b)$$

where

$$\sigma_{\varepsilon r_d}(d) = d^{0.850} \cdot 0.0072 \quad \text{[for d < 40 ft], and} \quad \sigma_{\varepsilon r_d}(d) = 40^{0.850} \cdot 0.0072 \quad \text{[for d ≥ 40 ft]} \quad (7.2c)$$

It is noted, however, that in-situ CSR (and r_d) can "jump" or transition irregularly within a specific soil profile, especially near sharp transitions between "soft" and "stiff" strata, and that CSR (and r_d) are also a function of the interaction between a site and each specific excitation motion. Accordingly, the best means of estimation of in-situ CSR within any given stratum is to calculate CSR directly by means of appropriate site-specific, and event-specific, seismic site response analyses, when this is feasible. As the new correlations were developed using both directly-calculated r_d values (from site response analyses) as well as r_d values from the statistically unbiased correlation of Equation 7.2, there is no intrinsic a priori bias associated with either approach.

In these new correlations, in-situ cyclic stress ratio (CSR) is taken as the "equivalent uniform CSR" equal to 65% of the single (one-time) peak CSR (from Equation 7.1) as

$$CSR_{eq} = (0.65) \cdot CSR_{peak} \quad (7.3)$$

In-situ CSR_{eq} was evaluated directly, based on performance of full seismic site response analyses (using SHAKE 90; Idriss and Sun, 1992), for cases where (a) sufficient sub-surface data was available, and (b) where suitable "input" motions could be developed from nearby strong ground motion records. For cases wherein full seismic site response analyses were not performed, CSR_{eq} was evaluated using the estimated a_{max} and Equations 7.1 and 7.2. In addition to the best estimates of CSR_{eq}, the variance or uncertainty of these estimates (due to all contributing sources of uncertainty) was also assessed (Cetin et al., 2001).

At each case history site, the critical stratum was identified as the stratum most susceptible to triggering of liquefaction. When possible, collected surface boil materials

were also considered, but problems associated with mixing and segregation during transport, and recognition that liquefaction of underlying strata can result in transport of overlying soils to the surface through boils, limited the usefulness of some of this data.

The $N_{1,60}$-values employed were "truncated mean values" within the critical stratum. Measured N-values (from one or more points) within a critical stratum were corrected for overburden, energy, equipment, and procedural effects to $N_{1,60}$ values, and were then plotted vs. elevation. In many cases, a given soil stratum would be found to contain an identifiable sub-stratum (based on a group of localized low $N_{1,60}$-values) that was significantly more critical than the rest of the stratum. In such cases, the sub-stratum was taken as the "critical stratum". Occasional high values, not apparently representative of the general characteristics of the critical stratum, were considered "non-representative" and were deleted in a number of the cases. Similarly, though less often, very low $N_{1,60}$ values (very much lower than the apparent main body of the stratum, and often associated with locally high fines content) were similarly deleted. The remaining, corrected $N_{1,60}$ values were then used to evaluate both the mean of $N_{1,60}$ within the critical stratum, and the variance in $N_{1,60}$.

For those cases wherein the critical stratum had only one single useful $N_{1,60}$-value, the coefficient of variation was taken as 20%; a value typical of the larger variances among the cases with multiple $N_{1,60}$ values within the critical stratum (reflecting the increased uncertainty due to lack of data when only a single value was available).

All N-values were corrected for overburden effects (to the hypothetical value, N_1, that "would" have been measured if the effective overburden stress at the depth of the SPT had been 1 atmosphere) [1 atm. $\approx$ 2,000 lb/ft^2 $\approx$ 1 kg/cm^2 $\approx$ 14.7 lb/in^2 $\approx$ 101 kPa] as

$$N_1 = N \cdot C_N \tag{7.4a}$$

where C_N is taken (after Liao and Whitman, 1986) as

$$C_N = \left(\frac{1}{\sigma'_v} \right)^{0.5} \tag{7.4b}$$

where σ'_v is the actual effective overburden stress at the depth of the SPT in atmospheres.

The resulting N_1 values were then further corrected for energy, equipment, and procedural effects to fully standardized $N_{1,60}$ values as

$$N_{1,60} = N_1 \cdot C_R \cdot C_S \cdot C_B \cdot C_E \tag{7.5}$$

where C_R = correction for "short" rod length,
C_S = correction for non-standardized sampler configuration,
C_B = correction for borehole diameter, and
C_E = correction for hammer energy efficiency.

The corrections for C_R, C_S, C_B and C_E employed correspond largely to those recommended by the NCEER Working Group (NCEER, 1997).

C_S was applied in cases wherein a "nonstandard" (though very common) SPT sampler was used in which the sampler had an internal space for sample liner rings, but the rings were not used. This results in an "indented" interior liner annulus of enlarged diameter, and reduces friction between the sample and the interior of the sampler, resulting in reduced overall penetration resistance (Seed et al., 1984 and 1985). The reduction in

penetration resistance is on the order of ~10 % in loose soils (N_1<10 blows/ft), and ~30 % in very dense soils (N_1>30 blows/ft), so C_S varied from 1.1 to 1.3 over this range.

Borehole diameter corrections (C_B) were as recommended in the NCEER Workshop Proceedings.

Corrections for hammer energy (C_E), which were often significant, were largely as recommended by the NCEER Working Group, except in those cases where better hammer/system-specific information was available. Cases where better information was available included cases where either direct energy measurements were made during driving of the SPT sampler, or where the hammer and the raising/dropping system (and the operator, when appropriate) had been reliably calibrated by means of direct driving energy measurements.

Within the Bayesian updating analyses, which were performed using a modified version of the program BUMP (Geyskens et al., 1993), all field case history data were modeled not as "points", but rather as distributions, with variances in both CSR and $N_{1,60}$ These regression-type analyses were simultaneously applied to a number of contributing variables, and the resulting proposed correlations are expressed in Equations 7.6 through 7.12.

The "clean sand" (Fines Content ≤ 5%) line of Seed et al. (1984) appears to correspond roughly to P_L≈50%. This is not the case, however, as the Seed et al. (1984) line was based on biased values of CSR (as a result of biased r_d at shallow depths, as discussed earlier.) The new correlation uses actual event-specific seismic site response analyses for evaluation of in situ CSR in 53 of the back-analyzed case histories, and the new (and statistically unbiased) empirical estimation of r_d (as a function of level of shaking, site stiffness, and earthquake magnitude) as presented in Equation 7.2 (Cetin and Seed, 2000) for the remaining 148 case histories. The new (improved) estimates of in-situ CSR tend to be slightly lower, typically of the order of ~ 5 to 15% lower, at the shallow depths that are critical in most of the case histories. Accordingly, the CSR's of the new correlation are also, correspondingly, lower by about 5 to 15%, and a fully direct comparison between the new correlation and the earlier recommendations of Seed et al. (1984) cannot be made.

It should be noted that the use of slightly biased (high) values of r_d was not problematic in the earlier correlation of Seed et al. (1984), so long as the same biased (r_d) basis was employed in forward application of this correlation to field engineering works. It was a slight problem, however, when forward applications involved direct, response-based calculation of in-situ CSR, as often occurs on major analyses of dams, etc.

It was Seed's intent that the recommended (1984) boundary should represent approximately a 10 to 15% probability of liquefaction, and with allowance for the "shift" in (improved) evaluation of CSR, the 1984 deterministic relationship for clean sands (<5% fines) does correspond to approximately $P_L \approx$ 10 to 30%, except at very high CSR (CSR > 0.3), a range in which data was previously scarce.

Yoshimi et al.(1984) is arguably unconservatively biased at very low densities (low N-values) as these loose samples densified during laboratory thawing and reconsolidation. Their testing provides potentially valuable insight, however, at high N-values where reconsolidation densification was not significant. In this range, the new proposed correlation provides slightly better agreement with the test data than does the earlier relationship proposed by Seed et al. (1984).

7.3.3 Adjustments for Fines Content

The new (probabilistic) boundary curve for P_L = 20% (again normalized to an effective overburden stress of σ'_v = 0.65 atm.) represents a suitable basis for illustration of the new correlation's regressed correction for the effects of fines content. Both the correlation as well as the mean values (CSR and $N_{1,60}$) of the field case history data are not corrected for fines (this time the N-value axis is not corrected for fines content effects, so that the (P_L=20%) boundary curves are, instead, offset to account for varying fines content.)

In these current studies, based on the overall (regressed) correlation, the energy- and procedure- and overburden-corrected N-values ($N_{1,60}$) are further corrected for fines content as

$$N_{1,60,CS} = N_{1,60} * C_{FINES} \tag{7.6}$$

where the fines correction was "regressed" as a part of the Bayesian updating analyses. The fines correction is equal to zero for fines contents of FC $\leq$ 5%, and reaches a maximum (limiting) value for FC $\geq$ 35%. The maximum fines correction results in an increase of N-values of about +6 blows/ft. (at FC $\geq$ 35%, and high CSR). This maximum fines correction is somewhat smaller than the earlier maximum correction of +9.5 blows/ft proposed by Seed et al. (1984).

The regressed relationship for C_{FINES} is

$$C_{FINES} = (1 + 0.004 \cdot FC) + 0.05 \cdot \left(\frac{FC}{N_{1,60}} \right) \quad \text{lim: FC} \geq 5\% \text{ and FC} \leq 35\% \tag{7.7}$$

where FC = percent fines content (percent by dry weight finer than 0.074 mm), expressed as an integer (e.g. 15% fines is expressed as 15), and $N_{1,60}$ is in units of blows/30 cm.

7.3.4 Magnitude-Correlated Duration Weighting

Both the probabilistic and "deterministic" (based on P_L=20%) new correlations are based on the correction of "equivalent uniform cyclic stress ratio" (CSR_{eq}) for duration (or number of equivalent cycles) to CSRN, representing the equivalent CSR for a duration typical of an "average" event of M_W = 7.5. This was done by means of a magnitude-correlated duration weighting factor (DWF_M) as

$$CSRN = CSR_{eq,M=7.5} = CSR_{eq} / DWF_M \tag{7.8}$$

This duration weighting factor has been somewhat controversial, and has been developed by a variety of different approaches (using cyclic laboratory testing and/or field case history data) by a number of investigators. In these current studies, this important and controversial factor could be regressed as a part of the Bayesian Updating analyses. Moreover, the factor (DWF_M) could also be investigated for possible dependence on density (correlation with $N_{1,60}$). As observed, the dependence on density, or $N_{1,60}$-values, was found to be relatively minor.

The duration weighting factors fall slightly below those recommended by the NCEER Working group, and slightly above (but very close to) recent recommendations of Idriss (2000). Idriss' recommendations are based on a judgmental combination of interpretation of high-quality cyclic simple shear laboratory test data and empirical assessment of "equivalent" numbers of cycles from recorded strong motion time histories, and are the only other values shown that account for the cross-correlation of r_d with magnitude. The close agreement of this very different (and principally laboratory data

based) approach, and the careful (field data based) probabilistic assessments of these current studies, are strongly mutually supportive.

7.3.5 Adjustments for Effective Overburden Stress

An additional factor not directly resolved in prior studies based on field case histories is the increased susceptibility of soils to cyclic liquefaction, at the same CSR, with increases in effective overburden stress. This is in addition to the normalization of N-values for overburden effects as per Equation 7.4.

The additional effects of reduction of normalized liquefaction resistance with increased effective initial overburden stress (σ'_v) has been demonstrated by means of laboratory testing, and this is a manifestation of "critical state" type of behavior (soils become less dilatant at increased effective stress). The NCEER Working Group (Youd et al., 2001) regarding the correction factor $K\sigma$ to be used to correct to the normalized resistance to liquefaction at an initial effective overburden stress of 1 atm. ($CSR_{liq,1atm}$) as

$$CSR_{liq} = CSR_{liq,1atm}. K_\sigma \quad (7.9)$$

These current studies were not very sensitive to $K\sigma$, as the range of σ'_v in the case history data base was largely between σ'_v = 600 to 2,600 lb/ft^2, but it was possible to "regress" K_σ as part of the Bayesian updating. These are in good agreement with the earlier recommendations, and it is recommended that $K\sigma$ can be estimated as

$$K_\sigma = (\sigma'_v)^{f-1} \quad (7.10)$$

where $f \approx 0.6$ to 0.8 (as $N_{1,60,cs}$ varies from 1 to 40 blows/ft.) The field case history data of these current studies are not a sufficient basis for extrapolation of K_σ. to much higher values of σ'_v, and the authors recommend use of $\sigma'_v > 2$ atm.

The earlier relationships proposed by Seed et al. (1984), Liao et al. (1988, 1998), Youd and Noble (1997), and Toprak (1999) were all stated to be normalized to an effective overburden stress of approximately σ'_v = 1 atm (2,000 lb/ft^2). The correlation of Seed et al. (1984) was never formally corrected to σ'_v = 1 atm., however, as it was noted that the field case histories of the database were "shallow", and approximately in this range. The database was, however, not centered at σ'_v = 1 atm., but rather at lesser overburden (Mean $\sigma'_v \approx$1,300 lb/ft^{2}or 0.65 atm), and this proves to render this earlier relationship slightly unconservative if taken as normalized to σ'_v = 1 atm. (The same is true of all of the previous relationships discussed.) It should be noted, however, that this unconservatism is minimized if the correlations are applied at shallow depths.

For correctness, and to avoid ambiguity, both the earlier relationship of Seed et al. (1984), and the correlations developed in these current studies, need to be formally normalized to σ'_v = 1 atm. Accordingly, in these studies, all data are corrected for K_σ-effects (by Equations 7.9 and 7.10); not just those data for which $\sigma'v$ was greater than 1 atm. A recommended limit is $K_\sigma \leq 1.5$ (at very shallow depths.)

The overall correlation can be expressed in parts, as in the previous sections (and Equations 7.6 - 12). It can also be expressed concisely as a single, composite relationship as shown in Equation 7.11.

$$P_L(N_{1,60}, CSR, M_w, \sigma'_v, FC) = \Phi\left(-\frac{\begin{pmatrix} N_{1,60}\cdot(1+0.004\cdot FC)-13.32\cdot\ln(CSR)- \\ 29.53\cdot\ln(M_w)-3.70\cdot\ln(\sigma'_v) \\ +0.05\cdot FC+44.97 \end{pmatrix}}{2.70}\right) \quad (7.11)$$

where
P_L = the probability of liquefaction in decimals (i.e. 0.3, 0.4, etc.)
Φ = the standard cumulative normal distribution. Also the cyclic resistance ratio, CRR, for a given probability of liquefaction can be expressed as:

$$CRR(N_{1,60}, CSR, M_w, \sigma'_v, FC, P_L) = \exp\left[\frac{\begin{pmatrix} N_{1,60}\cdot(1+0.004\cdot FC)-29.53\cdot\ln(M_w) \\ -3.70\cdot\ln(\sigma'_v)+0.05\cdot FC+44.97+2.70\cdot\Phi^{-1}(P_L) \end{pmatrix}}{13.32}\right] \quad (7.12)$$

where

$\Phi^{-1}(P_L)$ = the inverse of the standard cumulative normal distribution (i.e. mean=0, and standard deviation=1)

note: for spreadsheet purposes, the command in Microsoft Excel for this specific function is "NORMINV(P_L,0,1)"

7.4. GIS-BASED LIQUEFACTION TRIGGERING ASSESSMENT FOR SAKARYA AND GÖLCÜK CITIES

In this section of the report, potential applications of previously discussed methodologies for the assessment of liquefaction triggering potential will be presented. For this purpose, it was intended to assess liquefaction triggering potentials of the cities of Sakarya and Gölcük shaken by August 17, 1999 Kocaeli earthquake, M_w=7.4.

The geotechnical engineering parameters needed for the assessment were selected as soil classification parameters such as liquid limit (LL), plastic limit (PL), and fines content (FC) as well as SPT blow counts and depth to water table. For the estimation of these parameters over 500 boreholes and over 5000 SPT blow count values were reviewed as summarized in Table 7.1. After an intensive data quality screening studies based on the availability of LL, PL, and FC values, the resulting database was reduced to over 3000 SPT blow count values obtained from over 470 boreholes. Figures 7.5 presents the locations of the "high" quality boreholes used for liquefaction assessment studies for the cities of Sakarya and Gölcük, respectively. A detailed presentation of the individual boring logs as well as the geotechnical engineering parameters associated with each soil layer is available in GIS (Map-info) and MS Excel formats.

Table 7.1. A summary of reviewed and used borelog and SPT blowcount values for liquefaction assessment analyses

	BORELOG	
CITY	TOTAL #	USED #
SAKARYA	263	251
GÖLCÜK	306	220
	SPT BLOWCOUNTS	
	TOTAL	USED
SAKARYA	2334	2324
GÖLCÜK	3544	757

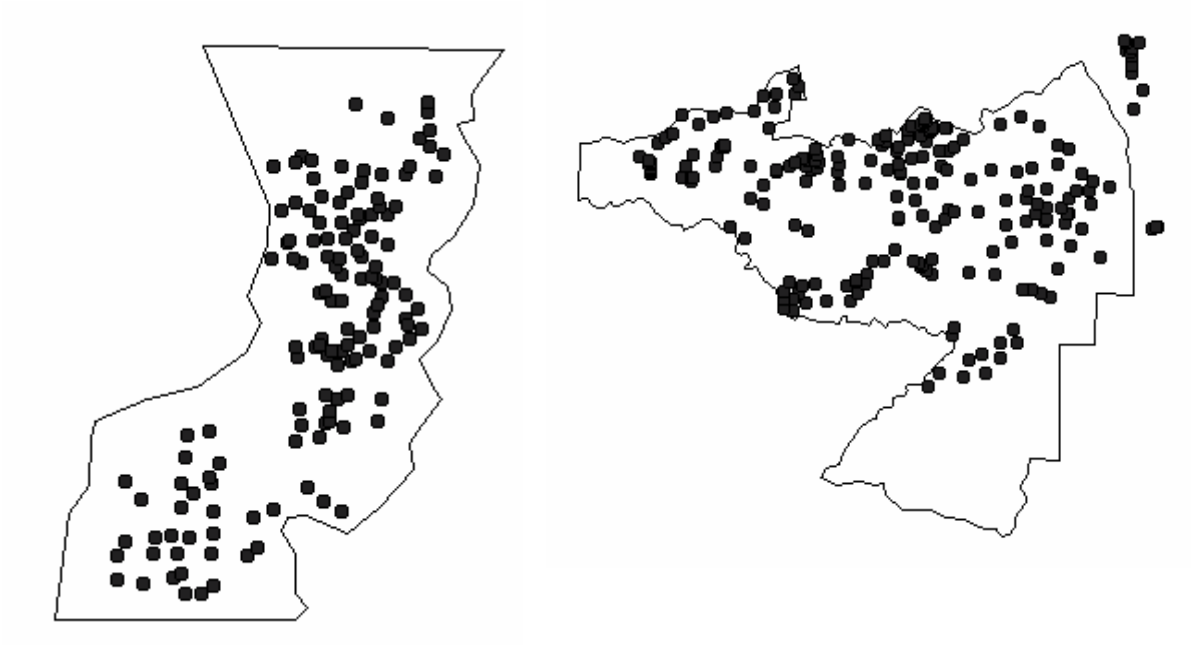

(a) (b)

Figure 7.5. Locations of the boreholes used for liquefaction triggering studies in (a) Sakarya and (b) Gölcük.

In addition to the geotechnical engineering parameters mentioned previously, for the estimation of CSR, the variation of peak ground acceleration and/or cyclic shear stresses values at soil sites after August 17, 1999 Kocaeli earthquake, within the cities of Sakarya and Gölcük need to be estimated. For the sake of presenting demonstration applications, peak ground acceleration at soil sites were adopted uniformly as 0.4 g for CSR estimations.

After having compiled geotechnical and earthquake engineering parameters, liquefaction triggering potential for both cities were performed as presented in the Liquefaction Assessment Section of the State of the Art Report. SPT blow counts were corrected for equipment, energy and procedural effects. The energy ratio was assumed to be 45% unless it was reported otherwise. CSR values were estimated based on the assumption of peak ground acceleration at soil sites to be 0.4 g. R_d values were adopted by following the mean curves as also presented in the Liquefaction Assessment Section of the State of the Art Report. The effects of soil structure interaction on the estimation of CSR as well as the liquefaction performance of soils were not incorporated for the sake of simplicity. This simplification is consistent with the potential use of these methodologies

since the main aim of this project is to assess liquefaction risk of undeveloped areas rather than the ones that have developed already contrary to our demonstration cases.

Once CSR, σ'_v, FC, $N_{1,60}$ values for each critical soil layer which were identified by checking the criteria summarized by Andrews and Martin (2000), probability of liquefaction values were estimated as defined in Eq. 7.11. Similarly, factor of safety values corresponding to 20 % probability of liquefaction-CRR contours can also be estimated as defined in Eq. 7.12. Figures 7.6 and 7.7 present maps of liquefaction triggering assessment studies for the cities of Sakarya and Gölcük, respectively. Red zones define the regions where liquefaction triggering probability after August 17, 1999 Kocaeli earthquake is predicted to be greater than 90 %. Similarly, orange and yellow zones define the regions, where liquefaction triggering probabilities after August 17, 1999 Kocaeli earthquake are predicted to be in the range of 70 % - 90 % and 50% to 70 %, respectively. Green, light and deep blue regions, listed in the order of higher to lower risk, are classified as the zones where liquefaction triggering probabilities are estimated to be less than 50 %.

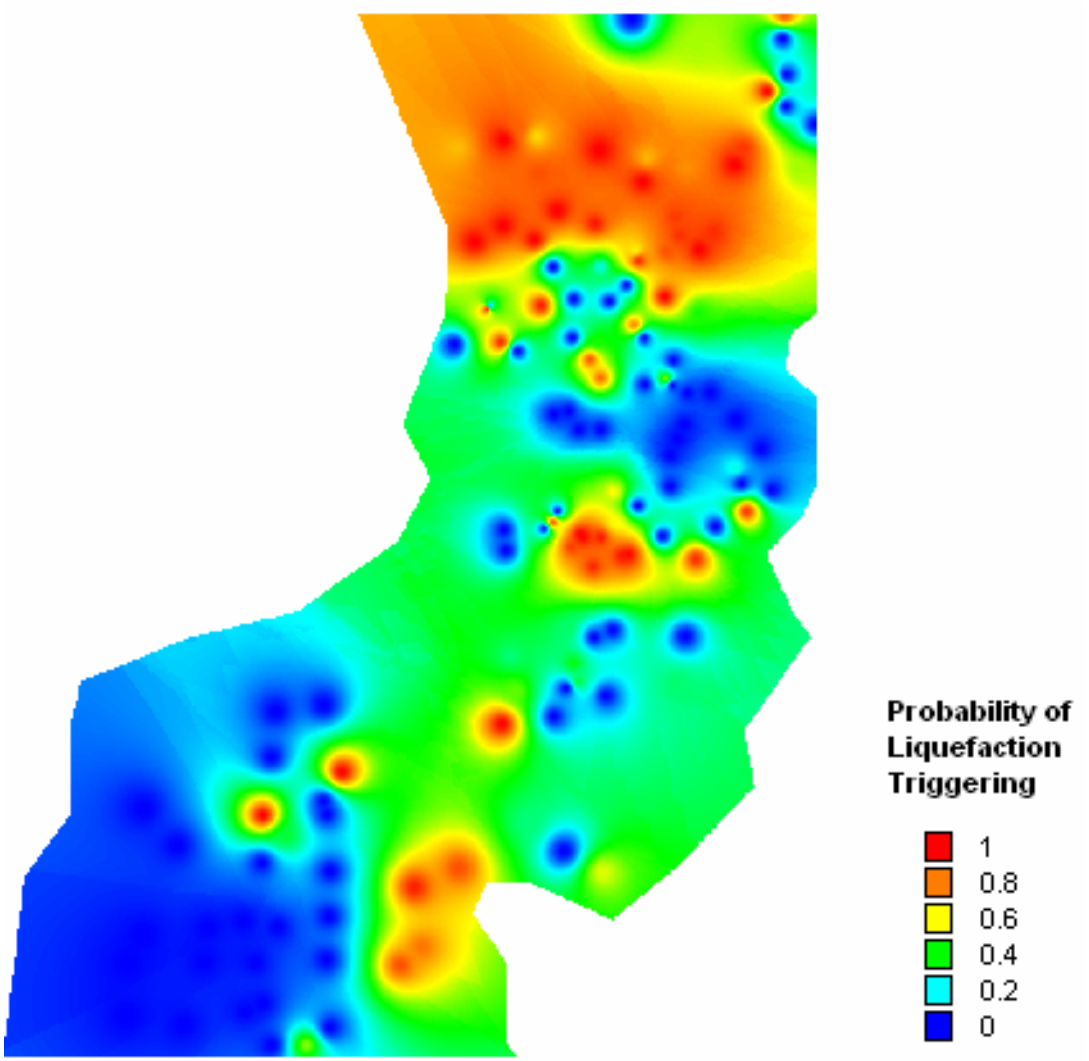

Figure 7.6. Liquefaction triggering potential of Sakarya after 17 August, 1999 Kocaeli earthquake, expressed in terms of probability of liquefaction

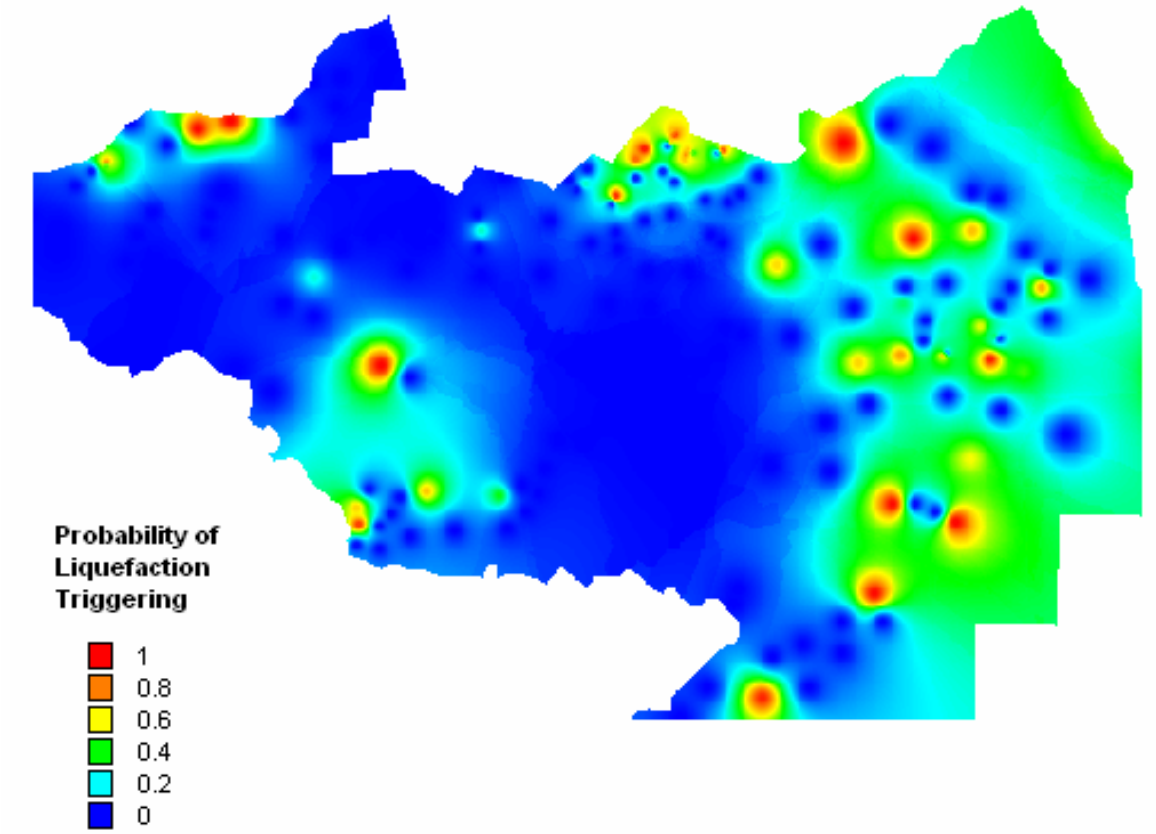

Figure 7.7. Liquefaction triggering potential of Gölcük after 17 August, 1999 Kocaeli earthquake

8. LANDSLIDE HAZARD

Bilge Siyahi and Yasin Fahjan, Department of Earthquake Engineering, Kandilli Observatory and Earthquake Research Institute, Boğaziçi University

8.1. INTRODUCTION

Siyahi and Ansal (1993) have proposed a procedure for investigating slope stability for microzonation purpose. This procedure is introduced in the "Manual for Zonation on Seismic Geotechnical Hazards" by TC4, ISSMFE (1999) as a Grade-3 method. Applicability of this procedure was confirmed against an earthquake that occurred in 1967 in the Adapazarı region, Turkey. The stability analysis method is a pseudo-static evaluation of slope stability utilizing a seismic coefficient A to account for the earthquake induced horizontal forces.

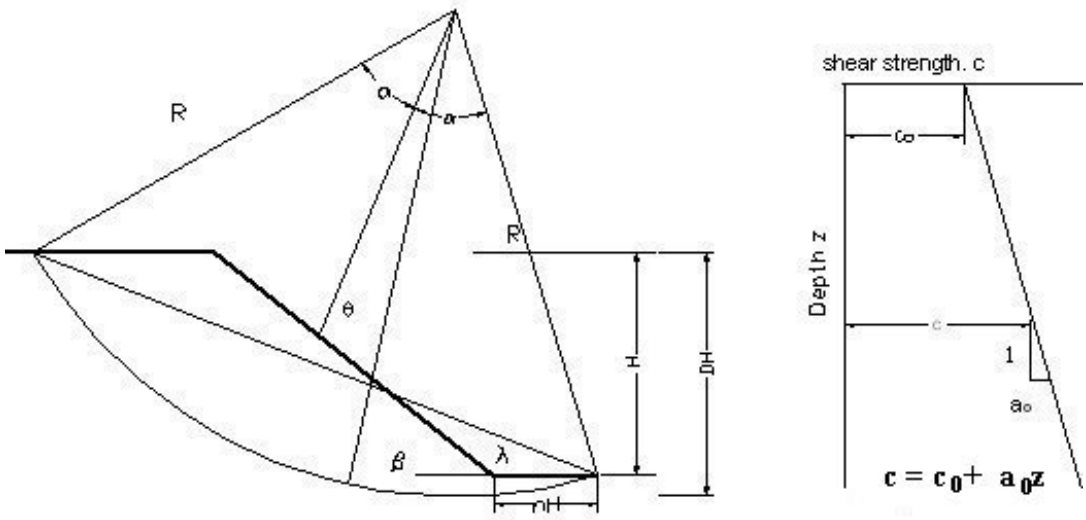

Figure 8.1. A typical section of a slope

A linear variation in shear strength τ with depth is assumed and the potential failure surface is taken as a circular arc, as shown in Figure 8.1.
The safety factor is calculated as

$$F_s = \frac{a_0}{\gamma} N_1 = \frac{\gamma \tan\phi}{\gamma} N_1 = N_1 \tan\phi \tag{8.1}$$

based on the angle of shear strength and stability number N_1 representing the configuration of the slope and failure surface. The minimum value of the stability number is determined by carrying out a parametric study in terms of α, β, γ, and n to find out the most critical failure surface as given in Figure 8.2. The variation of minimum N_1 can be expressed as a function of β (slope angle) and A (maximum ground acceleration on the surface). It becomes possible at this stage to calculate minimum safety factor Fs, if a ϕ value can be determined or estimated.

This procedure assumes a circular arc failure and normally consolidated soil. Although all the slopes are not of this type, it can be considered as the most critical condition. Because this procedure is simplified, the failure and parametric study approached is applied. There are generally varieties of slope characteristics in the areas

and it is difficult to identify slope failure parameters for every slope in detail. Therefore this procedure is applied to be able to make a qualitative evaluation of slope stability.

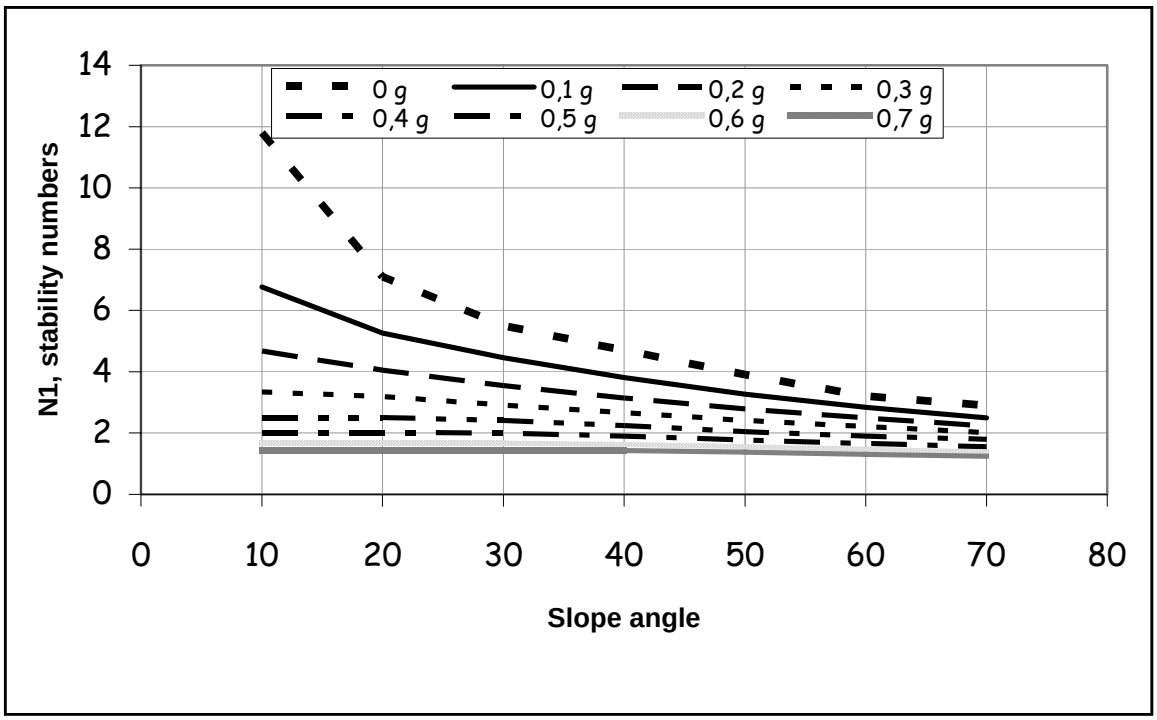

Figure 8.2. Relationship between slope angle (β), seismic coefficient (A) and minimum stability number (N1) (Siyahi,1998)

8.2. PROCEDURE OF ANALYSIS AND EVALUATION OF STABILITY

The outline of the evaluation method is described below and shown in Figure 8.3. The maximum slope gradient for each 50-m grid, that covers all of the area, is calculated at first. Then the slope stability of each point is judged, using Siyahi and Ansal (1993) procedure taking the maximum ground acceleration value and strength of soil into account.

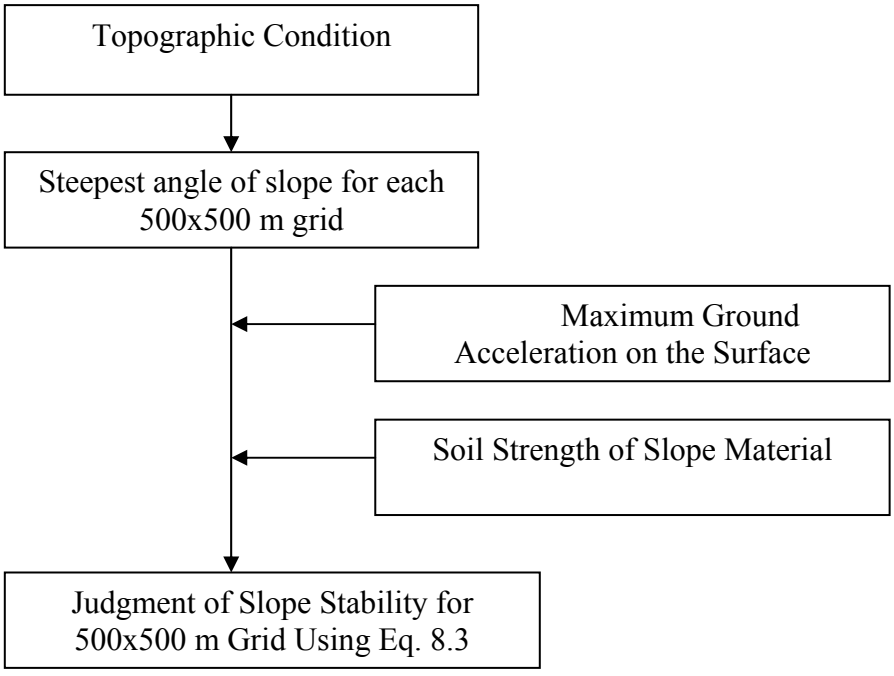

8.3. PARAMETERS FOR CALCULATION

8.3.1 Shear Strength of Slope Material

Shear strength is the most important parameters for applying this procedure. The values of strength adopted are summarized in Table 8.1 for the Adapazarı and Gölcük regions. These are evaluated from data obtained from boreholes in these regions. Since the borehole data covers laboratory and in-situ testing such as SPT, shear box, triaxial and uniaxial tests, for soil and rock deposits in the region, to find the actual values of shear strength, which is represented here such as shear strength angle, ϕ, or alternatively as the internal friction angle, is rather straightforward in this case.

Table 8.1. Shear strength angle for slope stability calculations in the Adapazarı and Gölcük regions.

Ages of the deposits	Formation	Shear strength angle, ϕ (°)	Description of soil and rock units
Quaternary	Alluvium in Adapazarı	25	Sand, gravel, silt, clay
Holocene	Alluvium in Gölcük	25	Sand, gravel, silt, clay
Upper Cretaceous	Akveren (Adapazarı)	35	Conglomerates, sandstone, limestone
Plioecene	Aslanbey (Gölcük)	30	Sand, gravel, silt and clay (loosely consolidated fluvial alluvium)
Recent	Fill (Gölcük)	15	Gravel and cobble-boulder blocks

8.3.2 Maximum Ground Acceleration on the Surface

Within a pseudo-static approach, the effects of an earthquake are represented by constant horizontal and vertical accelerations. Selection of an appropriate pseudo-static coefficient is the most important aspect of a pseudo-static stability analysis. In this procedure, maximum ground acceleration (A) on the surface can be accepted as a pseudo-static coefficient. Maximum ground acceleration on the surface is evaluated based on the one-dimensional ground response analysis as performed by ETHZ.

8.3.3 Slope Angle

The topographical contours are provided in terms of Mapinfo tables. The minimum distance among subsequent contours for each cell is computed using the (Ruler) option provided in Mapinfo. The relevant steepest slope gradient for each Geo-cell is calculated using the minimum distance and elevations difference in the subsequent contours.

8.4. SLOPE STABILITY COMPUTATION USING KOERISLOPE

KoeriSlope is application developed to estimate slope stability for microzonation purposes. KoeriSlope Version 1.0 in its current form is capable of performing slope stability estimation analysis based on the Siyahi and Ansal (1993) procedure. KoeriSlope is a user-friendly application that operates through Geo-cells systems. Geo-cells (Grids) facilitate the manipulation of data for soil type, slope gradient and earthquake hazards. The application is developed using the MapBasic language and runs efficiently under MapInfo software. The application is integrated with MapInfo and capable to utilizing the powerful features in displaying, querying, manipulating and mapping inventory databases.

KoeriSlope can be launched under MapInfo using the <Run MapBasic Program> feature from the standard menu bar of MapInfo. The main dialog of the application is shown below.

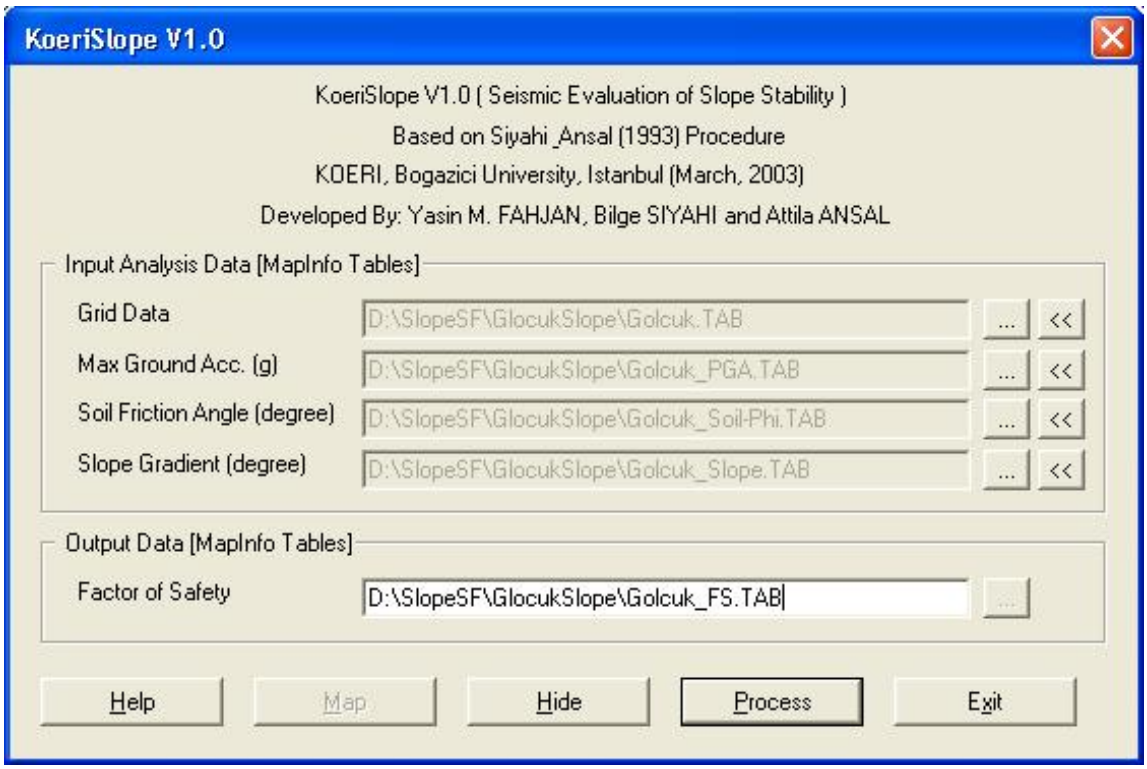

Figure 8.3. Main Dialog of KoeriSlope Application

8.4.1 Data Needed for the Slope Stability Study

In order to perform a slope stability analysis, the following input data should be provided for each Geo-cell.

- Maximum expected ground acceleration (seismic coefficient).
- Soil friction angle.
- Maximum slope gradient.

8.4.2 Output of the Analysis

The application computes the N1 stability number, based on the seismic coefficient of acceleration and slope gradient for each Geo-cell. Then slope stability safety factor for each Geo-cell is calculated, as it is described in Eq. (8.1). An output File is provided including all the input information for each Geo-cell in addition to the stability number (N1) and the slope stability factor of safety (FS). A thematic map of the results is also provided as shown in Chapter 11.

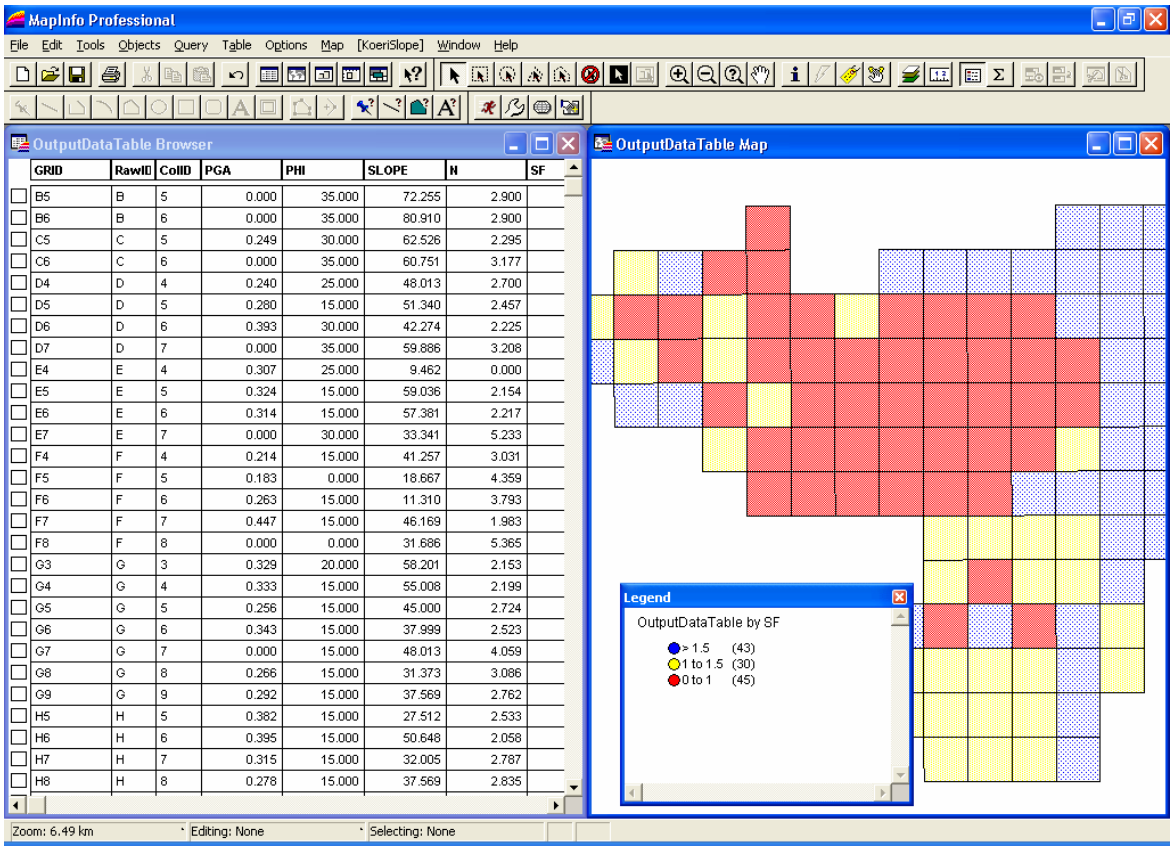

GRID	RawID	ColID	PGA	PHI	SLOPE	N	SF
B5	B	5	0.000	35.000	72.255	2.900	
B6	B	6	0.000	35.000	80.910	2.900	
C5	C	5	0.249	30.000	62.526	2.295	
C6	C	6	0.000	35.000	60.751	3.177	
D4	D	4	0.240	25.000	48.013	2.700	
D5	D	5	0.280	15.000	51.340	2.457	
D6	D	6	0.393	30.000	42.274	2.225	
D7	D	7	0.000	35.000	59.886	3.208	
E4	E	4	0.307	25.000	9.462	0.000	
E5	E	5	0.324	15.000	59.036	2.154	
E6	E	6	0.314	15.000	57.381	2.217	
E7	E	7	0.000	30.000	33.341	5.233	
F4	F	4	0.214	15.000	41.257	3.031	
F5	F	5	0.183	0.000	18.667	4.359	
F6	F	6	0.263	15.000	11.310	3.793	
F7	F	7	0.447	15.000	46.169	1.983	
F8	F	8	0.000	0.000	31.686	5.365	
G3	G	3	0.329	20.000	58.201	2.153	
G4	G	4	0.333	15.000	55.008	2.199	
G5	G	5	0.256	15.000	45.000	2.724	
G6	G	6	0.343	15.000	37.999	2.523	
G7	G	7	0.000	15.000	48.013	4.059	
G8	G	8	0.266	15.000	31.373	3.086	
G9	G	9	0.292	15.000	37.569	2.762	
H5	H	5	0.382	15.000	27.512	2.533	
H6	H	6	0.395	15.000	50.648	2.058	
H7	H	7	0.315	15.000	32.005	2.787	
H8	H	8	0.278	15.000	37.569	2.835	

Figure 8.4. Output of the KoeriSlope Application

9. BACKGROUND REPORT ON STRUCTURAL DAMAGE; DEVELOPMENT AND IMPLEMENTATION OF A BUILDING DAMAGE SURVEY FOR ADAPAZARI, TURKEY: INTERPRETATION AND SOILS CORRELATION

P. Gülkan, S. Bakır, A. Yakut, T. Yılmaz and U. Yazgan (METU) with Collaboration of M. Elmas (SU) and P. Lestuzzi (EPFL)

9.1. EXECUTIVE SUMMARY

Turkey is among countries that have long been affected by natural disasters, in particular earthquakes and floods. The most recent series of devastating earthquakes in 1999 have caused loss of lives of thousands and created an enormous financial burden on the economy, government, industry, insurance sector and public. Rigorous impact of these disasters led the Government of Turkey to initiate a legal revision to explore a natural catastrophe risk management strategy including ways of promoting disaster insurance. For this purpose, various studies financed under loans obtained from the World Bank have been completed. As a result, the Government of Turkey has decided to introduce a compulsory earthquake scheme making it mandatory for residences to take out insurance starting from September 27, 2000. The legal framework of the new scheme has been established by a decree (No. 587) with power of law for Compulsory Earthquake Insurance. A decree is a fast-track legal instrument that must be amended and adopted by parliament within a prescribed time limit. The decree has created the Turkish Catastrophe Insurance Pool (TCIP) for the purpose of relieving the Government of having to provide compensation to earthquake victims. A natural consequence of the creation of TCIP has been a renewed perception to set up a global damage assessment and quantification system for compensation of policy holders. Because of its past experience in such matters, the Disaster Management Research and Implementation Center at Middle East Technical University (DMC/METU) has been contracted by GDDA to train damage assessors. The present contract work described below has been an outgrowth of this experience to ascertain connections between local geological conditions and structural damage distribution patterns.

A parallel activity toward earthquake hazard mitigation was a study funded by the Government of Switzerland and executed through the World Institute for Disaster Risk Management (DRM) to produce a microzonation manual for local governments to follow when making land use decisions with the aim of minimizing seismic risks. The Government of Turkey is represented in this project through the General Directorate of Disaster Affairs because it is through this agency that regulations requiring such studies to be undertaken by municipalities can be issued. Microzonation is not an end to itself but a useful tool that facilitates reaching rational land-use decisions that safeguard public safety from the seismic peril. The region centered around the city of Adapazarı in northwestern Turkey was chosen as the natural site for the case studies because of extensive damages closely linked to improper consideration of local geology in the area. The global research teams are comprised of specialized groups, both international and Turkish, that carries out a coordinated set of activities to produce the Manual of Practice for Microzonation and its supporting documentation.

The World Institute for Disaster Risk Management engaged DMC/METU in order to perform services in respect of “Consultancy Services for Microzonation for Earthquake Risk Mitigation” in accordance with the following conditions:

- Provision of limited data for geotechnical studies in the case study regions (with the bulk of the data coming from other subcontractors in the project)
- Analysis of structural performance of buildings in case study regions
- Analysis of land use management practices at the municipal level
- Preparation of a report including recommendations for strengthening of land use management for earthquake safety

An itemization of the tasks required under this obligation is reproduced below:

- Collection and organization of relevant geological and geotechnical data for the case study areas
- Collection of structural damage data locally through services provided by Sakarya University (SU)
- Preparation of data in transportable GIS format
- Establishing liaison with IS-ENAC EPFL in data identification, definition of data format and review of literature

A great deal can be learned from the pattern of damage experienced in recent or historic earthquakes. Damage patterns correlate well with the distribution of shaking intensity and the relationship of structural conditions with site conditions. Within the corresponding phase of the services DMC/METU was to provide analysis of site conditions to structural performance, drawing from the data collected by SU. Preparation of maps of damage patterns from Adapazarı was an objective. Determination of specific procedures to assess the vulnerability of local construction and description of these practices for inclusion in the Manual were also cited as output from this work. A separate task was subsequently appended to the DMC/METU work package to study the liquefaction vulnerability of the municipal area of Adapazarı and Gölcük, expressing the output in terms of probability numbers.

DMC/METU is also committed to ensuring the sustained implementation of the set of good practices that will be identified in the Manual. To this end, the analytical evaluation of the legal bases for land use management and its regulatory practice will be submitted to DRM under a separate package. Training of municipal personnel and public information on land use management are also parts of this other package.

The present report is intended to answer the question of whether the damage patterns in Adapazarı are indicative of a consistent trend explicable in terms of local site conditions. For this purpose a total of 301 buildings that had collapsed fully were evaluated. This exercise was necessarily a desk study conducted from the design blueprints of the individual buildings. The data collection was done in accordance with the form reproduced in Appendix 5.1, and its interpretation is contained in Section 9.2. None of the buildings in this data set existed at the time of our studies, so there remain a good number of points that must be known if accurate projections for the cause of the damage were to be identified. As a complementary body of data we have also included in Section 9.3 an explanation of the rationale for the damage assessment form used by personnel of GDDA is outlined. The form used in customary practice is given in Appendix 5.2.

Can a correlation be established between structural damage observed in Adapazarı and site conditions? This question is tackled in Section 9.4 on the basis of borehole and laboratory data from soils investigations performed in Adapazarı municipal limits.

9.2. COLLAPSE DAMAGE SURVEY IN ADAPAZARI

9.2.1 Introduction

Adapazarı was the scene of spectacular structural damage as well as widespread liquefaction that occurred in the city. The damage survey was conducted during the summer of 2002, nearly three years after the actual event. By that time, extensive repairs had been done in surviving buildings, and many others had been demolished and removed. Homeowners were reluctant to permit another round of examinations to be conducted in their property, so the decision was reached to include those buildings that had collapsed during the earthquake, and had led to loss of human life. When such is the case, the law requires expert witnesses to prepare an affidavit that will establish who the culprits might be. The Department of Civil Engineering, Sakarya University, because of their proximity to the site, had served in this capacity for many buildings on the basis of design blueprints and structural calculations, so the decision was reached to utilize that information source under a new magnifier. The information was extracted through the form reproduced in Appendix 5.1, assuming that the drawings were an accurate replication of the as-built structure. The location coordinates of the buildings were determined by a hand-held GPS device, accurate to about 10 m. This was judged to be an acceptable error.

9.2.2 Building Morphology

The buildings reported by SU were situated in the locations in Figure 9.1. This figure is deliberately superposed on the analog map of the city because even with its poor legibility it allows urban features such as major roads and the Sakarya River banks on the east. The same information is repeated in Figure 9.2 where the districts in the city have been numbered, and the number of stories of these collapsed buildings coded to allow a rapid assessment of the building heights. Building heights are as much a function of the economics of the corresponding usage as it is of zoning laws enacted by the city government. In central urban areas in Turkey there is commonly a mixed form of occupation, where small businesses (small grocery shops, barber shops, lawyers or physicians offices, etc.) are dispersed among the residences under the same roof. The ground story is usually made as free of obstructions to human traffic as possible, and this leads to weak or soft stories at the level where the seismic demand is largest. Figure 9.3 shows that half of the buildings examined in this study were five stories in height. The next largest group is for six story buildings comprising 32 percent of the total, and this is typical for much of recent construction.

The information contained in Figures 9.1-9.3 is useful to establish the overall architectural characteristics of the housing stock in Adapazarı. We believe that extrapolations can safely be made from these figures for reaching general conclusions. There is also reason to believe that most of the buildings in the sample group dated from the post-1975 period, so that their earthquake designs were done according to the provisions of the 1975 edition of that code.

The total number of building in the data set was 301. Interpretation as absolute numbers of normalized graphs in the following will be facilitated when those figures are multiplied with this sum. All buildings were reinforced concrete frames.

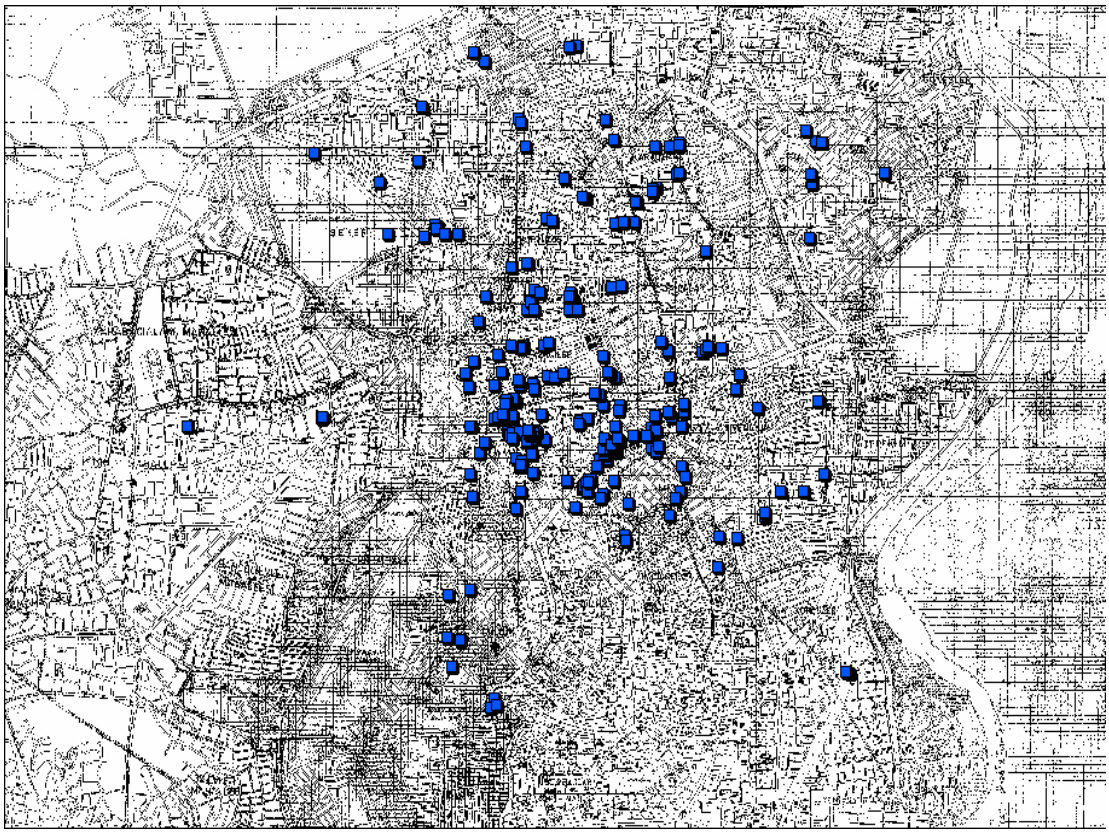

Figure 9.1. Building Locations

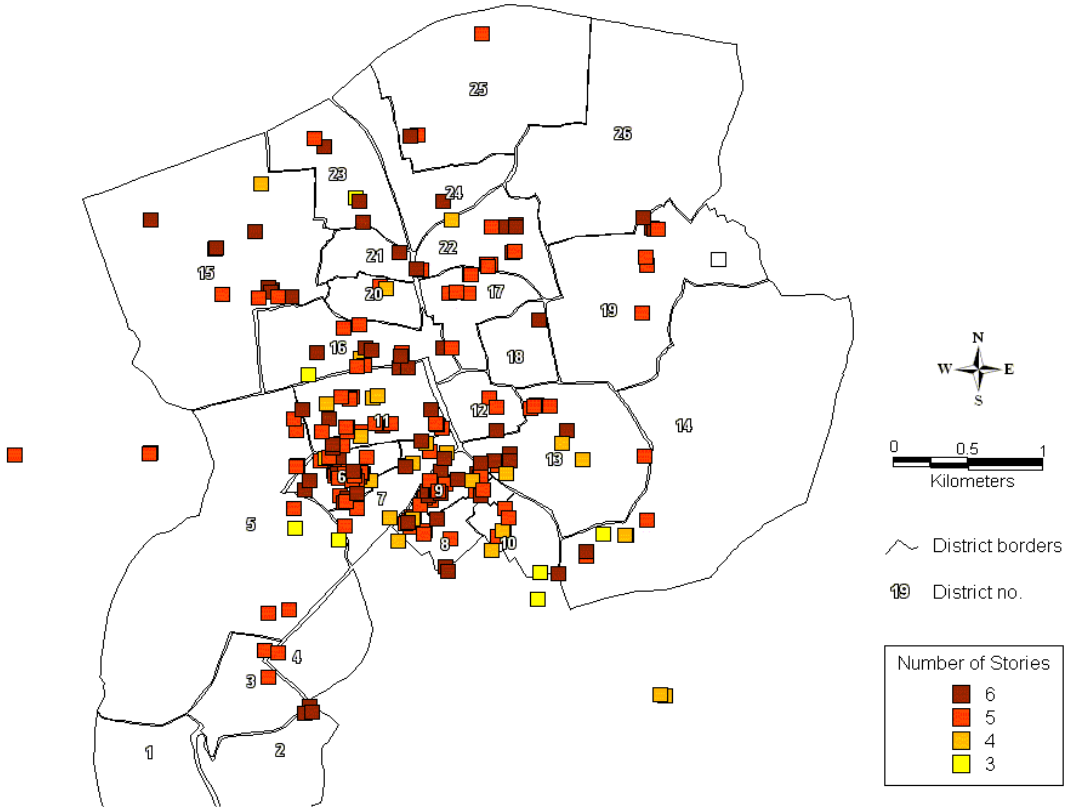

Figure 9.2. Building Locations Differentiated according to Height

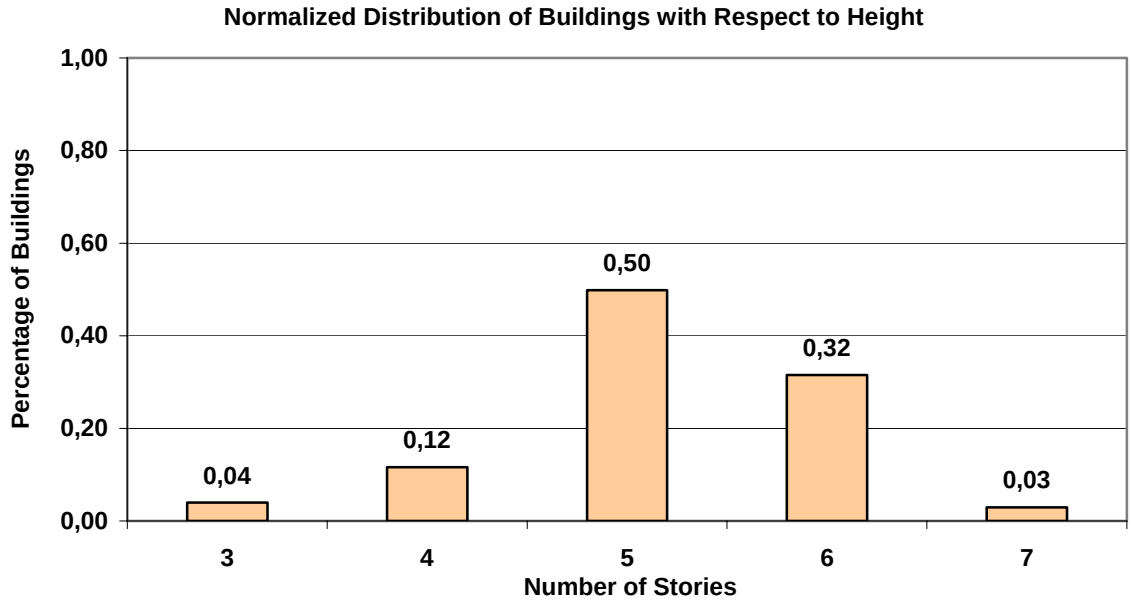

Figure 9.3. Distribution of Building Height in the Sample

9.2.3 Architectural and Structural Features

The current Turkish earthquake regulations make a clear definition of structural irregularities that lead to added earthquake vulnerability. In general, irregularities in plan are classified as being of type A, with sub-group designated as A1, A2, etc., and irregularities in elevation are described as being of type B. These are each described, and follow universal procedures for quantification. The questions listed under "Irregularities" in the form in Appendix 5.1 have been designed to clarify the prevalence of the distribution of these among the sample of buildings examined by SU.

It is instructive to examine first the distribution of soft stories. A soft story occurs when the lateral rigidity of the horizontal load resisting members at any level is such that the average lateral drift under the design load at that level is more than 50 percent larger than the same quantity calculated for the next story. This property needs a set of calculations to be made. With taller columns and no infill or structural walls, this situation usually is encountered at the ground level in Turkey. In Figure 9.4 we have shown the distribution of this situation in normalized fashion among the buildings in the sample set.

It can be assumed that taller buildings were of more recent dates of construction, and as building height limitations had been eased in recent times owners took advantage of the full height permitted in the zonation decisions. It is quickly seen that while (older) 3-story buildings were evenly distributed with respect to existence of soft stories, taller buildings were about 70 percent that way, and the seven story subset was entirely rated as having the property. In general, the situation for identifying a weak story where the lateral strength at a given story differs by more than 20 percent that at the neighboring story did not arise because designers accounted for that by varying the reinforcement details.

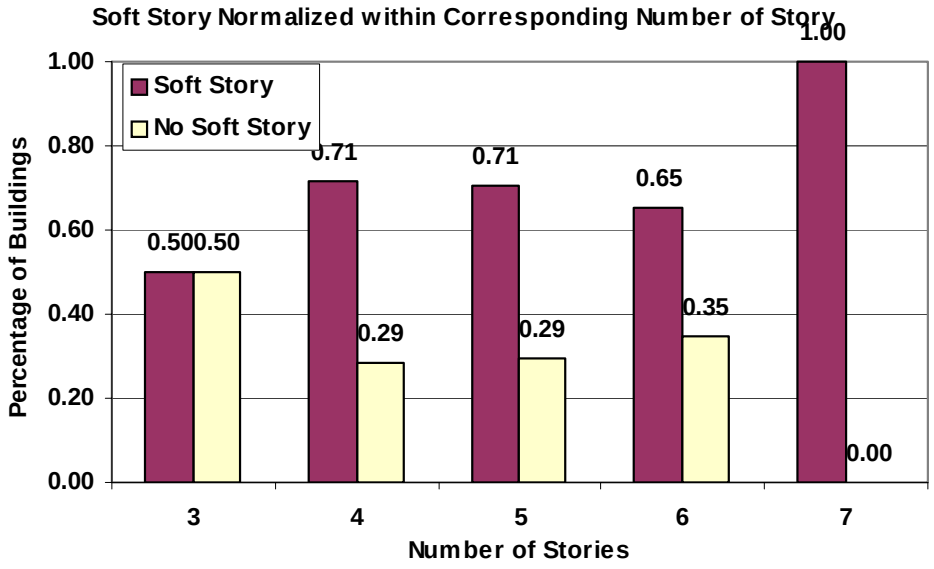

Figure 9.4. Distribution of Soft Stories

Torsional irregularity is defined in the Turkish code as the situation when the average lateral translation under the design forces at a given story differs by more than 20 percent the largest lateral situation at the same story. This usually occurs at the extreme ends of the floor slabs when L-, T- or similar shapes in plan exist. Land ownership patterns sometimes force architects to design such buildings when they wish to take advantage of utilizing the entire buildable footprint area of the land. Figure 9.5 describes the distribution of this property among our sample set.

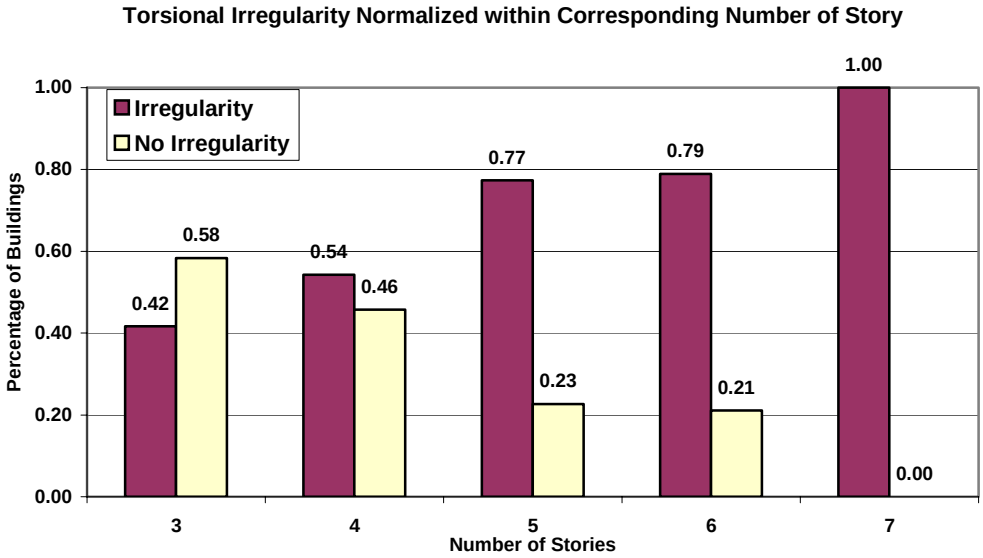

Figure 9.5. Existence of Torsional Irregularity

Plan irregularity refers to the situation when long projections in plan exist for the building. In addition to the increased likelihood of causing torsional irregularity this situation creates re-entrant corners where stresses are concentrated, and may cause unexpected distress. The data in Figure 9.6 describes this situation. Again taller buildings seem to be more likely to possess this characteristic.

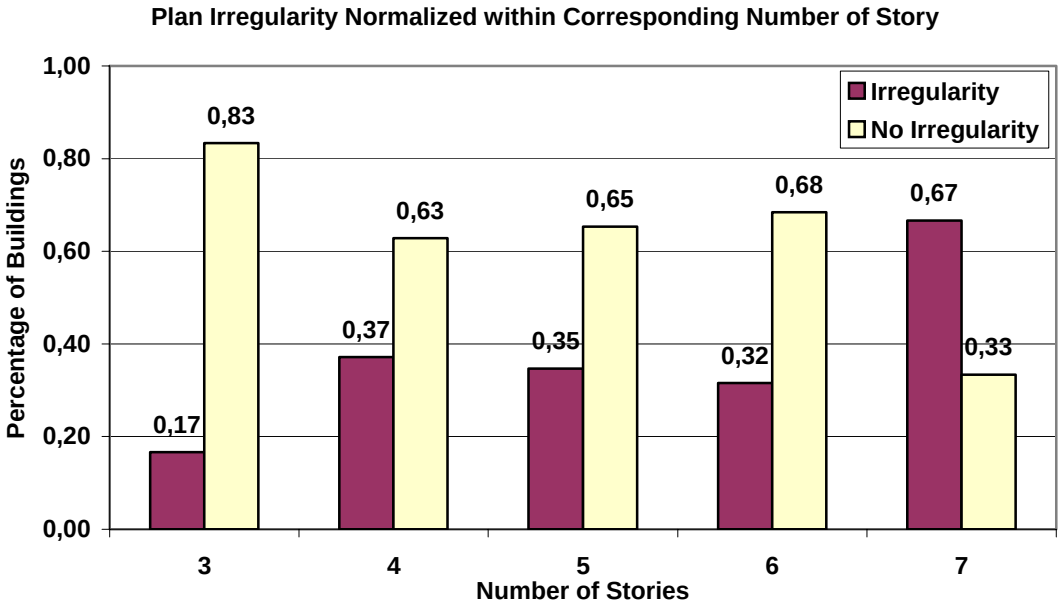

Figure 9.6. Existence of Plan Irregularity

From the structural viewpoint, mezzanines can prove to be trouble spots because the lateral strength of short and tall columns are different by large amounts, and the extra inertia effects transmitted to columns at their mid-height are difficult to account for. As Figure 9.7 shows, this situation appears not to have been a widespread practice.

While the post-collapse damage form in Appendix 5.1 has entries for material quality, workmanship and similar features it was not possible to conduct any tests on actual material coupons or cylinders to answer this with clarity. We have relied on the intended material qualities on the calculation sheets which was generally specified as 20 MPa. It is known that the actual strengths may differ by large margins from their intended values. We have also no factual data on whether plain or deformed bars had been used.

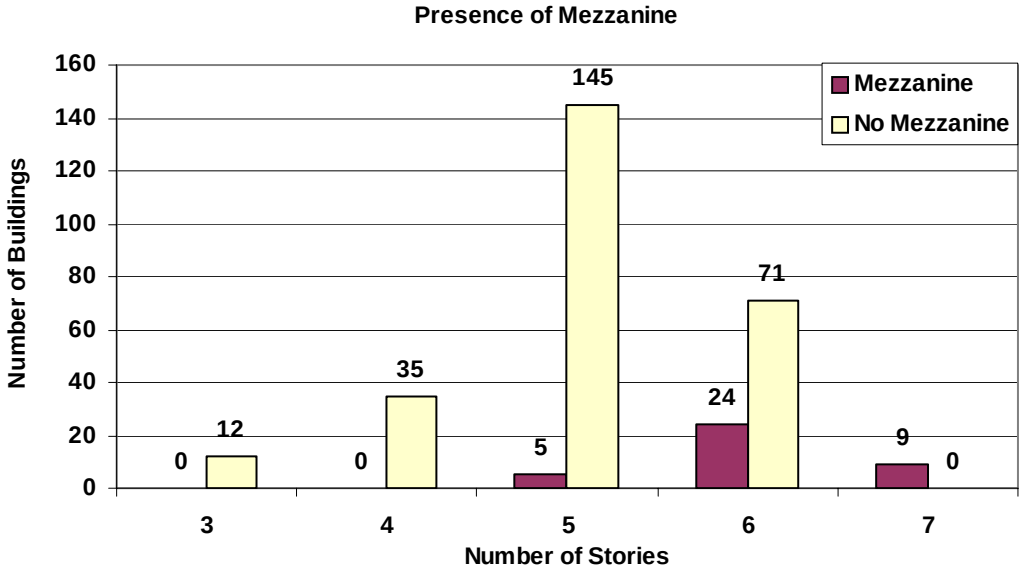

Figure 9.7. Occurrence of Mezzanine Floors at Ground Level

9.2.4 Column and Wall Indexes

Our experience with the seismic vulnerability of the housing stock in Turkey has taught us that the normalized column and wall areas a given building possesses can serve as a useful index (Shiga et al., 1968; Gülkan & Sözen, 1999). The central idea for expressing vulnerability is expressed as the weight of the structure (which is proportional to its total floor area) divided into the sum of the cross-sectional areas of the columns and walls at the base. This format is attractive because of the ease with which the data can be acquired. Lengthy calculations are not necessary. The outcome is a crisp numerical index that can be matched against a derived yardstick so that a judgment about the vulnerability can be stated. The paper by Shiga et al. is difficult to generalize because it was derived exclusively in relation to a particular group of buildings constructed in accordance with the Japanese practice of the 1960s. Recalibrating their format can best be accomplished by testing its predictive success against observed damage in a collection of buildings with dimensional and material properties based on random choices made during the design and construction stages. This way, the question of whether a rational explanation of the empirical evidence is contained in the theory can be answered with confidence.

Conventional design procedures focus on arriving at proper component dimensions that will accommodate prescribed forces, but a more important issue is to keep structural displacements within prescribed limits. This idea has gained popularity in recent years as the central principle of performance based earthquake design. The concept of limiting ground level drift to prescribed limits was tested against empirical data collected in Erzincan following a major earthquake there in 1992. The article by Gülkan & Sözen (1999) contains the rationalization of the concept of linking column and wall areas to drift, and its comparison with actual data. Basically, the column index is 0.5 times the total cross sectional area of columns at the base plus 1.0 times the area of structural walls divided by the total floor area of the building. Filler wall index is defined as 0.1 times the area of filler walls at the base divided by the total floor area. Because orientation of planar members such as walls is direction dependent, it is possible to express this ratio in the two principal directions of the building. The result of this exercise for the set of buildings in our sample has produced the diagrams in Figures 9.8 and 9.9. We stress that the directions have been defined arbitrarily.

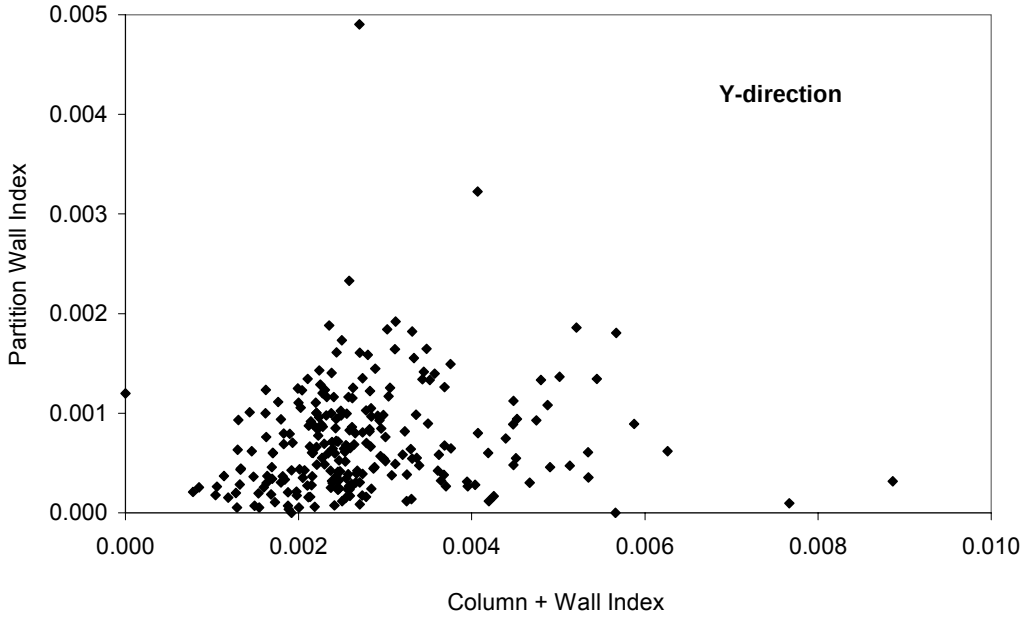

Figure 9.8. Wall and Column Indexes in y-Direction

Generally, when column index falls below 0.0025-0.003 the structure is rated as being vulnerable under conditions in Turkey. Both figures indicate that this was the median figure for the buildings in our population, so a clear indication of their collapse is difficult to rationalize on the basis of that information alone.

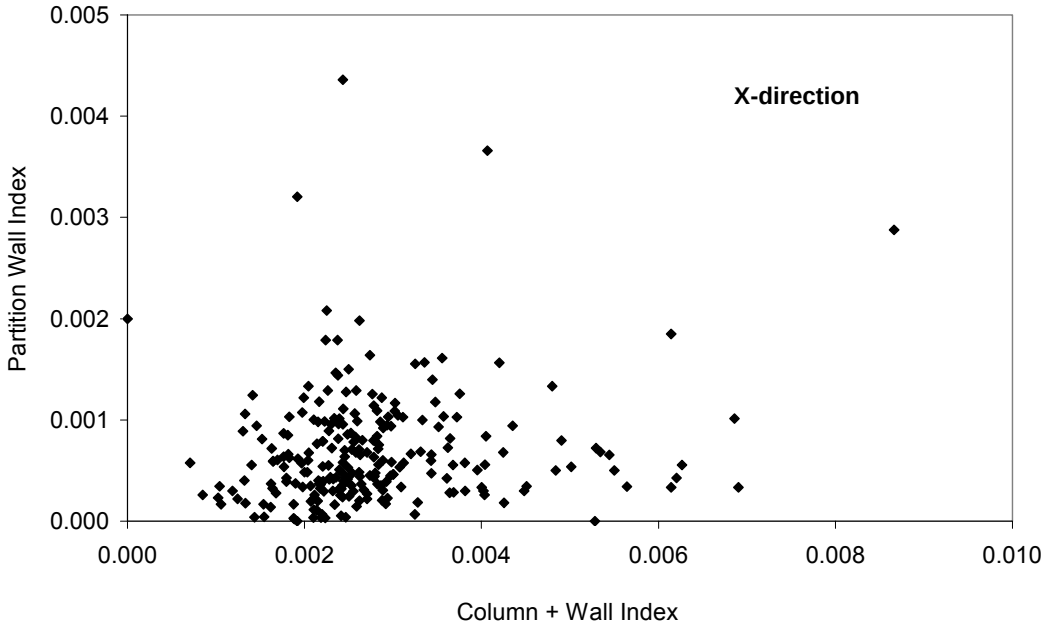

Figure 9.9. Wall and Column Indexes in x-Direction

In support of this observation Figures 9.10-9.12 show the results of a survey on 162 buildings that served as service facilities for a major bank in Turkey. The buildings were first entered on a form similar to that in Appendix 5.1, and then each was analyzed in the linear as well as the nonlinear mode. A good many other considerations entered the eventual decision regarding the adequacy of the load-carrying system but the figures encapsulate the decision in terms of the two indexes.

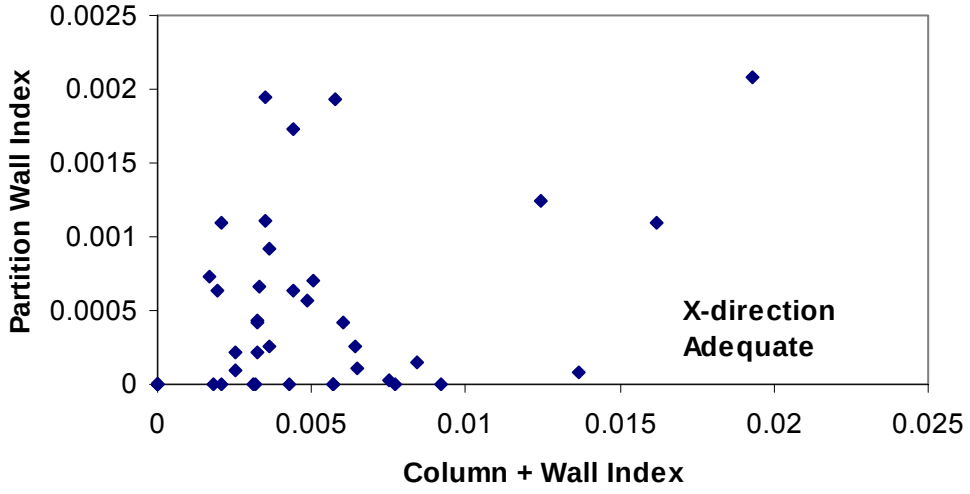

Figure 9.10. Buildings Rated as Adequate

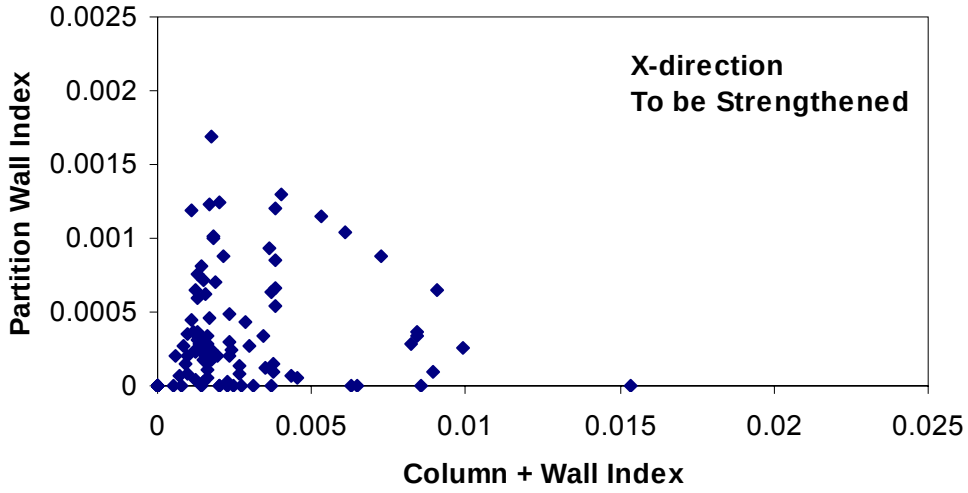

Figure 9.11. Buildings Rated as Requiring Strengthening

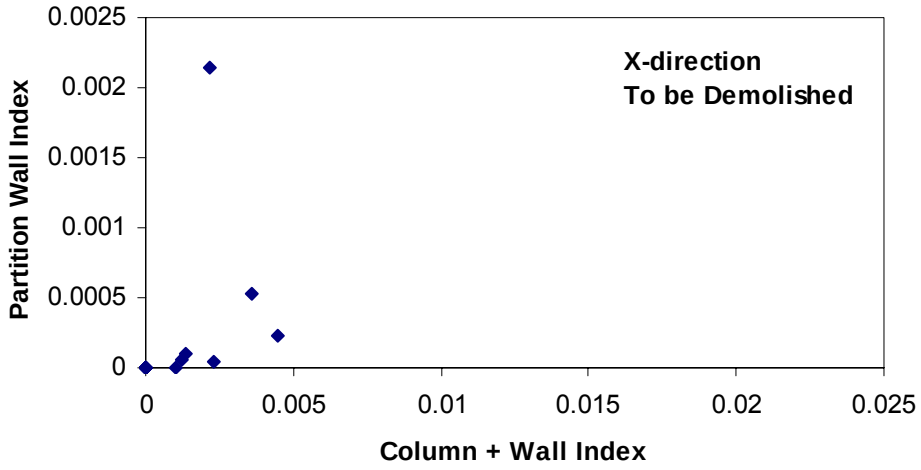

Figure 9.12. Buildings Rated as Requiring to Be Demolished

9.2.5 Conclusions

Attempting to piece together a clear post-fact statement for the collapse of the buildings in the data set assembled by SU and analyzed by the DMC/METU team appears to be a challenge. It is known that in Turkey many buildings are built in contravention of their design drawings, and records of these modifications usually do not exist. Buildings on soft and liquefaction-prone sites in Adapazarı were toppled or sunk into their foundations in spectacular ways, but these buildings did not usually suffer structural collapse leading to fatalities. As our building population had been examined for judicial purposes, there is reason to believe that most of them had been instigated by the public prosecutor following human life losses.

We believe that factors not identified in our investigations may have played just as important a role in these collapses. This is borne out by the inconsistency between Figures 9.8-9.9 and 9.10-9.12.

9.3. EARTHQUAKE DAMAGE ASSESSMENT IN TURKEY

9.3.1 Introduction

This chapter is intended as a resource for how damage assessment is conducted in Turkey following earthquakes. Until September 2000, this was the responsibility of the teams assigned to disaster areas by the General Directorate of Disaster Affairs. From that time on, this responsibility was transferred to damage assessors appointed by the Turkish Compulsory Insurance Pool (TCIP) through its operational arm DASK. Because of its immediate relevance we show the distribution of building types of the housing stock in Turkey in Figure 9.13. We note that nearly 7 out of every 8 buildings are fully or partly residential.

It is not yet known how this service will be performed by the teams empowered by TCIP because no major earthquake has occurred, but considerable experience had been accumulated over 40 years at GDDA. In 1994 GDDA had engaged DMC/METU to design a more advanced system of damage assessment to reduce the number of litigations against it by citizens in disagreement with the assessed damage of their property. The remainder of this chapter and Appendix 5.2 are devoted to a description of this new concept and the form that served as its underpinning.

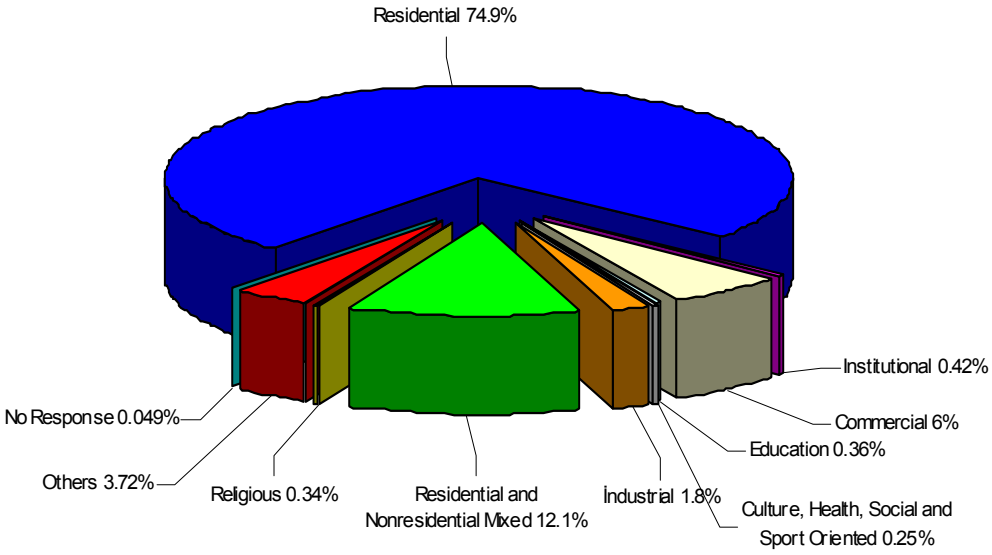

Figure 9.13. Breakdown according to Usage of the Housing Stock in Turkey

9.3.2 Post-Earthquake Damage Assessment

When a strong earthquake strikes a populated area, a good many buildings may suffer damages of various degrees, occasionally leading to partial or complete collapse in some of them. Building officials and damage inspection teams are then faced with confusing and chaotic circumstances when they must make quick and reliable judgments in assessing the degree of damage, the safety and continued usability of these buildings. This operation is referred to as Emergency Post Earthquake Damage Assessment (or EPEDA). It typically consists of a quick reconnaissance of the buildings in the area to determine whether they can still serve the functions they had been designed for without a substantial reduction in the safety conditions required for human occupancy.

The primary purpose of emergency damage inspection is to protect human lives and to prevent injuries by identifying buildings that have been weakened by the earthquake, and are therefore threatened by subsequent aftershocks. The other important objective of this operation is to avoid unnecessary squandering of resources by singling out habitable and easily repairable buildings. A parallel goal is the quantification of structural damage in a given structure after it has been exposed to a given ground motion so that projections useful for constructing vulnerability curves or insurance loss models. It is conceivable that compensation to insured property owners would be based on the results of this exercise. In fact, the exclusive purpose of damage assessment in Turkey has traditionally been to identify individuals to whom government subsidies would be conferred.

Following an earthquake, the demand for building experts far exceeds their availability. In many instances, inexperienced engineers or poorly trained technicians are assigned to perform this task without being given specific criteria on how to do it. The task of damage assessment is generally done in the following way: the inspection team fills out a form that consists of a series of questions covering general information on the type of structure, its location, and the state of damage of selected components of the building. The questionnaires are tools for the uniform gathering of data. There is no intention to guide the inspector in reasoning about the task he/she faces, nor is there a targeted attempt to assist in the evaluation and decision-making process. The quantitative assessment of the degree of damage in the entire structure is made difficult because it is described in vague or imprecise language, or is beyond their technical capabilities. An all-seeing system for post-earthquake damage assessment is difficult to design for this reason. It can also be the source of endless litigation if not used properly. The work described in this part (Gülkan et al., 1994) was designed initially to upgrade also the form for damage assessment in use in Turkey (Gülkan & Aykut, 1996). Its scope is broad enough to accommodate all forms of engineered construction that might be encountered in Turkey.

The remainder of this chapter is devoted to describing shortly features of the form which is based on visual material contained in the parent document cited in Gülkan et al., (1994). The references to figures or tables in the form given as Appendix 5.2 are in fact to that work. The rating of damage reflected in the form is related strictly to structural damage (Park & Arg, 1985) as expressed through a specific damage model suitable for reinforced concrete components.

We have attached the popularly preferred acronym of EPEDA also to this methodology.

9.3.3 Overview

EPEDA is an advisory system for the condition assessment of buildings hit by an earthquake. Its purpose is to assist the assessor during the emergency inspection phase following an earthquake by providing a rational and uniform set of guidelines for this purpose. Based on the inspector's observations, EPEDA helps in making quick and accurate decisions regarding the severity of the damage and occupancy state of the building. It is not intended to replace the inspector but to guide him through the reasoning process to ensure that the engineer's approach to the problem is correct. The system provides the background required in particular circumstances, and suggests a second inspection when the damage score is within the transition limits.

The knowledge base upon which the damage state for the entire building is based is the most heavily damaged floor level, which is usually the ground level. When the most heavily damaged floor is too large for the canvassing team to inspect fully, then this

difficulty is bypassed by requiring that only a representative sub-part of that floor should be examined because damage scores are based on ratios rather than on absolute numbers for damaged elements.

The visible part of EPEDA consists of a form (reproduced in Appendix 5.2) that has a number of question for the inspector to answer, and a booklet that serves as a background tool. Some of the questions in the form are answered with the aid of iconized diagrams drawn in detailed form in the booklet, and supported by verbal explanations based on structural theory and empirical data. The questions fall into four major categories:

- Administrative information (ownership, address, casualties, etc.)
- General information (geometric/architectural characteristics, structural features, irregularities, spans, etc.)
- Load-resisting mechanism features (type of framing, wall-frame, or box, type of floor system, whether poured in place or prefabricated, partition wall strengths, type of foundation system, workmanship quality, etc.)
- Attributes of damage and their extent for each type of member for each damage category (permanent drifts, wall crack widths, visible cracks in the horizontal and vertical members, etc.). The form is designed to work also in conjunction with a renewable relational data base.

9.3.4 Knowledge in EPEDA

The methodology embedded in EPEDA is based on the notion of Global Damage State, which is a qualitative measure of the safety of the building under inspection. The score of the Global Damage State directly dictates the decision that should be taken regarding the continued use of the structure. If it is severe, then the building should be immediately evacuated, and eventually demolished. If it is slight, then the building is declared as being safe for continued use, and may be occupied even as aftershocks are occurring. If it is in a state of moderate damage, then the building requires repair, and therefore can be occupied only after retrofit has been done. Any of the outcomes may apply only to the entire building, and not to parts of it. The damage state associated with the building is the result of a consistent reasoning involving three principal elements: evidence derived from the geotechnical state of the local site conditions in the immediate vicinity of the building and its foundations system, the state of the structural system, and additional hazards represented by its deformed configuration. The Global Damage State is determined by calculating the Total Damage Score (TDS), which consists, in the case of reinforced concrete systems, of contributory damage from five different damage sub-scores. The first is called the Damage Exacerbating Score (DES) that reflects the general architectural features of the building. For example, the presence of mezzanine floors or penthouses, plan or elevation irregularities, omission of adequate clearances from adjoining buildings, or having floor levels situated at different levels from them, or spans longer than 7 m, foundations on visibly poor soils, permanent settlements, inferior material or workmanship qualities each brings prescribed DESs. The summed upper limit score for DES is 5.

The System Damage Score (SDS) reflects the structural damage experienced by the framing elements. The inputs to this score are governed by the severity, extent (expressed as element type damage score) and relative importance of the members in question. Ranking of element-level severity falls into the following categories:

Category	Multiplier
No damage	0
Slight damage	1
Moderate damage	2
Severe damage	4

The inspector is guided in the booklet through elementary theory to facilitate his judgment for a particular damage category. We have determined that even civil engineers must be constantly trained to ensure that their judgments are logical and correct.

Extent reflects how widely spread the damage of all descriptions is in a given type of members, and varies between 0 (none affected) and 1 (all affected to some degree). Relative Element Importance (REI) differentiates between structural members or components serving different functions, particularly in resisting lateral forces. For example, girders are assigned an REI of 1 in reinforced concrete buildings, while columns are assigned 2, and structural walls 6. The Element Damage Score (EDS) is calculated as:

EDS = REI * (# slight damage + 2 # moderate damage + 4 # severe damage) /
Total # elements

The booklet contains explanatory discussions of what visual state in a given type of member corresponds to which damage state. We have utilized this form in many earthquake field assignments we have assumed since its development (i.e., Dinar, 1995; Ceyhan-Adana, 1998; Kocaeli, 1999), and found that a total novice can not be expected to use it in an error-free way from the very beginning. The damage descriptions themselves are really no more than expected values with much scatter about that value.

The SDS is then calculated as the sum of the EDSs, normalized with respect to the number of elements contributing to that score in accordance with their relative importance. The remaining three sub-score adding to the TDS are the permanent drift at the most severely distorted floor (PLDS, range 0-10), visible excessive foundation settlement (EFSS, range 0-3), and the visible damage in the stairs and the roof (RSDS, range 0-2). The permanent story displacement, or drift, at the most heavily racked floor (usually the ground level) is accorded a heavy score because it gives an indication of the deformation history of all elements there. The upper limit sum of these three additive sub-scores to TDS plus DES is 20. Inasmuch as the total score for a completely collapsed or very severely damaged building should be 100, 80 percent of SDS is considered in calculating TDS.

When TDS has been calculated, the verbal expressions for the possible damage state are as follows:

0 < TDS < 5	No damage
6 < TDS < 14	Slight damage
15 < TDS < 43	Moderate damage
44 < TDS < 100	Severe damage/collapse

A simple software has been coded to facilitate both the entering of data from inspectors, and calculation of scores for streets, districts, cities or regions. A second examination is recommended when the assessed score is within ±4 points around the transition bounds.

9.4. SITE-SPECIFIC GEOTECHNICAL CLASSIFICATION AND BUILDING DAMAGE INTERPRETATION IN ADAPAZARI

9.4.1 Introduction

Development and implementation of a site-specific geotechnical classification methodology (microzonation) for Adapazarı, aiming at estimation of surface response and interpretation of building damage associated with the 17 August 1999 İzmit earthquake are presented. The methodology is essentially a design spectrum approach in which the ground characteristics peculiar to Adapazarı are considered, and applied specifically for the ground surface response calculations based on the recorded motion at Adapazarı during the 17 August earthquake. Implementation was realized over the central municipality districts of the city utilizing the geotechnical data consisting of borehole logs, laboratory test results and in-situ shear wave velocities, provided by the General Directorate of Disaster Affairs (GDDA). Basic intentions considered during the development of the methodology were as follows:

- To include the effects of both, the alluvium thickness over bedrock and surficial soil characteristics, which appear to be the major factors controlling the site response during 17 August earthquake
- The approach could have used the presently available geotechnical data exhaustively and could be continuously improved through integration of new data that might later be available
- The approach would be rational and relatively easy to implement, thus it would constitute a model for future microzonation applications at sites for which a site-specific classification system is deemed necessary

Sites were categorized based on a consideration of the amplification and de-amplification characteristics of soil columns at the borehole locations, depending on depth to bedrock and existence of stiff or soft surficial deposits. Spectral accelerations corresponding to 0.2 s and 0.5 s periods, predicted by the site-specific classification methodology, were plotted over the area of central municipality districts. Building damage interpretation was based on the comparison of spectral acceleration distributions to the distribution of collapsed and heavily damaged buildings on the basis of districts, as well as to the distribution of available collapse cases.

9.4.2 Background

The city of Adapazarı is located at the edge of a sedimentary basin, which is a former lake bed, underlain by the thick sediments of clay (Figure 9.14). A Quaternary alluvium layer, up to a depth of about 15 m and primarily consisting of silt and fine sand deposited by Sakarya River and its tributaries overlay the lake sediments. Bedrock formation descends sharply through the north beneath alluvia and reaches depths in excess of 200 m within the city limits. Variation of the bedrock depth beneath the city is depicted in Figure 9.15. Most of the city is situated over the Quaternary alluvial sediments of the basin, where damage was highly concentrated during the 17 August earthquake.

The relatively shallow surficial deposits have rather low shear wave velocities and partly consist of liquefaction susceptible materials. Due to the pore pressure increase induced by dynamic loading, such materials exhibit further substantial reductions in shear wave velocities accompanied with very high damping capacities during earthquakes. NEHRP (2000) recommends no site-specific evaluations to determine spectral

accelerations for liquefiable soils, in case of structures having fundamental periods of vibration equal to or less than 0.5 second. This is due to the fact that the seismically induced forces are expected to reduce for such structures in case of soil liquefaction occurrence. Nevertheless, an associated reduction in demand cannot be recommended for design purposes, due to a long list of uncertainties involved in the assessment of soil liquefaction.

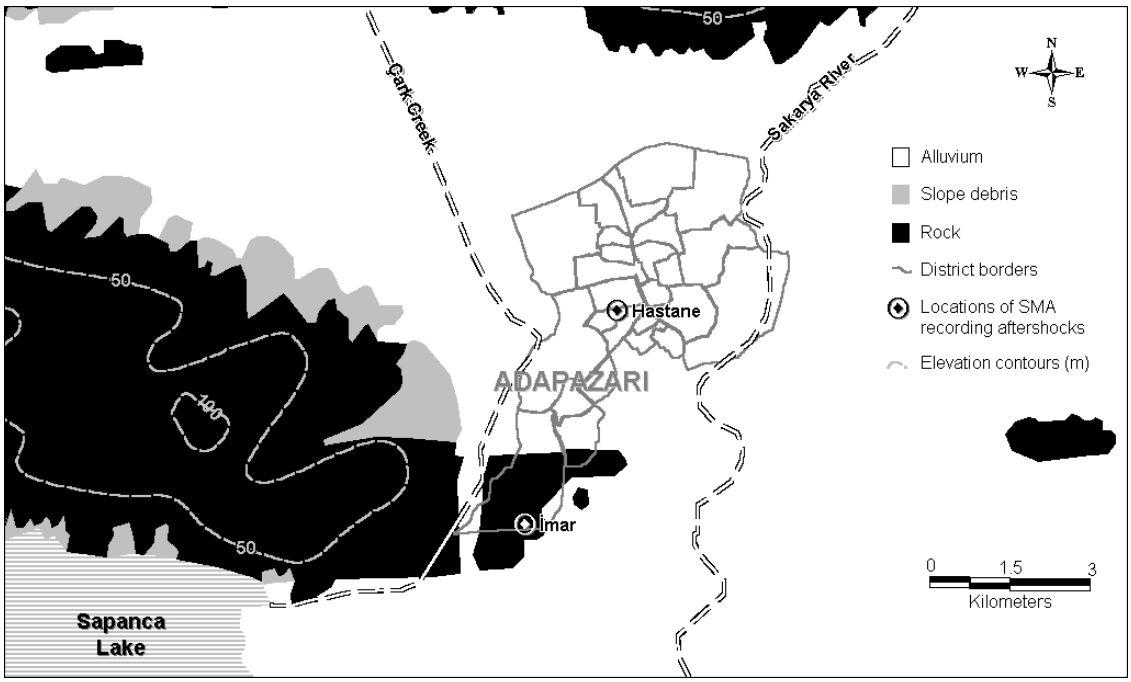

Figure 9.14. Main Geological Features of Adapazarı Area (after Bakır et al., 2002)

Soil liquefaction related phenomena are known to have had substantial influence on the seismic response and modes of damage of buildings during 17 August earthquake (Bakır et al., 2002). Accordingly, since the main goal of the present work is to ascertain the effects of local ground conditions on the trends of building damage distribution for a post-fact case, the impact of such phenomena has to be incorporated in the evaluation process. In this study, the spectral accelerations are assessed disregarding the impact of soil liquefaction on surface response, as recommended by NEHRP. However, such potential effects are evaluated subsequently, through contrasting the building damage distribution to the distribution of those areas having relatively higher liquefaction potential in the city.

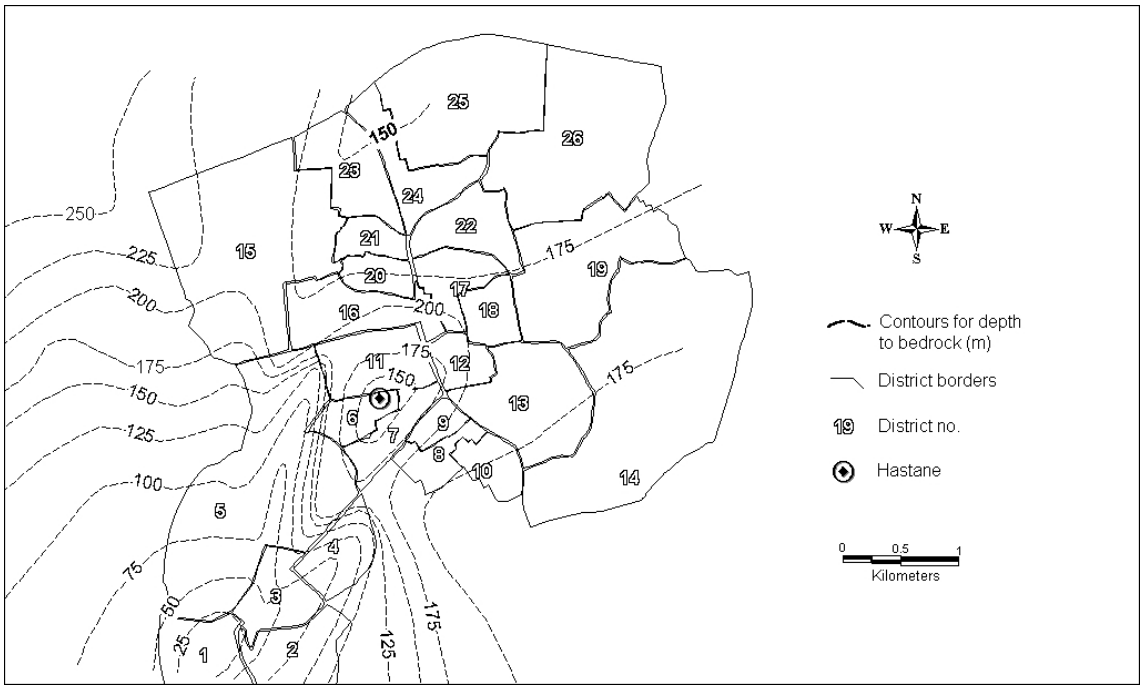

Figure 9.15. Variation of Bedrock Depth and Central Municipality Districts in Adapazarı (after Bakır et al., 2002)

The extent of the available geotechnical data from Adapazarı precludes the use of rigorous methods requiring detailed specific information (such as fines content throughout the profile) to estimate the liquefaction occurrence. In Figure 9.16, representative field Standard Penetration Test blow count (SPT-N_{45}) data from Adapazarı is compared to the backcalculated forms of liquefaction causing cyclic stress ratio (CSR) curves presented by Seed et al. (1985) for fine contents of 5, 15 and 35%. Back calculations were performed for a magnitude 7.4 earthquake and for 45% energy efficiency. An average PGA of 0.43g is assumed for the nonliquefied soil, based on the 1-dimensional soil response studies. It is observed from Figure 9.16 that a great majority of surface soils classified as silty sand and sand were not dense enough to resist liquefaction during 17 August earthquake. Accordingly, the significance of soil liquefaction on the surface response is characterized here as the percentage of deposits with relatively higher liquefaction susceptibility (sand and silty sand) observed from borehole logs pertaining to the top 10 m of the soil profile. Such an approach, in addition to being relatively easy to implement, provides a useful index to evaluate the impact of soil liquefaction on a relative basis among the sites.

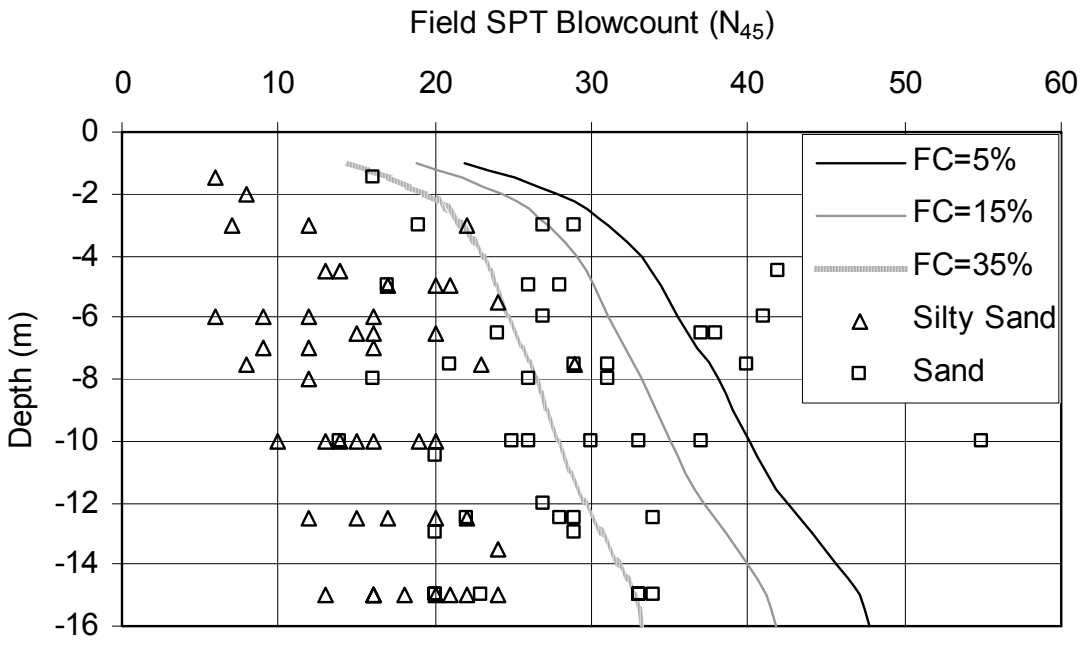

Figure 9.16. Liquefaction Occurrence Assessment in Adapazarı for the 17 August Earthquake (after Bakır et al., 2002)

Besides surficial deposits, the underlying thick medium-stiff clay sediments in Adapazarı have an extensive potential to modify the surface motion response. In NEHRP (2000), sites consisting of soft/medium stiff clays in excess of 120 ft (36 m) thickness are classified as site class F (soils requiring site-specific evaluations). Accordingly, in order to be able to relate the distribution of the observed building damage during 17 August earthquake in Adapazarı to the geotechnical factors, site-specific evaluation is required for a broader area of the city. For this purpose, following two important geotechnical factors are considered:

- Depth to bedrock, which is the fundamental component of the transfer function of motion that propagates from rock to surface through deep alluvial deposits.
- Characteristics of the surficial deposits, which can have a significant potential effect of amplification or de-amplification for specific period ranges.

Deep deposit properties can be assessed based on the results of the work by Bakır et al. (2002), while properties of surficial deposits will be evaluated utilizing the shallow geotechnical investigation database provided by the GDDA.

9.4.3 Effects of Surficial Deposits on Site Response

Database relating the range of recorded small strain shear wave velocities of surficial deposits to the Standard Penetration Test blow counts in Adapazarı, provided by GDDA, is presented in Figure 9.17. Where available, data provided by PEER is also included for comparison purposes. It is to be noted that, due to energy efficiency considerations in SPT-testing, SPT blow count numbers of PEER data are multiplied by 1.33, and no other corrections are utilized due to practical considerations.

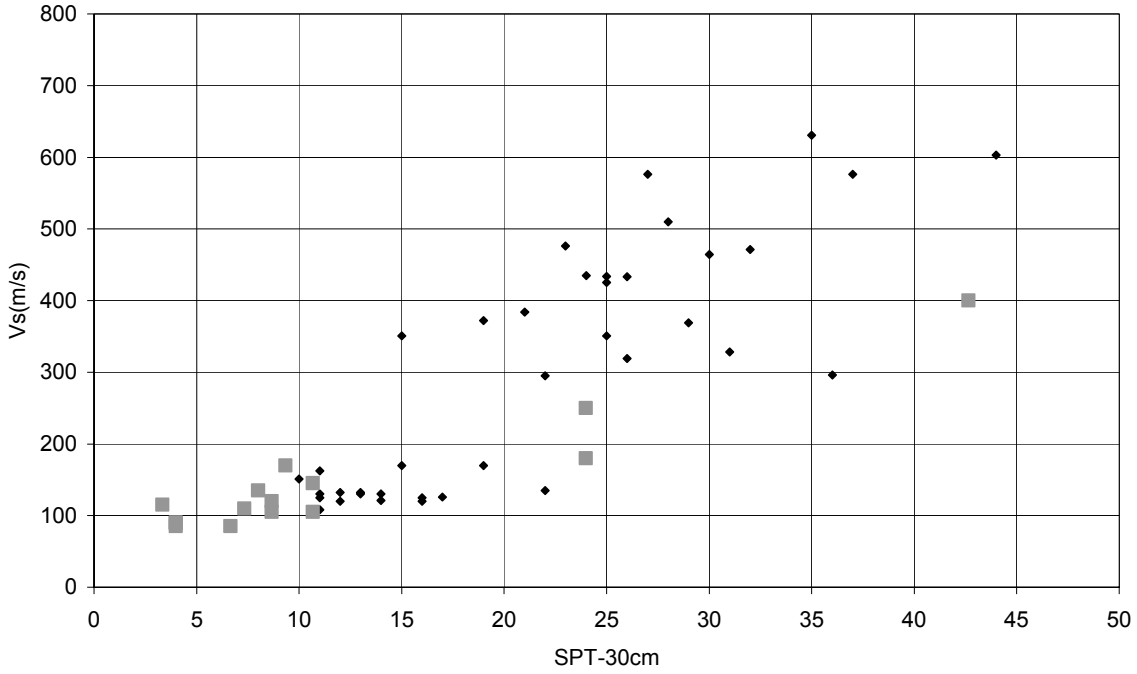

Figure 9.17. Available V_s versus SPT Correlation Data Extracted from the Geotechnical Database Provided by GDDA (PEER data is presented in gray squares)

As the next step, a regression analysis utilizing the GDDA data is performed, and the model suggested by Ohta and Goto (1976) for SPT-V_s correlation is applied for the analysis:

$$V_s = a \cdot N^b \tag{9.1}$$

where, V_s (m/s) is the shear wave velocity for small strain excitation and N is the uncorrected SPT blow-count. The parameters a and b are determined by the regression analysis as 5.83 and 1.26, respectively. Plot of the regression curve is presented in Figure 9.18.

It is observed that, for soft surficial deposits, the small strain shear wave velocity is in the range of 85-185 m/s, and significant scatter exists when their values are estimated based on SPT-N blow counts. The plasticity index (PI) ranges of these materials, extracted from the GDDA data, are presented in the form of histograms in Figure 9.19.

In order to develop the correlation curves providing equivalent shear wave velocity and damping ratio relationship, curves relating shear modulus degradation and damping variation to shear strain, provided by Vucetic and Dobry (1991) are utilized for PI=15. The range for such curves, corresponding to the range of low strain shear wave velocities observed in Adapazarı is presented in Figure 9.20. It is important to note that, when an approach based on equivalent linearization is utilized (e.g., SHAKE analyses), representative shear wave velocity and damping ratio values for soils will be represented by such curves, depending on the characteristics of input earthquake utilized in the analyses as well as the engineering properties of underlying deep deposits in the constructed site response models.

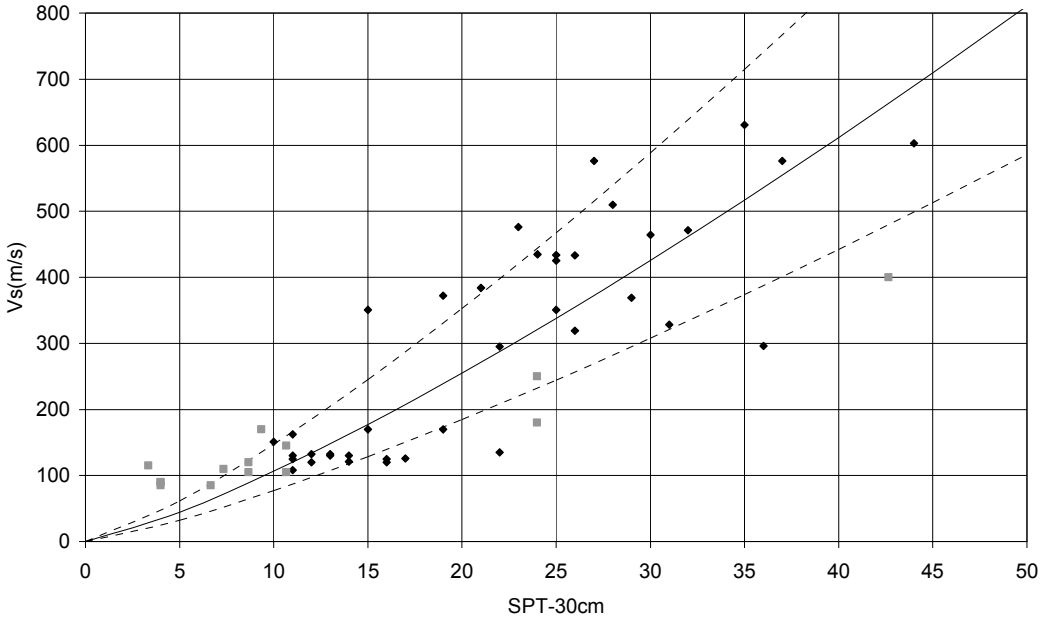

Figure 9.18. Regression Curve (with ±1 standard deviation) Plotted Using Available V_s - SPT Correlation Data, Extracted from the Geotechnical Database

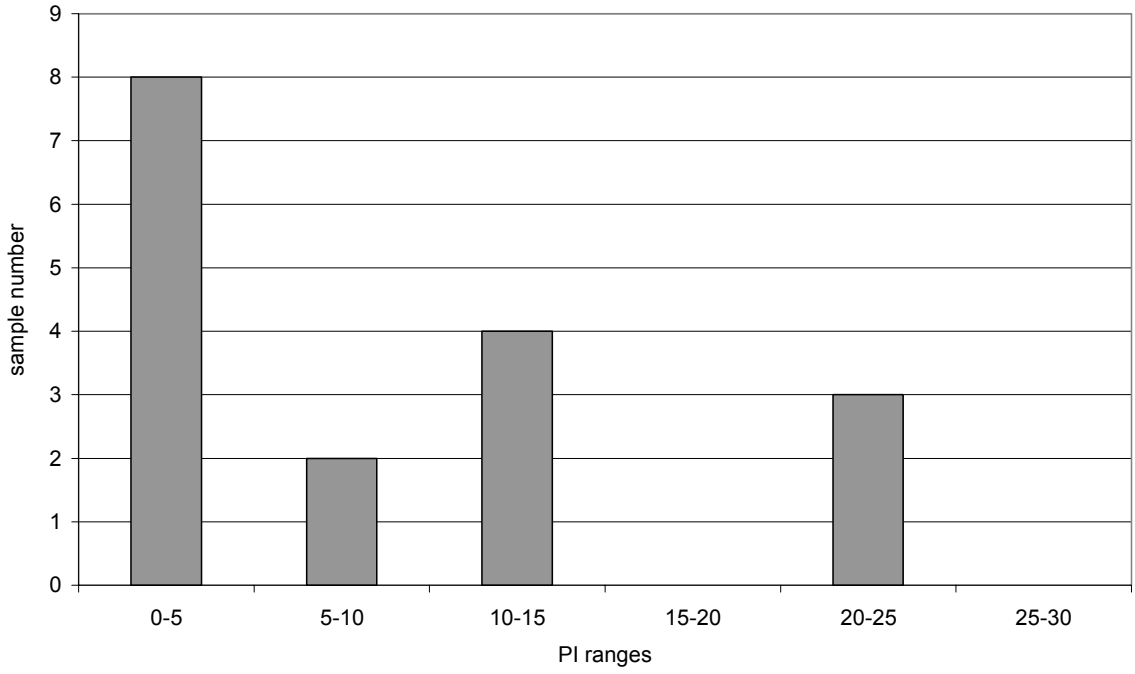

Figure 9.19. PI Ranges for Data Points in Figure 9.18

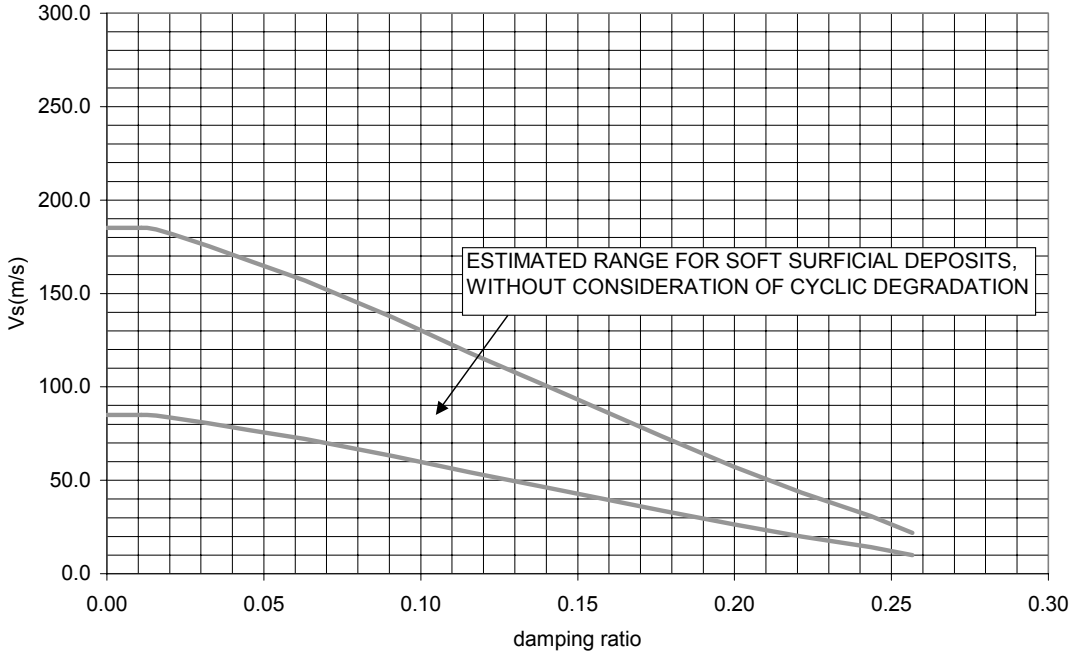

Figure 9.20. Estimated Range of Equivalent V_s and Damping Ratio for Soft Surficial Adapazarı Deposits

When the effect of surficial deposits on response spectra is investigated, different amplification or de-amplification capacities can be calculated depending on parameters such as shear wave velocity, damping, layer thickness, period of interest (representative of building fundamental periods) and earthquake input motion. In developing a site-specific geotechnical classification, it is of interest to ascertain the site conditions that yield amplification or de-amplification. An overview of such conditions can be attained relatively easily, assuming that the amplification factor for a harmonic incoming wave of period "T" is a reasonable estimate of response-spectrum amplification factor at period "T".

Based on this assumption, a routine that calculates the locations of specific amplification factors, for a site response model consisting of a damped elastic soil layer on a damped elastic half-space model, depicted in Figure 9.21, is developed utilizing Matlab software. The transfer function is defined as the ratio of the soil surface amplitude to the outcrop amplitude,

$$\frac{A_I(\omega)}{A_{II}(\omega)} = \frac{1}{\cos(\omega H/(V_S')_{top}) + i\alpha'\cos(\omega H/(V_S')_{top})} \qquad (9.2)$$

where, V_S' and α' indicate complex shear wave and impedance ratios, respectively.

Amplification and de-amplification capacities are determined corresponding to specific periods of interest for surficial layer depths of 5.0 and 10.0 m. In calculations, an average large strain shear wave velocity of 250 m/s and 5% damping are assigned for the elastic half-space, while a wide range of shear wave and damping values were utilized for the surficial layer. The results of the proposed approach were validated through comparison to spectral amplifications calculated by PROSHAKE utilizing Adapazarı and El Centro records. As a general trend, it is observed that the amplification ratios are over one (amplification) for the higher shear wave velocities of surficial deposits with the

accompanying low damping ratios, and reduce below one (de-amplification) with reducing shear wave velocities and increasing damping ratio, as would be expected.

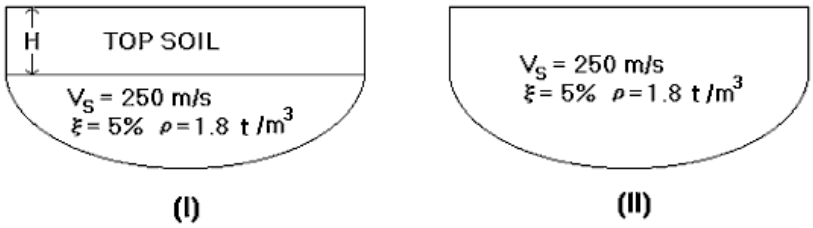

Figure 9.21. Idealized Site Response Model Used to Assess the Effects of Surficial Deposit on Surface Response

9.4.4 Idealized Soil Profile and Properties

The idealized soil column developed by Bakır et al. (2002) for Adapazarı is essentially utilized in this study. The model combines the highly consistent stratifications observed in the deep borehole logs and the generally loose silty, sandy character of the surface soils.

Available deep borehole logs, idealized soil profile and corresponding variation of the shear wave velocity of the model is presented in Figure 9.22. Depending on depth to bedrock, the idealized profile was truncated or extended at the base in 1-dimensional site response analyses. The shear wave velocities of surficial deposit and gravel layer intersecting the deep clay deposits were determined employing the empirical equations proposed by Ohta and Goto (1978). The indices used in equations include depth, soil type, geological epoch and Standard Penetration Test blow counts for the surficial deposits. In the analyses, the shear modulus and damping ratio versus shear strain curves presented by Ishibashi and Zhang (1993) are used for all soils. The plasticity indices of 10 and 35 are assigned as average representative values, respectively, for the surface soil and deep clay deposits. Records of aftershocks following 17 August earthquake, captured simultaneously on outcrop and deep alluvium were utilized to calibrate the model through adjustment of shear wave velocities of deep clay profiles dominating the profile. The model was validated to be capable of capturing the site response appropriately in the interval of fundamental vibration period range of the buildings in Adapazarı.

9.4.5 Development of Idealized Response Spectra

Based on the preliminary information obtained from the analytical model studies and using the idealized soil profile, numerous analyses were conducted with the computer program SHAKE for a series of combinations of surficial soil characteristics and alluvium depth. The east-west component of 17 August earthquake Adapazarı record, which was the only available lateral component from that station, was assigned as rock motion in the analyses. The surficial soil thickness was presumed to be 10 m, which is the depth of a considerable portion of the boreholes. The results were compiled to develop an idealized codification of site-specific spectra that can be utilized to assess the spectral accelerations associated with the 17 August earthquake throughout the city. Averaging and regression techniques were utilized in the idealization process.

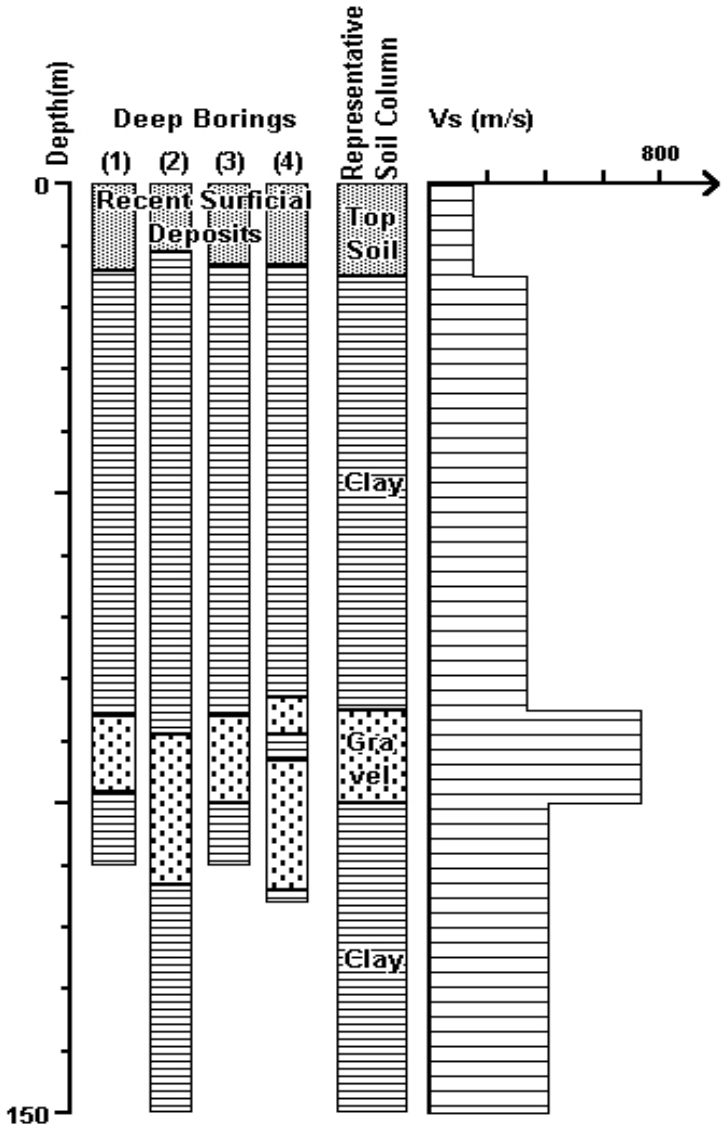

Figure 9.22. Deep Borehole Logs, Idealized Soil Profile and Variation of Shear Wave Velocity (after Bakır et al., 2002)

The codification is classified for two main categories of site conditions identified depending on the presence of soft surficial deposits. Such deposits, which impose a significant de-amplification, particularly over the short period range of the response spectra, are identified as follows:

- Sands and silty sands with uncorrected SPT-$N_{45} \leq 30$
- Silt- Clay mixtures with SPT-$N_{45} \leq 10$

Sites having such surficial soil deposits in extent of at least 50% of upper 10 m of borings (i.e., 5 m of total thickness) are referred to here as “soft sites”. Such deposits can develop relatively large damping capacities during strong shaking, and cause significant reductions in seismic demand on common building structures in Adapazarı.

The sites that do not comply with the definitions of “soft site” given above, are referred to here as “stiff site”. Idealized site-specific spectra for such sites, for which the spectral response is essentially dependent on the alluvium thickness, are defined by the following equations:

$$
\begin{aligned}
0 < T \le T_A \quad &: \quad SA(T) = 0.4 + \frac{0.5}{T_A} T \quad (g) \\
T_A < T \le T_B : \quad &SA(T) = 0.9 \quad (g) \\
T_B < T \quad &: \quad SA(T) = 0.9 \left(\frac{T_B}{T} \right)^n \quad (g)
\end{aligned}
\tag{9.3}
$$

where, T_A, T_B and n are provided in graphical form in Figure 9.23 as a function of depth to bedrock at the site locality. A set of sample spectra generated utilizing the developed codification is shown in Figure 9.24.

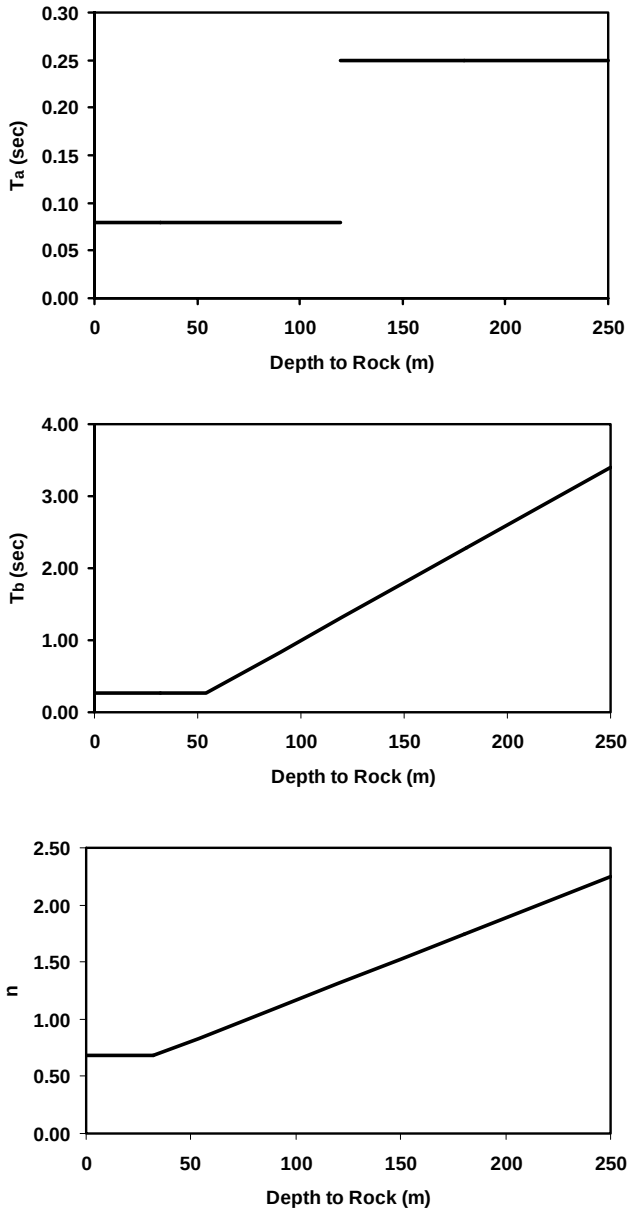

Figure 9.23. Set of Curves to Construct Site-Specific Spectra for Stiff Sites in Adapazarı

For the soft sites, idealized spectrum cannot be reliably developed utilizing equivalent linear site response approach, and true nonlinear analyses are required. On the other hand, a relatively conservative spectrum for such sites can be defined for the period

range up to 0.5 s, regardless of depth to bedrock, as the soft surficial deposit dominates the response. Such a spectrum is representative of site conditions corresponding to the boundary state between soft and stiff site definitions and forms an upper bound envelope spectral response for soft sites. The spectral response is observed to be very sensitive to further reductions in surficial soil stiffness, decreasing drastically at short period range, as surficial deposits get softer. Spectrum representative of soft sites is defined in Figure 9.24.

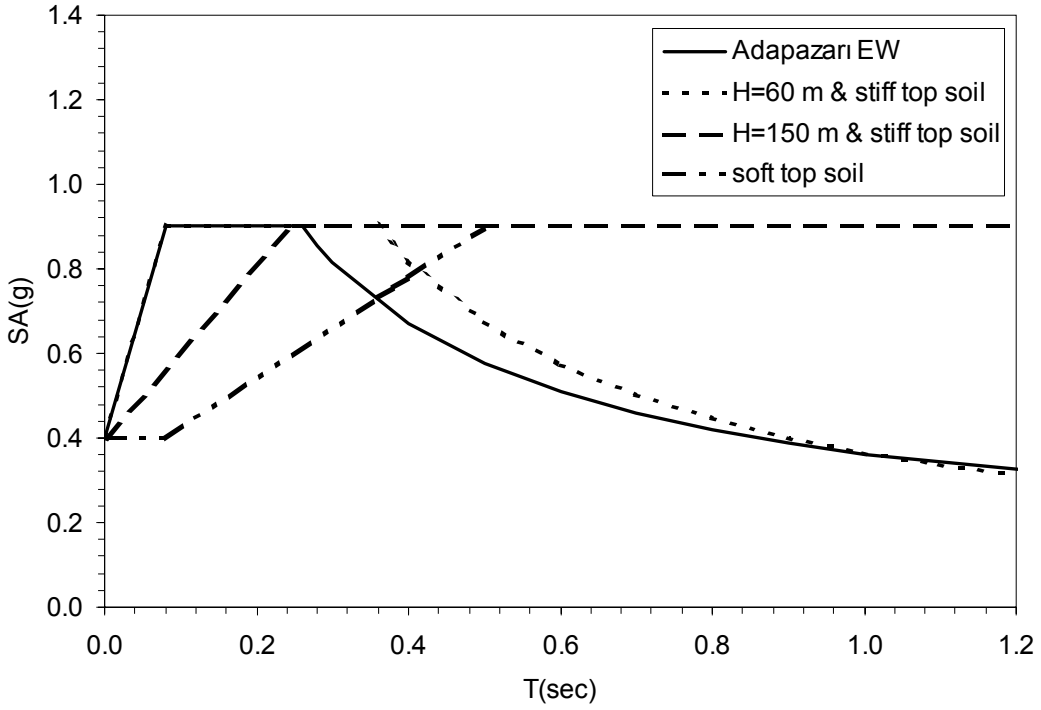

Figure 9.24. Sample Spectra for Soft and Stiff Sites (Outcrop spectrum is the smoothed response spectrum of Adapazarı record. Soft site spectrum is representative of upper bound envelope for spectral response)

9.4.6 Overview of Building Stock and Damage Distribution

After the earthquake, the Adapazarı Municipality conducted a comprehensive damage assessment survey in the city. Outcome of this survey is provided on the basis of districts within the central municipality area. The total number of buildings investigated in 26 districts covering an area of about 20 km^2, was 23,914. The damaged buildings were classified into two damage grades according to the criterion whether the building can be feasibly repaired (light or moderate damage) or has to be demolished and removed (collapse or heavy damage).

Figure 9.2 depicts the area covered during the survey, along with the 26 districts. Corresponding damage statistics are presented in Table 9.1 and the distribution of the ratio of collapsed and heavily damaged buildings to the total number of buildings is plotted in Figure 9.25 on the basis of districts. It can be observed that only few buildings collapsed or experienced heavy damage in the southernmost districts of the city, underlain by stiff and shallow soil deposits. Through north, over the deep alluvium, damage concentration increases significantly in the central districts where the buildings are generally taller compared to the rest of the city.

Table 9.1. Building Damage Statistics in Adapazarı (after Bakır et al., 2002)

District	Collapsed and Heavily Damaged buildings	Moderately and Slightly Damaged Buildings	Undamaged Buildings	Total
1-Maltepe	0 (0.0%)	38 (2.4%)	1514 (97.6%)	1552
2-Hızırtepe	7 (0.6%)	40 (3.3%)	1177 (96.2%)	1224
3-Şirinevler	15 (3.7%)	2 (0.5%)	391 (95.8%)	408
4-Güllük	14 (3.3%)	3 (0.7%)	403 (96.0%)	420
5-Mithatpaşa	100 (5.3%)	55 (2.9%)	1735 (91.8%)	1890
6-Yenidoğan	130 (24.6%)	69 (13.0%)	330 (62.4%)	529
7-Pabuççular	185 (28.8%)	51 (7.9%)	407 (63.3%)	643
8-Akıncılar	151 (20.3%)	155 (20.8%)	439 (58.9%)	745
9-Yenicami	83 (25.4%)	36 (11.0%)	208 (63.6%)	327
10-Çukurahmediye	68 (18.6%)	83 (22.7%)	214 (58.6%)	365
11-Semerciler	220 (24.2%)	88 (9.7%)	600 (66.1%)	908
12-Tığcılar	60 (11.4%)	150 (28.5%)	317 (60.2%)	527
13-Yenigün	338 (16.5%)	215 (10.5%)	1490 (72.9%)	2043
14-Tepekum	15 (1.7%)	25 (2.8%)	868 (95.6%)	908
15-Şeker	248 (12.5%)	188 (9.5%)	1550 (78.0%)	1986
16-Cumhuriyet	133 (15.4%)	145 (16.8%)	586 (67.8%)	864
17-Orta	114 (13.8%)	84 (10.2%)	626 (76.0%)	824
18-Yahyalar	48 (8.3%)	44 (7.6%)	488 (84.1%)	580
19-Yağcılar	151 (7.1%)	154 (7.2%)	1832 (85.7%)	2137
20-Kurtuluş	60 (10.7%)	44 (7.8%)	457 (81.5%)	561
21-İstiklal	205 (40.8%)	67 (13.3%)	230 (45.8%)	502
22-Karaosman	227 (30.0%)	117 (15.5%)	413 (54.6%)	757
23-Ozanlar	95 (8.6%)	84 (7.6%)	924 (83.8%)	1103
24-Sakarya	86 (8.6%)	63 (6.3%)	849 (85.1%)	998
25-Tekeler	56 (8.0%)	70 (9.9%)	578 (82.1%)	704
26-Tuzla	35 (8.6%)	6 (1.5%)	368 (90.0%)	409
Sum	2844 (11.9%)	2076 (8.7%)	18994(79.4%)	23914

Heavily damaged central part, which constitutes the business district as well as the bulk of residential and state buildings, has been developed rapidly over the past two decades. A great majority of the buildings constructed in this period are 4-5 story, rarely 6-7 story apartment buildings, typically with high entrance floor. They have reinforced concrete framing system with hollow brick infill walls, almost without an exception. This category of buildings experienced the greatest impact from the earthquake with a considerable portion of which either were totally collapsed or damaged heavily. Some of these buildings were classified as heavily damaged due to foundation displacements beyond tolerable limits, despite minor or no structural damage. Relatively older buildings, mostly 1- or 2-story, are either stone or brick masonry, or traditionally built with timber frame and brick infill. Such buildings, which constitute the majority in the outskirt districts of the city, are relatively fewer in the central section. Collapses in this category of buildings were notably less. With few exceptions, all of the buildings in Adapazarı are built over shallow foundations, while majority of the buildings with 3 or more stories have mat foundations. Evidently, the consistently high ground water level has been the primary controlling parameter over the foundation depth, which ranges between 1-1.5 m throughout the city, irrespective of building characteristics.

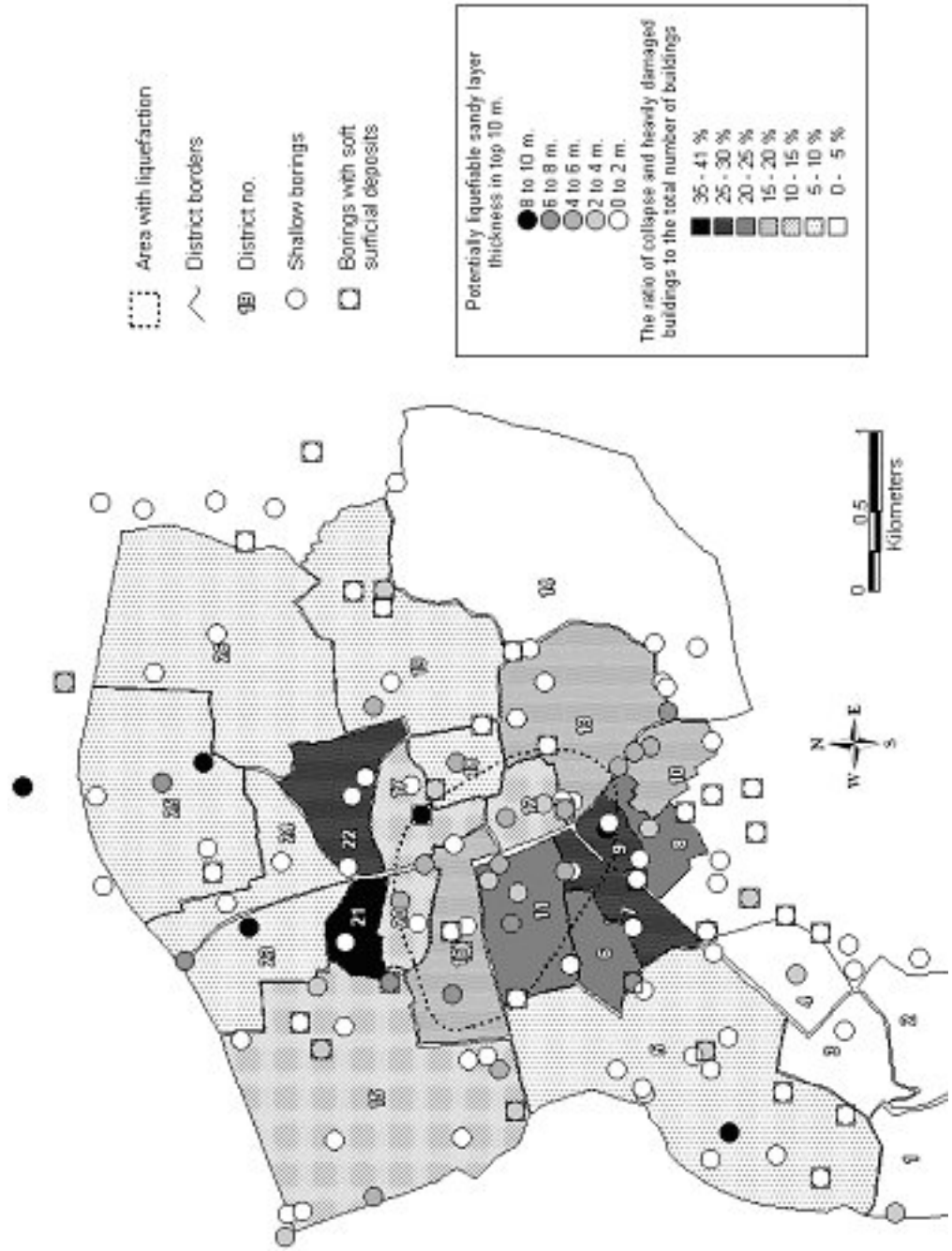

Figure 9.25. Borehole Locations and Comparison of Collapsed and Heavily Damaged Building Distribution to the Relevant Soil Stiffness Data in the Top 10 m of the Borehole Logs (the area marked by the dotted line covers where foundation displacements of various forms and levels were commonly observed)

The fundamental vibration periods of the building types encountered in Adapazarı can be estimated using the empirical expression, $T_1 \cong C_t H_N^{3/4}$ (where H_N is the total height of the building and C_t is a coefficient), provided in the 1998 Turkish Seismic Code. The coefficient C_t is specified as 0.05 and 0.07, respectively, for masonry and reinforced concrete frame buildings. Accordingly, the natural period ranges are estimated between 0.1s and 0.3 s for varieties of masonry buildings (1- to 3-story), and between 0.35 s and 0.65 s for reinforced concrete buildings (3- to 7-story).

Two entirely different modes of building damage were observed in the city depending on the stiffness of surficial soils. As a general trend, collapsed or structurally damaged buildings had no or comparatively less foundation displacements (Figure 9.26), while those buildings subjected to various forms of foundation displacements sustained relatively less or no structural damage at all (Figure 9.27). This observation suggests that the sites, which were soft or softened due to soil liquefaction, provided means of natural base isolation that reduced seismically induced forces transmitted to the superstructure during the earthquake. As a result, the number of collapse cases, and hence loss of life, must have been reduced to a certain extent over soft sites.

Figure 9.26. Building Damage on Stiff Sites along İzmit Street - Borderline between Districts 7 and 9

9.4.7 Assessment of Local Site Effects on Structural Damage

Two different sets of damage survey data are utilized here to correlate the local site conditions and the building damage observed in the city. One of these is the survey conducted comprehensively by the Adapazarı Municipality on the basis of districts, also utilized in the previous section to elucidate the general trends in the distribution of damage. The other set is the damage survey data provided by the Civil Engineering Department of Sakarya University (1998) covering part of collapse cases only, but including detailed information regarding building structural and architectural characteristics. The latter set, which has been discussed in detail in Section 9.2 of this document, contains the location coordinates of the buildings as well.

Figure 9.27. Building Damage on Soft Sites - District 12

To overview the potential effects of local sites on the observed structural damage, the distribution of collapsed and heavily damaged buildings is contrasted to the relevant soil stiffness data in the top 10 m of borehole logs in Figure 9.25. The percentage of liquefaction susceptible soils (sand and silty sand) in boreholes are indicated by gray scale circles and soft, non-liquefiable clayey deposits that comply with the soft site definition given in Section 9.4.5 are enclosed in squares.

From Figure 9.25, the heaviest concentrations of damage in the city are observed to be localized on deep alluvial deposits and generally coincide with surface soils that are either stiff or least sensitive to liquefaction (districts 7, 9, 21 and 22). Within the area enclosed by the dashed line in the figure, foundation displacements of various forms and levels were commonly encountered. Within this area, where the sites at borehole locations are generally either highly susceptible to soil liquefaction or already soft, the building damage is relatively reduced, despite the concentration of buildings with higher story numbers with potentially greater vulnerability to the excessive foundation displacements or seismically induced forces. On the other side, the general reduction trend observed in damage concentration through outskirt districts located over the deep alluvial soils can be largely attributed to the decreasing story numbers and thus to the generally reduced building vulnerability.

Utilizing the idealized spectra presented in Section 9.4.5 and depth to bedrock contours shown in Figure 9.2, distribution of spectral accelerations are computed for 0.2 s and 0.5 s periods, respectively representative of the fundamental period ranges of varieties of masonry (1–3 story) and reinforced concrete building (3-7 story) categories encountered in the city. Variations of spectral accelerations, smoothed and grouped by Inverse Distance Weighting algorithm, are contoured in Figure 9.28 for 0.2 s and in Figure 9.29 for 0.5 s. On Figure 9.29, the areas identified as soft sites, as well as the locations of collapsed buildings provided by Sakarya University are superimposed. The soft sites were developed

by the same algorithm, however with a greater resolution and by accepting 150 m as the representative radius for a boring.

As can be observed in Figure 9.28, two spectral acceleration zones were identified corresponding to the 0.2 s period in the city. The distribution is almost uniform with 0.9g in the southern section on relatively shallower deposits of alluvium and 0.8g in northern section where depth of alluvium reaches 200 m. It is to be noted that no buildings represented by the 0.2 s period (the masonry category) were included in the set of collapse cases investigated by Sakarya University. In fact, collapses in this category were markedly rare and more or less uniformly distributed throughout the city. This occurrence can be attributed to the smaller seismically induced forces in this category due to smaller building masses.

Spectral accelerations corresponding to the 0.5 s period, range between 0.6g and 0.9g, increasing through north with increasing alluvium depth, as depicted in Figure 9.29. Nearly all of the collapsed buildings are located within the highest spectral acceleration zone, clearly indicating the influence of alluvium depth on seismically induced force levels imposed over the buildings. Note that, due to the inherently greater building masses in this category, a greater impact in terms of seismically induced forces would result from spectral variations, compared to the category represented by 0.2 s. The other significant observation from Figure 9.29 is that the locations of collapsed buildings rarely coincide with the patches representing soft sites, which is consistent with the post-earthquake observations of significantly reduced levels of structural damage over soft surficial deposits.

9.4.8 Conclusions

The rather high degree of non-uniformity observed in the distribution of damage in Adapazarı following the 17 August earthquake clearly indicated the well-known local site effects associated with alluvial basins. These effects, such as motion amplification and low-frequency enhancement, are in general unfavorable to structures with longer periods. However, the remarkable aspect of the post-earthquake scene in the city was the foundation displacements of various forms and levels observed in numerous cases. This phenomenon, which can be largely attributed to the surficial soil characteristics, had a substantial influence on the response and modes of damage of buildings.

The general trends observed in the levels and distribution of damage associated with the 17 August earthquake in Adapazarı are successfully captured through implementation of the idealized spectra developed on the basis of site-specific geotechnical classification. Following are the main conclusions:

Ground response at a specific site in the city is controlled by the two major geotechnical factors: the alluvium thickness, which is highly variable throughout the city, and the presence of soft surficial deposits.

Distribution of spectral accelerations corresponding to 0.2 s period was almost uniform throughout the city, whereas for 0.5 s period the spectral response was relatively varied with the maximum level overlapping the zone where alluvium thickness is greater.

Significant de-amplification of spectral response for the period interval up to 0.5 s is predicted at the sites defined as “soft” according to the idealized site-specific spectra.

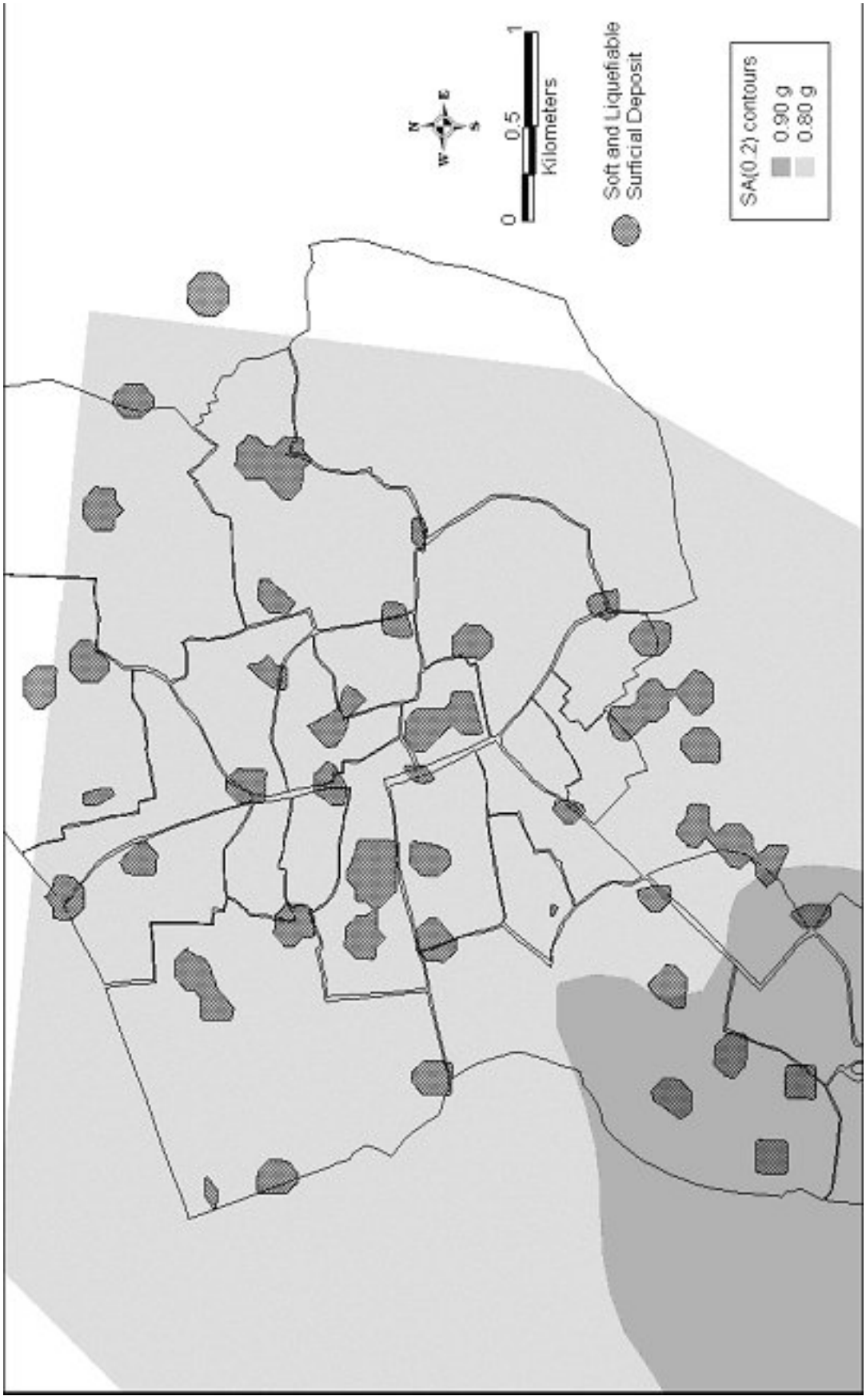

Figure 9.28. Variation of Spectral Acceleration for T = 0.2 s

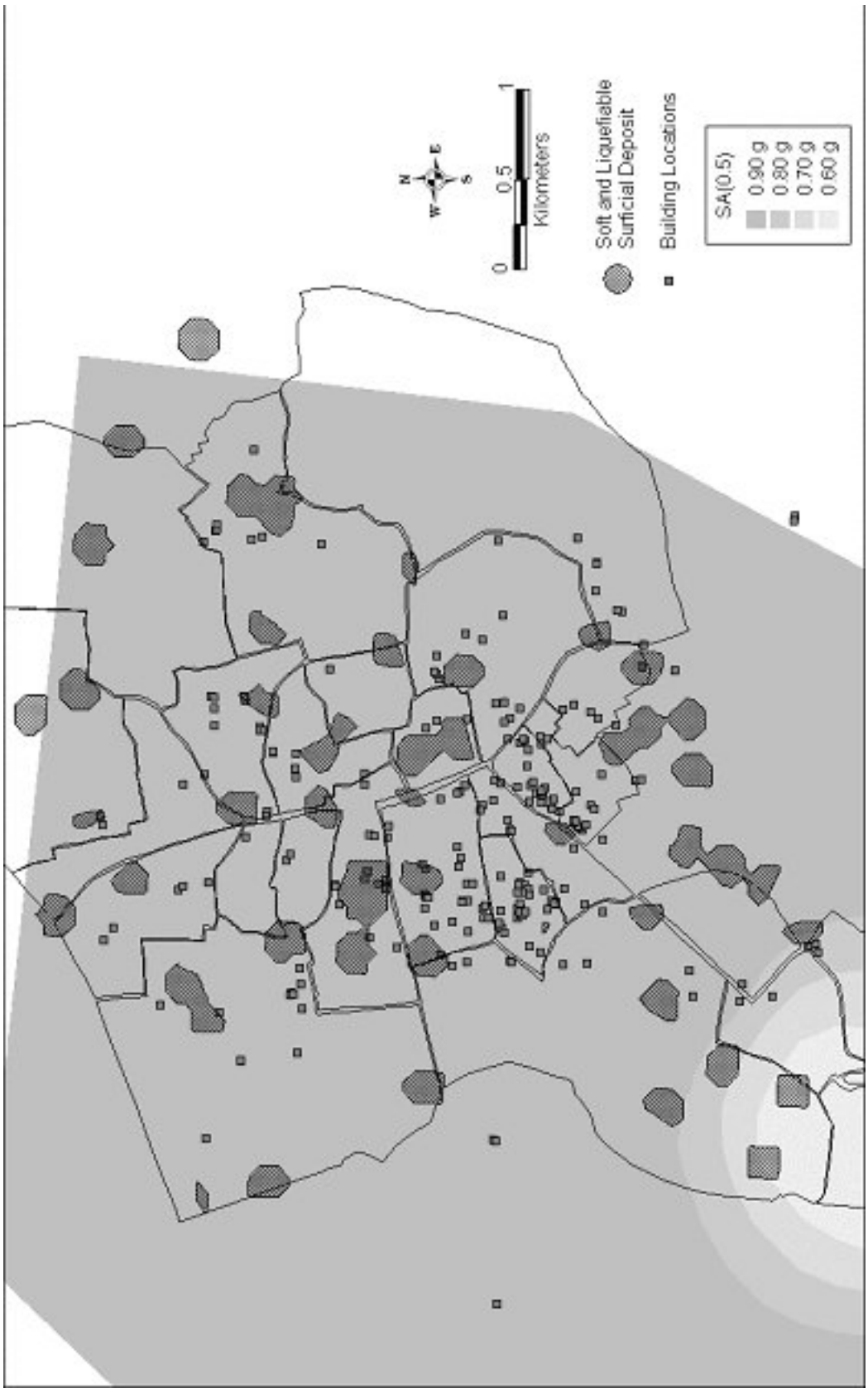

Figure 9.29. Variation of Spectral Acceleration for T = 0.5 s and Locations of Collapsed Buildings (dark gray patches mark the soft site

10. MAPPING BY USING GEOGRAPHIC INFORMATION SYSTEMS (GIS)

M.D.Köksal (World Institute for Disaster Risk Management - DRM, Virginia, USA), O.Gökçe (General Directorate of Disaster Affairs, GIS and Remote Sensing Project Center - GDDA, Ankara Turkey) with the contribution of M.K.Tüfekçi, K.Özener, S. Demir, A. Demir, S.Kök, S. Yağcı, İ. Kayakıran, E. Nebioğlu, A. Güldemir, M.E.Durgun (General Directorate of Disaster Affairs, GIS and Remote Sensing Project Center - GDDA, Ankara Turkey).

10.1. SUMMARY

All mapping operations for seismic microzonation and land use management purposes for the Project MERM concept were done by using GIS technology. Below is some brief information about the whole process.

10.2. INTRODUCTION

A centre has been established at General Directorate of Disaster Affairs, Ankara, Turkey for the mapping and GIS activities in the context of MERM. All activities including contracting, design, procurement, data collection, digitizing, transformations to GIS formats, training, exercising, final mapping and interpretations have been completed in one year (2002-2003). DRM were present during all stages at the Centre.

10.3. DESIGN AND PROCUREMENT

The DRM GDDA contract, establishment of the Centre and utility as well as the training program have been designed in nearly three months. The procurement, delivery and finalizing the setup operations lasted more than two months. All other real GIS activities lasted around eight months.

10.3.1 Office

GDDA have assigned a wide space at the Department of Disaster Investigations and Building Damage Assessment (Figure 10.1). The Office is a 200 m^2 room with and additional small space connected to the office for the server system. The office was later been restored. All furniture is modern and is laid out in suitable format so that the space is comfortable for around 20 people to work. The optimum number is 10 people working with computers only.

Figure 10.1. DRM GDDA MERM Geographic Information System and Remote Sensing Project Center, Ankara Turkey - Office view

10.3.2 Hardware

High tech instruments have been donated by DRM - DEZA to GDDA for the GIS Centre (Figure 10.2, 10.3). Brief information about this equipment includes:

- A good server system to easily handle the present work and expected to serve in the next 5 years period.
- Eight Workstations - 6 of them are 512 MB Ram, one is 1 GB, one is 2 GB Ram. All are Pentium 4 - 1.4 GHz. Well designed graphic utilities and components are available and all 21" monitors are very high quality.

One A0 Plotter

One A0 Scanner

One A3 color laser printer

Figure 10.2. DRM DEZA donated A0 size scanner and A0 size plotter + A3 color laser printer.

Figure 10.3. One of the eight workstations donated by DRM DEZA - P4 1.4 GHz, 2 GB Ram Software

The latest version of one of the world's leading GIS software package has been used for Project MERM. For script writing and special processes, additional software packages were provided. Eight GIS Licenses have been procured; one for each workstation.

For the server and workstations an advanced server software system has been used. Special scanning and copying of software packages were useful during the operations.

10.3.3 Service

All equipment has up to 3 year under warranty. Unlimited service, maintenance and training for all hardware and software has been made available (when needed) free of charge for one year through agreements.

10.3.4 Personnel

A nucleus team of ten GDDA Engineers have been trained during the project period. When necessary, additional basic lecturing has been done for an increment of trained engineers (up to thirty) when needed. The engineers are from different disciplines mainly geology, geodesy and photogrametry, city planning, geophysics and construction engineering.

10.4. TRAINING PROGRAM

Training programs have been planned for mainly the research tasks and GIS related activities. Also the sustainable implementation and manual commenting was an important exercise for the engineers. Valuable lecturing by the Project Professors has been organized every week systematically on a topic related to MERM.

10.5. RAW DATA

Half of the cartographic data were in paper format at various scales from 1:1000 to smaller scales, belonging to various dates, and the other half was digital. It took almost seven months to optimize and digitize for both pilot areas. More than 100 A0 paper maps were carefully cleaned and then digitized. The already digitized base (topographic) maps needed to be worked on for months because of the non standardized existing methods in the country. Since each part of a district has been digitized by different enterprises through the Municipality, they first had to be put in a same CAD format. After a good layout of CAD formatted base maps had been achieved, these then were transformed to GIS format. Tens of layers were studied carefully and finalized.

The other data group were the scientific data. Since there were a vast quantity of data but in paper format and unfortunately almost all with no coordinates, the work of data entry according to the approved GIS philosophy took plenty of time.

10.5.1 Process

Processing of raw data and transformation to GIS formats was based on tasks mentioned below.

10.5.2 Database Design

A careful study has been made to design the structure of the GIS process. For this purpose, firstly the relationships between the parameters have been determined (Figure 10.4). Then related forms and tables have been produced for raw data entry. Below are the samples of these studies (Figure 10.5). For beginning the process and using small amount of data, the most simple way to enter this data may be by a regular electronic tabular form such that entering the coordinates x and y and then the data to be mapped in the next column (So

three columns are enough). With this method, each measurement taken in a different location shall be stored in a different row. This is the easiest way of setting up a preliminary database. Simple sorting can be done in this type of format, but for serious query operations and professional work, a well designed database is recommended.

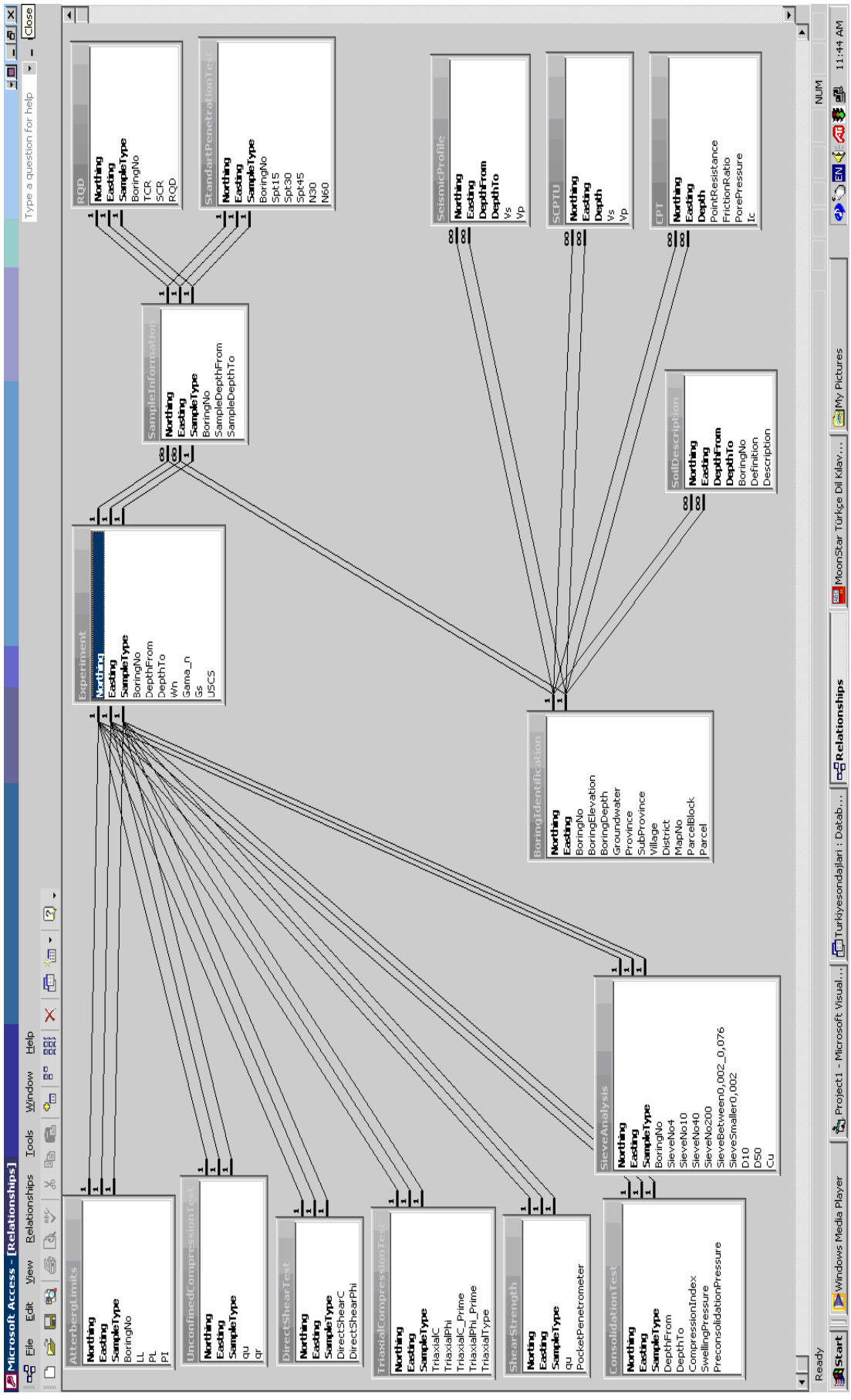

Figure 10.4. Relations among parameters

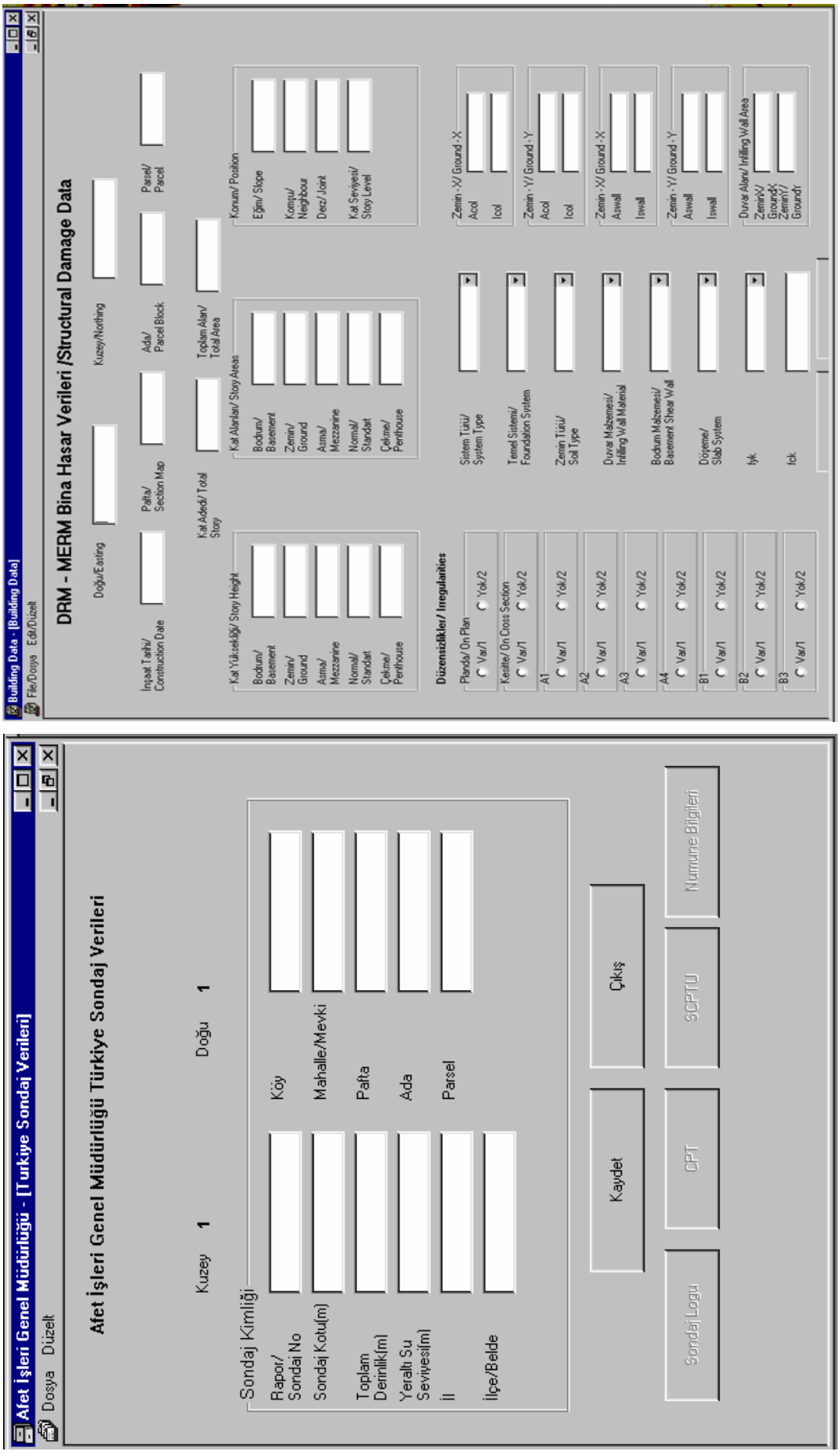

Figure 10.5. First frame of the borehole database and one page structural damage database form designed for MERM

10.5.3 Digitizing

Almost half of the cartographic data was in paper format and these were digitized for GIS purposes. The time required depended on the extent of the data, it needed a lot of time.

10.5.4 Other Operations

After the database had been designed, already compiled geo-data (in paper format) have been entered in to the database. Prior to this, coordinates have been assigned to all measurement points. Then geo-referencing, optimizations, sorting, filtering, corrections, smoothing, engineering judgement and review operations were carried out. First trial maps were produced and printed, then proper layouts have been designed, data and contours, colors checked, correlations and relations between the properties were reviewed on the map. For colors, red was selected to represent always risky or dangerous areas, whereas blue was adopted for safer areas.

10.6. COORDINATE SYSTEM

For MERM, the UTM (Universal Transverse Mercator - European Datum 1950 Central Meridian 30 - a 3 degree Turkish Coordinate System) is used.

10.7. RECOMMENDATIONS AND CONCLUSION

For GIS operations, the data to be mapped must be in digital format. The data must have a coordinate system. So every point of measurement or property has an identified place on the map by in terms of unique set of coordinates. The coordinate system and the type of projection must be carefully determined from the beginning. Any data which have no written coordinate must be matched from a known paper map or image and known points should be matched and coordinates must be assigned (geo-referencing). Since vast amount of time have been wasted on coordinate assignment operations for the unknown points, it is highly recommended for future studies that any investigation location or point done at any place must be precisely determined by giving coordinates at that point from the beginning (during investigation) by using proper GPS instruments.

One more recommendation would be that; in order to save time in the future; the number of layers in digital base (topographical) maps must be decreased to four or five at a maximum, by focusing on contours, buildings, roads and rivers.

All scientific data is recommended to be kept in digital electronic format for easy operation with GIS for the future.

Proper training for application of GIS is essential. The design of the GIS system for upcoming centres or offices should be such that the equipment and software packages must be easy to be handled and operated, efficient, fast, good quality, cheap and most important to have excellent maintenance and service as well as training when needed, preferably free of charge. So all agreements, prior to any purchasing of GIS technology, must be well studied. The system should go without any upgrade for at least 3-4 years.

Also it should be remembered that a safe back up system for the data must be established.

As a conclusion, for MERM Project, design of the process took 30% of time, data collection and optimization 60%, and mapping 10%. For already existing utilities, data collection and optimization may go up to 85% and mapping 15%.

11. INTERPRETATION AND ASSESSMENT

Atilla Ansal, Department of Earthquake Engineering, Kandilli Observatory and Earthquake Research Institute, Boğaziçi University

11.1. GENERAL

This chapter was prepared in accordance with the suggestions of the Technical Advisory Board (TAB, 2003) and along the consensus reached among the members of the Research Task Group. The main purpose was to provide case studies in full agreement with the procedures recommended in the Microzonation Manual (Part 2B).

The final stage of the study involved interpretation and assessment of all the available data to finalize the microzonation maps in the selected pilot areas. The pilot areas were divided into squares by a grid system of 500 x 500 meters. This approach is adopted for estimating the effects of site conditions at a scale of 1:5000 by assigning partly hypothetical boreholes at the centre of each grid. There were basically two reasons behind this approach (1) to utilize all the available data in each grid in order to have more comprehensive and reliable information about the soil profile; (2) to eliminate the effects of different distances among boreholes or site investigation points during the GIS mapping. The results obtained were mapped using GIS techniques by applying linear interpolation among the grid points, thus enabling a smooth transition of the selected parameters. Soft transition boundaries are preferred to show the variation of the mapped parameters. Better defined clear boundaries were not used and are not recommended due to the accuracy of the study and in addition to allow some flexibility to the city planners and to avoid misinterpretation by the end users that may consider the clear boundaries as accurate estimations of the different zones.

The initial boundaries of the pilot areas were the official boundaries of the cities considered in the in the pilot areas, as shown in Chapter 3. However, for both pilot areas there were no boreholes or in-situ tests mostly in the outer grids, as explained in Chapter 5, thus it was decided to modify the boundaries of the both regions for microzonation study, as will be shown in the maps given in this Chapter. The basic idea was to avoid the need for additional extrapolation that may not be very reliable.

The approach adopted in the assessment of the calculated zonation maps involves the division of the area into three zones as (A, B, and C) as defined in the Microzonation Manual (Part 2B). Since the site characterizations, as well as all the analysis performed, require various approximations as well as some assumptions, it was preferred not to present the numerical values for any parameter. In all cases, the variations of the calculated parameters are considered for each area separately and their frequency distributions were calculated. Thus the zone A shows the most unsuitable 33 percentile, zone B the medium 34 percentile and zone C shows the most favorable 33 percentile.

Thus in making suggestions for the municipalities and city planners who will be utilizing these microzonation maps for establishing the city plans, it is recommended that they should try to avoid A zones as much as possible.

11.2. SITE CLASSIFICATION

As explained in detail in Chapter 5, site characterization was conducted based on the boreholes and other related information available for each grid. Each selected soil profile was classified according to the Turkish Earthquake Code and NEHRP site classification, and equivalent shear wave velocities were calculated for each grid point.

11.2.1 Adapazarı Region

As explained in detail in the previous sections, the Adapazarı region is mostly located on alluvium deposits, as shown in the geological map in Figure 11.1. The thickness of the alluvial deposit at certain locations is estimated to extend approximately down to 1000 m, as given in Figure 1.3 (Komazawa et al., 2002). The elevation variation in the region is limited (Figure 11.2) and most of the area is flat.

The site conditions with respect to Turkish Earthquake Code and NEHRP site classification for the region are shown in Figures 11.3 and Figure 11.4. The majority of the area is classified as Z3 or Z4 according to the Turkish Earthquake Code and naturally as D or E according to NEHRP, indicating the dominance of loose and soft alluvial deposits in the region.

The variation of equivalent shear wave velocity for the Adapazarı region is shown in Figure 11.5 as described above in terms of three zones (A, B and C). The zone A shows the lower 33 percentile, zone B shows the medium 34 percentile, and zone C shows the upper 33 percentile with respect to equivalent shear wave velocities.

11.2.2 Gölcük Region

The geology is slightly more variable in the Gölcük region, as shown in the geological map in Figure 11.6. A large portion of the area is covered by stiffer geological formations and, as shown in the elevation map in Figure 11.7, it is hillier with flat areas located in the north by the Izmit Bay.

The site conditions with respect to the Turkish Earthquake Code and the NEHRP site classification for the region are shown in Figures 11.8 and Figure 11.9. The majority of the area is classified as Z1 or Z2 according to the Turkish Earthquake Code, and naturally as C according to NEHRP, indicating the dominance of stiffer and denser deposits in the region.

The variation of equivalent shear wave velocity for the Gölcük region is given in Figure 11.10 as described above in terms of three zones (A, B, and C). The zone A shows lower 33 percentile, zone B shows the medium 34 percentile, and zone C shows the upper 33 percentile with respect to equivalent shear wave velocities.

11.3. SITE AMPLIFICATION

Site response analyses were conducted for both pilot areas using the selected soil profiles and the input time histories obtained for each grid from the regional probabilistic earthquake hazard study. Unfortunately due to the time limitations, only one simulated time histories was used as an outcrop motion and site response analyses were conducted using EERA Excel routines, as explained in detail in Chapter 6.

The basic intention of the site response analysis is to estimate the effect of local site conditions in assessing the site amplification with respect to ground shaking. It would be logical to base this decision on all the available results obtained from site identification based on equivalent shear wave velocity, site response analysis as well as from microtremor measurements conducted in the region. In the case of site response analysis, a suitable parameter is considered to be the average spectral acceleration between 0.5 and 1.5 second periods based on the consensus reached among all parties including TAB (2003). Thus, instead of giving all the parameters obtained by site response analysis, such as peak ground or maximum spectral accelerations, only the variation of the average

spectral accelerations will be mapped in accordance with the relative mapping approach described above in terms of three zones (A, B and C).

The peak spectral amplifications based on equivalent shear wave velocity were calculated using the empirical relationship given by Midorikawa (1987);

$$A_k = 68 * V_s^{-0.6} \quad (11.1)$$

where A_k is the spectral amplification and V_s is the equivalent shear wave velocity. The peak spectral amplifications calculated based on Eq. (11.1) were evaluated and the variations were also mapped, as in the case of average spectral accelerations obtained by site response analyses.

Even though it is generally accepted that H/V ratios obtained from microtremor records would not lead to very reliable spectral amplification values, they can still be taken into consideration when finalising the microzonation with respect to site amplification. Therefore, the results obtained from the microtremor study (Chapter 4) were utilized to map the variation of the spectral amplifications only for Adapazarı region, since the number of microtremor measurements was very limited in the Gölcük pilot area. Since the results of the microtremor studies are plotted only for comparison purposes, original measurement locations were used at the mapping stage, neglecting the effects of the spacing between the measurement points.

11.3.1 Adapazarı Region

The results obtained from the site response analyses with respect to average spectral accelerations, and the peak spectral amplifications calculated using equivalent shear wave velocities, are shown in Figure 11.11 and Figure 11.12, respectively. The peak spectral amplifications calculated from H/V ratios obtained from the microtremor study are given in Figure 11.13.

11.3.2 Gölcük Region

The results obtained from site response analysis with respect to average spectral accelerations and the peak spectral amplifications calculated using equivalent shear wave velocities are shown in Figure 11.14 and Figure 11.15.

11.3.3 Seismic Microzonation with respect to ground motion

The final mapping with respect to ground shaking can be accomplished by comparing the average spectral accelerations obtained by site response analyses with the peak spectral amplifications calculated using equivalent shear wave velocity. In order to make this comparison, the results obtained from both approaches are shown in a consecutive order for both areas.

As can be seen from these maps, there are similarities and differences. After studying the soil profiles and site classifications, it was observed that at some grid points the site amplifications were relatively high and at some grid points the peak ground accelerations were very low based on the site response analyses. The site response analysis, whether it is conducted by EERA or Shake, would sometimes give unrealistically high spectral amplifications or very low peak ground acceleration values depending on the thickness of the deposit, estimated initial shear moduli, and also on the characteristics of the input acceleration time histories. On the other hand, even though they are more empirical, the spectral amplifications calculated using equivalent shear wave velocities

tend to give more consistent values that appear to be more realistic when compared with the selected soil profiles.

There are basically two possibilities in making the comparison between the average spectral accelerations obtained by site response analysis and peak spectral amplifications obtained from equivalent shear wave velocities.

1. The first option is to use the maps obtained for both parameters and determine the overlapping zones graphically using the GIS program. In the procedure that can be followed in carrying out this assessment, and since both maps were divided in to three zones, it was also essential to have three zones again in the final map. The zone A_{GS} corresponds to overlapping zones of A_S and A_V or A_S and B_V or B_S and A_V. The zone B_{GS} corresponds to overlapping zones of A_S and C_V or C_S and A_V or B_S and B_V. The zone C_{GS} corresponds to overlapping zones of B_S and C_V or C_S and B_V or C_S and C_V obtained from both approaches. Due to the methodology followed for the graphical evaluation, the final map can only be obtained in terms of clear boundaries.
2. The second alternative is to perform this assessment for each grid numerically by adopting the above criteria to determine the three zones and then perform the mapping using the new data. The resulting map obtained from this approach is shown in Figure 11.16.

Since it is easier, faster and less susceptible to errors, and since it has soft boundaries, it was decided to adopt the second alternative to obtain the ground shaking zonation map, as shown in Figure 11.16.

As a last step, the estimated map for the ground shaking is compared with the geology map for Gölcük, as shown in Figure 11.17. It is evident from this map that most part of the alluvium deposit, as expected, is in the zone A of high intensity of ground shaking. However, it is important to observe that certain sections of Aslanbey Formation which was described as "*It consists of loose and lightly cemented sandstones-siltstones-claystones and gravelstones (conglomerates). It often behaves as soil due to past extensive weathering and degradation. Its thickness is in the order of 100 m.*" (Chapter 2), are also located in zone A. This example demonstrates that zonation with respect to geological formations may not be very accurate due to different factors where in the case of Aslanbey formation it is very likely that the differences in the weathering and degradation requires to define different zones in the same formation for microzonation purposes.

The seismic zonation map with respect to ground shaking was obtained for Adapazarı region based on the second approach as explained above for the Gölcük region, as shown in Figures 11.18. Even though the peak spectral amplifications calculated based on microtremor H/V ratios are not considered very reliable, they seem to agree with the ground shaking zonation map in the case of Adapazarı as shown in Figure 11.13, thus supporting the decision to use the average spectral accelerations and peak spectral amplifications from shear wave velocities as the zonation criteria for the ground shaking microzonation maps.

11.4. LIQUEFACTION SUSCEPTIBILITY

The approach adopted to perform microzonation map in terms of the liquefaction susceptibility was based on the method developed by (Youd et al., 2001) and Iwasaki et al. (1982) as recommended in the Manual (Part 2B) and as suggested by TAB (2003). For the purpose of demonstrating the applicability of the proposed approach, the liquefaction susceptibility microzonation map was produced for the Adapazarı region.

A more refined and detailed analysis was presented in Chapter 7 with respect to liquefaction triggering probabilities where all available borehole information was used to assess the liquefaction susceptibility for both case study areas.

In the approach adopted in this chapter, the safety factors were determined for each representative borehole for the Adapazarı region based on the method proposed by Youd et al. (2001). Even though the details of this approach was explained in detail in Ansal et al (2001), it may be appropriate to review the basic steps followed in determining the variation of the safety factors with depth.

Step 1. *CSR* is calculated from Seed and Idriss (1971) as,

$$CSR = \frac{\tau_{av}}{\sigma'_v} = 0.65 \frac{a_{\max}}{g} \frac{\sigma_v}{\sigma'_v} r_d \tag{11.2}$$

where a_{max}= peak horizontal ground surface acceleration
g = acceleration of gravity
σ_v= total vertical overburden stress
σ'_v= effective vertical overburden stress
r_d= stress reduction factor.

The average values r_d is calculated by the expression (Youd, et al 2001),

$$r_d = \frac{(1.00 - 0.4113z^{0.5} + 0.04052z + 0.001753z^{1.5})}{(1.00 - 0.4177z^{0.5} + 0.05729z - 0.006205z^{1.5} + 0.001210z^2)} \tag{11.3}$$

where, z is the depth below ground surface in meters.

Step 2. Corrected $N_{1,60}$ values are calculated as,

$$N_{1,60} = NC_N C_R C_S C_B C_E \tag{11.4}$$

where N = measured standard penetration resistance,

C_N = factor to normalize N to a common reference effective overburden stress
C_R = correction for rod length,
C_S = correction for non-standardized sampler configuration,
C_B = correction for borehole diameter,
C_E = correction for hammer energy ratio.

C_N was calculated from Kayen et al. (1992), which limits its maximum value to 1.7,

$$C_N = \frac{2.2}{(1.2 + \sigma'_v / P_a)} \tag{11.5}$$

Taking into consideration the average borehole drilling experience in Turkey, it was assumed that C_E=0.5, C_B=1, C_S=1.1. C_R is corrected as suggested by Youd et al (2001) with respect the depth of the each individual location (C_R=0.75 for d<3 m, C_R=0.8 for d=3-4m, C_R=0.85 for d=4-6m, C_R=0.95 for d=6-10m, C_R=1 for d=10-30m).

Step 3. Even though the proposed method recommends a further correction to account for the influence of fines content, since there was not sufficient information, this correction was not applied for the present study. However, it is highly recommended that fines

correction should be applied in the future microzonation studies. Therefore it is crucial that fines content should be determined for all liquefiable soil layers.

Step 4. The resulting $N_{1,60,}$ is used with modified 5% or less fines content curve of Seed et al. (1985) to evaluate liquefaction resistance *CRR* using the equation of the curve as given by (Youd et al., 2001);

$$CRR_{7.5} = \frac{1}{34 - N_{1,60}} + \frac{N_{1,60}}{135} + \frac{50}{\left(10N_{1,60} + 45\right)^2} - \frac{1}{200} \tag{11.6}$$

Step 5. Since the curve given by Eq.(11.6) is valid only for magnitude 7.5 earthquakes magnitude scaling factor *MSF* need to be applied to adjust to the other magnitudes and the factor of safety may be calculated from,

$$FS = (CRR_{7.5} / CSR)MSF \tag{11.7}$$

where MSF would to be chosen from a range of recommended values (Youd et al., 2001). For the Adapazarı case study *MSF* is taken as 1.

The safety factors were calculated along the whole depth of the borehole for all liquefiable soil layers based on the available SPT-N blow counts using the surface peak ground accelerations calculated from site response analysis, explained in detail in Chapter 6. The liquefaction potential for each borehole was calculated based on the procedure proposed by Iwasaki et al. (1982) using the variation of the safety factors with depth.

Iwasaki et al. (1982) quantified the severity of possible liquefaction at any site by introducing a factor called the liquefaction potential index, P_L, defined as

$$P_L = \int F(z)w(z)dz \tag{11.8}$$

where *z* is the below the ground water surface, measured in meters; *F(z)* is a function of the liquefaction resistance factor, F_L, where *F(z)=1-* F_L but if F_L>1.0, *F(z)=0*; and *w(z)=10-0.5z.* Eq.(6.36) gives values of P_L ranging from 0 to 100.

Based on the results reported by Iwasaki et al. (1982) and in accordance with the Microzonation Manual (Part 2B) and TAB (2003), three zones (A, B, and C) were identified with respect to liquefaction potential index. Zone A is the where the liquefaction potential index is PL>15, zone B is the intermediate zone where the liquefaction potential index is 5>PL>15, and zone C is the safest zone where liquefaction potential index is PL<5. The microzonation map for liquefaction susceptibility determined by this approach is shown for Adapazarı region in Figure 11.19.

11.5. LANDSLIDE HAZARD

The zonation with respect to landslide hazard for the Adapazarı and Gölcük regions as explained in detail in Chapter 8 using the KoeriSlope program are given in Figures 11.20 and 11.21. The zonation was in accordance with the Microzonation Manual (Part 2B), where three zones (A, B, and C) were identified with respect to safety factors. Zone A is where the landslide hazard is very likely with a safety factor less than one, zone B is the intermediate zone where the safety factor is between one and two, and zone C is the safest zone, where landslide hazard is unlikely with a safety factor greater than two. As can be observed from the maps given, and as expected, the landslide hazard is negligible for Adapazarı but it needs to be take into account at certain locations in the Gölcük area.

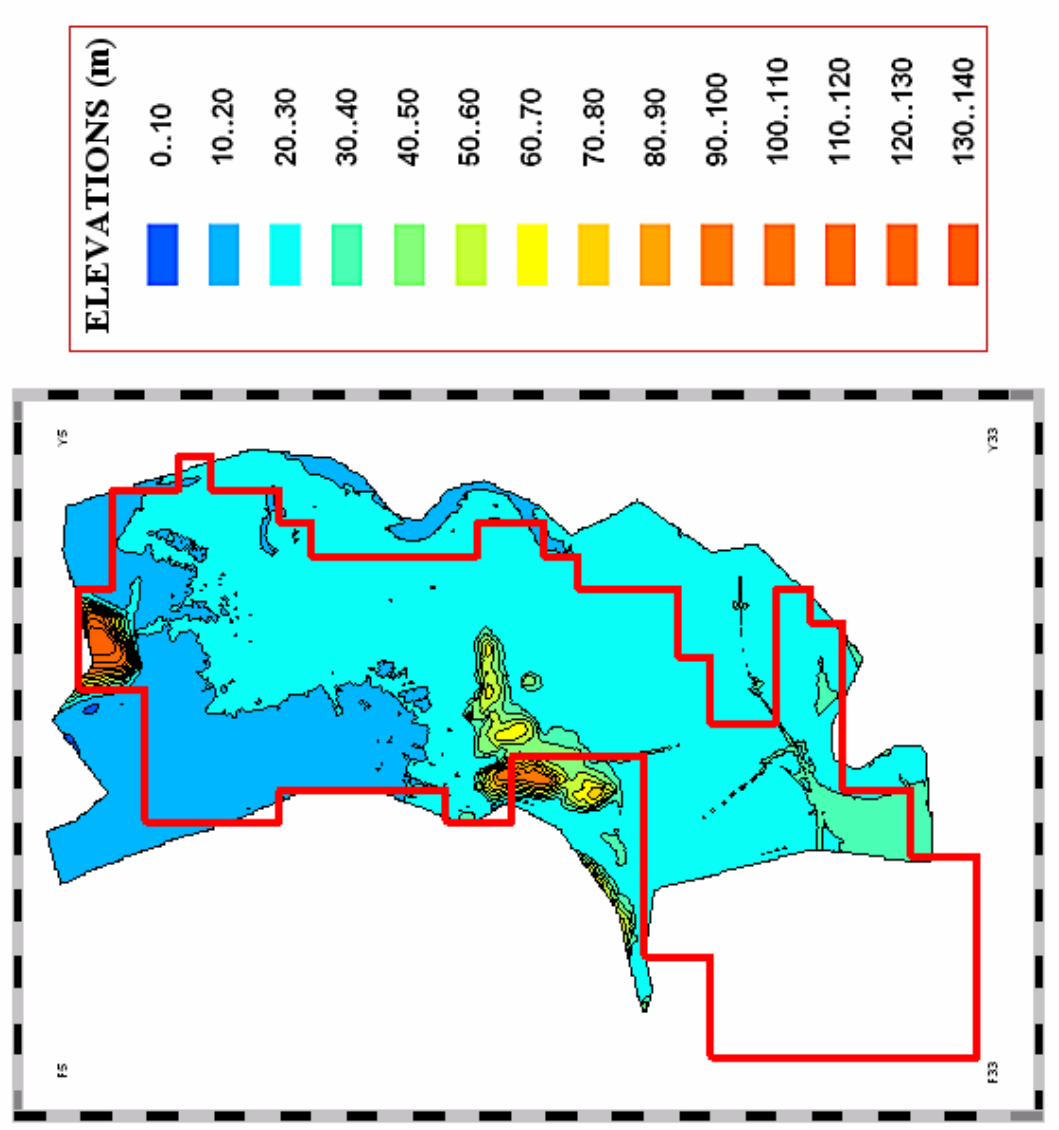

Figure 11.2. Variation of elevation in Adapazarı

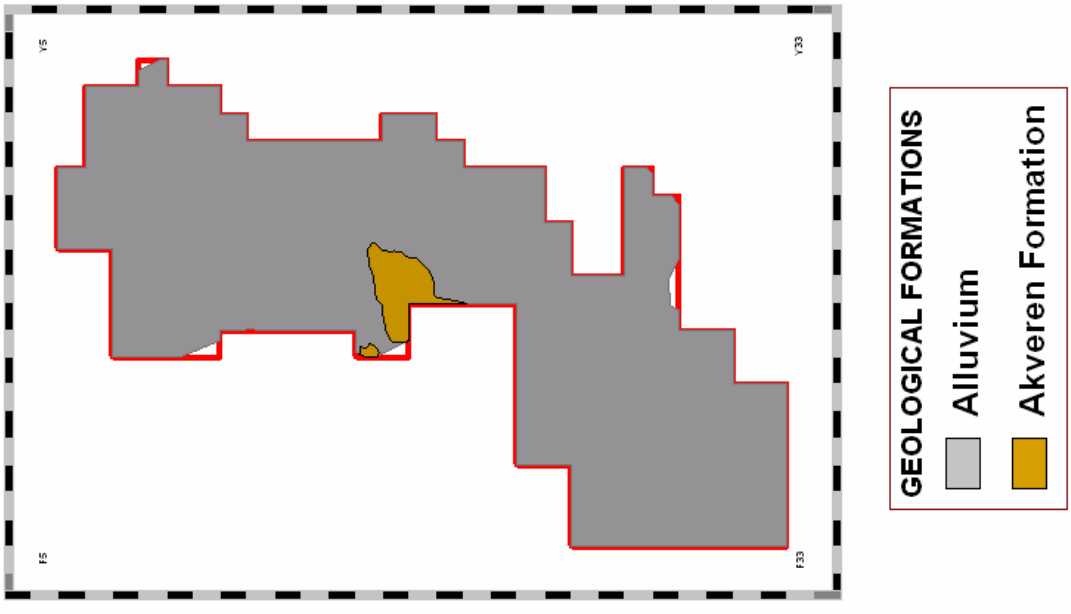

Figure 11.1. Geological units in the Adapazarı Region

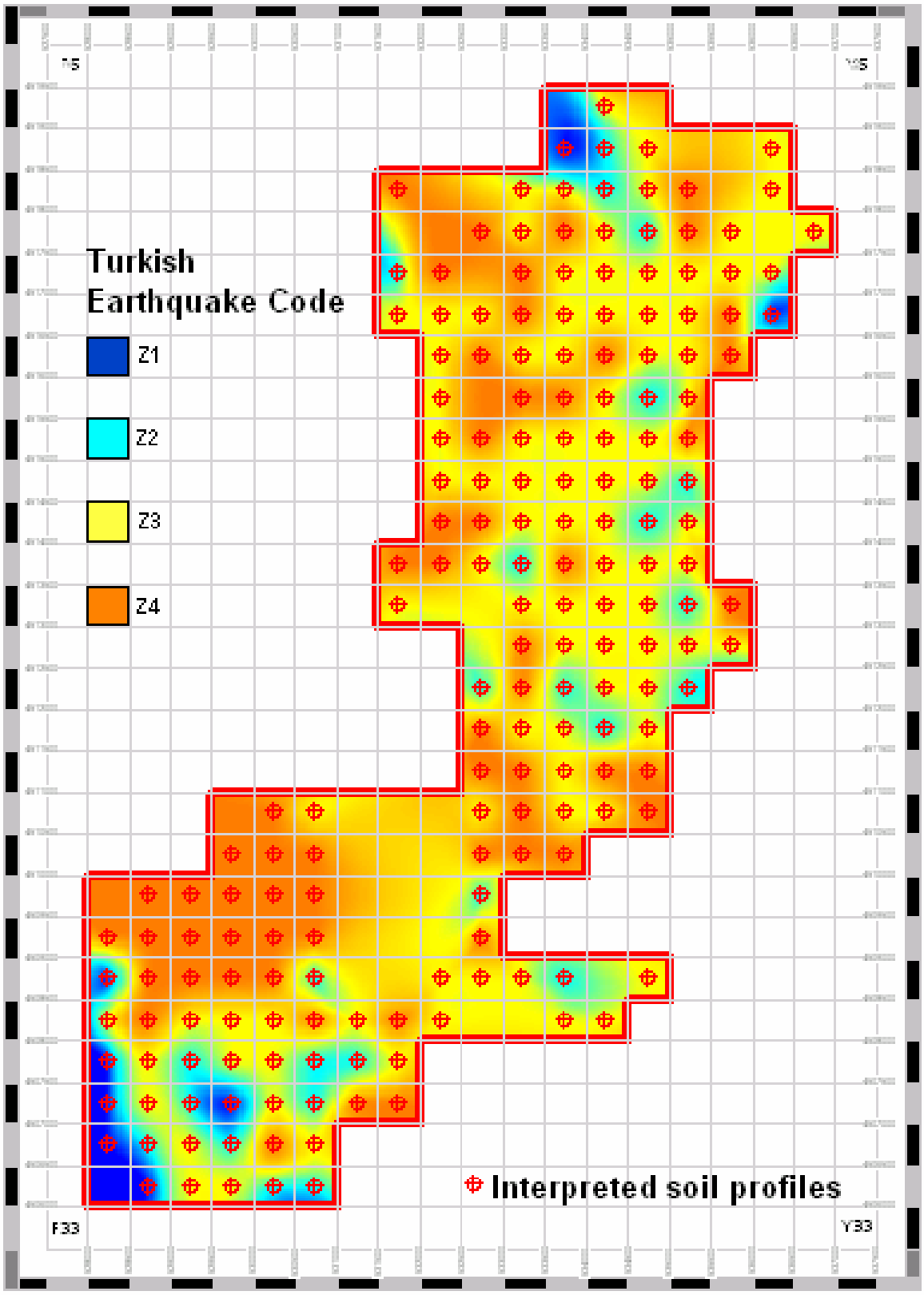

Figure 11.3. Site Classification according to the Turkish Earthquake Code for Adapazarı

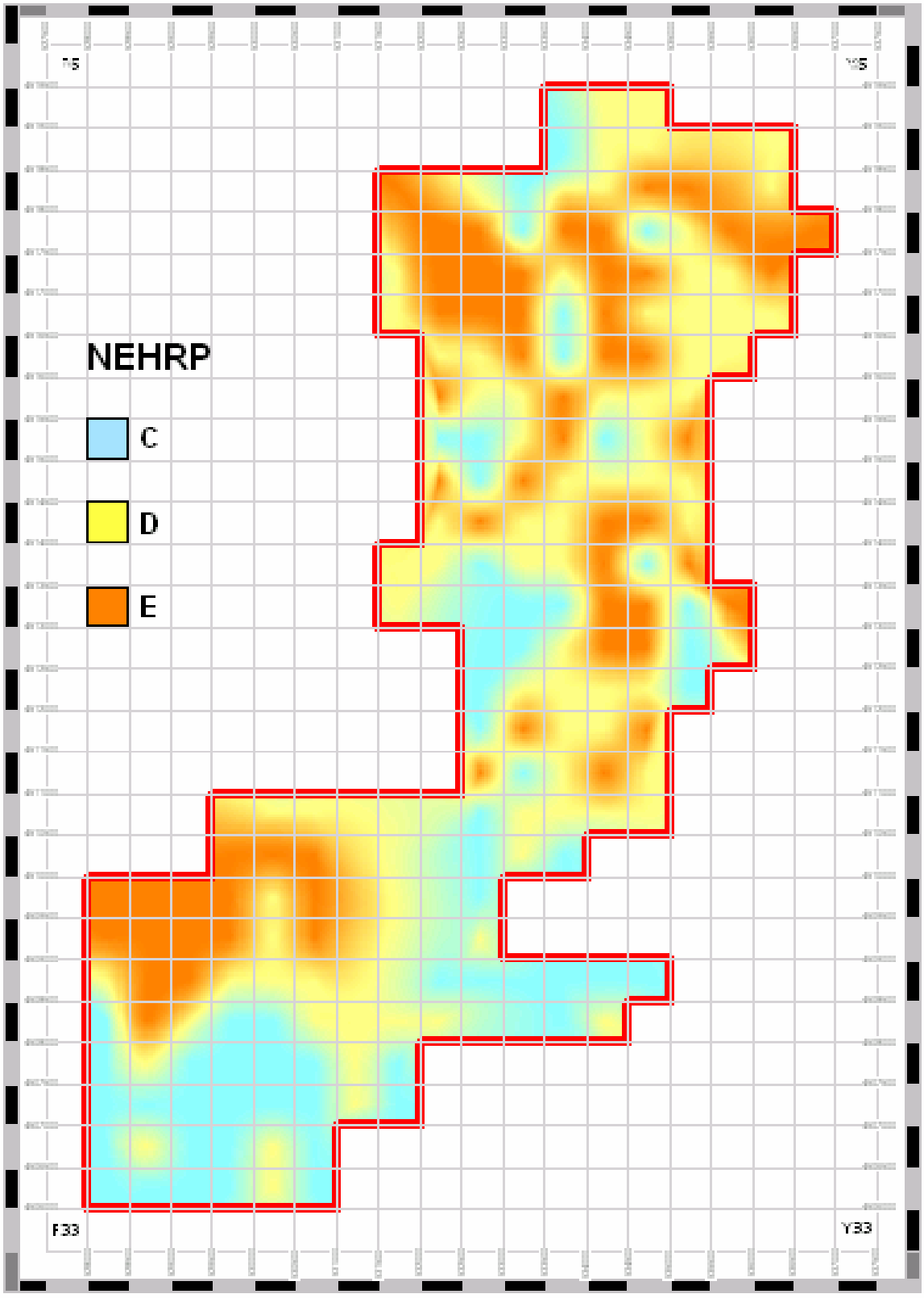

Figure 11.4. Site Classification according to NEHRP for Adapazarı

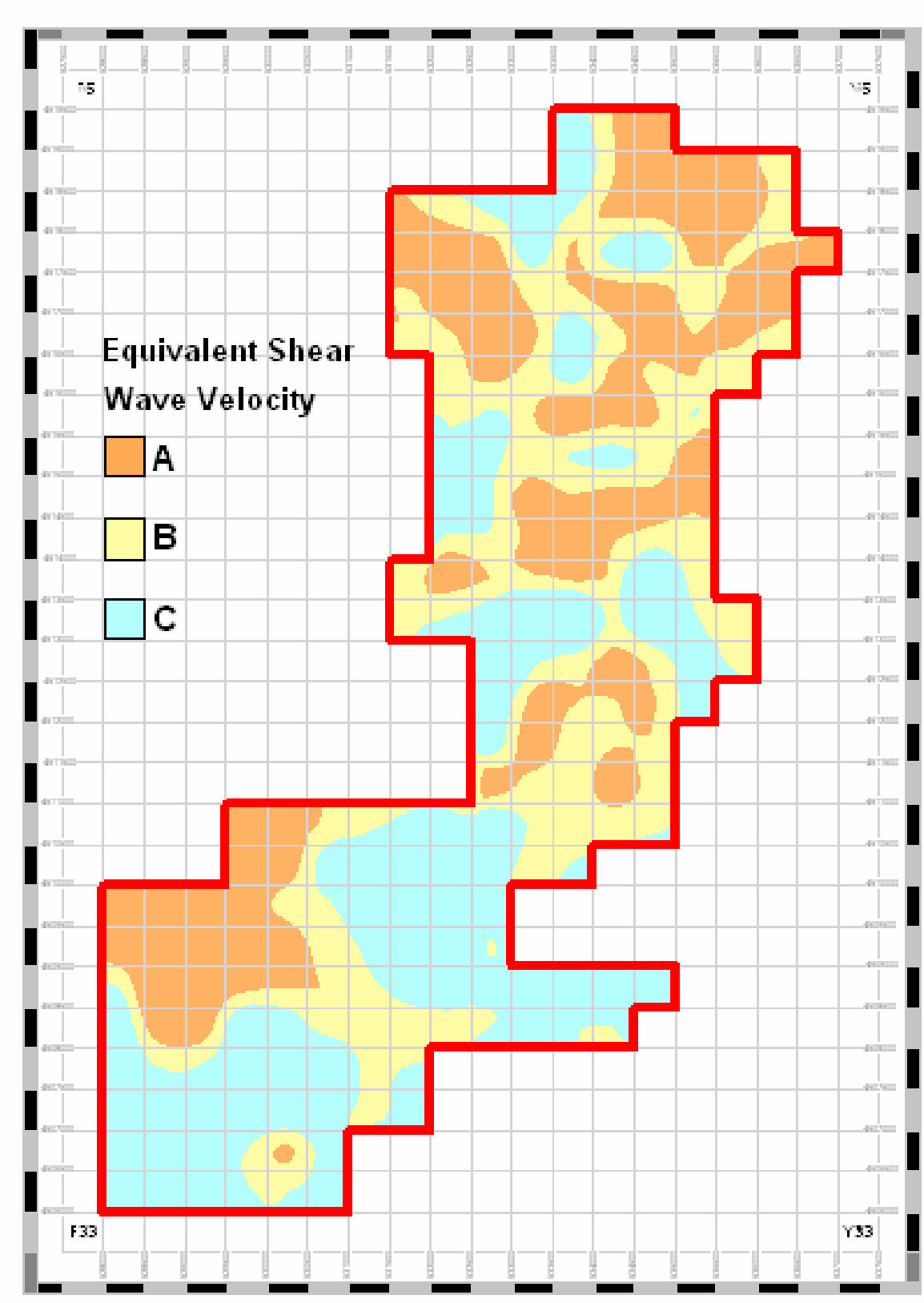

Figure 11.5. Site Classification according to equivalent shear wave velocity for Adapazarı

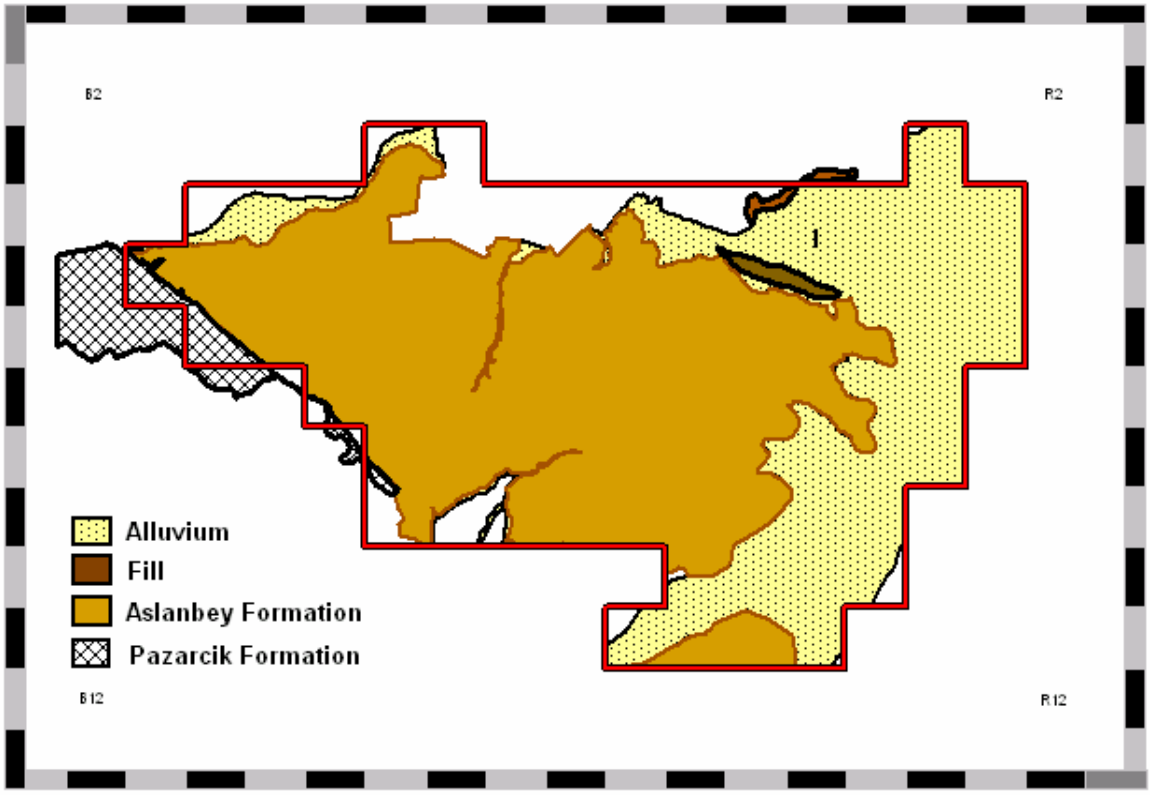

Figure 11.6. Geological units in the Gölcük Region

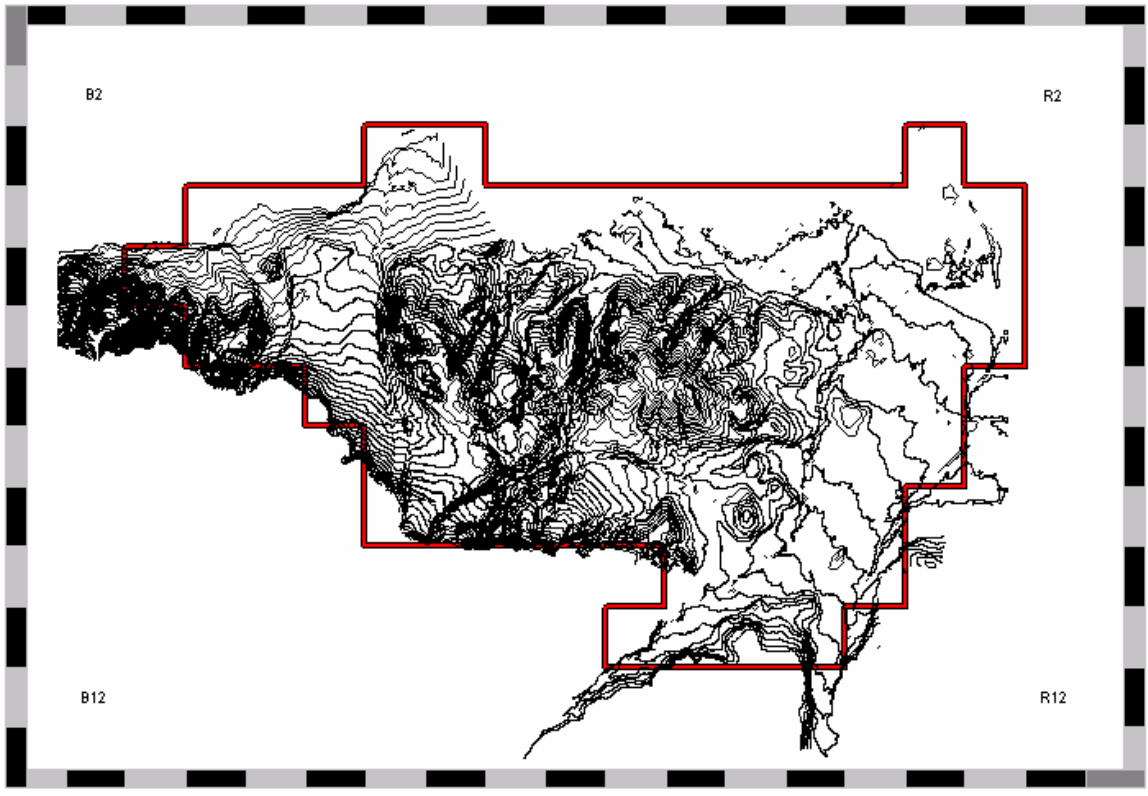

Figure 11.7. Variation of elevation in Gölcük

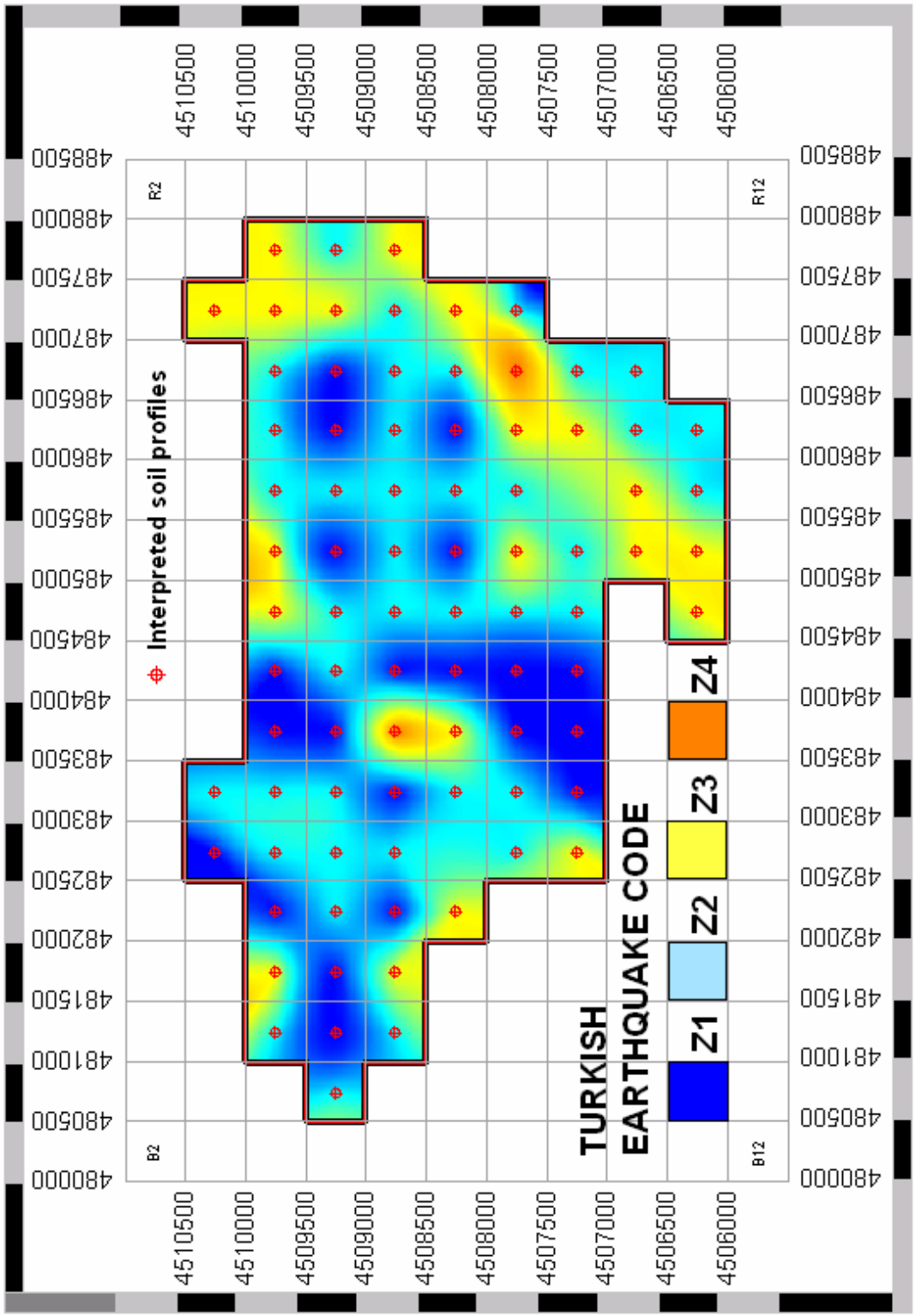

Figure 11.8. Site Classification according to Turkish Earthquake Code for Gölcük

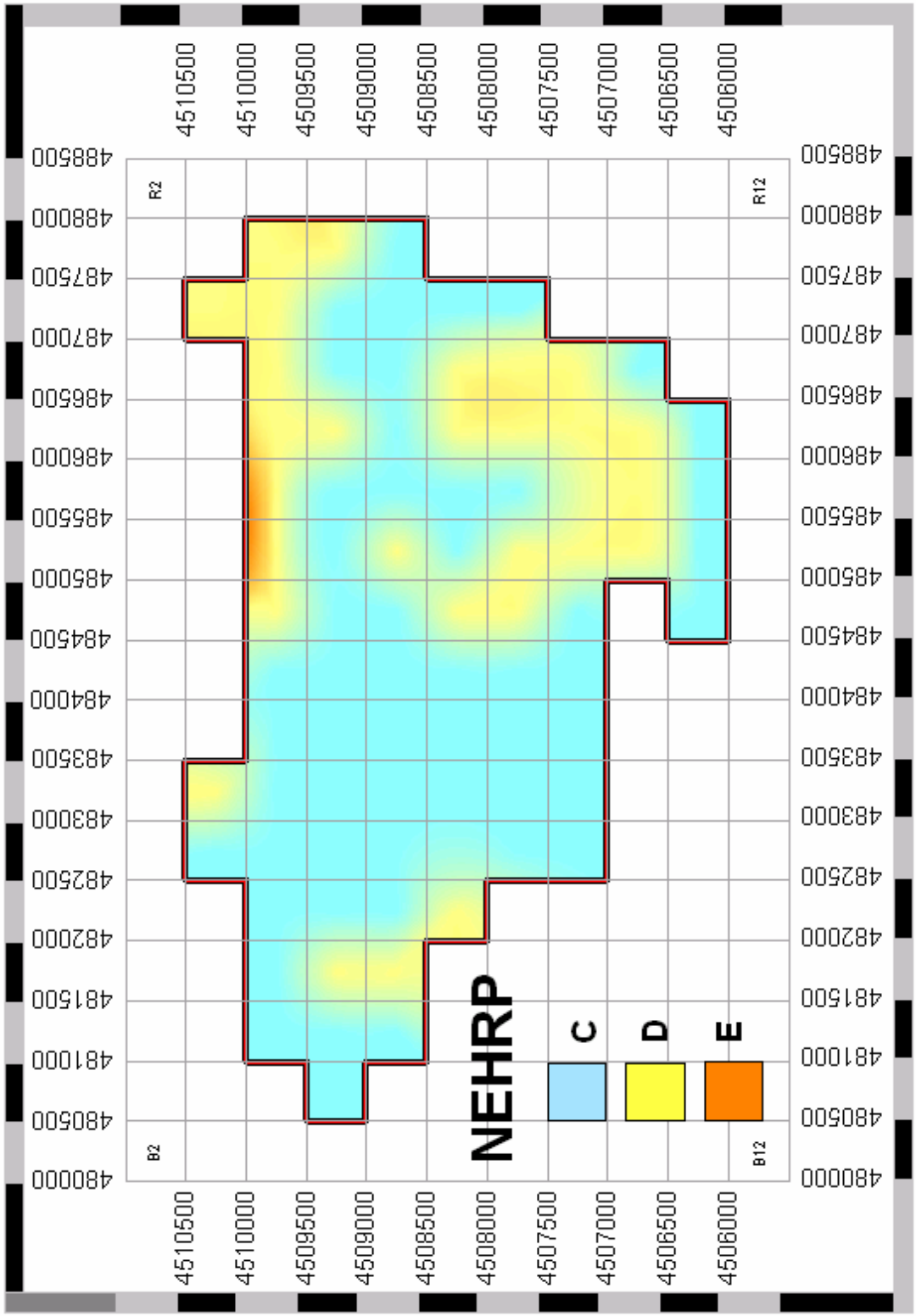

Figure 11.9. Site Classification according to NEHRP for Gölcük

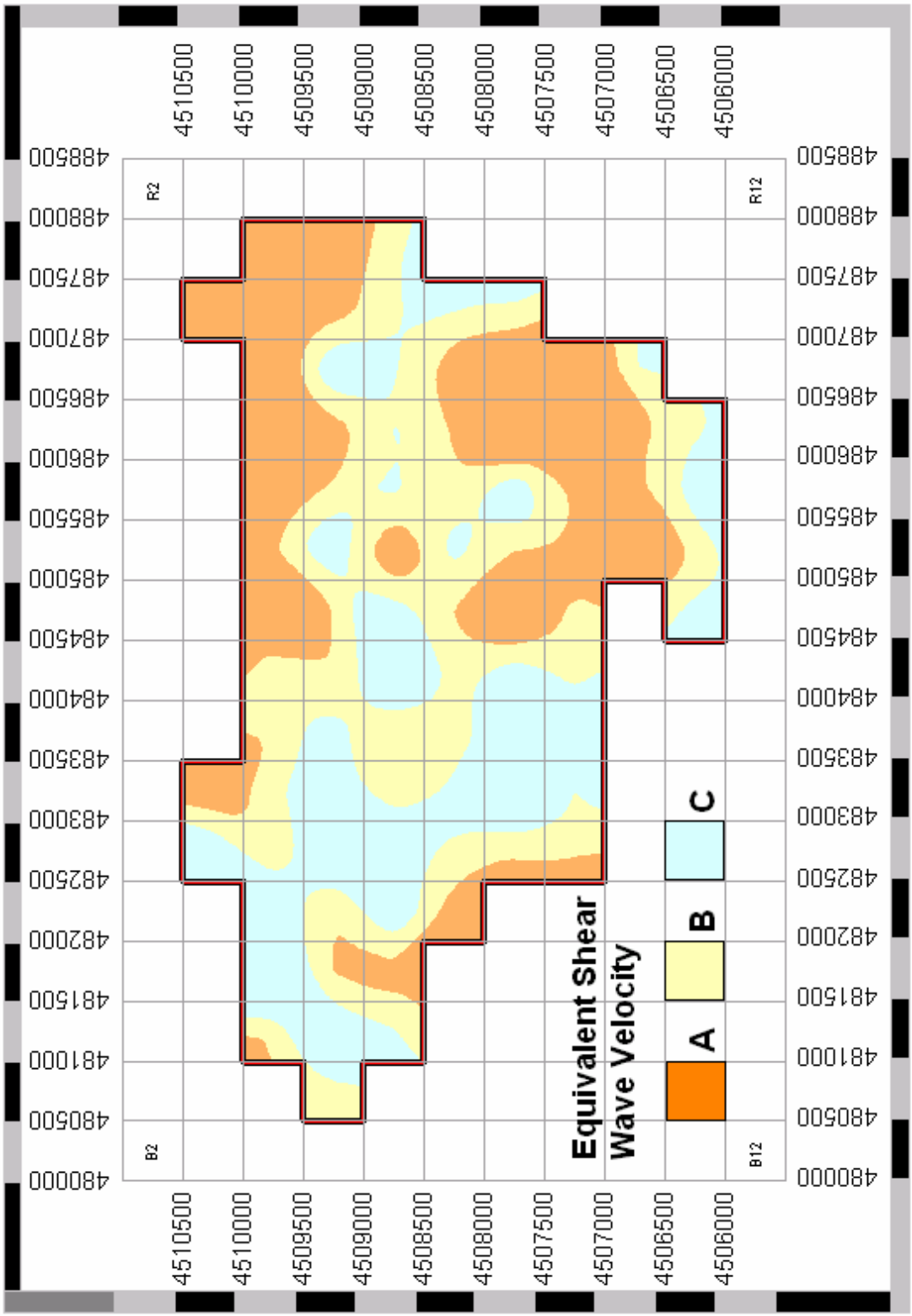

Figure 11.10. Site Classification according to equivalent shear wave velocity for Gölcük

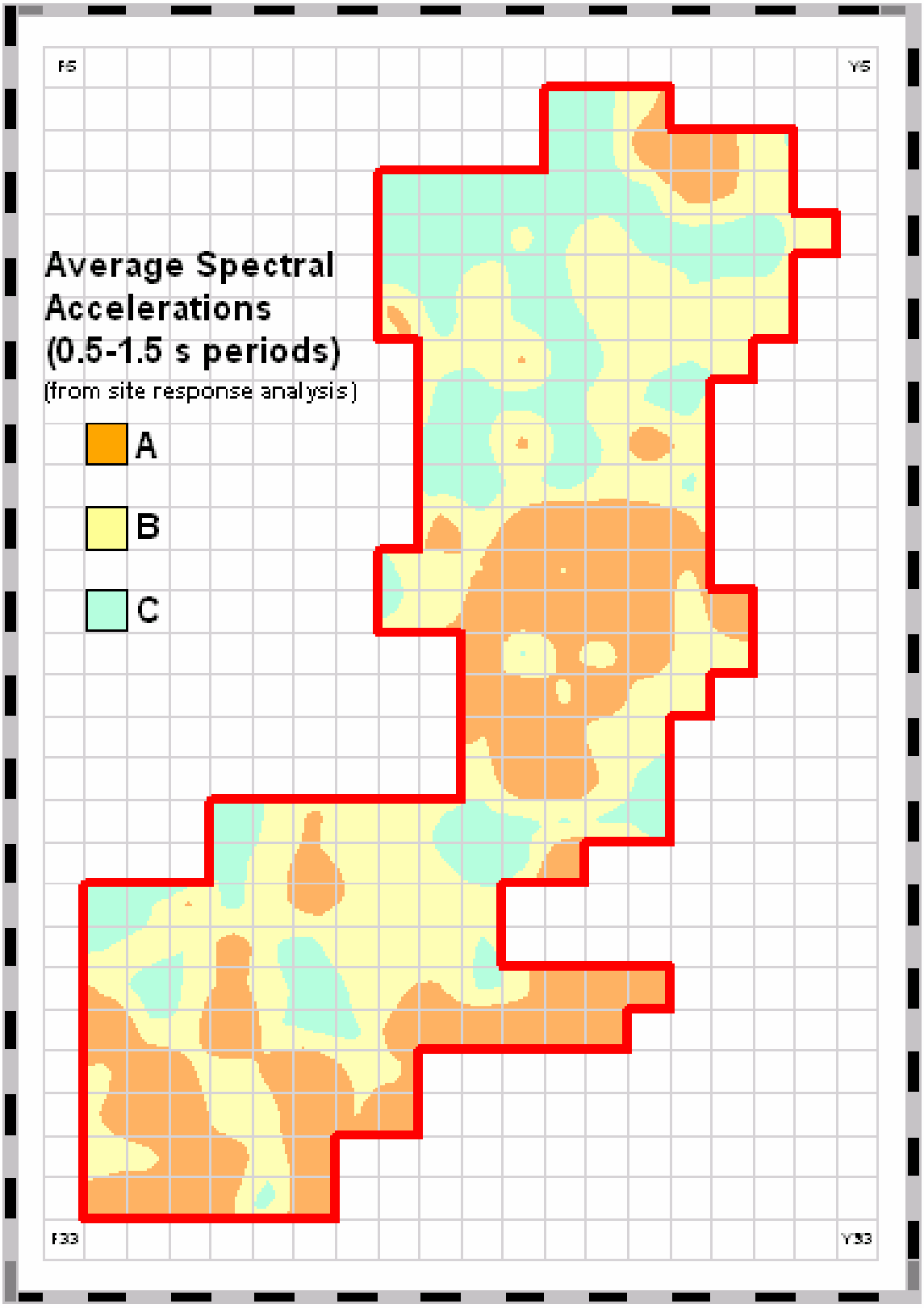

Figure 11.11. Variation of average spectral accelerations calculated by site response analysis in Adapazarı

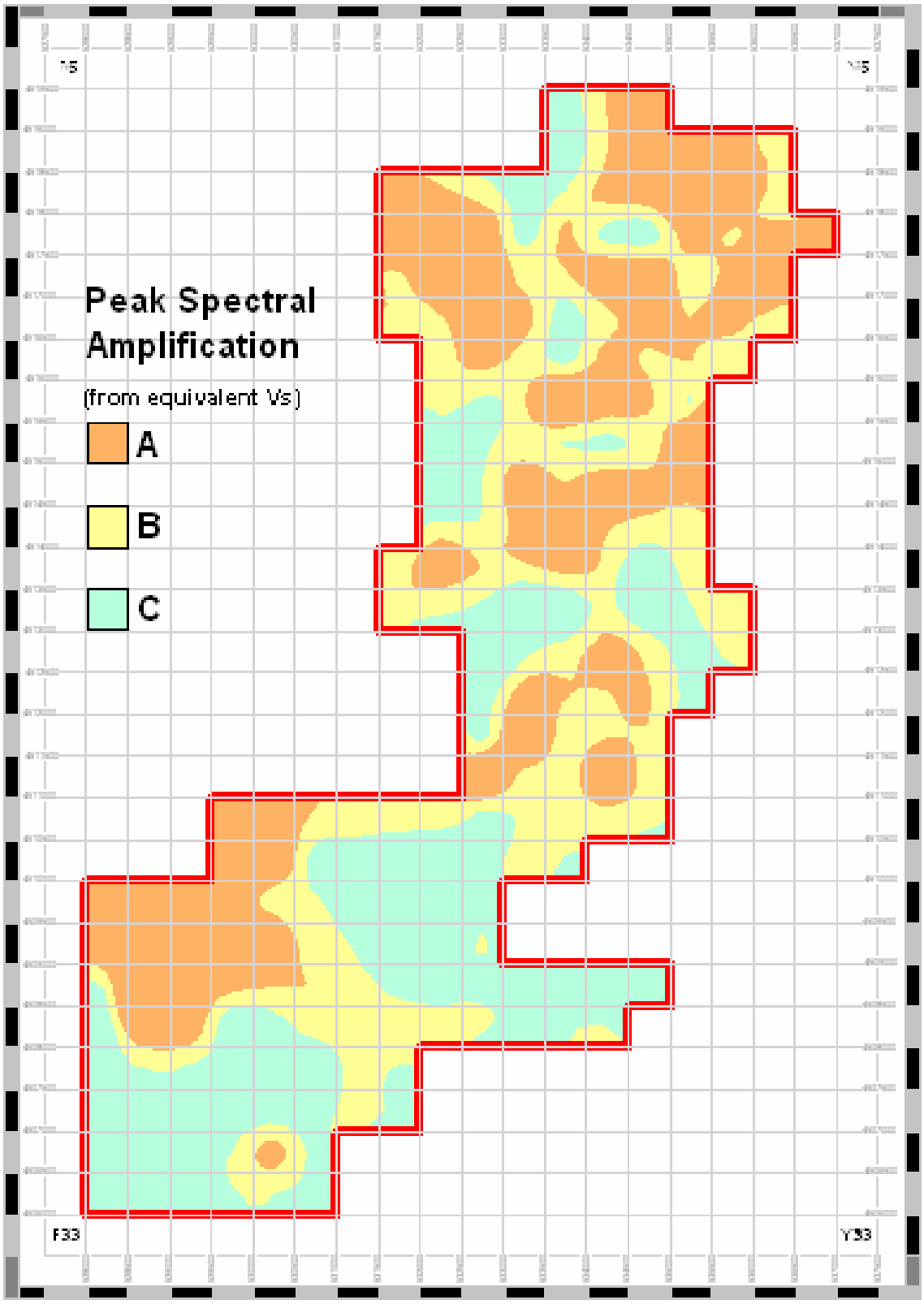

Figure 11.12. Spectral amplification from equivalent shear wave velocity for Adapazarı

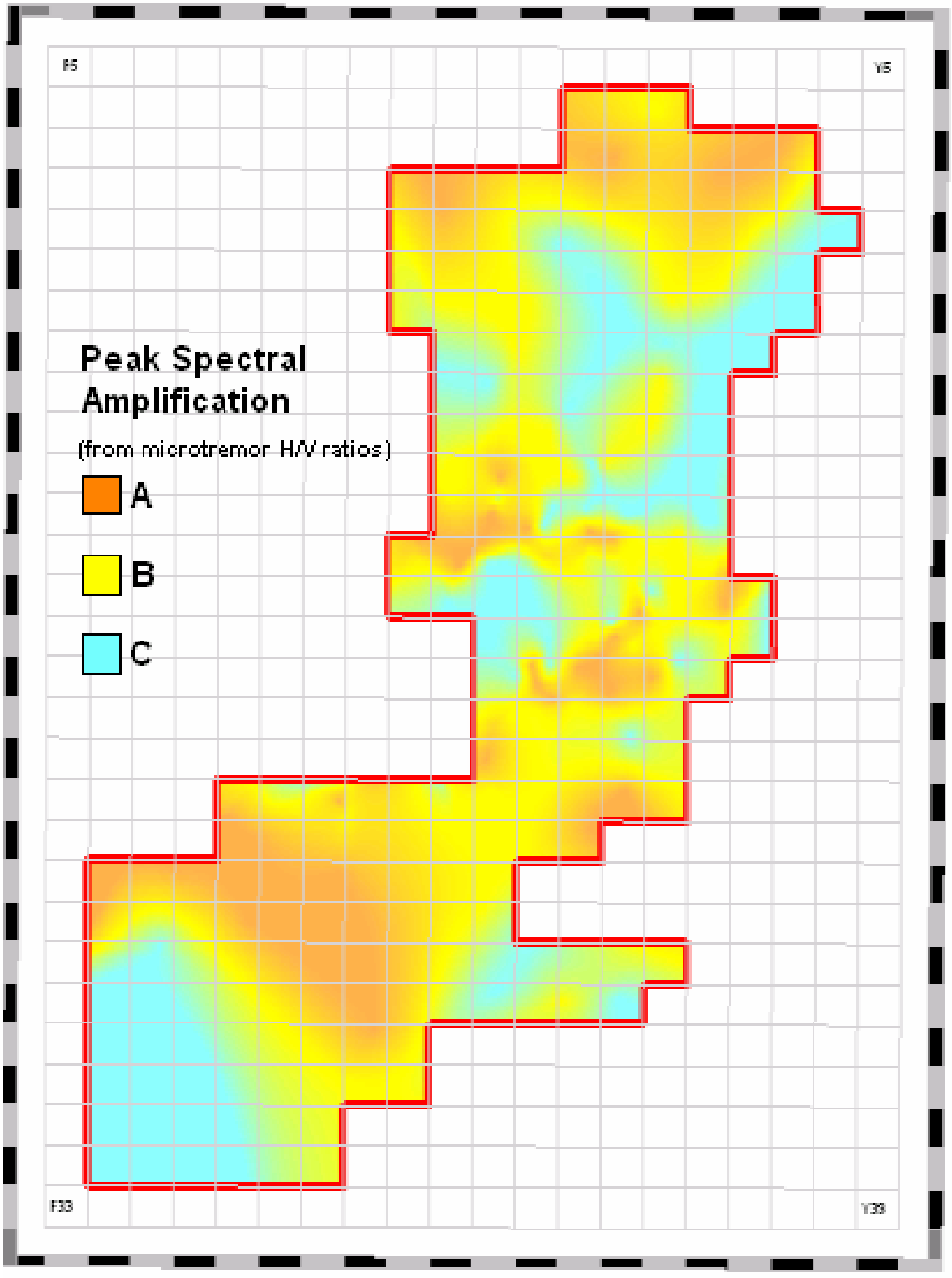

Figure 11.13. Spectral amplification from microtremor H/V ratios for Adapazarı

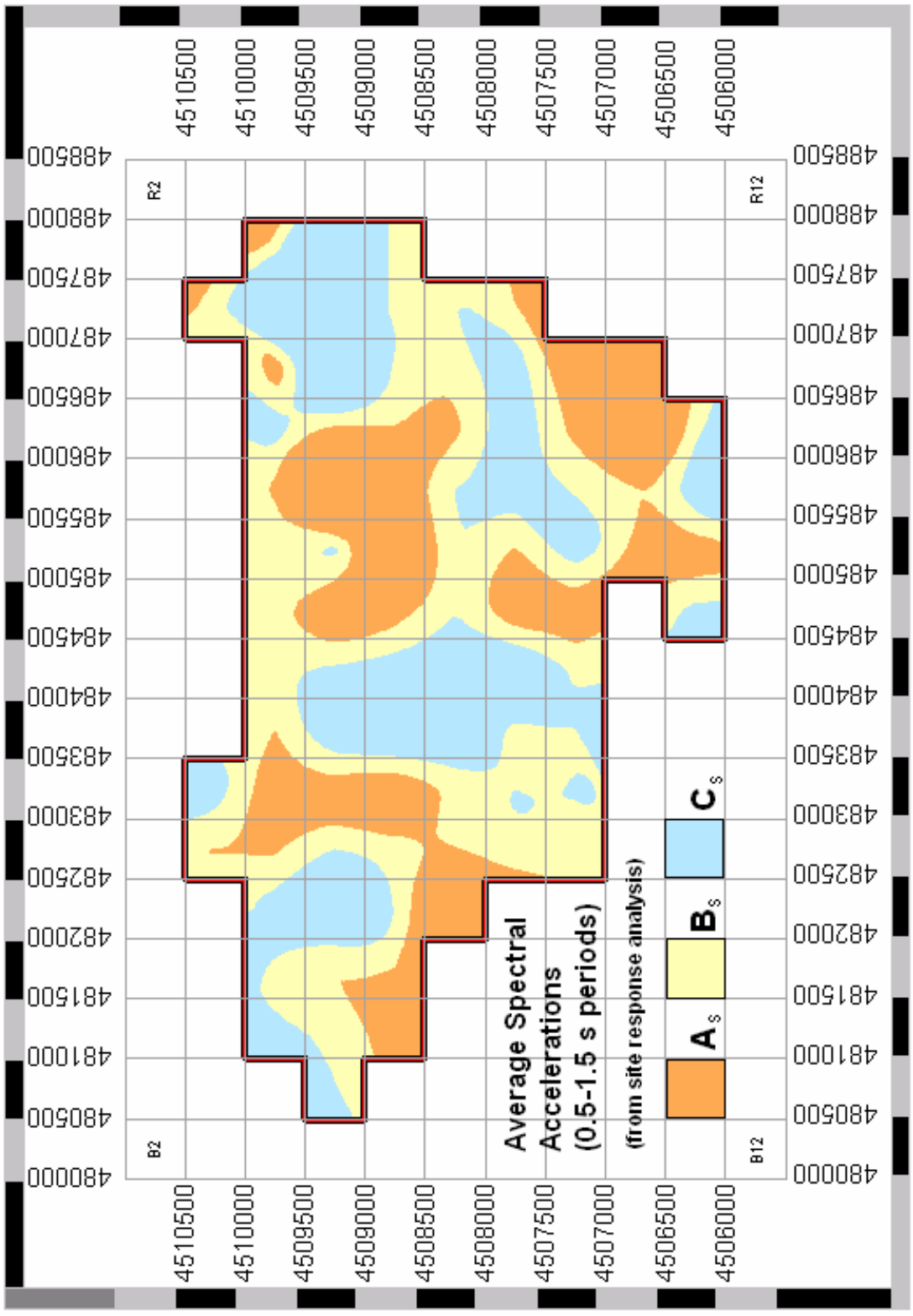

Figure 11.14. Variation of average spectral accelerations calculated by site response analysis in Gölcük

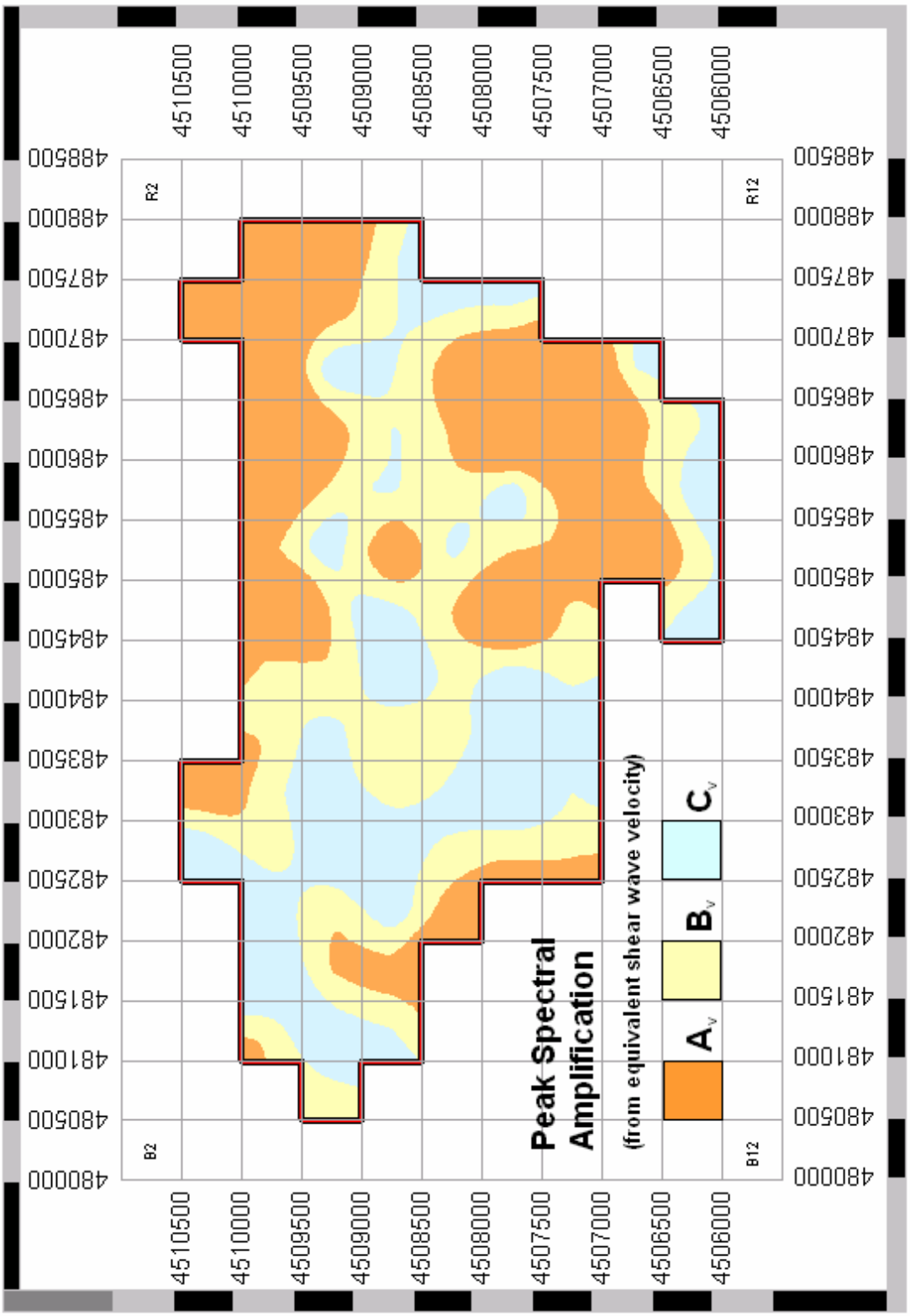

Figure 11.15. Spectral amplification from equivalent shear wave velocity for Gölcük

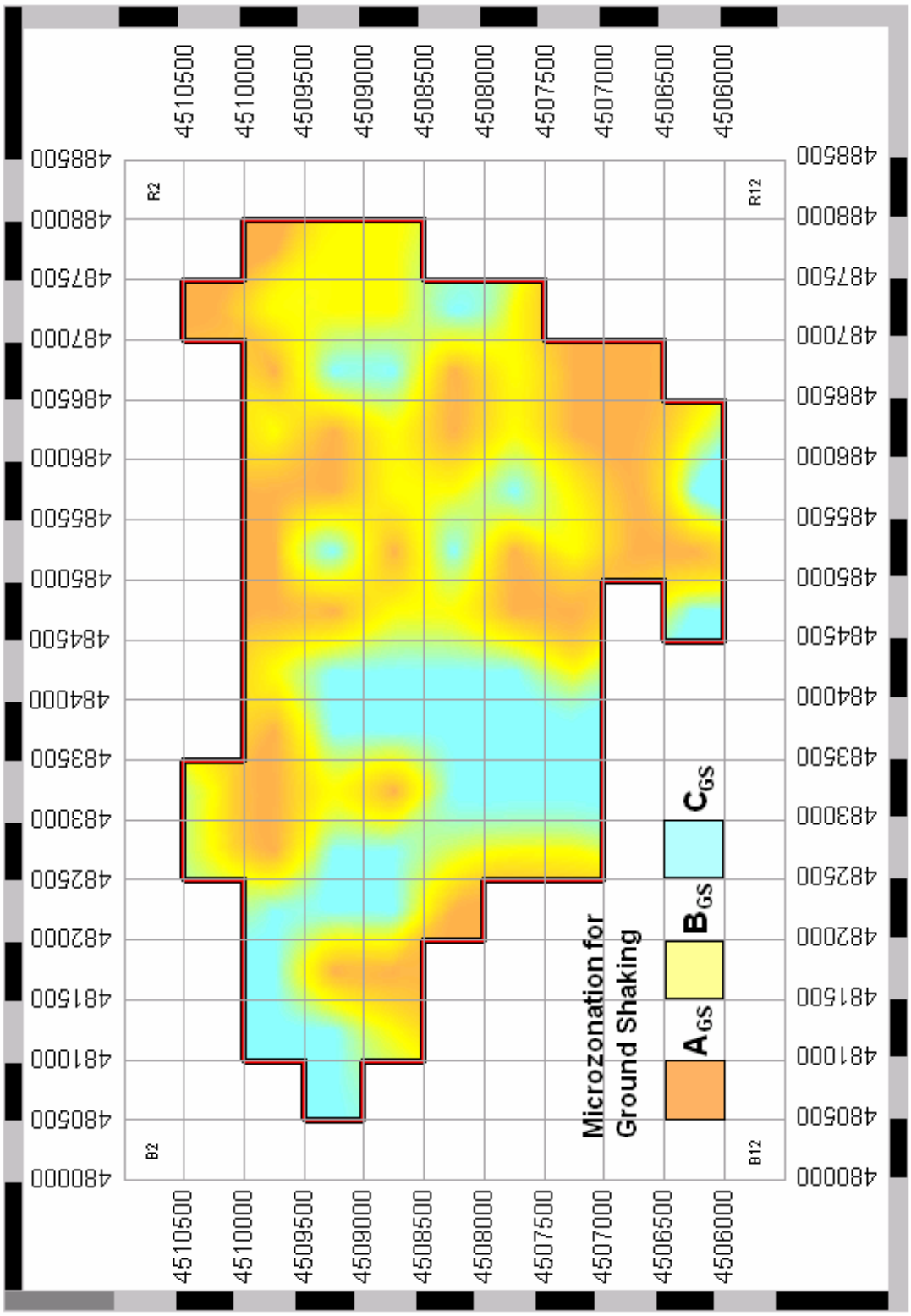

Figure 11.16. Ground shaking zonation map for Gölcük when overlapping zones are determined for each grid from average spectral acceleration map obtained from site response analysis and peak spectral amplification map calculated from equivalent

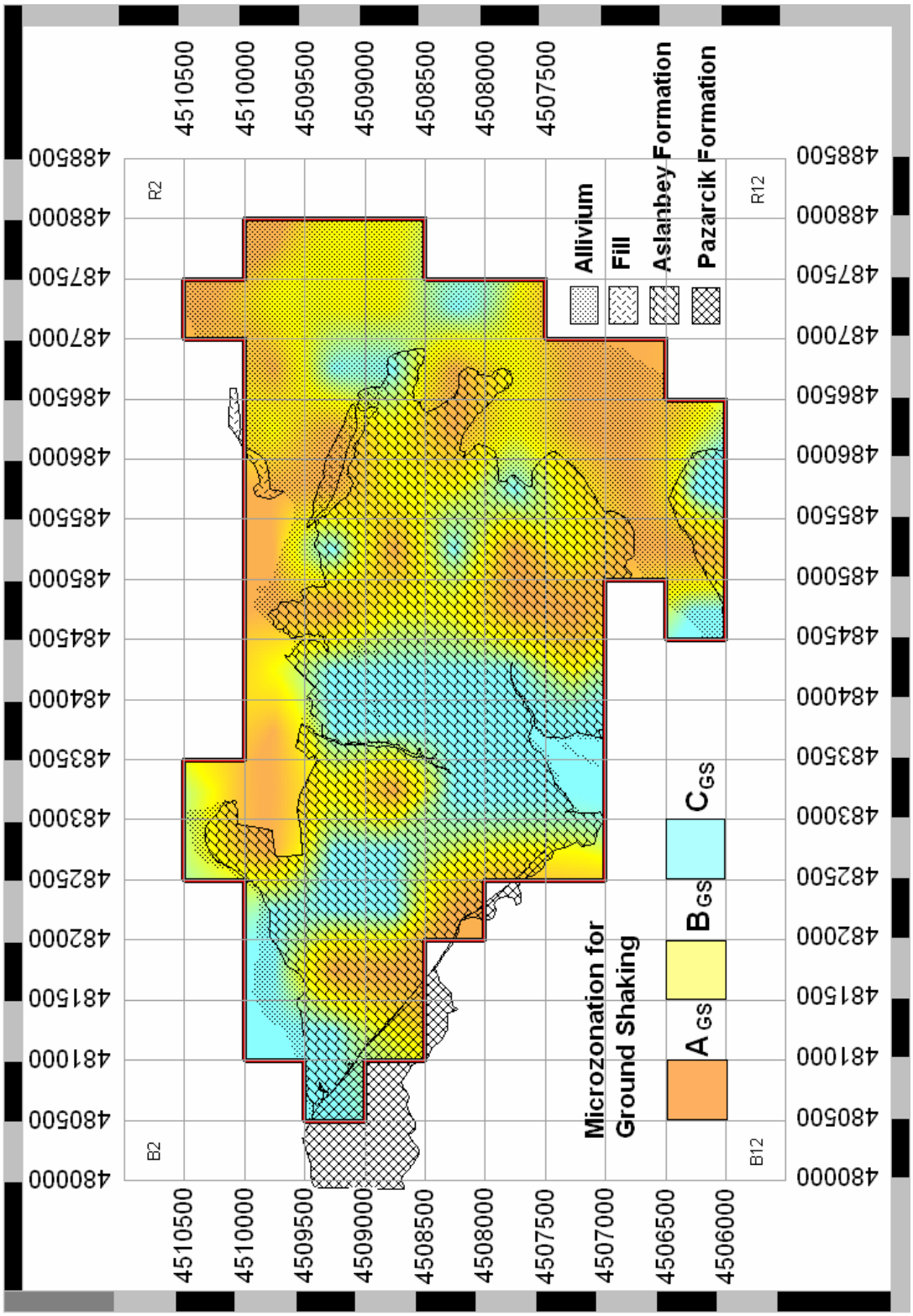

Figure 11.17. Comparison of ground shaking map with geological formations

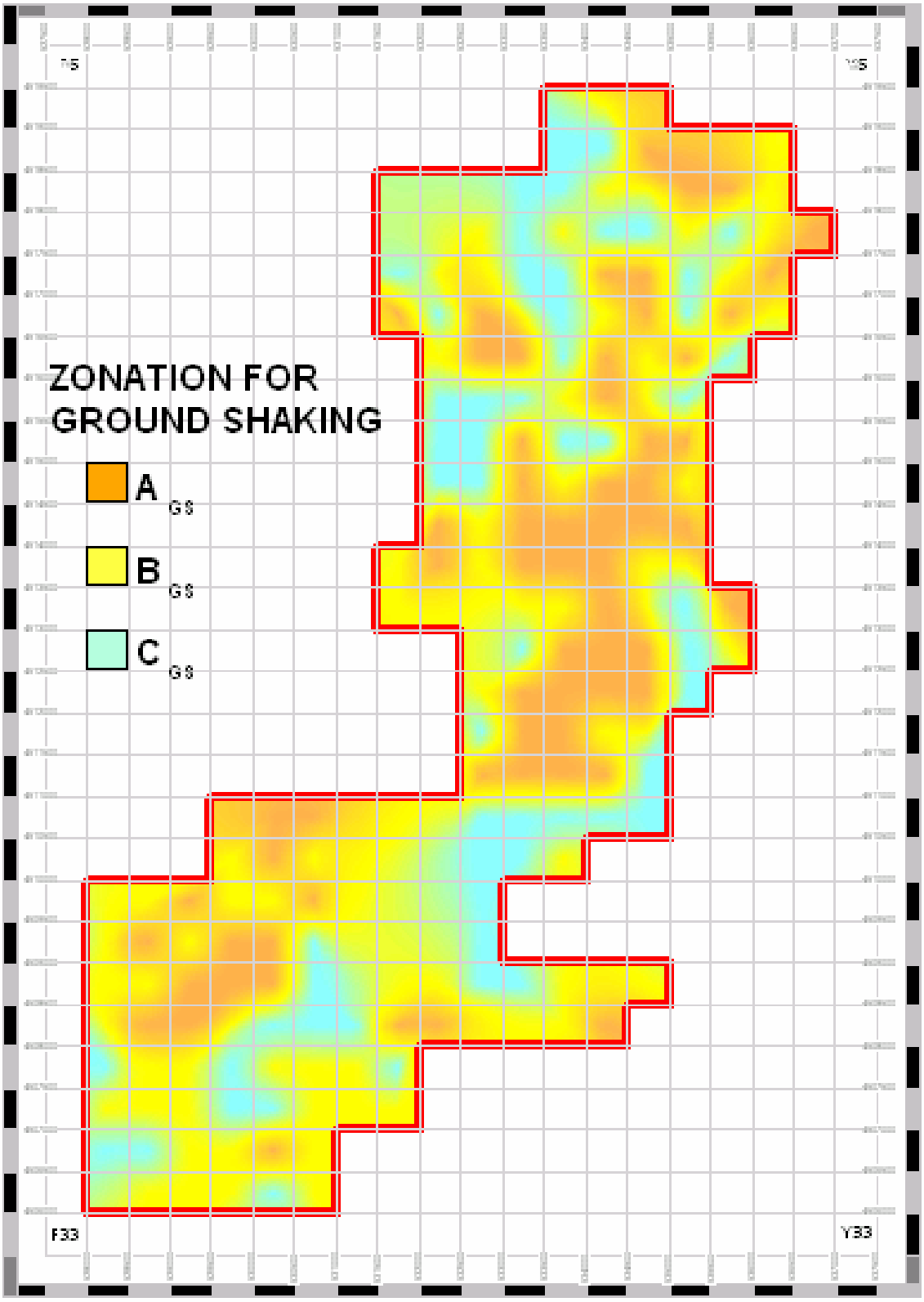

Figure 11.18. Ground shaking zonation map for Adapazarı when overlapping zones are determined for each grid from average spectral acceleration map obtained from site response analysis and peak spectral amplification map calculated from equivalent shear wave velocity

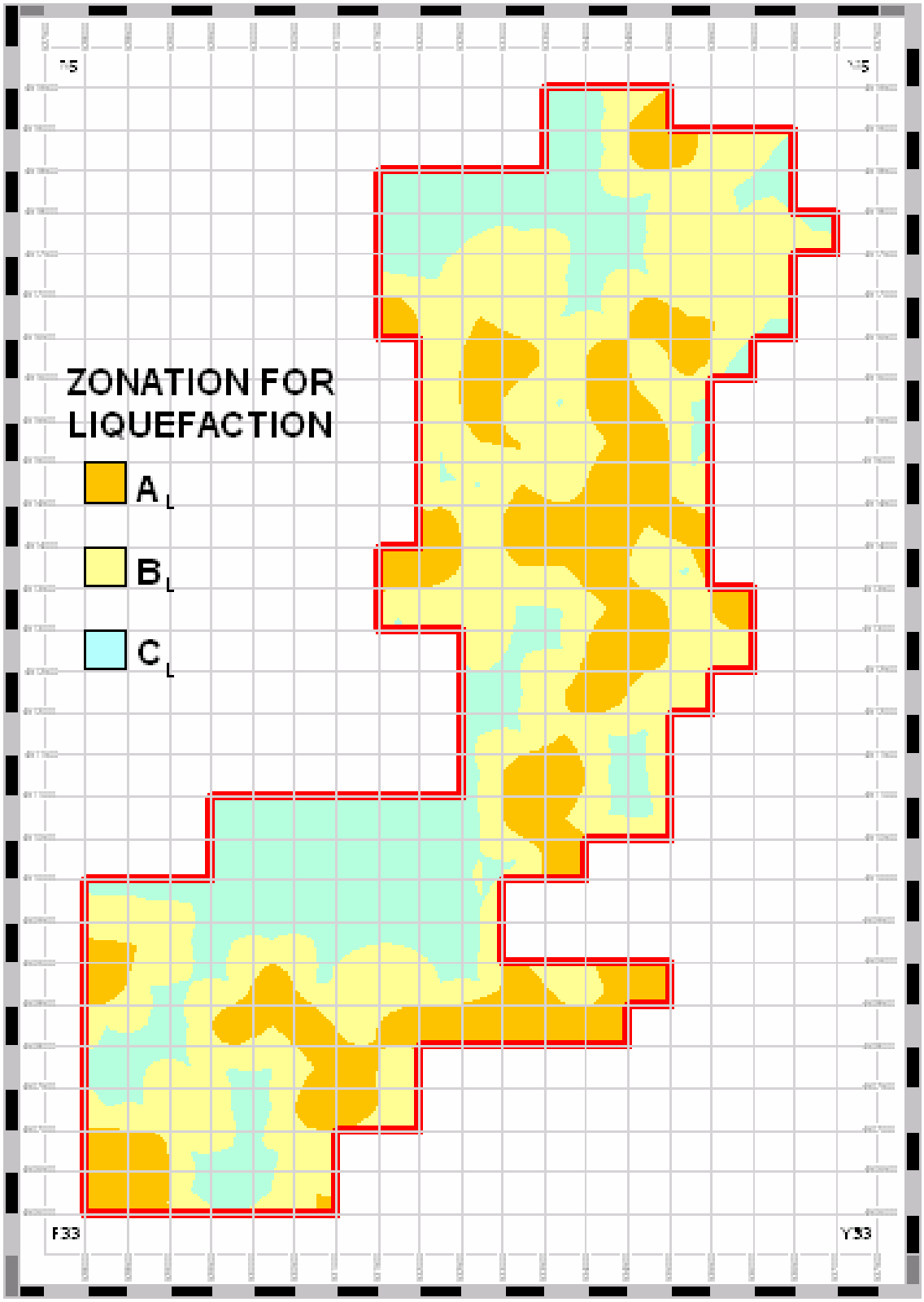

Figure 11.19. Variation of liquefaction susceptibility in Adapazarı

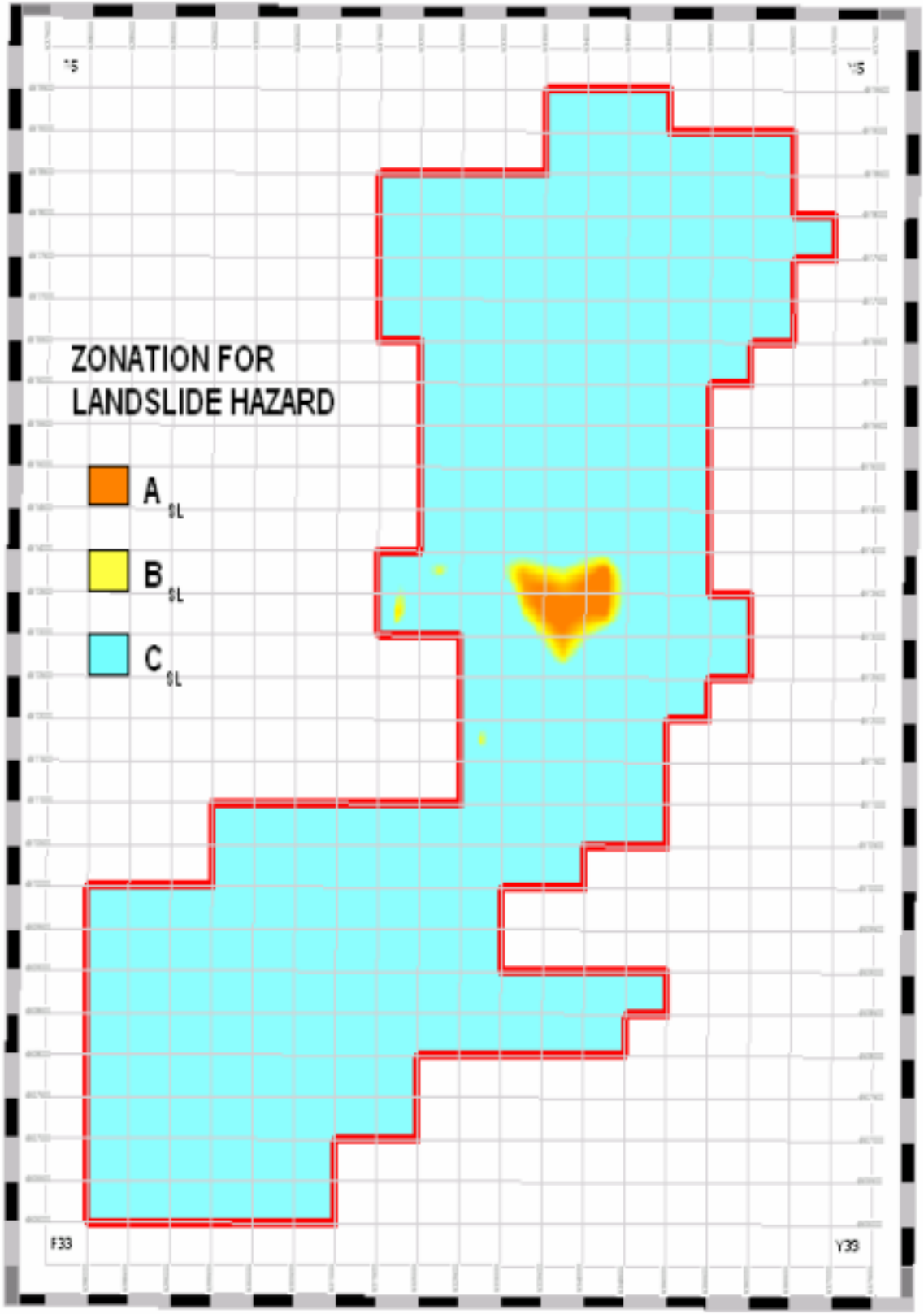

Figure 11.20. Variation of landslide hazard in Adapazarı

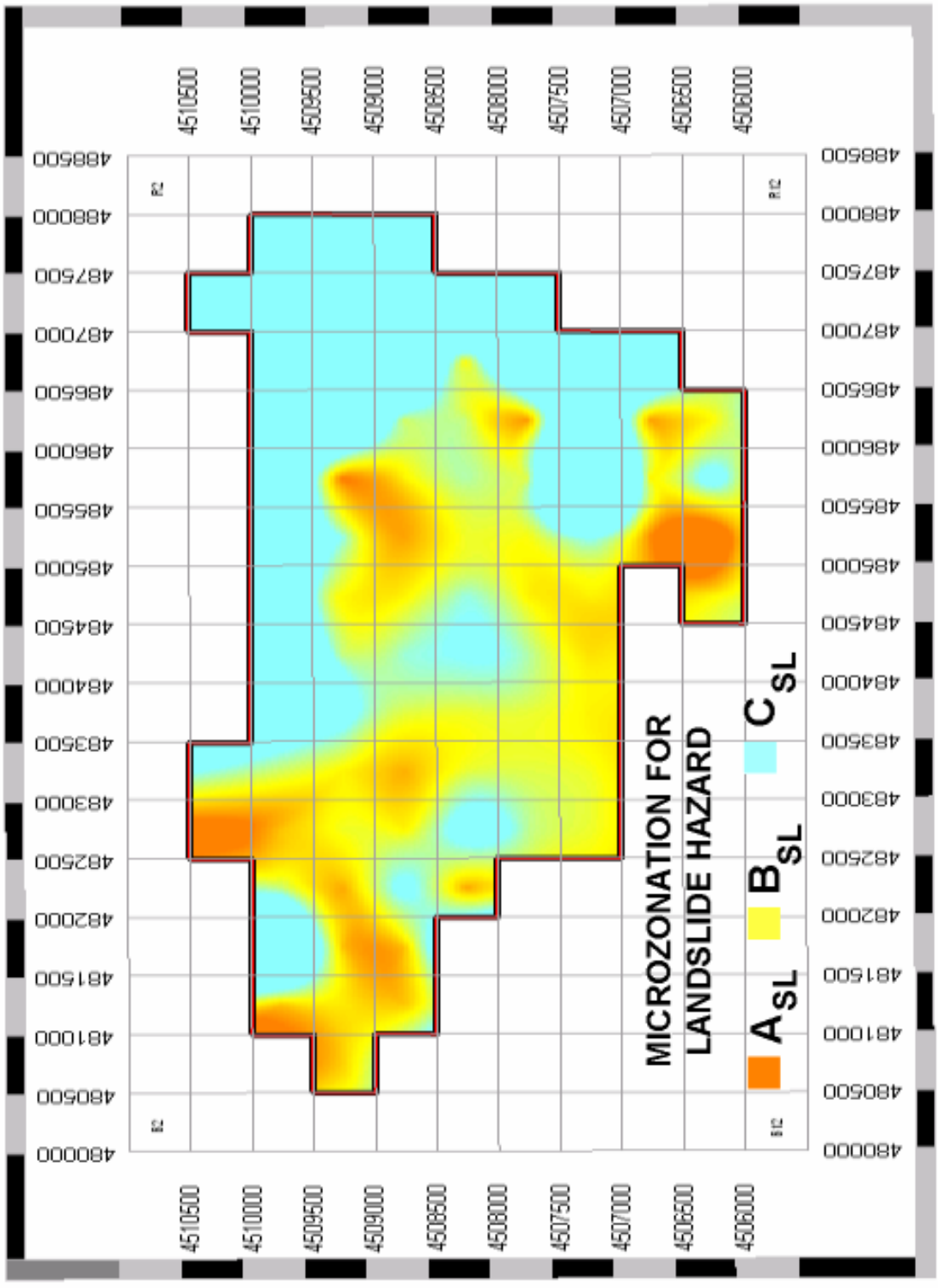

Figure 11.21. Variation of landslide hazard in Gölcük

12. REFERENCE

Abeki, A., Matsuda, I., Enomoto, T., Shigyo, V., Watanabe, K., Tanzawa, Y. & Nakajima, Y. (1995) "A Study of Seismic Microzonation Based on the Dynamic Characteristics of Subsurface Ground Conditions", Proc. 5th International Conference on Seismic Zonation, Nice, France, (3):2187-2194.

AFPS (1995) "Guidelines for Seismic Microzonation Studies", French Association for Earthquake Engineering, 18 pp.

Aki, K. (1957) "Space and time spectra of stationary stochastic waves with special reference to micro-tremors", Bull. Earthquake Res. Inst., Tokyo Univ. 35, 415-457.

Akyuz, H. S., A. Barka, E. Altunel, R. Hartleb, G. Sunal (2000), "Field Observations and Slip Distribution of the November 12, 1999 Duzce Earthquake (M=7.1), Bolu-Turkey", The 1999 Izmit and Duzce Earthquakes: Preliminary Results, A. Barka, O. Kozacı, S. Akyüz and E. Altunel, Istanbul Tech. Un. Press, Istanbul, pp. 61-70.

Ambraseys, N. N. and C. F. Finkel, (1991), "Long-term seismicity of Istanbul and of the Marmara Sea region", Terra Nova, 3, pp: 527-539.

Andrews, D. C. A. and Martin, G. R. (2000): "Criteria for Liquefaction of Silty Soils." 12th World Conference on Earthquake Engineering, Proceedings, Auckland, New Zealand

Andrus, R. D. (1994). "In situ characterization of gravelly soils that liquefied in the 1983 Borah Peak Earthquake." Ph.D. Dissertation, University of Texas at Austin

.Ansal, A., Çetin, K.Ö., Demirbaş, E., Elmas, M., Erdik, M., Fäh, D., Giardini, D., Köksal, D., Laue, J., Lestuzzı,P., Önalp, A., Siyahi, B., Sprıngman, S., Studer, J., (2002a) Report of the Meetıng On Concepts for Analyses and Interpretatıon of Results ın DRM-MERM Project by Research Task Group, Project Place Web Site

Ansal, A., Erdik, M., Kurtulus, A., Erken, A., Sesetyan, K., Siyahi, B. (2002b) Project MERM Microzonation for Earthquake Risk Mitigation, "Part E. State-of-the Art Report Review of Current Literature on Seismic Microzonation", Kandilli Observatory and Earthquake Research Institute, Bogaziçi University, Istanbul, Turkey

Ansal, A., Balamir, M., Bakır, S., Buchheister, J., Christen, A., Çetin, K.Ö., Demirbaş, E., Durgun. M., M., Erdik, M., Fäh, D., Giardini, D., Gülkan, P., Hammer, J., Köksal, D., Krimgold, F., Laue, J., Lestuzzi,P., Önalp, A., Siyahi, B., Sprıngman, S., Studer, J., Yasuda, S. (2003) Report of the Synthesis Meeting for the Research and Manual Task Groups in DRM-MERM Project by Research and Manual Task Groups, Project Place Web Site

Ansal,A.M., Şengezer,B.S., İyisan,R. & Gençoğlu,S. (1993) "The Damage Distribution in March 13, 1992 Earthquake and Effects of Geotechnical Factors", Soil Dynamics and Geotechnical Earthquake Engineering, Ed.P.Seco e Pinto, Balkema, 413-434.

Athanasopoulus, G.A., Pelekis, P.C. & Leonidou, E.A. (1999)."Effects of Surface Topography on Seismic Ground Response in the Egion (Greece) 15 June 1995 Earthquake", Soil Dynamics and Earthquake Engineering, (18):135-149.

Bakır, B.S., H. Sucuoğlu, and T. Yılmaz (2002). "An Overview of Local Site Effects and the Associated Building Damage in Adapazarı during the 17 August 1999 İzmit Earthquake", Bulletin of the Seismological Society of America, Vol.92, No.1, pp.509-526.

Bard, P.-Y. (1994) "Effects of Surface Geology on Ground Motion: Recent Results and Remaining Issues", Proc. 10th ECEE, Vienna, Austria, (1):305-323.

Barka A. A. and K. Kadinsky-Cade, (1988), "Strike-Slip Fault Geometry in Turkey and its influence on earthquake activity", Tectonics, Vol. 7, No. 3, pp: 663-684.

Barka, A. A., (1992), "The NAFZ", Annales Tectonicae, Special issue, Supplement to volume VI, pp: 164-195.

Boore, D. M., W. B. Joyner, T. E. Fumal (1997), "Equations for Estimating Horizontal Response Spectra and Peak Acceleration from Western North American Earthquakes: A Summary of Recent Work", Seismological Research Letters, Vol. 68, No. 1, pp. 128-153.

Borcherdt, R.D. (1994) "Estimates of Site Dependent Response Spectra for Design (Methodology and Justification)", Earthquake Spectra, (10)4:617-653.

Bray, J.D. et al. (2000) "Damage Patterns and Foundation Performance in Adapazarı" Earthquake Spectra, Supllement A to Vol. 16, 1999 Kocaeli, Turkey Earthquake Reconnaissance Reort, pp. 163-189

Building Seismic Safety Council (BSSC), 2001, "NEHRP (National Earthquake Hazards Reduction Program) Recommended Provisions for Seismic Regulations for new buildings and other structures", 2000 Edition, Part1: Provisions (FEMA 368), Chapter 4, BSSC Washington, D.C.

Campbell, K. W. (1997), "Empirical Near-Source Attenuation Relationships for Horizontal and Vertical Components of Peak Ground Acceleration, Peak Ground Velocity, and Pseudo-Absolute Acceleration Response Spectra", Seismological Research Letters, 68, January/February.

Çetin, K. O. and Seed, R. B. (2001a). "Nonlinear Shear Mass Participation Factor (rd) for Cyclic Shear Stress Ratio Evaluation.", Submitted to the Journal of Geotechnical and Geoenvironmental Engineering.

Çetin, K. O. and Seed, R. B. (2001b). "Nonlinear Shear Mass Participation Factor (Rd) for Cyclic Shear Stress Ratio Evaluation", Research Report No. UCB/GT-2000/08, University of California, Berkeley.

Çetin, K. O., Seed, R. B., Der Kiureghian, A., Tokimatsu, K., Harder, L. F., and Kayen, R. E. (2000). "SPT-Based Probabilistic and Deterministic Assessment of Seismic Soil Liquefaction Initiation Hazard", Research Report No. 2000/05, Pacific Earthquake Engineering Research Center.

Chavez-Garcia, F.J., Cuenca, J. & Sanchez-Sesma, F.J. (1996) "Site Effects in Mexico City Urban Zone. A Complementary Study", Soil Dynamics and Earthquake Engineering, (15):141-146.

Chin-Hsiung, L., Jeng-Yaw, H. & Tzay-Chyn, S. (1998) "Observed Variation of Earthquake Motion across a Basin-Taipei City", Earthquake Spectra, (14)1:115-134.

Deodatis, G. (1996), "Non-stationary Stochastic Vector Processes: Seismic Ground Motion Applications", Probabilistic Engineering Mechanics 11, pp.145-168.

DIN 4094 Beiblatt 1; Baugrund; Erkundung durch Sondierung; Anwendungshilfen, Erklärungen, Ausgabe:1990-12

Erdik et al. (2002), "Earthquake Risk Assessment for the Istanbul Metropolitan Area", Report prepared by B. U. Kandilli Observatory and Earthquake Research Ins., Dept. of Earthquake Engineering.

Evans, M. D. (1987). "Undrained Cyclic Triaxial Testing of Gravels: The Effect of Membrane Compliance." Ph.D. Thesis, University of California, Berkeley

Faccioli, E. (1991) Seismic Amplification in the Presence of Geological and Topographic Irregularities", Proc. 2nd International Conference on Recent Advances in Geotechnical Earthquake Engineering, St. Louis, Missouri, State-of-art paper, 1779-1797.

Fäh, D., Christen, A., Gülerce, Ü., Greifenhagen, C., Single-station ambient vibration measurements and interpretation for the cities of Adapazarı and Gölcük, Turkey 16.1.2003 report provided to the DRM-MERM project

Fäh, D., Kind, F. & Giardini, D. (2001) "A theoretical investigation of average H/V ratios", Geophysical Journal Int., 145, 535-549.

Fäh, D., Kind, F. & Giardini, D. (2001) "Inversion of local S-wave velocity structures from average H/V ratios, and their use for the estimation of site-effects", Journal of Seismology, in press.

Fäh, D., Rüttener, E., Noack, T. & Kruspan, P. (1997) "Microzonation of the City of Basel", Journal of Seismology, (1):87-102.

Field, E.H. & Hough, S.E. (1997) "The Variability of PSV Response Spectra across a Dense Array Deployed during the Northridge Aftershock Sequence", Earthquake Spectra, 13(2):243-257.

Finn, W. D. L., Ledbetter, R. H., and Wu, G. (1994) "Liquefaction in Silty Soils: Design and Analysis." Ground Failures under Seismic Conditions, Geotechnical Special Publication 44, ASCE, New York, pp. 51-76.

Frankel, A., C. Mueller, T. Barnhard, D. Perkins, E. V. Leyendecker, N. Dickman, S. Hanson and M. Hopper (1996), "National Seismic Hazard Maps: Documentation June 1996", Open File Report 96-532, U. S. Geological Survey, Denver , Colorado.

Frankel, A.D., Mueller, C.S., Barnhard, T.P., Leyendecker, E.V., Wesson, R.L., Harmsen, S.C., Klein, F.W., Perkins, D.M., Dickman, N.C., Hanson, S.L. & Hopper, M.G. (2000) "USGS National Seismic Hazard Maps", Earthquake Spectra, (16)1:1-15

Gazetas,G., Dakoulas, P. & Papageorgiou, A. (1990) "Local Soil and Source-Mechanism Effects in the 1986 Kalamata (Greece) Earthquake" Earthquake Engineering and Structural Dynamics, (19):431-453

Geyskens, P., Der Kiureghian, A., Monteiro, P. (1993), "Bayesian Updating of Model Parameters", Structural Engineering Mechanics and Materials Report No. UCB/SEMM-93/06, University of California at Berkeley

Gueguen, P., Chatelain, J-L., Guillier, B., Yepes, H. & Egred, J. (1998) "Site Effect and Damage Distribution in Pujili (Ecuador) after the 28 March 1996 Earthquake", Soil Dynamics and Earthquake Engineering, (17), 329-334.

Gülkan, P., A. Yakut, H. Sucuoğlu, M.S. Yücemen, and E. Çıtıpıtıoğlu, "A Damage Assessment Form for Engineered Buildings in Turkey," Earthquake Engineering Research Center Report No. 95-01, Middle East Technical University, December, 1994 (in Turkish).

Gülkan, P., and A. Yakut, "An Expert System for Reinforced Concrete Structural Damage Quantification," in Mete A. Sozen Symposium-A Tribute from His Students, Edited by J.K. Wight and M.E. Kreger, ACI Special Publication No. SP-162, 1996, pp.53-71.

Gülkan, P., and M.A. Sozen, "Procedure for Determining Seismic Vulnerability of Building Structures," ACI Structural Journal, 96, 3, May, 1999, pp. 336-342.

Harder, L. F. (1988). "Use of Penetration Tests to Determine the Cyclic Loading Resistance of Gravelly Soils During Earthquake Shaking." Ph.D. Thesis, University of California, Berkeley.

Hartzell, S., Carver, D. & Williams, R.A. (2001) "Site Response, Shallow Shear-Wave Velocity and Damage in Los Gatos, California, from the 1989 Loma Prieta Earthquake", BSSA, (91)3:468-478.

Hartzell, S., Cranswick, E, Frankel, A., Carver, D. & Meremonte, M. (1997a) "Variability of Site Response in the Los Angeles Urban Area", BSSA, (87)6:1377-1400.

Hartzell, S., Harmsen, S., Frankel, A., Carver, D., Cranswick, E. Meremonte, M. & Michael,J. (1997b) "First-Generation Site-Response Maps for the Los Angeles Region Based on Earthquake Ground Motions", BSSA, (88)2:463-472.

Horike, M. (1985) "Inversion of phase velocity of long-period microtremors to the S-wave-velocity structure down to the basement in urbanized areas", J. Phys. Earth 33, 59-96.

Hynes, M. E. (1988). "Pore Pressure Generation Characteristics of Gravel under Undrained Loading." Ph.D. Thesis, University of California, Berkeley

Idriss, I. M. (2000), "Personal Communication"

Idriss, I. M., Sun, J. I., (1992), "Users Manual for SHAKE91, A Computer Program for Conducting Equivalent Linear Seismic Response Analyses of Horizontally Layered Soil Deposits, Program Modified Based on the Original SHAKE Program Published in December 1972, by Schnabel, Lysmer and Seed, August.

Ishibashi, I. and X. Zhang (1993). Unified Dynamic Shear Moduli and Damping Ratios of Sand and Clay. Soils and Foundations, 33, 182-191

Iwasaki, T., Tokida, K., Tatsuoka, F., Watanabe, S., Yasuda, S., & Sato, H. (1982) "Microzonation of Soil Liquefaction Potential Using Simplified Methods", Proc. 3rd Int. Conf. On Microzonation, Seattle, 3:1319-1330

Kayen RE, Mitchell JK, Seed RB, Lodge A, Nishio A, Coutinho R. "Evaluation of SPT-, CPT-, and Shear Wave-Based Methods for Liquefaction Potential Assessment Using Loma Prieta Data." Proceedings of 4th Japan-US Workshop on Earthquake-Resistant Design of Lifeline Facilities and Countermeasures for Soil Liquefaction, 1992; (1):177-204.

Kawase, H. (1998) "The Cause of the Damage Belt in Kobe: 'The Basin Edge Effect', Constructive Interference of the Direct S-Wave with the Basin-induced Diffracted/Rayleigh Waves", Seismological Research Letters, (67):25-34.

Kind, F. (2002) "Development of microzonation methods: application to Basle, Switzerland", PhD the-sis No.14548, Swiss Federal Institute of Technology, Zurich.

Kishida, H. (1966), "Damage to Reinforced Concrete Buildings in Niigata City with Special Reference to Foundation Engineering", Soils and Foundations, Vol. VII, No. 1.

Koizumi, Y (1966), "Change in Density of Sand Subsoil caused by the Niigata Earthquake", Soils and Foundations, Vol. VIII, No. 2, pp. 38-44.

Komazawa,M., Morikawa,H., Nakamura,K., Akamatsu,J., Nishimura,K., Sawada, S., Erken,A., & Onalp, A.(2002) "Bedrock structure in Adapazarı, Turkey—a possible cause of severe damage by the 1999 Kocaeli earthquake" Soil Dynamics and Eartquake Engineering, (22):829-836

Kudo, K., Kanno, T., Okada, H., Özel, O., Erdik, M., Sasatani, T. Higashi, S, Takahashi, M., Yoshida, K. (2002) "Site-specific issues for strong ground motions during the Kocaeli, Turkey, earthquake of 17 August 1999, as inferred from array observations of microtremors and aftershocks", Bull. Seism. Soc. Am. 92, 448-465.

Lachet, C. & Bard, P.-Y. (1994) "Numerical and Theoretical Investigations on the Possibilities and Limitations of Nakamura's Technique", J. Phys. Earth, 42, 377-397.

Lachet, C., Hatzfeld, D., Bard, P.Y., Theodulidis, N., Papaioannou, C. & Savvaidis, A. (1996) "Site Effects and Microzonation in the City of Thessaloniki-Comparison of Different Approaches", BSSA, (86)6:1692-1703.

Le Pichon, X, A.M.C. Sengör, E. Demirbag, C. Rangin, C. Imren, R. Armijo, N. Görür, N. Çagatay, B. Mercier de Lepinay, B. Meyer, R. Saatçilar and B. Tok ,(2001), "The Active Main Marmara Fault", Earth and Planetary Science Letters, Vol. 192 (4) pp. 595-616.

Lermo, J. & Chavez-Garcia, J. (1994) "Are Microtremors Useful in Site Response Evaluation?", Bull. Seism. Soc. Am. 84, 1350-1364.

Leyendecker, E.V., Hunt, R.J., Frankel, A.D. & Rukstales, K.S. (2000) "Development of Maximum Considered Earthquake Ground Motion Maps", Earthquake Spectra, (16)1:21-40

Liao, S. S. C., Lum, K. Y. (1998), "Statistical Analysis and Application of the Magnitude Scaling Factor in Liquefaction Analysis", Geotechnical Earthquake Engineering and Soil Dynamics III, Vol. 1, 410-421.

Liao, S. S. C., Veneziano, D., Whitman, R.V. (1988), "Regression Models for Evaluating Liquefaction Probability", Journal of Geotechnical Engineering, ASCE, Vol. 114, No. 4, pp. 389-409.

Lungu, D., Aldea, A., Cornea, T. & Arion, C. (2000) "Seismic Microzonation of the City of Bucharest", 6th International Conference on Seismic Zonation, California, USA.

Midorikawa, S. (1987), Prediction of Isoseismal Map in the Kanto Plain due to Hypothetical Earthquake, Journal of Structural Eng. 33B, 43-48.

Ministry of Public Works and Settlement, Government of Republic Turkey 2.9.1997 Official Gazette No. 23098, "Specification for Structures to be Built in Disaster Areas" Part III – Earthquake Disaster Prevention (Chapter 5 through Chapter 13) English Translation, Chapter 12, Kandilli Observatory and Earthquake Research Institute

Marcellini, A., Bard, P.Y., Iannaccone, G., Meneroud, J.P., Mouroux, P., Romeo, R.W., Silvestri, F., Duval, A.M., Martin, C. & Tento, A. (1995b). The Benevento Seismic Risk Project. II- The microzonation", Proc. 5th International Conference on Seismic Zonation, Nice, France, (1):810-817.

Nakamura, Y. (1989) "A Method for Dynamic Characteristics Estimation of Subsurface using Micro-tremor on the Ground Surface", QR of RTRI, 30, 25-33.

National Earthquake Hazard Reduction Program (NEHRP) (1997) Recommended Provisions for Seismic Regulations for New Buildings and Other Structures, FEMA 302/303.

NCEER (1997), "Proceedings of the NCEER Workshop on Evaluation of Liquefaction Resistance of Soils", Edited by Youd, T. L., Idriss, I. M., Technical Report No. NCEER-97-0022, December 31, 1997.

NEHRP (1997), Recommended Provisions For Seismic Regulations For New Buildings and Other Structures, FEMA-303, Prepared by the Building Seismic Safety Council for the Federal Emergency Management Agency, Washington, DC.

Ohsaki, Y. (1966), "Niigata Earthquakes, 1964, Building Damage and Soil Conditions", Soils and Foundations, Vol. 6, No. 2, pp. 14-37.

Ohta, Y. and N. Goto (1978). Empirical Shear Wave Velocity Equations in Terms of Characteristic Soil Indexes. Earthq. Engng. Struct.Dynam., 6,167-187.

Ozbey C. (2001), "Empirical Peak Horizontal Acceleration Attenuation Relationship for Northwestern Turkey", M.Sc. Thesis, KOERI, Bogazici University.

Panza, G.F. & Suhadolc, P. (1987) "Complete strong motion synthetics", In: Seismic strong motion synthetics, B.A. Bolt (Ed.), Academic Press, Computational Techniques, 4, 153-204.

Panza, G.F. (1985) "Synthetic seismograms: The Rayleigh waves modal summation", J. Geophysics, 58, 125-145.

Papageorgiou, A., B.Halldorsson and G.Dong (2000), "Target Acceleration Spectra Compatible Time Histories", University of Buffalo, Dept. of Civil, Structural and Environmental Engrg., NY.

Park, Y.J., and A.H.-S. Ang, "Mechanistic Seismic Damage Model for Reinforced Concrete," J. Str. Eng., ASCE, 111, 4, April, 1985, pp. 722-739.

Parsons, T., S. Toda, R. S. Stein, A. Barka and J. H. Dieterich, "Heightened odds of large earthquakes near Istanbul: An interaction-based probability calculation", Science, 288, pp. 661-665, 2000.

Prinz, H., 1997, "Abriss der Ingenieurgeologie mit Grundlagen der Boden- und Felsmechanik, des Erd-, Grund- und Tunnelbaus sowie der Abfalldeponien", 3. Aufl, Ferdinand Enke Verlag, Stuttgart, Germany

Procedure for the Classification of hypothetical borings according to the National Earthquake Hazards Reduction Program (NEHRP)

Rathje, E. et al (2000) "Ground Motions and Site Effects" Earthquake Spectra, Supllement A to Vol. 16, 1999 Kocaeli, Turkey Earthquake Reconnaissance Reort, pp. 65-96

Riemer, M. F., Seed, R. B., and Sadek, S. (1993) "The SRS/RFT Soil Evaluation Testing Program." University of California, Berkeley Geotechnical Report No. UCB/GT-93/01

Sadigh, K., Chang, C.-Y., Egan, J.A., Makdisi, F., Youngs, R.R. (1997) "Attenuation Relationships for Shallow Crustal Earthquakes Based on California Strong Motion Data." Seismological Research Letters 1997; (68)1: 180-189.

Sakarya University (1998). Geology and Geomorphology of Adapazarı, Report No. 1 (in Turkish).

Saroğlu, F., O. Emre and I. Kuscu (1992), "Active Fault Map of Turkey", Mineral Res. Explor. Inst. Turkey.

Satoh, T., Kawase, H., Iwata, T. Higaski, S., Sato, T., Irikura, K. & Huang, H. C. (2001) "S-wave velocity structure of Taichung basin, Taiwan estimated from array and single-station records of microtremors", Bull. Seism. Soc. Am. 91, 1267-1282.

Seed, H. B., Idriss, I. M. (1971), "Simplified Procedure for Evaluating Soil Liquefaction Potential", Journal of the Soil Mechanics and Foundations Division, ASCE, Vol. 97, No SM9, Proc. Paper 8371, September 1971, pp. 1249-1273.

Seed, H. B., Tokimatsu, K., Harder, L. F., and Chung, R. M. (1985). "Influence of SPT Procedures in soil liquefaction resistance evaluations." Journal of Geotechnical Engineering, ASCE, 111(12), 1425-1445.

Seed, H. B., Tokimatsu, K., Harder, L. F., Chung, R. M. (1984), "The Influence of SPT Procedures in Soil Liquefaction Resistance Evaluations", Earthquake Engineering Research Center Report No. UCB/EERC-84/15, University of California at Berkeley, October, 1984.

Seed, R. B., Cetin, K. O., Der Kiureghian, A., Tokimatsu, K., Harder, L. F. Jr., and Kayen, R. E. (2001) "SPT-Based Probabilistic and Deterministic Assessment of Seismic Soil Liquefaction Potential." Submitted to the ASCE Journal of Geotechnical and Geoenvironmental Engineering.

Shiga, T., A. Shibata, and T. Takahashi, "Earthquake Damage and Wall Index of Reinforced Concrete Buildings," Proceedings of the Tohuku District Symposium, Architectural Institute of Japan, No. 12, Dec., 1968, pp. 29-32 (in Japanese).

Steimen, S., Fäh, D., Kind, F., Schmid, C. & D. Giardini (2003) "Identifying 2D resonance in microtremor wave fields", Bull. Seism. Soc. Am., in press.

Straub, C., H.-G. Kahle, and C. Schindler, (1997), "GPS and Geologic Estimates of the Tectonic Activity in the Marmara Sea region, NW Anatolia", Journal of Geophysical Research, Vol. 102, No. B12, pp: 27,587-27,601, Dec. 10.

TAB Technical Advisory Board (2003) Report of Technical Advisory Board, Zurich, Switzerland, Project Place Web Site

Technical Committee for Earthquake Geotechnical Engineering, TC4, ISSMGE (1999) "Manual for Zonation on Seismic Geotechnical Hazards", The Japanese Geotechnical Society.

Toprak, S., Holzer, T. L., Bennett, M. J., Tinsley, J. C. (1999), "CPT- and SPT-based Probabilistic Assessment of Liquefaction Potential, Proceedings of Seventh U.S.-Japan Workshop on Earthquake Resistant Design of Lifeline Facilities and Countermeasures Against Liquefaction.

Toprak, S., Holzer, T. L., Bennett, M. J., Tinsley, J. C. (1999), "CPT- and SPT-based Probabilistic Assessment of Liquefaction Potential, Proceedings of Seventh U.S.-Japan Workshop on Earthquake Resistant Design of Lifeline Facilities and Countermeasures Against Liquefaction.

Vucetic, M and R. Dobry (1991). "Effect of soil plasticity on cyclic response", Journal of Geotechnical Engineering, ASCE, Vol.117, No.1, pp.89-107

Weichert, D. H. (1980), "Estimation of the Earthquake Recurrence Parameters for Unequal Observation Periods for Different Magnitudes", Bull. Seism. Soc. Am., 70, pp. 1337-1346.

WGCEP94 (1995), "Seismic Hazards in Southern California: Probable Earthquakes, 1994 to 2024", Bull. Seism. Soc. Am. Vol. 85, pp. 379-439.

Wills, C.J. & Silva, W. (1998) "Shear Wave Velocity Characteristics of Geologic Units in California", Earthquake Spectra, (14)3:533-566.

Wills, C.J., Peterson, M., Bryant, W.A., Reichle, M., Saucedo, G.J., Tan, S., Taylor, G. & Treiman, J. (2000) "A Site Conditions Map for California based on Geology and Shear Wave Velocity", BSSA, (90)6B:S187-S208.

Yaltirak, C.(2002), Tectonic evolution of Marmara Sea and its surroundings, Marine Geology, pp.1-37

Yamanaka, H., Kato, M., Hashimoto, M., Gulerce, U., Iyisan, R., Ansal, A. (2002) "Microtremor and earthquake observations in Adapazarı and Duzce, Turkey, for estimation of site amplifications", Japanese Ministry of Education, Science, Sports and Culture, Grant No.11694134, Proceedings "Assessment of seismic local-site effects at plural test sites, March 2002, 129-145.

Yamanaka, H., Takemura, M., Ishida, H. & Niea, M. (1994) "Characteristics of long-period micro-tremors and their applicability in exploration of deep layers", Bull. Seism. Soc. Am. 84, 1831-1841.

Yoshimi, Y., Tokimatsu, K., Ohara, J. (1994), "In-situ Liquefaction Resistance of Clean Sands over a Wide Density Range", Geotechnique, Vol. 44, No. 3, pp. 479-494.

Youd, T. L., Idriss, I. M., Andrus, R. D., Arango, I., Castro, G., Christian, J. T., Dobry, R., Finn, W. D. L., Harder, L. F. Jr., Hynes, M. E., Ishihara, K., Koester, J. P., Liao, S. S. C., Marcuson, W. F. III., Martin, G, R., Mitchell, J. K., Moriwaki, Y., Power, M. S., Robertson, P. K., Seed, R. B., and Stokoe, K. H., II. (2001) "Liquefaction Resistance of Soils: Summary Report from the 1996 NCEER and 1998 NCEER/NSF Workshops on Evaluation of Liquefaction Resistance of Soils", ASCE Journal of Geotechnical and Geoenvironmental Engineering, 127(10):817-833

Youd et al. (2001) Personal Communıcations

Youd, T. L., Idriss, I. M., Andrus, R. D., Arango, I., Castro, G., Christian, J. T., Dobry, R., Finn, W. D. L., Harder, L. F. Jr., Hynes, M. E., Ishihara, K., Koester, J. P., Liao, S. S. C., Marcuson, W. F. III., Martin, G, R., Mitchell, J. K., Moriwaki, Y., Power, M. S., Robertson, P. K., Seed, R. B., and Stokoe, K. H., II. (1997) Summary Paper, Proc., NCEER Workshop on Evaluation of Liquefaction Resistance of Soils, NCEER-97-0022.

Youd, T. L., Noble, S. K. (1997), "Liquefaction Criteria Based on Statistical and Probabilistic Analyses", Proceedings of the NCEER Workshop on Evaluation of Liquefaction Resistance of Soils, December 31, 1997, pp. 201-205.

Young, R. R. and Coppersmith, K. J. (1985) "Implications of Fault Slip Rates and Earthquake Recurrence Models to Probabilistic Seismic Hazard Estimates." BSSA 1985; 75: 939-964.

Seismic Microzonation for Municipalities

Reference Information

Pilot Studies - Appendices

TABLE OF CONTENTS

1. CHAPTER 4

1.1. Appendix 1: Instrument set-up

Menu	Parameter	Wert
Configuration	Sampling	32 ms
Configuration	Scale_0	2 uV/c
Configuration	Scale_1	2 uV/c
Configuration	Scale_2	2 uV/c
Configuration	Exponent	3
Configuration	In channels	3
Configuration	Mon channel	on
Coincidence	weight_0	0
Coincidence	weight_1	0
Coincidence	weight_2	0
Coincidence	weight_ext	0
Coincidence	coinc_sum	0

1.2. Appendix 2: Dataset description

The measurements have a unique identifier for naming the measurement points. The teams are:
Team C:
Christian Greifenhagen (EPFL), Ali Zeynel Denizlioglu (GDDA), Ismail Kocak (SAU)
Team R:
Andreas Christen (ETH), Sadullah Yagci (GDDA), Eray Yildrim (SAU)
Team U:
Ümit Gülerce (ITU), Hatice Erguven (SAU), Coskun Bal (SAU)

The point names have a structure corresponding to the following example AC05_R01

A	stands for Adapazarı (G would be for Gölcük)
C	raster field in east-west direction
05	raster field in north-south direction
R	name of the group that made the measurement
01	this group's first measurement in this raster field.

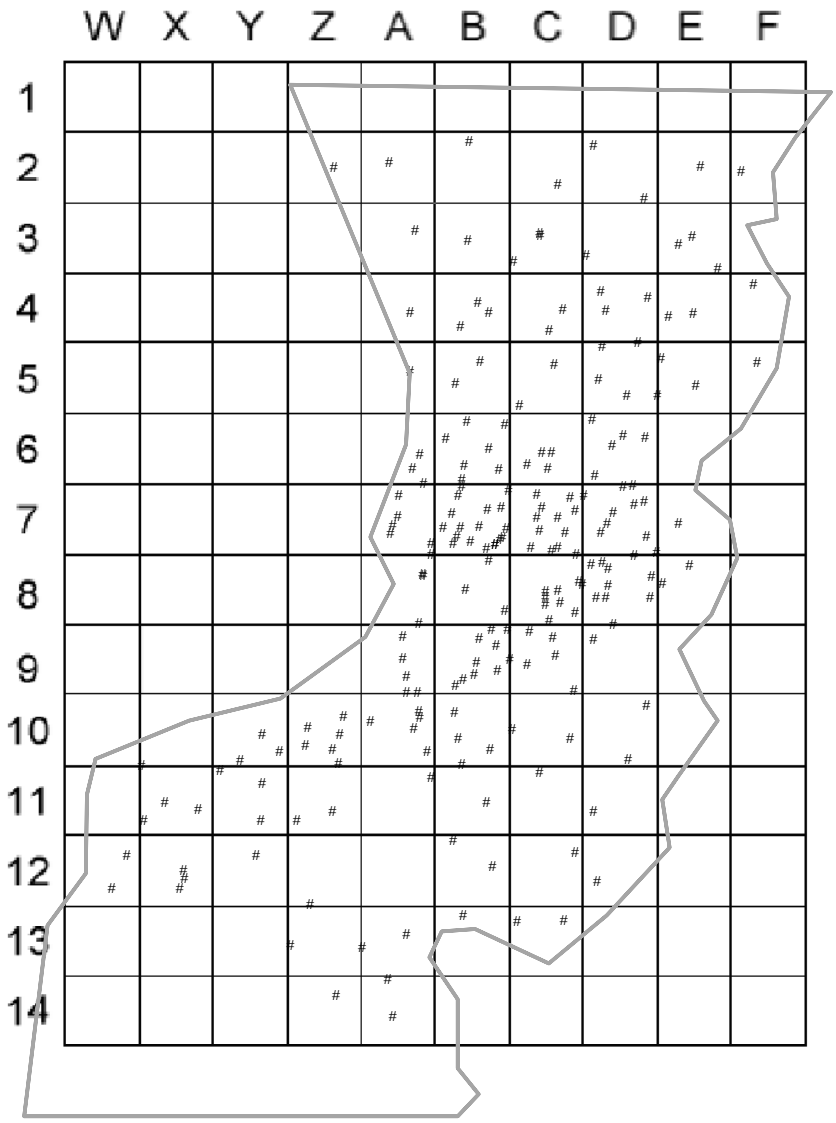

Figure 1.1. Grid used for the Adapazarı area.

The coordinates of the sites are provided in tabular form in the files Adapazarı_Results.xls and Gölcük_Results.xls on the CD-ROM.

1.3. Appendix 3: SAF Data Format

This format has been defined within the European Commission SESAME project (EVG1-CT-200-00026) for the exchange of ambient vibration data.

SESAME ASCII data format (saf) v. 1 (this line must not be modified)
The SESAME ASCII Format can contain an arbitrary number of comment
lines starting with '#' in the header. Parameters are specified on
lines starting without # character, followed by a keyword separated
with a '=' sign from the value of the key. The keyword name can be in
lower or upper case letters, no distinction is made in the
interpretation.
No empty lines are allowed in the header.
The first line indicates the name of the file format,
for automatic format identification tools.

```
#
# Two compulsory parameters have to be specified
# the sampling rate and the number of points.
#
# All other parameters are optional, but the response and saturation
# information
# is highly recomended.
#
# Data begin after this line : "####--------------------------------"
# Data are organized in colums in this order : Vertical, Horizontal_1,
# Horizontal_2
# Horizontal_1 generally is N-S, for different orientation parameter
# NORTH_ROT can
# be set.
# Data can be real or integer
#
#
# sampling frequency in Hertz
SAMP_FREQ = 125
# number of samples (integer)
NDAT = 1200
# date and time of the first sample, read as 5 integers, one real
START_TIME=2002 4 26 17 03 12.1233324
# accuracy of the timing, in seconds
#very large values indicate manual time setting
# GPS ~0.001, DCF ~0.01
TIME_ACCURRACY= 0.001
# Sensor type (accelerometer, seismometer)
SENSOR_TYPE = accelerometer
# Sensor serial number (character string)
SENSOR_ID = Q332
# Sensor name (character string)
SENSOR_NAME = Lennartz 5s
# Response file code (name of the file in the response directory)
RESPFILE = mark1s_098
# Acquisition system (character string)
ACQ_SYSTEM = MARS88
# Digitizer serial number (interpreted as character string)
DIGITIZER_ID = 345
# saturation value of the digitizer in UNITS
SATURATION = 23056
# conversion factor ( V/count)
CONV_FACTOR = 1234.5
# transduction factor (Volts/m/s or Volts/m/s^2)
TRANS_FACTOR = 12345.6
# Eigen frequency of the sensor
SENS_EIGFREQ = 1
# Damping factor of the sensor
SENS_DAMPING = 0.7
# Code for the site (exactly 6 characters)
STA_CODE= NCE_12
# Station coordinate type, 0= lat/lon, 1= km of local coordinate,
# elevation is always in km
STA_COORD_TYPE = 0
# coordinates are one real number: 45 30' -> 45.5
STA_X = 45.73
STA_Y = 7.009
```

```
STA_Z = 0.235
# project name
PROJECT_NAME = example data format project
#
# Earthquake data can be specified with the Pitsa keywords:
#
# Event coordinate type, as station coordinate type
EVT_COORD_TYPE = 0
# Event location
EVT_X = 34.5432
EVT_Y = 5.876
EVT_Z = 0.786
# Event time (origin time)
EVT_TIME = 1989 3 23 17 4 12.345
# Event comment
EVT_COMMENT = Lisbon quake
# Station comment
STA_COMMENT = bedrock
# event azimuth (from north clockwise)
EVT_AZ = 270
# event backazimuth (from north clockwise)
EVT_BACK_AZ = 23.345
# event hypocentral distance (km)
EVT_HYPO_DIST = 30
# event epicentral distance (km)
EVT_EPI_DIST = 3000
# Event magnitude definitions:
EVT_MAG = 7.3
# magnitude definitions with specific magnitudes
# possible keys: EVT_LOCAL_MAG, EVT_BODY_MAG, EVT_SURFACE_WAVE_MAG,
#       EVT_DURATION_MAG, EVT_MOMENT_MAG
# Orientation of Horizontal_1 component from North clockwise (degrees)
NORTH_ROT
# units of the values below in the data (label)
UNITS = m/s
#
# Vert, NS, EW
####------------------------------------------------------
13      214     898
13      214     898
13      214     898
13      214     898
13      214     898
13      214     898
13      214     898
13      214     898
13      214     898
13      214     898
13      214     898
13      214     898
13      214     898
13      214     898
13      214     898
13      214     898
13      214     898
13      214     898
13      214     898
13      214     898
13      214     898
13      214     898
```

1.4. Appendix 4: Content of the CD-ROM:

- Raw Data of all measurement points in SAF format
- Report (PDF File)
- Matlab Routines used for the analysis
- Excel file containing the coordinates and results (fundamental frequency & amplitude) for all measurement points in Adapazarı and Gölcük.

1.5. Microtremor Measurements

1.5.1 Adapazari region

Station	Mesurement								Coordinates		Date			Results	
	p	x	y		r				Latitude	Longitude	dd	mm	yy	Frequency	Amplitude
	a	a	02	_	c	01			40.8035N	30.3669E	09	08	02	0.42	0.64
	a	a	02	_	r	01			40.8041N	30.3761E	23	08	02	0.39	0.72
	a	a	03	_	r	01			40.7955N	30.3805E	26	08	02	0.33	0.72
sek	a	a	04	_	c	01	_	sek	40.7851N	30.3796E	07	08	02	0.25	0.65
	a	a	05	_	r	01			40.7777N	30.3795E	12	08	02	0.33	0.57
	a	a	06	_	r	01			40.7670N	30.3811E	12	08	02	0.50	0.68
	a	a	06	_	r	02			40.7654N	30.3798E	23	08	02	0.74	0.59
	a	a	07	_	r	01			40.7558N	30.3828E	10	08	02	2.45	0.79
	a	a	07	_	r	02			40.7593N	30.3773E	12	08	02	1.14	0.78
	a	a	07	_	r	03			40.7582N	30.3765E	23	08	02	1.54	0.72
	a	a	07	_	r	04			40.7571N	30.3761E	23	08	02	3.31	0.63
	a	a	07	_	r	05			40.7620N	30.3775E	23	08	02	1.09	0.76
	a	a	07	_	r	06			40.7635N	30.3818E	23	08	02	0.93	0.71
	a	a	08	_	r	01			40.7518N	30.3815E	08	08	02	n/a	n/a
	a	a	08	_	r	02			40.7519N	30.3813E	09	08	02	4.70	0.28
	a	a	08	_	r	03			40.7544N	30.3828E	09	08	02	n/a	n/a
skr	a	a	09	_	r	01	_	skr	40.7370N	30.3805E	07	08	02	12.20	0.34
	a	a	09	_	r	02			40.7390N	30.3787E	08	08	02	n/a	n/a
	a	a	09	_	r	03			40.7414N	30.3780E	08	08	02	n/a	n/a
	a	a	09	_	r	04			40.7442N	30.3781E	08	08	02	4.38	0.22
	a	a	09	_	r	05			40.7457N	30.3808E	08	08	02	3.25	0.42
	a	a	10	_	r	01			40.7370N	30.3786E	08	08	02	8.45	0.54
	a	a	10	_	r	02			40.7347N	30.3806E	27	08	02	5.06	0.73
	a	a	10	_	r	03			40.7325N	30.3798E	27	08	02	1.02	0.58
	a	a	10	_	r	04			40.7295N	30.3820E	27	08	02	0.83	0.63
	a	a	10	_	r	05			40.7339N	30.3810E	27	08	02	2.51	0.60
	a	a	11	_	r	01			40.7262N	30.3827E	27	08	02	0.54	0.67
	a	a	13	_	u	01			40.7064N	30.3785E	27	08	02	1.45	0.66
	a	a	13	_	u	02			40.7007N	30.3755E	27	08	02	1.69	0.63
	a	a	14	_	u	01			40.6959N	30.3763E	19	08	02	1.57	0.69
	a	b	02	_	r	01			40.8067N	30.3894E	26	08	02	0.43	0.73
	a	b	03	_	r	01			40.7941N	30.3893E	12	08	02	0.33	0.68
babali	a	b	04	_	c	01	_	bab	40.7864N	30.3908E	08	08	02	0.25	0.64
gen	a	b	04	_	c	02	_	gen	40.7851N	30.3927E	08	08	02	0.27	0.68
	a	b	04	_	r	01			40.7832N	30.3879E	13	08	02	0.24	0.59
	a	b	05	_	r	01			40.7789N	30.3911E	12	08	02	0.22	0.59
	a	b	05	_	r	02			40.7761N	30.3871E	14	08	02	0.27	0.57
	a	b	06	_	r	01			40.7657N	30.3885E	10	08	02	0.45	0.74
	a	b	06	_	r	02			40.7639N	30.3881E	10	08	02	0.62	0.57

	a	b	06	_	r	03			40.7713N	30.3889E	10	08	02	0.33	0.66
	a	b	06	_	r	04			40.7709N	30.3952E	13	08	02	0.30	0.61
	a	b	06	_	r	05			40.7679N	30.3926E	14	08	02	0.38	0.67
	a	b	06	_	r	06			40.7690N	30.3853E	23	08	02	0.40	0.71
sic	a	b	06	_	u	01	_	sic	40.7651N	30.3942E	08	08	02	0.41	0.62
	a	b	07	_	c	01			40.7556N	30.3935E	10	08	02	1.18	0.44
	a	b	07	_	c	02			40.7551N	30.3921E	10	08	02	1.11	0.40
	a	b	07	_	c	03			40.7566N	30.3948E	10	08	02	1.53	0.76
	a	b	07	_	c	04			40.7562N	30.3943E	12	08	02	2.27	0.66
	a	b	07	_	r	01			40.7578N	30.3849E	09	08	02	1.55	0.73
	a	b	07	_	r	02			40.7618N	30.3875E	09	08	02	1.11	0.74
	a	b	07	_	r	03			40.7595N	30.3863E	10	08	02	1.29	0.74
	a	b	07	_	r	04			40.7604N	30.3945E	13	08	02	0.91	0.57
	a	b	07	_	r	05			40.7630N	30.3880E	13	08	02	0.99	0.62
	a	b	07	_	r	06			40.7560N	30.3895E	14	08	02	1.40	0.40
	a	b	07	_	r	07			40.7580N	30.3909E	14	08	02	1.52	0.65
	a	b	07	_	r	08			40.7624N	30.3958E	14	08	02	0.90	0.52
	a	b	07	_	r	09			40.7601N	30.3924E	23	08	02	1.01	0.74
	a	b	07	_	r	10			40.7559N	30.3866E	28	08	02	5.06	0.50
	a	b	07	_	r	11			40.7578N	30.3878E	28	08	02	1.95	0.44
	a	b	07	_	r	12			40.7568N	30.3871E	28	08	02	1.78	0.73
	a	b	08	_	c	01			40.7537N	30.3925E	10	08	02	1.13	0.42
	a	b	08	_	r	01			40.7501N	30.3885E	09	08	02	3.77	0.15
	a	b	08	_	r	02			40.7474N	30.3952E	16	08	02	7.46	0.57
	a	b	09	_	c	01			40.7429N	30.3936E	23	08	02	1.31	0.81
	a	b	09	_	c	02			40.7379N	30.3870E	23	08	02	2.30	0.76
	a	b	09	_	c	03			40.7386N	30.3882E	23	08	02	2.17	0.69
	a	b	09	_	c	04			40.7449N	30.3954E	23	08	02	6.91	0.44
	a	b	09	_	c	05			40.7409N	30.3903E	26	08	02	3.06	0.69
	a	b	09	_	c	06			40.7437N	30.3909E	27	08	02	4.17	0.58
	a	b	09	_	c	07			40.7397N	30.3939E	27	08	02	1.15	0.69
	a	b	09	_	r	01			40.7392N	30.3900E	16	08	02	1.77	0.71
	a	b	09	_	r	02			40.7449N	30.3929E	16	08	02	1.56	0.85
	a	b	10	_	r	01			40.7345N	30.3867E	15	08	02	0.93	0.72
	a	b	10	_	r	02			40.7312N	30.3872E	15	08	02	0.89	0.67
	a	b	10	_	u	01			40.7297N	30.3926E	27	08	02	0.88	0.68
	a	b	11	_	r	01			40.7279N	30.3879E	15	08	02	0.63	0.60
	a	b	11	_	r	02			40.7231N	30.3918E	15	08	02	0.48	0.71
	a	b	11	_	u	01			40.7183N	30.3864E	27	08	02	0.50	0.70
	a	b	12	_	r	01			40.7149N	30.3930E	15	08	02	0.46	0.46
	a	b	13	_	u	01			40.7088N	30.3880E	27	08	02	1.15	0.48
	a	c	02	_	c	01			40.8012N	30.4043E	09	08	02	0.37	0.75
	a	c	03	_	c	01			40.7947N	30.4013E	09	08	02	0.31	0.69
tek	a	c	03	_	u	01	_	tek	40.7951N	30.4011E	08	08	02	0.34	0.63
	a	c	04	_	r	01			40.7827N	30.4028E	12	08	02	0.30	0.39
srf	a	c	04	_	u	01	_	srf	40.7915N	30.3968E	08	08	02	0.33	0.58
	a	c	04	_	u	02			40.7854N	30.4051E	13	08	02	0.28	0.53
	a	c	05	_	r	01			40.7784N	30.4036E	13	08	02	0.24	0.39
hastane	a	c	05	_	u	01	_	has	40.7732N	30.3978E	08	08	02	0.25	0.50
	a	c	06	_	c	01			40.7652N	30.4024E	14	08	02	0.37	0.56
	a	c	06	_	r	01			40.7673N	30.4013E	14	08	02	0.34	0.58
	a	c	06	_	r	02			40.7657N	30.3990E	28	08	02	0.40	0.64
	a	c	06	_	u	01			40.7674N	30.4030E	10	08	02	0.30	0.62
	a	c	07	_	c	01			40.7556N	30.3936E	10	08	02	1.01	0.70

	a	c	07	_	c	02			40.7621N	30.4005E	13	08	02	0.84	0.55
	a	c	07	_	c	03			40.7571N	30.4052E	13	08	02	1.40	0.62
	a	c	07	_	c	04			40.7577N	30.3955E	14	08	02	1.07	0.70
	a	c	07	_	c	05			40.7549N	30.4030E	14	08	02	1.35	0.52
	a	c	07	_	c	06			40.7554N	30.4040E	14	08	02	1.96	0.66
ere	a	c	07	_	u	01	_	ere	40.7615N	30.4060E	08	08	02	0.83	0.58
	a	c	07	_	u	02			40.7603N	30.4013E	23	08	02	0.91	0.78
	a	c	07	_	u	03			40.7591N	30.4006E	23	08	02	1.01	0.75
	a	c	07	_	u	04			40.7553N	30.3995E	23	08	02	2.06	0.64
	a	c	07	_	u	05			40.7590N	30.4040E	26	08	02	0.99	0.77
	a	c	07	_	u	06			40.7575N	30.4010E	26	08	02	1.23	0.71
	a	c	07	_	u	07			40.7599N	30.4069E	26	08	02	0.91	0.70
	a	c	08	_	c	01			40.7481N	30.4020E	12	08	02	1.77	0.69
	a	c	08	_	c	02			40.7497N	30.4019E	14	08	02	10.01	0.58
	a	c	08	_	c	03			40.7489N	30.4020E	15	08	02	2.48	0.80
	a	c	08	_	c	04			40.7460N	30.4025E	15	08	02	1.58	0.78
	a	c	08	_	u	01			40.7482N	30.4044E	20	08	02	1.33	0.83
	a	c	08	_	u	02			40.7498N	30.4039E	20	08	02	6.45	0.33
	a	c	08	_	u	03			40.7471N	30.4068E	20	08	02	1.03	0.69
	a	c	09	_	c	01			40.7440N	30.4031E	15	08	02	1.10	0.92
	a	c	09	_	c	02			40.7415N	30.4035E	16	08	02	1.10	0.75
	a	c	09	_	c	03			40.7371N	30.4065E	16	08	02	1.03	0.57
	a	c	09	_	c	04			40.7405N	30.3988E	23	08	02	1.29	0.63
	a	c	09	_	c	05			40.7447N	30.3993E	23	08	02	2.59	0.81
	a	c	09	_	r	01			40.7412N	30.3959E	16	08	02	1.38	0.73
	a	c	10	_	c	01			40.7312N	30.4059E	15	08	02	0.86	0.74
	a	c	10	_	u	01			40.7322N	30.3963E	19	08	02	0.89	0.71
	a	c	11	_	u	01			40.7267N	30.4008E	16	08	02	0.94	0.76
	a	c	12	_	u	01			40.7166N	30.4066E	16	08	02	0.96	0.69
	a	c	13	_	r	01			40.7078N	30.3970E	15	08	02	1.06	0.64
	a	c	13	_	u	01			40.7080N	30.4047E	16	08	02	1.05	0.53
	a	d	02	_	r	01			40.7994N	30.4186E	27	08	02	0.33	0.72
	a	d	02	_	u	01			40.8061N	30.4102E	12	08	02	0.49	0.69
	a	d	03	_	u	01			40.7922N	30.4090E	12	08	02	0.31	0.59
	a	d	04	_	u	01			40.7853N	30.4122E	09	08	02	0.26	0.59
	a	d	04	_	u	02			40.7877N	30.4113E	13	08	02	0.25	0.71
	a	d	04	_	u	03			40.7806N	30.4114E	14	08	02	0.31	0.46
yen	a	d	05	_	u	01	_	yen	40.7765N	30.4110E	09	08	02	0.24	0.60
	a	d	05	_	u	02			40.7811N	30.4175E	10	08	02	0.31	0.42
	a	d	05	_	u	03			40.7744N	30.4156E	14	08	02	0.24	0.53
	a	d	06	_	u	01			40.7628N	30.4148E	09	08	02	1.00	0.50
	a	d	06	_	u	02			40.7714N	30.4098E	10	08	02	0.26	0.61
	a	d	06	_	u	03			40.7695N	30.4149E	13	08	02	0.26	0.57
	a	d	06	_	u	04			40.7630N	30.4166E	23	08	02	0.96	0.57
	a	d	06	_	u	05			40.7643N	30.4102E	26	08	02	0.36	0.53
	a	d	06	_	u	06			40.7681N	30.4131E	26	08	02	0.28	0.50
	a	d	07	_	c	01			40.7582N	30.4123E	12	08	02	1.11	0.65
	a	d	07	_	c	02			40.7618N	30.4084E	13	08	02	1.12	0.42
	a	d	07	_	u	01			40.7526N	30.4124E	15	08	02	1.72	0.67
	a	d	07	_	u	02			40.7542N	30.4167E	15	08	02	1.33	0.60
	a	d	07	_	u	03			40.7610N	30.4185E	15	08	02	0.98	0.51
	a	d	07	_	u	04			40.7543N	30.4070E	23	08	02	6.14	0.71
	a	d	07	_	u	05			40.7596N	30.4132E	23	08	02	1.00	0.62
	a	d	07	_	u	06			40.7607N	30.4167E	26	08	02	0.93	0.51

	a	d	07	_	u	07			40.7571N	30.4111E	28	08	02	1.43	0.65
	a	d	07	_	u	08			40.7566N	30.4187E	28	08	02	1.17	0.69
adc	a	d	08	_	c	01	_	adc	40.7534N	30.4114E	08	08	02	2.28	0.71
	a	d	08	_	c	02			40.7488N	30.4118E	12	08	02	1.00	0.71
	a	d	08	_	c	03			40.7509N	30.4075E	26	08	02	4.32	0.91
	a	d	08	_	c	04			40.7505N	30.4081E	26	08	02	2.93	0.91
	a	d	08	_	c	05			40.7532N	30.4096E	26	08	02	3.12	0.50
	a	d	08	_	c	06			40.7504N	30.4124E	26	08	02	1.54	0.59
	a	d	08	_	c	07			40.7489N	30.4193E	26	08	02	1.50	0.71
	a	d	08	_	u	01			40.7488N	30.4102E	28	08	02	1.13	0.69
	a	d	09	_	u	01			40.7436N	30.4098E	20	08	02	1.11	0.83
	a	d	09	_	u	02			40.7454N	30.4132E	28	08	02	1.20	0.52
	a	d	10	_	c	01			40.7285N	30.4156E	16	08	02	1.04	0.70
	a	d	10	_	u	01			40.7353N	30.4186E	19	08	02	1.14	0.65
	a	d	11	_	c	01			40.7219N	30.4097E	15	08	02	1.07	0.74
	a	d	12	_	c	01			40.7130N	30.4103E	15	08	02	1.08	0.60
	a	e	02	_	r	01			40.8034N	30.4280E	26	08	02	0.43	0.73
	a	e	03	_	r	01			40.7936N	30.4242E	26	08	02	0.31	0.61
	a	e	03	_	r	02			40.7904N	30.4309E	26	08	02	0.29	0.55
	a	e	03	_	u	01			40.7945N	30.4266E	12	08	02	0.34	0.61
adu	a	e	04	_	c	01	_	adu	40.7869N	30.4192E	08	08	02	0.32	0.59
	a	e	04	_	u	01			40.7848N	30.4268E	10	08	02	0.31	0.50
	a	e	04	_	u	02			40.7843N	30.4225E	14	08	02	0.35	0.45
	a	e	05	_	u	01			40.7756N	30.4270E	12	08	02	0.34	0.37
	a	e	05	_	u	02			40.7743N	30.4207E	13	08	02	0.27	0.47
	a	e	05	_	u	03			40.7791N	30.4214E	13	08	02	0.29	0.46
	a	e	06	_	u	01			40.7691N	30.4187E	09	08	02	0.27	0.58
	a	e	07	_	u	01			40.7581N	30.4240E	14	08	02	0.99	0.71
	a	e	07	_	u	02			40.7545N	30.4203E	15	08	02	1.17	0.75
	a	e	08	_	u	01			40.7507N	30.4214E	14	08	02	1.59	0.71
	a	e	08	_	u	02			40.7516N	30.4196E	15	08	02	1.30	0.72
	a	e	08	_	u	03			40.7529N	30.4259E	15	08	02	1.16	0.27
	a	f	02	_	c	01			40.8028N	30.4349E	09	08	02	0.46	0.70
	a	f	04	_	u	01			40.7884N	30.4369E	12	08	02	0.34	0.41
	a	f	05	_	u	01			40.7785N	30.4374E	12	08	02	0.37	0.36
	a	w	10	_	r	01			40.7279N	30.3344E	20	08	02	0.74	0.83
	a	w	11	_	r	01			40.7209N	30.3349E	19	08	02	0.38	0.98
	a	w	12	_	r	01			40.7165N	30.3320E	19	08	02	0.36	0.78
	a	w	12	_	r	02			40.7123N	30.3295E	20	08	02	1.30	0.62
	a	x	11	_	c	01			40.7232N	30.3384E	28	08	02	0.50	0.73
	a	x	11	_	r	01			40.7222N	30.3439E	19	08	02	0.40	0.89
	a	x	11	_	r	02			40.7273N	30.3476E	20	08	02	0.62	0.81
	a	x	12	_	r	01			40.7147N	30.3415E	19	08	02	0.87	0.48
	a	x	12	_	r	02			40.7124N	30.3408E	20	08	02	1.34	0.56
	a	x	12	_	r	03			40.7135N	30.3416E	20	08	02	0.99	0.22
	a	y	10	_	c	01			40.7318N	30.3547E	19	08	02	1.77	0.59
	a	y	10	_	c	02			40.7295N	30.3575E	20	08	02	0.91	0.60
	a	y	10	_	c	03			40.7285N	30.3509E	27	08	02	0.61	0.83
	a	y	11	_	c	01			40.7208N	30.3544E	19	08	02	0.41	0.92
	a	y	11	_	c	02			40.7255N	30.3546E	20	08	02	0.50	0.80
	a	y	11	_	c	03			40.7208N	30.3603E	28	08	02	0.42	0.88
	a	y	12	_	r	01			40.7165N	30.3535E	19	08	02	0.46	0.74
	a	y	13	_	c	01			40.7051N	30.3592E	20	08	02	n/a	n/a
	a	z	10	_	c	01			40.7299N	30.3664E	19	08	02	0.88	0.83

	a	z	10	_	c	02			40.7326N	30.3622E	20	08	02	2.44	0.50
	a	z	10	_	c	03			40.7334N	30.3726E	27	08	02	1.36	0.77
	a	z	10	_	c	04			40.7318N	30.3675E	27	08	02	1.74	0.64
	a	z	10	_	c	05			40.7303N	30.3618E	27	08	02	0.97	0.66
	a	z	10	_	c	06			40.7281N	30.3673E	28	08	02	0.70	0.62
	a	z	10	_	r	01			40.7341N	30.3682E	27	08	02	n/a	n/a
	a	z	11	_	c	01			40.7221N	30.3663E	19	08	02	0.42	0.86
	a	z	12	_	c	01			40.7102N	30.3626E	19	08	02	n/a	n/a
	a	z	13	_	u	01			40.7047N	30.3710E	19	08	02	1.37	0.74
	a	z	14	_	u	01			40.6987N	30.3667E	19	08	02	1.66	0.59

1.5.2 Golcuk region

Station	**Mesurement**								**Coordinates**		**Date**			**Results**	
	p	x	y		r				Latitude	Longitude	dd	mm	yy	Frequency [Hz]	Amplitude
DMD	G	D	01	_	R	01	_	DMD	40.7261N	29.7981E	21	08	02	0.30	0.37
PIR	G	E	02	_	R	01	_	PIR	40.7226N	29.8201E	21	08	02	0.26	0.50
	G	E	02	_	R	02			40.7197N	29.8184E	21	08	02	0.25	0.55
	G	E	02	_	R	03			40.7213N	29.8195E	22	08	02	0.28	0.35
	G	E	02	_	R	04			40.7188N	29.8183E	22	08	02	0.29	0.36
	G	F	02	_	R	01			40.7193N	29.8334E	22	08	02	0.31	0.27
	G	F	02	_	R	02			40.7193N	29.8280E	22	08	02	0.27	0.35
	G	G	01	_	C	01			40.7247N	29.8400E	22	08	02	0.33	0.55
	G	G	01	_	U	01			40.7224N	29.8418E	22	08	02	0.33	0.46
	G	G	02	_	C	01			40.7177N	29.8381E	22	08	02	0.25	0.40
	G	G	02	_	C	02			40.7154N	29.8368E	22	08	02	0.26	0.40
	G	G	02	_	C	03			40.7143N	29.8363E	22	08	02	0.27	0.41
	G	G	02	_	R	01			40.7212N	29.8339E	21	08	02	0.25	0.43
	G	G	02	_	R	02			40.7177N	29.8335E	21	08	02	0.26	0.51
	G	G	02	_	R	03			40.7200N	29.8338E	22	08	02	0.24	0.36
	G	G	02	_	R	04			40.7220N	29.8334E	22	08	02	0.28	0.37
GYM	G	G	02	_	U	01	_	GYM	40.7206N	29.8399E	21	08	02	0.24	0.56
GEM	G	G	02	_	U	02	_	GEM	40.7199N	29.8444E	21	08	02	0.26	0.46
	G	G	02	_	U	03			40.7157N	29.8409E	22	08	02	0.23	0.48
	G	G	02	_	U	04			40.7182N	29.8409E	22	08	02	0.27	0.25
GLH	G	G	03	_	U	01	_	GLH	40.7078N	29.8338E	21	08	02	0.27	0.57
	G	G	03	_	U	02			40.7136N	29.8426E	22	08	02	0.27	0.38
	G	G	03	_	U	03			40.7112N	29.8451E	22	08	02	0.27	0.38
	G	G	03	_	U	04			40.7089N	29.8429E	22	08	02	0.27	0.45
	G	G	03	_	U	05			40.7121N	29.8435E	22	08	02	0.24	0.41
GLF	G	H	02	_	C	01	_	GLF	40.7216N	29.8482E	21	08	02	0.22	0.50
FOC	G	H	02	_	C	02	_	FOC	40.7173N	29.8542E	21	08	02	0.24	0.33
LOJ	G	H	03	_	C	01	_	LOJ	40.7129N	29.8504E	21	08	02	0.25	0.49
	G	H	03	_	C	02			40.7050N	29.8496E	21	08	02	0.28	0.59
	G	H	03	_	C	03			40.7102N	29.8501E	22	08	02	0.29	0.36
	G	H	03	_	C	04			40.7083N	29.8507E	22	08	02	0.28	0.46

2. CHAPTER 5 AND CHAPTER 6

2.1. NEHRP RECOMMENDED PROVISIONS FOR SEISMIC REGULATIONS FOR NEW BUILDINGS AND OTHER STRUCTURES

BUILDING SEISMIC SAFETY COUNCIL

Program on Improved Seismic Safety Provisions

Of the National Institute of Building Sciences

2000 Edition

NEHRP RECOMMENDED PROVISIONS FOR SEISMIC REGULATIONS FOR NEW BUILDINGS AND OTHER STRUCTURES

Part 1: Provisions (FEMA 368)

The **Building Seismic Safety Council** (BSSC) was established in 1979 under the auspices of the National Institute of Building Sciences as an entirely new type of instrument for dealing with the complex regulatory, technical, social, and economic issues involved in developing and promulgating building earthquake hazard mitigation regulatory provisions that are national in scope. By bringing together in the BSSC all of the needed expertise and all relevant public and private interests, it was believed that issues related to the seismic safety of the built environment could be resolved and jurisdictional problems overcome through authoritative guidance and assistance backed by a broad consensus.

The BSSC is an independent, voluntary membership body representing a wide variety of building community interests. Its fundamental purpose is to enhance public safety by providing a national forum that fosters improved seismic safety provisions for use by the building community in the planning, design, construction, regulation, and utilization of buildings.

To fulfill its purpose, the BSSC: (1) promotes the development of seismic safety provisions suitable for use throughout the United States; (2) recommends, encourages, and promotes the adoption of appropriate seismic safety provisions in voluntary standards and model codes; (3) assesses progress in the implementation of such provisions by federal, state, and local regulatory and construction agencies; (4) identifies opportunities for improving seismic safety regulations and practices and encourages public and private organizations to effect such improvements; (5) promotes the development of training and educational courses and materials for use by design professionals, builders, building regulatory officials, elected officials, industry representatives, other members of the building community, and the public; (6) advises government bodies on their programs of research, development, and implementation; and (7) periodically reviews and evaluates research findings, practices, and experience and makes recommendations for incorporation into seismic design practices.

See the back of the *Commentary* volume for a full description of BSSC activities.

BOARD OF DIRECTION: 2000

Chairman	William W. Stewart, Stewart-Schaberg Architects, Clayton, Missouri
Vice Chairman	Charles Thornton, Ph.D., PE, The Thornton P Tomasetti Group, Inc., New York, New York (representing the Applied Technology Council)
Secretary	Jack Prosek, PE, Turner Construction Company, San Francisco, California (representing the Associated General Contractors of America)
Ex-Officio	Eugene Zeller, PE, City of Long Beach, California
Members	J. Gregg Borchelt, PE, Brick Institute of America, Reston, Virginia; Charles Carter, PE, American Institute of Steel Construction, Chicago, Illinois; Bradford K. Douglas, PE, American Forest and Paper Association, Washington, D.C.; S. K. Ghosh, Ph.D., S. K. Ghosh Associates, Inc., Northbrook, Illinois (representing the Portland Cement Association); Gerald H. Jones, PE, Kansas City, Missouri (representing the National Institute of Building Sciences); Do Y. Kim, PE, Institute for Business and Home Safety, Tampa, Florida (through October 2000); H. S. Lew, Ph.D., PE, National Institute of Standards and Technology, Gaithersburg, Maryland (representing the Interagency Committee for Seismic Safety in Construction); Joseph Nicoletti, PE, URS/John A. Blume and Associates, San Francisco, California (representing the Earthquake Engineering Research Institute); W. Lee Shoemaker, Ph.D., Metal Building Manufacturers Association, Cleveland, Ohio; Howard Simpson, Sc.D., P.E., Simpson, Gumpertz and Heger, Arlington, Massachusetts (representing the National Council of Structural Engineers Associations); Charles Spitz, NCARB, AIA, CSI, Architect/Planner Code Consultant, Wall, New Jersey (representing the American Institute of Architects); John C. Theiss, PE, Theiss Engineers, Inc., St. Louis, Missouri (representing the American Society of Civil Engineers); David Wismer, PE, CBO, Department of Licenses and Inspections, Philadelphia, Pennsylvania (representing the Building Officials and Code Administrators International)
BSSC Staff	Claret M. Heider, Acting Executive Director; Bernard Murphy, PE, Director, Special Projects; Patricia Blasi, Administrative Assistant; Carita Tanner, Administrative Assistant; Kelly Harris, Summer Intern

BSSC Program on Improved Seismic Safety Provisions

NEHRP RECOMMENDED PROVISIONS
(National Earthquake Hazards Reduction Program)

FOR SEISMIC REGULATIONS

FOR NEW BUILDINGS AND

OTHER STRUCTURES

2000 EDITION

Part 1: PROVISIONS
(FEMA 368)

Prepared by the
Building Seismic Safety Council
for the
Federal Emergency Management Agency

BUILDING SEISMIC SAFETY COUNCIL
Washington, D.C.
2001

This report was prepared under Contract EMW-97-CO-0481 between the Federal Emergency Management Agency and the National Institute of Building Sciences.

Building Seismic Safety Council activities and products are described at the end of this report. For further information, contact the Building Seismic Safety Council, 1090 Vermont, Avenue, N.W., Suite 700, Washington, D.C. 20005; phone 202-289-7800; fax 202-289-1092; e-mail bssc@nibs.org.

Copies of this report may be obtained by contacting the FEMA Publication Distribution Facility at 1-800-480-2520.

Chapter 4

GROUND MOTION

4.1 PROCEDURES FOR DETERMINING MAXIMUM CONSIDERED EARTHQUAKE AND DESIGN EARTHQUAKE GROUND MOTION ACCELERATIONS AND RESPONSE SPECTRA: Ground motion accelerations, represented by response spectra and coefficients derived from these spectra, shall be determined in accordance with the general procedure of Sec. 4.1.2 or the site-specific procedure of Sec. 4.1.3. The general procedure in which spectral response acceleration parameters for the *maximum considered earthquake ground motions* are derived using Maps 1 through 24, modified by site coefficients to include local site effects and scaled to design values, are permitted to be used for any *structure* except as specifically indicated in the *Provisions*. The site-specific procedure also is permitted to be used for any *structure* and shall be used where specifically required by the *Provisions*.

4.1.1 Maximum Considered Earthquake Ground Motions: The *maximum considered earthquake ground motions* shall be as represented by the mapped spectral response acceleration at short periods, S_S, and at 1 second, S_1, obtained from Maps 1 through 24 of the *Provisions*, respectively, and adjusted for *Site Class* effects using the site coefficients of Sec. 4.1.2.4. When a site-specific procedure is used, *maximum considered earthquake ground motion* shall be determined in accordance with Sec. 4.1.3.

4.1.2 General Procedure for Determining Maximum Considered Earthquake and Design Spectral Response Accelerations: The mapped *maximum considered earthquake* spectral response acceleration at short periods, S_S ,and at 1 second ,S_1, shall be determined from Maps 1 through 24.

For *structures* located within those regions of the maps having values of the short period spectral response acceleration, S_S, less than or equal to 0.15 and values of the 1 second period spectral response acceleration, S_1, less than or equal to 0.04, accelerations need not be determined. Such *structures* are permitted to be directly categorized as *Seismic Design Category* A in accordance with Sec. 4.2.1.

For all other *structures*, the *Site Class* shall be determined in accordance with Sec. 4.1.2.1. The *maximum considered earthquake* spectral response accelerations adjusted for *Site Class* effects, S_{MS} and S_{M1}, shall be determined in accordance with Sec. 4.1.2.4 and the design spectral response accelerations, S_{DS} and S_{D1}, shall be determined in accordance with Sec. 4.1.2.5. The general response spectrum, when required by the *Provisions*, shall be determined in accordance with Sec. 4.1.2.6.

4.1.2.1 Site Class Definitions: For all *structures* located within those regions of the maps having values of the short period spectral response acceleration, S_S, greater than 0.15 or values of the 1 second period spectral response acceleration, S_1, greater than 0.04, the site shall be classified as one of the following classes:

A Hard rock with measured shear wave velocity, $\overline{v}_s$ > 5,000 ft/sec (1500 m/s)

B Rock with 2,500 ft/sec < $\overline{v}_s$ ≤ 5,000 ft/sec (760 m/s < $\overline{v}_s$ ≤ 1500 m/s)

C Very dense soil and soft rock with 1,200 ft/sec < $\overline{v}_s$ ≤ 2,500 ft/sec (360 m/s < $\overline{v}_s$ ≤ 760 m/s) or with either $\overline{N}$ > 50 or $\overline{s}_u$ > 2,000 psf (100 kPa)

D Stiff soil with 600 ft/sec ≤ $\overline{v}_s$ ≤ 1,200 ft/sec (180 m/s ≤ $\overline{v}_s$ ≤ 360 m/s) or with either 15 ≤ $\overline{N}$ ≤ 50 or 1,000 psf ≤ $\overline{s}_u$ ≤ 2,000 psf (50 kPa ≤ $\overline{s}_u$ ≤ 100 kPa)

E A soil profile with $\overline{v}_s$ < 600 ft/sec (180 m/s) or with either

$\overline{N}$ < 15 $\overline{s}_u$ < 1,000 psf or any profile with more than 10 ft (3 m) of soft clay defined as soil with PI > 20, w ≥ 40 percent, and s_u < 500 psf (25 kPa)

F Soils requiring site-specific evaluations:

1. Soils vulnerable to potential failure or collapse under seismic loading such as liquefiable soils, quick and highly sensitive clays, and collapsible weakly cemented soils.

   Exception: For structures having fundamental periods of vibration equal to or less than 0.5 second, site-specific evaluations are not required to determine spectral accelerations for liquefiable soils. Rather, the *Site Class* may be determined in accordance with Sec. 4.1.2.2 and the corresponding values of F_a and F_v determined from Tables 4.1.2.4a and 4.1.2.4b.

2. Peats and/or highly organic clays (H > 10 ft [3 m] of peat and/or highly organic clay where H = thickness of soil)
3. Very high plasticity clays (H > 25 ft [8 m] with PI > 75)
4. Very thick soft/medium stiff clays (H > 120 ft [36 m])

When the soil properties are not known in sufficient detail to determine the *Site Class*, *Site Class* D shall be used. *Site Classes* E or F need not be assumed unless the authority having jurisdiction determines that *Site Classes* E or F could be present at the site or in the event that *Site Classes* E or F are established by geotechnical data.

4.1.2.2 Steps for Classifying a Site (also see Table 4.1.2.2 below):

Step 1: Check for the four categories of *Site Class* F requiring site-specific evaluation. If the site corresponds to any of these categories, classify the site as *Site Class* F and conduct a site-specific evaluation.

Step 2: Check for the existence of a total thickness of soft clay > 10 ft (3 m) where a soft clay layer is defined by: s_u < 500 psf (25 kPa), w ≥ 40 percent, and PI > 20. If these criteria are satisfied, classify the site as *Site Class* E.

Step 3: Categorize the site using one of the following three methods with $\overline{v}_s$, $\overline{N}$, and $\overline{s}_u$ computed in all cases as specified by the definitions in Sec. 4.1.2.2:

a. $\overline{v}_s$ for the top 100 ft (30 m) ($\overline{v}_s$ method)

b. $\overline{N}$ for the top 100 ft (30 m) ($\overline{N}$ method)

c. $\bar{N}_{ch}$ for cohesionless soil layers (PI < 20) in the top 100 ft (30 m) and average $\bar{s}_u$ for cohesive soil layers (PI > 20) in the top 100 ft (30 m) ($\bar{s}_u$ method).

TABLE 4.1.2.2 Site Classification

Site Class	$\bar{v}_s$	$\bar{N}$ or $\bar{N}_{ch}$	$\bar{s}_u$
E	< 600 fps (< 180 m/s)	< 15	< 1,000 psf (< 50 kPa)
D	600 to 1,200 fps (180 to 360 m/s)	15 to 50	1,000 to 2,000 psf (50 to 100 kPa)
C	> 1,200 to 2,500 fps (360 to 760 m/s)	> 50	> 2,000 (> 100 kPa)

NOTE: If the $\bar{s}_u$ method is used and the $\bar{N}_{ch}$ and $\bar{s}_u$ criteria differ, select the category with the softer soils (e.g., use *Site Class* E instead of D).

The shear wave velocity for rock, *Site Class* B, shall be either measured on site or estimated for competent rock with moderate fracturing and weathering. Softer and more highly fractured and weathered rock shall either be measured on site for shear wave velocity or classified as *Site Class* C.

The hard rock category, *Site Class* A, shall be supported by shear wave velocity measurements either on site or on profiles of the same rock type in the same formation with an equal or greater degree of weathering and fracturing. Where hard rock conditions are known to be continuous to a depth of 100 ft (30 m), surficial shear wave velocity measurements may be extrapolated to assess $\bar{v}_s$.

The rock categories, *Site Classes* A and B, shall not be used if there is more than 10 ft (3 m) of soil between the rock surface and the bottom of the spread footing or mat foundation.

4.1.2.3 Definitions of Site Class Parameters: The definitions presented below apply to the upper 100 ft (30 m) of the site profile. Profiles containing distinctly different soil layers shall be subdivided into those layers designated by a number that ranges from 1 to n at the bottom where there are a total of n distinct layers in the upper 100 ft (30 m). The symbol i then refers to any one of the layers between 1 and n.

v_{si} is the shear wave velocity in ft/sec (m/s).

d_i is the thickness of any layer between 0 and 100 ft (30 m),

$\bar{v}_s$ is:

$$\bar{v}_s = \frac{\sum_{i=1}^{n} d_i}{\sum_{i=1}^{n} \frac{d_i}{v_{si}}} \qquad (4.1.2.3\text{-}1)$$

where $\sum_{i=1}^{n} d_i$ is equal to 100 ft (30 m)

N_i is the Standard Penetration Resistance (ASTM D1586-84) not to exceed 100 blows/ft as directly measured in the field without corrections.

$\overline{N}$ is:

$$\overline{N} = \frac{\sum_{i=1}^{n} d_i}{\sum_{i=1}^{n} \frac{d_i}{N_i}} \qquad (4.1.2.3\text{-}2)$$

$\overline{N}_{ch}$ is:

$$\overline{N_{ch}} = \frac{d_s}{\sum_{i=1}^{m} \frac{d_i}{N_i}} \qquad (4.1.2.3\text{-}3)$$

where $\sum_{i=1}^{m} d_i = d_s$.

(Use only d_i and N_i for cohesionless soils.)

d_s is the total thickness of cohesionless soil layers in the top 100 ft (30 m).

s_{ui} is the undrained shear strength in psf (kPa), not to exceed 5,000 psf (250 kPa), ASTM D2166-91 or D2850-87.

2.2. SITE CLASSIFICATIONS

2.2.1 In terms of Turkish Earthquake Code

ADAPAZARI			TURKISH CODE		
GRID	X (UTM)	Y (UTM)	Soil group	Local Site Class	Remarks
G 26	528250	4509250	D	Z4	
G 27	528250	4508750	B	Z1	
G 28	528250	4508250	D	Z3	interpolated boring
G 29	528250	4507750	B	Z1	
G 30	528250	4507250	B	Z1	
G 31	528250	4506750	B	Z1	
H 25	528750	4509750	D	Z4	
H 26	528750	4509250	D	Z4	
H 27	528750	4508750	D	Z4	
H 28	528750	4508250	D	Z4	interpolated boring
H 29	528750	4507750	D	Z3	interpolated boring
H 30	528750	4507250	D	Z3	interpolated boring
H 31	528750	4506750	B-C	Z1-Z2	
H 32	528750	4506250	B	Z1	
I 25	529250	4509750	D	Z4	interpolated boring
I 26	529250	4509250	D	Z4	interpolated boring
I 27	529250	4508750	D	Z4	interpolated boring
I 28	529250	4508250	D	Z3	interpolated boring
I 29	529250	4507750	B	Z1-Z2	
I 30	529250	4507250	B	Z1-Z2	
I 31	529250	4506750	D	Z3	interpolated boring
I 32	529250	4506250	D	Z3	interpolated boring
J 24	529750	4510250	D	Z4	
J 25	529750	4509750	D	Z4	
J 26	529750	4509250	D	Z4	interpolated boring
J 27	529750	4508750	D	Z4	
J 28	529750	4508250	D	Z3	
J 29	529750	4507750	C	Z2-Z3	
J 30	529750	4507250	B	Z1	
J 31	529750	4506750	B	Z1-Z2	
J 32	529750	4506250	C	Z3	
K 23	530250	4510750	D	Z4	
K 24	530250	4510250	D	Z4	interpolated boring
K 25	530250	4509750	D	Z4	interpolated boring
K 26	530250	4509250	D	Z3-Z4	
K 27	530250	4508750	D	Z4	
K 28	530250	4508250	C	Z2-Z3	
K 29	530250	4507750	D	Z3	interpolated boring
K 30	530250	4507250	D	Z3	interpolated boring
K 31	530250	4506750	D	Z3-Z4	interpolated boring
K 32	530250	4506250	B	Z1-Z2	

L 23	530750	4510750	C	Z2-Z3	
L 24	530750	4510250	D	Z4	
L 25	530750	4509750	D	Z4	interpolated boring
L 26	530750	4509250	D	Z4	
L 27	530750	4508750	C	Z2	
L 28	530750	4508250	D	Z3-Z4	
L 29	530750	4507750	C	Z2	
L 30	530750	4507250	C	Z2	
L 31	530750	4506750	D	Z3	interpolated boring
L 32	530750	4506250	B	Z2	
M10	531500	4517300	C	Z2-Z3	
M 28	531250	4508250	D	Z3	interpolated boring
M 29	531250	4507750	C	Z2	
M 30	531250	4507250	D	Z4	
N 10	531750	4517250	C	Z2	
N 11	531750	4516750	D	Z3	
N 17	531750	4513750	D	Z3-Z4	
N 18	531750	4513250	C	Z2-Z3	
N 28	531750	4508250	D	Z3-Z4	
N 29	531750	4507750	D	Z3	interpolated boring
N 30	531750	4507250	D	Z4	
O 10	532250	4517250	D	Z4	
O 11	532250	4516750	D	Z3	
O 12	532250	4516250	C	Z3	
O 13	532250	4515750	D	Z3	
O 14	532250	4515250	D	Z3	
O 15	532250	4514750	D	Z3	
O 16	532250	4514250	D	Z3-Z4	
O 17	532250	4513750	D	Z4	
O 27	532250	4508750	D	Z3	
O 28	532250	4508250	D	Z3	
P 09	532750	4517750	D	Z3-Z4	
P 10	532250	4517250	D	Z3-Z4	
P 11	532750	4516750	D	Z3	
P 12	532750	4516250	D	Z4	
P 13	532750	4515750	D	Z3-Z4	
P 14	532750	4515250	D	Z3-Z4	
P 15	532750	4514750	D	Z3	
P 16	532750	4514250	D	Z4	
P 17	532750	4513750	C	Z2-Z3	
P 20	532750	4512250	C	Z2	
P 21	532750	4511750	D	Z4	interpolated boring
P 22	532750	4511250	D	Z3-Z4	
P 23	532750	4510750	D	Z3	
P 24	532750	4510250	D	Z4	
P 25	532750	4509750	C	Z2	interpolated boring
P 26	532750	4509250	D	Z3-Z4	

P 27	532750	4508750	D	Z3	
Q 08	533250	4518250	C	Z2-Z3	
Q 09	533250	4517750	D	Z3	
Q 10	533250	4517250	D	Z3-Z4	
Q 11	533250	4516750	D	Z3-Z4	
Q 12	533250	4516250	D	Z3	
Q 13	533250	4515750	D	Z4	
Q 14	533250	4515250	C	Z2-Z3	
Q 15	533250	4514750	D	Z3	
Q 16	533250	4514250	C	Z2-Z3	
Q 17	533250	4513750	C	Z2	
Q 18	533250	4513250	D	Z3	attention: difference between spt N30 values and defined layers
Q 19	533250	4512750	D	Z4	
Q 20	533250	4512250	D	Z4	
Q 21	533250	4511750	D	Z3	interpolated boring
Q 22	533250	4511250	D	Z3-Z4	
Q 23	533250	4510750	D	Z4	
Q 24	533250	4510250	D	Z4	
Q 27	533250	4508750	D	Z3	
R 07	533750	4518750	A	Z1	
R 08	533750	4518250	D	Z3	interpolated boring
R 09	533750	4517750	D	Z3-Z4	
R 10	533750	4517250	B-C	Z1-Z3	
R 11	533750	4516750	D	Z3	
R 12	533750	4516250	D	Z3	
R 13	533750	4515750	D	Z3-Z4	
R 14	533750	4515250	D	Z3	
R 15	533750	4514750	D	Z3	
R 16	533750	4514250	D	Z3	
R 17	533750	4513750	D	Z3-Z4	
R 18	533750	4513250	D	Z3	
R 19	533750	4512750	B	Z2-Z3	
R 20	533750	4512250	C	Z2	
R 21	533750	4511750	D	Z3	
R 22	533750	4511250	D	Z3	
R 23	533750	4510750	D	Z3	
R 24	533750	4510250	D	Z4	
R 27	533750	4508750	C	Z2	interpolated boring
R 28	533750	4508250	D	Z3	
S 06	534250	4519250	C	Z2-Z3	
S 07	534250	4518750	C	Z2	
S 08	534250	4518250	C	Z2	
S 09	534250	4517750	D	Z3	
S 10	534250	4517250	D	Z3	interpolated boring
S 11	534250	4516750	D	Z3	

S 12	534250	4516250	D	Z3-Z4	
S 13	534250	4515750	D	Z3	
S 14	534250	4515250	D	Z3	
S 15	534250	4514750	D	Z3	
S 16	534250	4514250	D	Z3	
S 17	534250	4513750	D	Z3	
S 18	534250	4513250	D	Z3	
S 19	534250	4512750	D	Z3	
S 20	534250	4512250	D	Z3	
S 21	534250	4511750	C	Z2	
S 22	534250	4511250	D	Z3-Z4	interpolated boring
S 23	534250	4510750	D	Z3	interpolated boring
S 27	534250	4508250	D	Z3	
T 07	534750	4518750	D	Z3	
T 08	534750	4518250	D	Z3	
T 09	534750	4517750	B	Z1-Z2	
T 10	534750	4517250	D	Z3	interpolated boring
T 11	534750	4516750	D	Z3	
T 12	534750	4516250	D	Z3	
T 13	534750	4515750	C	Z2	
T 14	534750	4515250	D	Z3	
T 15	534750	4514750	D	Z3	
T 16	534750	4514250	C	Z2	
T 17	534750	4513750	D	Z3	
T 18	534750	4513250	D	Z3	
T 19	534750	4512750	D	Z3	
T 20	534750	4512250	D	Z3	
T 21	534750	4511750	D	Z3	
T 22	534750	4511250	D	Z4	
T 23	534750	4510750	D	Z4	
T 26	534750	4508750	D	Z3	
U 08	535250	4518250	D	Z3-Z4	
U 09	535250	4517750	D	Z3-Z4	
U 10	535250	4517250	D	Z3-Z3	interpolated boring
U 11	535250	4516750	D	Z3	
U 12	535250	4516250	D	Z3	
U 13	535250	4515750	D	Z3	
U 14	535250	4515250	D	Z4	
U 15	535250	4514750	C	Z2	
U 16	535250	4514250	D	Z3	
U 17	535250	4513750	D	Z3	
U 18	535250	4513250	C	Z2	
U 19	535250	4512750	D	Z3	interpolated boring
U 20	535250	4512250	C	Z2	
V 08	535,750	4,518,250	D	Z3-Z4	
V 09	535750	4517750	D	Z3	
V 10	535750	4517250	D	Z3	

V 11	535750	4516750	D	Z3-Z4	
V 12	535750	4516250	D	Z3-Z4	interpolated boring
V 18	535750	4513250	D	Z4	
V 19	535750	4512750	C	Z2-Z3	
W 07	536250	4518750	C	Z2-Z3	
W 08	536250	4518250	C	Z2-Z3	
W 09	536750	4517750	D	Z3	
W 10	536250	4517250	D	Z3	
W 11	536250	4516750	B	Z1	

GÖLCÜK			TURKISH CODE		
GRID	X (UTM)	Y (UTM)	Soil group	Local Site Class	Remarks
C5	480750	4509250	B	Z1-Z2	
D4	481250	4509750	C	Z2	
D5	481250	4509250	B	Z1	
D6	481250	4508750	C-B	Z1-Z2	
E4	481750	4509750	D	Z3	
E5	481750	4509250	C	Z1	
E6	481750	4508750	C	Z2-Z3	
F4	482250	4509750	A	Z1	
F5	482250	4509250	B	Z1-Z2	
F6	482250	4508750	A	Z1	
F7	482250	4508250	D	Z3	
G3	482750	4510250	A	Z1	
G4	482750	4509750	C	Z2	
G5	482750	4509250	C	Z2	
G6	482750	4508750	C	Z2	
G8	482750	4507750	C	Z2	
G9	482750	4507250	C	Z2-Z3	
H3	483250	4510250	C	Z2	
H4	483250	4509750	C	Z2	interpolated boring
H5	483250	4509250	C	Z2	
H6	483250	4508750	B	Z1	
H7	483250	4508250	C	Z2	
H8	483250	4507750	B	Z1-Z2	interpolated boring
H9	483250	4507250	B	Z1	
I4	483750	4509750	B	Z1	
I5	483750	4509250	B	Z1	
I6	483750	4508750	D	Z3-Z4	
I7	483750	4508250	C	Z2-Z3	interpolated boring
I8	483750	4507750	A	Z1	
I9	483750	4507250	A	Z1	
J4	484250	4509750	B	Z1	
J5	484250	4509250	C	Z2	
J6	484250	4508750	A	Z1	
J7	484250	4508250	B	Z1	
J8	484250	4507750	A	Z1	

J9	484250	4507250	B	Z1	
K11	484750	4506250	D	Z3	
K4	484750	4509750	C	Z2-Z3	
K5	484750	4509250	C	Z2	
K6	484750	4508750	C	Z2	
K7	484750	4508250	C	Z2	
K8	484750	4507750	C	Z2	
K9	484750	4507250	B-C	Z1-Z2	interpolated boring
L10	485250	4506750	C	Z2-Z3	
L11	485250	4506250	D	Z3	
L4	485250	4509750	D	Z3	
L5	485250	4509250	A	Z1	
L6	485250	4508750	C	Z2	
L7	485250	4508250	A	Z1	
L8	485250	4507750	D	Z3	
L9	485250	4507250	C	Z2	interpolated boring
M10	485750	4506750	D	Z3	
M11	485750	4506250	C	Z2	
M4	485750	4509750	C	Z2	
M5	485750	4509250	C	Z2	
M6	485750	4508750	C	Z2	
M7	485750	4508250	B	Z2	
M8	485750	4507750	C	Z2	
N10	486250	4506750	C	Z2	
N11	486250	4506250	C	Z2	
N4	486250	4509750	C	Z2	
N5	486250	4509250	B	Z1	
N6	486250	4508750	C	Z2	
N7	486250	4508250	B	Z1	
N8	486250	4507750	D	Z3	interpolated boring
N9	486250	4507250	D	Z3	
O1O	486750	4506750	B-C	Z1-Z2	
O4	486750	4509750	C	Z2	
O5	486750	4509250	B	Z1	
O6	486750	4508750	C	Z2	
O7	486750	4508250	C	Z2	
O8	486750	4507750	D	Z4	
O9	486750	4507250	C	Z2	
P3	487250	4510250	D	Z3	
P4	487250	4509750	D	Z3	
P5	487250	4509250	D	Z3	
P6	487250	4508750	C-B	Z2	
P7	487250	4508250	C	Z2-Z3	
P8	487250	4507750	C	Z2	
Q4	487750	4509750	D	Z3	
Q5	487750	4509250	C	Z2	
Q6	487750	4508750	B-C	Z1-Z3	

2.2.2 In terms of NEHRP Site Classes

ADAPAZARI			NEHRP		
GRID	X (UTM)	Y (UTM)	v_S 30 m (m/s)	Site class	Remarks
G 26	528250	4509250	169	E	
G 27	528250	4508750	343	D	
G 28	528250	4508250	491	C	interpolated boring
G 29	528250	4507750	485	C	
G 30	528250	4507250	390	C	
G 31	528250	4506750	391	C	
H 25	528750	4509750	157	E	
H 26	528750	4509250	150	E	
H 27	528750	4508750	125	E	
H 28	528750	4508250	165	E	interpolated boring
H 29	528750	4507750	360	D	interpolated boring
H 30	528750	4507250	396	C	interpolated boring
H 31	528750	4506750	370	D	
H 32	528750	4506250	512	C	
I 25	529250	4509750	125	E	interpolated boring
I 26	529250	4509250	123	E	interpolated boring
I 27	529250	4508750	156	E	interpolated boring
I 28	529250	4508250	190	D	interpolated boring
I 29	529250	4507750	386	C	
I 30	529250	4507250	376	C	
I 31	529250	4506750	364	C	interpolated boring
I 32	529250	4506250	456	C	interpolated boring
J 24	529750	4510250	209	D-E	
J 25	529750	4509750	171	E	
J 26	529750	4509250	145	E	interpolated boring
J 27	529750	4508750	219	D	
J 28	529750	4508250	517	C	
J 29	529750	4507750	420	C	
J 30	529750	4507250	496	C	
J 31	529750	4506750	361	C	
J 32	529750	4506250	374	C	
K 23	530250	4510750	190	D	
K 24	530250	4510250	173	E	interpolated boring
K 25	530250	4509750	317	D	interpolated boring
K 26	530250	4509250	188	D	
K 27	530250	4508750	253	D	
K 28	530250	4508250	455	C	
K 29	530250	4507750	365	C	interpolated boring
K 30	530250	4507250	488	C	interpolated boring
K 31	530250	4506750	210	D	interpolated boring
K 32	530250	4506250	358	D	
L 23	530750	4510750	275	D	
L 24	530750	4510250	449	C-E	
L 25	530750	4509750	337	D-E	interpolated boring
L 26	530750	4509250	310	D-E	
L 27	530750	4508750	265	D	
L 28	530750	4508250	296	D	
L 29	530750	4507750	588	C	
L 30	530750	4507250	529	C	
L 31	530750	4506750	422	C	interpolated boring
L 32	530750	4506250	403	C	
M10	531500	4517300	204	D	
M 28	531250	4508250	317	D	interpolated boring
M 29	531250	4507750	307	D	
M 30	531250	4507250	263	D	

N 10	531750	4517250	272	D	
N 11	531750	4516750	269	D	
N 17	531750	4513750	322	D	
N 18	531750	4513250	329	D	
N 28	531750	4508250	287	D	
N 29	531750	4507750	375	C	interpolated boring
N 30	531750	4507250	454	C	
O 10	532250	4517250	228	D-E	
O 11	532250	4516750	267	D-E	
O 12	532250	4516250	298	D	
O 13	532250	4515750	295	D-E	
O 14	532250	4515250	489	C	
O 15	532250	4514750	543	C-E	
O 16	532250	4514250	327	D	
O 17	532250	4513750	197	D	
O 27	532250	4508750	448	C	
O 28	532250	4508250	308	D	
P 09	532750	4517750	178	E	
P 10	532250	4517250	203	D-E	
P 11	532750	4516750	227	D-E	
P 12	532750	4516250	229	D	
P 13	532750	4515750	382	C	
P 14	532750	4515250	403	C	
P 15	532750	4514750	379	C	
P 16	532750	4514250	345	D-E	
P 17	532750	4513750	266	C	
P 20	532750	4512250	525	C	
P 21	532750	4511750	475	C	interpolated boring
P 22	532750	4511250	143	E	
P 23	532750	4510750	481	C	
P 24	532750	4510250	440	C	
P 25	532750	4509750	414	C	interpolated boring
P 26	532750	4509250	342	D	
P 27	532750	4508750	389	C	
Q 08	533250	4518250	501	C	
Q 09	533250	4517750	463	C	
Q 10	533250	4517250	284	D-E	
Q 11	533250	4516750	217	D-E	
Q 12	533250	4516250	295	D-E	
Q 13	533250	4515750	279	D	
Q 14	533250	4515250	319	D	
Q 15	533250	4514750	202	D-E	
Q 16	533250	4514250	238	D	
Q 17	533250	4513750	279	D	
Q 18	533250	4513250	547	C	attention: difference between spt N30 values and defined layers
Q 19	533250	4512750	426	C	
Q 20	533250	4512250	223	D	
Q 21	533250	4511750	152	E	interpolated boring
Q 22	533250	4511250	303	C	
Q 23	533250	4510750	344	D	
Q 24	533250	4510250	303	D	
Q 27	533250	4508750	445	C	
R 07	533750	4518750	543	C	
R 08	533750	4518250	353	D	interpolated boring
R 09	533750	4517750	242	D-E	
R 10	533750	4517250	280	D	
R 11	533750	4516750	461	C	
R 12	533750	4516250	446	C	

R 13	533750	4515750	152	E	
R 14	533750	4515250	376	C-E	
R 15	533750	4514750	257	D	
R 16	533750	4514250	241	D	
R 17	533750	4513750	230	D	
R 18	533750	4513250	685	C	
R 19	533750	4512750	309	D	
R 20	533750	4512250	255	D	
R 21	533750	4511750	321	D	
R 22	533750	4511250	347	D	
R 23	533750	4510750	297	D	
R 24	533750	4510250	367	C	
R 27	533750	4508750	422	C	interpolated boring
R 28	533750	4508250	368	C	
S 06	534250	4519250	262	D	
S 07	534250	4518750	268	D	
S 08	534250	4518250	231	D	
S 09	534250	4517750	446	C-E	
S 10	534250	4517250	187	D-E	interpolated boring
S 11	534250	4516750	302	D-E	
S 12	534250	4516250	217	D-E	
S 13	534250	4515750	213	D	
S 14	534250	4515250	432	C	
S 15	534250	4514750	206	D	
S 16	534250	4514250	258	D-E	
S 17	534250	4513750	284	D-E	
S 18	534250	4513250	307	D-E	
S 19	534250	4512750	213	D-E	
S 20	534250	4512250	268	D	
S 21	534250	4511750	278	D	
S 22	534250	4511250	161	E	interpolated boring
S 23	534250	4510750	326	D	interpolated boring
S 27	534250	4508250	357	D	
T 07	534750	4518750	205	D	
T 08	534750	4518250	202	D-E	
T 09	534750	4517750	540	C	
T 10	534750	4517250	174	E	interpolated boring
T 11	534750	4516750	199	D	
T 12	534750	4516250	285	D-E	
T 13	534750	4515750	240	D	
T 14	534750	4515250	328	D	
T 15	534750	4514750	231	D	
T 16	534750	4514250	289	D-E	
T 17	534750	4513750	574	C	
T 18	534750	4513250	543	C-E	
T 19	534750	4512750	290	D-E	
T 20	534750	4512250	252	D	
T 21	534750	4511750	269	D-E	
T 22	534750	4511250	323	D	
T 23	534750	4510750	337	D	
T 26	534750	4508750	597	C	
U 08	535250	4518250	159	E	
U 09	535250	4517750	214	D	
U 10	535250	4517250	334	D	interpolated boring
U 11	535250	4516750	263	D	
U 12	535250	4516250	256	D	
U 13	535250	4515750	374	D	
U 14	535250	4515250	154	E	
U 15	535250	4514750	227	D	
U 16	535250	4514250	316	D	

U 17	535250	4513750	295	D-E	
U 18	535250	4513250	374	C	
U 19	535250	4512750	407	C	interpolated boring
U 20	535250	4512250	425	C	
V 08	535,750	4,518,250	156	E	
V 09	535750	4517750	281	D-E	
V 10	535750	4517250	234	D	
V 11	535750	4516750	211	D	
V 12	535750	4516250	360	D	interpolated boring
V 18	535750	4513250	303	D-E	
V 19	535750	4512750	329	D	
W 07	536250	4518750	296	D	
W 08	536250	4518250	296	D	
W 09	536750	4517750	236	D-E	
W 10	536250	4517250	158	E	
W 11	536250	4516750	303	D	

GÖLCÜK			NEHRP		
GRID	X (UTM)	Y (UTM)	v_S 30 m (m/s)	Site class	Remarks
C5	480750	4509250	394	C	
D4	481250	4509750	380	C	
D5	481250	4509250	462	C	
D6	481250	4508750	420	C	
E4	481750	4509750	487	C	
E5	481750	4509250	355	D	
E6	481750	4508750	330	D	
F4	482250	4509750	470	C	
F5	482250	4509250	363	C	
F6	482250	4508750	472	C	
F7	482250	4508250	319	D	
G3	482750	4510250	493	C	
G4	482750	4509750	385	C	
G5	482750	4509250	466	C	
G6	482750	4508750	457	C	
G8	482750	4507750	369	C	
G9	482750	4507250	362	C	
H3	483250	4510250	328	D	
H4	483250	4509750	396	C	interpolated boring
H5	483250	4509250	437	C	
H6	483250	4508750	394	C	
H7	483250	4508250	426	C	
H8	483250	4507750	470	C	interpolated boring
H9	483250	4507250	414	C	
I4	483750	4509750	370	C	
I5	483750	4509250	431	C	
I6	483750	4508750	374	C	
I7	483750	4508250	394	C	interpolated boring
I8	483750	4507750	459	C	
I9	483750	4507250	502	C	
J4	484250	4509750	403	C	
J5	484250	4509250	364	C	
J6	484250	4508750	492	C	
J7	484250	4508250	393	C	
J8	484250	4507750	442	C	
J9	484250	4507250	384	C	
K11	484750	4506250	437	C	
K4	484750	4509750	225	D	
K5	484750	4509250	364	C	

K6	484750	4508750	445	C	
K7	484750	4508250	356	D	
K8	484750	4507750	268	D	
K9	484750	4507250	373	C	interpolated boring
L10	485250	4506750	298	D	
L11	485250	4506250	377	C	
L4	485250	4509750	339	D	
L5	485250	4509250	449	C	
L6	485250	4508750	289	D	
L7	485250	4508250	430	C	
L8	485250	4507750	356	D	
L9	485250	4507250	317	D	interpolated boring
M10	485750	4506750	345	D	
M11	485750	4506250	449	C	
M4	485750	4509750	253	D	
M5	485750	4509250	372	C	
M6	485750	4508750	417	C	
M7	485750	4508250	376	C	
M8	485750	4507750	464	C	
N10	486250	4506750	332	D	
N11	486250	4506250	402	C	
N4	486250	4509750	239	D	
N5	486250	4509250	321	D	
N6	486250	4508750	415	C	
N7	486250	4508250	346	D	
N8	486250	4507750	234	D	interpolated boring
N9	486250	4507250	240	D	
O1O	486750	4506750	405	C	
O4	486750	4509750	263	D	
O5	486750	4509250	472	C	
O6	486750	4508750	418	C	
O7	486750	4508250	314	D	
O8	486750	4507750	287	D	
O9	486750	4507250	281	D	
P3	487250	4510250	295	D	
P4	487250	4509750	294	D	
P5	487250	4509250	324	C	
P6	487250	4508750	406	C	
P7	487250	4508250	417	C	
P8	487250	4507750	400	C	
Q4	487750	4509750	259	D	
Q5	487750	4509250	287	D	
Q6	487750	4508750	401	C	

2.3. SITE RESPONSE ANALYSIS

2.3.1 AdazarıRegion

GRID	X(UTM)	Y(UTM)	PGA (g)	Pre-dominant T (s)	S_A (g)	max strain (%)	Depth (m)	remarks
G 26	528250	4509250	0.128	0.70	0.50	0.540	41	
G 27	528250	4508750	0.370	0.92	1.48	0.031	20	two peaks
G 28	528250	4508250	0.751	0.42	3.21	0.711	7	interpolated, two peaks, max strain in upper 10m
G 29	528250	4507750	0.314	0.92	1.29	0.031	20	two peaks
G 30	528250	4507250	0.369	0.72	1.41	0.546	36	two peaks
G 31	528250	4506750	0.270	0.92	1.13	0.865	36	
H 25	528750	4509750	0.101	0.94	0.38	0.825	42	
H 26	528750	4509250	0.189	0.94	0.88	2.041	29	max strain in the upper 30m
H 27	528750	4508750	0.106	2.50	0.35	1.678	29	max strain in the upper 30m
H 28	528750	4508250	0.166	0.94	0.81	2.006	29	interpolated, max strain in the upper 30m
H 29	528750	4507750	0.480	0.70	2.04	0.579	9	interpolated, max strain in the upper 10m
H 30	528750	4507250	0.493	0.94	2.92	4.120	5	interpolated, max strain in the upper 5m
H 31	528750	4506750	0.267	0.94	1.14	0.832	36	
H 32	528750	4506250	0.689	0.20	2.58	0.077	12	max strain in the upper 15m
I 25	529250	4509750	0.321	0.49	1.14	0.568	32	interpolated, Resp Spectra: 2.peak at 0,94/1,14
I 26	529250	4509250	0.134	0.94	0.65	2.917	29	interpolated, max strain in the upper 30m
I 27	529250	4508750	0.172	0.94	0.58	1.130	29	interpolated, max strain in the upper 30m
I 28	529250	4508250	0.160	0.94	0.75	1.919	29	interpolated, max strain in the upper 30m
I 29	529250	4507750	0.384	0.70	1.42	0.550	36	
I 30	529250	4507250	0.430	0.94	1.60	0.203	36	
I 31	529250	4506750	0.380	0.94	2.01	4.638	8	interpolated, max strain in the upper 10m
I 32	529250	4506250	0.649	0.70	2.57	1.221	8	interpolated, max strain in the upper 10m
J 24	529750	4510250	0.063	2.50	0.28	0.872	42	
J 25	529750	4509750	0.074	0.70	0.29	1.274	42	interpolated
J 26	529750	4509250	0.410	0.70	1.47	1.022	11	max strain in the upper 15m
J 27	529750	4508750	0.365	0.94	1.80	2.406	9	interpolated, max strain in the upper 10m
J 28	529750	4508250	0.674	0.42	2.73	9.660	3	max strain in the upper 10m
J 29	529750	4507750	0.183	0.94	0.60	0.967	32	
J 30	529750	4507250	0.167	0.94	0.56	1.014	32	
J 31	529750	4506750	0.412	0.94	1.83	0.446	29	interpolated, max strain in the upper 30m
J 32	529750	4506250	0.365	0.94	1.26	0.252	36	
K 23	530250	4510750	0.194	0.94	0.06	0.812	29	max strain in the upper 30m
K 24	530250	4510250	0.256	0.94	0.92	0.584	22	interpolated, max strain in the upper 30m
K 25	530250	4509750	0.263	0.47	0.96	0.648	32	interpolated

K 26	530250	4509250	0.180	0.92	0.59	0.605	29	interpolated, max strain in the upper 30m
K 27	530250	4508750	0.194	0.94	0.70	0.867	32	
K 28	530250	4508250	0.164	0.95	0.57	0.951	32	
K 29	530250	4507750	0.409	0.94	2.10	2.369	11	interpolated, max strain in the upper 15m
K 30	530250	4507250	0.217	0.94	0.84	0.951	32	interpolated, great strain also in the upper 10m
K 31	530250	4506750	0.170	0.92	0.64	1.023	29	max strain in the upper 30m
K 32	530250	4506250	0.108	2.50	0.38	1.405	36	
L 23	530750	4510750	0.321	0.94	1.43	1.156	16	max strain in the upper 20m
L 24	530750	4510250	0.357	0.94	1.60	3.514	9	max strain in the upper 10m
L 25	530750	4509750	0.397	0.47	1.46	1.164	32	interpolated
L 26	530750	4509250	0.082	2.50	0.30	0.625	32	
L 27	530750	4508750	0.130	2.50	0.39	1.332	32	
L 28	530750	4508250	0.136	2.50	0.38	1.317	36	
L 29	530750	4507750	0.650	0.19	2.01	0.104	3	max strain in the upper 10m
L 30	530750	4507250	0.808	0.48	3.86	0.702	12	max strain in the upper 15m
L 31	530750	4506750	0.539	0.94	2.40	3.130	4	interpolated, max strain in the upper 5m
L 32	530750	4506250	0.554	0.48	1.91	0.250	36	
M 10	531250	4517250	0.095	0.94	0.27	0.359	32	
M 28	531250	4508250	0.106	2.50	0.35	3.600	11	interpolated, max strain in the upper 15m
M 29	531250	4507750	0.238	0.94	1.13	0.519	36	
M 30	531250	4507250	0.277	0.92	1.19	0.815	36	
N 10	531750	4517250	0.073	0.94	0.21	0.429	32	
N 11	531750	4516750	0.367	0.92	0.76	0.330	42	
N 17	531750	4513750	0.171	0.94	0.61	0.709	36	
N 18	531750	4513250	0.169	0.94	0.59	0.792	32	
N 28	531750	4508250	0.401	0.72	1.67	0.516	8	max strain in the upper 10m
N 29	531750	4507750	0.275	0.94	1.21	4.472	11	max strain in the upper 15m
N 30	531750	4507250	0.541	0.48	2.20	0.570	8	max strain in the upper 10m
O 10	532250	4517250	0.088	0.94	0.24	0.412	32	
O 11	532250	4516750	0.074	2.50	0.22	0.442	32	Resp Spectra: 2.peak 0.94/ 0.22
O 12	532250	4516250	0.181	0.94	0.71	0.499	37	
O 13	532250	4515750	0.065	0.94	0.23	0.440	32	high peaks
O 14	532250	4515250	0.067	2.50	0.22	0.447	32	two peaks
O 15	532250	4514750	0.067	2.50	0.23	0.466	32	
O 16	532250	4514250	0.389	0.70	1.34	0.224	29	max strain in the upper 30m (twice)
O 17	532250	4513750	0.227	0.94	0.84	0.372	25	max strain in the upper 30m
O 27	532250	4508750	0.356	0.70	1.21	0.465	36	
O 28	532250	4508250	0.510	0.24	1.58	0.258	2	max strain in the upper 5m
P 09	532750	4517750	0.104	0.70	0.33	0.313	32	
P 10	532250	4517250	0.116	0.94	0.36	4.038	9	max strain in the upper 10m, high peaks
P 11	532750	4516750	0.211	0.92	0.75	0.449	32	
P 12	532750	4516250	0.162	0.94	0.57	0.351	32	
P 13	532750	4515750	0.120	0.70	0.38	1.276	32	kein vs+Bohrprofil
P 14	532750	4515250	0.070	2.50	0.21	0.432	32	

P 15	532750	4514750	0.068	2.50	0.22	0.443	32	
P 16	532750	4514250	0.208	0.94	0.89	0.683	36	
P 17	532750	4513750	0.270	0.48	1.33	2.707	32	
P 20	532750	4512250	0.592	0.20	2.21	0.102	11	max strain in the upper 15m
P 21	532750	4511750	0.274	0.94	1.38	1.535	11	max strain in the upper 15m
P 22	532750	4511250	0.164	0.94	0.91	1.705	29	max strain in the upper 30m
P 23	532750	4510750	0.110	2.50	0.33	1.190	36	
P 24	532750	4510250	0.050	2.50	0.15	17.115	42	
P 25	532750	4509750	0.197	0.92	0.84	0.255	42	interpolated
P 26	532750	4509250	0.125	0.94	0.38	0.594	32	
P 27	532750	4508750	0.126	0.94	0.39	0.629	37	interpolated
Q 08	533250	4518250	0.064	2.50	0.20	0.406	32	
Q 09	533250	4517750	0.168	0.92	0.62	0.450	37	
Q 10	533250	4517250	0.124	0.94	0.38	0.728	32	
Q 11	533250	4516750	0.094	0.47	0.27	0.406	32	
Q 12	533250	4516250	0.310	0.94	1.62	1.227	5	max strain in the upper 5m
Q 13	533250	4515750	0.079	0.94	0.23	0.442	32	two peaks
Q 14	533250	4515250	0.342	0.92	1.32	0.292	37	
Q 15	533250	4514750	0.155	0.94	0.57	0.620	21	max strain in the upper 30m
Q 16	533250	4514250	0.458	0.94	1.38	0.391	27	max strain in the upper 30m
Q 17	533250	4513750	0.354	0.70	1.36	0.182	29	
Q 18	533250	4513250	0.408	0.42	1.81	0.504	7	max strain in the upper 10m
Q 19	533250	4512750	0.123	0.93	0.34	1.060	36	
Q 20	533250	4512250	0.412	0.94	1.79	0.411	29	max strain in the upper 30m
Q 21	533250	4511750	0.301	0.94	1.11	0.641	19	interpolated, max strain in the upper 20m
Q 22	533250	4511250	0.477	0.94	1.95	0.910	3	max strain in the upper 5m
Q 23	533250	4510750	1.270	2.50	0.34	1.170	36	
Q 24	533250	4510250	0.061	2.50	0.27	0.659	32	
Q 27	533250	4508750	0.267	0.94	1.02	0.735	36	
R 07	533750	4518750	0.064	0.94	0.20	0.390	37	two peaks
R 08	533750	4518250	0.068	0.94	0.20	0.407	32	interpolated, two peaks
R 09	533750	4517750	0.114	0.47	0.33	0.436	32	
R 10	533750	4517250	0.119	0.94	0.41	0.443	32	
R 11	533750	4516750	0.068	2.50	0.21	0.425	31	
R 12	533750	4516250	0.067	2.50	0.21	0.418	32	
R 13	533750	4515750	0.130	2.40	0.47	-		two constant values for shear strain (0.2; 65535)
R 14	533750	4515250	0.072	0.94	0.21	0.427	33	
R 15	533750	4514750	0.077	0.94	0.23	0.458	32	
R 16	533750	4514250	0.645	0.70	2.37	0.861	2	max strain in the upper 5m
R 17	533750	4513750	0.270	0.94	1.17	0.583	29	max strain in the upper 30m
R 18	533750	4513250	0.498	0.24	0.94	0.014	1	high peaks
R 19	533750	4512750	0.330	0.72	1.28	0.384	36	
R 20	533750	4512250	0.263	0.94	1.03	0.802	25	max strain in the upper 30m
R 21	533750	4511750	0.410	0.92	1.77	0.594	26	max strain in the upper 30m
R 22	533750	4511250	0.541	0.48	1.69	0.201	36	high peaks
R 23	533750	4510750	0.131	0.94	0.35	1.027	36	

R 24	533750	4510250	0.545	0.48	1.80	0.213	36	
R 27	533750	4508750	0.458	0.94	1.83	0.221	36	interpolated
R 28	533750	4508250	0.742	0.17	2.62	0.455	2	max strain in the upper 30m
S 06	534250	4519250	0.075	0.94	0.23	0.389	32	
S 07	534250	4518750	0.077	0.94	0.23	0.392	32	
S 08	534250	4518250	0.073	0.94	0.22	0.148	32	
S 09	534250	4517750	0.205	0.92	0.86	0.225	42	
S 10	534250	4517250	0.287	0.92	1.33	0.350	24	interpolated, max strain in the upper 30m
S 11	534250	4516750	0.214	0.92	0.91	0.201	42	
S 12	534250	4516250	0.154	0.94	0.60	0.511	19	max strain in the upper 20m
S 13	534250	4515750	0.196	0.47	0.71	0.438	32	
S 14	534250	4515250	0.168	0.94	0.65	0.473	37	
S 15	534250	4514750	0.213	0.94	0.63	0.347	32	high peaks
S 16	534250	4514250	0.429	0.94	1.95	0.780	22	max strain in the upper 30m
S 17	534250	4513750	0.618	0.70	2.09	0.500	16	max strain in the upper 20m
S 18	534250	4513250	0.488	0.84	2.20	1.996	7	max strain in the upper 10m
S 19	534250	4512750	0.219	0.94	0.91	0.130	19	max strain in the upper 20m
S 20	534250	4512250	0.476	0.94	2.16	2.551	4	max strain in the upper 10m
S 21	534250	4511750	0.172	0.94	0.70	0.719	32	
S 22	534250	4511250	0.227	0.92	0.94	0.927	19	interpolated, max strain in the upper 20m
S 23	534250	4510750	0.125	0.94	0.34	1.055	36	interpolated, Resp Spectra: 2.peak at 02.50/.34
S 27	534250	4508250	0.457	0.94	1.48	0.196	36	
T 07	534750	4518750	0.444	0.94	1.50	0.312	24	two high peaks, max strain in the upper 30m
T 08	534750	4518250	0.081	0.41	0.48	0.441	31	high peaks
T 09	534750	4517750	0.063	2.50	0.20	0.395	37	Resp Spectra: 2.peak at 0,94/0,19
T 10	534750	4517250	0.193	0.94	0.72	0.789	19	interpolated, max strain in the upper 20m
T 11	534750	4516750	0.264	0.94	1.00	0.614	23	max strain in the upper 30m
T 12	534750	4516250	0.195	0.92	0.73	0.492	37	
T 13	534750	4515750	0.130	0.94	0.44	0.442	32	
T 14	534750	4515250	0.395	0.72	1.93	2.461	4	max strain in the upper 5m
T 15	534750	4514750	0.170	0.50	0.42	0.481	32	high peaks
T 16	534750	4514250	0.481	0.70	1.86	0.460	9	max strain in the upper 10m
T 17	534750	4513750	0.565	0.20	2.42	0.242	3	max strain in the upper 5m
T 18	534750	4513250	0.675	0.28	2.46	0.437	3	max strain in the upper 5m
T 19	534750	4512750	0.494	0.27	1.76	0.285	3	max strain in the upper 5m
T 20	534750	4512250	0.181	0.94	0.72	0.406	32	
T 21	534750	4511750	0.195	0.94	0.79	0.660	32	
T 22	534750	4511250	0.127	0.94	0.35	1.060	36	
T 23	534750	4510750	0.123	0.94	0.33	1.117	36	Resp Spectra: 2.peak at 02.50/.33
T 26	534750	4508750	0.685	0.12	2.04	0.081	2	
U 08	535250	4518250	0.432	0.94	1.38	-		two constant values for shear strain (0.2; 65535)
U 09	535250	4517750	0.085	0.94	0.23	0.402	32	high peaks
U 10	535250	4517250	0.131	0.94	0.45	0.455	32	interpolated

U 11	535250	4516750	0.145	0.94	0.43	0.466	32	
U 12	535250	4516250	0.143	0.94	0.45	0.456	33	
U 13	535250	4515750	0.058	2.50	0.22	0.535	32	
U 14	535250	4515250	0.282	0.94	1.23	1.859	13	max strain in the upper 15m
U 15	535250	4514750	0.086	0.94	0.24	0.432	32	high peaks
U 16	535250	4514250	0.352	0.72	1.36	0.329	36	
U 17	535250	4513750	0.287	0.94	1.20	0.492	29	max strain in the upper 30m
U 18	535250	4513250	0.166	0.94	0.59	0.709	36	
U 19	535250	4512750	0.184	0.94	0.76	0.672	36	interpolated, max strain in the upper 10m
U 20	535250	4512250	0.198	2.50	0.52	1.582	32	high peaks
V 08	535750	4518250	0.292	0.94	1.06	0.584	19	
V 09	535750	4517750	0.075	0.94	0.23	0.405	32	
V 10	535750	4517250	0.143	0.94	0.44	0.450	32	
V 11	535750	4516750	0.240	0.94	0.91	0.608	23	max strain in the upper 30m
V 12	535750	4516250	0.207	0.94	1.04	0.763	10	interpolated, max strain in the upper 10m
V 18	535750	4513250	0.697	0.94	2.54	1.118	20	max strain in the upper 20m
V 19	535750	4512750	0.174	0.94	0.65	0.741	36	
W 07	536250	4518750	0.169	0.94	0.66	0.419	37	
W 08	536250	4518250	0.174	0.92	0.70	0.451	37	
W 09	536750	4517750	0.200	0.94	0.75	0.448	37	
W 10	536250	4517250	0.149	0.92	0.56	0.625	29	max strain in the upper 30m
W 11	536250	4516750	0.180	0.94	0.69	0.474	37	

2.3.2 Golcuk Region

GRID	X(UTM)	Y(UTM)	PGA (g)	predominant T (s)	S_A (g)	max strain	remarks
C5	480750	4509250	0.249	0.92	0.87	0.081	interpolated
D4	481250	4509750	0.240	0.92	0.83	0.071	
D5	481250	4509250	0.280	0.94	0.92	0.081	
D6	481250	4508750	0.393	0.24	1.23	0.069	
E4	481750	4509750	0.307	0.17	0.92	0.084	double peak
E5	481750	4509250	0.324	0.27	1.02	0.078	
E6	481750	4508750	0.314	0.70	1.28	0.210	interpolated
F4	482250	4509750	0.214	0.94	0.80	0.071	
F5	482250	4509250	0.183	0.92	0.72	0.129	interpolated
F6	482250	4508750	0.263	0.92	0.90	0.092	interpolated
F7	482250	4508250	0.447	0.48	1.38	0.159	max strain in upper 6m
G3	482750	4510250	0.329	0.94	1.02	0.072	
G4	482750	4509750	0.333	0.36	1.13	0.144	
G5	482750	4509250	0.256	0.92	0.90	0.090	
G6	482750	4508750	0.343	0.19	1.01	0.097	
G8	482750	4507750	0.266	0.94	0.91	0.075	interpolated
G9	482750	4507250	0.292	0.27	0.95	0.076	interpolated
H3	483250	4510250	0.227	0.92	0.80	0.113	
H4	483250	4509750	0.395	0.24	1.20	0.071	interpolated
H5	483250	4509250	0.382	0.28	1.09	0.104	some high peaks
H6	483250	4508750	0.395	0.27	1.21	0.074	
H7	483250	4508250	0.315	0.19	1.03	0.087	
H8	483250	4507750	0.278	0.72	0.93	0.170	interpolated
H9	483250	4507250	0.275	0.72	0.97	0.149	
I4	483750	4509750	0.316	0.92	1.01	0.077	some high peaks
I5	483750	4509250	0.198	0.92	0.73	0.121	

I6	483750	4508750	0.209	0.94	0.88	2.958	max strain in upper 10m
I7	483750	4508250	0.190	0.92	0.74	0.125	interpolated
I8	483750	4507750	0.269	0.92	0.92	0.079	
I9	483750	4507250	0.256	0.94	0.89	0.079	
J4	484250	4509750	0.284	0.92	0.95	0.089	
J5	484250	4509250	0.254	0.92	0.84	0.095	
J6	484250	4508750	0.214	0.92	0.80	0.106	
J7	484250	4508250	0.196	0.94	0.75	0.124	
J8	484250	4507750	0.181	0.92	0.72	0.121	
J9	484250	4507250	0.275	0.92	0.92	0.090	
K4	484750	4509750	0.301	0.94	1.41	0.343	
K5	484750	4509250	0.384	0.70	1.35	0.163	
K6	484750	4508750	0.339	0.94	1.10	0.071	
K7	484750	4508250	0.251	0.70	0.93	0.090	
K8	484750	4507750	0.374	0.70	1.36	0.167	
K9	484750	4507250	0.392	0.24	1.11	0.066	
K11	484750	4506250	0.249	0.92	0.82	0.090	
L4	485250	4509750	0.309	0.28	0.93	0.095	
L5	485250	4509250	0.253	0.92	0.86	0.113	
L6	485250	4508750	0.475	0.70	1.67	0.205	max strain in the upper 10m
L7	485250	4508250	0.256	0.92	0.90	0.087	two high peaks
L8	485250	4507750	0.334	0.28	1.01	0.084	
L9	485250	4507250	0.213	0.94	0.83	0.099	two high peaks
L10	485250	4506750	0.335	0.70	1.35	0.419	max strain in the upper 10m
L11	485250	4506250	0.363	0.36	1.21	0.108	
M4	485750	4509750	0.339	0.94	1.63	0.572	max strain in the upper 30m
M5	485750	4509250	0.603	0.48	1.73	0.150	max strain in the upper 15m, high peaks
M6	485750	4508750	0.392	0.27	1.34	0.075	
M7	485750	4508250	0.255	0.70	0.90	0.096	two high peaks
M8	485750	4507750	0.244	0.92	0.82	0.105	
M10	485750	4506750	0.317	0.70	1.01	0.079	high peaks
M11	485750	4506250	0.208	0.92	0.74	0.104	
N4	486250	4509750	0.238	0.92	0.91	0.210	two high peaks
N5	486250	4509250	0.330	0.70	1.20	0.108	
N6	486250	4508750	0.337	0.27	1.04	0.101	
N7	486250	4508250	0.337	0.36	1.08	0.089	high peaks
N8	486250	4507750	0.232	0.94	0.94	0.580	max strain in the upper 30m
N9	486250	4507250	0.359	0.94	1.36	0.966	max strain in the upper 15m
N10	486250	4506750	0.417	0.36	1.52	0.185	max strain in the upper 15m
N11	486250	4506250	0.278	0.70	0.98	0.144	two high peaks, max strain in upper 30m
O4	486750	4509750	0.249	0.94	0.87	0.245	max strain in the upper 30m
O5	486750	4509250	0.116	0.94	0.53	0.336	
O6	486750	4508750	0.271	0.92	0.91	0.090	
O7	486750	4508250	0.307	0.92	1.27	0.401	max strain in the upper 30m
O8	486750	4507750	0.248	0.94	1.19	0.981	max strain in the upper 20m
O9	486750	4507250	0.417	0.36	1.37	0.097	
O1O	486750	4506750	0.358	0.70	1.15	0.160	max strain in the upper 30m
P3	487250	4510250	0.339	0.93	1.69	3.377	max strain in the upper 10m
P4	487250	4509750	0.116	0.94	0.49	0.453	
P5	487250	4509250	0.165	0.92	0.58	0.224	
P6	487250	4508750	0.281	0.94	0.95	0.307	
P7	487250	4508250	0.261	0.94	0.87	0.070	
P8	487250	4507750	0.306	0.70	1.14	0.234	max strain in the upper 30m
Q4	487750	4509750	0.282	0.70	0.98	0.225	high peaks, max strain in upper 20m
Q5	487750	4509250	0.175	0.92	0.82	1.278	max strain in the upper 30m
Q6	487750	4508750	0.277	0.94	0.98	0.170	max strain in the upper 30m

3. CHAPTER 8- KOERISLOPE MANUAL (KOERISLOPE V1.0)

Yasin Fahjan and Bilge Siyahi, Department of Earthquake Engineering, Kandilli Observatory and Earthquake Research Institute, Boğaziçi University

KoeriSlope is application developed to estimate slope stability for microzonation purposes. KoeriSlope Version 1.0 in its current form is capable to perform slope stability estimation analysis based on Siyahi and Ansal (1993) procedure. KoeriSlope is user-friendly application that operates through Geo-cells systems. Geo-cells (Grids) facilitate the manipulation of data for soil type, slope gradient and earthquake hazards. The application is developed using the MapBasic language and runs efficiently under MapInfo software. The application is integrated with MapInfo and capable to utilize the powerful features in displaying, querying, manipulating and mapping inventory databases.

3.1. KOERISLOPE DIALOG FORM

KoeriSlope is a MapBasic application with a standard Windows interface. The application can be launched under MapInfo using the <Run MapBasic Program> feature from the standard menu bar of MapInfo. The main dialog of the application is shown below.

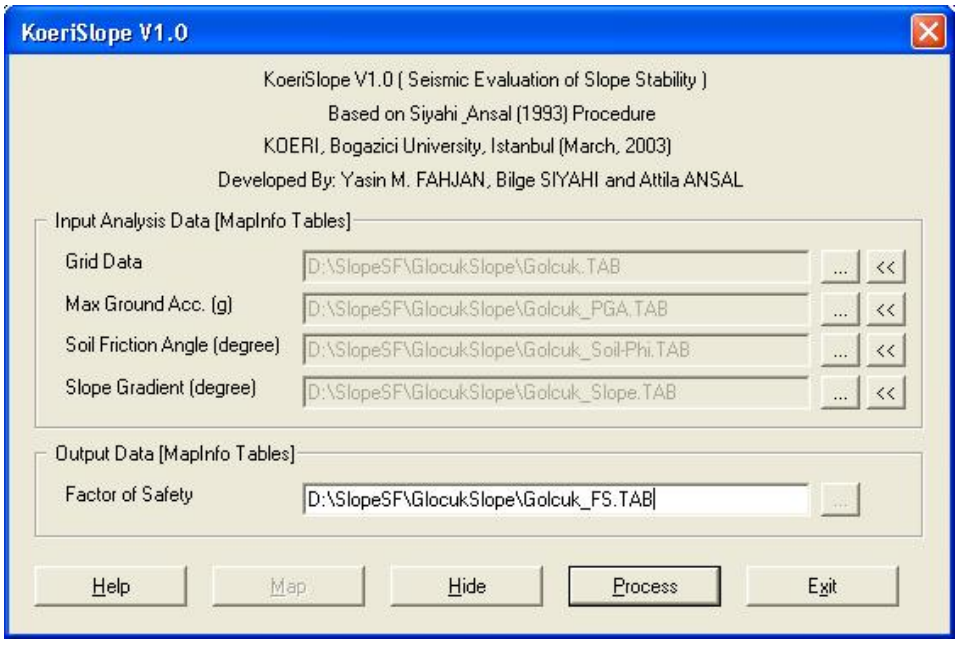

The main dialog provides the user different features like the ... icon which is used to setup the input data tables' filenames using the standard Windows Open File Dialog, and << icon to open input data files as MapInfo tables. To manipulate the data using MapInfo features, main dialog can be inactivated using the <Hide> icon. To start performing the analysis <Process> icon can be used.

3.1.1 KoeriSlope Menu Bar Item

The main function of the menu bar item [KoeriSlope] is to provide extra features to provides the ability to reactivate the main dialog form using <Show Main Dialog> menu item.

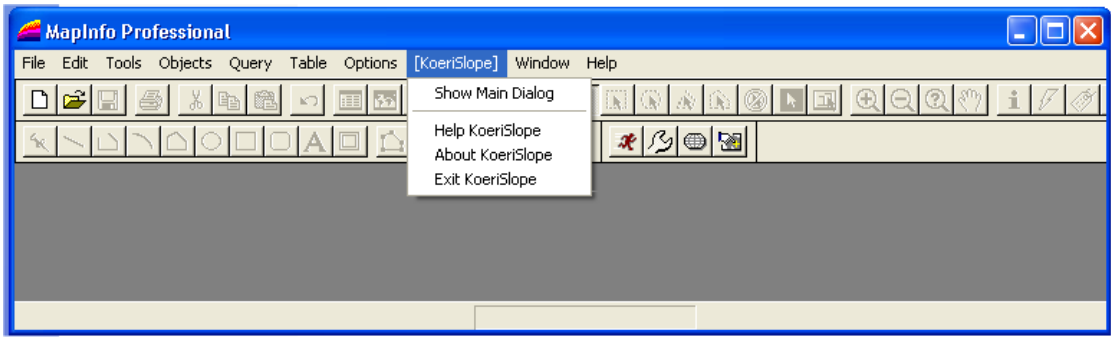

3.1.2 Data Needed for Slope Stability Study

In order to perform slope stability analysis, the following input data should be provided for each Geo-cell.

- Maximum expected ground acceleration (seismic coefficient).
- Soil friction angle.
- Maximum slope gradient.

The analysis will be performed for the Geo-cells presented in Grid data table. If Grid data is a mappable table, the <Map> icon in Main dialog will be activated and the analysis results can be mapped. The data should be provided as MapInfo data tables with the specific headers as it is shown below.

InputGridData Browser

GRID	Col_Name	Row_Name
B5	B	5
B6	B	6
C5	C	5
C6	C	6
D4	D	4
D5	D	5
D6	D	6
D7	D	7
E4	E	4
E5	E	5
E6	E	6

Grid Data Input Data

InputSpPGAData Browser

GRID	Col_Name	Row_Name	PGA
D4	D	4	0.24
D5	D	5	0.28
D6	D	6	0.393
E4	E	4	0.307
E5	E	5	0.324
E6	E	6	0.314
F4	F	4	0.214
F5	F	5	0.183
F6	F	6	0.263
F7	F	7	0.447
G3	G	3	0.329
G4	G	4	0.333
G5	G	5	0.256

Maximum Expected Ground Acceleration Input Data

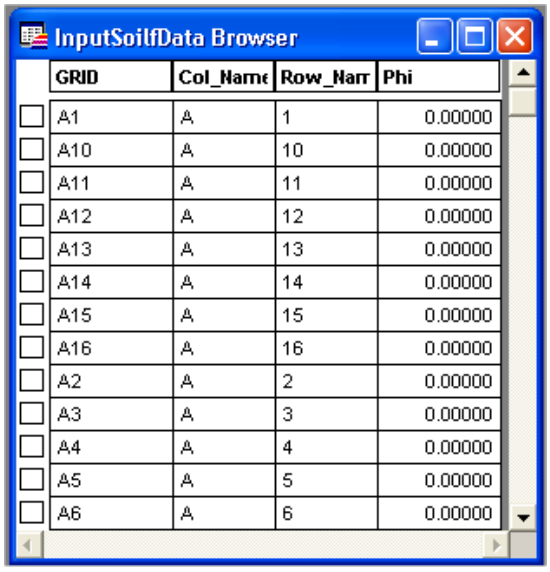

Soil Friction Angle Input Data

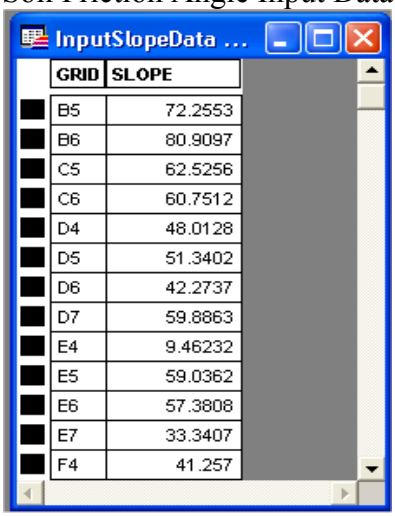

Maximum Slope Gradient Input Data

3.1.3 Processing Analysis Status Dialog

Status bar demonstrates the analysis processing status in percentages. The analysis can be halted by using the <Cancel> icon.

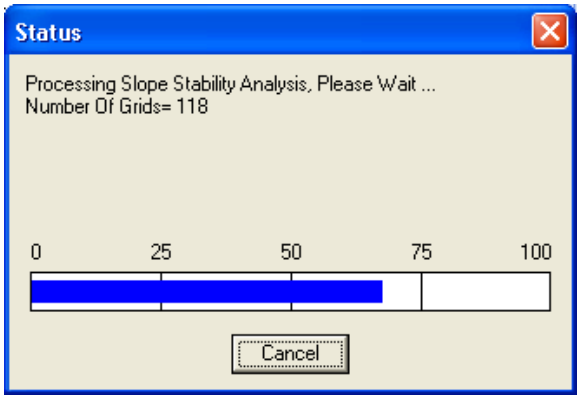

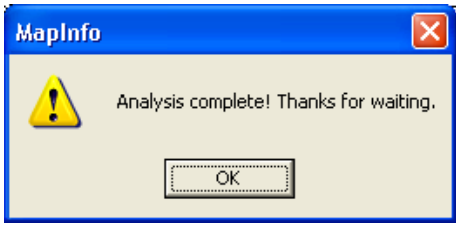

3.1.4 Output of the Analysis

The application computes N1 stability number based on seismic coefficient acceleration and slope gradient for each Geo-cell. Then slope stability safety factor for each Geo-cell is calculated. Output File is provided included all the input information for each Geo-cell in addition to stability number (N1) and the slope stability factor of safety (FS). Thematic map of the results is also provided as it is shown below.

OutputDataTable Browser

GRID	RawID	ColID	Xc	Yc	PGA	PHI	SLOPE	N	SF
B5	B	5	29.76626600	40.71699700	0.000	35.000	72.255	2.900	2.031
B6	B	6	29.76628200	40.71249500	0.000	35.000	80.910	2.900	2.031
C5	C	5	29.77218400	40.71700900	0.249	30.000	62.526	2.295	1.325
C6	C	6	29.77219900	40.71250700	0.000	35.000	60.751	3.177	2.225
D4	D	4	29.77808600	40.72152300	0.240	25.000	48.013	2.700	1.259
D5	D	5	29.77810100	40.71702100	0.280	30.000	51.340	2.457	1.418
D6	D	6	29.77811600	40.71251800	0.393	30.000	42.274	2.225	1.285
D7	D	7	29.77813100	40.70801600	0.000	35.000	59.886	3.208	2.246
E4	E	4	29.78400400	40.72153400	0.307	25.000	9.462	0.000	3.500
E5	E	5	29.78401800	40.71703200	0.324	30.000	59.036	2.154	1.243
E6	E	6	29.78403300	40.71252900	0.314	30.000	57.381	2.217	1.280
E7	E	7	29.78404700	40.70802700	0.000	30.000	33.341	5.233	3.021
F4	F	4	29.78992100	40.72154500	0.214	30.000	41.257	3.031	1.750
F5	F	5	29.78993500	40.71704300	0.183	0.000	18.667	4.359	1.168
F6	F	6	29.78995000	40.71254000	0.263	30.000	11.310	3.793	2.190
F7	F	7	29.78996400	40.70803800	0.447	30.000	46.169	1.983	1.145
F8	F	8	29.78997800	40.70353600	0.000	0.000	31.686	5.365	1.438
G3	G	3	29.79582500	40.72605800	0.329	20.000	58.201	2.153	0.784
G4	G	4	29.79583900	40.72155600	0.333	30.000	55.008	2.199	1.270
G5	G	5	29.79585300	40.71705300	0.256	30.000	45.000	2.724	1.573
G6	G	6	29.79586600	40.71255100	0.343	30.000	37.999	2.523	1.456
G7	G	7	29.79588000	40.70804900	0.000	30.000	48.013	4.059	2.343

Output Data of KoeriSlope Application

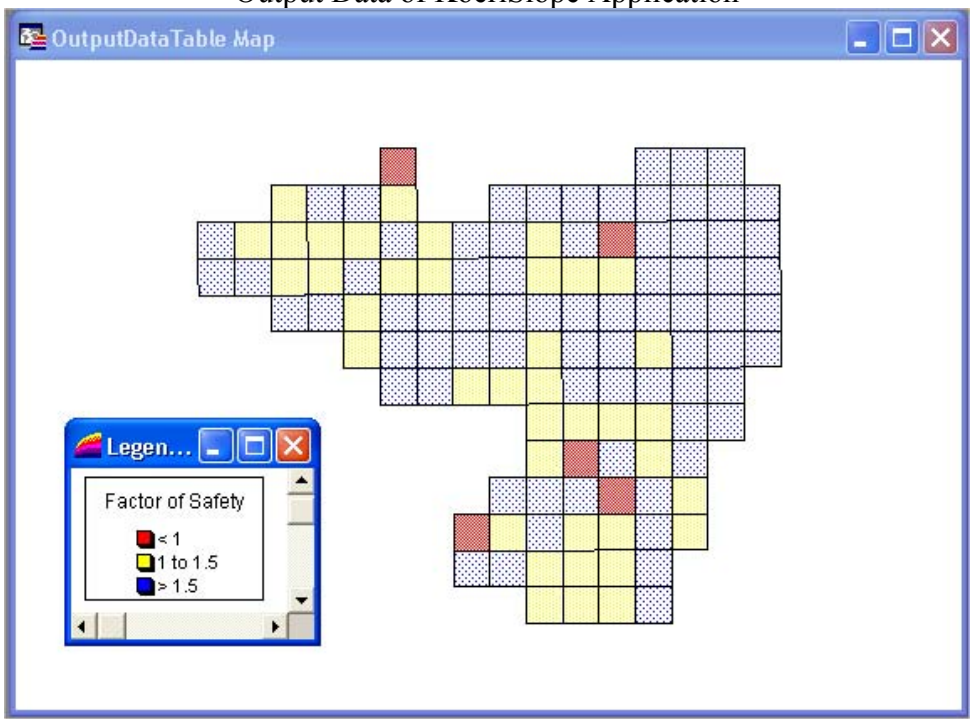

Slope Stability Factor of Safety (FS) Thematic Map

4. CHAPTER 9 -VULNERABILITY CURVES OF TYPICAL RC BUILDINGS

Pierriono Lestuzzi, Structural engineering Institute of the Swiss Federal Institute of Technology, Loussane,

4.1. INTRODUCTION

The present contribution focuses on the vulnerability curve concept, which is a very efficient tool for the prediction of structural damage affecting buildings hit by an earthquake. In contrast to Chapter 9, which deals with post event assessment, the subject discussed here is intended for the preventive assessment of structures. It is of interest to check if the predictions drawn from that procedure actually match the observations made in Adapazari after the earthquake struck on August 17, 1999.

Based on the blueprints of ten typical reinforced concrete buildings, three structural types are defined. The influence of the number of stories and the material strengths are also considered when computing the vulnerability curves.

4.2. DEFINITION OF THE TYPICAL RC STRUCTURES

Prof. Elmas at the Sakarya University selected ten RC buildings representative of the structural systems commonly used in Adapazari. For the sake of simplification and in order to assure that the results be usable in other places in Turkey, three typical structural systems were defined based on the ten RC buildings. But before focusing on those types, it is worthwhile to point out general features regarding the structures encountered in Adapazari:

- A great deal of buildings is made of RC frames
- Those frames are similar in both x and y directions
- The slabs always have a depth of 12 cm with 20 cm x 60 cm underbeams but only along the columns (walls) axis.
- The buildings are typically five stories high, with a constant story height of 2.80 m
- Due to trade activities, the story height may reach 4.00 m on the ground floor
- Masonry infills are very widespread in the upper stories but are lacking in the ground story, favouring thus soft story mechanisms
- Irregularities in the plan view are common
- Based on the main features of the ten RC buildings, the three types of typical RC buildings are the following:
- Type 1: RC frames with classical columns (representing four buildings)
- Type 2: RC frames with small walls (representing two buildings)
- Type 3: RC frames with both columns and walls (representing three buildings)

The subsequent material properties were used:

		Lower bound	*Upper boun*d
Cylinder compressive strength of concrete:	f'_c =	15 MPa	20 MPa
Tensile strength of concrete:	f_{ct} =	4 MPa	4 MPa
Yield strength of steel:	f_y =	235 MPa	500 MPa
Ultimate strength of steel:	f_k =	360 MPa	500 MPa

The geometry and reinforcement properties are given here below.

4.2.1 Columns alone, type 1

This case represents classical RC frames.

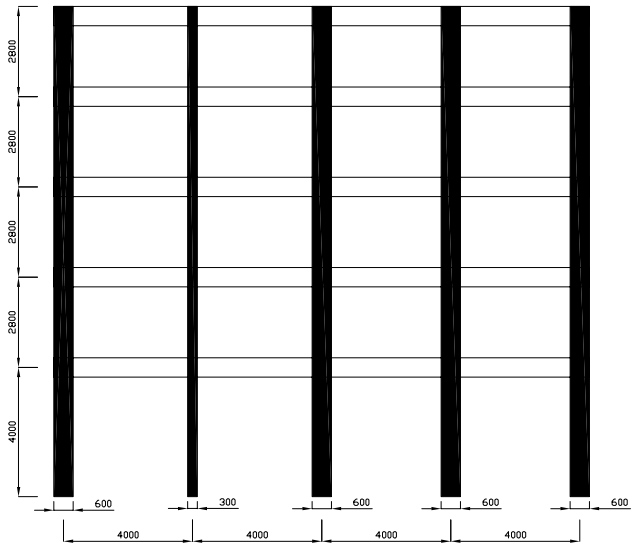

Cross sections of the columns:

0.6 m x 0.4 m and
0.3 m x 0.7 m

Reinforcement:

4∅16 on both long sides

Figure 4.1. Sketch of structural type 1 - dimensions in [mm]

Note that second column is purposefully oriented along its weak axis, modelling thus at best the real structures.

4.2.2 Small walls, type 2

In opposition to the first type, the vertical elements can now be considered as walls even if their length does not exceed 1.0 m. This choice was made based upon reinforcement detailing that clearly showed higher reinforcement ratios at the ends of the elements.

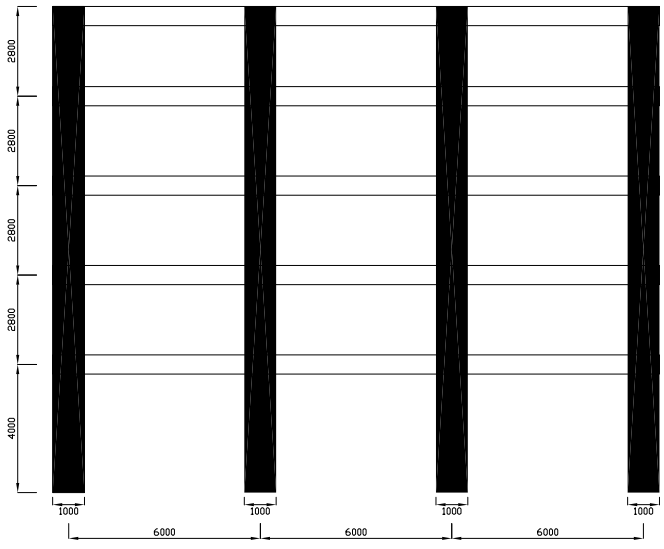

Cross sections of the walls:

1.0 m x 0.25 m

Reinforcement:

1 % - 2 % for the whole section with

3 % - 4 % in the edges

0.4 % - 1.3 % in the web

Figure 4.2. Sketch of structural type 2 - dimensions in [mm]

4.2.3 Columns and small walls, type 3

This case actually combines columns and small walls in order to create a frame.

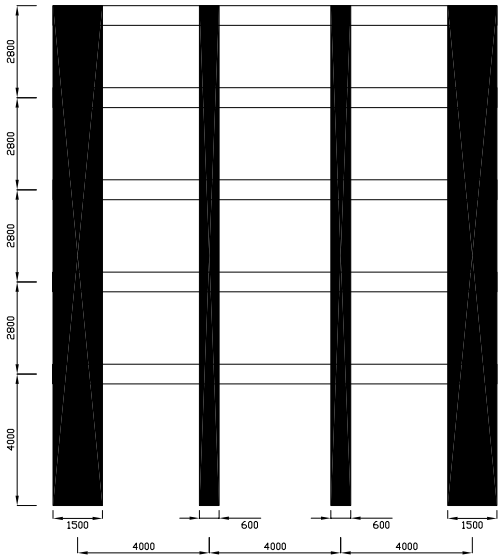

Cross sections of the columns:

0.6 m x 0.4 m

Cross sections of the walls:

1.5 m x 0.2 m

Reinforcement:

0.95 % for the wall section with

3.8 % in the edges

0.5 % in the web

3∅22 on both sides of the columns

Figure 4.3. Sketch of structural type 3 - dimensions in [mm]

It is interesting to notice that none of the above-defined types relates to structural systems that are based on shear walls alone. This is a characteristic that applies to the whole country. In fact, only a single building among the ten selected ones features a 3.8 m long shear wall. It was decided not to consider such a type of structure, as it is not very representative.

4.2.4 Column and wall indexes

The column and wall indexes of the typical buildings described above have been computed by means of simplified formulas derived from [GS 99]. The column and wall index varies between 0.009 and 0.024, while the partition wall index features values between 0.002 and 0.006. Those values are rather high compared to the results obtained for the 301 buildings investigated in Chapter 9: *Collapse damage survey in Adapazari* section. This is not very surprising since the latter sample focuses exclusively on buildings that actually collapsed.

4.3. METHODOLOGY

Vulnerability curves are being used to predict the damage a given structure will undergo. The underlying methodology is thoroughly described in [Lang 02]. The major ideas are recalled here, though.

In general, a vulnerability function is a relationship which defines the expected damage for a building or a class of buildings as a function of the ground motion.

In the present study and because of a lack of information regarding the ground motion, it was chosen to use a plot of the displacement at the top floor Δ_{top} of the examined building (defined by its fundamental frequency), versus the spectral displacement S_d. This curve is solely dependent on the buildings characteristics and can thus easily be plotted with the help of the relation that exists, for the first mode of vibration of a building, between a multiple degree of freedom system and its corresponding equivalent single degree of freedom system. The graphic and algebraic version of the curve are shown in Figure 3.5.

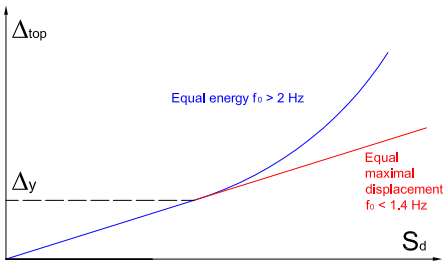

$$\Delta_{top} = \frac{\mu_\Delta}{R} \cdot \Gamma \cdot S_d(f_1)$$

Top displacement – spectral displacement relationship

Figure 4.4. Top displacement – spectral displacement relationship

Note that for a given ground motion, the curve begins at ($S_d(f_0)$; Δ_y) which corresponds to the elastic state. In the current discussion however, the intensity of the earthquake is not set, it varies as one moves along the x axis.

The damage information is then added on this Δ_{top} - S_d curve by the means of dots which show when a given damage grade is reached, see Figure 3.6. The latter are defined in a way that the degradation of the structure (cracking, creation of plastic hinges), under increased loading, is well caught.

A pushover analysis yields the necessary values of the displacement on the top floor for which a specific event occurs. The nonlinear behavior under lateral loading is thus pointed out.

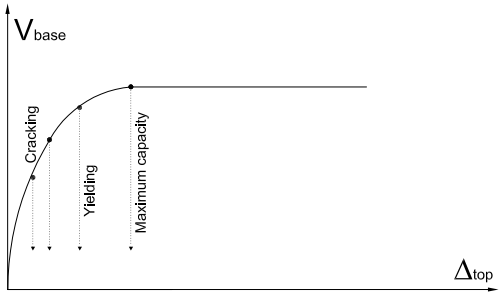

Figure 4.5. Catching the static nonlinear behavior by means of a pushover analysis

Figure 3.7 shows the "vulnerability" curve that is obtained by combining the two previous figures.

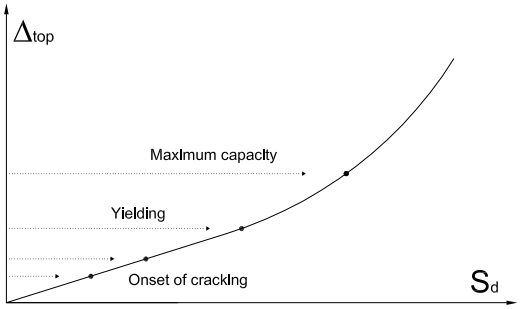

Figure 4.6. Vulnerability curve

For a given building, and without further information regarding the ground motion, the seismic demand can yet be varied: assuming a design spectrum, one only has to change the PGA used to construct the spectrum to get various values of S_d.

4.4. COMPUTATION OF THE VULNERABILITY CURVES

4.4.1 Hypotheses

All geometric and material features are based, in a simplified way, on the blueprints of the ten buildings. The simplification both facilitates the computation and assures that the obtained vulnerability curves can easily be used to analyze other buildings.

Due to the irregularities in the plan layout, it is sensible to limit the computations to a single frame, instead of the whole building, for each structure. That way, complex torsion computations can be avoided.

On top of gravity loads, 30% of the total dead load, set as 12 KPa, was taken into account to compute the masses and axial forces acting upon the vertical elements.

The masonry infills were neglected in the model because they are either isolated from the structure by joints or are subjected to very heavy damage during the strong motion phase.

The damage grades are defined as follows:

- Damage grade 1 (DG1): onset of concrete cracking
- Damage grade 2 (DG2): yielding of the first vertical element
- Damage grade 3 (DG3): all vertical elements on the ground floor have developed a plastic hinge at their base
- Damage grade 4 (DG4): point after which the stiffness tends to zero
- Damage grade 5 (DG5): the top story drift reaches 3 %

4.4.2 Method

As mentioned in the methodology, the vulnerability curve of a given building is obtained by plotting the seismic demand and the capacity of the building to withstand lateral loading in the same graph.

The capacity of the building to withstand lateral loading is usually described by means of a bilinear approximation in the base shear – top displacement (Δ_{top}) plane. Such a curve can be obtained with any program that performs nonlinear static analyses. IDARC 4.0 [Valles et al.] was used here. Once the structure is modelled, one only has to choose the shape of the lateral force distribution (usually triangular). The outputs include the base shear – top displacement curve, but also the loading steps for which a given element cracks or yields. This is indeed very useful to define the damage grades.

The bilinear approximation is mainly constructed to compute the fundamental frequency of the multistory building, which corresponds of course to the frequency of the equivalent single degree of freedom system. The capacity reached after the stiffness drops dramatically, defines the plateau value $V_{b\ max}$. The slope of the linear part is given by the point DG2, where the first vertical element yields.

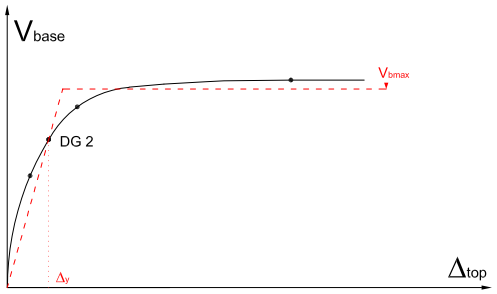

Figure 4.7. Bilinear approximation of the static nonlinear behavior

Now, the relation between the displacement on the top floor (Δ_{top}) of a multistory building and the spectral displacement (S_d) of the equivalent single degree of freedom system representing the first mode of vibration, is driven by the modal participation factor Γ and the kind of R – μ_Δ rule used to model the nonlinear behavior as shown in Figure 3.9.

In the current case, the equal maximum displacement rule was applied for frequencies up to 1.4 Hz. Beyond 2 Hz; the principle of equal energy was applied. Note that the definition of these limits is yet to be subject of the discussion among specialists.

Between those two boundaries, an interpolation was used.

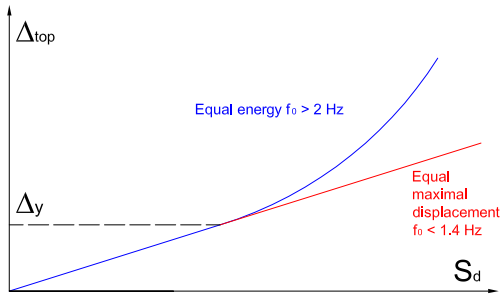

Figure 4.8. Top displacement – spectral displacement relationship

4.5. RESULTS

4.5.1 Computed cases

A total amount of 16 structures were modeled and their vulnerability curves computed.

	3 storeys	5 storeys	7 storeys
Type 1	1a3 – 1b3	1a5 – 1b5	1a7 – 1b7
Type 2	2a3 – 2b3	2a5 – 2b5 / 2ah5 – 2bh5	2a7 – 2b7
Type 3	3a2 – 3a4		

The letter *a* respectively *b* stands for an optimistic respectively pessimistic hypothesis regarding the material's strength. The letter *h* means that the reinforcement ratio is especially high. For type 3, the last figure gives the number of columns that are added to the two walls.

4.5.2 Results

Due to a lack of information regarding the ground motion intensity of the earthquakes, only limited conclusions can be drawn so far. It is, however, possible for a preliminary investigation to predict the damage each structure will suffer. The seismic demand was based on the Turkish code [EDP 97]. The design spectra are given in Figure 3.10 for a PGA of 4 m/s^2.

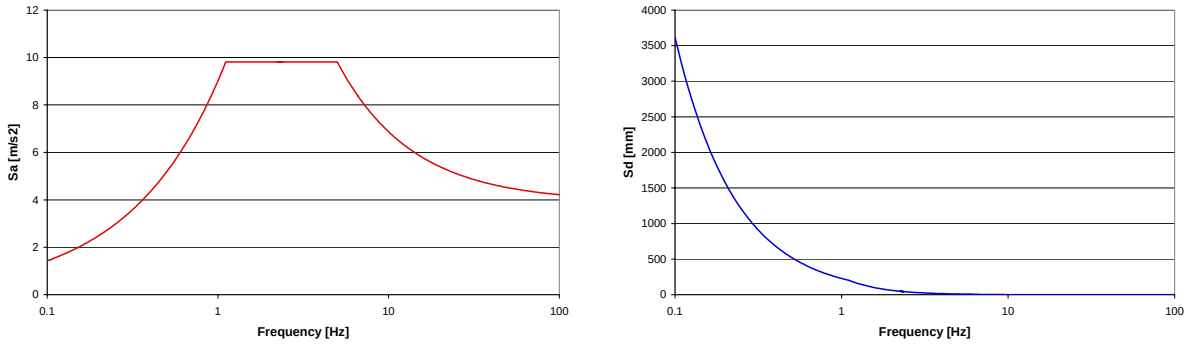

Figure 4.9. Acceleration (left) and displacement (right) spectra based on the Turkish code

Figure 3.11 shows, for a specific case, how the damage evolves from damage grade 1 to damage grade 5. The shaded regions represent cracks while the black circles emphasize the plastic hinges.

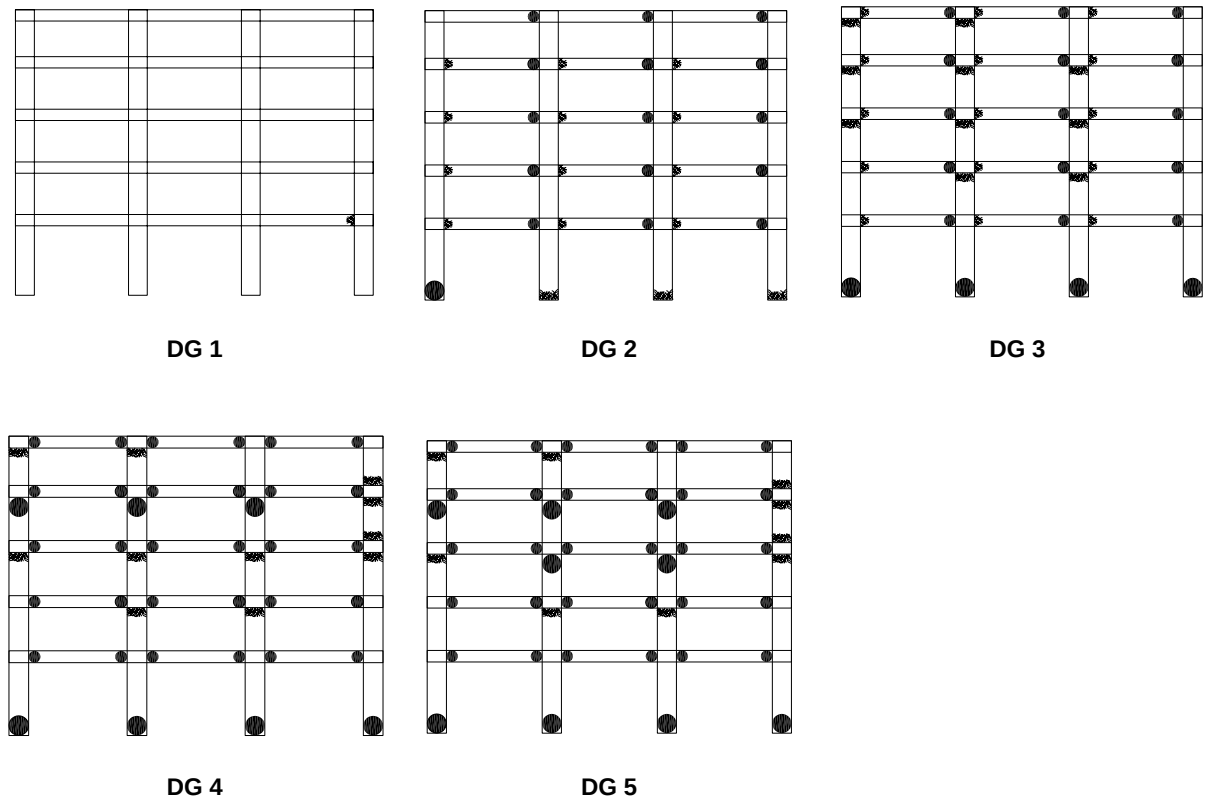

Figure 4.10. The five damage grades

Each computed structure is described by its capacity and spectral displacement versus normalized (by the building height) top displacement curves. The latter are shown hereafter in Figures 13.12 to 13.17. The squares represent the various damage grades, while the crosses show the stage reached for the following PGA values: 2 m/s^2, 4 m/s^2 and 6 m/s^2.

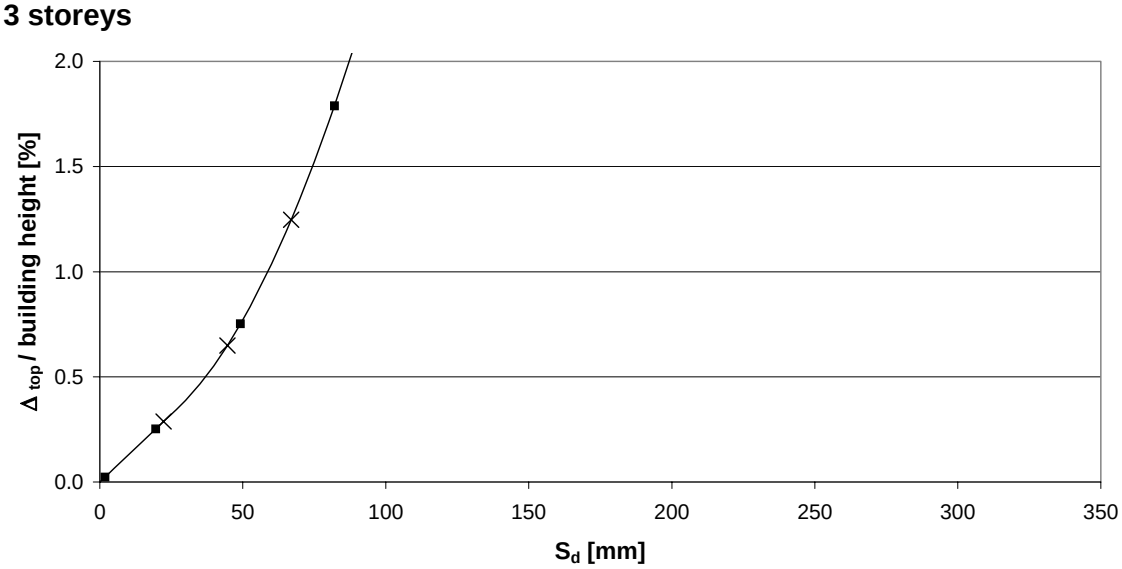

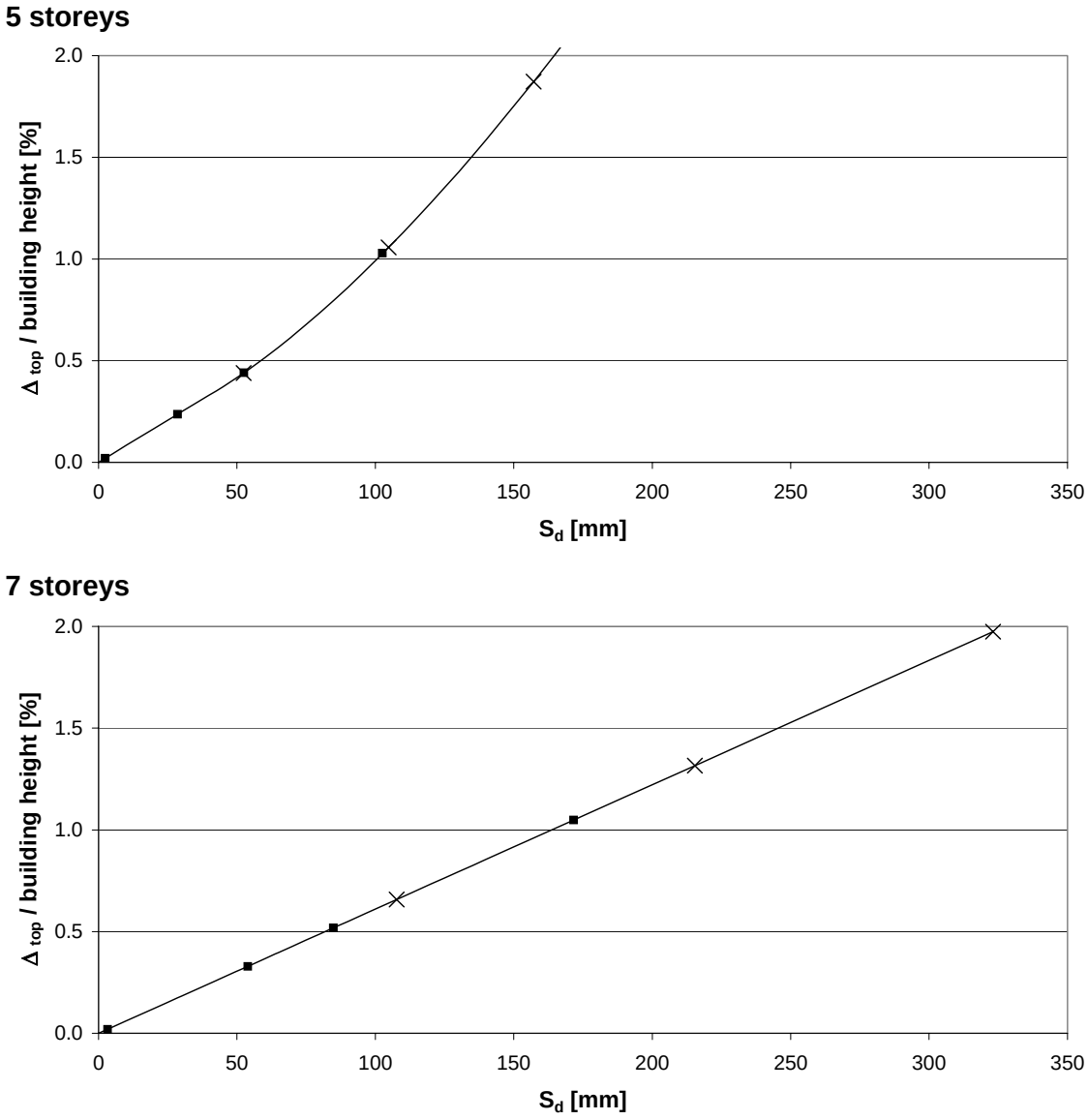

Figure 4.11. Spectral displacement versus normalized top displacement curves for classical RC frame buildings – high material strengths

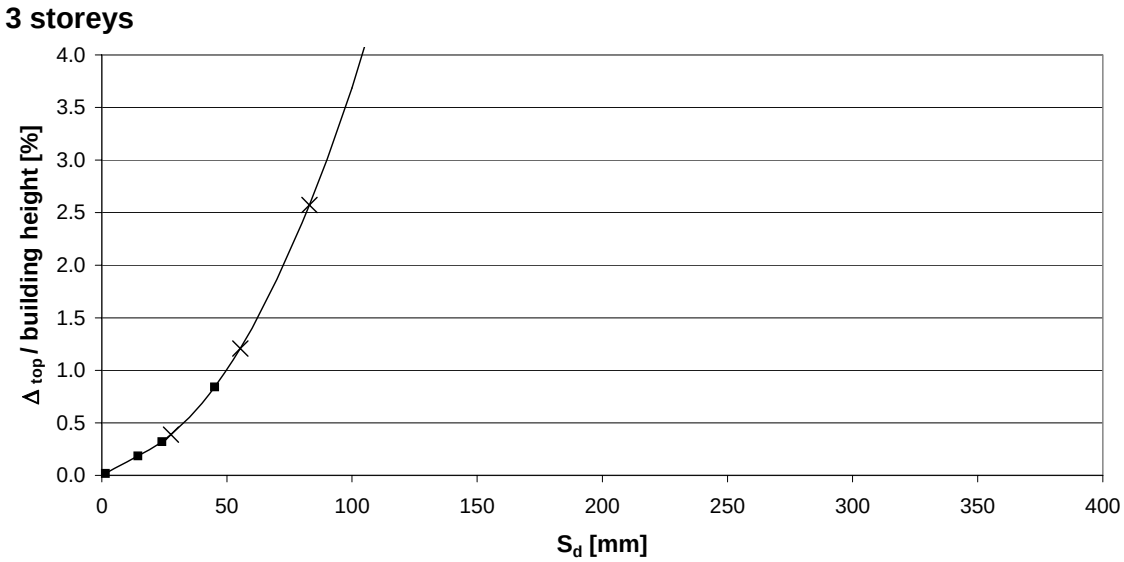

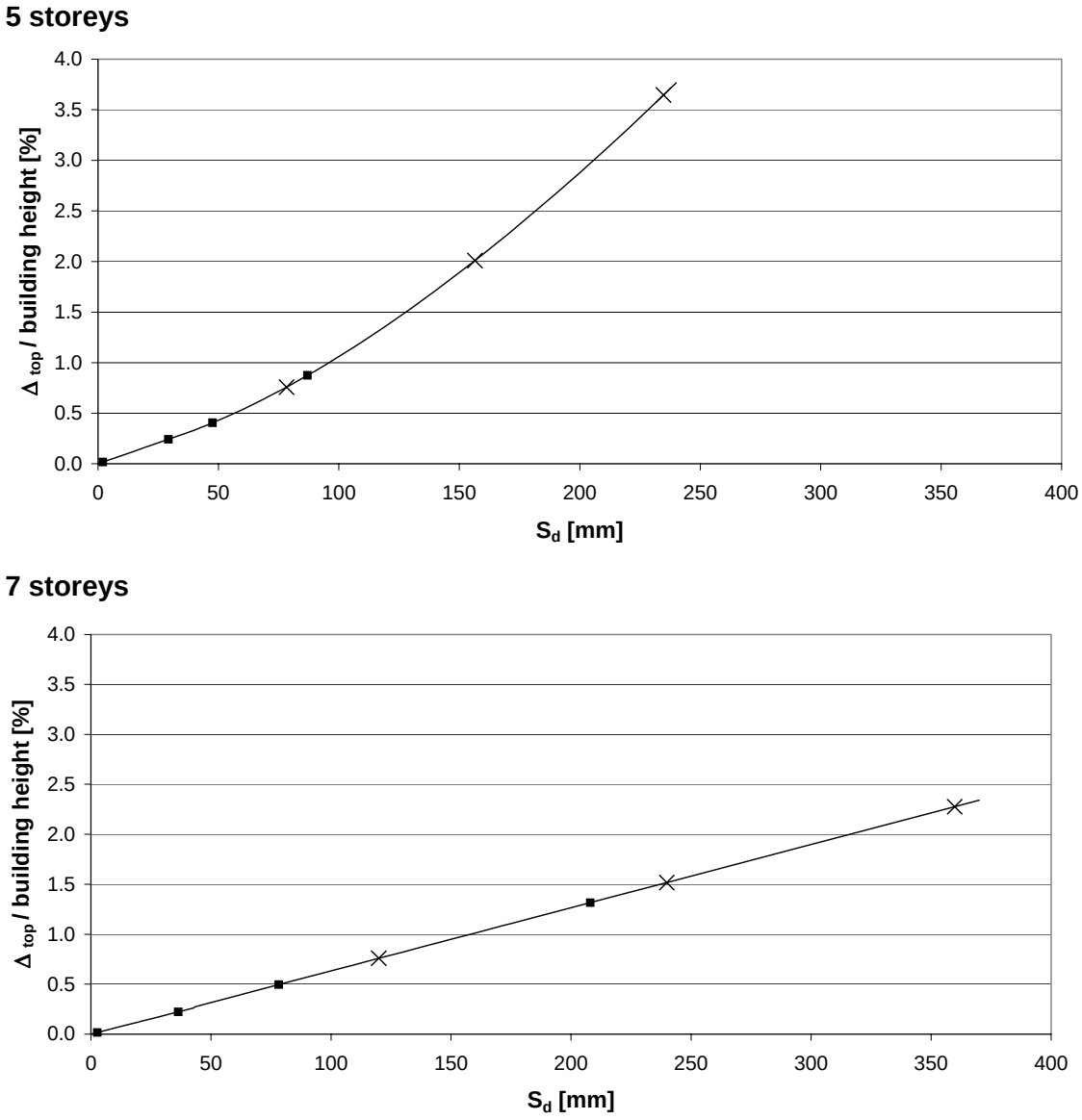

Figure 4.12. Spectral displacement versus normalized top displacement curves for classical RC frame buildings – low material strengths

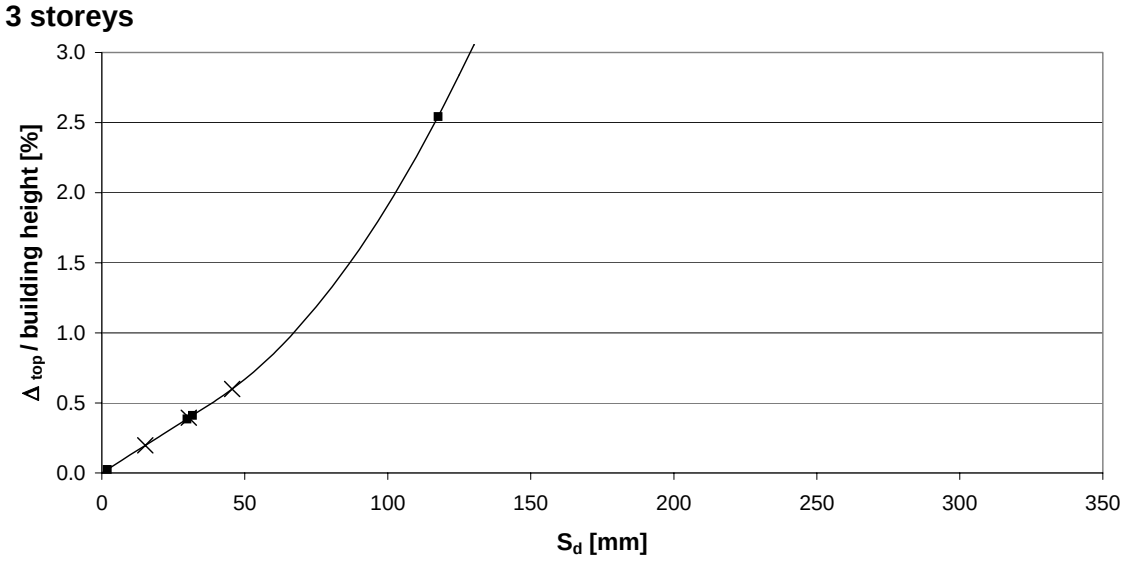

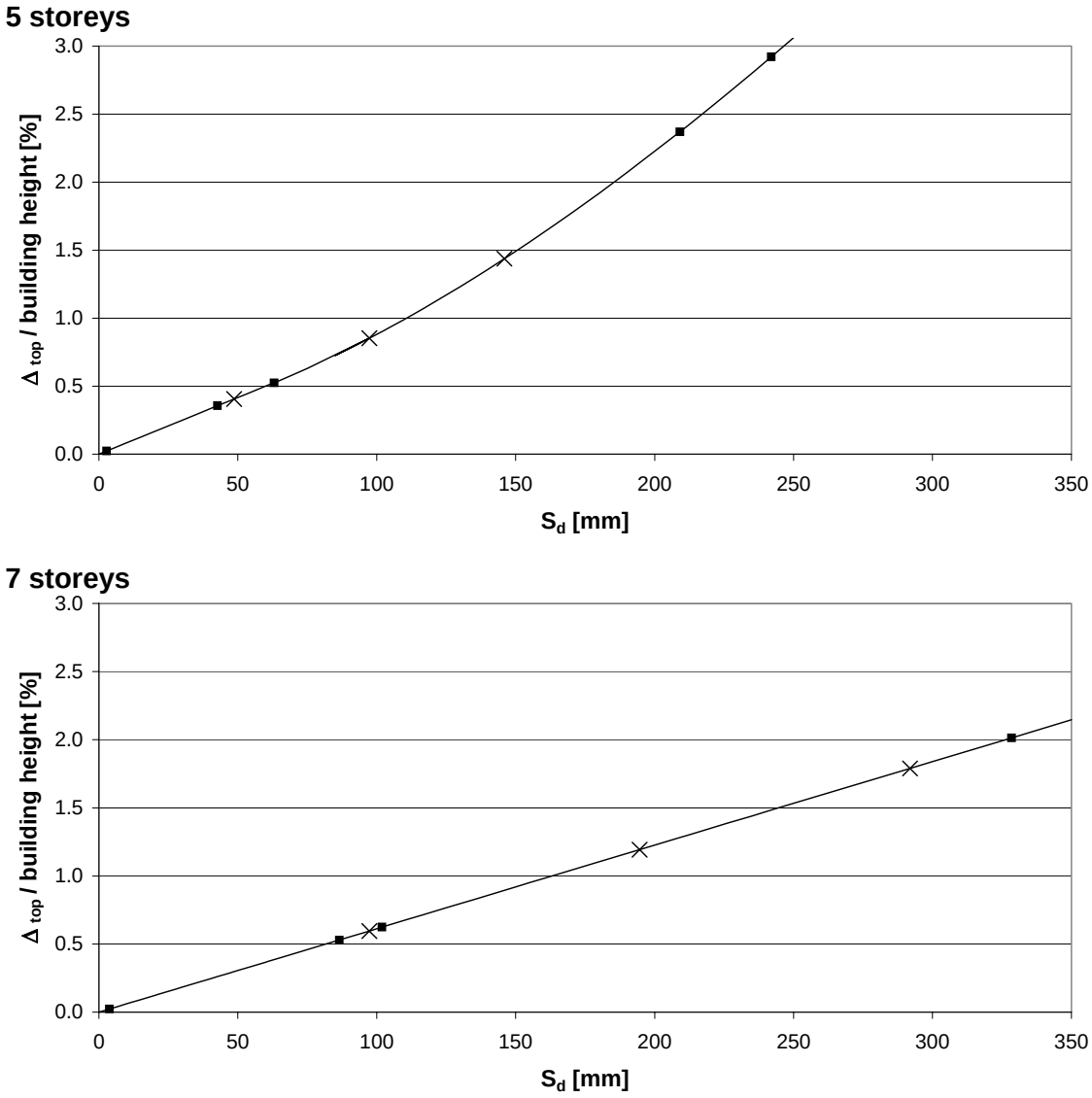

Figure 4.13. Spectral displacement versus normalized top displacement curves for RC frame buildings with small walls – high material strengths

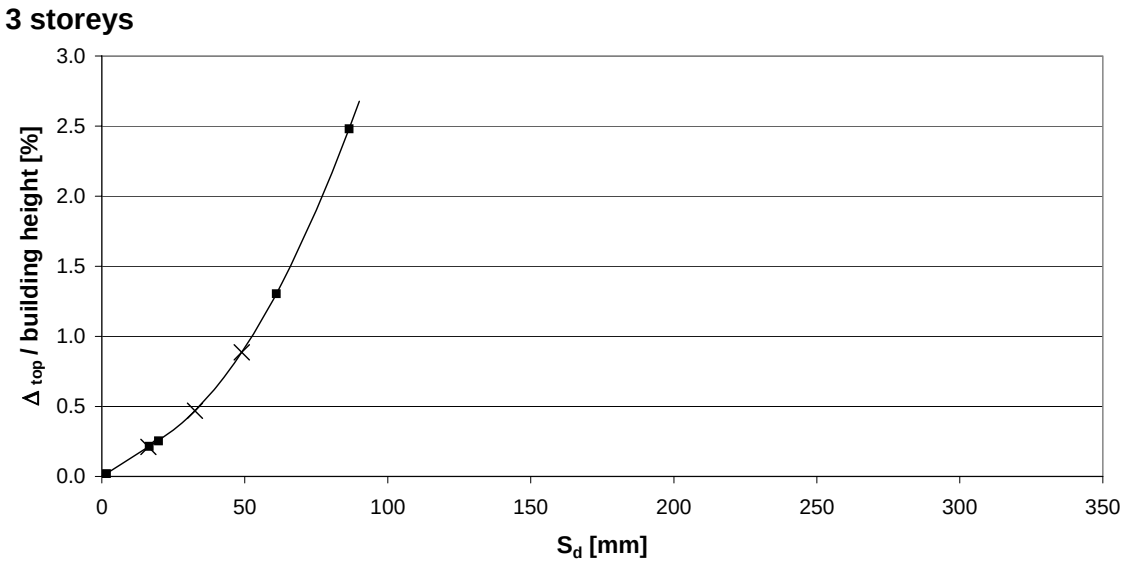

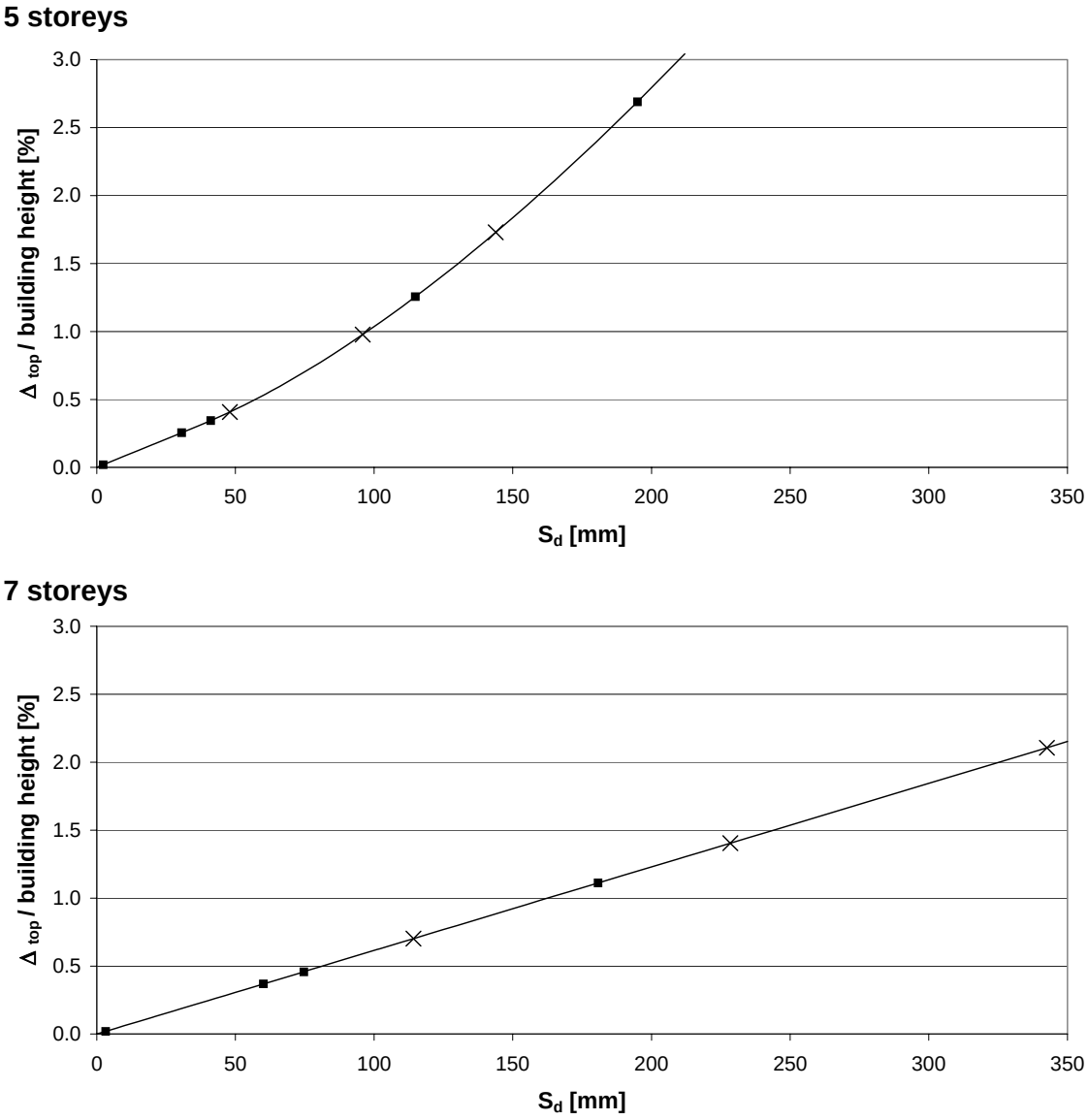

Figure 4.14. Spectral displacement versus normalized top displacement curves for RC frame buildings with small walls – low material strengths

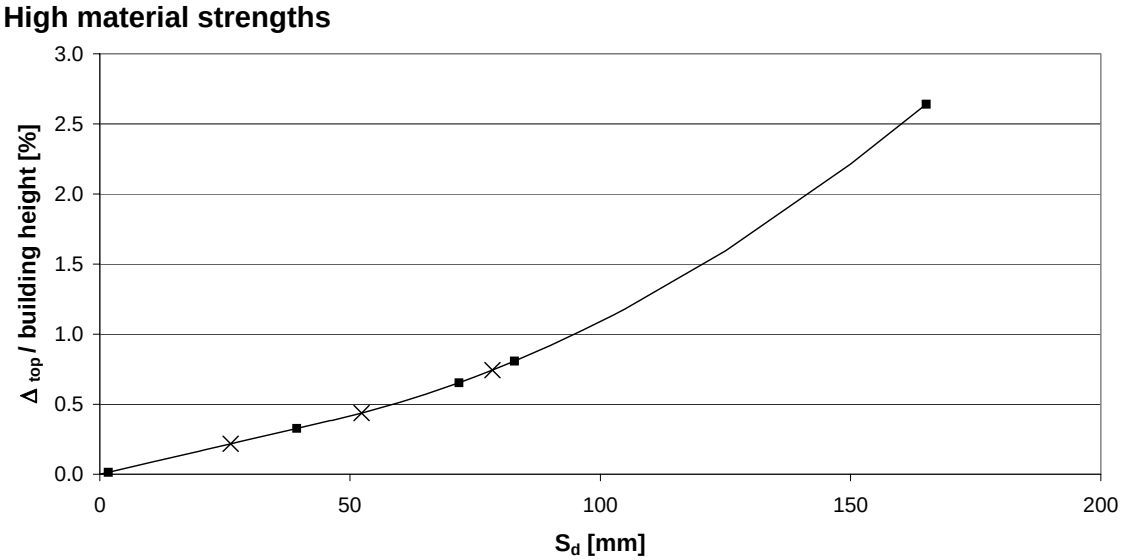

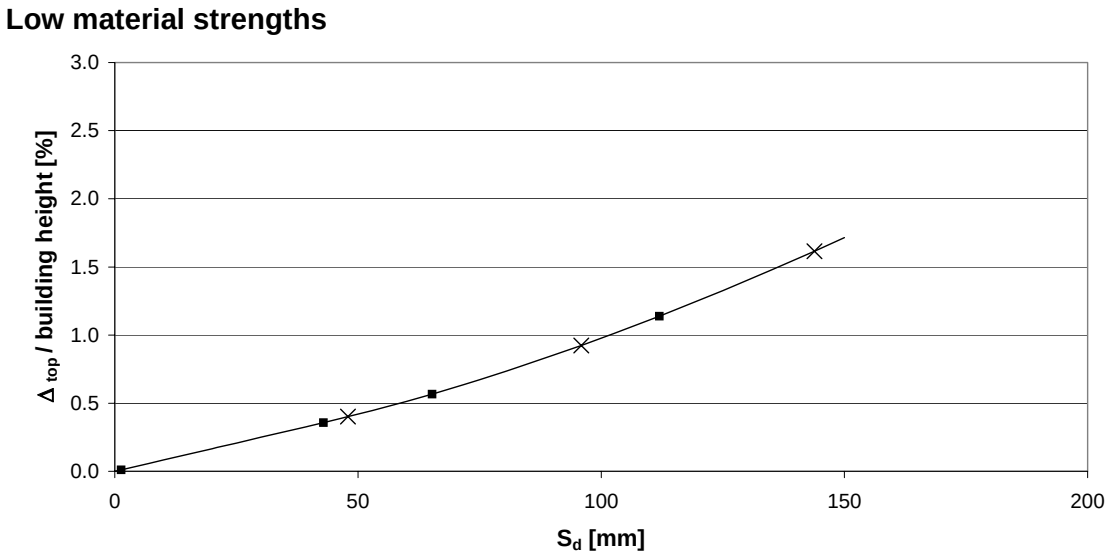

Figure 4.15. Spectral displacement versus normalized top displacement curves for a 5 storey RC frame building with small walls – especially high reinforcement ratio

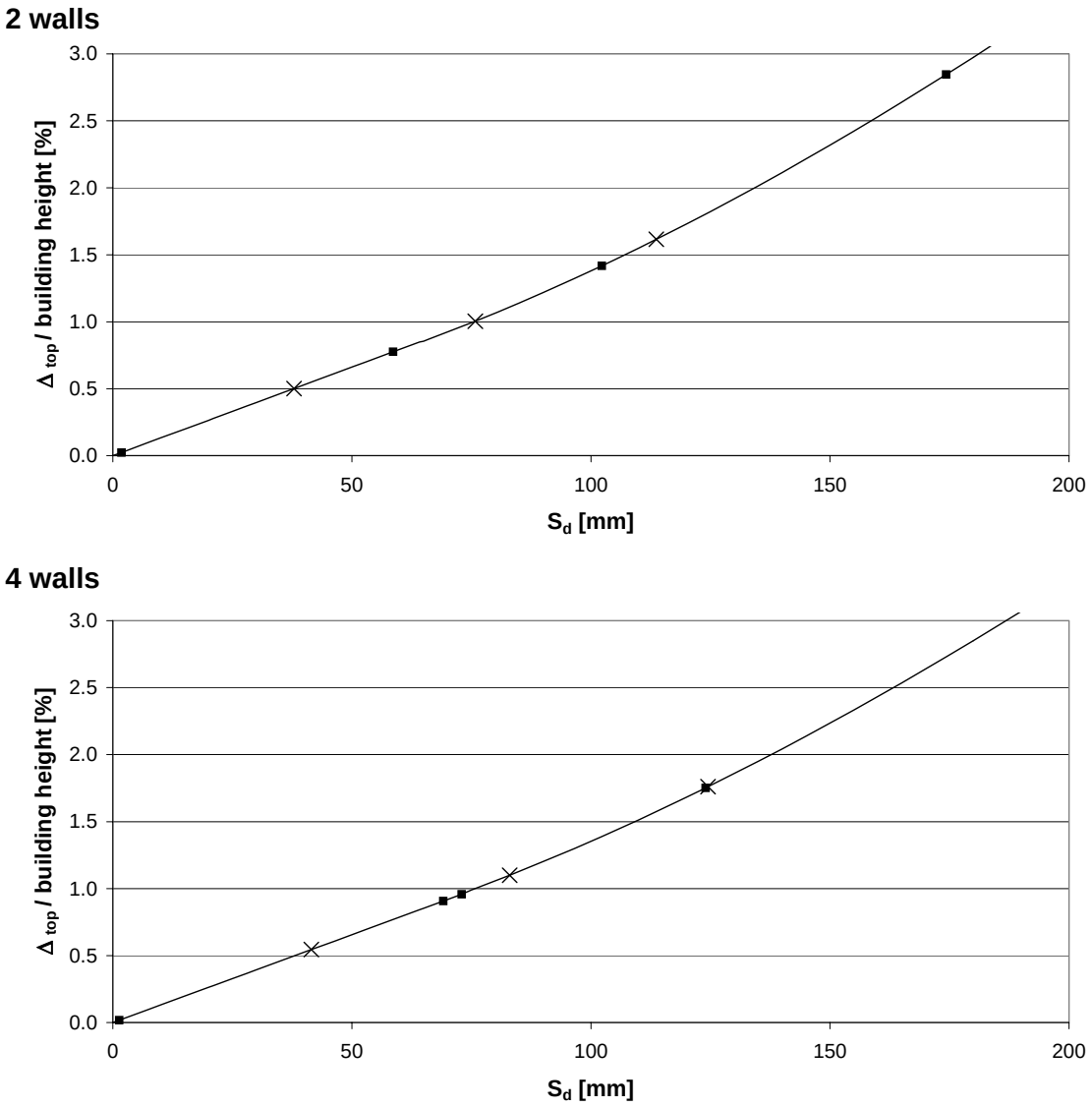

Figure 4.16. Spectral displacement versus normalized top displacement curves for a 3 storey RC frame building with both columns and walls

By considering the Turkish code for the seismic demand and PGA values of 2 m/s^2, 4 m/s^2 and 6 m/s^2, the following damage grade is reached for the investigated buildings:

Damage grades		**PGA [m/s^2]**		
Structure	f_0 [Hz]	**2**	**4**	**6**
1a3	2.36	2	2	3
1a5	1.54	3	4	4
1a7	1.05	3	4	4
1b3	2.12	3	4	4
1b5	1.26	3	4	4
1b7	0.96	3	4	4
2a3	2.86	1	2	3
2a5	1.77	2	3	3
2a7	1.13	2	3	3
2b3	2.76	1	3	3
2b5	1.61	3	3	4
2b7	1.0	3	4	4
2ah5	2.18	1	2	3
2bh5	1.61	2	3	4
3a2	1.81	1	2	3
3a4	1.73	1	3	4

4.5.3 Discussion

The current investigation clearly shows that

- as expected, compared to columns (type 1), small walls (type 2) delay the degradation.
- the use of good material featuring high values of f'_c and f_y, enables the wall to withstand a given earthquake with less damage.

Stocky structures are less exposed to heavy damage than 7 storey buildings.

4.6. OUTLOOK

The next step would be the transformation of the x axis of the vulnerability curve from the spectral displacement into the intensity. Such a graph would then enable damage predictions, for a given building, as a function of the seismic demand to be made.

4.7. BIBLIOGRAPHY

[EDP 97] Ministry of Public Works and Settlement Government of Republic of Turkey: “Specifications for Structures to be built in Disaster Areas, part III - Earthquake Disaster Prevention”. Official Gazette No.23390.

[GS 99] Gülkan P., Sozen M. A.: “Procedure for Determining Seismic Vulnerability of Building Structures”. ACI Structural Journal, 96, 3 May, 1999, pp.336-342.

[Lang 02] Lang K.: ”Seismic vulnerability of existing buildings”. Institut für Baustatik und Konstruktion, ETH Zürich, Dissertation No. 14446, 2002.

[Valles et al.] Valles R. E. et al.: “IDARC 2D Version 4.0: A Program for Inelastic Damage Analysis of Buildings”. Technical Report NCEER-96-0010. State University of New York at Buffalo, NY. January 1996.

5. CHAPTER 9

5.1. STRUCTURAL DAMAGE DATA FORM FOR BUILDINGS IN ADAPAZARI

MICROZONATION FOR EARTHQUAKE MITIGATION
DAMAGE SURVEY FOR THE HOUSING STOCK IN ADAPAZARI

1. GENERAL INFORMATION

Building Ref. No.	:		**Date Examined**	: / /	**2002**
Building Address	:				
Date of Construction	:	/ /	**Date of Design**	: / /	
Building GPS Coord.	:				
Survey Team	:				

View 1 **View 2**

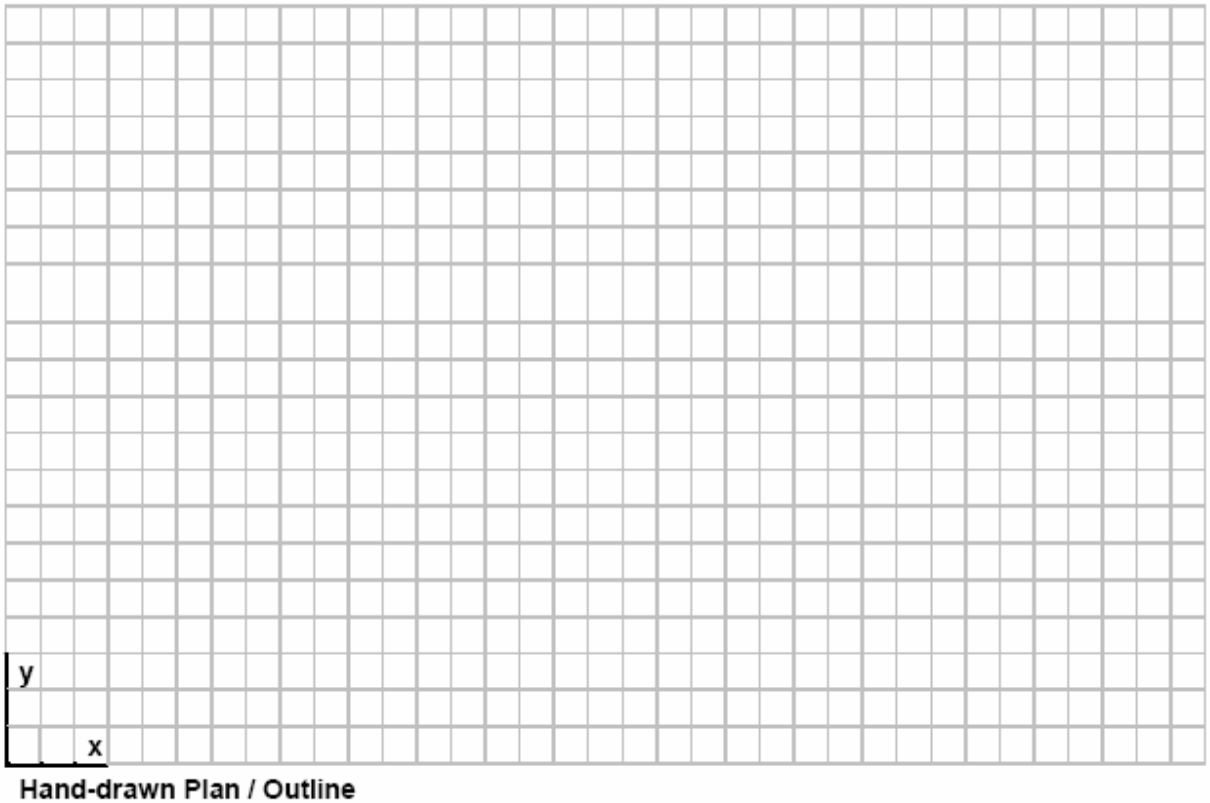

Hand-drawn Plan / Outline

2. BUILDING INFORMATION

Stories	Times Repeated	Story Height (m)	Story Area (m^2)	Annotation
Basement				
Ground Fl.				
Mezzanine				
Regular Story				
Penthouse				

Have additional stories been built due to building regulation revisions?	Yes		No	

Situation:	Detached		Row, end building		Row, middle building	
	Is building on inclined terrain?	Yes			No	

Irregularities					
				Yes	No
In plan					
In elevation					
A1 :	Torsional irregularity				
A2 :	Oversize openings in floor slab				
A3 :	Extreme projections in plan				
A4 :	Non-parallel framing				
B1 :	Weak story existence				
B2 :	Soft story existence				
B3 :	Discontinuities of vertical load carrying members				
Number of continous frames in two orthogonal axes?		X-dir.		Y-dir.	

Joints with adjoining buildings:	Yes		No		Uncertain	

Floor elevation comparison with adjoining buildings:	Same		Different	

3. LOAD CARRYING SYSTEM CHARACTERISTICS

Type :	Reinforced concrete	
	Reinforced concrete + structural shear wall	

Partititon wall types:	Clay tile with cavities	
	Solid clay bricks	
	Concrete masonry units	
	Terra cotta	
	Autoclaved concrete or panel	
	Other (give details) :	

Basement peripheral wall materials:	Stone masonry (cut or natural)	
	Reinforced concrete	
	Solid masonry units or terra cotta	
	Concrete masonry units	
	Other (give details) :	

Floor slab system:	Slab supported by beams	
	Joist floor with concrete block infill	
	Joist floor with no infill	
	Flat plate	
	Other (give details) :	

Materials Test Results				
No.	Impact Hammer Test		Ultrasonic Test	
	Member	Hammer Count	Member	Sound Velocity (m/s)

Design compressive strength, f_{ck} :	MPa	Tested by :	
Design modulus of elasticity, E_c :	GPa	Date :	

Steel type as built : *	S220 (Stl)		S420 (St III)		S500 (St IV)		
Reinforcement type as built: *	Plain		Deformed				

* In case this can be established at the time of inspection.

Statistical Indices for the Load Carrying System		
(1) Footprint area at ground level	:	m^2
(2) Total floor area (Excluding basements)	:	m^2
(3) Total cross section area of columns at ground floor in x-direction	:	m^2
(4) Total moment of inertia of columns at ground floor in x-direction	:	m^4
(5) Total cross section area of columns at ground floor in y-direction	:	m^2
(6) Total moment of inertia of columns at ground floor in y-direction	:	m^4
(7) Total cross section area of shear walls at ground floor in x-direction	:	m^2
(8) Total moment of inertia of shear walls at ground floor in x-direction	:	m^4
(9) Total cross section area of shear walls at ground floor in y-direction	:	m^2
(10) Total moment of inertia of shear walls at ground floor in y-direction	:	m^4
(11) Total cross section area of filler walls at ground floor in x-direction	:	m^2
(13) Total cross section area of filler walls at ground floor in y-direction	:	m^2

Lower and upper limits of the slenderness ratios in bending about x-axis of columns at ground floor	$\leq H/d_x \leq$	Avg. :
Lower and upper limits of the slenderness ratios in bending about y-axis of columns at ground floor	$\leq H/d_y \leq$	Avg. :

4. OVERALL RATING OF STRUCTURE

Evaluation Criteria		Notes and Clarifications	Points 0=inferior 5=good
Overall quality of as built structures			
Material quality	Concrete		
	Reinforcement		
	Filler walls		
Systemic defects	Short columns		
	Soft story		
	Weak story		
Do vertical mismatches exist at girder/column joints?			
Do a minimum of two spans exist in each direction?			
Is there a high probability of hammering adjacent buildings?			
Are story plans very disparate?			
Do filler wall discontinuities exist ?			
Does corrosive effects in reinforcement exist?			
Do discontinuities exist in the vertical load carrying system?			
Is the lateral force resisting system adequate?			

5.2. DAMAGE ASSESSMENT FORM

MINISTRY OF PUBLIC WORKS AND SETTLEMENT

GENERAL DIRECTORATE OF DISASTER AFFAIRS

DAMAGE ASSESSMENT FORM FOR ENGINEERED BUILDINGS

1. ADMINISTRATIVE INFORMATION

Province :
Subdistrict :
Village/neighborhood:
Street :
No. :

Team Members ..... Signature .....
....
....

Date prepared :
Photo available? :
Disaster type :
Date of occurrence :
Life loss (if known) :

Type of Occupancy :
☐ Residential ☐ Business ☐ Institutional (Purpose .....)
☐ Industrial ☐ Hotel, restaurant ☐ Hospital, health facility ☐ Other (give details)

Number of independent units in building ☐

Independent Unit No.	Legal Owner Surname, name	Used by Surname, name
1.		
2.		
3.		
4.		

.
.
.
(Add as needed)

Date of design :
Date constructed :
Architectural design : ☐Yes ☐No
Structural design : ☐Yes ☐No

2. GENERAL INFORMATION

*Note: In Parts 2 and 3 a **damage exacerbating factor** is entered next to some of the boxes. The sum of these factors is utilized in Part 5.*

Plan Geometry:
☐Rectangular ☐T-shaped
☐L-shaped ☐U-shaped ☐Other

Scheme:
Plan (Approx. Dim.)

Direction of Building x-axis (show on scheme):
☐N-S ☐E-W
☐N45E ☐N45W

Elevation (Approx. Dim.)

Number of stories: ..... Basement + ... Stories =
Mezzanine : ☐Yes (**0.25**) ☐No
Penthouse : ☐Yes (**0.25**) ☐No
(See Fig. 1)

Story height:
Basement : ..... m
Ground : ..... m
Regular stroy : ..... m

Plan Irregularity: ☐Yes(**0.5**) ☐No
(See Fig. 3)

Section Irregularity: ☐Yes(**0.5**) ☐No

Building Situation : (**0.25**)
☐Detached ☐Edge (**0.25**) ☐Central
(See Fig. 4)

Floor elevation dissimilarity:
Floor slabs at same Elev.
Flor slabs at different Elev. (**0.5**)

Separation Jt.: ☐Yes ☐No

Longest span in Buildg.:
☐ ≤ 4 m ☐ 4-6 m ☐ > 6 m (**0.5**)

3. LOAD CARRYING SYSTEM FEATURES

Type :
☐Reinf. Conc. Frame
☐Reinf. Conc. Frame + Wall ☐Cast in place ☐Prefab
☐Betonarme Kutu (tamamen perde, tünel kalıp vs.)

☐Masonry ☐Stone ☐Clay tiles (Cavity Orient. : ☐Vertical ☐Hor.)
☐Solid terra cotta ☐Concrete masonry units

☐Steel frame ☐Moment resisting + braced ☐Industrial type

☐Timber ☐Timber frame filled with masonry ☐Timber frame + timber strips ☐Prefab

☐Hybrid (explain)

Slab system: ☐Slab on girders ☐Two-way joist
☐Joist infilled with Conc. ☐Timber ☐Uniform at all levels
☐One way joist ☐Steel ☐Nonuniform (explain)
☐Flat slab ☐Flat plate
(See Fig. 5)

Roof System :

Material : Geometry :
☐Reinf. Cons. ☐Galvanized tin (composite) ☐A ☐B ☐C ☐D
☐Roof tiles ☐Other (See Fig. 6)

Walls:
Basement peripheral walls: ☐Stone masonry ☐Concrete masonry
☐Reinf. Conc. ☐Clay units/Solid terra cotta ☐Other

Non-bearing partition walls at all levels:
☐Solid terra cotta ☐Clay masonry units ☐Other
☐Autoclaved concrete masonry unit

Load-bearing walls in masonry buildings :
☐ Solid terra cotta ☐ Concrete masonry ☐Stone masonry ☐Autoclaved units ☐Other
☐ Clay units (☐Cavities vertical ☐Cavities horizontal)

Intermediate tie beams in walls: Wall mortar :
☐Upper end of walls, continuous ☐Above openings only ☐Cement ☐Lime
☐Partial above openings (lintel) ☐Vertical tie beam ☐Under sills

Short columns :
☐Yes (**1.0**) ☐No
(See Fig. 7)

Site geology : Foundation system :
☐Rock/hard clay / Dense sand ☐Sand / hard clay ☐Indiv. Ftgs. ☐Cont. Ftg.
☐Loose sand / Soft clay (**0.25**) ☐Unknown (**0.25**) ☐Pile ☐Other
☐Mat ☐Unknown

Material quality: Workmanship :
☐1 ☐2 ☐3 (**0.5**) ☐4 (**0.5**) ☐1 ☐2 ☐3 (**0.5**) ☐4 (**0.5**)
(See Fig. 8) (See Fig. 9)

Additional Information for Reinforced Concrete Buildings:

Reinf.: ☐St I ☐StIII ☐Unknown

Concrete: If impact hammer is feasible ☐$\sigma_b < 100$ (**1.0**) ☐$100 < \sigma_b < 150$ (**1.0**) ☐$150 < \sigma_b < 225$ ☐$\sigma_b > 225$ Visual inspection: ☐Good ☐Inferior (**1.0**) ☐Unknown / variable (**1.0**)

4. DAMAGE RATING

Note : For hybrid buildings fill this section for the dominant material type or system.

Partial or total collapse in building: ☐Yes ☐No
If Yes then Heavy damage ☐ should be marked.

At ground or most everely damaged story level:

Permanent drift :	Drift-related damage	
☐$\delta/h \leq 0.0015$	0	
☐$0.0015 \leq \delta/h \leq 0.005$	2	δ = Permanent drift
☐$0.005 \leq \delta/h \leq 0.020$	5	h = Column or story height
☐$\delta/h \geq 0.020$	10	

Column Damage Distribution Matrix : (Show axes in plan scheme, add rows or columns as needed.)

This table is to be utilized only for marking column damage.

Y - DIRECTION	X - DIRECTION									
	1	2	3	4	5	6	7	8	9	10
A										
B										
C										
D										
E										
F										
G										

In this table enter 0 No damage 1 Light damage 2 Moderate damage 4 Severe damage
(See Fig. 10)

Cast in place reinforced concrete frame or frame + wall systems:

	Total No. (TN)	No Damage (N)	Light Damage (L)	Moderate Damage (M)	Severe Damage (S)	REI	EDS	TN*REI
Columns						2		
Girders (Fig. 11)						1		
Wall (Fig. 12)						6		
JoinTN (Fig. 13)						1		
Partition walls (Fig. 14)						0.5		
						TOTAL 1		TOTAL 2

Element Damage Score (EDS) = REI * (L*1 + M*2 + S*4)
System Damage Score (SDS) = 25* TOTAL 1 / TOTAL 2

Reinforced Concrete Box (Tunnel Form or Prefab) :

	Total No. (TN)	No damage (N)	Light damage (L)	Moderate damage (M)	Severe damage (S)	REI	EDS	TN*REI
Hor./Vert. Joints						2		
Interior walls						4		
Exterior walls						1		
						TOTAL 1		TOTAL 2

(See Figure 15)
EDS = REI * (L*1 + M*2 + S*4)
SDS = 25* TOTAL 1 / TOTAL 2

Load Bearing Masonry :

	Total No. (TN)	No damage (N)	Light damage (L)	Moderate damage (M)	Severe damage (S)
Walls					

(See Figure 16)
SDS = (L*1 + M*2 + S*4)*100/(4*TN)

Prefabricated Concrete Frame (Tunnel Form or Prefabricated) :

	Total No. (TN)	No damage (N)	Light damage (L)	Moderate damage (M)	Severe damage (S)	REI	EDS	TN*REI
Columns						3.5		
Beams						2		
Connections						6		
						TOTAL 1		TOTAL 2

(See Figure 17)
EDS = REI * (L*1 + M*2 + S*4)
SDS = 25* TOTAL 1 / TOTAL 2

Steel Frame :

	Total No. (TN)	No damage (N)	Light damage (L)	Moderate damage (M)	Severe damage (S)	REI	EDS	TN*REI
Columns						2		
Beams						1		
Col.-Beam Connections						6		
Infill walls						1		
Bracings						0.5		
						TOTAL 1		TOTAL 2

(See Figure 18)
EDS = REI * (L*1 + M*2 + S*4)
SDS = 25* TOTAL 1 / TOTAL 2

Timber :

	Wall Type	Total No. (TN)	No damage (N)	Light damage (L)	Moderate damage (M)	Severe damage (S)
Diaphram Walls						

(See Figure 19)
SDS = (L*1 + M*2 + S*4)*100/(4*TN)

Roof :

☐No damage *(0)* ☐ Light damage *(0)* ☐ Moderate damage *(0.75)* ☐ Sever damage *(1.5)*

(See Figure 20)

Staircase:

☐No damage *(0)* ☐ Cracking or Collapse *(1.0)*

(See Figure 20)

Amount of Excessive Foundation Settlement:

☐ ≤ 0.5 m *(0)* ☐ > 0.5 m *(1.5)*

5. CALCULATION OF TOTAL DAMAGE SCORE

1. Permanent Lateral Displacement Score (PLDS) :
2. SDS for given building type :
3. Damage Exacerbating Score (≤5) (DES) :
4. Rood and Staircase Damage Score (RSDS) :

Total Damage Score (TDS) = SDS*0.80 + RSDS + PLDS + DES + EFSS

0 ≤ TDS ≤ 5	No Damage
6 ≤ TDS ≤ 14	Slight Damage
15 ≤ TDS ≤ 43	Moderate Damage
TDS > 43	Severe Damage